“Forward modelling of petrological crust-forming processes on the early Earth”

Dissertation
zur Erlangung des Grades
„Doktor
der Naturwissenschaften“
im Promotionsfach Geowissenschaften

am Fachbereich Chemie, Pharmazie und Geowissenschaften
der Johannes Gutenberg-Universität
in Mainz

Karen Ziaja
geb. in Lehrte

Mainz, 21. Mai 2012

Dekan:

1. Berichterstatter:
2. Berichterstatter:

Tag der mündlichen Prüfung: 20.07.2012

Versicherung

für das Gesuch um Zulassung zur Promotion in dem Fachbereich 09

Hiermit versichere ich gemäß § 10 Abs. 3d der Promotionsordnung vom 24.07.2007

a) Ich habe die jetzt als Dissertation vorgelegte Arbeit selbst angefertigt und alle benutzten Hilfsmittel (Literatur, Apparaturen, Hilfsmittel) in der Arbeit angegeben.

b) Ich habe oder hatte die jetzt als Dissertation vorgelegte Arbeit nicht als Prüfungsarbeit für eine staatliche oder andere wissenschaftliche Prüfung eingereicht.

c) Ich hatte weder die jetzt als Dissertation vorgelegte Arbeit noch Teile davon bei einer anderen Fakultät bzw. einem anderen Fachbereich eingereicht.

______________________ ______________________

Datum Unterschrift

Acknowledgements

Abstract

Tonalite-trondhjemite-granodiorite (TTG) gneisses form up to two-thirds of the preserved Archean continental crust and there is considerable debate regarding the primary magmatic processes of the generation of these rocks. The popular theories indicate that these rocks were formed by partial melting of basaltic oceanic crust which was previously metamorphosed to garnet-amphibolite and/or eclogite facies conditions either at the base of thick oceanic crust or by subduction processes.

This study investigates a new aspect regarding the source rock for Archean continental crust which is inferred to have had a bulk compostion richer in magnesium (picrite) than present-day basaltic oceanic crust. This difference is supposed to originate from a higher geothermal gradient in the early Archean which may have induced higher degrees of partial melting in the mantle, which resulted in a thicker and more magnesian oceanic crust.

The methods used to investigate the role of a more MgO-rich source rock in the formation of TTG-like melts in the context of this new approach are mineral equilibria calculations with the software THERMOCALC and high-pressure experiments conducted from 10–20 kbar and 900–1100 °C, both combined in a forward modelling approach. Initially, *P–T* pseudosections for natural rock compositions with increasing MgO contents were calculated in the system NCFMASHTO (Na_2O–CaO–FeO–MgO–Al_2O_3–SiO_2–H_2O–TiO_2) to ascertain the metamorphic products from rocks with increasing MgO contents from a MORB up to a komatiite. A small number of previous experiments on komatiites showed the development of pyroxenite instead of eclogite and garnet-amphibolite during metamorphism and established that melts of these pyroxenites are of basaltic composition, thus again building oceanic crust instead of continental crust.

The *P–T* pseudosections calculated represent a continuous development of their metamorphic products from amphibolites and eclogites towards pyroxenites. On the basis of these calculations and the changes within the range of compositions, three picritic **M**odels of **A**rchean **O**ceanic **C**rust (MAOC) were established with different MgO contents (11, 13 and 15 wt%) ranging between basalt and komatiite. The thermodynamic modelling for MAOC 11, 13 and 15 at supersolidus conditions is imprecise since no appropriate melt model for metabasic rocks is currently available and the melt model for metapelitic rocks resulted in unsatisfactory calculations. The partially molten region is therfore covered by high-pressure experiments. The results of the experiments show a transition from predominantly tonalitic melts in MAOC 11 to basaltic melts in MAOC 15 and a solidus moving towards higher temperatures with increasing magnesium in the bulk composition. Tonalitic melts were generated in MAOC 11 and 13 at pressures ≥ 12.5 kbar in the presence of garnet + clinopyroxene + plagioclase ± quartz (± orthopyroxene in the presence of quartz and at lower pressures) in the absence of amphibole but it could not be explicitly indicated whether the tonalitic melts coexisting with an eclogitic residue and rutile at 20 kbar do belong to the Archean TTG suite. Basaltic melts were generated predominantly in the presence of granulite facies residues such as amphibole ± garnet ± plagioclase + orthopyroxene that lack quartz in all MAOC compositions at pressures ≤ 15 kbar.

The tonalitic melts generated in MAOC 11 and 13 indicate that thicker oceanic crust with more magnesium than that of a modern basalt is also a viable source for the generation of TTG-like melts and therefore continental crust in the Archean. The experimental results are related to different geologic settings as a function of pressure. The favoured setting for the generation of early TTG-like melts at 15 kbar is the base of an oceanic crust thicker than existing today or by melting of slabs in shallow subduction zones, both without interaction of tonalic melts with the mantle. Tonalitic melts at 20 kbar may have been generated below the plagioclase stability by slab melting in deeper subduction zones that have developed with time during the progressive cooling of the Earth, but it is unlikely that those melts reached lower pressure levels without further mantle interaction.

Zusammenfassung

Die heute noch erhaltene archaische kontinentale Kruste besteht bis zu zwei Dritteln aus Tonalit-Trondhjemit-Granodiorit (TTG)-Gneisen. Die Entstehung von Schmelzen, die zur Bildung der primären magmatischen Gesteine und somit zu ersten archaischen kontinentalen Krusten führten, steht jedoch erheblich zur Diskussion. Die verbreitetsten Theorien besagen, dass diese Gesteine nach metamorpher Umwandlung zu Granat-Amphibolith oder Eklogit und anschließendem partiellen Aufschmelzen entweder an der Unterseite von mächtiger ozeanischer Kruste oder durch Prozesse an Subduktionszonen entstanden sind.

Die vorliegende Arbeit stellt einen neuen Untersuchungsansatz hinsichtlich des Ausgangsgesteins für die erste kontinentale Kruste im Archaikum dar. Im Gegensatz zu heutiger basaltischer Ozeankruste könnte als Ausgangszusammensetzung eine magnesiumreichere Ozeankruste mit pikritischer Zusammensetzung in Frage kommen. Diese Annahme liegt darin begründet, dass im frühen Archaikum ein höherer Geothermischer Gradient vorhanden war, welcher eine stärkere partielle Aufschmelzung des Mantels und somit eine magnesiumreichere und mächtigere ozeanische Kruste zur Folge hatte.

In dieser Arbeit wurden thermodynamische Gleichgewichtsmodellierungen mit THERMOCALC sowie Hochdruckexperimente bei Drücken von 10–20 kbar und Temperaturen von 900–1100 °C in einem „forward modelling“ Ansatz miteinander kombiniert, um den möglichen Beitrag eines magnesiumreicheren Ausgangsgesteins während der Entstehung von ersten TTG-ähnlichen Schmelzen zu untersuchen. Im ersten Schritt wurden *P–T* Pseudosections für metamorphe Produkte von natürlichen Gesteinszusammensetzungen mit zunehmendem Magnesiumgehalt von Mittel-ozeanischem Rücken Basalt bis zu Komatiit im System NCFMASHTO (Na_2O–CaO–FeO–MgO–Al_2O_3–SiO_2–H_2O–TiO_2) modelliert. Eine geringe Anzahl an Experimenten mit Komatiiten haben im Vorfeld gezeigt, dass deren metamorphe Produkte Pyroxenite, und keine Granat-Amphibolithe oder Eklogite sind. Partielle Schmelzen von diesen Pyroxeniten sind wiederum basaltisch und würden daher weitere ozeanische Kruste anstatt kontinentaler Kruste bilden.

Die *P–T* Pseudosections bestätigen eine kontinuierliche Entwicklung der metamorphen Produkte von Amphibolith und Eklogit bis hin zu Pyroxenit. Auf dieser Basis sind drei **M**odelle für **a**rchaische **o**zeanische **K**ruste (MAOC) mit verschiedenen Gehalten an MgO (11, 13 und 15 Gew%) berechnet worden. Thermodynamische Mineralgleichgewichtsmodellierungen im Supersolidus-bereich von MAOC 11, MAOC 13 und MAOC 15 sind nicht zufriedenstellend möglich, da derzeit noch kein entsprechendes Schmelzmodell für metabasische Gesteine fertiggestellt ist. Das an dieser Stelle verwendete Schmelzmodell für metapelitische Gesteine ist in diesem Rahmen sehr ungenau. Um die partiell geschmolzenen Bereiche zu untersuchen wurden Hochdruckexperimente durchgeführt. Die Ergebnisse dieser Experimente zeigen einen Übergang von überwiegend tonalitischen Schmelzen in MAOC 11 zu basaltischen Schmelzen in MAOC 15 sowie eine Zunahme der Solidus-Temperatur mit zunehmendem Magnesiumgehalt der Ausgangszusammensetzungen.

Tonalitische Schmelzzusammensetzungen treten in MAOC 11 und 13 bei Drücken ≥ 12.5 kbar in Paragenese mit Granat + Klinopyroxen + Plagioklas ± Quarz (± Orthopyroxen in Gegenwart von Quarz bei niedrigem Druck) in der Abwesenheit von Amphibol auf. Inwiefern tonalitische Schmelzen, die bei 20 kbar im Gleichgewicht mit einem eklogitischen Residuum und Rutil gebildet wurden, zu den archaischen TTG-Gneisen gehören, kann im Rahmen dieser Arbeit nicht ausdrücklich bestimmt werden. Schmelzen mit basaltischer Zusammensetzung treten in allen MAOC Zusammensetzungen bei Drücken ≤ 15 kbar überwiegend in granulitischen Residuen mit Amphibol ± Granat ± Plagioklas ± Orthopyroxen und in der Abwesenheit von Quarz auf.

Die tonalitischen Schmelzen in MAOC 11 und 13 zeigen, dass ozeanische Kruste mit einem höheren MgO-Gehalt als heutige Mittelozeanische Rücken Basalte, mögliche Ausgangsgesteine für die Bildung von TTG-ähnlichen Schmelzen darstellen und somit auch für die Entstehung erster kontinentaler Kruste verantwortlich sind. Die Ergebnisse der Experimente können auch aufgrund der residualen Mineralparagenesen bei verschiedenen Drücken unterschiedlichen geologischen Bildungsbedingungen zugeordnet werden. Für die Experimente bei 12.5 und 15 kbar ist die Theorie wahrscheinlicher, dass das partielle Schmelzen an der Unterseite mächtiger ozeanischer Kruste oder in flachen Subduktionszonen stattfand, wobei die Schmelze anschließend nicht mit Mantelmaterial reagieren konnte. Die tonalitischen Schmelzen, die in den Experimenten bei 20 kbar in der Abwesenheit von Plagioklas gebildet wurden, sind tieferen Subduktionszonen, wie sie sich während der progressiven Abkühlung der Erde entwickelt haben können, zuzuordnen. Ein Aufstieg dieser tonalitischen Schmelzen ohne Interaktion mit dem Mantel ist jedoch unwahrscheinlich.

Table of contents

List of Figures

List of Tables

List of Abbreviations

amph	amphibole
gl	glaucophane
hb	hornblende
act	actinolite
parg.	pargasite
tscherm.	tschermakite
mg-hbl.	magnesiohornblende
cpx	clinopyroxene
di	diopside
o	omphacite
Ae	aegirine
Jd/jd	jadeite
En/en	enstatite
Fs/fs	ferrosilite
Wo/wo	wollastonite
C	corundum
chl	chlorite
g	garnet
py	pyrope
alm	almandine
andr	andradite
grs	grossular
ma	majorite
ep	epidote
Mag	magnetite
opx	orthopyroxene
Hyp	hypersthene
pl	plagioclase
Ab/ab	albite
An/an	anorthite
Or/or	orthoclase

oli	oligoclase
and	andesine
labr	labrodorite
by	bytownite
Ol/ol	olivine
Ilm/ilm	ilmenite
sp	spinel
law	lawsonite
Neph	nepheline
ru	rutile
sph	sphene
ky	kyanite
Q/q	quartz
ta	talc
liq	silica melt
α	asymmetry parameter
asf	asymmetric formalism
av	average
BSE	backscattered-electron
c	components in a system
DQF	Darken´s quadratic formalism
E–HPG	eclogite-high-pressure granulite
EOS	equations of state
ΔG^0	standard-state Gibbs energy of a reaction
Ga	Giga Annum (billion years)
GPa	Giga Pascal
G–UHT	ultrahigh-temperature granulite
HREE	heavy rare earth elements
HSA	high-silica adakites
HT–LP	high-temperature low-pressure
HP	high-pressure
K	equilibrium constant
LSA	low-silica adakites
LT–HP	low-temperature-high-pressure

Ma	Mega Annum (million years)
MAOC	Model of Archean oceanic crust
Mg#	Magnesium number (molecular Mg/Mg + Fe)
mol%	mole percent
MORB	mid-ocean ridge basalt
n	moles
$\mathrm{n}A$	nano Ampere
P	pressure
p	end-member proportion
p	phases in a system
pfu	per formula unit
$\mathrm{P}_{\mathrm{H2O}}$	water pressure
S	entropy
sd	standard deviation
sf	symmetric formalism
TTG	tonalite-trondhjemite-granodiorite
UHP	ultrahigh pressure
V	molar volume
v	variance
W	interaction energies
wt%	weight percent
X	composition
μ	chemical potential

Chapter 1

Introduction and outline

1.1 Introduction to the study

The understanding of the formation and evolution of the continental crust is a fundamental topic in petrological research. The evolution of continental crust occurred during continued processes of crust formation by melt extraction from the mantle and by further modification and reworking of former continental and oceanic crust, which in turn induced modifications of the mantle and the atmosphere. The associated melting processes led to an enrichment of incompatible elements in the melts from which the continental crust has formed. This chemically evolved crust was long regarded as an unique feature in our Solar System (e.g. Taylor, 1989; Rudnick, 1995) but it was shown that also the Martian crust is felsic in part (Christensen *et al.*, 2005). Although the continental crust is composed of a broad spectrum of magmatic, metamorphic and sedimentary rock types, its average composition is broadly andesitic (e.g. Taylor & McLennan, 1981, 1985; Rudnick & Gao, 2003) and it represents only 0.57 % of the mass of the Earth´s mantle (Rudnick, 1995; Hawkesworth & Kemp, 2006). Nevertheless, the continental crust covers ca. 40 % of the Earth´s surface area (Rudnick, 1995) and therefore hosts the best exposed rocks on Earth. There is evidence that 50 % of the continental crust was formed before the end of the Archean at 2.5 Ga (Rollinson, 2007) and that the formation occurred episodically with peaks at 2.7, 1.9 and 1.2 Ga (Hawkesworth & Kemp, 2006 and references therein). Several crustal growth curves based on different isotopic ratio investigations have been published, all indicating that the crustal growth rate decreases with time as a result of decreasing radioactive decay, especially since 2.0 Ga (e.g. Allègre & Rousseau, 1984; Taylor & McLennan, 1995; Nagler & Kramers, 1998; Collerson & Kamber, 1999; Condie, 2000). The oldest rocks on Earth are preserved in Archean cratons, e.g. the 4.03 Ga Acasta Gneiss in Canada (Bowring and Williams, 1999) and the 3.9–3.6 Ga Itsaq gneiss complex of Greenland

(Nutman *et al.*, 1996). A 4.4 Ga old detrital zircon in the Australian Jack Hills indicates the earliest evidence for continental crust and oceans on the Earth (Wilde *et al.*, 2001).

Up to two-thirds (e.g. Condie, 1981; Martin, 1994) of the Archean continental crust is composed of rocks of the tonalite-trondhjemite-granodiorite (TTG) suite with variable bulk rock compositions. Major differences may account from different source rock compositions or from the evolution through time during the secular cooling of the Earth (e.g. Martin & Moyen, 2002). There is general agreement that TTGs formed by partial melting of basaltic oceanic crust with 4–8 wt% MgO, which was previously hydrothermally altered and metamorphosed to garnet-amphibolite and/or eclogite facies rocks but there is still considerable debate regarding the generation of those rocks. The popular theories indicate that they were formed either by subduction zone processes with partial melting of the subducted slab or at the base of thick oceanic crust and subsequent partial melting.

1.2 The aim of the study

This study aims to contribute to the solution of the continued debate concerning the generation of TTG-like melts on the early Earth by using a forward modelling approach, combining mineral equilibria calculations with the software THERMOCALC and high-pressure partial melting experiments as well as the comparison of the two approaches. Former experiments concerning this topic were conducted for basaltic rocks, whereas the present study embodies a new aspect regarding the source rock, which is inferred to have a bulk rock compostion richer in MgO (picrite) than present-day basaltic oceanic crust. A higher geothermal gradient in the early Archean may have induced higher degrees of partial melting, which may then have resulted in thicker and more MgO-rich oceanic crust. This study is focused on partial melting of those primary picritic compositions and the approach used is based on the assumption of a picritic early oceanic crust, which evolved to lower magnesium content during the secular cooling of the Earth. The aim of this study is to ascertain the maximum magnesium content of oceanic crust, from which TTG-like melts can be generated at different *P*–*T* conditions as well as the relation of these conditions to geologic settings.

1.3 Outline of the study

Chapter 2 provides a general overview of the formation of oceanic and continental crust and the related metamorphism from modern times to estimates for the early Earth. The main focus lies on the genesis of early continental crust of the tonalite-trondhjemite-granodiorite suite, their potential modern analogues as well as on previous experimental work concerning the question of the generation of TTG under conditions prevailing during the early Earth.

Chapter 3 outlines the methods used to obtain the data presented in this study. These are thermodynamic equilibrium calculations with the software THERMOCALC, high-pressure partial melting experiments in a 650 ton 1-inch endloaded piston-cylinder press and mineral chemistry analysis with an electron microprobe.

Chapter 4 provides pseudosections for MORB, picritic and komatiitic rocks as well as for synthesised rock compositions. The synthesised rock compositions are based on the results of the previous modelling for the natural ones in the scope of the primary question of this thesis. The pseudosections were calculated with THERMOCALC to provide fundamental constraints of the metamorphic assemblages in regard to the intended high-pressure experiments.

Chapter 5 presents the results of the high-pressure partial melting experiments conducted on synthesised starting materials, whose compositions were ascertained on the basis of thermodynamic modelling and relates the results to potential geologic settings, in which early continental TTG-like crust from picritic materials may have formed.

Chapter 6 compares and discusses the thermodynamic modelling with the results of the high-pressure experiments.

Chapter 7 gives concluding remarks und suggestions for future research.

Chapter 2

Crust-forming processes during the history of the Earth and former experimental work

2.1 Introduction

This chapter presents a review of modern oceanic and continental crust-forming processes, the development of metamorphic conditions during the evolution of the Earth, considerations about crust forming processes on the early Earth as well as potential links from modern to Archean rocks. The chapter closes with an overview of previous experimental work.

2.2 Formation of crust and related metamorphism

2.2.1 Introduction to metamorphism

Metamorphism is the mineralogical and structural alteration of rocks in Earth´s crust with the exception of the alteration at or beneath the surface by weathering and early diagenesis (Vernon & Clarke, 2008). A fundamental tenet of metamorphism is the assumption that each rock with a specified composition (X) tends to reach the thermodynamic equilibrium with the lowest Gibbs energy at given pressure and temperature (subchapter 3.1.3.4.2). Changes in these variables (P, T, X) induced by vertical and lateral tectonic movement and percolating volatile fluids or melt lead to a readjustment of minerals under superimposed conditions. The preserved rock depends on the protolith and on the type of metamorphism which in turn is dependent on the peak P–T conditions, the P–T path and the deformation experienced. The preserved mineral assemblage normally reflects the inferred peak metamorphic conditions, which may have also experienced retrograde reaction. A qualitative subdivision of the P–T range is the concept of metamorphic facies defined by Escola (1915, 1921) and advanced by Turner (1981), who subdivided rocks due to their formation under broadly equivalent P–T conditions. The classification was drawn for modern mafic rock compositions with names on the basis of their metamorphic mineral assemblages, e.g.

greenschist, amphibolite, blueschist, eclogite and granulite facies with several subdivisions, e.g. garnet-amphibolite (subchapter 4). The intensity of metamorphism is specified by the “grade”, which is either low, medium or high (Vernon & Clarke, 2008).

2.2.2 Oceanic and continental crust-formation on the modern Earth and related metamorphism

2.2.2.1 Formation of modern oceanic crust

Basaltic oceanic crust is generated by decompression melting of the upwelling mantle below a mid-ocean ridge (MOR). It is also known as adiabatic melting, which occurs where hot lherzolitic mantle material (α-olivine + orthopyroxene + clinopyroxene + aluminous mineral) ascends passively towards lower levels with nearly no heat loss or gain and starts to partially melt when the material crosses the mantle solidus. Melting occurs in a triangular area directly beneath and several hundred kilometers on either side of a ridge and the first melt collects along grain boundaries until it reaches a critical proportion, which predominantly depends on the viscosity of melt (McKenzie, 1985). The melt may then migrate upwards, leaving depleted residues of harzburgite after the loss of clinopyroxene, and then dunite (only olivine) through further partial melting of the residue. Petrological analyses indicate a partial melting of 15 % to 20 % lherzolite to form the plagioclase-lherzolite and harzburgite residues (Mysen & Kushiro, 1977; Jaques & Green, 1980; Nicolas, 1989). Related to the mantle flow, the collected melt migrates below the suboceanic lithosphere. It then either merges with the oceanic crust by thermal accretion or coalescent melt channels build a network to convey the melt beneath the ridge into a magma chamber. The eruption at mid-ocean ridges produces the typical patterns of oceanic crust, which is composed of about 7 km mafic rocks in a characteristic sequence of basaltic pillow lavas, sheeted dyke complexes, layered gabbros and ultramafic cumulates with a various thickness of underlying ultramafic asthenosphere. The modern mantle has a potential temperature near 1430 °C (Green *et al.*, 2001) which is responsible for the 7 km thick modern oceanic crust. However, the hotter the mantle, the earlier the melting starts and the more melt with higher MgO will be produced. In modern fast-spreading ridges these primitive melts can approach the crust (Coogan *et al.*, 2002). Nicolas (1989) describes the differences between slow and fast spreading ridges by referring to them as lherzolite- and the more common harzburgite-type. The harzburgite-type is associated with higher degrees of partial melting and results in a thicker crustal section with quartz-tholeiites, whereas alkali-basalts occur in slow spreading ridges with thin crust (Ishiwatari, 1985; Nicolas, 1989). Nicolas (1989) infers that the distinction between the two types is not adaptive to the case of an unusal cold or hot mantle and gives the example of a hot spot, where the harzburgitic mantle as well as the crust are abnormally thick regardless of the spreading rate.

Large Igneous Provinces, especially oceanic plateaux made up of Ocean Island basalt (OIB) represent a particular form of oceanic crust. They occur over near stationary mantle plumes (hot spots) with unusually thick crust (e.g. up to 35 km for the Ontong Java plateau; Farnetari *et al.*, 1996) and originate by high-degree melts with very low water-contents (Arndt *et al.*, 1998; Foley *et al.*, 2002). This allows metamorphism to produce granulites and eclogites but not the more hydrous amphibolites (Foley *et al.*, 2002). The plateaux are dominated by tholeiitic basalts with small proportions of picrite (Farnetari *et al.*, 1996) and the underside of such thick oceanic crust may have rocks of high Mg# due to the high proportion of cumulates (Saunders *et al.*, 1996). However, the undersides of modern oceanic plateaux are not deep enough to cross the solidus in typical oceanic settings and hence they are not affected by partial melting processes.

2.2.2.2 Formation of modern continental crust

Present day formation of continental crust generally takes place at convergent plate boundaries where two plates converge against each other. On the one hand, subduction zones cause accretionary orogens like the Pacific rim with accompanied arc generation, and on the other hand there are subduction-to-collision orogens, where the collision of continents is superimposed on the accretionary complex, e.g. the Himalaya-Tibet system (Brown, 2006). The processes of continental crust formation in subduction zones are described first.

Oceanic crust, generated at modern mid-ocean ridges, becomes denser with time and with increasing distance from the mid-ocean ridge. At some time the crust becomes negatively buoyant and starts to subduct and then descends into the mantle (Forsyth & Uyeda, 1975). The oldest oceanic lithosphere is up to 160–180 Ma old (e.g. Müller *et al.*, 2008), e.g. parts of the Jurassic Izu Bonin Arc south of Japan (Condie, 1997) and the present mean age of subducted material is 60 Ma (Bickle, 1978). The subduction zone metamorphism of the descending plate is generally characterised by low-temperature-high-pressure (*LT–HP*) blueschist to eclogite facies rocks, achieving a *dT/dP* of 300–400 °C/GPa, which is approximately equivalent to 9–11 °C/km (Brown, 2006). Modern subduction-zones involve mid-ocean ridge basalt (MORB) with 4–8 wt% MgO and typical metamorphic products with increasing depth are greenschist, amphibolite and eclogite/blueschist facies rocks, given that the crust experienced hydrothermal alteration close to the mid-ocean ridge. If dry, these are granulite, garnet-granulite and eclogite facies rocks.

The generation of crust in oceanic arcs is summarised on the basis of an ordinary subduction zone, where oceanic crust descends under the arc (Macdonald *et al.*, 2000; Rollinson, 2007). At 50–60 km depth in the subduction zone, the amphibolitic oceanic crust starts to devolatilise, allowing fluids to penetrate the overlying mantle wedge where amphiboles form, which results in amphibole-peridotite. This is coupled to the subducted plate, which drags it to depth of around 110 km, where the breakdown of amphibole in the altered layer initiates partial melting of the mantle wedge. The partial melting zone migrates upwards and initiates further melting in the hotter regions of the overlying mantle wedge. The fact that these partial melts are basaltic, and that the avarage arc magmas are andesitic leads to the conclusion that the basaltic magmas fractionate in the lower continental crust by leaving a cumulatic mafic to ultramafic residue (Rollinson, 2007). This "wedge model" is the most likely model of today´s continental crust formation, supported by experimental studies of Pichavant *et al.* (2002), who showed that primitive arc basalts originated in the mantle in the presence of water. Melting of sediment and subducted slabs are further subordinate contributors for present day arc magma generation.

The second scenario for the generation of modern continental crust are subduction-to-collision orogens where metamorphism takes places in the collision zones. Brown (2006) highlighted a duality of thermal regimes, which he interprets to be the hallmark of plate tectonics and pointed out that two contrasting types of metamorphism at convergent plate boundaries are characteristic for the modern style of plate tectonics. These are on the one hand the *LT–HP* metamorphism in subduction zones as described above and on the other hand the high-temperature low-pressure (*HT–LP*) metamorphism in arc-backarc systems where granulites develop. Granulites are characterised by high *dT/dP* (>> 750 °C/GPa), equivalent to >> 20 °C/km (Brown, 2007). Today, granulites are likely being generated under orogenic plateaux (Gregoire *et al.,* 1994; Shafer *et al.*, 2005; Brown, 2006, 2007) and are exposed in middle to lower crust of young continental arcs (Lucassen & Franz, 1996; Brown, 2006).

Ultrahigh-pressure (*UHP*) metamorphism and lawsonite-bearing blueschists and eclogites (high-pressure (*HP*) metamorphism) are related to deep subduction of continental lithosphere in subduction-to-collision orogens (Brown, 2007). This is triggered by a previous subduction of oceanic rocks, whose slab pull leads the attached continental rocks also descending some distance into the subduction zone. After the slab pull ends, e.g. by slab-breakoff, the continental rocks become exhumed rapidly due to their buoyancy and are likely to be preserved. *UHP* terranes show *dT/dP* from 150–350 °C/GPa (4–10 °C/km) with hairpin-like *P–T–t* paths (syn-subduction exhumation) to 350–750 °C/GPa (10–20 °C/km) with near-isentropic decompression segments resulting from fast exhumation to Moho depth followed by thermal relaxation (Brown, 2007).

2.2.3 Metamorphism during the history of the Earth

The metamorphic rock record has evolved over time and reflects different conditions of crustal evolution throughout the Earth´s history, induced by secular changes of the thermal conditions on Earth. It is supposed that plate tectonics in its present form could not have operated since the beginning and that the tectonic style must have evolved as the planet cooled (Stern, 2007). The thermal gradients become higher with increasing age and reflect the higher temperatures and heat production in the early Earth (Fig. 2.2.1b, e.g. Bickle, 1978; Abbott & Hoffman, 1984; Brown, 1986; Martin, 1986; Martin & Moyen 2002). Granulite facies metamorphism in its different forms is common during the whole timespan and those rocks also occur in the Archean cratons. It is noteworthy that the established facies concept is based on modern metabasaltic rocks (subchapter 2.2.1) and that the mineral assemblages developed vary if magmatic rocks of different compositions experience metamorphism. However, the areas of the facies still cover the previously defined *P–T* ranges. By going back in time the main types of metamorphism are high-pressure to ultrahigh-pressure (*HP–UHP*) metamorphism, medium-temperature eclogite-high-pressure granulite (*E–HPG*) metamorphism and ultrahigh-temperature granulite (*G–UHT*) metamorphism (Fig. 2.2.1a, b).

High-pressure to ultrahigh-pressure (*HP–UHP*) metamorphism is characterised by blueschist and eclogite belts, which are recorded since the Neoproterozoic (Ediacaran) until today with thermal gradients of 150–350 °C/GPa (4–10 °C/km) and may be associated with low-temperature eclogites (Maruyama *et al.*, 1996;

Brown, 2007). It is a defining feature of modern plate tectonic processes and the absence of *HP–UHP* metamorphism before the Neoproterozoic implies a switch from an Archean mode of tectonics to a “Proterozoic plate tectonics” regime (Brown, 2006).

Medium-temperature eclogite high-pressure granulite (*E–HPG*) metamorphism is predominantely known from Proterozoic and Phanerozoic rocks and includes three periods coinciding with the first formation of supercratons (Superior/Sclavia) and supercontinents (Nuna, Rodinia). These rocks represent higher geotherms than those for modern subduction zones (Brown, 2006) in a thermal regime around 350–750 °C/GPa (10–20 °C/km). The oldest *E–HPG* metamorphic record dates the Neoarchean (in the 2.72 Ga old Fennoscandian Shield, Volodichev *et al.*, 2004; Brown, 2007) and exposed post-Carboniferous record of *E–HPG* is rare, which may reflect a lack of complete exhumation since that time. An example for younger (Jurassic to Early Cretaceous) high-pressure granulite metamorphism are rocks in New Zealand, metamorphosed at the Gondwana Pacific margin (Clarke *et al.*, 2000).

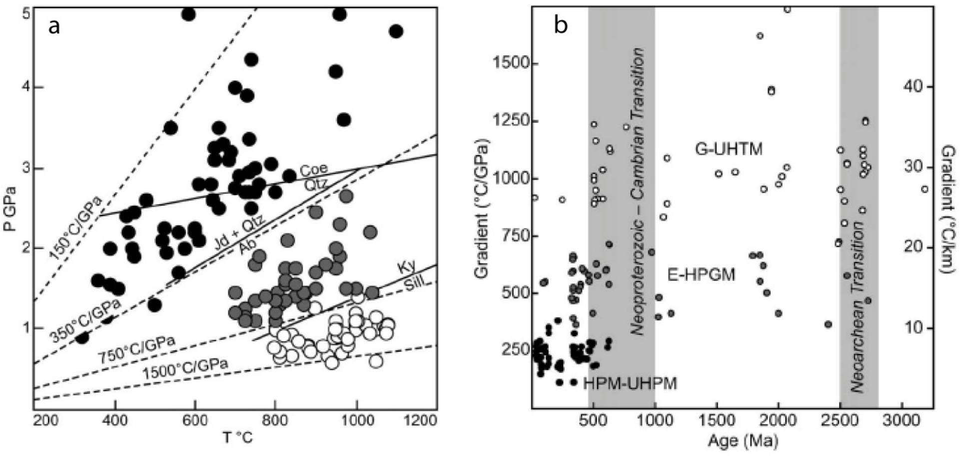

Figure 2.2.1a, b: Metamorphic patterns based on representative *P–T* data by belt in apparent thermal gradients (a) and apparent thermal gradients versus age of peak *P–T* and for three main types of metamorphic belts (b) (Brown, 2006, figs 1, 2). Open circles: granulite and ultrahigh-temperature (UHT) granulite metamorphic belts, gray circles: medium-temperature eclogite-high-pressure granulite (EHP–G) metamorphic belts, and filled circles: high-pressure–ultrahigh-pressure (HP–UHP) metamorphic belts.

Unlike common granulite facies metamorphism, ultrahigh-temperature granulite (*G–UHT*) metamorphism is largely restricted to Proterozoic rocks, of which the four main periods from the Neoarchean to the Lower Cambrian reflect the formation of supercratons (Superior/Sclavia) and supercontinents (Nuna, Rodinia, Gondwana) by crustal aggregation. The thermal regime is assumed to be >> 750 °C/GPa (>> 20 °C/km) with tight clockwise *P–T* paths.

2.3 Continental crust formation in the past, modern counterparts and previous experimental work

2.3.1 Introduction

The metamorphic rock record has evolved during the history of the Earth (subchapter 2.2.3) and this implies changes in the processes of rock formation, especially on the early Earth. Only little knowledge is given from the sparse rock record from the early Archean and the application of uniformitarianism, predicting that "the present is the key to the past" is adaptive only to physical and chemical processes and not to processes related to changing conditions on Earth (Stern, 2007). The potential compositions of rocks involved in building Archean oceanic crust and hence the first continental crust are supposed to have been different from the present-day ones as well as the crust-forming processes itself.

The next subchapter introduces the tonalite-trondjhemite-granodiorite (TTG) suite, which represents the major component (two-thirds) of the Archean continental crust (e.g. Condie, 1981; Martin & Moyen, 2002). TTGs occur in Archean cratons, which are generally composed of the three main lithological associations granite-gneiss terrains, greenstone belts and late Archean sedimentary basins (Rollinson, 2007), of which granite-gneiss terrains and greenstone belts host rocks of the TTG suite. The potential generation of TTGs is deduced on the basis of expected modern counterparts (subchapter 2.3.3) and experimental studies (subchapter 2.3.4).

2.3.2 Rocks of the Tonalite-Trondhjemite-Granodiorite Suite (TTG)

Rocks of the TTG suite are dominantly sodic granitoids (Moyen & Stevens, 2006) in Archean high-grade metamorphic (grey gneiss) and low-grade granite-greenstone terranes (Rapp *et al.*, 2003 and references therein), and their genesis is significant to early continental crust development (Jahn *et al.*, 1981). The magmatic TTG suites are characterised by low potassium and high silica contents (Rollinson, 2007), by paired low Nb/Ta and high Zr/Sm ratios (Foley *et al.*, 2002, 2003) and by an absent Sr-anomaly which indicates that plagioclase may have been a residual phase during the genesis of TTGs (Martin, 1999). The low concentrations of HREE and Y can be explained by the stability of garnet in the residue of melting from rocks like garnet-amphibolite or eclogite (e.g. Drummond & Defant, 1990; Rapp *et al.*, 1991;

Martin, 1999). The presence of amphibole is inferred using several arguments, e.g. low Nb/Ta, high Zr/Sm-ratios and concave REE-patterns. Furthermore, the presence of amphibole indicates a hydrated source (Foley *et al.*, 2002).

It is generally accepted that TTG suites were generated by partial melting of a hydrous metabasaltic source (e.g Barker & Arth, 1976; Jahn *et al.*, 1981; Rapp *et al.*, 1991; Sen & Dunn, 1994; Rapp & Watson, 1995; Martin, 1999; Rapp *et al.*, 1999; Smithies, 2000; Martin & Moyen, 2002, Moyen & Stevens, 2006), but there is debate whether the residue was either garnet-amphibolite (e.g. Foley *et al.*, 2002, 2003; Schmidt *et al.*, 2004; Moyen & Stevens, 2006) or eclogite (e.g. Rapp *et al.*, 2003). Furthermore, the geodynamic context in which this melting occured is still subject to debate (e.g. Martin, 1999; Smithies, 2000). Some workers argue for slab-melting in subduction-zones (e.g. Martin, 1986; Defant & Drummond, 1990; Zegers & van Keken, 2001; Foley, 2002), which most likely took place in a slab window along the thinned edge of a broken slab (Thorkelson & Breitsprecher, 2005) in an unusually warm slab (Peacock *et al.*, 1994), e.g. during subduction of young oceanic crust or of spreading ridges. Other arguments indicate melting at the base of a thick basaltic crust in several settings, e.g. overthickened oceanic crust, possibly related to delamination of the lower eclogitic part (e.g. Kröner, 1985; Kay & Mahlburg-Kay, 1991; Atherton & Petford, 1993; Muir *et al.*, 1995; Rudnick, 1995; Petford & Atherton, 1996; Johnson *et al.*, 1997; Albarède, 1998; Smithies, 2000; Zegers & van Keken, 2001; Moyen and Stevens, 2006). An approximate modern analogue for the underside of a thick crust are oceanic plateaux (Saunders *et al.*, 1996; subchapter 2.2.2.1), but the lower thermal gradients today prevent them from melting (Foley *et al.*, 2002). The modern oceanic plateau which best fits the high geothermal regime in the early Archean is Iceland (Martin *et al.,* 2008). Willbold *et al.* (2009, 2010) proposed that TTG-like dacitic melts were generated by plume- and rift axis-related high-pressure partial melting of basaltic lower crust after hydration of the basalt. This hypothesis is questioned by Martin *et al.* (2008, 2010) who argued that the pressures under Iceland are too low to stabilise garnet and that the felsic magmas on Iceland are unlike TTG.

Foley *et al.* (2002) stated that the formation of TTG-like continental crust requires slab-melting after the metamorphism of parts of the slab into garnet-amphibolite, which is achieved if the upper 3–4 km of the oceanic crust were previously hydrothermally altered (subchapter 2.3.3). Only melting of garnet-amphibolite is able to produce low Nb/Ta-ratios typical for TTG-like melts and melting of rutile-bearing eclogite produces melts with Nb/Ta ratios which are too high for TTG (Schmidt *et al.*, 2004; Foley *et al.*, 2002). In contrast, the view of Rapp *et al.* (2003) is that Nb/Ta-ratios in TTGs are either low or variable, and that compositionally appropriate TTG granitoids were produced by partial melting at the base of thickened, „arc-like“ crust in equilibrium with eclogite residues of basaltic source material. However, Moyen & Stevens (2006) surmised that the essential geochemical factor for the Nb/Ta-ratio is the presence or absence of rutile during melting and that TTGs of both origins are known. The question whether melting of garnet-amphibolite or eclogite may account for TTG-like melts is still debated. Moyen & Stevens (2006) also pointed out that melting of "amphibolite" or "eclogite" is somewhat misleading because incipient melting of amphibolite quickly results in melts in equilibrium with amphibole-free eclogitic assemblages also at amphibolite-facies depth.

2.3.3 Adakites as modern counterparts for Archean TTG genesis and their implications for early continental crust formation

A potential process which is proposed to have generated TTG-like melts in the Archean is slab melting. Rocks in modern slab melting environments are adakites which are comparable to TTGs and originate from melting of young (< 25 Ma), hot subducted slabs with variable degrees of interaction with the overlying mantle. This process is rare in modern arc environments due to the required high geotherms, which are normally not obtained in modern subduction zones (Peacock *et al.*, 1994) and it is in contrast to the dominant "wedge model" process (subchapter 2.2.2.2). Modern analogues for Archean continental crust formation by slab melting exist in geodynamic settings where young hot oceanic crust was subducted, e.g. at the circum-Pacific margin (fig. 1 in Martin, 1999). Adakites, as defined by Defant & Drummond (1990), are intermediate to felsic rocks with a compositional range between hornblende-andesite to dacite and rhyolite. These rocks are termed adakites after the Aleutian Adak Island (Kay, 1978) and exhibit the major element compositions ≥ 56 % SiO_2, ≥ 15 % Al_2O_3 (rarely lower) and usually < 3 % MgO (rarely above 6 % MgO). If adakites result from partial melting of a subducted slab, they must have aquired a number of their distinctive characteristics by a significant interaction with the mantle and possibly with the crust (Sen & Dunn, 1994). High-silica adakites (HSA, SiO_2 > 60 wt%) are thought to be slab melts from basaltic rocks which have interacted with the mantle to a small degree, whereas low-silica adakites (LSA, SiO_2 < 60 wt%) have higher MgO due to their increased interaction with the mantle peridotite (Martin *et al.*, 2005). The modern HSA are rare arc magmas, but they show geochemical similarities to middle and late Archean (< 3.3 Ga) TTG magmas (Fig. 2.3.1a). This leads to the conclusion that TTGs also have formed by slab melting that may have been more common in a hotter Archean environment (Martin, 1986, 1999). Martin *et al.* (2005) proposed that low-silica adakites show significant differences to TTG (Fig. 2.3.1a) and that they are rather similar to late Archean sanukitoids, which may have formed by a two-stage process where slab-derived melts metasomatised the overlying mantle prior to mantle melting. Sanukitoids were described for the first time by Shirey & Hanson (1984) and their temporal occurrence marks the transition to an environment where slab-melting was only a minor constituent to arc magma generation. Martin *et al.* (2005) conclude that the transition from early Archean TTG through Archean TTG to late Archean sanukitoids proceeded progressivly due to the increasing amount of interaction between the magmas and the mantle peridotite reflecting the origin of different adakites.

An alternative model for the generation of adakitic melt is proposed by Macpherson *et al.* (2006), who stated that any subduction zone has the potential to produce adakitic magma if the basaltic precursor was generated from fluid-modified mantle and then differentiated within the garnet-stability field.

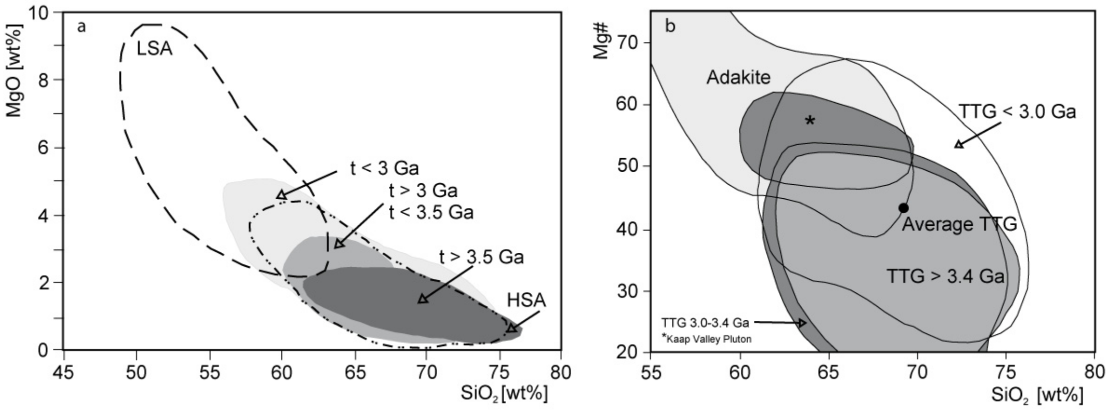

Figure 2.3.1a, b: Compositional ranges of SiO_2 vs. MgO (a, after Martin *et al.*, 2005, fig. 10) and Mg# (b, after Smithies 2000, fig. 4) for TTGs of several ages and different types of adakite. High-silica-adakites (HSA) are similar to early TTG whereas low-silica-adakites (LSA) overlap the fields of younger TTG in (a). Mg# increases from early to late Archean TTG and adakites (b).

Smithies (2000) stated that the generation of TTG magmas by subduction and slab-melting processes was only possible for pre-3.0 Ga TTGs due to the lack of overlap between adakites and TTG > 3.5 Ga in terms of SiO_2 vs. Mg#. He suggests that earlier TTG are rather formed by melting of hydrous basaltic material at the base of a thickened crust (e.g. Kay & Mahlburg-Kay, 1991; Atherton & Petford, 1993; Muir *et al.*, 1995; Petford & Atherton, 1996; Johnson *et al.*, 1997).

Martin & Moyen (2002) also state that the progressive cooling of the Earth led to secular changes in the compositions of TTG and that first melts from slabs were generated at 4.0 Ga by shallow melting in the stability field of plagioclase. The melting occured at greater depth during time due to the lowering geothermal gradient and more interaction of the slab melts with the mantle material during ascent. Therefore, the evolution of the TTG composition may have been coupled to the increasing mantle-interaction, expressed by increasing values of #Mg, Ni and Cr. Furthermore, Martin & Moyen (2002) link the enrichment in (Na_2O + CaO) and Sr to the limited residual stability of plagioclase during melting at increasing depth in response to the higher pressures of the deepened subduction zones. As already mentioned, TTGs > 3.5 Ga could be consistent with melting at the base of oceanic plateaux and these early Archean TTGs have relatively low Mg# with no evidence for interactions with the mantle wedge. They are inferred to have formed at shallow depth, e.g. in a low angle dipping slab or in a thick basaltic lava pile, but their origin is not yet resolved (Rollinson, 2007). Melting at these shallow depths was facilitated by the higher heat production in the early Archean (e.g. Bickle, 1978; Abbott & Hoffman, 1984; Brown, 1986; Martin, 1986; Martin & Moyen, 2002) and the resulting higher geothermal gradients (e.g. Bickle, 1978; Abbott & Hoffman, 1984; Martin, 1986), which permit melting within the plagioclase stability field. Bickle (1978) and Abbott & Hoffman (1984) infer faster spreading rates, a thicker oceanic crust, smaller plates (Hargraves, 1986) and therefore, if subduction occured, a younger average age (20 Ma) of the subducted crust. The high heat flow in the early Earth may have also caused higher degrees of melting at mid-ocean ridges (e.g. Bickle, 1994). Foley *et al.* (2003) proposed that the early Archean oceanic crust was more magnesian than today´s mid-ocean ridge basalt due to the higher proportion of melting in spreading centres, being probably comparable to komatiites (Arndt, 1983; Nisbet & Fowler, 1983). In modern fast-spreading ridges (e.g. Oman ophiolite), primitive MgO-rich melts are able to approach the crust (Coogan *et al.*, 2002), which leads to the inference that the supposed fast-spreading Archean ridges were also composed of more primitive (high MgO) components (Foley *et al.*, 2003).

High-pressure experiments conducted on a komatiite from Gorgona Island (17.5 wt% MgO) showed that metamorphic products of komatiites and ultramafic cumulates are plagioclase-free (garnet-) amphibole-pyroxenites and that the incoming of garnet lies at higher pressures than those for MORB (Foley *et al.* 2003). Partial melts of these pyroxenites would have led to basaltic and nephelinitic melts that do not resemble TTG (Foley *et al.*, 1999) and would again building oceanic crust. These results exclude a komatiitic source for metamorphism to garnet-amphibolite (or eclogite) and suggest that there may be important differences in magmatic processes in subduction zones as a function of time. The differences might have been a thicker ultramafic crust which was too thick to be subducted or buried as a coherent unit (Abbott & Mooney, 1995) and therefore a delamination of just the lower unaltered part was likely. Metamorphism and melting of this lower unaltered ultramafic part, metamorphosed to pyroxenite, led to basaltic melts (Foley *et al.*, 1999) in a pre-subduction stage. Hydrothermal alteration at ridges along faults is not likely to reach deeper than the uppermost 3 or 4 km (Bickle *et al.*, 1994) and therefore partial melting of the complete oceanic crust, including the hydrated upper part, as a slab could not have taken place if the crust was too thick. During the progressive cooling of the Earth, when the oceanic crust became progressively thinner and poorer in magnesium, it may have became possible to subduct or bury the complete and partially hydrated crust (Abbott & Mooney, 1995; Foley, 2003), metamorphosed to garnet-amphibolite (Foley *et al.,* 2002) or eclogite (Rapp *et al.,* 2003) before partial melting and generation of TTG-like melts (e.g Barker & Arth, 1976; Jahn *et al.*, 1981; Rapp *et al.*, 1991; Sen & Dunn, 1994; Rapp & Watson, 1995; Martin, 1999; Rapp *et al.*, 1999; Smithies, 2000; Martin & Moyen, 2002; Foley *et al.*, 2002, 2003; Rapp *et al.*, 2003; Schmidt *et al.*, 2004; Moyen & Stevens, 2006).

The stability diagrams for the metamorphic products of komatiite (pyroxenites) and MORB (amphibolites) are illustrated in Fig. 2.3.2 (fig. 2 in Foley *et al.*, 2003). However, the details of the compositional change in bulk compositions of the rocks involved in these processes and the transition of their metamorphic products from pyroxenites to amphibolites remain poorly understood.

2.3.4 Experimental investigations on the genesis of TTG

The genesis of TTG has been investigated by several partial melting experimental studies on amphibolites and eclogites. The starting materials were broadly basaltic (basalts to basaltic andesites) and generally belonging to the tholeiitic series (Moyen & Stevens, 2006). With the exception of Foley *et al.* (2003), who investigated a komatiite, no picritic or komatiitic source rocks have been investigated with the expressed intention of testing melting of more magnesian Archean oceanic crust. Based on evidence of isotope and trace elements the mantle is supposed to be inhomogeneous and may include old oceanic crust in addition to the typical mantle peridotite (Pertermann & Hirschmann, 2003) and there have been many studies of mafic lithologies (pyroxenites) to figure out the contribution of pyroxenite in the upper mantle to the generation of basalt (summarised by Kogiso *et al.*, 2004).

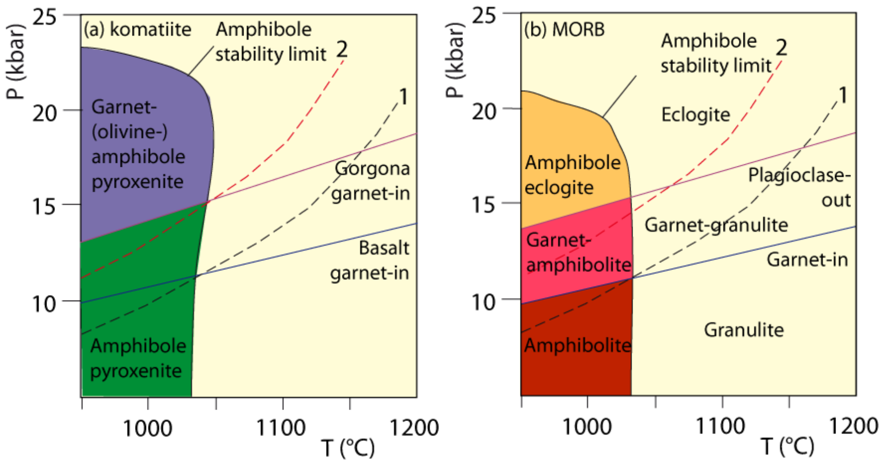

Figure 2.3.2a, b: Stability diagrams for metamorphic products of potential Archean oceanic crust with geotherms for early (1) and late (2) Archean after Foley *et al.* (2003, fig. 2). The coloured regions represent rocks produced by subduction metamorphism of the Gorgona komatiite (a) and MORB (b). Garnet-amphibolite, as required for the generation of TTG-like partial melts by slab melting is not developed for the metamorphosed komatiite but in the metamorphosed MORB.

The previous experiments on amphibolites and eclogites were conducted under different water saturation conditions. Fluid-absent melting occurs in metabasalts when less than ca. 1.8 wt% water is present in the rock (Zamora, 2000; Moyen & Stevens, 2006), and when all water in the system is accommodated in hydrous minerals. The hydrous minerals have to be stable at least to the conditions of the relevant solidus (Moyen & Stevens, 2006). Fluid-absent melting is the type of melting used also for the experiments in this study (Chapter 5). Further types of melting are: H_2O-free or anhydrous melting, fluid-present melting with water-saturated starting compositions and melting without a free fluid phase (Vielzeuf & Schmidt, 2001).

Rapp *et al.* (1991) and Rapp & Watson (1995) studied a spectrum of Archean tholeiites, high-alumina basalts, low-potassium tholeiites and alkali-rich basalts at pressures between 8 and 32 kbar and temperatures of 1000–1150 °C under fluid-absent conditions. Partial melting experiments in roughly the same *P*–*T* range as used for the experiments in the present study (10–20 kbar and 900–1050 °C), but with varying water-saturation conditions, were done by Winther & Newton (1991), Sen & Dunn (1994), Winther (1996), Springer & Seck (1997) and, with an eclogitic starting composition, by Skjerle & Patino-Douce (2002). Eclogitic starting material was also used by Laurie & Stevens (2010) for experiments at lower temperatures than investigated in this study. Other essential studies with lower *P–T* conditions than used in this study were done by Rushmer (1991), Wolf & Wyllie (1994) and by Beard and Lofgren (1989, 1991), who showed that adakitic magmas form during dehydration melting and not under water-saturated conditions (Martin, 1999). In summary, melting of alkali-basalts and tholeiites under various P_{H2O}-conditions lead to rather tonalitic rather than trondhjemitic melts (e.g. Holloway & Burnham, 1972; Helz, 1976; Martin, 1999).

The studies summarised above involve investigations regarding the stability of phases and for major and trace element partitioning to achieve conclusions about the boundary parameters for the genesis of TTG at pressures above 15 kbar and temperatures from 900–1100 °C (Moyen & Stevens, 2006). The pressure is limited by the stability of plagioclase (on the basis of Sr and Eu), by the garnet-stability (on the basis of Yb), and by the presence or absence of rutile (subchapter 2.3.2) in the residuum during melting. The stability fields of the observed phases and the position of the solidus in the precedent studies are further discussed in the scope of the experiments conducted in this study (subchapter 5.4.2).

Moyen & Stevens (2006) pointed out that some studies have used lithologies that were too felsic as starting material to adress the question of TTG formation and that a depleted MORB or komatiite can not account for the compositions of major and trace elements in TTGs. On the basis of the major and trace element investigations they also concluded that Archean TTGs were products of fluid-absent partial melting of metabasites (relatively enriched basalts) at pressures above 15 kbar and temperatures between 900–1100 °C. They proposed low geothermal gradients (ca. 20 °C/km at 50 km or more) in subduction zones that were hotter than today. Moyen & Stevens (2004) referred to unusually low pressure TTG genesis early in the cratonic history probably formed by melting of underplated basalts at the base of thick oceanic plateaus or in a stack of oceanic crust “slices” (De Wit & Hart, 1993) at geothermal gradients of ca. 30 °C/km and Moyen and Stevens (2006) also do not exclude further mechanisms of TTG genesis.

Chapter 3

Methods

3.1 Thermodynamic equilibrium calculations for metamorphic rocks with the software THERMOCALC

3.1.1 Introduction

Several computer software packages can be used for thermodynamic calculations on metamorphic rocks such as thermobarometry or the definition of the thermodynamically stable mineral assemblages for a specific rock composition in a chemical system. A stable equilibrium mineral assemblage for imposed conditions is represented by the assemblage with the lowest Gibbs energy. In an equilibrium model of metamorphism, changes in assemblages, mineral proportions and compositions occur in response to varying *P*–*T* conditions during metamorphism, in an attempt to achieve thermodynamic equilibrium. The reactions predominantly occur on the prograde path where fluid is produced from the breakdown of hydrous phases, e.g. amphibole. The peak assemblage as well as the textures formed along the prograde path of a rock are generally preserved during the retrograde path due to the absence of fluids or melt to allow retrograde reaction (Fyfe, 1973; Guiraud *et al.,* 2001; White & Powell, 2002). The study of the preserved assemblages commonly utilises thermodynamic equilibrium calculations. Powell & Holland (2010) summarise two types of modelling, these are *inverse* and *forward* modelling, of which the first one is based on minerals and their measured compositions to constrain the *P* and *T* of formation of a rock (conventional thermobarometry). With the development of thermodynamic datasets, *forward* modelling became common, especially by using the bulk rock compositions to calculate *P*–*T* pseudosections (subchapter 3.1.3.2.5 and 3.1.3.5).

Previous studies showed good agreement between thermodynamic calculations and experiments, e.g. Zen (1972), Helgeson *et al.* (1978) and Wood & Holloway (1984). Powell & Holland (Powell & Holland, 1985, 1988; Holland & Powell, 1985) introduced THERMOCALC to the field of metamorphic petrology and further software for performing thermodynamic modelling are Theriak-Domino (de Capitani & Brown, 1987) and Perplex (Connolly, 1990). They all are based on internally consistent thermodynamic datasets of mineral end-members based on experimentally-determined mineral equilibria. This chapter tracks the development, methology and application of THERMOCALC covering primarily the required topics of this study, in which the software is used to construct *P–T* and *T–X* pseudosections for metabasic rocks in the context of the evolution of the first continental crust. For further information the THERMOCALC homepage is available at http://www.metamorph.geo.mainz.de/thermocalc/index.html.

3.1.2 The theory of thermodynamic equilibrium calculations

The software THERMOCALC is used for equilibrium thermodynamic calculations on metamorphic rocks. This chapter outlines a number of different methods and thermodynamic descriptions that are used for the determination of the required data. Holland & Powell (1985) created a thermodynamic database and stated that, as long as the dataset covers the reliable data for all phases in the desired reaction, any equilibrium reaction may be calculated from this internally consistent thermodynamic dataset. It combines and makes consistent constraints from experimentally determined phase equilibria with calorimetric data from the thermodynamic properties of the end-members of phases (Tab. 3.1.1). The internally consistent database can be combined with activity-composition (*a–x*) relationships (subchapter 3.1.2.2) of the combined end-members to form a solid-solution phase (Powell & Holland, 2010).

3.1.2.1 The development of internally consistent thermodynamic datasets and the required data

3.1.2.1.1 Introduction

An internally consistent dataset for end-members is required to undertake thermodynamic calculations with the software THERMOCALC. It is made up of thermodynamic properties for the mineral end-members with information about volume, enthalpy, entropy, heat capacity, compressibility and expansibility. It was presumed that the thermodynamic data for end-members needed for the dataset were available or could be reliably estimated with the exception of the enthalpies of formation of the mineral end-members (Helgeson *et al.*, 1978; Powell & Holland, 1985). Initially, Powell & Holland (1985) accepted the methodology of Holland (1981) concerning heat capacities, volumes and entropies. Thermal expansion and isothermal compressibility were fitted by linear equations and Darken´s quadratic formalism (DQF) was used to describe volume- and enthalpy-composition relationships (Powell, 1987). This subchapter introduces the development and advancement of the methods used to create an internally consistent thermodynamic dataset and provides information about the internally consistent thermodynamic datasets itself and the software THERMOCALC.

3.1.2.1.2 Enthalpy of formation

There is no absolute enthalpy for a particular substance but it was possible to calculate differences in enthalpies from a defined anchor phase (Holland & Powell, 1985). Values for enthalpies of formation derived from experimental (phase equilibrium studies) bracketing data (notation adopted from Demarest & Haselton, 1981) and experimental *P–T* brackets were used to determine enthalpy of reaction brackets, which then were processed to achieve an overall enthalpy of one reaction bracket for each reaction (Powell & Holland, 1985).

3.1.2.1.3 Least squares approach and the internally consistent dataset

Powell & Holland (1985) set up an internally consistent dataset with the knowledge about the enthalpy of formation and they chose a weighted least squares approach (using covariance matrices in the process), which allowed the simultaneous generation of all thermodynamic data. An important difference of the least squares approach to previous alternatives (linear programming, e.g. Halbach & Chatterjee, 1982; and incremental approach, e.g. Helgeson *et al.*, 1978; Powell, 1978) was the ability to determine the uncertainties on, and correlations between, the enthalpies of formation for all phases in the set. In addition, the ability to determine uncertainties in any phase equilibrium calculations performed by simple error propagation techniques was given (Holland & Powell, 1985).

By application of a least squares approach, involving 60 reaction equilibria among 43 phases in the system K_2O–Na_2O–CaO–MgO–Al_2O_3–TiO_2–SiO_2–H_2O–CO_2, Holland & Powell (1985) demonstrated that it is possible to attain a well-constrained internally consistent set of thermodynamic data and that there is an impressive consistency among many experimental studies and high-temperature calorimetric data.

3.1.2.1.4 The software THERMOCALC

Powell & Holland (1988) made recommendations for uncertainties on activities and showed applications for the internally consistent dataset, which can be used for various thermodynamic calculations using the Pascal computer program THERMOCALC (subchapter 3.1.3.4). The program can be applied to recalibrate conventional barometers such as the garnet-pyroxene-plagioclase-quartz barometry of Newton & Perkins (1982) or to construct phase diagrams to determine variations of phase relationships with pressure and temperature for specified bulk compositions.

3.1.2.1.5 Calculations involving solid solutions

Holland & Powell (1990) presented an enlarged and updated internally consistent thermodynamic dataset within the system K_2O–Na_2O–CaO–MgO–MnO–FeO–Fe_2O_3–Al_2O_3–TiO_2–SiO_2–C–H_2–O_2. It consisted of 123 mineral and fluid end-members. This larger set of mineral end-members permit the calculation of compositions of complex solid solutions involving invariant, univariant and divariant equilibria, rather than being restricted to “end-member” phase diagrams. Whereas in Powell & Holland (1985) the mixing properties of CO_2–H_2O fluids had not yet been well known, the fugacity polynomials for CO_2 and H_2O are improved in Holland & Powell (1990). Other new features included Tschermak´s substitutions in orthopyroxene, clinopyroxene, amphibole, white mica, biotite, chlorite and talc by using the approach of ideal mixing on sites for mineral solid solutions. Ideal charge balance was assumed only for aluminous pyroxenes. According to magnetic disordering at high temperatures, some iron-bearing minerals have lambda heat capacity anomalies, so they applied simple Landau theory for the handling of Si–Al order-disorder in equilibrium feldspars. Landau theory describes the disordered state at high temperatures relative to the ordered state of minerals at low temperatures. To extract the enthalpies of formation for iron-silicates and carbonate end-members, Fe/Mg partitioning-experiments among pairs of those minerals were used and some natural data (Fe/Mg and Al/Fe^{3+}-partitioning) were employed to incorporate mineral end-members for which no experimental date were available. The H_2O and CO_2 contents of cordierites were explicitly defined as a function of pressure and temperature and Holland & Powell (1990) took the equations of Kurepin (1985) to model the uptake of volatiles from Fe-cordierite assuming an identical behaviour of Fe- and Mg-cordierite, whereas the behaviour of the magnesian counterpart was determined experimentally.

The enthalpies of formation of the end-members remained constant except for clinochlore and phlogopite, whereas the method of conversion to one *cumulative* enthalpy bracket was refined (Powell & Holland, 1985). Entropies for some minerals have changed according to new measurements of Berman (1988) who presented another internally consistent dataset. Berman (1988) improved the state of knowledge for many minerals, but he used a linear programming method, which unlike the approach of Holland and Powell did not allow the derivation of uncertainties and correlations between end-member thermodynamics.

The anchor-approach was no longer required in the new dataset from Holland & Powell (1990) because there has been a consistency between calorimetric measurements and phase equilibrium data; hence most of the data were included as separate calorimetric constraints.

According to the new dataset, many calculations were done for metamorphic rocks, e.g. a petrogenetic grid for ultramafic rocks from Will *et al.* (1990). Methods used to obtain the data required for petrological calculations have always been, and still are in a progress of developing and advancement. These are, for instance, the appliance of Landau theory for modelling activities of components in omphacitic solid solutions (Holland, 1990) or the modified appliance of the least squares approach due to an increasing volume of experimental and calorimetric data (Powell & Holland, 1993a).

3.1.2.1.6 The internally consistent dataset used in this study

Holland & Powell (2011) introduced a new dateset for thermodynamic calculations but the dataset used in this study is that from Holland & Powell (1998). The dataset from Holland & Powell (1998) includes 154 mineral end-members, 13 silicate liquid end-members and 22 aqueous fluids. Holland & Powell (1998) introduced new end-members for the subsystems and presented a modified methology adjusted to changes in thermodynamic data and to the equations of state (EOS) that had been used. The changes in methology occurred in thermal expansion, compressibility, extrapolation of heat capacity, EOS for fluid phases, hydrous cordierite and for pressure dependence in Landau theory disordering as well as for aqueous and melt species. The new data set allows calculations up to pressures higher than 100 kbar for mineral-fluid equilibria. The included melt end-members enabled calculations of melt mixing models in NCKFMASH for the first time. Holland & Powell (1998) tried to avoid uncertainties derived by using mixing models in solid solutions, but some end-member enthalpies may only be derived from equilibria with the end-member concerned occuring as part of a solid solution. Activity models for solid solutions were described for phengite, biotite, tremolite-tschermakite amphibole, clinozoisite-epidote, chlorite, aluminous talc, sapphirine, pyroxene, cummingtonite-grunerite and for Fe–Mg non-ideality. They applied the symmetric formalism in cases where non-ideality was involved. Together with the software THERMOCALC (Powell & Holland, 1988) this new data set enables the user to do phase equilibrium calculations in which natural systems can be more closely modelled. The dataset ds55 was updated on 22 November 2003.

3.1.2.2 Activity composition *(a–x)* models

3.1.2.2.1 Introduction

The *a–x* relationships describe the distribution of elements on sites between the end-members of a phase as well as the interaction energies between those end-members and are needed for reliable calculation of conditions of rock formation and for the calculation of phase diagrams (Holland & Powell, 1996a). There are two key aspects of the *a–x* models. First, the distribution of components on multiple sites is either done by equipartition or by order-disordering in minerals (subchapter 3.1.2.2.2) and second, the thermodynamics of mixing are ideal, symmetric or asymmetric (subchapter 3.1.2.2.3).

Powell (1987) characterised Darken´s quadratic formalism as a model for consistent descriptions of these *a–x* relationships for binary mineral solid solutions. Activity data for H_2O–CO_2-fluids were taken from Kerrick & Jacobs (1981), who assumed a non-ideal mixing (subregular model) involving mixtures of H_2O and CO_2.

The *a–x* models used in this study are those for amphibole (Diener *et al.*, 2007), clinopyroxene (Green *et al.*, 2007), chlorite (Holland *et al.*, 1998), garnet (White *et al.*, 2007), epidote (Holland & Powell, 1998), plagioclase (Holland & Powell, 2003), talc (Holland & Powell, 1998), ilmenite and hematite (White *et al.*, 2000) and olivine (Holland, unpublished).

3.1.2.2.2 Distribution of elements on sites

Where a component occupies more then one site, the distribution of components on sites is either done by equipartition or by order-disorder in minerals. Equipartition was initially used for many minerals (pyroxenes, amphiboles, micas, chlorites) particularly with respect to Fe–Mg distribution, but this was a common default option for thermodynamic calculations in petrology where limited data existed. For Fe–Mg distribution, equipartition involved keeping the same xFe (xFe = Fe/Fe + Mg) on each site (Holland & Powell, 2006). A slightly different form of equipartition was used for minor components (e.g. Mn) in phases where the minor component was equally distributed between sites such that the amount on each site was the same. Problems with equipartition are shown in Holland & Powell (2006).

Order-disorder models in contrast have order parameters (e.g. “N”, “Q”) to handle the different distributions of one or more elements on different sites. Holland & Powell (1996a, b) applied the symmetric formalism (subchapter 3.1.2.2.3) to order-disorder in minerals of fixed compositions and to solid solutions. In handling order-disorder in a mineral, a fully ordered end-member is developed and the mineral is treated as a solid solution between an independent set of end-members that includes this ordered end-member. A set of independent end-members is a group of end-members representing a mineral solid solution, which is able to depict a complete thermodynamic description of a phase. Thus the range of composition and ordering states of the phase can be represented (Holland & Powell, 1996a, b).

3.1.2.2.3 Thermodynamics of mixing: Ideal mixing, symmetric and asymmetric formalism

Powell & Holland (1993b) stated that a simple and powerful way of handling the thermodynamics of cation-dominated order-disorder in minerals is presented by the symmetric formalism. One important aspect of this model is that it is a “macroscopic” model where *a–x* relationships are written between end-members rather than complex mixing “on-sites”, which would represent a “microscopic” model. Holland & Powell (1996a) extended the symmetric formalism to minerals, in which the state of order varies with parameters like temperature and composition.

In contrast to the assumption about ideal mixing, where ideal interactions between end-members exist, most minerals have non-ideal interactions between their end-members, expressed through interaction parameters (W´s). If these are symmetric ($Wij = Wji \neq 0$), the symmetric formalism is described as a powerful instrument for putting thermodynamics of mixing into practice as the representation of thermodynamics is simple as well as flexible due to the small number of adjustable parameters required. It represents an important simplification to ascertain the *a–x* relationships between minerals with end-members whose sites contain more than one element, e.g. hornblende (Powell & Holland, 1993b). Previous models used thermodynamic mole fractions written in terms of ideal mixing with activity-composition terms written separately (Holland & Powell, 1996a). The simplification related to the formulation of non-ideality with symmetric enthalpic interactions involving all sites (including same-site (regular) and cross-site (reciprocal, Bragg-Williams) interactions). The *a–x* relationships were specified by an interaction energy for the constituent binary joins used to represent a phase (Holland & Powell, 2003). Due to the macroscopic nature of the symmetric model, problems with formulating many pairwise microscopic ("on-site") interactions in complex multisite phases are avoided (Holland & Powell, 2003). This is important for paired exchanges, e.g. CaAl=SiNa in plagioclase, where the microscopic exchanges cannot be considered separately.

The asymmetric formalism is a further modification of the *a–x* methodology (Holland & Powell, 2003) and extends the symmetric formalism from Powell & Holland (1993b). For the asymmetric formalism they reformulated the van Laar model into a convenient form for multicomponent asymmetric solutions. The van Laar formulation involves a modification of a symmetric parameter via a size rather than having to specify two interaction parameters such as Wij $\neq$ Wji. The size parameter α for every end-member adapted for fluid mixtures, minerals and silicate liquid determines the degree of asymmetry: if αi = αj, the binary remains symmetric, but is asymmetric if αi $\neq$ αj.

3.1.2.2.4 *a–x* coding - an example using garnet

The *a–x* coding used for the calculations with the software THERMOCALC involves definitions of compositional variables and the definition of end-member proportions and site fractions by using these variables. The code includes the ideal activties of each end-member and any non-ideal interaction parameters. The *a–x* coding for garnet is described here as an example: Informations in a line following "%" are not read by THERMOCALC and contain additional information for the user. The *a–x* coding file "tc-NCFMASHTO" with all phases is presented in the electronic Appendix A7.

At first the mineral name and reference are given:

```
% ============================================================
% Garnet:
% White, RW, Powell, R & Holland, TJB (2007) Progress relating to calculation
% of partial melting equilibria for metapelites. Journal of Metamorphic Geology,
% 25, 511-527.
%
% this model is somewhat less asymmetric than used in the calculations
% of the above paper, but this is our currently preferred model
```

The definition of the compositional variables *x, z* and *f* are:

```
% x= Fe2/(Fe2 + Mg), z= Ca/(Fe2 + Mg + Ca), f = Fe3/2
```

The mineral abbreviation (g), number of end-members (4) and starting guesses for the compositional variables *x, z* and *f* are:

```
g 4         % garnet with ferric (and van Laar)

x(g)        0.87
z(g)        0.235
f(g)        0.046
```

The definitions of the end-member proportions (p) are the "terms" and the end-members always occur in the same order. The end-members for garnet are almandine (alm), pyrope (py), grossular (gr) and andradite (andr). The terms for the end-members are arranged in blocks, of which the first one, e.g. for almandine "1 2" gives the information that the term for alm is composed of "1" line with "2" blocks of functions after the first one. Block 2 is: "1-z" and Block 3 is "1x" Due to their appearance in the same line they have to be multiplied with each other such that p(alm) = (1-z)x. If a term consists of several lines, the first function block of the next line have to be added.

```
% -------------------------------------------------
  p(alm)  1  2    1  1 -1  z    0  1  1  x
  p(py)   1  2    1  1 -1  z    1  1 -1  x
  p(gr)   1  1    0  2  1  z -1  f
  p(andr) 1  1    0  1  1  f
% -------------------------------------------------
```

The type of mixing model is defined as "ideal", "symmetric formalism" (sf) or "asymmetric formalism" (asf). The symmetric part of the mixing is defined through the interaction energies (W for each pair in the form a + bT + cP) and the asymmetric aspects via the parameters (α) for each end-member in the same form.

```
asf

 W(alm,py)      2.5  0  0
 W(alm,gr)       10  0  0
 W(alm,andr)     75  0  0
 W(py,gr)        45  0  0
 W(py,andr)      90  0  0
 W(gr,andr)       0  0  0
```

The site parameters (α) show that interactions between alm–py and gr–andr are symmetric, the other pairs (alm–gr, alm–andr, py–gr and py–andr) are asymmetric:

```
 alm      1 0 0
 py       1 0 0
 gr       3 0 0
 andr     3 0 0
% -------------------------------------------------
```

The number of site fractions is 5 and their occupancies are listed below, they are called “terms” and are also subdivided into blocks.

```
 5     % no of site fractions
 xFeX   1  2    1  1 -1   z    0  1  1  x
 xMgX   1  2    1  1 -1   z    1  1 -1  x
 xCaX   1  1    0  1  1   z
 xAlY   1  1    1  1 -1   f
 xFe3Y  1  1    0  1  1   f
% --------------------------------------------------
```

These are the ideal mixing activities for the end-members:

```
alm     1  2      xFeX  3   xAlY 2
py      1  2      xMgX  3   xAlY 2
gr      1  2      xCaX  3   xAlY 2
andr    1  2      xCaX  3   xFe3Y 2
```

A useful script for achieving the *a–x* codes in the log-file (subchapter 3.1.3.4.3) in a standard mathematical format is “incax yes” of which the output is shown here:

```
%---------------------------------------
g
starting guesses
    x(g) =      0.8700
    z(g) =      0.2350
    f(g) =      0.04600

 site fractions
   xFeX = (1 - z) x
   xMgX = (1 - z) (1 - x)
   xCaX = z
   xAlY = 1 - f
   xFe3Y = f

 proportions
   alm  = (1 - z) x
   py   = (1 - z) (1 - x)
   gr   = z - f
   andr = f
```

This information allows the user to illustrate a site box diagram for the elements in a phase with specified starting guesses of a phase, in this case garnet (Fig. 3.1.1).

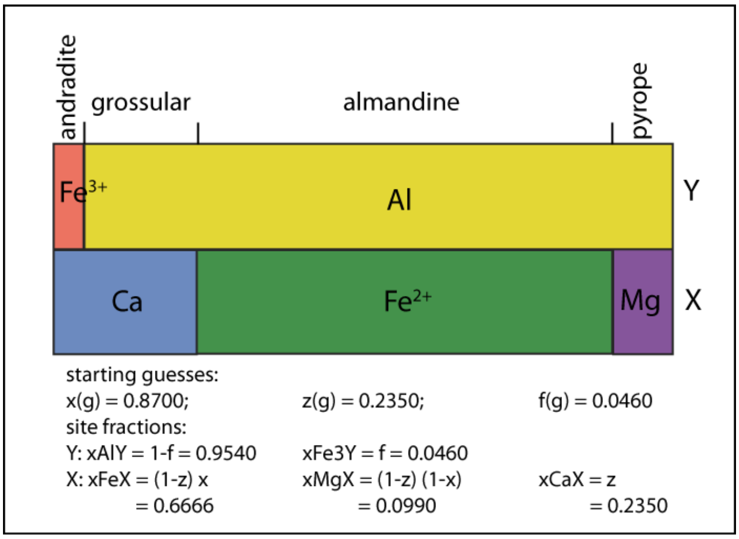

starting guesses:
x(g) = 0.8700; z(g) = 0.2350; f(g) = 0.0460
site fractions:
Y: xAlY = 1-f = 0.9540 xFe3Y = f = 0.0460
X: xFeX = (1-z) x = 0.6666 xMgX = (1-z) (1-x) = 0.0990 xCaX = z = 0.2350

Figure 3.1.1: Site box diagram for a garnet with end-member proportions for the given starting guesses and end-member proportions determined by the site fractions. The end-members are given in Tab.3.1.1.

The following information gives the ideal mixing activities and the non-ideal interaction parameters:

```
 ideal mixing actvities
   alm =   xFeX^3 xAlY^2
    py =   xMgX^3 xAlY^2
    gr =   xCaX^3 xAlY^2
  andr =   xCaX^3 xFe3Y^2

 non-ideality by van laar
  W(alm,py) = 2.5
  W(alm,gr) = 10.0
  W(alm,andr) = 75.0
  W(py,gr) = 45.0
  W(py,andr) = 90.0
  v(alm) = 1.00
  v(py) = 1.00
  v(gr) = 3.00
  v(andr) = 3.00
```

3.1.2.2.5 Site box diagram for orthopyroxene

A more complicated example of a site box diagram is shown for orthopyroxene (Fig. 3.1.2), where the order-disorder parameter “N” is added to the composition variables *x, y* and *f* . White *et al.* (2002) defines the compositional variables and the order-disorder parameter as followed:

$x_{\mathrm{opx}} = [(\mathrm{Fe}^{2+})/(\mathrm{Fe}^{2+}+\mathrm{Mg})]$

$y_{\mathrm{opx}} = x_{AlM1} = \mathrm{Al}^{oct}$

$f_{\mathrm{opx}} = x_{Fe3+M1} = \mathrm{Fe}^{3+oct}$

$N_{\mathrm{opx}} = 2(x_{Fe2+M2} - x_{\mathrm{opx}})$

By using the script „incax yes“ during a calculation, the starting guesses of an orthopyroxene are shown as first in the tc-log file:

```
starting guesses
   x(opx) =     0.2022
   y(opx) =     0.1035
   N(opx) =     0.2126
   f(opx) =     0.003516
```

The site distributions in orthopyroxene are:

```
site fractions
   x(Al,M1) = y
   x(Fe3,M1)= f
   x(Mg,M1) = 1 - y - f + 1/2 N + (-x) (1 - y - f)
   x(Fe,M1) = -1/2 N + x (1 - y - f)
   x(Mg,M2) = 1 - x - 1/2 N
   x(Fe,M2) = x + 1/2 N
```

The end-member proportions in orthopyroxene are:

```
proportions
   en   = 1 - x - y - 1/2 N - f
   fs   = -1/2 N + x (1 - y - f)
   mgts = y
   fm   = N + x (y + f)
   mots = f
```

The site box diagram for orthopyroxene for the given starting guesses is shown in Fig. 3.1.2. The end-members are ferrosilite (fs; $FeFeSi_2O_6$), enstatite (en; $MgMgSi_2O_6$), Fe–Mg-ordered pyroxene (fm; $FeMgSi_2O_6$), Mg-Tschermaks pyroxene (mgts; $MgAlAlSiO_6$) (Powell & Holland, 1999) and the Fe^{3+}-bearing orthopyroxene end-member mots ($MgFe^{3+}AlSiO_6$) from White *et al.* (2002).

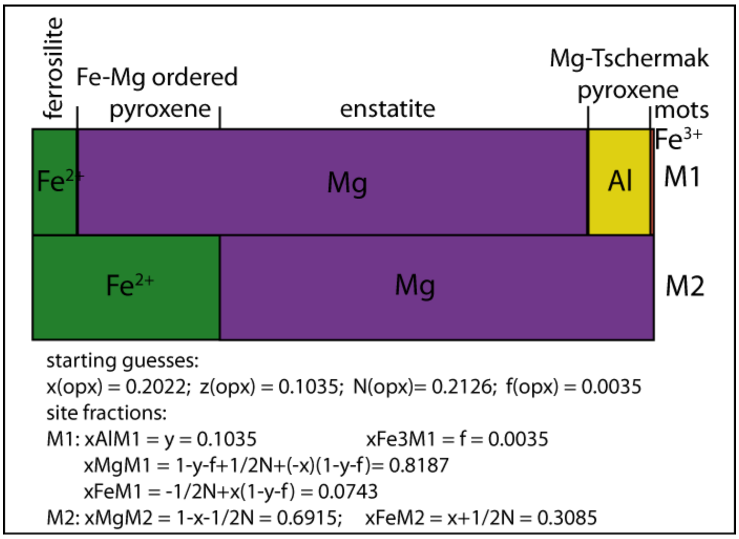

starting guesses:
x(opx) = 0.2022; z(opx) = 0.1035; N(opx)= 0.2126; f(opx) = 0.0035
site fractions:
M1: xAlM1 = y = 0.1035 xFe3M1 = f = 0.0035
xMgM1 = 1-y-f+1/2N+(-x)(1-y-f)= 0.8187
xFeM1 = -1/2N+x(1-y-f) = 0.0743
M2: xMgM2 = 1-x-1/2N = 0.6915; xFeM2 = x+1/2N = 0.3085

Figure 3.1.2: Site box diagram for an orthopyroxene with end-member proportions for the given starting guesses and end-member proportions determined by the site fractions. The end-members are given in Tab.3.1.1.

The remaining information is about the ideal and non-ideal mixing activities as well as the dependent end-members and their DQF-increments (subchapter 3.1.2.2.1).

```
ideal mixing actvities
    en =    x(Mg,M1) x(Mg,M2)
    fs =    x(Fe,M1) x(Fe,M2)
  mgts =    x(Al,M1) x(Mg,M2)
    fm =    x(Mg,M1) x(Fe,M2)
  mots =    x(Fe3,M1) x(Mg,M2)

 non-ideality by symmetric formalism
  W(en,fs)    = 6.8
  W(en,fm)    = 4.5
  W(en,mots)  = -14.0
  W(fs,mgts)  = -1.0
  W(fs,fm)    = 4.5
  W(fs,mots)  = 6.0
  W(mgts,fm)  = 1.2
  W(fm,mots)  = 6.0

 dependent ("make") end-members
  fm = 1/2 en + 1/2 fs
  mots = 2/2 mgts + -1/2 cor + 1/2 hem

 DQF increments
  fm = -6.95
  mots = 22.00
```

The phases appearing in the thermodynamic modelling of this study are listed in Tab. 3.1.1, which includes the symbols used for the labelling of the pseudosections in Chapter 4 and 6, the end-member names and their chemical formulae.

Table 3.1.1: Phases appearing in the thermodynamic calculations in Chapter 4 with their end-members, symbols and formulae. The coding for the 4 clinoamphiboles, the 3 clinopyroxenes and ilmenite/hematite are the same, only distinguished by their starting guesses.

Phase	symbol	End-member name	Formula
Amphibole (amph)	tr	tremolite	$Ca_2Mg_5Si_8O_{22}(OH)_2$
(clinoamphiboles)	ts	tschermakite	$Ca_2Mg_3Al_4Si_6O_{22}(OH)_2$
hb (hornblende)	parg	pargasite	$NaCa_2Mg_4Al_3Si_6O_{22}(OH)_2$
gl (glaucophane)	gl	glaucophane	$Na_2Mg_3Al_2Si_8O_{22}(OH)_2$
act (actinolite)	cumm	cummingtonite	$Mg_7Si_8O_{22}(OH)_2$
cu (cummingtonite)	grun	grunerite	$Fe_7Si_8O_{22}(OH)_2$
	A (camo1)	camo1	$Fe_2Mg_3Fe_2Si_8O_{22}(OH)_2$
	B (camo2)	camo2	$Fe_2Fe_3Mg_2Si_8O_{22}(OH)_2$
	mrb	Mg-riebeckite	$Na_2Mg_3Fe^{3+}{}_2Si_8O_{22}(OH)_2$
clinopyroxene (cpx)	jd	jadeite	$NaAlSi_2O_6$
di (diopside)	di	diopside	$CaMgSi_2O_6$
o (omphacite)	hed	hedenbergite	$CaFeSi_2O_6$
	acm	acmite	$NaFeSi_2O_6$
	om	ordered omphacite	$Ca_{0.5}Na_{0.5}Mg_{0.5}Al_{0.5}Si_2O_6$
	cfm	Ca-Fe-Mg end-member	$CaFe_{0.5}Mg_{0.5}Si_2O_6$
	jac	ordered end-member	$NaAl_{0.5}Fe^{3+}{}_{0.5}Si_2O_6$
chlorite (chl)	afchl	Al-free chlorite	$Mg_6Si_4O_{10}(OH)_4$
	clin	clinochlore (ordered)	$Mg_5Al_2Si_3O_{10}(OH)_4$
	daph	daphnite	$Fe_5Al_2Si_3O_{10}(OH)_4$
	ames	amesite	$Mg_4Al_4Si_2O_{10}(OH)_4$
garnet (g)	alm	almandine	$Fe_3Al_2Si_3O_{12}$
	py	pyrope	$Mg_3Al_2Si_3O_{12}$
	gr	grossular	$Ca_3Al_2Si_3O_{12}$
	andr	andradite	$Ca_3Fe_2Si_3O_{12}$
epidote (ep)	cz	clinozoisite	$Ca_2Al_3Si_3O_{12}(OH)$
	ep	epidote	$Ca_2FeAl_2Si_3O_{12}(OH)$
	fep	Fe-epidote	$Ca_2Fe_2AlSi_3O_{12}(OH)$
orthopyroxene (opx)	en	enstatite	$Mg_2Si_2O_6$
	fs	ferrosilite	$Mg_2Si_2O_6$
	mgts	Mg-Tschermaks pyroxene	$MgAl_2Si_2O_6$
	fm	Fe-Mg pyroxene	$FeMgSi_2O_6$
	mots	Fe^{3+} end-member	$MgFe^{3+}AlSiO_6$
plagioclase (pl)	ab	albite	$NaAlSi_3O_8$
	an	anorthite	$CaAl_2Si_2O_8$
olivine (ol)	fa	fayalite	Fe_2SiO_4
	fo	forsterite	Mg_2SiO_4
ilmenite (ilm)-hematite	oilm	ordered ilmenite	$Fe^{2+}TiO_3$
	dilm	disordered ilmenite	$(Fe_{1/2}^{2+}Ti_{1/2})\ (Fe_{1/2}^{2+}Ti_{1/2})\ O_3$
	hem	hematite	Fe_2O_3
spinel (sp)	he	hercynite	$FeAl_2O_4$
	sp	spinel	$MgAl_2O_4$
	mt	magnetite	Fe_3O_4
	ulv	ulvospinel	Fe_2TiO_4
talc (ta)	ta	talc	$Mg_3Si_4O_{10}(OH)_2$
	fta	Fe-talc	$Fe_3Si_4O_{10}(OH)_2$
	tats	Tschermak-talc	$Mg_2Al_2Si_3O_{10}(OH)_2$
lawsonite (law)	law		$CaAl_2Si_2O_7(OH)2{*}H2O$
albite (ab)	ab		$NaAlSi_3O_8$
rutile (ru)	ru		TiO_2
sphene (sph)	sph		$CaTiSiO_5$
kyanite (ky)	ky		Al_2SiO_5
quartz (q)	q		SiO_2
Gas species	H_2O	water fluid	H_2O

3.1.2.2.6 Melt model adopted from metapelitic rocks

There is currently no appropriate model for silicate melt (liquid) for metabasic rocks and for this study a melt model for metapelitic rocks (White *et al.*, 2001, 2007) was used to locate the solidus in the calculated metabasic compositions. The model used here is written in the system NCFMASH, representing the melt-model in the largest system without K and it is based on 5 end-members. The consistence of this model with to the actual results from the high-pressure experiments conducted in this study is discussed in subchapter 6. 2.

3.1.2.2.7 The importance of developing new *a–x* models

Based on the theory described in 3.1.2.2, many new order-disorder models have been recently derived, e.g. for mafic minerals like amphiboles (subchapter 3.1.2.3, Diener *et al.*, 2007) and omphacitic pyroxenes (Green *et al.*, 2007), which both are essential phases in the scope of this study. For the first time it is now possible to model mafic rocks including amphiboles in the largest chemical system available (NCFMASHTO) for those rocks.

3.1.2.3 Deriving a new *a–x* model - an example using amphiboles

The advancements in methology allow the development of more and better *a–x* relationship models, e.g. for amphiboles. Models for amphiboles are difficult to validate due to the relatively high variance of amphibole-bearing equilibria in natural rocks (Dale *et al.*, 2005). The amphibole model from Diener *et al.* (2007) is an advancement from that of Dale *et al.* (2005), who presented an *a–x* model for Na–Ca clinoamphiboles in NCFMASHO, which allowed calculations of phase equilibria in metabasic and amphibole-bearing rock compositions using a single thermodynamic description for the first time. It is the first model that could predict coexisting of amphiboles in thermodynamic calculations. Previous models (Ghiorso & Evans, 2002; Okamoto & Tourimi, 2004; Dale *et al.*, 2005) were less useful for phase diagram calculations because coexisting amphiboles (glaucophane and barroisitic amphibole/hornblende), for example, did not have identical descriptions and thus their co-existence was superimposed by the user rather than be a consequence of the thermodynamics of the phases. Dale *et al.* (2005) used an independent set of the end-members tremolite, tschermakite, pargasite, glaucophane, ferroactinolite (for FeO) and ferritschermakite (for Fe_2O_3), a mixing-on-sites model for ideal-mixing activities and a macroscopic van

Laar model for activity coefficients. 15 pairwise interaction energies as well as six asymmetry parameters were used in the model-formulation. The size and shape of the amphibole solvi were calibrated on the basis of a dataset including 71 coexisting amphibole pairs from rocks on which the *a–x* relationships could be calibrated independently from thermodynamic properties of end-members. After first calibrations were done for the subsystem NCMASH, the model was extended and combined to NCFMASHO, considering "O" for the portion of Fe_2O_3 in FeO total.

The new model (Diener *et al.*, 2007) extended the model of Dale *et al.* (2005) by including the clinoamphiboles cummingtonite-grunerite and the orthoamphiboles (anthophyllite and gedrite). In addition, order-disorder Fe–Mg-partitioning in different sites (Holland & Powell, 2006) was introduced, calibrated using experimental data from cummingtonite-grunerite. The formulation of the clinoamphiboles in NCMASH is based on Dale *et al.* (2005), but the enlargement to FeO- and Fe_2O_3 bearing systems was revised. The independent set of end-members for clinoamphiboles now consists of tremolite, tschermakite, pargasite, glaucophane, cummingtonite, grunerite (for FeO) and magnesioriebeckite (for Fe_2O_3). The formulation of ideal-mixing activities is still the same, but some activity coefficients using the asymmetric formalism (Holland & Powell, 2003) have been modified. This includes pairwise interactions between the end-members in the independent set, interaction energies between the pairs of end-members and an asymmetry parameter for each end-member. Calibration of the coexisting pairs to constrain the shape and size of amphibole solvi has been advanced for subsystems and, with respect to other phases, new constraints on stability of the amphiboles have been provided. Hence, it has been necessary to adjust enthalpies via a DQF parameter and add *a–x* models for end-members of these phases.

3.1.3 Thermodynamic calculations

3.1.3.1 Introduction

This subchapter outlines the application of THERMOCALC to calculate *P–T* and *T–X* pseudosections in this study. Thermodynamic calculations for phase diagrams are computer intensive, therefore an example of calculating a *P–T* pseudosection is given at the end of this subchapter. Compatibility diagrams, petrogenetic grids and *P–X* or $T–XCO_2$ pseudosections are further types of phase diagrams that can be constructed using the THERMOCALC software. Firstly, information is given concerning chemical systems and thermodynamic variables, followed by an outline of phase diagrams in general: the rules that control the shape as well as a documentation of how THERMOCALC is used. Further, the required files, their structure and scripting are introduced to produce a *P–T* pseudosection in the chemical system NCFMASHTO. For any other calculation and description of scripts, further information is given on the THERMOCALC homepage (http://www.metamorph.geo.uni-mainz.de/thermocalc/documentation/index.html).

3.1.3.2 Phase diagrams

3.1.3.2.1 Introduction

A phase diagram that shows all the thermodynamic dimensions is called the "total phase diagram". Such diagrams can typically only be drawn for very simple systems where the number of dimensions considered is three or less. For larger systems the phase relationships have to be rendered in two or three dimensions. To introduce useful 2D representations of mineral equilibria in a chemical system, projections and sections are used, whose axes are defined by thermodynamic variables. In this subchapter the types of phase diagrams, the rules for construction of a phase diagram as well as the application of the software THERMOCALC are given.

3.1.3.2.2 Chemical systems and thermodynamic variables

The thermodynamic calculations in this study were done in the system NCFMASHTO for metabasic rocks, representing the largest system available for this rock type. The bigger the system the better it represents a natural rock, whereas smaller systems are commonly more useful to describe general processes. By adding a chemical component to a system, the variances of identical reactions change by one, e.g. an univariant line becomes a divariant field and a divariant becomes a trivariant field.

Thermodynamic variables always come in conjugate pairs of intensive variables like pressure (P), temperature (T) or chemical potential (μ) that are independent of the amount of material involved and as extensive variables like volume (V), entropy (S) or moles (n) whose values are dependent on the amount of material, though extensive variables may be given in their normalised form, e.g. X for n. The commonly considered conjugate pairs are P & V, T & S and μ & n. From each pair only one variable is represented on a phase diagram as an axis, e.g. P, T and X for a *P–T* pseudosection at a fixed composition (X).

3.1.3.2.3 Compatibility diagrams

Triangular diagrams showing mineral compositions and stable assemblages at given *P* and *T* for specific chemical systems, simplified to three components, e.g. an AFM diagram (Al_2O_3–FeO–MgO) for metapelitic rocks that uses projection from excess phases to reduce the dimensions.

3.1.3.2.4 Petrogenetic grids

Petrogenetic grids are general diagrams showing stable univariant reactions and invariant points in a given chemical system for all bulk compositions in the defined system.

3.1.3.2.5 Pseudosections

Phase diagrams for a specified bulk composition are pseudosections. “Pseudo” is used because it represents a constant bulk composition instead of a constant chemical potential (i.e. the total phase diagram is sectioned with respect to an extensive variable (*X*) and thus the compositions of the phases do not lie on the plane of the section). These phase diagrams involve three variables (*P*, *T* and *X*) with one of them fixed, e.g. a *P–T* pseudosection with the composition (*X*) fixed. In contrast to petrogenetic grids, *P–T* pseudosections do not show all possible reactions in a system but only those “seen” by a given bulk rock composition. Thus, reactions on a *P–T* grid are often only present in a pseudosection with a part of their total stability range or may be completely absent from a pseudosection. Pseudosections illustrate stable multivariant assemblages for a specified bulk composition in a *P–T* coordinate system, each field bounded by effective invariant points and zero-mole proportion boundaries. *T–X* pseudosections are calculated at a constant pressure and show the changes occurring as a result of a change in the bulk composition (*X*) along the x-axis. The rules controlling the constructing of phase diagrams as well as examples using THERMOCALC for calculating *P–T* and *T–X* pseudosections are given below.

3.1.3.3 Construction of phase diagrams

3.1.3.3.1 The phase rule

The assemblages in a *P–T* pseudosection have different variances (*v*) or degrees of freedom depending on the components in the system (*c*) and the number of phases (*p*) involved in the reaction (Eq. 3.1.1).

$$v = c - p + 2 \qquad \text{[Equation 3.1.1]}$$

The system used in this thesis is NCFMASHTO with the 9 components Na_2O–CaO–FeO–MgO–Al_2O_3–SiO_2–H_2O–TiO_2 and O as a factor for the amount of Fe_2O_3 (Eq. 4.1.1). In this system the variances relate to the number of phases involved in a reaction (Tab. 3.1.2).

Table 3.1.2: Variances and related number of phases in the 9-component system NCFMASHTO.

Phase rule:	***v* = *c* –*p* + 2**	**NCFMASHTO**
***v*= variance**	***p*= phases**	***c* = 9**
0	11	invariant
1	10	univariant
2	9	divariant
3	8	trivariant
4	7	quadrivariant
5	6	quinivariant
6	5	hexivariant
7	4	septivariant
8	3	octivariant

3.1.3.3.2 The Schreinemarkers rule

This rule controls the topology of petrogenetic grids (i.e. univariant and invariant equilibria). Each reaction stops at an invariant point and has a stable and a metastable extension, whereby the metastable extension lacks a given phase [phase] which lies between reactions that produce this phase. Furthermore a mineral assemblage cannot exist in an angle greater than 180 °.

3.1.3.3.3 The multivariant boundary rule

Intersections of boundaries across a point involve four boundaries, two boundaries for each phase. In compatibility diagrams and pseudosections the variance across a boundary between two assemblages always changes by one and the change through a point is zero or two.

3.1.3.4 Calculating phase diagrams with THERMOCALC

3.1.3.4.1 Introduction

Using the software THERMOCALC requires a set of files and applications in a single folder. The software is built around a non-linear equation solver which is outlined in the next part. The file structures and the application of the program are described in subchapter 3.1.3.4.3–3.1.3.4.8 and 3.1.3.5.

3.1.3.4.2 Non-linear equation solver

The software THERMOCALC is built around a non-linear equation solver to calculate user-specified equilibria (Powell *et al.*, 1998) and it carries out equilibrium calculations for balanced reactions between end-members of minerals in the dataset. Equation 3.1.2 represents the equilibrium relationship and displays a non-linear equation in temperature and pressure defining a line (potential barometer) on a *P–T* diagram, if *a–x* relations and compositions of phases, whose end-members are involved, are given.

$$\Delta G^0 + RT\ln K = 0 \qquad \text{[Equation 3.1.2]}$$

lnK is the natural logarithm of the equilibrium constant for the reaction (calculated from the activities of the end-members in the phases in which these end-members occur) and ΔG^0 is the standard-state Gibbs energy of a reaction (calculated from the Gibbs energies of the participating end-members in the reactions).

Powell & Holland (1988) characterised a multiple reaction approach which allows the calculation of average pressures from a set of independent reactions, where the number of independent reactions depicts the difference between the number of applied end-members and the number of components in a system which are needed to represent their compositions (Holland & Powell, 1990). THERMOCALC is able to scan all available equilibrium reactions to figure out the set of relevant independent end-member reactions describing the specified equilibria (Powell & Holland, 1988).

Powell *et al.* (1998) describe the calculation of phase diagrams with THERMOCALC: the calculation of pseudosections is possible once a bulk composition is specified and the lines and points of a pseudosection can be calculated directly by setting one or two modes to zero.

An example is given for the NCFMASHTO effective invariant point “garnet diopside rutile quartz H_2O [hornblende plagioclase]” of the *P–T* pseudosection in Fig. 3.1.3. The point becomes effectively invariant for a fixed bulk rock composition by setting the two modes of hornblende and plagioclase to zero. This point is described by the following independent set of reactions written between the end-members of the phases involved:

```
1)  jd + q = abh
2)  7tr = 3cumm + 14di + 4q + 4H2O
3)  7a = 3cumm + 4grun
4)  7b = 2cumm + 5grun
5)  py + 2gr + 3q = 3di + 3an
6)  alm + 2gr + 3q = 3hed + 3an
7)  2cfm = di + hed
8)  cumm + 2gr = ts + 4di
9)  3tr + 2py = ts + 2cumm + 4di
10)  6grun + 11gr = 27hed + 5alm + 6an + 6H2O
11)  7gl = 3cumm + 10jd + 4abh + 4H2O
12)  2om = jd + di
13)  2jac = jd + acm
14)  2parg + 6abh = tr + ts + 8jd
15)  2jd + andr = 2acm + gr
16)  gl + 2acm = mrb + 2jd
```

Corresponding to Eq. 3.1.2 , a set of equilibrium relationships is given with the end-member activities of the phases involved in each reaction for the equilibrium constant *K*. The first two resulting equilibrium reactions are given here as an example:

$$0 = \Delta G_{1)}{}^{0} + RT\ln\left[\frac{(\alpha_{abh})}{(\alpha_{jd})(\alpha_{q})}\right]$$

$$0 = \Delta G_{2)}{}^{0} + RT\ln\left[\frac{(\alpha_{cumm})^{3}(\alpha_{di})^{14}(\alpha_{q})^{4}(\alpha_{h2o})^{4}}{(\alpha_{tr})^{7}}\right]\ldots\ldots$$

The end-member activities are substituted by the activity expressions (for example α_{jd} = $(X^{M1m}_{Al}\ X^{M1a}_{Al}\ X^{M2c}_{Na}\ X^{M2n}_{Na})^{1/2}$, which in turn are expressed by the site fractions (Figs 3.1.1 and 3.1.2). THERMOCALC then solves these equations with the information from the dataset to get information about the unknown equilibrium compositions of the phases listed below. Given that each ΔG^{0} is a function of *P* and *T*, these are also unknowns THERMOCALC solves for. For this example, the solved unknowns, also designated as starting guesses are:

```
% calculated at P = 17.9, T = 918; for (hb di g pl ru q H2O  with hb = 0, pl = 0)
xyzguess x(hb)       0.07988
xyzguess y(hb)        0.6402
xyzguess z(hb)        0.1478
xyzguess a(hb)        0.5909
xyzguess c(hb)        0.7334
xyzguess f(hb)       0.04925
xyzguess Q1(hb)      0.01286  range -1.000 1.000
xyzguess Q2(hb)      0.03298  range -1.000 1.000
xyzguess x(di)       0.07593
xyzguess j(di)        0.2497
xyzguess f(di)        0.1726
xyzguess Q(di)       0.01448
xyzguess Qaf(di)    0.005024  range -0.500 0.500
xyzguess Qfm(di)    -0.02008  range -0.500 0.500
xyzguess x(g)         0.2802
xyzguess z(g)         0.1462
xyzguess f(g)       0.006163
xyzguess ca(pl)       0.3060
% ----------------------------------------------------------
```

3.1.3.4.3 Applications and files for using THERMOCALC

The applications needed for calculations with THERMOCALC are:

the current version of THERMOCALC: 3.30 or 3.33 (tc330i or tc333i in this study)
the drawpd application for the graphic illustration of the calculated phase diagrams

The THERMOCALC input files for phase diagram calculations are:

the current internally consistent dataset: “tc-ds55.txt”
the global preferences file: “tc-prefs.txt”
the system activity-composition file: “tc-NCFMASHTO.txt” for metabasites
the script file: “tc-<name>.txt”

The output files are created in each run of THERMOCALC and contain all designated information in different formats. After running THERMOCALC again, these files will be overwritten. The results in these files depend on the requested information and the phase diagram the user likes to calculate and they are described in the context of the calculation of a *P–T* pseudosection (subchapter 3.1.3.5):

tc-log.txt
tc-<name>-o.txt
tc-<name>-dr.txt

The files needed for drawing a phase diagram are:

the information for drawing a diagram with drawpd are in: “dr d <name>.txt”
the prefs-file

3.1.3.4.4 The file structures of the input files

THERMOCALC is computing by reading the information in the input files (“tc-prefs.txt”, “tc-<name>.txt”). Two general commands in all THERMOCALC files are <%> and <*>. Inputs following a “%” in a line are not read by THERMOCALC and may contain additional information for the user, a “*” indicates the end of a file.

3.1.3.4.5 The internally consistent dataset

The dataset used in this study is “tc-ds55.txt” (Holland & Powell, 1998), updated 22 November 2003. Detailed information about the dataset is given in subchapter 3.1.2.1.6.

3.1.3.4.6 The global preference file

This file allows the user to control how THERMOCALC operates. In this file it is determined which dataset and scriptfile are to be used, as well as the calcmode which defines the type of calculation. Further, the size of window is defined and whether the output is wrapped or not.

```
        setpagewidth 195                          % for Mac; 80 on a PC
        dontwrap   yes                            % out put is not wrapped
        dataset 55                                % dataset is tc-ds55
        calcmode 1                                % mode 1 calcs ie phase diagram calculations
        scriptfile MAOC15                         % the script file MAOC15 is used
        strictsyntax no                           % strict syntax rules for a-x models not used
        *                                         % end of file
```

3.1.3.4.7 The script-file

The script file defines how the calculations will be done by THERMOCALC. The example below is a script file for a *P–T* pseudosection calculated in this study, “tc-MAOC15.txt” (Figs 3.1.2 and 4.3.4a). It defines parameters about the calculation, e.g. *P–T* windows and the information which will be written into the output files. The explanations of the scripts (used in this study) are given in the following excerpt:

```
axfile NCFMASHTO                          % defining the ax file to use

ignore                                    % tells thermocalc which minerals in the ax file can be
                                          % automatically ignored

setdefTwindow yes   500.001 1200.001      % default T window, allows just to hit return when
                                          % prompted for T window
setdefPwindow yes   8 25                  % default P window, allows just to hit return when
                                          % prompted for P window

%setPwindow yes   13 13                   % defining the P range for calculations, e.g. for a T-X
                                          % pseudosection at constant P

calctatp ask                              % whether to set P´s and calc T´s or vice versa at each
                                          % run, or always set P´s or T´s

setexcess                                 % set any phases to excess

seta no                                   % whether to set any activities

usecalcq yes                              % solve the state of order in order-disorder minerals
                                          % prior to solving for the specified equilibria

samecoding act hb gl                      % same coding for coexisting amphiboles
samecoding jd o di                        % same coding for coexisting clinopyroxenes

pseudosection yes                         % whether to generate pseudosection information or not,
                                          % if <yes>, thermocalc expects a bulk composition
% MAOC15
% ----------------------------------------------------------------
%                   H2O   SiO2   Al2O3  CaO    MgO    FeO    Na2O TiO2  O
  setbulk yes       1.478 47.058 8.688 12.134 22.024 6.667 1.470 0.481 0.3
% ---------------------------------------------------------------
                                          % defines a bulk composition in mol%
                                          % for a T-X pseudosection two compositions are required

setmodeiso yes                            % whether to set any modes for boundaries or contours

zeromodeiso yes                           % whether to set zero modes for field boundaries,
                                          % for contouring modes of a phase this has to be <no>

setiso no                                 % whether to calculate composition isopleths

%dogmin yes                               % do Gibbs energy minimisation, if “yes”, thermocalc
                                          % gives the assemblage with the lowest Gibbs energy from
                                          % the entered phases for specified P-T
```

```
drawpd yes                                % whether to format the output file "tc-<name>-dr.txt"
                                          % for drawpd
project no                                % whether to do a compatibility projection

%printbulkinfo yes                        % whether to include a bulk composition matrix in
                                         % the logfile

printxyz yes                              % whether to include the output mineral compositions in
                                          % form of starting guesses in the logfile. This can be
                                          % copied and pasted into the script file as new starting
                                          % guesses, overwriting starting guesses in the ax file

%incax no                                 % includes ax relationships in the datafile

smath no                                  % whether to format the output file for mathematica
```

```
% The starting guesses stem from the log file if "printxyz yes":
% calculated at P = 8.5, T = 795; for (hb di g opx pl lm sp  with sp = 0)
xyzguess x(hb)         0.1293
xyzguess y(hb)         0.6943
xyzguess z(hb)        0.02434
xyzguess a(hb)         0.8463
xyzguess c(hb)         0.8794
xyzguess f(hb)        0.09787
xyzguess Q1(hb)       0.01675  range -1.000 1.000
xyzguess Q2(hb)       0.05749  range -1.000 1.000
xyzguess x(di)         0.1019
xyzguess j(di)        0.08845
xyzguess f(di)         0.3604
xyzguess Q(di)       0.003826
xyzguess Qaf(di)     0.003213  range -0.500 0.500
xyzguess Qfm(di)     -0.03130  range -0.500 0.500
xyzguess x(g)          0.4083
xyzguess z(g)          0.1601
xyzguess f(g)        0.008319
xyzguess x(opx)        0.2022
xyzguess y(opx)        0.1035
xyzguess N(opx)        0.2126
xyzguess f(opx)      0.003516
xyzguess ca(pl)        0.7196
xyzguess x(lm)         0.9511
xyzguess Q(lm)         0.8639  range -0.990 0.990
xyzguess x(he)         0.4005
xyzguess y(he)         0.9799
xyzguess z(he)        0.01537
```

3.1.3.4.8 The activity-composition *(a–x)* file

In this file the activity-composition models (subchapter 3.1.2.2) for each solid solution phase and the pure end-member phases are given. The complete *a–x* file „tc-NCFMASHTO“ is presented in the Appendix A7. The first section in the file is a documentation about the minerals coded in it and the associated literature of the activity-composition relationships:

```
% ------------------------------------------------------------------------------------
%
% This is a NCFMASHTO datafile for metabasic rocks that contains coding for:
% gl, act, hb, cu, ged, anth, di, o, jd, chl, g, ep, pl, mt, ilm, hem.
%
% ------------------------------------------------------------------------------------
%
% When using this datafile, please cite the following references:
%
% Amphiboles:
% Diener, JFA, Powell, R, White, RW & Holland, TJB (2007) A new thermo-
% dynamic model for clino- and orthoamphiboles in Na2O-CaO-FeO-MgO-Al2O3-
% SiO2-H2O-O. Journal of Metamorphic Geology, 25, 631-656.
%
% Clinopyroxenes:
% Green, ECR, Holland, TJB & Powell, R (2007) An order-disorder model for
% omphacitic pyroxenes in the system jadeite-diopside-hedenbergite-acmite,
% with applications to eclogite rocks. American Mineralogist, 92, 1181-1189.

....next citation....etc.
```

Additional information is given:

```
% ------------------------------------------------------------------------------------
%
% The coding for the 4 clinoamphiboles is identical - the different amphiboles are
% distinguished by different starting guesses. The same goes for the 2 ortho-
% amphiboles, the 3 clinopyroxenes and ilmenite and hematite.
%
% With all these minerals, watch that the calculated mineral composition hasn't
% "jumped" a solvus (ie check that the calculated mineral composition matches the
% mineral name)
%
% ------------------------------------------------------------------------------------
%
% WARNING: AMPHIBOLES ARE NOT GOOD FOR YOU.
% McDonald, J.C., Gibbs, G.W., Liddell, F.D.K and McDonald, A.D. (1978)
% Mortality after long exposure to cummingtonite-grunerite,
% American Review of Respiratory Disease, 118, 271-277.
%
% ====================================================================================
```

The activity-composition models for each mineral are listed finally, whereas plagioclase is given as an easy example for the structure af an *a–x* model. Minerals without coding (i.e. pure end-members) are written at the end of the file.

```
Several models….

% =============================================================
% Plagioclase:
% Holland, TJB & Powell, R (2003) Activity-composition relations for phases in
% petrological calculations: an asymmetric multicomponent formulation. Contributions
% to Mineralogy and Petrology, 145, 492-501.
%
% from ternary plag mode for Cbar1 ASF

pl 2

   ca(pl) 0.3

% --------------------------------------------------

  p(ab)    1 1    1 1 -1 ca
  p(an)    1 1    0 1  1 ca

% --------------------------------------------------
  asf

    w(aban)   3.1   0     0

   ab   0.643  0  0
   an   1.0    0  0

% --------------------------------------------------
  2

  x(Na)    1 1    1 1 -1 ca
  x(Ca)    1 1    0 1  1 ca

% --------------------------------------------------

  abh      1 1     x(Na) 1
  an       1 1     x(Ca) 1
     DQF   7.03  -0.00466   0

....next model....etc.
```

The following pure phases are also included:

```
% =====================================================================
pa law ab ru sph ky q H2O

% end of file
```

With the four files described above, set up in the required form, THERMOCALC is able to do calculations for a designated phase diagram. An example of calculating points and lines for a *P–T* pseudosection and using the information of the created output files to draw a pseudosection is given in the next subchapter.

3.1.3.5 Calculation of a *P–T* pseudosection - an example

3.1.3.5.1 Introduction

Each zero-mole proportion boundary and each invariant point in a *P–T* pseudosection requires a single calculation by the user. Therefore a series of questions, based on the setting descibed in subchapter 3.1.3.4.7, are prompted by the program and have to be answered by the user. On the basis of the quadrivariant assemblage garnet-hornblende-diopside-plagioclase-rutile-quartz-H_2O the calculation of the high pressure effective invariant point [hb pl] and the plagioclase-out boundary between the quadri - and quinivariant fields are documentated in this subchapter. The points and boundaries have to be fitted together under consideration of the rules described in subchapter 3.1.3.3. A helpful instrument is to draw a sketch of the calculated boundaries, points and the emerging fields of stable mineral assemblages with their different variances.

3.1.3.5.2 Calculation of an effective invariant point

After opening the terminal application („tc333i“) the following lines appear:

```
Last login: Tue Apr  6 15:53:00 on ttys000
mcziaja:~ karenziaja$
```

First of all the user types in <cd> and drag the folder including all requied files into the application, hitting <return> and types in <./tc333i>

```
mcziaja:~ karenziaja$ cd /Users/karenziaja/Documents/PHD\ 30.03.10/Diss06.03.10/MAOC15
mcziaja:MAOC15 karenziaja$ ./tc333i
THERMOCALC 3.33 (Free Pascal version)
```

The program generates files including the results, these are: „tc-<name>-o.txt“ as a complete documentation of all questions and inputs of the user. “tc-log.txt” gives additional user specified information, if the generation is intended in the script file. In „tc-<name>-dr.txt“ the output for generating the *P–T* pseudosection with “dr d <name>.txt” is given in a special form.

```
the main output is in the file, "tc-MAOC15-o.txt"
other (eg drawpd) output is in the file, "tc-MAOC15-dr.txt"

reading a-x datafile, "tc-NCFMASHTO.txt"...
gl  act  hb  cu  ged  anth  di  o  jd  chl  g  ep  opx  ta  pl  ol
mt  lm  hem  sp  pa  law  ab  ru  sph  ky  q  H2O  zo  cz
choose from: gl  act  hb  cu  ged  anth  di  o  jd  chl  g  ep  opx  ta  pl  ol  mt  lm  hem
sp  pa  law  ab  ru  sph  ky  q  H2O  zo  cz
```

The first question concerns the minerals involved in the reaction, chosen from the list above. The given mineral abbreviations (Tab. 3.1.1) have to be typed in in any order separated by a space:

```
which phases : g hb di pl ru q H2O
```

The scriptfile defines that no phases are in excess:

```
no phases in excess (from script)
```

The variance is 4, due to the phase rule (Eq. 3.1.1 and Tab. 3.1.2). THERMOCALC offers a suggestion and the user hits <return> to confirm it or type in the variance again.

```
variance of required equilibrium (4?) :
you may set zero modal proportions, from:hb di g pl ru q H2O
```

The next question is which phases the user intends to set to zero. For calculating an effective invariant point one needs two phases set to zero, in this case hornblende and plagioclase, whose zero mole proportion boundaries are crossing in this example.

```
which to set : hb pl
specification of PT window:
PT window within which invariant points expected to lie
```

Here, the *P–T* window in which the invariant point should occur can be defined. Answering this question is not required in most cases and the solver is able to find the point just by hitting <return> and THERMOCALC uses the default *T* and *P* windows in the script file.

```
T low,high, P low,high : 900 950 17 19
fluidtype = H2O
```

The following output is the answer where the point is located in *P–T* space, including the mineral compositions of the minerals involved in this point which are given in form of defining composition variables, e.g. *x(hb)*. The form of the notation of these variables is given in 3.1.2.2.4 and 5. The proportions of the modes of all phase considered in the calculation are given at the end of the output.

```
composition (from script)
    H2O   SiO2  Al2O3    CaO    MgO    FeO   Na2O   TiO2      O
  1.474 46.917  8.662 12.098 21.958  6.647  1.466  0.480  0.299
<===================================================>
phases : hb, di, g, pl, ru, q, H2O

--------------------------------------------------------------------
 P(kbar)     T(?C)    x(hb)    y(hb)    z(hb)    a(hb)    c(hb)    f(hb)   Q1(hb)   Q2(hb)
   17.95     918.4  0.07988   0.6402   0.1478   0.5909   0.7334  0.04925  0.01286  0.03298
                      x(di)    j(di)    f(di)    Q(di)  Qaf(di)  Qfm(di)
                    0.07593   0.2497   0.1726  0.01448 0.005024 -0.02008
                       x(g)     z(g)     f(g)   ca(pl)
                     0.2802   0.1462 0.006163   0.3060

  mode       hb       di        g       pl       ru        q      H2O
              0   0.4454   0.5256        0 0.004796 0.009501  0.01474

more phase diagram calculations ?
```

Hitting <return> after this prompt allows further calculations.

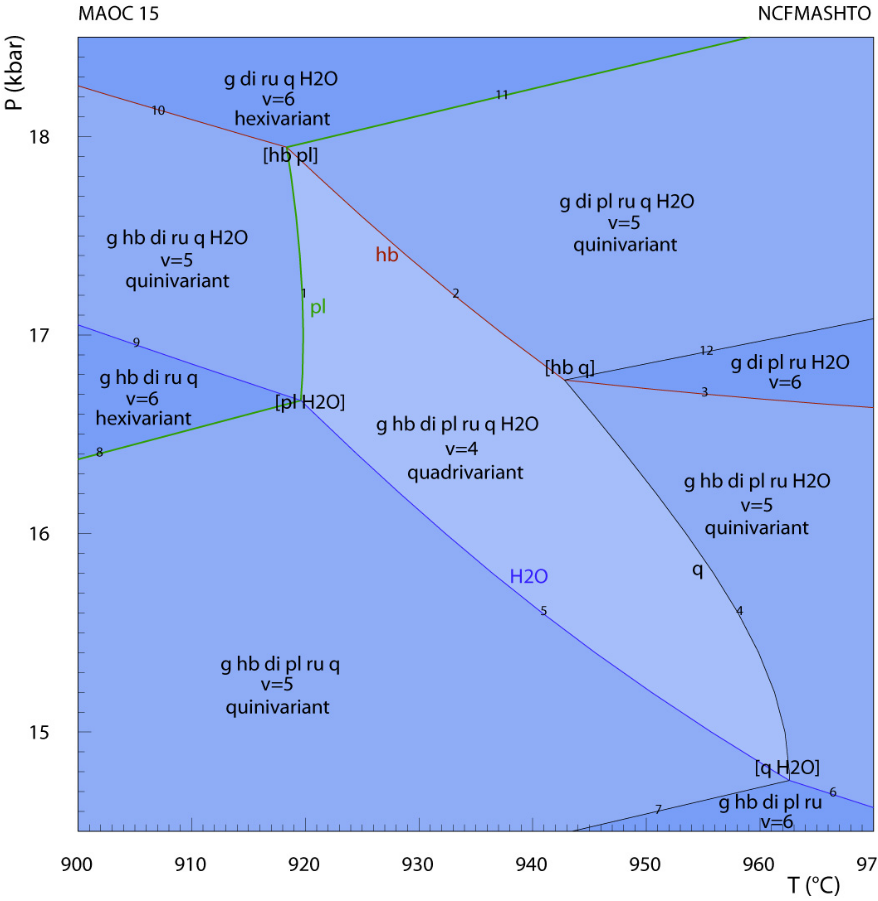

Figure 3.1.3: The Figure illustrates a cutout of the *P*–*T* pseudosection for “MAOC15” (Fig. 4.3.4a) to show the relationships between zero mole proportion boundaries (lines), invariant points and mineral assemblages of different variances, brought together by following the phase rule and the multivariant boundary rule. The calculated examples are the plagioclase line “1” (green) and the adjacent [hb pl] point. Variances change by one across a line and by zero or two across a point.

3.1.3.5.3 Calculation of a zero-mole proportion boundary (line)

The calculation of the plagioclase-out line emanating from the invariant point in the last subchapter is described here: Hence the minerals involved in the following calulation are the same as for the invariant point, the user can type in “=” and THERMOCALC will use the same phases as in the previous calcultaion. If a mineral shall be added or removed from the previous assemblage, the commands are “+” or “-“ plus the abbreviation of the mineral.

```
reading a-x datafile, "tc-NCFMASHTO.txt"...
gl  act  hb  cu  ged  anth  di  o  jd  chl  g  ep  opx  ta  pl  ol
mt  lm  hem  sp  pa  law  ab  ru  sph  ky  q  H2O  zo  cz
choose from: gl  act  hb  cu  ged  anth  di  o  jd  chl  g  ep  opx  ta  pl  ol  mt  lm  hem
sp  pa  law  ab  ru  sph  ky  q  H2O  zo  cz

which phases : =
using the previous phases: hb  di  g  pl  ru  q  H2O
no phases in excess (from script)
variance of required equilibrium (4?) :
you may set zero modal proportions, from:hb di g pl ru q H2O
```

The next question is about the phases the user intends to set to zero. For calculating a zero-mole proportion boundary one needs one phase set to zero, in this case plagioclase, to define the boundary between the quadri- and quinivariant fields.

```
which to set : pl
```

THERMOCALC prompts whether the user intends to calculate the boundary with *T* at *P* or with *P* at *T*. The latter is useful for nearly horizontal boundaries and the user types in “no”. Most boundaries can be calculated with *T* at *P* and the user types in “yes” or hit “return”.

```
calculate T at  P (rather than P at T) ? yes

specification of PT window:
P range over which T of reactions to be calculated
```

The following inputs set limits for the *P* and *T* range in which THERMOCALC shall search for results. Increments need to be adjusted to the length of the boundaries. For very lines the interval spacing must be small.

```
P window: P low,high : 16 18.5
T window within which reactions expected to lie
T window: T low,high :
fluidtype = H2O
P window :16 <-> 18.5kbar : P interval : 0.2
```

THERMOCALC indicates an answer for every specified increment with the same information as described before for the invariant point, if it finds a result. If no results are found, every failed calculation appears in form of a cipher. In the case of the higher variant plagioclase boundary emanating from the calculated point, only the stable part of the boundary is calculable. In contrast, the calculation of the plagioclase-out boundary between the quini- and hexivariant fields without hornblende would also give results for the metastable parts of the boundary. The boundary calculated here starts at the first increment above the lower point where it intersects the H_2O-out boundary. A hint for the disappearance of H_2O is given by the decreasing mode of H_2O along the line towards the lower point. At higher pressure the mode of hornblende decreases towards the effective invariant point calculated above.

```
composition (from script)
H2O   SiO2  Al2O3    CaO    MgO    FeO   Na2O   TiO2      O
1.474 46.917  8.662 12.098 21.958  6.647  1.466  0.480  0.299
<==================================================>
phases : hb, di, g, pl, ru, q, H2O

8888---------------------------------------------------------------------

P(kbar)     T(?C)    x(hb)    y(hb)    z(hb)    a(hb)    c(hb)    f(hb)   Q1(hb)   Q2(hb)
  16.80     919.7  0.09417   0.5950   0.1169   0.5623   0.7548  0.05155  0.01446  0.03846
                       x(di)    j(di)    f(di)    Q(di)  Qaf(di)  Qfm(di)
                     0.08853   0.2043   0.2010  0.01011 0.004528 -0.02361
                        x(g)     z(g)     f(g)   ca(pl)
                      0.3178   0.1538 0.006995   0.3569

mode       hb       di         g      pl       ru         q      H2O
         0.1977   0.3509   0.4266        0 0.004796  0.01867 0.001389
---------------------------------------------------------------------
 P(kbar)     T(?C)    x(hb)    y(hb)    z(hb)    a(hb)    c(hb)    f(hb)   Q1(hb)   Q2(hb)
   17.00     919.8  0.09165   0.6021   0.1222   0.5672   0.7508  0.05123  0.01422  0.03752
                      x(di)    j(di)    f(di)    Q(di)  Qaf(di)  Qfm(di)
                    0.08628   0.2116   0.1963  0.01072 0.004623 -0.02297
                       x(g)     z(g)     f(g)   ca(pl)
                     0.3111   0.1519 0.006836   0.3464

  mode       hb       di         g      pl       ru         q      H2O
          0.1652   0.3666   0.4425        0 0.004796  0.01734 0.003571
---------------------------------------------------------------------
 P(kbar)     T(?C)    x(hb)    y(hb)    z(hb)    a(hb)    c(hb)    f(hb)   Q1(hb)   Q2(hb)
   17.20     919.7  0.08914   0.6095   0.1276   0.5722   0.7469  0.05086  0.01397  0.03657
                      x(di)    j(di)    f(di)    Q(di)  Qaf(di)  Qfm(di)
                    0.08405   0.2191   0.1915  0.01138 0.004714 -0.02235
                       x(g)     z(g)     f(g)   ca(pl)
                     0.3045   0.1502 0.006682   0.3365

  mode       hb       di         g      pl       ru         q      H2O
          0.1320   0.3826   0.4590        0 0.004796  0.01590 0.005808
---------------------------------------------------------------------
 P(kbar)     T(?C)    x(hb)    y(hb)    z(hb)    a(hb)    c(hb)    f(hb)   Q1(hb)   Q2(hb)
   17.40     919.5  0.08665   0.6173   0.1330   0.5771   0.7431  0.05047  0.01369  0.03562
                      x(di)    j(di)    f(di)    Q(di)  Qaf(di)  Qfm(di)
                    0.08185   0.2269   0.1866  0.01210 0.004802 -0.02173
                       x(g)     z(g)     f(g)   ca(pl)
                     0.2979   0.1488 0.006533   0.3273

  mode       hb       di         g      pl       ru         q      H2O
         0.09790   0.3989   0.4759        0 0.004796  0.01435 0.008105
---------------------------------------------------------------------
 P(kbar)     T(?C)    x(hb)    y(hb)    z(hb)    a(hb)    c(hb)    f(hb)   Q1(hb)   Q2(hb)
   17.60     919.2  0.08417   0.6254   0.1384   0.5821   0.7394  0.05004  0.01340  0.03466
                      x(di)    j(di)    f(di)    Q(di)  Qaf(di)  Qfm(di)
                    0.07967   0.2350   0.1815  0.01290 0.004886 -0.02112
                       x(g)     z(g)     f(g)   ca(pl)
                     0.2914   0.1476 0.006390   0.3189

  mode       hb       di         g      pl       ru         q      H2O
         0.06292   0.4156   0.4935        0 0.004796  0.01269  0.01047
---------------------------------------------------------------------
 P(kbar)     T(?C)    x(hb)    y(hb)    z(hb)    a(hb)    c(hb)    f(hb)   Q1(hb)   Q2(hb)
   17.80     918.7  0.08169   0.6338   0.1439   0.5872   0.7359  0.04959  0.01310  0.03369
                      x(di)    j(di)    f(di)    Q(di)  Qaf(di)  Qfm(di)
                    0.07750   0.2434   0.1764  0.01378 0.004967 -0.02052
                       x(g)     z(g)     f(g)   ca(pl)
                     0.2849   0.1467 0.006255   0.3111

  mode       hb       di         g      pl       ru         q      H2O
         0.02693   0.4327   0.5118        0 0.004796  0.01089  0.01291
8888
more phase diagram calculations ?
```

3.1.3.5.4 Drawing a *P–T* pseudosection with data from the output-file

The output file „tc-<name>-dr.txt“ will be created, if the script „drawpd“ is activated. The file contains information about the points and boundaries in a form, which is readable for the drawpd software.

The point calculated above is given as:

```
i<k>   di g ru q H2O  - hb pl

17.946 918.36  % hb = 0pl = 0
```

The plagioclase boundary is given as:

```
% ------------------------------
u<k>   hb di g ru q H2O  - pl

begin  end

16.800 919.75  % pl = 0
17.000 919.82  % pl = 0
17.200 919.74  % pl = 0
17.400 919.52  % pl = 0
17.600 919.19  % pl = 0
17.800 918.75  % pl = 0
```

This information needs to be copied into „dr d<name>“ which is arranged as followed and gives information about the number of variables (“2”) and which column has to be drawn on which axes (x-axis: “2”; y-axis: “1”) on the pseudosection:

```
2                                  % no of variables in each line of data in this case, P, T

9                                  % 9 (NCFMASHTO)

2 1                                % which columns to be x,y in phase diagram
```

Points “i<k>” as well as the lines “u<k>” have to be renamed with chronologic numbers. A boundary ends and begins at different i and the user needs to change “begin” and “end” to the names of the points which border the line unless the line runs to the edge of the diagram.

```
% ------------------------------
i1   di g ru q H2O  - hb pl

17.946 918.36  % hb = 0pl = 0

i2, i3....

% ------------------------------
u1   hb di g ru q H2O  - pl

i4  i1

16.800 919.75  % pl = 0
17.000 919.82  % pl = 0
17.200 919.74  % pl = 0
17.400 919.52  % pl = 0
17.600 919.19  % pl = 0
17.800 918.75  % pl = 0

u2, u3....
*
%AREAS
```

Each field can be be coloured to reflect its variance in a shaded nuance of a defined colour. The lower the variance the lighter the field, e.g. for the highest variance area in this example (v = 4) the value of 0.6 is written before the names of the field bordering lines, which are arranged in a continuous order. The higher variant fields have lower numbers for darker fields.

```
%v=4
0.6 u1 u2 u4 u5
%v=5
0.5 u11 u2 u12
0.5 u3 u4 u6
0.5 u7 u5 u8
0.5 u9 u1 u10
%v=6
0.4 u10 u11
0.4 u3 u12
0.4 u6 u7
0.4 u8 u9
% ---------------------------------------------
*
```

This section defines the *P–T* area and the labelling of a *P–T* pseudosection. The drawn area ranges from 900–970 °C and 14.4–18.5 kbar.

```
window 900 970 14.5 18.5         % T,P window
```

The user types in information about the intervals of big and small ticks for *T* and *P* as well as the beginning of these ticks:

```
bigticks 10 900 1 15             % main T ticks at 10° intervals, starting at 900°

                                 % main P ticks at 1 kbar intervals, starting at 15

smallticks 1 0.1                 % minor T,P ticks
```

The chosen RGB dark colour for the highest variant fields is defined here and all other variances are nuances of this colour.

```
darkcolour 29 93 242             % red green blue in 0<->255 => Illustrator RGB
```

If numbering is set to <yes> or <y> the numbers of lines are drawn in the diagram.

```
numbering yes                    % each line is labelled with its number

*                                % end of file
```

3.1.3.6 *T–X* pseudosections

A *T–X* pseudosection is calculated at a fixed pressure and it connects two different bulk rock compositions by illustrating the changes occurring in mineral assemblages from one (X_1) to another (X_2) bulk rock composition (e.g. Fig. 4.3.1). The calculation differs from that of a *P–T* pseudosection in several ways: Firstly, the script file requires a second bulk rock composition below the first one and the user needs to specify a fixed pressure. By running THERMOCALC, the program asks for the assemblage and the phase intended to set to zero, for the *P* window (using the default option by hitting <return>), the *T* window (the user has the possibility to specify) and the start and finish proportions of the bulk composition range. By hitting <return> THERMOCALC calculates for the total range by using the specified number of increments, or the user can specify the range where the line should occur. In this study, points in *T–X* pseudosections were calculated by running a line in a small range with many increments with one phase phase going to zero and the last point of those lines is taken as the point. Another possibility of calculating a point is to interpolate it, but this was not applied here.

The data for drawing a pseudosection are split in three colums (mode, *P* and T), so the adjustment in „tc-<name>-dr.txt“ is:

```
3                          % no of variables in each line of data, in this case,
                           mode, P, T

9                          % 9 (NCFMASHTO)

1 3                        % which columns to be x,y in phase diagram
```

This gives the information that from 3 variables in each line the first and third need to be read to draw the pseudosection.

3.2 High-pressure partial melting Experiments

3.2.1 Introduction

The experiments were conducted in a 650 ton 1-inch endloaded piston-cylinder press at the Institute of Geoscience, Johannes-Gutenberg University of Mainz. The pressure is generated by a tungsten carbide piston which is hydraulically driven into the cylindrical bore of the pressure vessel. The uniaxial pressure transmitted by the piston is converted into a hydrostatic pressure by a solid pressure medium (CaF_2) (Fig. 3.2.1).

Figure 3.2.1: Schematic assembly of the Piston-cylinder apparatus.

3.2.2 Sample assemblies

For the experiments Ca-fluoride (CaF_2) cell assemblies were used. Inner and outer spacers were machined from sintered Ca-fluoride bits to perfectly fit (+/- 0.02 mm) the graphite heater and pressure vessel walls and the lower spacer was holding the three capsules in 120 °-geometry (Fig. 3.2.2). The B-type thermocouple (subchapter 3.2.4) wires were isolated by a two-hole mullite tube. To ensure good electric contact, a graphite disk was placed between furnace and piston.

3.2.3 Capsules

A gold-palladium-alloy was used as capsule material. Platinum was avoided to reduce the loss of iron by alloying with Pt and hydrogen diffusion through the capsule walls. The lower melting point of that alloy (around 1400 °C) is still far about the experimental conditions (up to 1100 °C).

The capsules were prepared by cutting off pieces of ca. 8 mm length from a Au80/Pd20 tube, the outer diameter of the capsules was 4 mm and the inner diameter was 3.6 mm. A small lid was then welded into the one end of the tube and subsequently pressed flat with a piston. The capsules were filled with the sample mix (subchapter 5.2), manually pressed to high density with a small tube and covered with a small graphite disk which acted as CCO oxygen buffer and separated the sample powder from the welding area.

After the top portion was cleaned with acetone and dried overnight at 110 °C a second lid was welded into the open end of the capsule. The whole capsule was then inserted into the 4 mm die and compressed with a steel piston to obtain its flat cylindrical shape and a high initial density (Fig. 3.2.2). This densification reduces the deformation of the whole cell assembly during pressurisation.

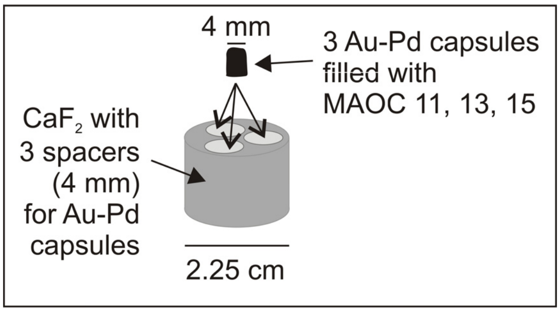

Figure 3.2.2: Capsule assembly in the CaF_2 capsule holder. Each of the three 4 mm Au-Pd capsules filled with MAOC 11, 13 and 15 is inserted in one of three 4 mm holes.

3.2.4 Pressure control

After loading the cell assembly into the cylindrical bore of the bomb, only the endload pressure was raised gently up to 60 bar oil pressure to ensure that the bomb is properly aligned. After the cooling circuit was connected to the bomb the piston pressure was slowly raised at a rate of 10 bar oil-pressure/min (0.5 kbar/min sample pressure) until the final run load was reached. The pressure is controlled by a Siemens SPS unit, compensating for the pressure rise during the subsequent heating phase and the pressure drop during the run of the experiment. Although all hydraulic parts are optimised for low internal friction, a pressure error of 0.5 kbar is assumed.

3.2.4 Temperature control

The temperature was measured with a B-type thermocouple which was positioned 0.5 mm on top of the capsule. It consists of a pair of Pt/Rh wires (Pt/Rh 70/30 and 6/94) which are led through a double bore tube of mullite (1.6 mm o.d.) and was welded at one end to form a thermal junction.

The experimental charge is heated at a rate of 50 °C/min by leading a high current through a graphite sleeve. The temperature is kept stable to +/- 1 °C by a PMA controller. The experiments were terminated by shutting off the power supply to the heating circuit. The temperature was < 300 °C after 15–20 seconds, depending on the experimental temperature condition.

3.2.5 Polishing

After the experiments, each capsule was recovered from the assemblies and cut into halves before being embedded into epoxy resin (araldite). The sample pucks were first ground on a wet SiC-paper (#500) until the experimental charge was exposed and subsequently polished on 9 μm, 3 μm an finally 1 μm polishing cloths. The sample was cleaned in an ultrasonic bath between each polishing step and kept dry in a vacuum furnace before the carbon coating for the subsequent electron microprobe analysis (subchapter 3.3). An overview of a polished half of a capsule taken during microprobe analysis is illustrated in Fig. 5.3.11a.

3.3 Mineral chemistry analyses

The mineral chemistry of the experimentally-grown phases (Chapter 5) was analysed by using the *Jeol JXA 8900 PL electron probe micro analyser* (EPMA) at the Institute of Geoscience, Johannes-Gutenberg University of Mainz. The analyser crystals and element standards are given in Table 3.3.1 and the analytical program used for the analyses of silicate and melt phases was *SilUMainz* with 15 kV accelerating voltage and a 12 nA beam current (2 μm diameter). The results for analyses on garnet, amphibole, clinopyroxene, orthopyroxene, plagioclase and melt are presented in subchapter 5.3.3 (averaged analyses) and in the Appendix B. Backscattered-electron (BSE) images were additionally taken during the analyses.

Table 3.3.1: Elements analysed with the program *SilUMainz*. Standards, wavelength-dispersive spectrometers and analyser crystals are presented.

Program: SilUMainz			
accelerate voltage: 15 kV			beam current: 2nA
Element	**Standard**	**Spectrometer**	**analyser crystal**
Na	albite	1	TAP
Al	corundum	1	TAP
Si	wollastonite	2	TAP
Mg	periclase	2	TAP
K	orthoclase	3	PET
Ca	wollastonite	3	PET
Ti	MnTi	4	PET
Cr	chromite	4	PET
Fe	hematite	5	LIFH
Mn	MnTi	5	LIFH

Chapter 4

Mineral equilibria modelling for mafic and ultramafic rocks and models for Archean oceanic crust

4.1 Introduction

The Archean bulk rock compositions and processes responsible for the generation of oceanic and TTG-like continental crust are supposed to have differed from today and there is debate of the crust-forming processes on the early Earth (subchapter 2.3). The aim of calculating phase equilibria of metamorphosed mafic and ultramafic rocks is to evaluate potential bulk rock compositions, which may have existed on the early Earth and which are able to account for the genesis of TTG. It is generally accepted that the first continental crust-like partial melts with a TTG-like composition were generated by partial melting of a hydrous metabasaltic source (e.g. Barker & Arth, 1976; Jahn *et al.*, 1981; Rapp *et al.*, 1991; Sen & Dunn, 1994; Rapp & Watson, 1995; Martin, 1999; Rapp *et al.*, 1999; Smithies, 2000; Martin & Moyen, 2002; subchapter 2.3.2) metamorphosed to plagioclase-bearing garnet-amphibolite (Foley, *et al.*, 2002, 2003, Schmidt *et al.,* 2004) or eclogite (Rapp *et al.*, 2003). Compared to early komatiites and ultramafic rocks, whose metamorphic products (plagioclase-free pyroxenites) produce basaltic or nephelinitic partial melts (Foley *et al.*, 1999), basalt transforms into either garnet-amphibolite or eclogite during metamorphism with corresponding TTG-like melts, generated in subduction zone settings by slab-melting or on the base of thick oceanic crust. The approach in this study follows the assumption of Foley *et al.* (2003; subchapter 2.3.3), that the generation of voluminous TTG was already possible at some stage after the transition from magnesium-rich komatiitic crust to a less magnesium stage of picritic oceanic crust, whereas in previous studies modern basaltic sources were assumed for the genesis of TTG (subchapter 2.3.4). Forward modelling is used here to locate the first-order transition from plagioclase-free (pyroxenite) to plagioclase-dominated (amphibolite) melting conditions performed with the help of thermodynamic calculations on intermediate (picritic) bulk rock compositions as a function of a decreasing MgO-content.

Based on today´s mid-ocean ridge basalt (MORB), several *P–T* pseudosections with different MgO-contents for natural bulk rock compositions up to a komatiite were calculated with the software THERMOCALC (subchapter 3.1). The compositions were chosen on the basis of comparability to the potential Archean development of the oceanic crust´s bulk rock composition from a komatiitic composition to a composition which may have been a potential precursor for the first continental crust, modelled via a decreasing MgO-content. In contrast to MORB, whose contribution to today´s subduction metamorphism is well studied (e.g. Green & Ringwood, 1967a; Schmidt & Poli, 1998; Macdonald *et al.*, 2000; subchapter 2.2.2.2), the behaviour of more magnesium-rich compositions in the Archean settings are less well known (subchapter 2.3.4). The *P–T* pseudosections presented here were used to evaluate appropriate compositions for models of Archean oceanic crust (subchapter 4.3 and Chapter 5).

The software used was THERMOCALC 3.30 and 3.33 (Powell & Holland, 1988) with the internally consistent data set “tc-ds55” (Holland & Powell 1998, updated 22 November 2003). The mineral abbreviations for the *P–T* and *T–X* pseudosections are given in Tab. 3.1.1.

Mineral equilibria calculations were undertaken in the system NCFMASHTO (Na_2O–CaO–FeO–MgO–Al_2O_3–SiO_2–H_2O–TiO_2–O), the largest system available for calculations on metabasic rocks (e.g. Diener *et al.*, 2007). The absence of K_2O from the system is not critical in the scope of this work since TTGs generally are sodic rocks where potassium is rather a trace element reflecting source differences (Moyen & Stevens, 2006). “O” is the factor for the amount of Fe^{3+}, according to Eq. 4.1.1 with x for the chosen percental amount of Fe_2O_3 from FeO.

$$\frac{\left(\frac{FeO_{tot}}{100} * x\right)}{2} = O \qquad \text{[Equation 4.1.1]}$$

Subchapter 4.2 introduces the *P–T* pseudosections for existing mafic and ultramafic rock compositions calculated with H_2O in excess. Subchapter 4.2.6 is a summary and discussion of the pseudosections and in subchapter 4.2.7 the *P–T* pseudosection for the komatiite composition is related to the experimental results of Foley *et al.* (2003). Under consideration of the results from these bulk rock compositions in Tab. 4.2.1, several models for Archean oceanic crust (MAOC) with low H_2O contents were calculated and subchapter 4.3 introduces *P–T* pseudosections for these models. The models for Archean oceanic crust were established for conducting high-pressure partial melting experiments since there is no melting model for mafic and ultramafic rocks in THERMOCALC (subchapter 3.1.2.2.6). The experiments are appropriate to determine the solidus, the melting rock-type (amphibolite, eclogite or pyroxenite) as well as the resulting melt-compositions (chapter 5).

4.2 Forward modelling of metamorphosed mafic and ultramafic rock compositions in the system Na_2O–CaO–FeO–MgO–Al_2O_3–SiO_2–H_2O–TiO_2–O (NCFMASHTO)

4.2.1 *P–T* pseudosections for existing bulk rock compositions in the system NCFMASHTO

This subchapter presents *P–T* pseudosections for different natural bulk rock compositions (Tab. 4.2.1), primarily differing in their varying MgO-contents (8.38 wt% for MORB to 17.5 wt% for Gorgona komatiite). The bulk rock compositions (Tab. 4.2.1) are given in wt% and mol%, whereas the latter is required for the THERMOCALC script-file (subchapter 3.1.3.4.7)

The initial *P–T* pseudosection in this study is taken from Diener *et al.* (2007, fig. 18b), calculated for a typical MORB composition (Sun & McDonough, 1989) in the system NCFMASHTO with H_2O in excess. The effect of the increasing MgO-content is illustrated by further *P–T* pseudosections for picritic bulk rock compositions with approximately 11 and 13 wt% MgO as well as for the Gorgona komatiite (subchapter 2.3.4). The two picrites from Keweenawan (Shirey *et al.*, 1994) and the Deccan Traps (Krishnamurthy *et al.*, 2000) were chosen; (1) because of their applicable MgO-content, (2) due to their flood basalt origin, which may be the best modern analogue to the thick Archean oceanic crust (Farnetari *et al.*, 1996; Foley *et al.*, 2003; Zegers & van Keken, 2001), (3) their initially low K_2O-content as proven for TTG-compositions (Moyen & Stevens, 2006) and to allow a more direct comparison to the K-free model-system NCFMASHTO and (4) their lack of olivine-accumulation, which would account for ultramafic cumulates from which TTG-like melts cannot be generated (Foley *et al.*, 1999).

Table 4.2.1 : Bulk rock compositions of existing mafic and ultramafic rocks used for the calculation of *P–T* pseudosections in this subchapter. The compositions are given in wt% and mol%, the latter required for the calculation with the software THERMOCALC. “O” is the amount of ferric iron from total FeO (Eq. 4.1.1)

Rock composition	Unit	SiO_2	Al_2O_3	CaO	MgO	FeO	Na_2O	TiO_2	O
MORB	wt%	51.61	15.19	11.21	8.38	9.59	2.66	1.37	
	mol%	53.40	9.26	12.43	12.93	8.29	2.66	1.07	0.50
Keweenawan	wt%	49.16	13.03	10.01	11.23	11.85	2.64	1.19	
	mol%	50.34	7.86	10.98	17.15	10.13	2.62	0.92	0.50
Deccan Traps	wt%	47.41	10.07	13.19	13.20	11.11	1.65	2.00	
	mol%	47.63	5.96	14.20	19.77	9.32	1.61	1.51	0.50
Gorgona	wt%	46.30	10.10	10.20	17.50	11.57	1.24	0.66	
	mol%	46.01	5.92	10.86	25.93	9.60	1.20	0.49	0.20

The classification of the rock types in the following *P–T* pseudosections is adopted from the stability diagrams for amphibolites and pyroxenites (Foley *et al.*, 2003, Fig. 2.3.2). Partial melting of garnet-amphibolite is proposed to be required for the generation of early continental crust and garnet-amphibolite assemblages typically contain garnet, hornblende, diopside, plagioclase and quartz in the pseudosections. The boundary to amphibolite at low pressure is marked by garnet-out, the boundary to amphibole-eclogite is marked by plagioclase-out and the boundary to (garnet-) granulite is marked by hornblende-out at high pressures and/or orthopyroxene-in at low pressures. Hornblende is also the critical phase for the transition between amphibole-eclogite and eclogite assemblages. The boundary to blueschist assemblages at low temperature is marked by the stability of either chlorite, glaucophane, lawsonite and actinolite at different conditions with varying combinations.

Several overall patterns of mineral stabilities are similar in each pseudosection. The garnet-in curve is generally characterised by a steep gradient at low temperature, flattening at lower pressures with increasing temperatures, whereas the plagioclase-stability is restricted to high-*T* low-*P* assemblages below a positively-sloped boundary.

The assemblages in the eclogite realm of the more MgO-rich picritic compositions contain no omphacite but diopside and these are referred to diopside-amphibole-eclogite. These assemblages are not pyroxenites due to the absence of orthopyroxene compared to the pyroxenites described in Foley *et al.* (2003). These pyroxenites are defined as plagioclase-free rocks containing clinopyroxene, orthopyroxene with or without olivine and/or garnet but lacking chlorite and/or actinolite, as appearing in the metamorphosed komatiite from Gorgona (subchapter 4.2.5). The appearance of chlorite and actinolite restricts the stability field of pyroxenite at low temperature.

Minerals with identically coded *a–x* models such as diopside and omphacite as well as the clinoamphiboles hornblende, glaucophane and actinolite (Appendix A1) are distinguished by their composition variables as described in Diener *et al.* (2007) and in the tutorial for calculating metabasic rocks (Diener, 2009), available on the THERMOCALC website (url: http://www.metamorph.geo.uni-mainz.de/thermocalc/ tutorials/ index.html).

For example, clinopyroxenes are distinguished by the variables *j(di)* and *j(o) = (xNaM2c + xNaM2n) / 2* respectively, expressing the amount of the Na-rich jadeite in the pyroxene. From $0 < j < 0.25$ the pyroxene is diopside, whereas omphacite is stable in the calculation if $0.35 < j < 0.6$ and jadeite is stable if $0.8 < j < 1$. Composition isopleths to distinguish diopside from omphacite are shown exemplarily in Fig. 4.2.2b for the picrite from Keweenawan. The coding of the amphiboles is more complicated, nevertheless the names of amphiboles specified in the pseudosections match the composition variables classification (Diener *et al.,* 2007 and Appendix A1).

P–T pseudosections with H_2O mode contours (i.e. fluid content) for all bulk rock compositions are illustrated additionally (Figs 4.2.3 and 4.2.6). The amount of free H_2O in them corresponds to the water released with changing pressure and temperature. To calculate this, a fixed amount of H_2O (instead of H_2O in excess) had to be chosen in each bulk rock composition with the constraint that all assemblages in the pseudosections contain at least a small amount of H_2O. This is achieved for approx. 16.6 mol% H_2O in each bulk rock composition. If the amount of H_2O is below this value, fluid-absent assemblages would develop at low *P–T* conditions (Fig. 6.4.2c, d). In contrast, a higher amount of H_2O in the bulk rock composition has no further influence on calculated phase-boundaries or mineral compositions as the system is now thermodynamically saturated in H_2O fluid making $aH_2O = 1$. As illustrated in Fig. 4.3.1 no changes occur in the assemblages by adding more H_2O once an assemblage is H_2O-saturated. The left part of Fig. 4.3.1 illustrates the transition from H_2O in excess to H_2O-undersaturation in the MORB composition. The assemblage fields start to change at low temperature once a specified value of H_2O is reached (here around 12 wt% H_2O at 15 kbar). The high amounts of H_2O used here are only chosen for comparison of all assemblages in the pseudosections with H_2O in excess and they do not resemble realistic H_2O-contents for a rock. However, the amount of free H_2O increases due to the breakdown of water-bearing phases like chlorite, lawsonite, epidote and amphibole. The final amount of free H_2O in the modelled rock depends on the initial defined H_2O-

content. This allows these pseudosections to be used to define the potential *P–T* conditions of dehydration of hydrous phases and it allows a comparison of the *P–T* range where water is released from a rock during metamorphism (e.g. Elmer *et al.*, 2006). However, it is unlikely that the fluid released during prograde metamorphism persists in the rock but rather migrates upwards in the crust.

4.2.2 Mid-ocean ridge basalt

According to the *P–T* pseudosection for MORB (Sun & McDonough, 1989; Diener *et al.* 2007, fig. 18b), pseudosections from 8–25 kbar and 500–900 °C are illustrated in Figs 4.2.1, 4.2.3a and 4.2.7a, the last with a coloured rock-type scheme following that of Fig. 2.3.2. The small amounts of K_2O and MnO in the whole rock analyses were ignored and recalculated assuming that 12% of Fe_{total} was present as Fe_2O_3, a typical value for wet-chemical analyses (e.g. Schilling *et al.*, 1983; Diener *et al.*, 2007). According to this and Eq. 4.1.1 “O” is set to 0.5. The pseudosection for MORB was calculated with H_2O in excess and it contains several univariant reactions from 18 to 25 kbar and 530 to 640 °C surrounded by divariant white-coloured assemblage fields.

The dominating garnet-amphibolite assemblage in this pseudosection is the quadrivariant g–hb–di–pl–ru–q–H_2O, which is bordered by several related assemblages from 700–900 °C up to 17 kbar which all contain at least garnet, hornblende and plagioclase. The disappearance of plagioclase, according to the reaction albite <=> jadeite + quartz, marks the boundary to amphibole-eclogite, e.g. g–hb–di–ep–ru–q–H_2O, whereas both become eclogite when hornblende disappears from the assemblages at higher *P–T*. At around 17 kbar at 625 °C a solvus top between diopside and omphacite is developed, leading to a solid solution of the phases with names given accordant to the particular composition variables *j(di)* and *j(o)* (subchapter 4.2.1). The direction of the elongation of the solvus-loop approximately determines the boundary between diopside and omphacite towards higher *P–T*.

At $P < 10$ kbar the loss of garnet restricts the stability of garnet-amphibolite, passing into amphibolite assemblages at lower pressure. (Garnet-) granulite assemblages arise with the appearance of orthopyroxene at high temperatures. The boundary towards the blueschist assemblages at low temperature is marked by a sequence of narrow, primarily trivariant fields emanating from < 10 kbar at 500 °C to > 600 °C at 20 kbar, made up of three amphiboles (glaucophane, hornblende and actinolite) among other minerals. At low *T*, glaucophane and actinolite are stable, whereas hornblende and actinolite occur at the high-*T* side of the trivariant assemblages. Actinolite quickly disappears at the high-*T* side of the narrow fields. At about 16 kbar at 580 °C a solvus closes between hornblende and glaucophane. According to the calculated composition variables the amphibole at the high-*T* side of the solvus is hornblende (sensu lato). The low-*T* blueschist assemblages contain glaucophane, lawsonite and/or epidote as well as chlorite at the lower grades and/or omphacite at higher grades. Quartz is absent at $P > 22$ kbar and $T < 520$ °C. At low *P–T* conditions (< 14 kbar at 550 °C) some clinopyroxene-free assemblages occur at the transition to the greenshist assemblages, where also albite occurs. The stability field of rutile covers nearly the whole area with the exception of the low-*P* area.

Important water-bearing phases are lawsonite, chlorite and amphibole, which dehydrate in the low-temperature assemblages and cause fluid-release to the system (Fig. 4.2.3a). At first, a rapid breakdown of lawsonite, emanating from the trivariant assemblage di–o–law–ep–chl–ru–q–H_2O (field no. 13 in Figs 4.2.1 and 4.2.3a) up to the trivariant assemblage g–o–law–ta–ru–ky–q–H_2O at 25 kbar is calculated. The transition from blueschist to amphibole eclogite assemblages is marked by the breakdown of glaucophane and epidote to form omphacite, garnet, quartz and H_2O, which is followed by the breakdown of hornblende and a further release of H_2O at higher *P–T* conditions. This may be linked to the intensive fluid release into the overlying mantle-keel during subduction with thermal gradients of 300–400 °C/GPa (Brown, 2006) according to the area between the two gradients in Fig. 4.2.3a. The fluid release establishes the conditions for partial melting of the mantle and the creation of arcs above subduction zones (subchapter 2.2.2.2). The breakdown of lawsonite shown in this pseudosection is restricted to lower *dT/dP*, but at lower *T* the lawsonite breakdown occurs between 300–400 °C/GPa (not shown). Chlorite breaks down subsequently at lower pressure and releases H_2O in broader temperature intervals. The steeper contours in the assemblage g–hb–di–pl–ep–ru–q–H_2O could be induced by the breakdown of epidote. Whilst passing into the amphibole-eclogite and amphibolite assemblages the slope of the contours adjusts to the amphibole-out boundary.

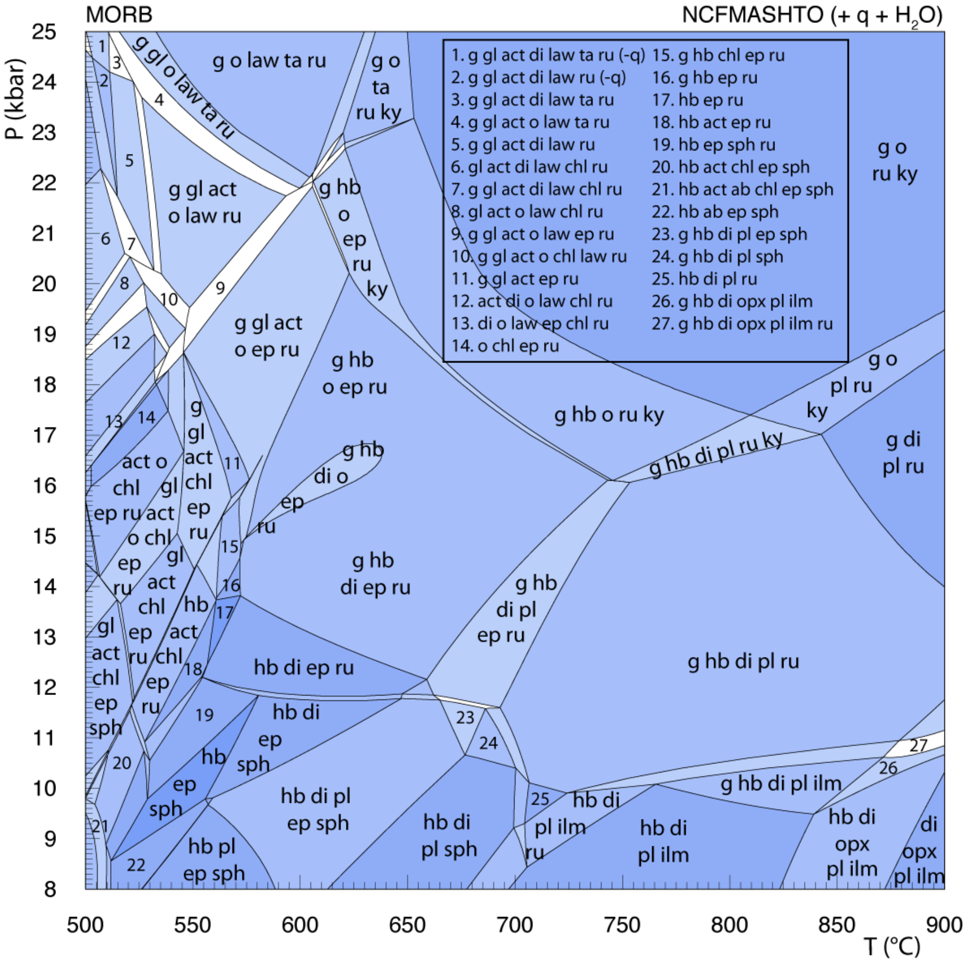

Figure 4.2.1: *P–T* pseudosection for MORB, calculated in NCFMASHTO with q and H_2O in excess for the composition taken from Tab. 4.1.1. The description is given in the text and mineral abbreviations are given in Tab. 3.1.1.

4.2.3 Picrite from Keweenawan

The bulk rock composition used for the pseudosections shown in Figs 4.2.2, 4.2.3b and 4.2.7b is taken from a study about flood basalt from the Keweenawan Mamainse Point Formation in Ontario, Canada (Shirey *et al.*, 1994). The sample DSC-3 contains 11.23 wt% MgO and belongs to Group 1, which Shirey *et al.* (1994) refer to be the more primitive and higher temperature lavas reflecting the initial stages of deep melting in an ascending mantle plume source. The *P–T* pseudosection was calculated with H_2O in excess and contains two univariant reactions, one of them is very short in extension (22.36–22.44 kbar at 606 °C) and the second one exists between 18.86 and 19.44 kbar at around 550 °C.

The amphibolite assemblages extend below the garnet-in boundary where also plagioclase is stable at high temperature. Garnet-amphibolite assemblages are located at pressures above the amphibolite assemblages and the change to (garnet-) granulite is initiated with the appearance of orthopyroxene at higher temperatures.

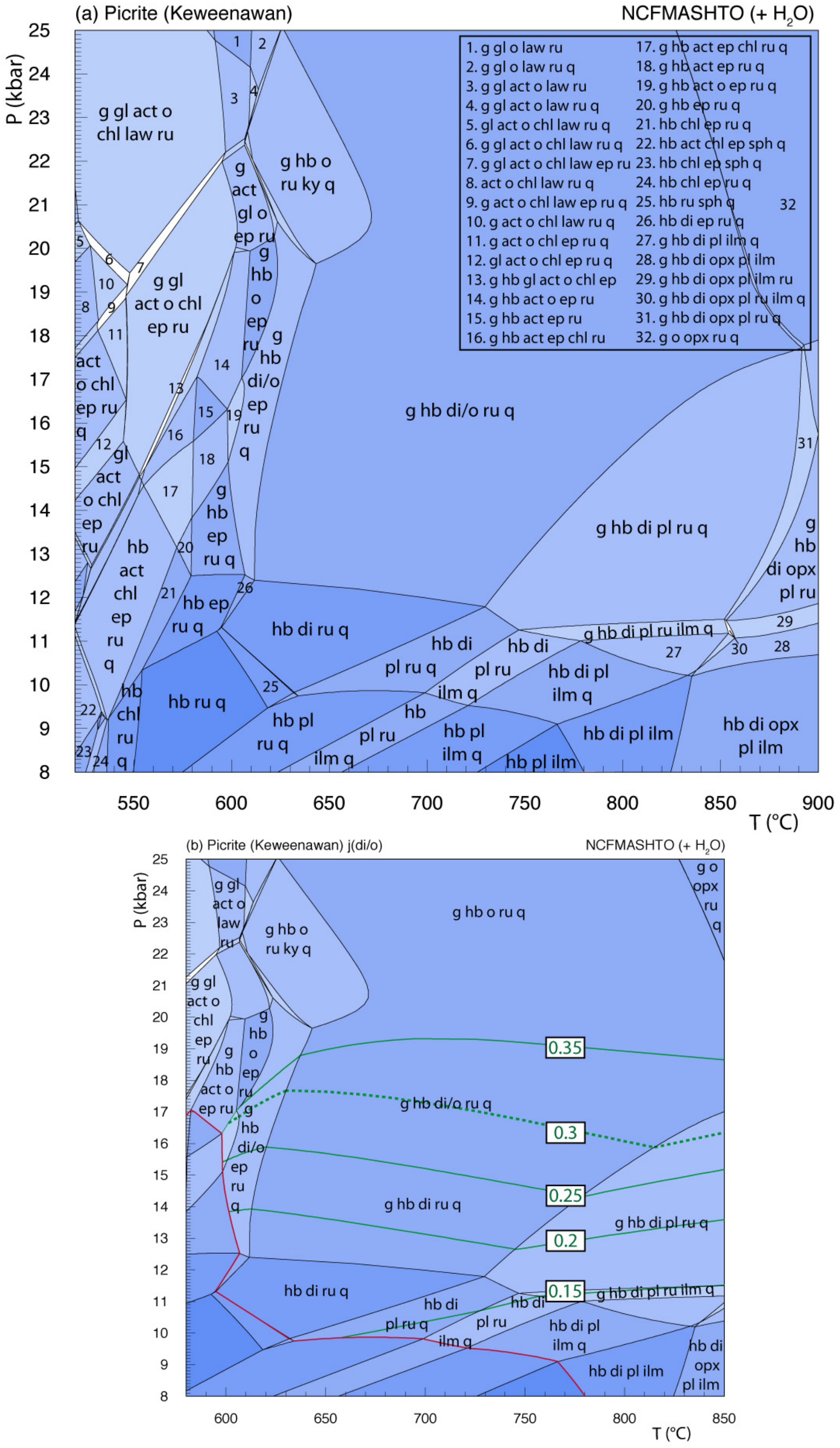

Figure 4.2.2a, b: (a) *P–T* pseudosection for a picrite from Keweenawan, calculated in NCFMASHTO with H_2O in excess for the composition taken from Tab. 4.1.1. (b) The same *P–T* pseudosection as (a) but with isopleths for the composition variable *j(di)/j(o),* indicating the stability of diopside (< 0.25) and omphacite (> 0.35). The red curve marks the stability of clinopyroxene. Further descriptions are given in the text and mineral abbreviations are given in Tab. 3.1.1.

The disappearance of plagioclase at higher pressure gives rise to amphibole-eclogite with the most striking quinivariant assemblage g–hb–di/o–ru–q–H_2O, extending from approximately 600 °C to the breakdown of hornblende at $T > 850$ °C at the beginning of the eclogite facies.

There is no clinopyroxene-solvus present in Fig. 4.2.2, but a composition variable diagram (Fig. 4.2.2b) illustrates the stability of diopside below $j(di) = 0.25$ and the stability of omphacite above $j(di) = 0.35$ with intermediate compositions in between. The conversion from diopside to omphacite depends on pressure. Omphacite is also stable next to the clinopyroxene-absent fields at low temperature.

The low-*T* blueschist assemblages include glaucophane, lawsonite, actinolite and chlorite among phases also appearing in the other facies. Several assemblages in narrow di- and trivariant fields contain three amphiboles (actinolite, hornblende, glaucophane), arranged in a sequence emanating from around 12 kbar at the lowest temperatures up to 20 kbar and 600 °C (field no. 13; Figs 4.2.2 and 4.2.3b). Glaucophane and actinolite are stable at low temperature up to 25 kbar, hornblende and actinolite occur on the high-*T* side of the three-amphibole fields until the actinolite is lost. The high-*T* boundary of field no. 14 (g–hb–act–o–ep–ru–H_2O) is a closing solvus between actinolite and hornblende at around 19 kbar and 600 °C. Except at low *T*, the blueschist assemblages above 15 kbar contain no quartz. Rutile is absent at low pressure and $T > 650$ °C where also garnet is absent.

The release of H_2O from the blueschist assemblages is induced by the breakdown of chlorite and lawsonite (Fig. 4.2.3b). The final breakdown of lawsonite occurs in the divariant fields emanating from the univariant reaction at 19 kbar. After the breakdown of chlorite at lower pressures and higher temperatures (e.g. from fields no. 16, 17), the H_2O mode contours change their slope from near vertical to diagonal and become more widely spaced in temperature in the amphibole-eclogite assemblages reflecting the broad field of the breakdown of epidote (steep contours in g–hb–di/o–ep–ru–q–H_2O) and amphibole.

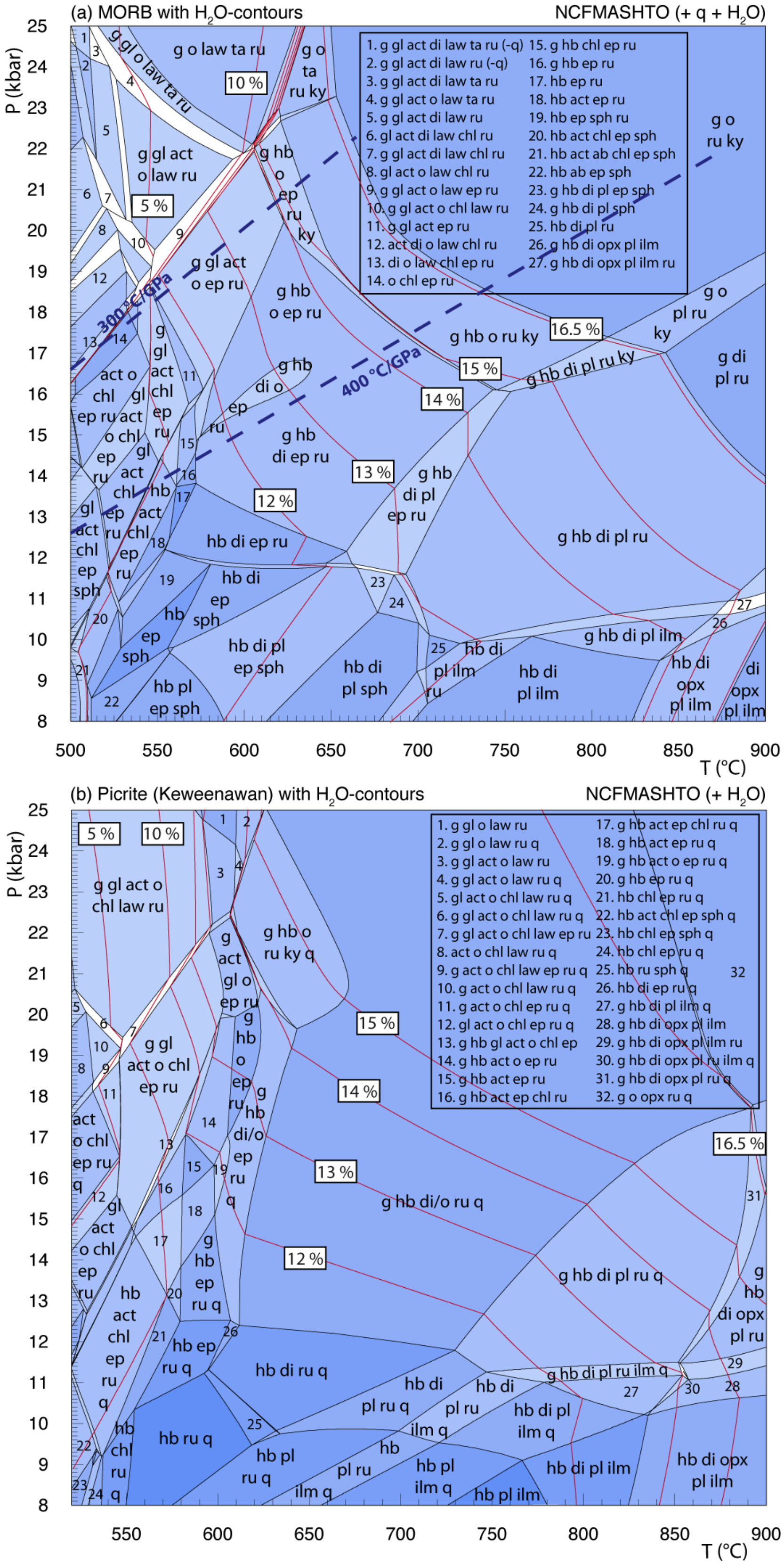

Figure 4.2.3a, b: *P*–*T* pseudosections for MORB (a, cf. Fig. 4.2.2) and the picrite from Keweenawan (b, cf. Fig. 4.2.2), calculated with H_2O in excess, illustrate the differences between the two bulk rock compositions. The main garnet-amphibolite assemblage g-hb-di-pl-ru-q-H_2O is stable in both, and the contours show the increasing amount of H_2O during the breakdown of the water-bearing phases, especially hornblende at high temperature up to the breakdown of this phase. Thermal gradients of 300 and 400 °C/GPa show the range of subduction gradients. Further descriptions are given in the text and mineral abbreviations are given in Tab. 3.1.1.

4.2.4 Picrite from the Deccan Traps

The second picritic bulk rock composition from the Deccan Traps (Krishnamurthy *et al.*, 2000) has a higher MgO-content than that of the Keweenawan composition. The sample 244 from the Dhandhuka location, Flow D-12 contains 13.20 wt% MgO and the appropriate *P–T* pseudosection is illustrated in Figs 4.2.4, 4.2.6a and 4.2.7c.

According to the restricted stability of plagioclase in this pseudosection, plagioclase-bearing garnet-amphibolite and amphibolite assemblages occur below 8 kbar at 710 °C and 12.4 kbar at 900 °C. The stability of quartz is restricted to a narrow area around 800 °C and 11 kbar. Since all clinopyroxenes show diopsidic compositions in the calculations, the assemblages in the *P–T* range of eclogite, e.g. g–hb–di–ru–H_2O ± ilm and g–hb–di–ru–q are diopside-amphibole-eclogite, introduced in subchapter 4.2.1. These assemblages constitute a transition to plagioclase-free pyroxenites, which stabilise with the appearance of orthopyroxene towards higher temperatures.

The transition to the low-*T* assemblages is marked by the appearance of chlorite through a conspicuous, steep boundary from 8 kbar at 540 °C to 25 kbar at 740 °C. A characteristic feature in the low-*T* area is the solvus between actinolite and hornblende at 19 kbar and 650 °C. The amphibole above the solvus-top is hornblende according to the calculated composition variables. Below this, a nearly 100 °C wide needle-shaped area of hornblende- and actinolite-bearing assemblages is located. The stability of glaucophane is restricted to one assemblage between 11 and 15 kbar at low temperature. The stability field of rutile nearly covers the complete pseudosection with the exception of two assemblages in the lower right corner and the low *P–T* area where it is replaced by sphene.

The main water-release (Fig. 4.2.6a) is coupled to the breakdown of lawsonite (P > 16 kbar) and epidote (P < 21 kbar), followed by the breakdown of chlorite at increasing temperature. Beyond that to higher *T*, the more or less vertical H_2O mode contours broadly parallel the hornblende-out boundary at the high-*T* side in the diopside-amphibole-eclogite and pyroxenite assemblages.

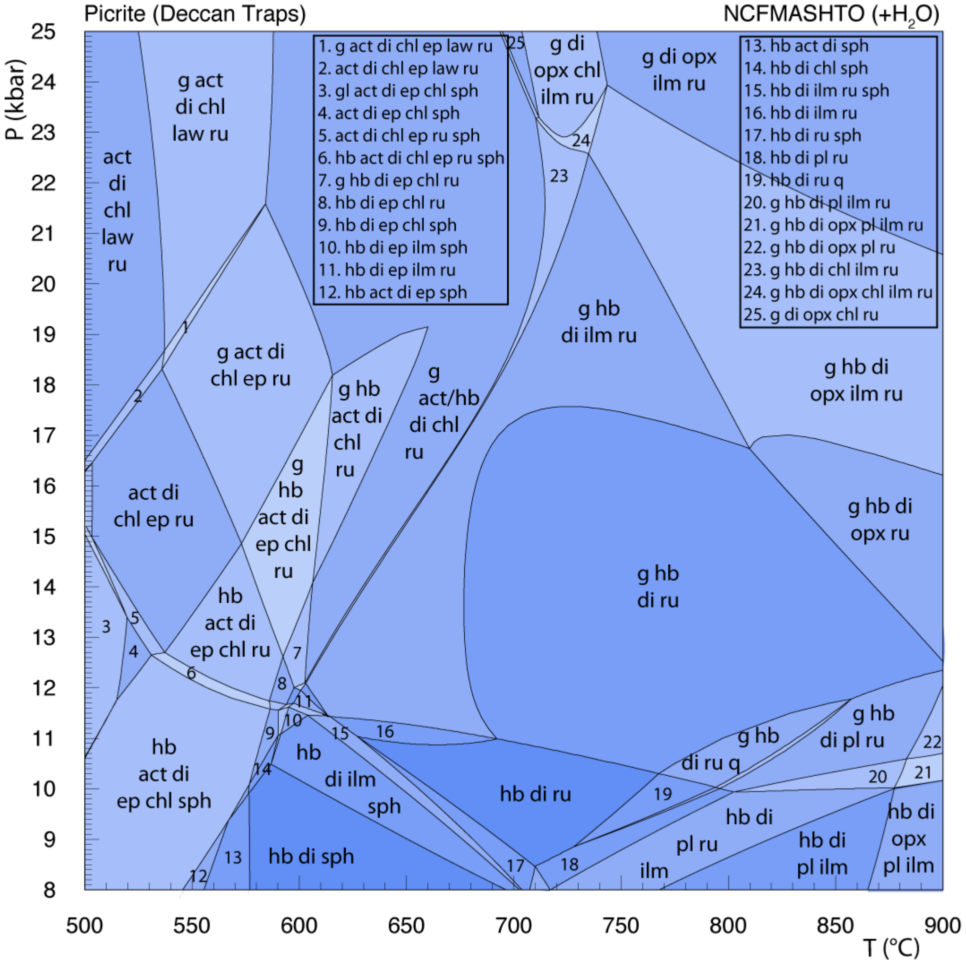

Figure 4.2.4: *P–T* pseudosection for a picrite from the Deccan Traps, calculated in NCFMASHTO with H_2O in excess for the composition taken from Tab. 4.1.1. The description is given in the text and mineral abbreviations are given in Tab. 3.1.1.

4.2.5 Komatiite from Gorgona

The *P–T* pseudosection illustrated in Figs 4.2.5, 4.2.6b and 4.2.7d is calculated for a komatiitic bulk rock composition from Gorgona island (Columbia), sample GOR-94-1, from which high-pressure experiments were already conducted (Foley *et al.*, 2003; subchapter 2.3.4). The amount of Fe_2O_3 was assumed to be low (“O” = 0.2).

The pseudosection is effectively divided into two parts by chlorite-out, and the assemblages at *T* > 750 °C are pyroxenitic (either amphibole or garnet-olivine-amphibole pyroxenite). The dominant pyroxenitic assemblage g–hb–di–opx–ol–ilm–H_2O is quadrivariant and hornblende breaks down completely at high *P–T* (*P* > 23 kbar at 850 °C). Rutile is not stable in the pyroxenites but becomes stable at *T* < 690 °C and *P* > 11 kbar.

The low-temperature assemblages are characterised by relatively simple fields of chlorite-bearing assemblages, and a solvus-top of actinolite and hornblende is located at around 16.5 kbar and 625 °C which constitutes the elongation of the two-amphibole assemblages below. The border between the calculated actinolite and hornblende composition variables proceeds from the solvus top up to about 750 °C at 25 kbar. Typical blueschist assemblages with lawsonite or glaucophane are not stable in the komatiitic bulk rock composition.

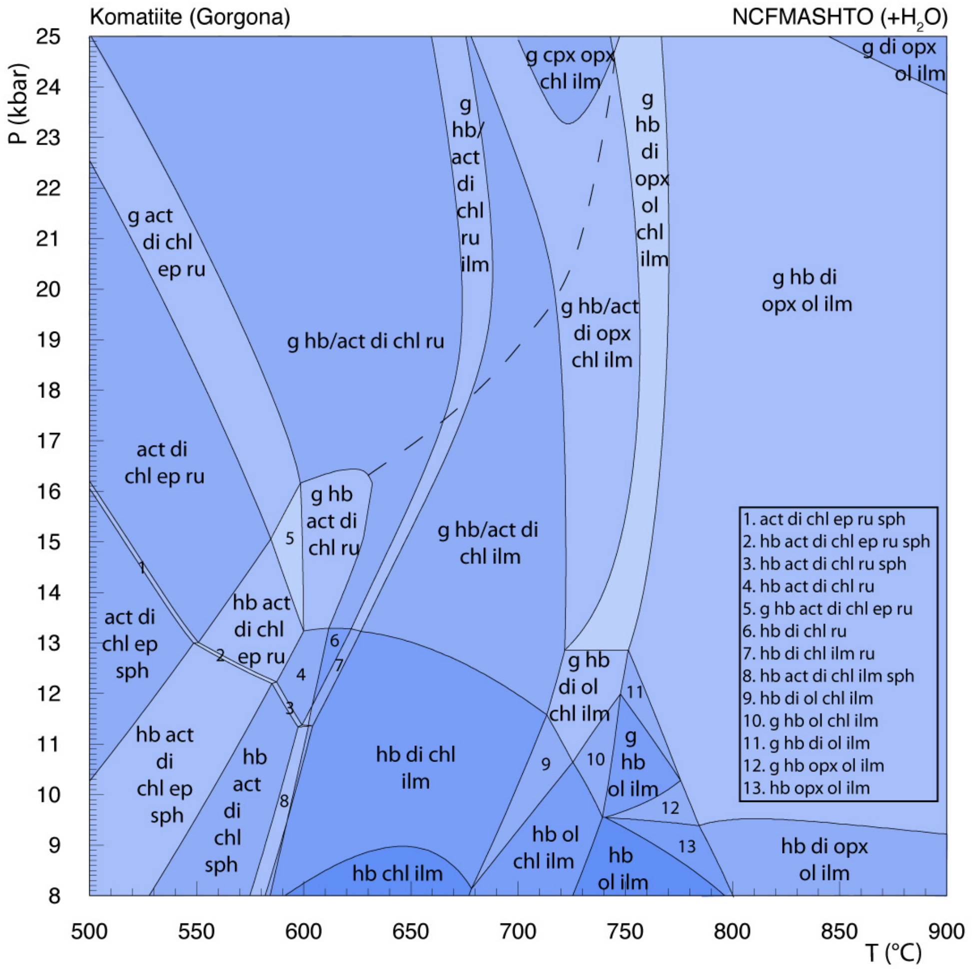

Figure 4.2.5: *P–T* pseudosection for a komatiite from Gorgona Island, calculated in NCFMASHTO with H_2O in excess for the composition taken from Tab. 4.1.1. The description is given in the text and mineral abbreviations are given in Tab. 3.1.1.

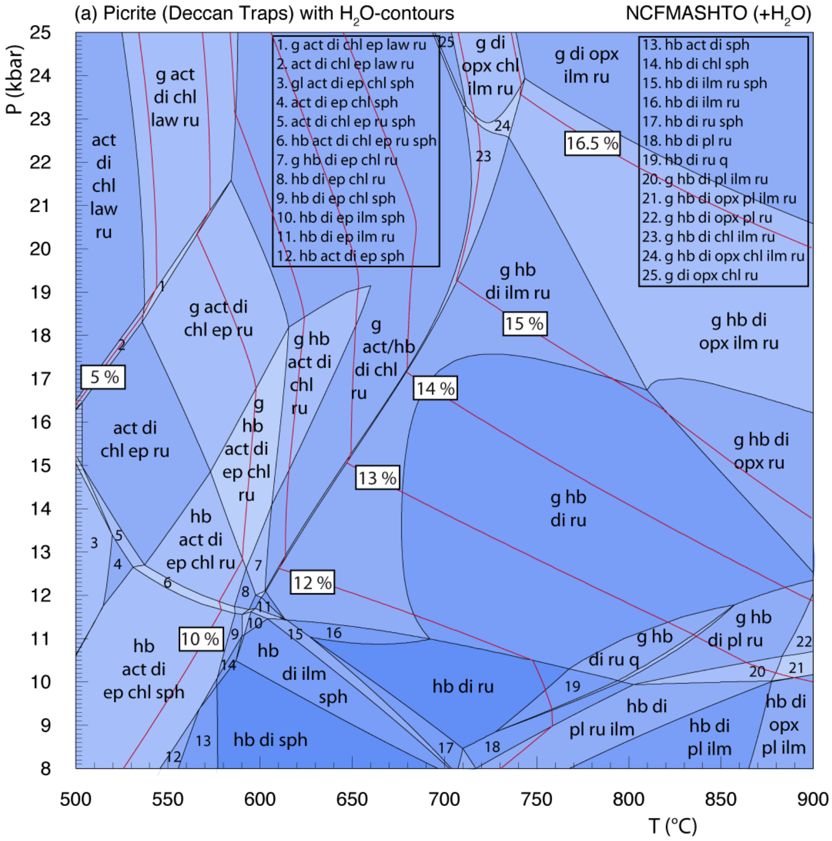

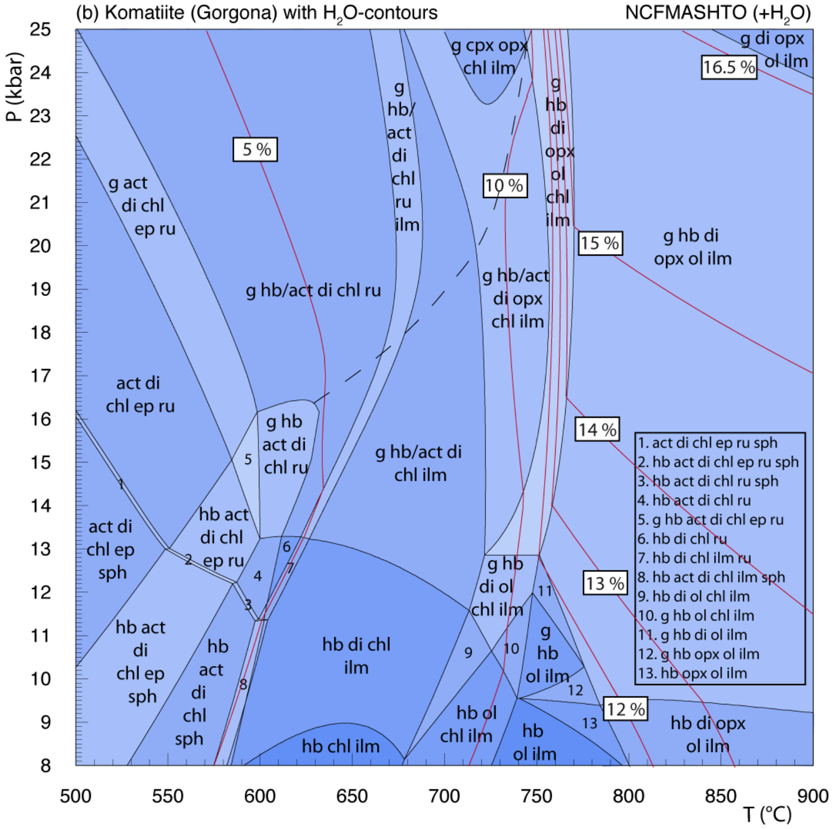

Figure 4.2.6a, b: *P*–*T* pseudosections for the picrite from the Deccan Traps (a, cf. Fig. 4.2.4) and for the komatiite from Gorgona Island (b, cf. Fig. 4.2.5), calculated with H_2O in excess, illustrate the differences between the two bulk rock compositions. The contours show the increasing amount of H_2O during the breakdown of the water-bearing phases, especially hornblende at high temperatures up to the breakdown of this phase. Further descriptions are given in the text and mineral abbreviations are given in Tab. 3.1.1.

The release of H_2O at low temperature is constantly small as a function of temperature and is largely independent of pressure (Fig. 4.2.6b). However, the final breakdown of chlorite generates a high amount of a free fluid phase over a short temperature interval at the final stages after orthopyroxene and olivine become stable. The H_2O mode contours in the pyroxenite fields are subparallel to the hornblende-out boundary.

4.2.6 Discussion of the changes during the transition from MORB to komatiite

The *P–T* pseudosections for the bulk rock compositions given in Tab. 4.2.1 illustrate the trend of metamorphosed products from a MORB through two picrites to a komatiite. They show a change from amphibolites to pyroxenites delineated by the changing stability of the main indicator mineral plagioclase. With increasing MgO, the field of garnet-amphibolite decreases due to the restriction of the plagioclase stability to lower pressures (Keweenawan and Deccan Traps picrites), and finally to the complete disappearence of plagioclase in the pseudosection for the komatiite from Gorgona.

The classification of rock types in the *P–T* pseudosections follows that of Foley *et al.* (2003; Fig. 2.3.2) and relates MORB and the picrite from Keweenawan to the basaltic stability diagram, whereas the Deccan Traps picrite and, of course, the komatiite are related to the stability diagram for the Gorgona komatiite (Figs 2.3.2, 4.2.7).

The effect of increasing MgO is seen for the first time in the pseudosection calculated for the picrite from Keweenawan. Characteristic garnet-amphibolite assemblages as defined for MORB are still stable but within a smaller *P–T* window due to the restricted plagioclase stability at higher temperatures. Garnet-amphibolite and amphibolite assemblages are restricted by the emergence of orthopyroxene at high *T*, whereas orthopyroxene is stable at higher pressures in the pseudosection for the picrite from Keweenawan.

Three quadrivariant assemblages are stable in the pseudosections for MORB and the Keweenawan picrite. These are the conspicuous g–hb–di–pl–ru–q–H_2O garnet-amphibolite assemblage as well as the amphibole-eclogite assemblages g–hb–di–ep–ru–q–H_2O and g–hb–di–ru–ky–q–H_2O above plagioclase-out. The *P–T* range of amphibole-eclogite in the picritic Keweenawan composition is larger than for MORB and the quinivariant amphibole-eclogite assemblage g–hb–di–ru–q–H_2O is only developed for Keweenawan where it covers a large proportion of the pseudosection until the disappearance of hornblende gives rise to the eclogite assemblages. Amphibole-free eclogite (MORB, Keweenawan picrite) and amphibole-free pyroxenite (Deccan Traps picrite, Gorgona komatiite) assemblages are generally located in the upper right corner of all pseudosections, shrinking with increasing MgO until only a small amphibole-free assemblage is located in the pseudosection for the komatiitic composition.

Whereas a solvus between glaucophane and hornblende occurs in the pseudosection for MORB, in the pseudosection for Keweenawan an actinolite-hornblende solvus is developed. The solvus between actinolite and hornblende also occurs in the pseudosections for the Deccan Traps picrite and the Gorgona komatiite. The pseudosections for the Deccan Traps picrite and the Gorgona komatiite are similar to each other and generally differ from the pseudosections for MORB and the Keweenawan picrite. Around the amphibole-solvus in the pseudosections for the komatiite and Deccan Traps picrite nine identical assemblages appear in both. Furthermore, almost no quartz is developed in the two pseudosections. Due to the absence of glaucophane in both, and of lawsonite in the komatiite, typical blueschist assemblages are not developed in these compositions. This is a potential link to the fact that blueschists are not recorded before the Neoproterozoic (> approx. 1000 Ma) (Maruyama *et al.*, 1996; Brown, 2007). Hence, independent of the *P–T* path or the tectonic setting, there is no opportunity to develop blueschists from those MgO-rich compositions, which may have been dominant on the early Earth. The effective blueschist facies assemblages of the modern MORB and the picrite from Keweenawan differ slightly from each other, especially by the decreased stability of quartz and the increased stability of chlorite in the Keweenawan picrite above 15 kbar.

Although the pseudosections for the Gorgona komatiite and the Deccan Traps picrite show the similarities mentioned above, obvious differences between them are the enlarged orthopyroxene-stability from 700 °C upwards, the stability of olivine as well as the increasing chlorite-stability to higher temperatures in the komatiite. The area of clino- and orthopyroxene bearing pyroxenite in the Gorgona komatiite is enlarged to T > 750 °C, whilst the stability of pyroxenite assemblages in the Deccan Traps pseudosection is restricted due to the emergence of plagioclase at low pressure and the disappearance of orthopyroxene at low temperature. Pyroxenites, as developed in the komatiite and in the picrite from the Deccan Traps, do not resemble possible sources for

TTG-like melts (Foley *et al.*, 1999) and they are not discussed further. Nevertheless, these two compositions would be interesting for Hadean to early Archean processes.

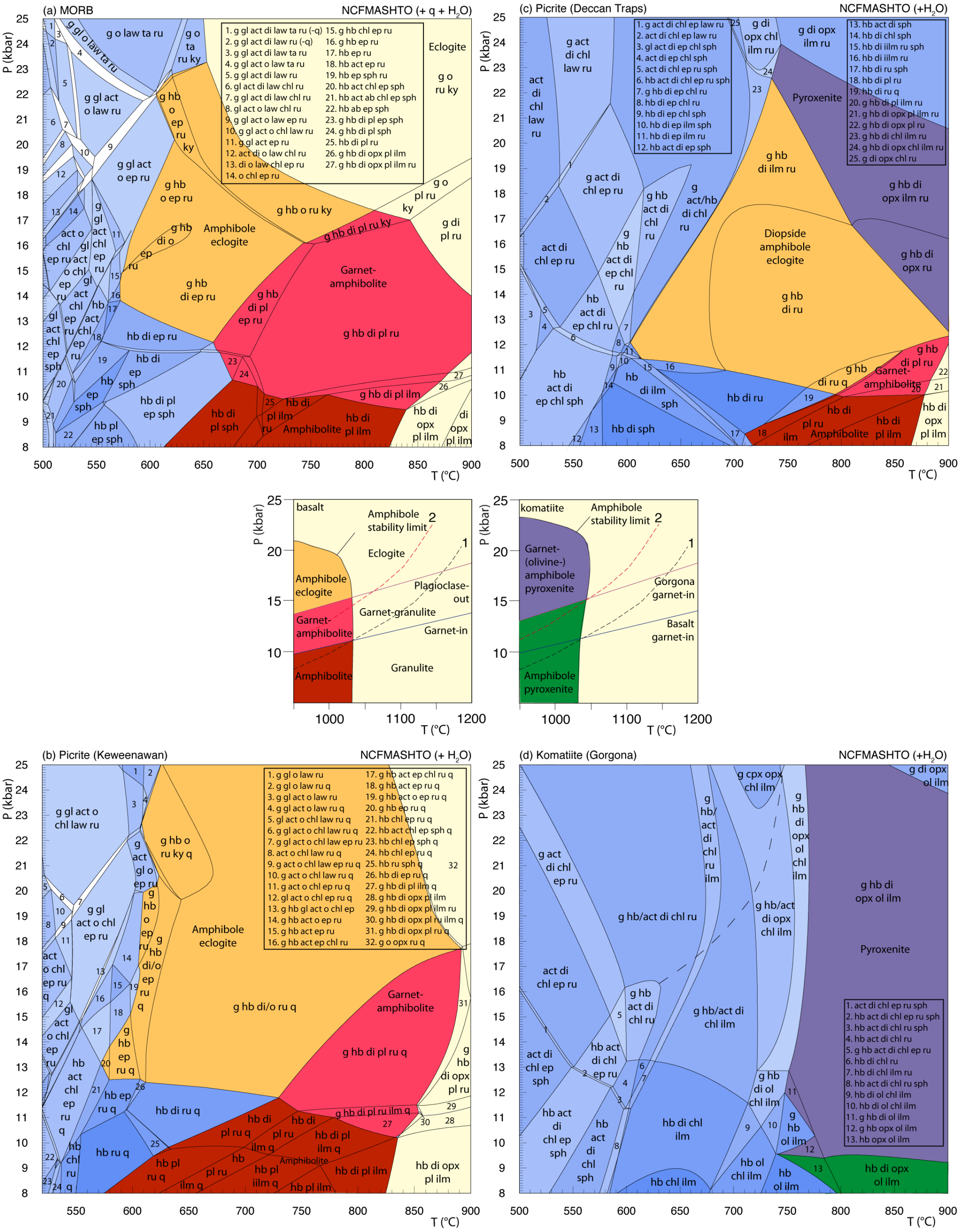

Figure 4.2.7a-d: The overview over the *P–T* pseudosections in subchapter 4.2 shows the transition of the metamorphic products from MORB (a) to komatiite (d) in the context of the previous work from Foley *et al.* (2003). The rock-types and assemblages in the picrite from Keweenawan (b) are similar to the classical MORB, while the range of (garnet-) amphibolite is restricted to a small area in the picritic Deccan Traps (c) composition due to the emergence of plagioclase-free pyroxenite, which also is developed in the Gorgona compostion. Diopside-amphibole-eclogite in the Deccan Traps pseudosection (c) contains diopside instead of omphacite in the eclogite facies area and it is supposed to be on the transition to pyroxenite.

Garnet-amphibolite or amphibole-eclogite are the proposed rocks for the generation of TTG-like melts. Garnet-amphibolite assemblages occur in the pseudosections for MORB, for the Keweenawan picrite and in the pseudosection for the Deccan Traps picrite, where these assemblages are reduced to a small, ellipsoidal *P–T* area around 11 kbar at 850 °C. It is unlikely that a potential melting would be constrained to this small area, especially at these *P–T* conditions.

Typical amphibole-eclogite assemblages, as defined for MORB and the picrite from Keweenawan do not occur in the pseudosection for the Deccan Traps picrite because the clinopyroxene is diopside instead of omphacite. This indicates a transition in the eclogite facies realm from typical (amphibole-) eclogite through diopside-amphibole-eclogite to pyroxenite with a transition to pyroxenites around 13 wt% MgO at high *P–T*. On the basis of thermodynamic modelling this value is proposed to mark the compositional threshold for the beginning of TTG-formation from garnet-amphibolite or some type of eclogite. Since rutile is stable in all assemblages considered to be potentially involved in melting, high Nb/Ta ratios (Foley *et al.*, 2002; Moyen & Stevens, 2006) in the potential melts would be achieved which does not resemble TTG-like melts with their low Nb/Ta ratio. However, the thermodynamic modelling predicts marginal amounts of rutile (< 0.05 %) and TiO_2, which is incorporated in the experimental grown amphiboles (Tab. 5.3.3), is not considered in the *a–x* model for amphibole. The differences between mineral equilibria modelling and experimental results are discussed in Chapter 6.

The rocks illustrated in these pseudosections were calculated for subsolidus *P–T* conditions to show the developing assemblages and the actual melting will start at higher temperatures (e.g. 975 °C for MORB, calculated with a melt model for metapelitic rocks; Fig. 6.3.3a). For MORB-like rocks the onset of melting is not a critical constraint because in modern settings slab melting is not common in contrast to the release of H_2O from the blueschist facies rocks which induces partial melting in the overlying mantle wedge.

4.2.7 Comparison of high-pressure experiments and calculated results from the Gorgona komatiite

The results from the high-pressure experiments conducted for the komatiitic Gorgona composition (Foley *et al.*, 2003) are compared to the results from the thermodynamic calculations (Fig. 4.2.8). Since the experiments were conducted under water-undersaturated conditions (0.2–0.3 wt% H_2O), the H_2O-content for the *P–T* pseudosection was fixed to 0.25 wt% (0.82 mol%) to allow a comparison between the two approaches. A reduced H_2O-content causes water-free assemblages together with a H_2O-in boundary at $T > 750$ °C and the topologies of the pseudosection at low temperatures are somewhat simpler where H_2O does not form a discrete fluid phase. Thereafter, the H_2O-bearing assemblages are identical to the assemblages with H_2O in excess illustrated in Fig. 4.2.5. The insertion in Fig. 4.2.8 illustrates the same pseudosection calculated with low bulk H_2O in the same *P–T* range as used for the Gorgona komatiite pseudosection with H_2O in excess (Fig. 4.2.5).

The experimental and calculated results for the komatiite from Gorgona are consistent regarding the main phases garnet, hornblende, clino- and orthopyroxene. Most of the *P–T* conditions where the experiments were conducted are located within the large quinivariant assemblage g–hb–di–opx–ol–ilm, and most experimental assemblages in this field (14–18 kbar at 950 °C and 1000 °C) are made up of at least g–hb–cpx–opx with additionally spinel at 950 °C. Ilmenite does not occur in the experiments and olivine is stable only at 1150 °C and at 1000 °C at high pressure. One of the possible reasons for ilmenite in the pseudosection but not in the experiments is that Ti is not yet incorporated into the amphibole model, whereas amphibole and other minerals in the experiments do have Ti. Further discussion about the differences and similarities of the experiments and calculations of the models for Archean oceanic crust in this study are given in subchapter 6.2. Garnet-absent assemblages are located in the experiments at 10 and 12 kbar, showing that the incoming of garnet occurs at higher pressures than in the calculated pseudosection. Amphibole-free and melt-bearing assemblages occur at 1150 °C where garnet first becomes stable at 18 kbar.

The experimental results at 1150 °C differ from the calculated assemblages obviously by the stability of melt, which cannot be calculated in the metabasic system NCFMASHTO. This causes incorrect calculations of the remaining phases where no liquid is considered. Adopting the haplogranite melt-model of White *et al.* (2007) in the system FMASH ($FeO–MgO–Al_2O_3–SiO_2–H_2O$) suggests that the melting in the Gorgona komatiite would begin at 10 kbar at 1050 °C which indicates a good agreement with the experimental solidus determinations (not illustrated). Calculations of the solidus were done for the bulk rock compositions used for the high-pressure partial melting experiments in the scope of this work (Fig. 6.3.1).

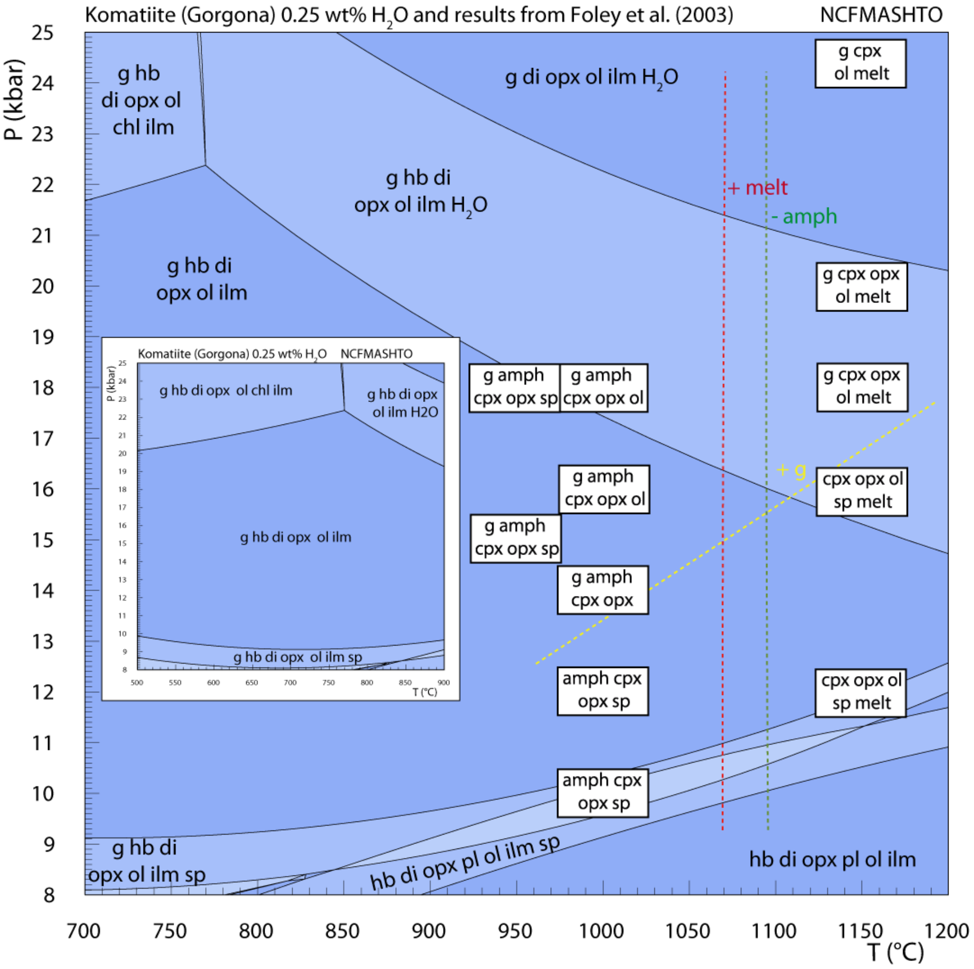

Figure 4.2.8: *P–T* pseudosection for the komatiite from Gorgona Island, calculated with 0.25 wt% H_2O and extended to the *P–T* conditions of the high-pressure experiments from Foley *et al.* (2003). The results of the high-pressure experiments are given at the appropriate *P–T* condition. The insertion is the extension to lower *T*, calculated for the same *P–T* range used for the pseudosection with H_2O in excess in Fig. 4.2.5, and illustrates the differences, less assemblages in the H_2O-free realm, depending on the amount of H_2O in the system. Further description is given in the text and mineral abbreviations are given in Tab. 3.1.1.

4.3 *P–T* pseudosections for models of Archean oceanic crust

4.3.1 Ascertaining the bulk rock compositions for high-pressure experiments

The mineral equilibria calculations for natural rock compositions in subchapter 4.2 indicate a transition from amphibolite and different types of eclogite to pyroxenite dominated metamorphic products between MORB and the komatiite from Gorgona. The transition between the metamorphic products occurs around 13 wt% MgO. Since there is no melt model for metabasic rocks, the calculations are imprecise at the conditions where melting generally takes place. A comparison between the thermodynamic calculations and earlier experimental results on the komatiite (Foley *et. al*, 2003) shows good agreement between the two approaches until melt was developed in the experiments (subchapter 4.2.7). To cover the range of the *P–T* conditions for partial melting, high-pressure partial melting experiments (chapter 5) extend the reliable *P–T* range of mineral equilibrium modelling.

To ensure a good comparability of the designated **M**odels of **A**rchean **O**ceanic **C**rust (MAOC), the amount of the essential oxide in this study, MgO, was varied, i.e. keeping the other oxides constant relative to each other. This was achieved by using an initial composition of an appropriate experimental partial melt composition of a MORB pyrolite (Falloon & Green, 1988), changing it by subtracting and adding an olivine composition to cover the range of MgO-contents from MORB to komatiite. This also led to small changes in SiO_2 and FeO. Pyrolite is a model composition for fertile mantle rocks of which basaltic melts can be extracted (Green & Ringwood, 1967b). Subchapter 5.2 introduces the calculation and synthesis of these models.

Since there are many studies concerning modern MORB in subduction zone metamorphism (e.g. Green & Ringwood, 1967a; Schmidt & Poli, 1998; Macdonald *et al.*, 2000), the initial MgO-content of 11 wt% MgO (MAOC 11, Tab. 4.3.1) used for the experiments in this study was higher than in a typical MORB, but resembles the MgO-content for the Keweenawan picrite pseudosection which is topologically similar to MORB (Fig. 4.2.3). Since the calculations in subchapter 4.2 indicate a transition between the two picrites with 11 and 13 wt% MgO, a model with 13 wt% MgO (MAOC 13, Tab. 4.3.1) was also used for an experimental composition to compare if there is also a transition between these two MgO contents. To cover a sensitive range between MORB and the already described komatiite (Foley *et al.*, 2003), 15 wt% MgO was used for the third model composition (MAOC 15, Tab. 4.3.1). This value is close to the beginning of a relatively constant development of assemblages to lower MgO in a coupled $T–X_{H2O}/T–X_{MgO}$ pseudosection at 15 kbar (Fig. 4.3.1). The left hand part of this figure illustrates the changes from MORB with H_2O in excess to MORB with 0.5 wt% H_2O (similar to the intended MAOC water-contents, left dotted line) over MAOC 11 to MAOC 17 at the right hand side. MAOC 17 (17 wt% MgO, Tab. 4.3.1) exhibits a similar MgO-content to that of the Gorgona komatiite and completes the series of MAOC, but no experiments were conducted on this composition. In the right hand part of Fig. 4.3.1 many assemblages are stable over a wide range of bulk rock compositions. The stability of the main assemblages shifts towards lower temperatures and the high-temperature assemblages become unstable with decreasing MgO. $T–X_{MgO}$ pseudosections at 10, 12.5, 16, 17, 19 and 20 kbar are presented in Appendix A2.

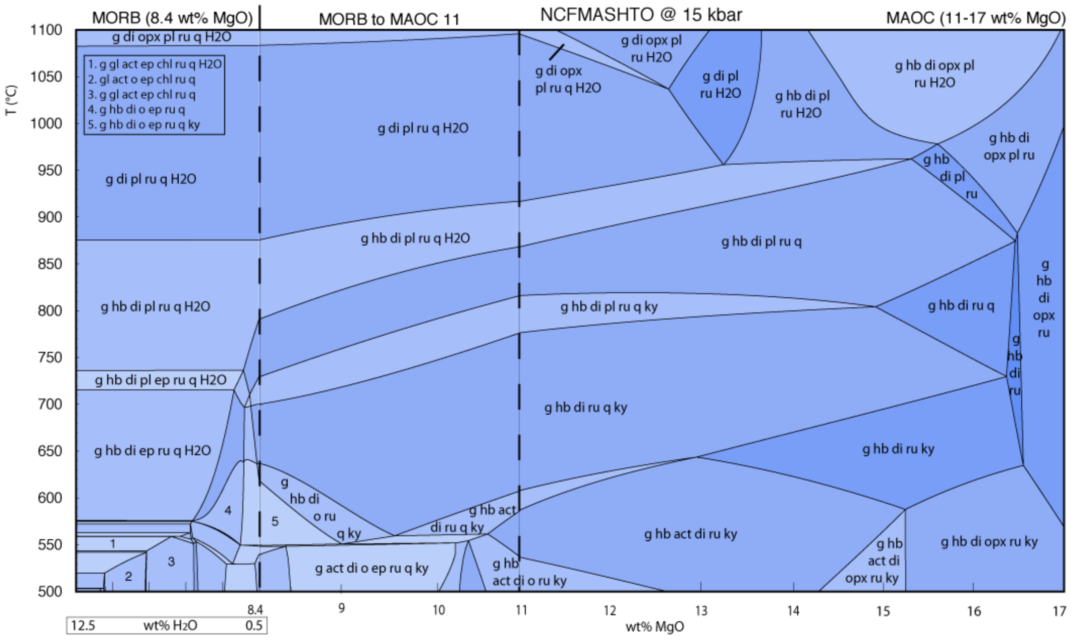

Figure 4.3.1: Coupled $T–X_{H2O}/T–X_{MgO}$ pseudosection illustrating the development of the assemblages from the H_2O-saturated MORB via the MORB with low H_2O to MAOC 11 and to the composition of MAOC 17 at 15 kbar. The decreasing water-content in MORB causes a rising of the water-free assemblages towards higher T, followed by a further decreasement of the stability of water-bearing assemblages with increasing MgO. The plagioclase-stability curve around 800 °C shows no significant changes between MAOC 11 and 15.

The *P–T* pseudosections for the models of Archean oceanic crust were calculated with THERMOCALC 3.33 in the same *P–T* range as used for the natural bulk rock compositions (subchapter 4.3.2–4.3.5). The rock-classification is based on the same parameters used for the natural compositions and the pseudosections are summarised in this context in Fig. 4.3.6. Again, due to the overall appearance of diopside instead of omphacite the *P–T* range covering the eclogite facies comprises a diopside-amphibole-eclogite.

Since a small amount of H_2O (approx. 0.5 wt%) was added to the experimental bulk rock compositions to perform fluid-absent melting, the *P–T* pseudosections for MAOC 11–17 were consequently calculated with low H_2O in the bulk composition. Due to this fact, the MAOC pseudosections are not directly comparable with the pseudosections for the natural existing bulk rock compositions in subchapter 4.2 until H_2O forms a discrete phase in the MAOC pseudosections at high *P–T*. H_2O-contours are exemplarily illustrated for MAOC 15 (Fig. 4.3.4b). Direct comparisons between pseudosections calculated with H_2O in excess and with low H_2O in the bulk composition (Fig. 6.4.2) are discussed later in the context of a comparison with the high-pressure partial melting experiments (subchapter 6.2).

Table 4.3.1: Bulk rock compositions of MAOC 11, 13 and 15 used for the calculation of *P–T* pseudosections in this subchapter. The compositions are given in wt% and mol%, the latter required for the calculation with the software THERMOCALC. “O” is the amount of ferric iron from total FeO (Eq. 4.1.1).

Rock composition	**Unit**	**H_2O**	**SiO_2**	**Al_2O_3**	**CaO**	**MgO**	**FeO**	**Na_2O**	**TiO_2**	**O**
MAOC 11	wt %	0.50	48.50	16.65	12.78	11.00	8.13	1.71	0.72	
	mol %	1.68	48.96	9.90	13.82	16.56	6.85	1.67	0.55	0.30
MAOC 13	wt %	0.47	48.14	15.81	12.14	13.00	8.12	1.63	0.69	
	mol %	1.56	48.00	9.29	12.97	19.33	6.76	1.58	0.52	0.30
MAOC 15	wt %	0.45	47.78	14.97	11.50	15.00	8.11	1.54	0.65	
	mol %	1.38	46.14	8.10	11.31	24.66	6.59	1.37	0.45	0.30
MAOC 17	wt %	0.42	47.41	14.13	10.85	17.00	8.11	1.45	0.62	
	mol %	1.38	46.14	8.10	11.31	24.66	6.59	1.37	0.45	0.30

The results of these models cover a range of MgO contents and give an overview of the behaviour of MgO-richer rock compositions during metamorphism, their potential contribution to continental TTG-like crust formation in the Archean, and to possible *P–T* conditions and geologic settings required for the formation of such rocks from MgO-rich oceanic crust.

4.3.2 MAOC 11

The *P–T* pseudosection for MAOC 11 was calculated for a fixed H_2O content giving rise for predominantly water-undersaturated assemblages in the pseudosections (Figs 4.3.2 and 4.3.6a). H_2O-bearing fields occur at $T > 600$ °C, reflecting the breakdown of amphibole. Both amphibole and H_2O occur together in an area up to 50 °C wide including the assemblages g–hb–di–ru–ky–H_2O ± q. Together with g–hb–di–ru–ky–q, these assemblages are designated as diopside-amphibole-eclogite assemblages or diopside-eclogite at higher *P–T* conditions. Plagioclase is stable up to 9.4 kbar at 500 °C and 18.2 kbar at 900 °C and its stability gives way to several garnet-amphibolite assemblages (g–hb–di–pl–ru–q ± ky ± H_2O). The occurrence of the garnet-amphibolite assemblages is constrained by the appearance of orthopyroxene at lower pressure in the granulite facies.

The appearance of actinolite at low temperature marks the transition to generally smaller fields and different assemblages than those occuring at high *T*, especially two-amphibole assemblages including hornblende and actinolite up to 19 kbar. Lawsonite is not developed in the water-undersaturated part of the MAOC 11 composition. However, MAOC 11 calculated with H_2O in excess (Fig. 6.4.2b), contains lawsonite- and chlorite-bearing blueschist assemblages at low temperature.

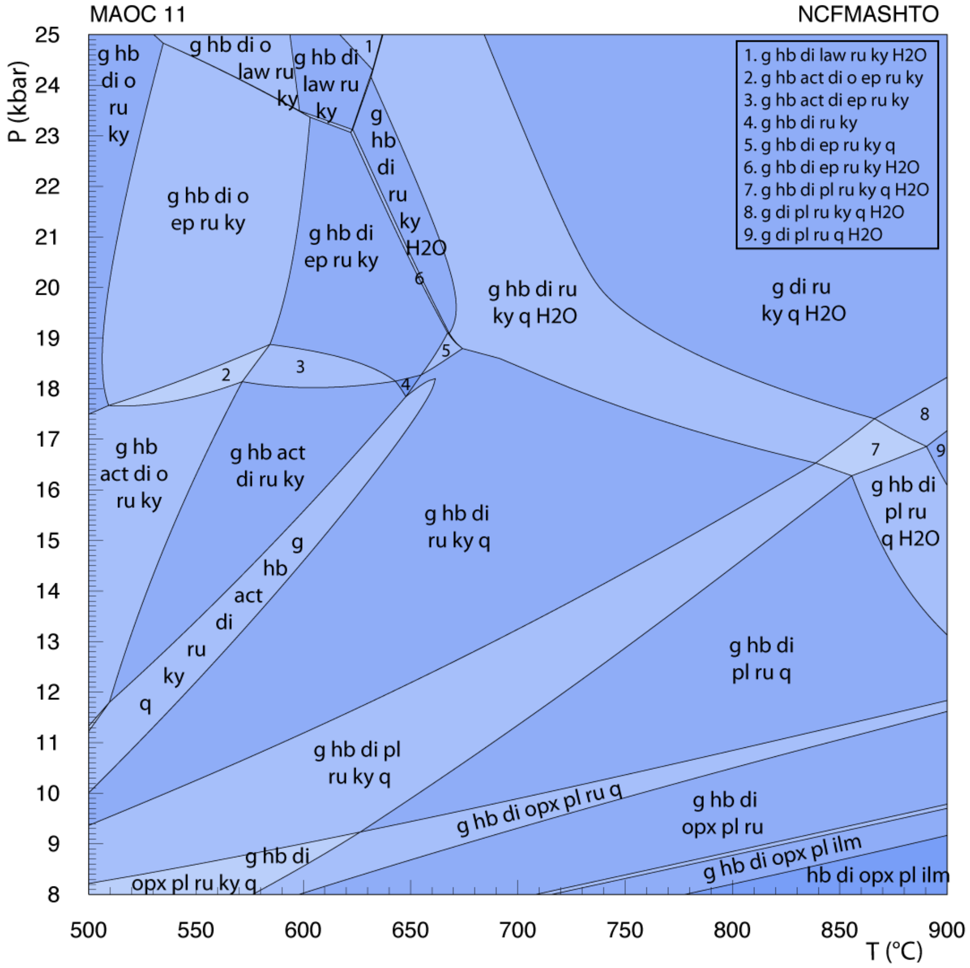

Figure 4.3.2: *P–T* pseudosection for MAOC 11, calculated in NCFMASHTO for the composition taken from Tab. 4.3.1. The description is given in the text and mineral abbreviations are given in Tab. 3.1.1.

4.3.3 MAOC 13

Since MAOC 13 (Figs 4.3.3 and 4.3.6b) differs predominantly by the amount of MgO from MAOC 11, the pseudosections have similar assemblages and a similar topology, especially at low pressure and high *P–T*. The garnet-amphibolite and diopside-amphibole-eclogite assemblages differ in their stability-ranges and occur here at slightly higher *P–T* due to the increasing stability of orthopyroxene at higher pressures (up to 13 kbar at 500 °C). This restricts the size of garnet-amphibolite assemblage fields at low *P–T*. However, at higher grades, the breakdown of hornblende at higher *T* accounts for a higher *P–T* stability of diopside-amphibole-eclogite and of garnet-amphibolite to a lesser extent. The stability field of plagioclase is similar to that of MAOC 11. The extension of the two-amphibole assemblages up to 22.5 kbar and to slightly higher temperature is a significant difference to MAOC 11.

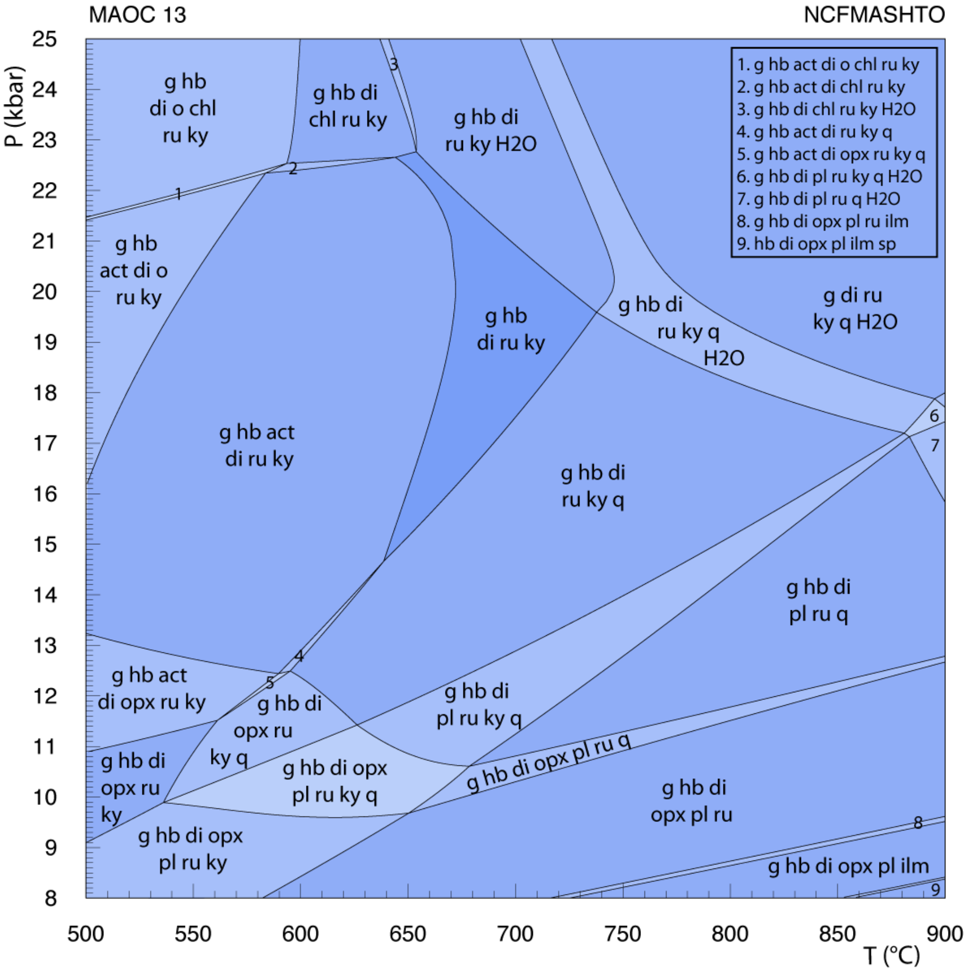

Figure 4.3.3: *P–T* pseudosection for MAOC 13, calculated in NCFMASHTO for the composition taken from Tab. 4.3.1. The description is given in the text and mineral abbreviations are given in Tab. 3.1.1.

4.3.4 MAOC 15

The trend from MAOC 11 to MAOC 13 described earlier continues in the pseudosection for MAOC 15 (Figs 4.3.4 and 4.3.6c). Most of the assemblages are similar to MAOC 13, and the increasing stability of orthopyroxene at low *P–T* leads to a further shrinking of the garnet-amphibolite assemblages (g–hb–di–pl–ru–q ± ky). The instability of plagioclase below 8 kbar at 510 °C and 16 kbar at 900 °C additionally causes a reduction of those assemblages, whereas the further increase of hornblende stability has no effect on the extent of the garnet-amphibolite assemblages.

Figure 4.3.4b illustrates additionally H_2O mode contours for MAOC 15 with 1.38 wt% H_2O. Once H_2O forms a discrete phase at high *P–T* the amount of H_2O increases up to the bulk rock value (1.38 mol%) and only anhydrous minerals are present. A further increase of the amount of H_2O is not possible after the achievement of this maximum value.

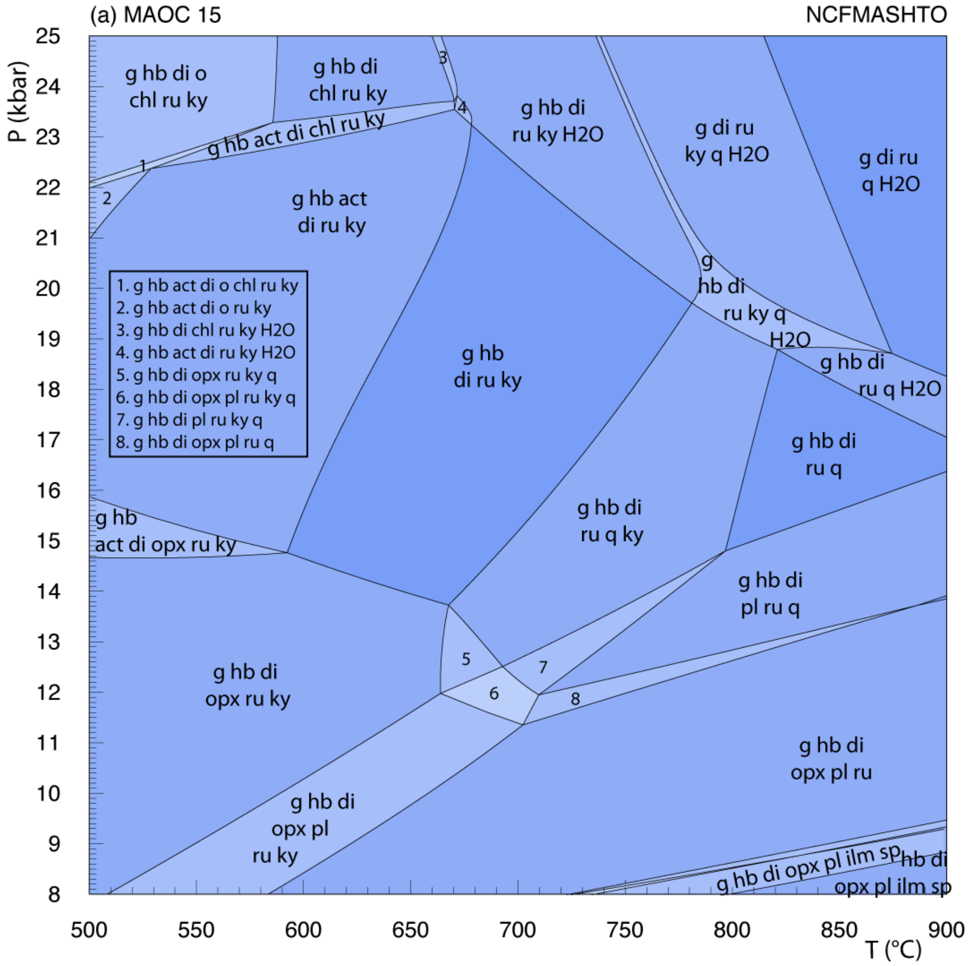

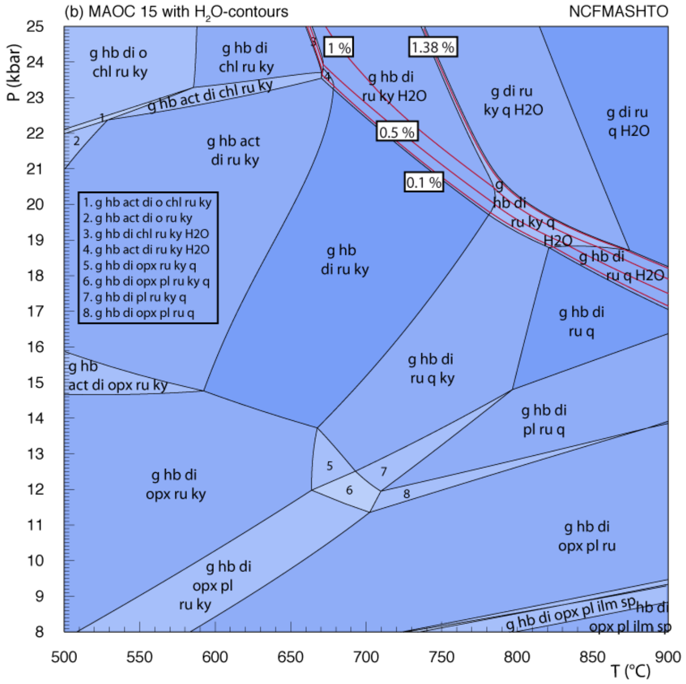

Figure 4.3.4a, b: *P*–*T* pseudosection for MAOC 15, calculated in NCFMASHTO for the composition with 1.38 mol% H_2O taken from Tab. 4.3.1. (b) shows the H_2O mode contours after the appearance of a free H_2O-phase. Further description is given in the text and mineral abbreviations are given in Tab. 3.1.1.

4.3.5 MAOC 17

A pseudosection for MAOC 17 with a similar MgO-content to the komatiite from Gorgona (Fig. 4.2.5) is illustrated in Figs 4.3.5 and 4.3.6d, but no experiments were conducted on this rock composition for comparison. The plagioclase-stability field is further reduced to below 8 kbar at 540 °C and 14 kbar at 900 °C, where the assemblages equal those of the MAOC 15 granulite ones. Due to the strong increase in orthopyroxene-stability up to 22 kbar, the most striking hexivariant assemblage g–hb–di–opx–ru resembles a garnet-amphibole pyroxenite. Hornblende is stable at all *P*–*T* conditions.

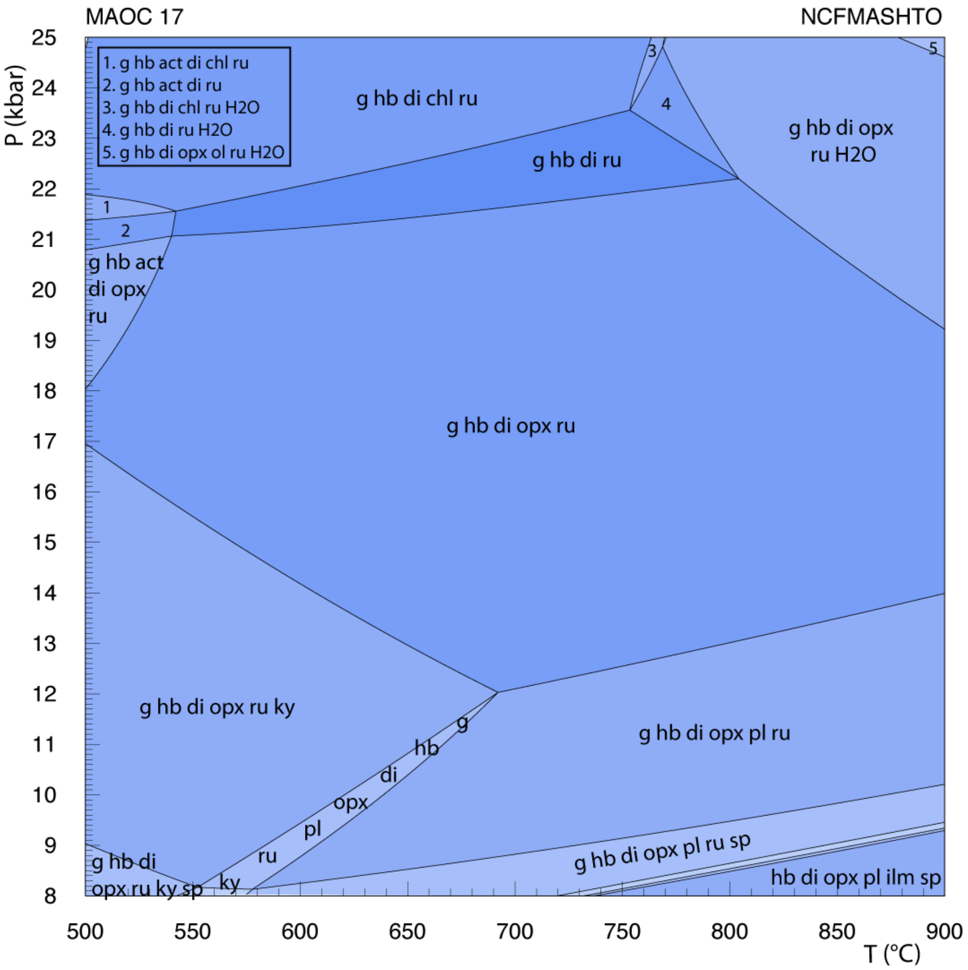

Figure 4.3.5: *P*–*T* pseudosection for MAOC 17, calculated in NCFMASHTO for the composition taken from Tab. 4.3.1. The description is given in the text and mineral abbreviations are given in Tab. 3.1.1.

4.3.6 Discussion

4.3.6.1 The changes from MAOC 11 to MAOC 17

The *P*–*T* pseudosections for MAOC 11 to MAOC 15 generally have a similar topology with an obvious shrinking of garnet-amphibolite and diopside-amphibole-eclogite at higher grades. Pyroxenite assemblages without plagioclase are first achieved in MAOC 17.

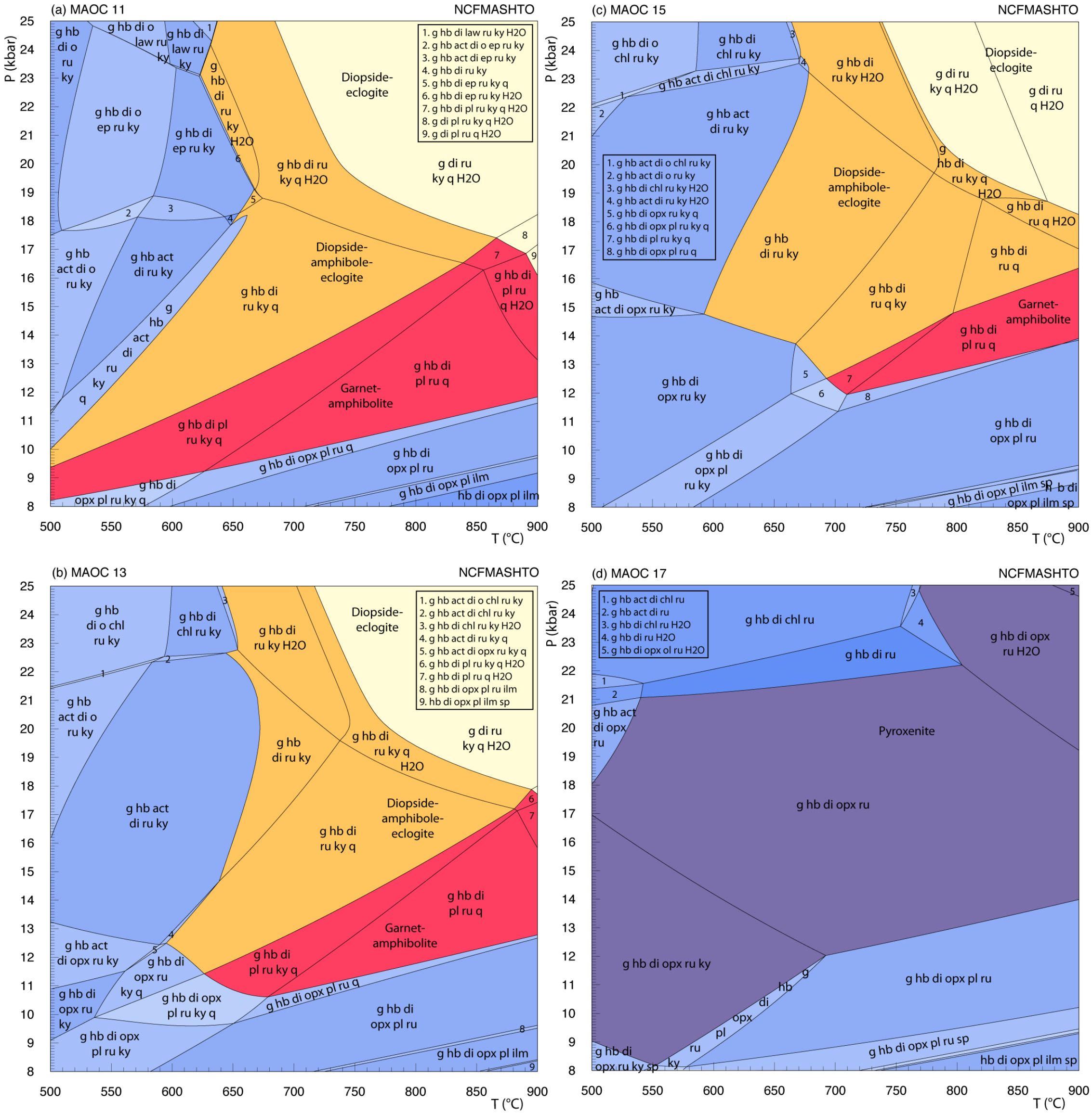

Figure 4.3.6a-d: Comparison of *P*–*T* pseudosections for MAOC 11–17, calculated with low H_2O and with the colour scheme introduced for the natural compositions. The field of plagioclase-bearing garnet-amphibolite reduces with increasing MgO, lowering the possibility of TTG-extraction by melting of this. Hornblende-clinopyroxenite occurs above the plagioclase-out, being no real eclogite due to the stability of diopside instead of omphacite. In MAOC 17 (d), a huge area is covered by clino-and orthopyroxene bearing pyroxenite.

All garnet-amphibolite and diopside-amphibole-eclogite assemblages contain rutile. Typical eclogite is not developed in the eclogite facies realm, the assemblages contain diopside instead of omphacite (hornblende-clinopyroxenite). Since the generation of TTG is inferred by several studies (subchapter 2.3.2) to occur from garnet-amphibolite or eclogite, the shift of garnet-amphibolite assemblages to higher pressure with increasing MgO limits the possibility of TTG-formation at lower pressures from such rocks. Furthermore, the shrinking of the *P–T* extent of these assemblages makes it difficult for such assemblages to reach solidus conditions (> 1000 °C, cf. Fig. 6.3.1) and undergo partial melting. However, the models of garnet-amphibolite or eclogite in the source of melting for the generation of TTG-like melts are based on limited experimental data for basaltic compositions and do not preclude other possible source rocks (e.g. metamorphosed picrites) and the calculated MAOC compositions have features of both inferred TTG sources. Plagioclase-free pyroxenite, as defined in subchapter 4.2.1 is not developed in the *P–T* pseudosections for MAOC 11, 13 and 15 due to the stability of plagioclase in the orthopyroxene-bearing assemblages. The unusually high *P–T* stability of plagioclase in the pseudosections is discussed in the comparison between the mineral equilibria calculations and the high-pressure partial melting experiments (subchapter 6.2).

4.3.6.2 MAOC compositions compared to natural existing rock compositions

The comparison of H_2O-bearing assemblages in pseudosections with similar MgO-contents (MAOC 11, Fig. 4.3.2 versus Keweenawan picrite, Fig. 4.2.2 and MAOC 13, Fig. 4.3.2 versus Deccan Traps picrite, Fig. 4.2.4) shows differences in the assemblages and the developed rock types, which probably reflect the influence of different amounts of the remaining oxides in the rocks. The compositions with ca. 11 wt% MgO have similar plagioclase-stabilities at higher *T*, but they differ predominantly by the occurrence of orthopyroxene up to 25 kbar in the natural picrite. MAOC 11 has a higher CaO which may reduce the stability field of orthopyroxene to the benefit of clinopyroxene in MAOC 11. The clinopyroxene in MAOC 11 is diopside whereas the natural picrite with slightly more Na_2O in the bulk rock composition stabilises omphacite at high pressure. The presence of kyanite in MAOC 11 likely reflects its higher Al_2O_3 content.

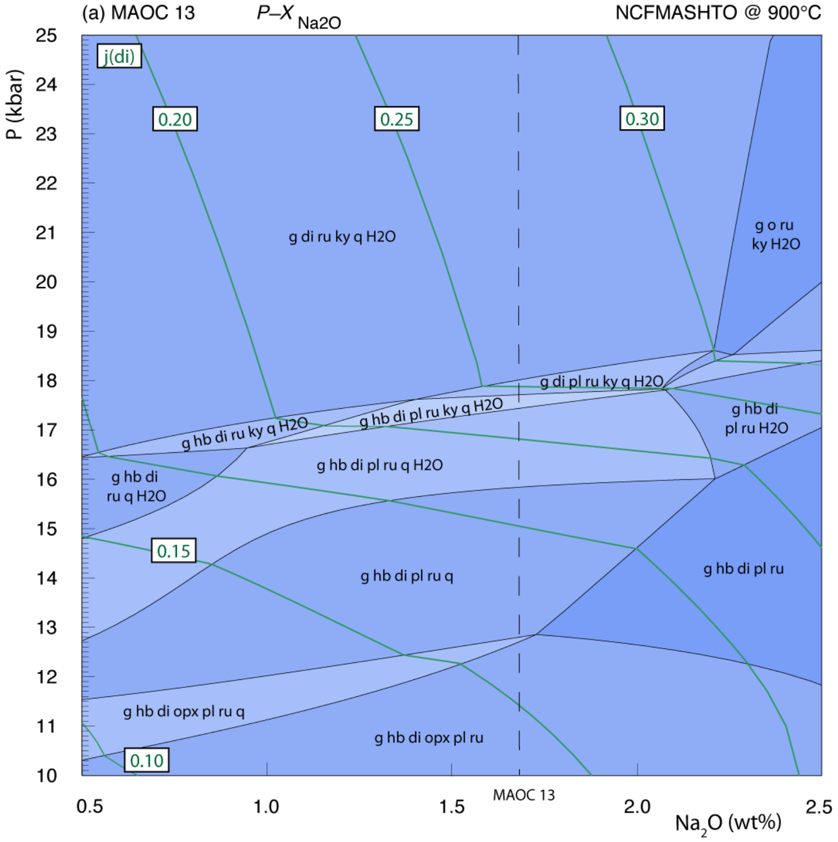

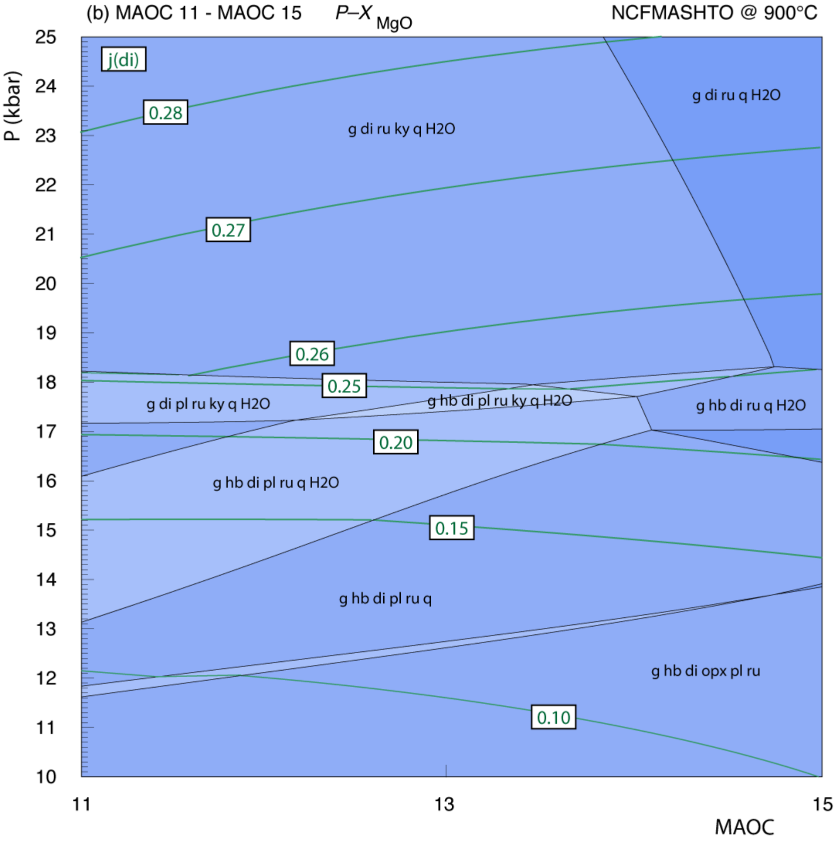

Figure 4.3.7a, b: *P–X* pseudosections for variable Na_2O in MAOC 13 (a) and from MAOC 11 to MAOC 15 (b) at 900 °C illustrate the dependence of the composition variable *j(di)* from the amount of Na_2O instead of the amount of MgO at high pressure in the eclogite facies realm.

The two compositions with 13 wt% MgO differ strongly by the presence of pyroxenite assemblages in the natural composition, whereas the stability of orthopyroxene is reduced to below 12 kbar in MAOC 13. The MAOC-composition is again richer in CaO which may account for the reduced orthopyroxene-stability. The stability field of plagioclase is much smaller in the natural picrite than in MAOC 13, restricting the area of garnet-amphibolite in the first below ca. 12 kbar. Na_2O is similarly low in both and diopside is developed in each pseudosection. Figure 4.3.7a is a P–X_{Na2O} pseudosection at 900 °C calculated for MAOC 13 with different values from 0.5 to 2.5 wt% Na_2O. The near vertical composition variable lines for *j(di)* indicate an increasing jadeite component towards higher bulk Na_2O, whereas an increase in MgO does not have a large effect on *j(di)*, and the variable rather depends on pressure in Fig. 4.3.7b. Therefore, the content of Na_2O can be regarded as the key factor for the development of either diopside or omphacite instead of a variable amount of MgO. The absence of omphacite and the stability of diopside in the eclogite facies realm is a consequence of the lower Na_2O content in the MAOC models, which may have consequences for melts generated from those rocks, which may also have too little Na_2O to resemble the elevated contents in TTGs.

Chapter 5

High-pressure partial melting experiments

5.1 Introduction

This chapter presents the results of a series of high-pressure partial melting experiments at pressures up to 20 kbar and 1100 °C conducted in a piston-cylinder press at the University of Mainz under fluid-absent conditions. Details of the experimental procedure are outlined in subchapter 3.2. The thermodynamic calculations in subchapter 4.2 predicted a transition from amphibolite- to pyroxenite-dominated metamorphic products with increasing MgO within the range between MORB and komatiite. On the basis of these findings, different models for Archean oceanic crust (MAOC) with 11, 13 and 15 wt% MgO were calculated on the basis of a partial melt from a MORB pyrolite (Falloon & Green, 1988), which is a model of fertile mantle rocks from which basaltic melts can be extracted (Green & Ringwood, 1967b). The synthesis of the model composition mixtures is presented in subchapter 5.2. The temperatures for the experiments are higher (900–1100 °C) than those used for the thermodynamic calculations for MAOC 11, 13 and 15 (up to 900 °C, subchapter 4.3) because the partial melting experiments are conducted to constrain the position of the solidus and the composition of the melt. The range of pressures was restricted to $P \geq 10$ kbar to determine the first appearance of garnet, which is inferred to be present in the source of melting for the generation of TTG-like melts (subchapter 2.3.2). An overview of the stable mineral assemblages for each of the 27 experiments and of the appropriate mineral chemistry is given in subchaper 5.3, which is followed by a discussion in subchapter 5.4.

5.2 Synthesis of the starting material

5.2.1 Calculation of the Models of Archean Oceanic Crust (MAOC)

The preparation of the MAOC oxide mixes was done in several steps. Firstly, an initial composition of a model of Archean Oceanic crust with 11 wt% MgO (MAOC 11) was calculated on the basis of an experimental partial melt composition of a MORB pyrolite with initially 14.45 wt% MgO (Falloon & Green 1988, tab. 3, No. 7). This composition was chosen due to the initial low potassium content to maintain the composition constant after eliminating K_2O from the system for the calculations in NCFMASHTO. The designated proportion of 11 wt% MgO was attained by a theoretically subtraction of an olivine composition (SiO_2 = 41.28 wt%; FeO = 8.00 wt%; MgO = 50.73 wt%) from the MORB pyrolite (Tab. 5.2.1). This was done via a least-squares-fit with the Excel function "solver" by calculating the amount of subtracted olivine to that value (0.09) that is necessary to reach 11 wt% MgO in column 4. Column 4 represents the bulk composition after the normalisation from column 3 which comprises the bulk composition after extracting 0.09 olivine from the MORB pyrolite in column 1.

Table 5.2.1: Conversion from MORB pyrolite (column 1) to MAOC 11 (column 4) by subtraction of olivine (column 2), conversion to the amount of the effectively oxide weight (g) (column 5), conversion of FeO, CaO, Na_2O and H_2O to $Mg(OH)_2$, Fe_2SiO_4, $CaCO_3$ and Na_2CO_3 (column 7) and the effective net weight (column 8).

oxide	Falloon & Green, 1988	olivine composition	substracted olivine (0.09 %)	normalised to 11wt% MgO	startmix normalised	conversion to:	target weight	effective weight
SiO_2	47.88	41.28	44.17	48.50	1.09517		1.01844	1.01842
TiO_2	0.66		0.66	0.72	0.01637		0.01637	0.01632
Al_2O_3	15.16		15.16	16.65	0.37591		0.37591	0.37604
FeO	8.12	8.00	7.40	8.13	0.18351	Fe_2SiO_4	0.26024	0.26024
MgO	14.58	50.73	10.02	11.00	0.24837		0.22312	0.22314
CaO	11.64		11.64	12.78	0.28863	$CaCO_3$	0.51515	0.51517
Na_2O	1.56		1.56	1.71	0.03868	Na_2CO_3	0.06615	0.06615
H_2O	0.00		0.50	0.50	0.01129		-	-
$Mg(OH)_2$			-	-	0.00000	$Mg(OH)_2$	0.03655	0.03415
Total	99.60		90.60	100.00	2.25790		2.51193	2.47548

The amount of oxides for ca. 2 g of a MAOC 11 mix was calculated from the MAOC 11 bulk composition (column 5) and then recalculated for the incorporation of Fe_2SiO_4 (fayalite) and the carbonates $CaCO_3$, Na_2CO_3 instead of FeO, CaO and Na_2O (column 7). Column 8 shows the effective weights of oxides in the MAOC 11 mix. Water was added as $Mg(OH)_2$ (brucite) to ensure a fixed water content in the powder because brucite stays stable during the storage of the oxide mix and during the fusing of the Au-Pd capsule even if the heating of the sample is not reproducible. The excess Si, Mg and Fe emerging from adding fayalite and brucite were subtracted from the MAOC composition.

The MAOC 11 mix (2.475 g) was split into 3 parts of which one was left unmodified (MAOC 11). The “solver” function in Excel was used again to calculate the amount of MAOC 11 mix and olivine powder which had to be mixed together to attain 13 and 15 wt% MgO in the particular parts. Tab. 5.2.2 shows the calculated start weights of MAOC 11 mix (column 1 and 4) and the addition of olivine powder (column 2 and 5) to reach 0.7 g of MAOC 13 and MAOC 15 mixes (column 3 and 6). The bulk compositions of MAOC 13 and MAOC 15 were calculated in the same way, They are listed in Tab. 5.2.3 with their CIPW-normative minerals (after Herrmann & Berry, 2002).

Table 5.2.2: Conversion from 0.66 g MAOC 11 (column 1) to 0.7 g of MAOC 13 (column 3) and from 0.63 g MAOC 11 (column 4) to 0.7 g of MAOC 15 (column 6) by adding the required amount of the olivine-mix (columns 2 and 5) to the original oxide mix.

oxide	original MAOC (g)	added olivine for 13 wt% MgO (g)	MAOC 13 (g)	original MAOC (g)	added olivine for 15 wt% MgO (g)	MAOC 15 (g)
SiO_2	0.32243	0.01455	0.33698	0.30534	0.02909	0.33443
TiO_2	0.00482		0.00482	0.00456		0.00456
Al_2O_3	0.11067		0.11067	0.10481		0.10481
FeO	0.05403	0.00282	0.05684	0.05116	0.00564	0.05680
MgO	0.07312	0.01788	0.09100	0.06925	0.03575	0.10500
CaO	0.08498		0.08498	0.08047		0.08047
Na_2O	0.01139		0.01139	0.01078		0.01078
H_2O	0.00332		0.00332	0.00315		0.00315
Total	0.66476	0.03524	0.70000	0.62952	0.07048	0.70000

Table 5.2.3: Bulk rock compositions for MAOC 11, 13 and 15 in wt% and mol% as well as the CIPW normalised minerals (identical abbreviations as in Tab. 5.3.7 plus olivine (Ol)). Mol% is the required for the mineral equilibrium calculations with THERMOCALC.

	MAOC 11		**MAOC 13**		**MAOC 15**	
oxide	**wt%**	**mol%**	**wt%**	**mol%**	**wt%**	**mol%**
SiO_2	48.50	48.96	48.14	48.00	47.78	47.06
TiO_2	0.72	0.55	0.69	0.52	0.65	0.48
Al_2O_3	16.65	9.90	15.81	9.29	14.97	8.69
FeO	8.13	6.85	8.12	6.76	8.11	6.67
MgO	11.00	16.56	13.00	19.33	15.00	22.02
CaO	12.78	13.82	12.14	12.97	11.50	12.13
Na_2O	1.71	1.67	1.63	1.58	1.54	1.47
H_2O	0.50	1.68	0.47	1.56	0.45	1.48
Total	99.99	100.00	100.00	100.00	100.00	100.00
CIPW-normalised						
An	37.96		35.97		34.08	
Di	20.88		19.79		18.65	
Hyp	9.46		8.83		8.38	
Ab	14.55		13.88		13.12	
Ol	15.78		20.22		24.55	
Ilm	1.37		1.31		1.23	
Total	100.01		100.00		100.01	

5.2.2 Preparation of the starting material for the Models of Archean Oceanic Crust (MAOC)

In a first step, fayalite (Fe_2SiO_4) was prepared at the Institute of Geoscience at the Goethe University in Frankfurt for the appliance in two several ways: Firstly, fayalite was used for the preparation of the oxide mix instead of FeO to avoid oxidation and secondly, to assemble the olivine powder.

Preparation of fayalite and olivine

Fayalite was prepared from 1 g pellets of a homogeneous mix of Fe_2O_3 and SiO_2 in a gas-mixing furnace at 1100 °C (log f_{O2} -13; flow: CO 130 and CO_2 070) and was formed by the following reaction: $SiO_2 + Fe_2O_3 + CO \rightarrow Fe_2SiO_4 + CO_2$. The composition was verified via diffractometry and the powder was mortared and stored dry in a desiccator before use.

The olivine composition was prepared from SiO_2, Fe_2SiO_4 (fayalite) and MgO (Tab. 5.2.4). The powder ground in a mortar and pestle under acetone, dried and stored in an desiccator until it was used to attain the MAOC compositions with 13 and 15 wt% MgO. The olivine powder was then used for the enrichment of the MAOC 11 oxide mix to reach 13 and 15 wt% MgO by keeping the oxides TiO_2, Al_2O_3, CaO and Na_2O constant relative to each other (Tab. 5.2.1). Before the enrichment a synthesised mix of 34 trace elements (Tab. 5.2.5) was added to the original MAOC composition.

Table 5.2.4: Composition of olivine, converted to 0.2 g with FeO converted to fayalite. The target and the effictive weights are presented.

oxide	olivine (wt%)	olivine normalized to 0.2 g	FeO → Fe_2SiO_4	Weight (g) target	Weight (g) effective
SiO_2	41.27770	0.06680	SiO_2	0.06230	0.06231
FeO	7.99600	0.01080	Fe_2SiO_4	0.01530	0.01539
MgO	50.72620	0.12240	MgO	0.12240	0.12234
Total	100.00	0.20		0.20000	0.20004

Preparation of the trace element mix

A mix of 34 trace elements (100 ppm of each trace element) was prepared by adding the elements mainly as oxides and in a few cases as carbonates or chlorides (Tab. 5.2.5) with occasional homogenisation through being ground in a mortar and pestle. The complete mix finally ground in a mortar and pestle under acetone and dried in a furnace at 500 °C (5 hours) in an evaporating dish and then ground in a mortar and pestle again dry.

Table 5.2.5: Target and effective weight of the 34 trace-elements to achieve 1 g of cations of the trace-elements, respectively 0.0294 g of each trace-element.

element	**compound**	**Weight (g)** **target**	 **effective**
Li	$LiNO_3$	0.29215	0.29210
Sc	Sc_2O_3	0.04511	0.04515
V	V_2O_5	0.04327	0.04321
Co	Co_2O_3	0.04139	0.04145
Cu	CuO	0.03684	0.03706
Zn	ZnO	0.03661	0.03669
Ga	Ga_2O_3	0.03954	0.03955
Rb	RbCl	0.04161	0.04163
Sr	$Sr(NO_3)_2$	0.07104	0.07122
Y	Y_2O_3	0.04700	0.04694
Zr	ZrO_2	0.03973	0.03971
Nb	$LiNbO_3$	0.04681	0.04678
Mo	MoO_3	0.04413	0.04420
Cs	CsCl	0.03726	0.03720
Ba	$Ba(NO_3)_2$	0.05597	0.05613
La	La_2O_3	0.03449	0.03458
Ce	CeO_2	0.03613	0.03622
Pr	Pr_6O_{11}	0.03553	0.03558
Nd	Nd_2O_3	0.03431	0.03425
Sm	Sm_2O_3	0.03411	0.03416
Eu	Eu_2O_3	0.03406	0.03409
Gd	Gd_2O_3	0.03390	0.03389
Tb	Tb_4O_7	0.03459	0.03471
Dy	Dy_2O_3	0.03376	0.03378
Ho	Ho_2O_3	0.03369	0.03372
Er	Er_2O_3	0.03363	0.03384
Tm	Tm_2O_3	0.03359	0.03363
Yb	Yb_2O_3	0.03349	0.03358
Lu	Lu_2O_3	0.03345	0.03360
Hf	HfO_2	0.03468	0.03465
Ta	Ta_2O_5	0.03591	0.03596
W	WO_2	0.03453	0.03450
Th	ThO_2	0.03347	0.03344
U	$UO_2(CH_3COO)_2 \cdot 2H_2O$	0.04796	0.04799
Total normalised to 1 g cations		1.58372	1.58519

Preparation of the MAOC oxide mixes

The MAOC 11 composition was prepared from oxides, faylite and carbonates (Tab. 5.2.1), which were dried at 300 °C for 24 hours. The chemicals (Tab. 5.2.1) were ground under acetone and subsequently decarbonated (by first heating to 1000 °C over 4 hours, keeping at 1000 °C for 2 hours and then at 1200 °C for 2 hours). The volatile-free mixture was recovered from the platinum-crucible and mortared under acetone and then dried at 300 °C for 2 hours. Finally brucite and the trace-element mix (Tab. 5.2.5) were added. The doped mixture was ground in a mortar and pestle for 30 minutes under acetone and dried at 250 °C for 2 hours. The brucite remains stable under these conditions because it breaks down at about 350 °C.

The mixes of MAOC 13 and 15 (Tab. 5.2.2) ground in a mortar and pestle for 30 minutes under acetone, then stored dry (110 °C).

5.3 Results of the high-pressure experiments

5.3.1 Overview

The experiments with the three model compositions for Archean oceanic crust (MAOC 11, MAOC 13 and MAOC 15) were conducted at different *P–T* conditions from 10 to 20 kbar and 900 to 1100 °C. In each run, three capsules were run simultaneously, resulting in a total number of 27 experiments, summarised in Tab. 5.3.1. The next subchapter provides general information of the observed phases and their appearances including detailed textural descriptions of each experiment and the composition of the melt compositions. Averaged microprobe analyses with calculations of mineral formulae and figures for further classification of mineral compositions are presented in subchapter 5.3.3 and single analyses are given in Appendix B. Backscattered-electron (BSE) images in the subchapters 5.3.1 and 5.3.2 show the different phases distinguished by grey scales based on the mean atomic mass of the elements in the phases.

The phases identified via microprobe analyses for each experiment are presented in Tab. 5.3.1. The phases are garnet (g), amphibole (amph), clinopyroxene (cpx), orthopyroxene (opx), plagioclase (pl), quartz (q), rutile (ru) and glass of various compositions. Single crystals of the phases are generally small with an average size on a μm-scale and they do not exceed 100 μm. Glass is the quenched melt which has developed during the experiments and "melt" compositions in this thesis correspond to analyses of glass. The proportion of melt listed in Tab. 5.3.1 is divided on the basis of estimations during the microprobe analyses (including BSE images) in combination with a mass-balance approach if the assemblages were well homogenised (subchapter 5.3.3.9). The broad division is made between a high, medium or low degree of melt. A high degree of melt implies up to ca. 25 % melt which is usually located at the upper rim as well as in the part halfway down a capsule. A medium amount of melt is characterised by generally smaller areas where melt has developed, but still with good potential to find appropriate areas to analyse it via microprobe, especially at the upper rim. A low degree of melt is defined if only small and sparse spots are common. If "low" is additionally set in brackets, appropriate areas big enough to analyse are rare or the small and sparse parts of melt were too small to analyse via microprobe.

Examples for each degree of melt are illustrated in the figures. Whereas a high degree of melt is shown in Figs 5.3.1a, b, d, 5.3.3, 5.3.7 and 5.3.9b, a medium amount of melt is shown in Figs 5.3.1c, e, 5.3.5b, 5.3.6b, 5.3.8 and and a low degree of melt is illustrated in Figs 5.3.1f, 5.3.5a, 5.3.6a and 5.3.10.

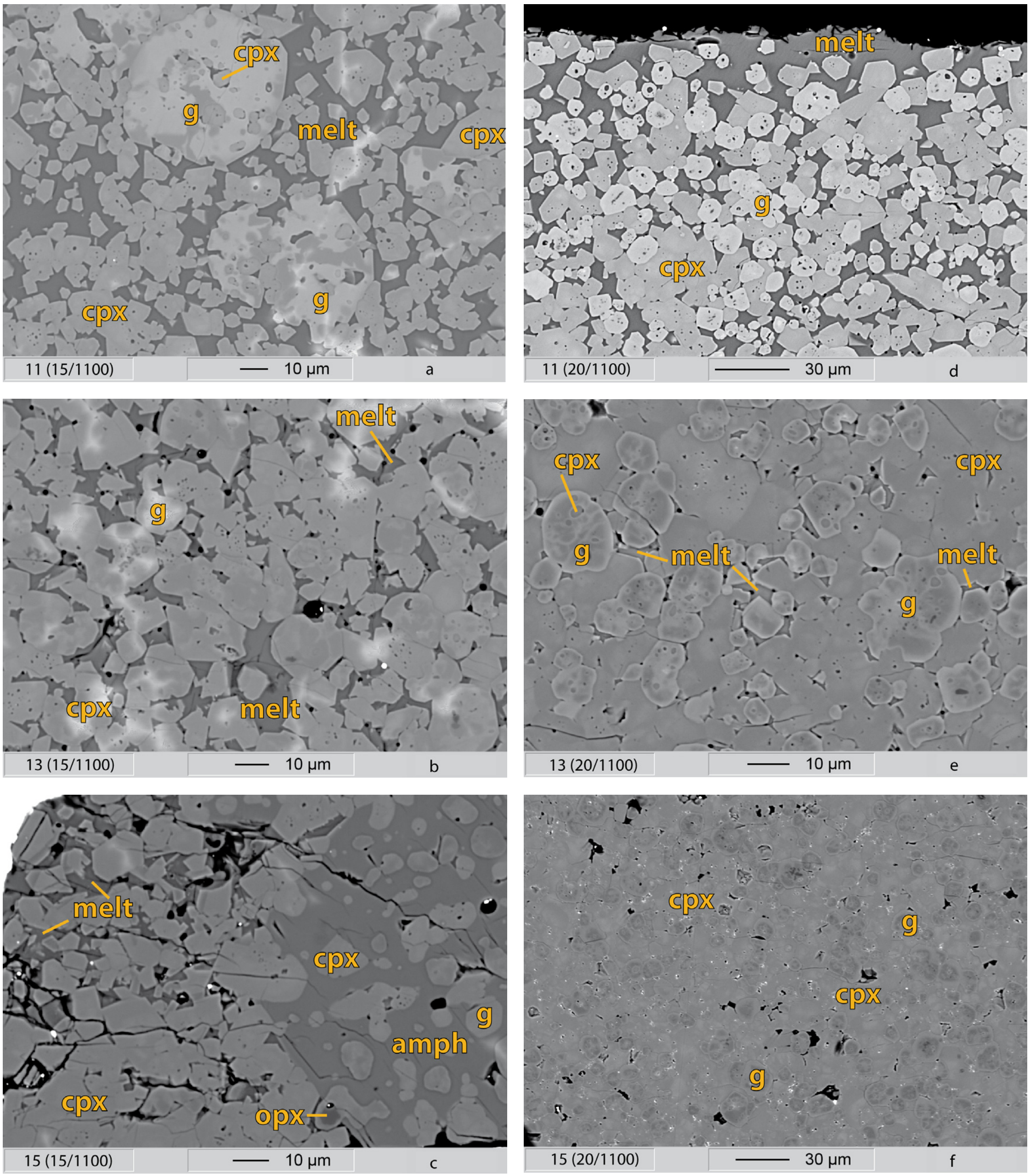

Figure 5.3.1a-f: A decreasing degree of partial melting from MAOC 11 to MAOC 15 at 15 kbar/ 1100 °C (a), (b), (c) and 20 kbar/1100 °C (d), (e), (f) is shown. Melt occurs everywhere in (a), (b), (c), but the assemblages change from g-cpx-melt to g-amph-cpx-opx-melt with increasing MgO. The change from d to f occurs only due to the absence of melt in MAOC 15 (f). The garnets in (a), (b), (d) and (f) show inclusions of clinopyroxene and inhomogeneities with different compositions. Analyses on (a) indicate that the darker parts in the middle are higher in Mg with lower Fe than in the lighter part.

A general result from the experiments is that the highest melt fraction occurs in MAOC 11 at higher *P*, whereas in MAOC 15 the melt fraction is generally very small. The degree of melting also depends on the temperature, e.g. it does not occur in the experiments conducted at 900 °C (Figs 5.3.2a, 5.3.9a). Melt commonly collected on the top of the capsule (Figs 5.3.1d, 5.3.3, 5.3.5b, 5.3.8a) and to a lesser extend in the middle of the capsules (Figs 5.3.1a, b, d, 5.3.7, 5.3.9b). The composition is divided by the SiO_2 content and it is either TTG-like (> 60 wt% SiO_2), basaltic (< 55 wt% SiO_2) or intermediate and it is generally quartz-normative (Tab. 5.3.7).

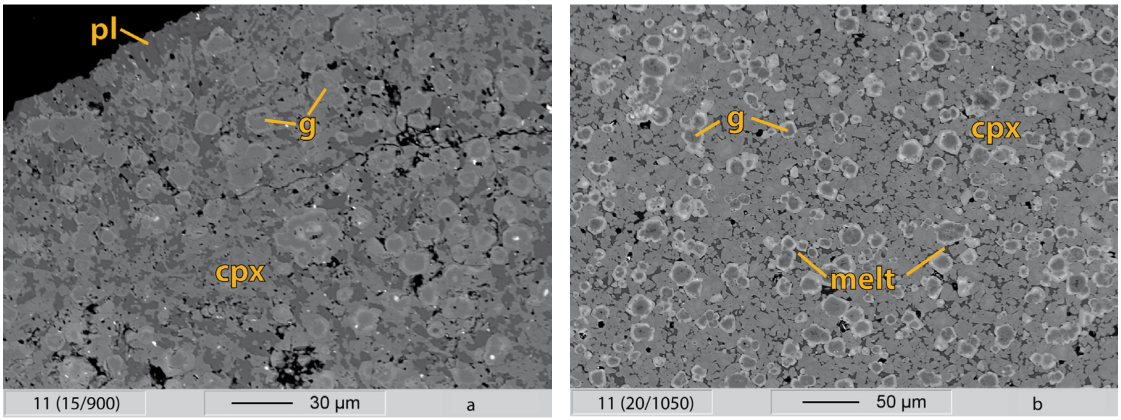

Figure 5.3.2a, b: (a) and (b) show zoned garnet-crystals with Mg-rich, dark cores and lighter Fe-richer rims in MAOC 11 at 15 kbar/900 °C and 20 kbar/1050 °C. Garnets are surrounded by clinopyroxene and interstitial plagioclase (a) or melt (b).

The experimentally-grown phases are generally small and may be aggregated and/or intergrown with each other (e.g. Fig. 5.3.4) and in places may not be clearly distinguishable from the other phases in the BSE images. For example, plagioclase and melt are commonly difficult to distinguish (e.g. Fig. 5.3.7a).

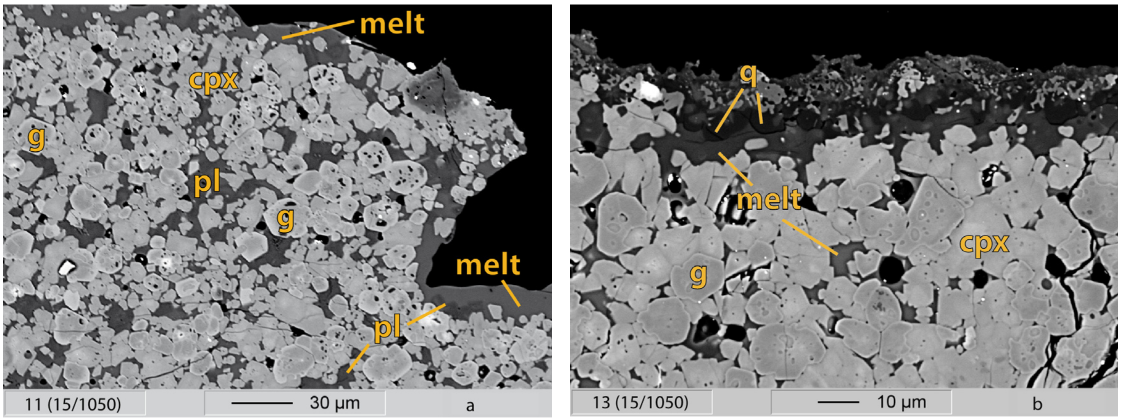

Figure 5.3.3a, b: BSE images for MAOC 11 (a) and MAOC 13 (b) at 15 kbar/1050 °C. Bigger areas of melt usually occur on the top of a capsule, where also quartz occurs in some experiments, e.g. in MAOC 13 (b). Plagioclase and melt sometimes are hard to distinguish due to their similar interstitial grow. Aggregtaed and single clinopyroxene crystals as well as heterogeneous garnet crystals are developed in (a) and (b).

The melt-free assemblages, especially in MAOC 15, are not well equilibrated and mostly form a mush with indistinguishable crystals with the exception of some indistinct garnet crystals (e.g. Figs 5.3.4a, b, 5.3.9a). For these reasons a representative percentage indication of the mineral modes was difficult and therefore was executed in combination with a mass-balance approach (subchapter 5.3.3.9) using the mineral compositions in subchapter 5.3.3. Clinopyroxene is stable in each assemblage, garnet occurs at pressures greater than 12.5 kbar and plagioclase is generally found at the lower *P–T* conditions. Plagioclase shows a decrease in its abundance from MAOC 11 towards MAOC 15, whereas the general amount of amphibole and orthopyroxene increases towards MAOC 15.

Table 5.3.1: Overview of the high-pressure partial melting experiments, including pressure, temperature and duration of each run as well as the observed phases. Phases in brackets indicate three or less analyses. The degree of melt is estimated to be high (up to ca. 25 % melt), medium or low (small and sparse areas). “Low” in brackets denotes no or only one analysable part of melt. Melt written in grey was generated in an untight capsule and therefore affected by material from the capsule holder. Mineral abbrevations are given in Tab. 3.3.1.

P [kbar]	*T* [°C]	Duration [h]		g	amph	cpx	opx	pl	q	ru	degree of melt	SiO_2 > 60 wt%
10	1050	240	MAOC 11			x		x			low	
			MAOC 13		x	x	x	x			low	
			MAOC 15		x	x	x	x			(low)	
10	1100	240	MAOC 11			x	x	x			medium	
			MAOC 13			x	x	(x)			medium	
			MAOC 15			x	x				low	
12.5	1050	240	MAOC 11	x	(x)	x	x	x			low	
			MAOC 13	x	(x)	x	x	x			-	
			MAOC 15	x	x	x	x	(x)			-	
12.5	1100	240	MAOC 11	x		x	x	x	(x)		medium	x
			MAOC 13	x		x	x	x			medium	
			MAOC 15	x		x	x	x			-	
15	900	336	MAOC 11	x	(x)	x		x			-	
			MAOC 13	x	x	x	(x)	x			-	
			MAOC 15	x	x	x	(x)	(x)			-	
15	1050	240	MAOC 11	x		x		x			high	x
			MAOC 13	x		x		(x)	(x)		high	x
			MAOC 15	x		x	x	x			(low)	
15	1100	240	MAOC 11	x		x					high	
			MAOC 13	x		x					high	
			MAOC 15	x	x	x	x				medium	
20	1050	240	MAOC 11	x		x			(x)	(x)	high	x
			MAOC 13	x		x			(x)	(x)	medium	x
			MAOC 15	x		x	(x)			(x)	(low)	
20	1100	240	MAOC 11	x		x					high	x
			MAOC 13	x		x					(low)	
			MAOC 15	x		x					-	

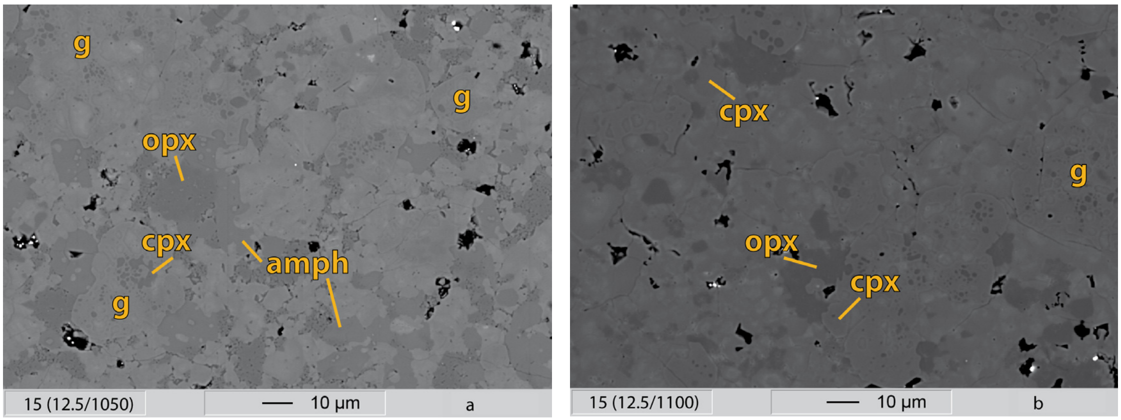

Figure 5.3.4a, b: Examples for bad homogenised melt-free assemblages of MAOC 15 at 12.5 kbar and 1050 °C (a) and 1100 °C (b). The phases in (a) are mostly hypidiomorphic, and in most cases they are clearly distuingishable from each other, even though they are intergrown with each other. Most areas in (b) are a mush of undefinable and not balanced phases. These areas contain no observable crystals instead of heterogeneous and indistict garnet crystals and pyroxene.

5.3.2 Mineral assemblages in MAOC 11, 13 and 15

This subchapter gives an overview of each experimental assemblage including the inferred stable phases and their appearance as well as the composition of melt developed. The averaged microprobe analyses and detailed information to the mineral chemistry are given in subchapter 5.3.3.

5.3.2.1 MAOC11

MAOC 11 at 10 kbar

Assemblage at 1050 °C

clinopyroxene - plagioclase - melt

This experiment was affected by the material from outside the capsule because the capsule seal had failed in the upper part where a light-coloured area occurs in the BSE image (Fig. 5.3.5a). This area includes a substantial proportion of the Ca-phase larnite (Ca from the surrounding CaF of the capsule holder) in addition to the usual assemblage. The melt is concentrated in the upper region of the capsule where the diffusion occurred and no analysis of unaffected melt could be done. In the area that was not contaminated by the CaF-diffusion, most of the clinopyroxene crystals are xenomorphic with crystals up to 25 μm in diameter and plagioclase occurs interstitially, both were analysed and fit the analyses of the other experiments. There was no replication of this run due to the fact that this *P–T* condition was not considered critical to the aim of this study because of the absence of garnet in the run products.

Mineral compositions of the unaffected area are given in subchapter 5.3.3 and the melt at the upper rim was affected by CaF showing very high Ca values representing biased results and are not considered further.

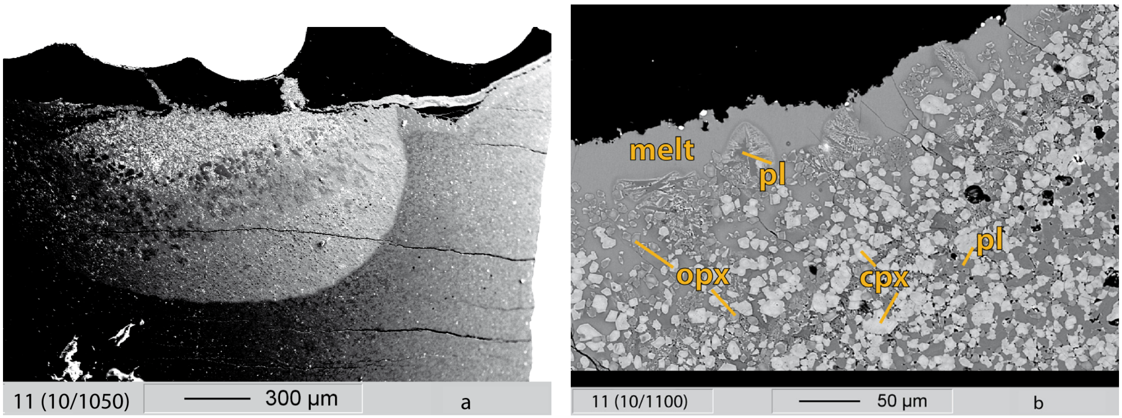

Figure 5.3.5a, b: (a) is an overview of the untight capsule at 10 kbar/1050 °C of MAOC 11, showing the affected area (light), which also extends to the right top of the capsule, in which melt also occurs. The phases in the part below are unaffected and could be determined. (b) shows the assemblage cpx–opx–plag–melt at 10 kbar and 1100 °C implying different plagioclase compositions in the bubbles and in the main part.

Assemblage at 1100 °C

clinopyroxene - orthopyroxene - plagioclase - melt (basaltic)

The run at this temperature produced more melt compared to that at 1050 °C and orthopyroxene was present in the melt at the upper rim (Fig. 5.3.5b). The clinopyroxene crystals are up to 30 μm across, whereas orthopyroxene crystals are smaller (< 15 μm in size). Where pyroxenes are surrounded by melt at the upper margin of the capsule, they are hypidiomorphic to idiomorphic. They are generally smaller halfway down the capsule, where they form xenomorphic to hypidiomorphic crystals and appear together with xenomorphic plagioclase crystals. Plagioclase of different composition (Tab. 5.3.6) also occurs as radial crystals in diffuse bubbles in the melt (Fig. 5.3.5b).

MAOC 11 at 12.5 kbar

Assemblage at 1050 °C

garnet - clinopyroxene - orthopyroxene - plagioclase - melt (basaltic) ± amphibole

Garnet is stable at this pressure and constitutes a major phase together with clinopyroxene and plagioclase (Fig. 5.3.6a). Additionally, a minor proportion of < 20 μm diameter orthopyroxene crystals occur, which form clusters with up to 20 μm diameter clinopyroxene grains. The clusters are surrounded by interstitial plagioclase in interstices up to 50 μm wide. Garnet crystals are hypidiomorphic and up to 50 μm across, their compositions commonly are patchy and the crystals also contain inclusions of clinopyroxene and plagioclase in places. Small amounts of amphibole and melt also occur in this assemblage. The melt-composition is *basaltic* with one of three analyses indicating a nepheline-normative basalt.

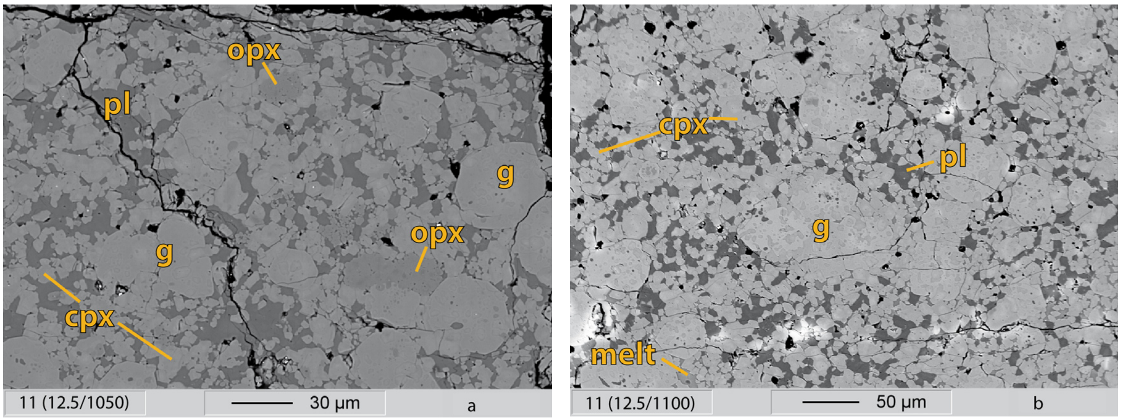

Figure 5.3.6a, b: MAOC 11 at 12.5 kbar is mainly made up of garnet, clinopyroxene and interstitial plagioclase, the small amounts of melt and amphibole are not shown here. Clusters of garnet are bigger at 1100 °C (b). At 1050 °C (a) orthopyroxene occurs everywhere whereas at 1100 °C it is assembled on the top of the capsule (not shown).

Assemblage at 1100 °C

garnet – clinopyroxene – orthopyroxene – plagioclase - melt (tonalitic) ± quartz

The assemblage is mainly composed of garnet, clinopyroxene and plagioclase, the latter occurs in up to 50 μm wide interstitial areas between garnet and clinopyroxene crystals (Fig. 5.3.6b). The grain size of plagioclase is larger on the upper margin of the capsule where small amounts of melt, quartz and xenomorphic orthopyroxene (up to 20 μm across) are also present. Orthopyroxene and melt are not in contact with each other and always separated by plagioclase (cf. Fig. 5.4.2), melt also occurs interstitially between the plagioclase crystals in the part half way down the thin section to a minor amount. Clinopyroxene crystals are xenomorphic and $\leq$ 30 μm in diameter, they are commonly intergrown with plagioclase or enclosed in garnets. The predominantly xenomorphic garnet crystals generally have inclusions of clinopyroxene and plagioclase and commonly aggregate to form clusters > 100 μm across.

MAOC 11 at 15 kbar

Assemblage at 900 °C

garnet - clinopyroxene - plagioclase ± amphibole

The products of this run are generally not well equilibrated as no melt was produced. The main phases are garnet, clinopyroxene and plagioclase with a very small proportion of amphibole (Fig. 5.3.2a). The phases were hard to distinguish, i.e. the areas with intergrown xenomorphic clinopyroxene and plagioclase. Hypidiomorphic garnet crystals up to 30 μm across in most cases are chemically zoned, with Mg-rich cores and Fe-richer rims (dark core and light rim in BSE image), and commonly contain inclusions of clinopyroxene.

Assemblage at 1050 °C

garnet - clinopyroxene - plagioclase - melt (tonalitic)

This assemblage differs from that at 900 °C due to the absence of amphibole and the presence of melt (Fig. 5.3.3a). Clinopyroxene and garnet occur as hypidiomorphic crystals (all sizes $\leq$ 30 μm) and small clinopyroxene inclusions in garnet are common (Fig. 5.3.7a). Garnet commonly shows a similar core to rim compositional zoning to that described for the experiment at 900 °C but here the rim was too thin to analyse and the compositional changes are smooth. The crystals may form aggregates or occur as single crystals surrounded by interstitial melt and/or plagioclase in up to 40 μm wide interstices. Melt is more common at the upper part of the capsule and the differentiation between plagioclase and melt here was possible in most cases only via quantitative analysis.

Assemblage at 1100 °C

garnet - clinopyroxene - melt (intermediate)

The mineral assemblage at 1100 °C differs from that at 1050 °C by a higher amount of interstitial melt and the absence of plagioclase. It is made up of xenomorphic to hypidiomorphic, internally inhomogeneous garnet crystals up to 60 μm across with randomly dispersed dark and light areas in the BSE images and smaller hypidiomorphic clinopyroxene grains. The crystals are surrounded by melt and clinopyroxene may also be included in garnet (Fig. 5.3.1a).

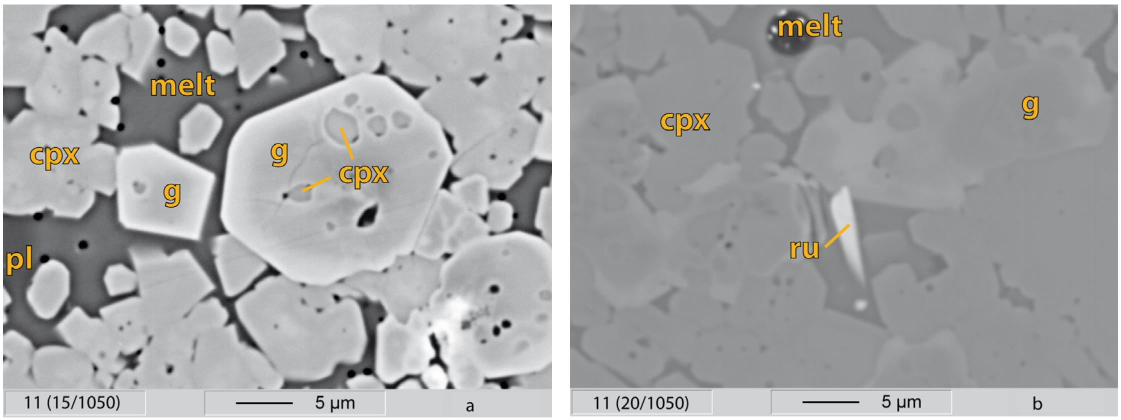

Figure 5.3.7a, b: MAOC 11 at 15 kbar/1050 °C and 20 kbar/1050 °C with high magnification. (a) and (b) show clinopyroxene and inhomogeneous garnet crystals with inclusions of clinopyroxene (a) and a grain of rutile, embedded in a melt pool (b). Interstitial melt is also present in both, whereas in (a) also plagioclase (darker than melt) occurs. The phases are distinguishable via microprobe analysis.

MAOC 11 at 20 kbar

Assemblage at 1050 °C

garnet - clinopyroxene - melt (tonalitic) ± quartz ± rutile

The main phases are garnet, clinopyropyene and melt with a small amount of quartz and an acicular Ti-phase, which is presumably rutile (Fig. 5.3.7b). The melt occurs interstitially between garnet crystals up to 25 μm in diameter. Garnet commonly occurs as hypidiomorphic to idiomorphic crystals, especially if they are surrounded by melt at the upper border of the capsule and they display the same zoning as described earlier (Fig. 5.3.2b). Most of the clinopyroxene grains are xenomorphic and form aggregates in areas with smaller amounts of melt and are developed in a broad range of sizes up to 40 μm. Quartz occurs at the upper margin of the capsule in the melt-rich portion. The acicular Ti-phase (rutile) occurs in interstitial melt pools and reaches up to 5 μm in length. The Ti-phase was too small to analyse without the interference of the surrounding material.

Assemblage at 1100 °C

garnet - clinopyroxene - melt (tonalitic)

This assemblage is similar to that at 1050 °C with the exception that more melt occurs between the zoned garnet (< 20 μm in diameter) and clinopyroxene crystals (Fig. 5.3.1d). Clinopyroxene crystals are commonly hypidiomorphic, but xenomorphic clinopyroxene grains are also present and form aggregates up to 70 μm across. The composition of the garnet crystals again varies slightly due to patchy variations in composition and they have inclusions of clinopyroxene grains.

5.3.2.2 MAOC 13

MAOC 13 at 10 kbar

Assemblage at 1050 °C

amphibole - clinopyroxene - orthopyroxene - plagioclase - melt

Compared to the equivalent MAOC 11 assemblage, this assemblage additionally contains amphibole and orthopyroxene and a slightly lower proportion of melt. Melt was identified on the upper margin, but the composition is also affected by the CaF from the capsule holder as described for MAOC 11 at this *P–T* condition. Clinopyroxene is developed as a network of xenomorphic crystals, intergrown with plagioclase and amphibole in the area below the contamination. Amphibole grains form up to 60 μm wide xenomorphic areas, which enclose xenomorphic clinopyroxene and plagioclase crystals as illustrated in Fig. 5.3.1c. Hypidiomorphic and idiomorphic orthopyroxene crystals up to 10 μm in size occur sporadically between clinopyroxene. A large amount of unreacted material is located between the xenomorphic minerals. Mineral compositions from the not affected area are given in subchapter 5.3.3 and the melt-composition must have been affected by CaF from the capsule holder (analyses not presented).

Assemblage at 1100 °C

clinopyroxene - orthopyroxene - melt (basaltic) ± plagioclase

The mineral assemblage differs from that at 1050 °C by the absence of amphibole and the decrease in the amount of < 30 μm in diameter clinopyroxene crystals. Orthopyroxene crystals between the clinopyroxene crystals are smaller but both pyroxenes are developed as hypidiomorphic to idiomorphic crystals in between the melt at the upper margin (Fig. 5.3.8a). Compared to the equivalent MAOC 11 assemblage at the same *P–T* condition, small xenomorphic orthopyroxene grains are located in melt pools and in the melt at the upper margin of the capsule. In the middle of the capsule unreacted material occurs between the pyroxenes instead of plagioclase. Small ragged quench crystals also exist in melt at the upper margin.

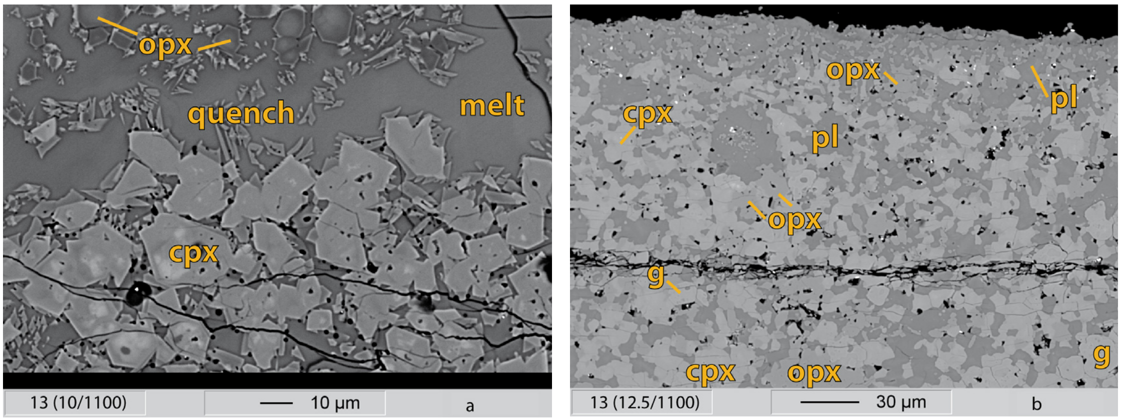

Figure 5.3.8a, b: MAOC 13 at 10 (a) and 12.5 kbar (b) at 1100 °C. The assemblage in (a) is cpx–opx–(pl)–melt with small quench crystals in the melt, which sometimes grew around bigger cores. At higher pressure garnet becomes stable and the amount of melt decreases (b), where melt only occurs as small parts halfway down the capsule and it is not present in this figure.

MAOC 13 at 12.5 kbar

Assemblage at 1050 °C

garnet - clinopyroxene - orthopyroxene - plagioclase ± amphibole

The assemblage is similar in its texture to its MAOC 11 equivalent but differs in the absence of melt and the higher amount of garnet. In comparison to that at 10 kbar, garnet is stable here but no melt occurs. The xenomorphic orthopyroxene crystals reach sizes up to 20 μm, they are mainly surrounded by xenomorphic clinopyroxene crystals and commonly aggregated into clusters with hypidiomorphic garnet crystals ranging widely in size from 10–60 μm in diameter. Smaller crystals of clinopyroxene occur with interstitial plagioclase in interstices of up to 20 μm across or as inclusions in garnet. Unreacted material is rarely present.

Assemblage at 1100 °C

garnet – clinopyroxene – orthopyroxene – plagioclase - melt (basaltic)

Compared with the equivalent assemblage of MAOC 11 the amount of plagioclase is lower in this experimental run. Figure 5.3.8b illustrates the different appearance of the pyroxenes in a BSE image: the orthopyroxene crystals are slightly darker than those of clinopyroxene. The interstitial plagioclase areas are up to 30 μm wide, but they are usually smaller between the aggregates of pyroxene crystals (all sizes ≤ 30 μm in diameter), especially in the upper part of the capsule (Fig. 5.3.8b). Garnet crystals up to 50 μm in size with inclusions of clinopyroxene form aggregates in the middle part of the capsule with clinopyroxene, interstitial melt (< 10 μm in space) and a small proportion of plagioclase and orthopyroxene.

MAOC 13 at 15 kbar

Assemblage at 900 °C

garnet - amphibole - clinopyroxene - plagioclase ± orthopyroxene

Texturally, this experimental run does not appear well equilibrated (Fig. 5.3.9a), similar to that of the equivalent *P–T* conditions in MAOC 11. In comparison to MAOC 11, here amphibole is more common and a small amount of orthopyroxene exists. All phases are internally compositionally heterogeneous. Amphibole and orthopyroxene are intergrown and occur with clinopyroxene and plagioclase, only garnet is developed in larger hypidiomorphic crystals greater than 15 μm. Garnet crystals are less common than in MAOC 11 but show the same zoning from core to rim as well as less structured internal compositional inhomogeneities and inclusions of clinopyroxenes.

Assemblage at 1050 °C

garnet - clinopyroxene - melt (tonalitic) ± plagioclase ± quartz

In addition to the prevailing phases a small amount of quartz occurs in the melt at the upper margin of the capsule. The experimental run products differ from that at 900 °C by the presence of melt and the absence of amphibole and orthopyroxene as well as by a decreased amount of plagioclase (Fig. 5.3.3b). The phases have similar appearance to that at 900 °C with the exception of garnet, where a zoning is not well pronounced here. However, the crystals and interstitial phases are smaller than those at 15 kbar and 900 °C and than those of the equivalent MAOC 11 assemblage at the same *P–T* conditions.

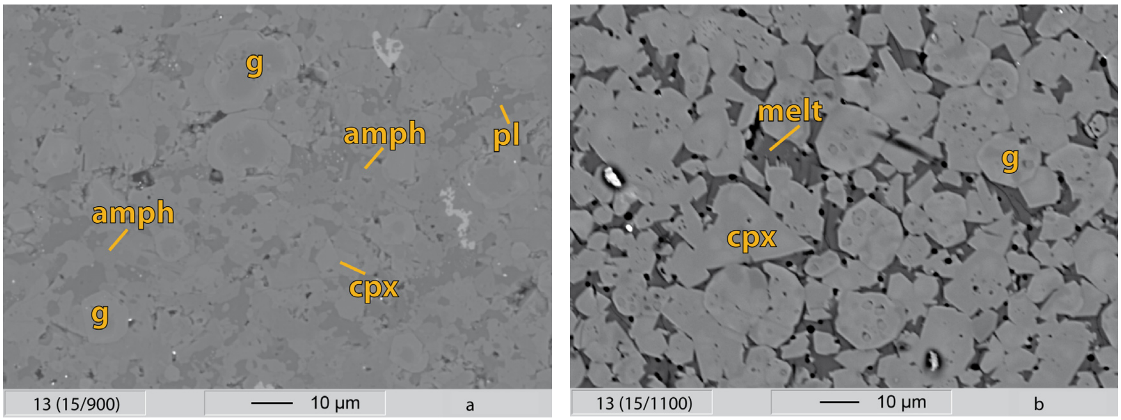

Figure 5.3.9a, b: Comparison of the melt-free, amphibole- and plagioclase-bearing assemblage at 900 °C (a) to the assemblage g–cpx–melt at 1100 °C in MAOC 13 at 15 kbar (b). In (a), only the zoned garnets are hypidiomorphic, whereas the other phases are intergrown and show poorly defined crystals. The light phase in (a) is not ascertained. For comparison, Fig. 5.3.3b shows the assemblage at 1050 °C containing melt and plagioclase.

Assemblage at 1100 °C

garnet - clinopyroxene - melt (basaltic)

This mineral assemblage is made up of less phases compared to 15 kbar and 1050 °C. Patchy variabilities ocuur in the hypidiomorphic (up to 60 μm in size) garnet crystals. The size of the clinopyroxene crystals ranges up to 40 μm across and the crystals are hypidiomorphic to idiomorphic if they are neither enclosed by melt nor aggregated (Fig. 5.3.9b).

MAOC 13 at 20 kbar

Assemblage at 1050 °C

garnet - clinopyroxene - melt (tonalitic) ± quartz ± rutile

The experimental run products are similar to the equivalent MAOC 11 *P–T* condition but the garnet crystals here are smaller and more rounded. Additionally, the composition is patchy and the crystals contain inclusions of clinopyroxene. The amount of melt is smaller and the clinopyroxene crystals are more aggregated than those of the equivalent MAOC 11 assemblage. Quartz is enclosed by melt especially at the upper margin of the capsule and a second accessory phase is presumably rutile (similar as shown in Fig. 5.3.7b).

Assemblage at 1100 °C

garnet - clinopyroxene ± melt

This assemblage is similar to that at 20 kbar and 1050 °C but with a much smaller proportion of interstitial melt pools. Some clinopyroxene crystals on the top of the capsule are idiomorphic and in the middle part clinopyroxenes usually form aggregates. Some garnet crystals reach sizes of up to 30 μm across with smooth compositional variations. The garnet crystals are generally smaller than those at 1050 °C and they are intergrown with clinopyroxene grains to form aggregates (Fig. 5.3.1e). In areas without garnet crystals at the upper margin of the capsule, the aggregated clinopyroxene grains appear to be arranged in a nearly plane surface. The presence of clinopyroxene in a plane surface is comparable to the way melt generally is present in the assemblages where melt is collected at the upper margin (e.g. Fig. 5.3.5 b). The sparse melt pools generally were too small to analyse but a basaltic melt composition was determined by a single analysis.

5.3.2.3 MAOC 15

MAOC 15 at 10 kbar

Assemblage at 1050 °C

amphibole - clinopyroxene - orthopyroxene - plagioclase ± melt (basaltic)

The products of this experimental run contain a higher proportion of unreacted material which indicates a poorly equilibrated assemblage (Fig. 5.3.10 a). The xenomorphic phases are predominantly pyroxene, which along with amphibole form aggregates and intergrowth. These are surrounded by the unreacted material. Clinopyroxene crystals are larger (< 30 μm in diameter) than orthopyroxene and amphibole (< 10 μm in size) and minor melt is present at the upper margin of the capsule.

Assemblage at 1100 °C

clinopyroxene - orthopyroxene - melt (basaltic)

The product of this experimental run is characterised by a large proportion of unequilibrated material, which is intergrown with pyroxene grains (Fig. 5.3.10b; similar to 10 kbar/1050 °C and MAOC 13 at this *P–T* condition). The pyroxenes occur as xenomorphic to hypidiomorphic crystals with varying sizes up to 40 μm across. Melt is present at the lateral rim and at the upper margin of this capsule in very small pools, which are intermingeled with a network of unreacted material. Idiomorphic orthopyroxene and hypidiomorphic clinopyroxene crystals (both < 15 μm in size) are also present in these areas. The melt is of basaltic composition.

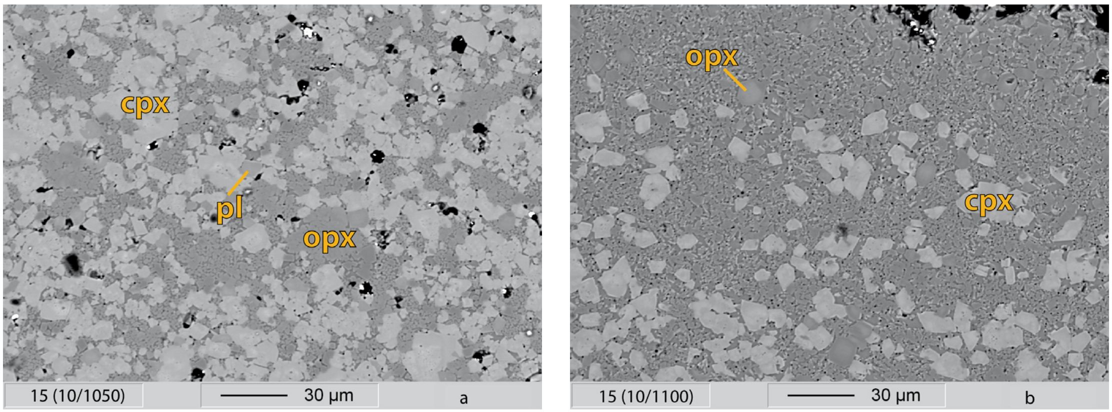

Figure 5.3.10a, b: MAOC 15 at 10 kbar and 1050 °C (a) and 1100 °C (b). At 1050 °C, intergrown clino- and orthopyroxene grains, plagioclase and a lot of unbalanced material are illustrated. The assemblage at 1100 °C consists of crystals of ortho- and clinopyroxene, whereas idiomorphic orthopyroxene and hypidiomorphic clinopyroxene crystals occur intermingled with small melt-pools and unreacted material.

MAOC 15 at 12.5 kbar

Assemblage at 1050 °C

garnet - amphibole - clinopyroxene - orthopyroxene ± plagioclase

The difference between this experiment and the equivalent assemblage of MAOC 13 is an increased abundance of amphibole. Compared to 10 kbar and 1050 °C in MAOC 15, garnet is stable here and melt does not occur (Fig. 5.3.4a). The poorly equilibrated assemblage contains unreacted material and it is characterised by xenomorphic intergrown crystals of different size which were difficult to analyse. The clinopyroxene grains form aggregates and are intergrown with amphibole, orthopyroxene and plagioclase (at the upper margin). Garnet is present as up to 40 μm across hypidiomorphic crystals, which are patchy in composition and host inclusions of clinopyroxene grains. Amphiboles form up to 30 μm across xenomorphic areas also enclosing clinopyroxenes.

Assemblage at 1100 °C

garnet - clinopypoxene - orthopyroxene - plagioclase

This experimental run is characterised by a cloudy mush of unequilibrated phases, which are usually finely intergrown with other phases and they are difficult to distinguish in the BSE images. These phases are garnet, clino- and orthopyroxene. Garnet crystals in places are present as xenomorphic grains with discernible grain boundaries and they contain many inclusions (Fig. 5.3.4b). In the upper plagioclase-bearing part xenomorphic pyroxene crystals are also present between the interstitial plagioclase areas. The pyroxenes are internally compositionally heterogeneous and consist of parts of clino- and orthopyroxene in a single grain.

MAOC 15 at 15 kbar

Assemblage at 900 °C

garnet - amphibole - clinopyroxene ± orthopyroxene ± plagioclase

The assemblage is similar to that of MAOC 13 at the equivalent *P–T* conditions, but the phases are less well equilibrated here and the amount of plagioclase is markedly reduced. Zoned garnet crystals up to 10 μm in diameter are present in a heterogeneous mushy matrix of aggregated and intergrown xenomorphic crystals of amphibole, pyroxene and plagioclase as well as with unreacted material. The minerals are internally inhomogeneous and intergrown with each other. Each phase analysed in this assemblage has varying compositions, given in subchapter 5.3.3.

Assemblage at 1050 °C

garnet - clinopyroxene - orthopyroxene - plagioclase ± melt

Compared to 15 kbar/900 °C, this assemblage lacks amphibole and the phases are more easily distinguishable from each other. Garnet crystals are rounded and up to 30 μm in diameter with numerous inclusions of the accompanying minerals. Garnet crytals occur between aggregated clinopyroxenes and small implemented crystals of plagioclase and orthopyroxene which all commonly have non-defined boundaries. Melt is present as an accessory phase. The melt composition could not be determined via microprobe analyses because the melt pools were too small.

Assemblage at 1100 °C

garnet - amphibole - clinopyroxene - orthopyroxene - melt (basaltic)

The products of this experimental run are garnet, amphibole, clinopyroxene and a small proportion of melt and orthopyroxene (Fig. 5.3.1c). In comparison to 15 kbar and 1050 °C, the phases are present as discrete crystals. Most of the < 10 μm small clinopyroxene crystals are hypidiomorphic if they are surrounded by interstitial amphibole (around 100 μm across). If clinopyroxenes are not surrounded by amphibole, the crystals aggregate in larger clusters. The internally heterogeneous garnet crystals with smoothly varying compositions are up to 30 μm in size, they are generally rounded and have typical grain boundaries in places. Some clinopyroxene grains include small orthopyroxen patches.

MAOC 15 at 20 kbar

Assemblage at 1050 °C

garnet - clinopyroxene ± orthopyroxene ± rutile ± melt (basaltic)

In this assemblage only a small proportion of interstitial melt pools is present between the two main phases garnet and clinopyroxene. Clinopyroxenes build an inhomogeneous groundmass hosting garnet crystals. Garnet crystals are < 10 μm in size and patchy in composition and exhibit inclusions of clinopyroxene as illustrated in Fig. 5.3.11b. An accessory Ti-rich phase, which is presumably rutile (similar as shown in Fig. 5.3.7b) is also present. The melt pools were too small to analyse but one analyses indicates a basaltic melt composition.

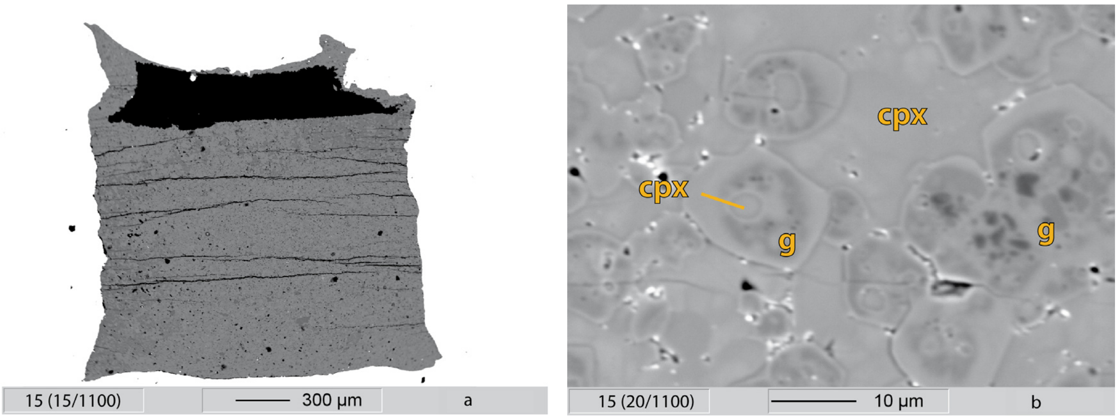

Figure 5.3.11a, b: MAOC 15 at 15 kbar (a) and 20 kbar (b) at 1100 °C. (a) is an overview of one half of the capsule and the black area above the upper margin of the assemblage is the graphite buffer. The surrounding area is white and represents the Au-Pd capsule. The assemblage at 20 kbar (b) is made up of clinopyroxene and garnet, the latter are inhomogeneous with patchy compositions and inclusions of clinopyroxenes.

Assemblage at 1100 °C

garnet - clinopyroxene

The texture of this assemblage is similar to 20 kbar and 1050 °C but this assemblage here lacks melt and rutile. Internally compositionally inhomogeneous garnet crystals with patchy compositions are arranged in a groundmass of clinopyroxene areas, and clinopyroxene grains are in turn enclosed in garnet crystals (Fig. 5.3.11b).

5.3.2.4 Summary

The mineral assemblages determined in the 27 experimental runs from 10–20 kbar and 900–1100 °C conducted on MAOC 11, 13 and 15 are described above. The assemblages generally consist of garnet, amphibole, clinopyroxene, orthopyroxene, plagioclase and melt and the chemistry of these phases is presented in subchapter 5.3.3. Accessory phases are quartz and rutile.

The amount of melt generally decreases from MAOC 11 to MAOC 15 (Tab. 5.3.1) and it commonly occurs at the upper rim of the experimental run capsules. In experiments with a high amount of melt, the melt pools are also located in the middle of the capsule between the other phases, which then are present commonly as idiomorphic to hypidiomorphic crystals. Subsolidus assemblages or assemblages with a minor proportion of melt are commonly not well homogenised and minerals are present as xenomorphic and intergrown grains, which are difficult to distinguish from each other in some assemblages. In many of these experimental run products, especially in MAOC 15, unreacted material is present.

Garnet is present in every assemblage at $P \geq$ 12.5 kbar. The crystals reach sizes of up to 60 μm across in MAOC 11 and 13 and of up to 40 μm in diameter in MAOC 15. Garnet crystals are frequently internally compositionally inhomogeneous with patchy zoning or are concentrically zoned into dark cores and light rims. In most of the zoned garnets (15 kbar/900 °C in MAOC 11, 13 and 15, and at 20 kbar/1050 °C in MAOC 11) and in one assemblage with randomly dispersed dark and light areas (15 kbar/1100 °C) it was possible to determine two types of garnet with higher (dark) and lower (light) amounts of MgO (Tab. 5.3.2), whereas in some assemblages the garnet crystals are patchy zoned and no compositional determination could be done. The grains vary between xenomorphic, hypidiomorphic and idiomorphic forms depending on the development of the experimental runs and they frequently host inclusions of other phases, especially clinopyroxene.

The highest abundance of amphibole is reached in the experimental run products from MAOC 15, whereas the phase is accessory in MAOC 11. Amphibole grains are commonly xenomorphic and intergrown with other phases or include them, with sizes of up to 100 μm across in MAOC 15 but generally smaller with sizes similar to the surrounding crystals in the assemblage. The coexistence of amphibole and melt is restricted to MAOC 15 at 15 kbar/1100 °C.

Clinopyroxene is present in all experimental run assemblages and commonly forms xenomorphic crystals with sizes from < 10 μm up to 40 μm across, whereas the bigger crystals are present in the assemblages formed at high pressures. Xenomorphic and idiomorphic clinopyroxene grains are also present and all crystals are frequently aggregated, especially in assemblages with a minor proportion of melt.

Orthopyroxene crystals have sizes up to 20 μm across and are generally present at 10 and 12.5 kbar in all MAOC compositions, whereas orthopyroxene is also present in MAOC 15 assemblages at higher pressures. The crystals are commonly xenomorphic and occur together with minor amounts of hypidiomorphic and idiomorphic grains. Orthopyroxene grains are frequently embedded in aggregates of clinopyroxene or they are intergrown with other phases.

The plagioclase stability is restricted to pressures up to 15 kbar in MAOC 11 to 15 and in MAOC 15 plagioclase is usually an accessory phase. The xenomorphic and interstitially plagioclase grains are present in up to 90 μm across interstices and they are frequently intergrown with other phases.

Quartz as an accessory phase occurs in MAOC 11 (12.5 kbar/1100 °C and 20 kbar/1050 °C) and MAOC 13 (15 kbar/1050 °C and 20 kbar/1050 °C) at the upper rim in assemblages where tonalitic melt occurs and is in contact with these melts and/or plagioclase. The assemblages at 20 kbar/1050 °C all contain rutile associated to interstical melt pools.

5.3.3 Mineral chemistry in MAOC 11, 13 and 15

5.3.3.1 Introduction

This subchapter presents the averaged analyses for the minerals and melt in terms of oxides and mineral formula calculations. Graphic classifications for garnet, amphibole, clinopyroxene, orthopyroxene, plagioclase and melt are also presented. The chemistry of the phases developed in the experiments (subchapter 5.3.3) was quantitatively determined via an electron microprobe (subchapter 3.3). The estimated amount of Fe^{3+} in garnet, pyroxene and plagioclase is calculated stoichiometrically on the basis of the particular number of oxygen in the phase, whereas the approach of Schumacher (1997; in: Leake *et al.*, 1997, their Appendix 2) was used for the amphiboles. Some composition variables used by THERMOCALC are additionally given for comparison with the thermodynamic calculations (subchapter 6.2). The individual analyses are presented in Appendix B. Small amounts of quartz and rutile were detected via EDS (Energy-dispersive X-ray spectroscopy) during the microprobe-analyses of the main phases.

5.3.3.2 Garnet

Garnet is stable in the MAOC assemblages 12.5 kbar. The average values of microprobe analyses with formulae calculated on the basis of 12 oxygen in terms of $X^{2+}{}_3Y^{3+}{}_2Z_3O_{12}$ and the distribution of elements on sites is given in Tab. 5.3.2. The proportions of the end-members pyrope Mg_3Al_2 (py), almandine $Fe^{2+}{}_3Al_2$ (alm), andradite $Ca_3Fe^{3+}{}_2$ (andr), grossular Ca_3Al_2 (grs) (Deer *et al.*, 1992) and majorite $Mg_3(Fe^{3+},Al,Si)_2$ (ma) (Smith & Mason, 1970) are given as well as Mg# = Mg/Mg + Fe^{2+} (molecular ratio) and the composition variable *x(g) = Fe2/Fe2 + Mg* as applied by THERMOCALC (subchapter 3.1.2.2.4).

The high standard deviation of the total values at 15 kbar/900 °C (MAOC 11, 13, 15), 15 kbar/1100 °C and 20 kbar/1050 °C (both in MAOC 11) originates from the presence of two types of garnets in assemblages with the zoned or compositionally inhomogeneous garnet crystals. The garnets from these experimental runs are seperated into dark Mg-rich parts and light Mg-poorer parts Tab. 5.3.2). In other assemblages with internally compositionally inhomogeneous garnet crystals the differences were indeterminable due to the patchy zoning in the crystals in which the standard deviation of the averaged values is lower than those of the total standard deviations resulting from the summary of two types.

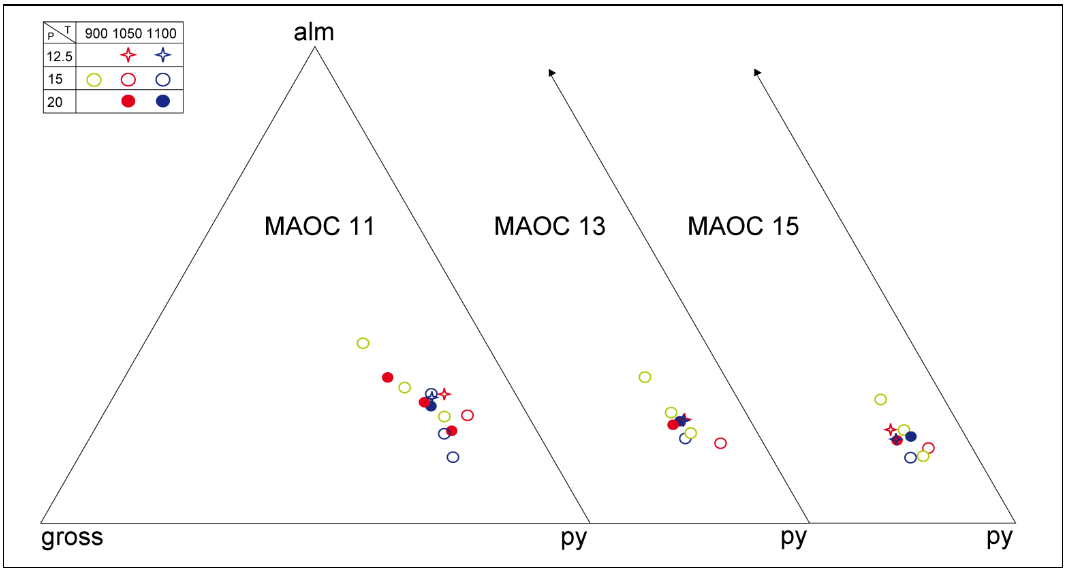

Figure 5.3.12: Almandine–grossular–pyrope triangular plots for garnets from MAOC 11, 13 and 15 at 12.5, 15 and 20 kbar. The pyrope content of garnet increases from MAOC 11 to MAOC 15. For the splitted garnet compositions in MAOC 11 and 13 three marks for each *P*–*T* condition are illustrated, of which the pyrope-rich ones indicate the dark Mg-rich parts, the centered marks are the average values and the marks with a low pyrope content illustrate the light Mg-poor parts.

Table 5.3.2: Garnet in MAOC 11 at 12.5 and 15 kbar. Oxides are given in wt%, # is the number of the accordant analyses, sd is standard deviation. The formulae with ions on the basis of 12 O and the proportions of the end-members pyrope (py), almandine (alm), andradite (andr), grossular (gross) and majorite (ma), Mg# and the composition variable *x(g)* are calculated for the average values. Individual analyses are presented in Appendix B.

	MAOC 11 - garnet																	
P	**12.5**				**15**													
T	**1050**		**1100**		**900**						**1050**				**1100**			
#/sd	10	sd	9	sd	25 tot	sd	15 dark	sd	10 light	sd	16	sd	20 tot	sd	12 dark	sd	8 light	sd
SiO_2	40.936	0.685	40.993	0.189	41.082	1.214	41.399	0.583	40.508	1.652	41.438	0.384	41.459	1.027	42.092	0.765	40.509	0.476
TiO_2	0.580	0.199	0.529	0.103	0.608	0.261	0.482	0.160	0.726	0.257	0.677	0.100	0.434	0.281	0.220	0.072	0.755	0.104
Al_2O_3	21.628	0.772	21.892	0.659	21.220	1.198	21.844	0.675	20.320	1.287	22.207	0.335	22.548	1.047	22.979	1.154	21.900	0.292
FeO	14.288	0.560	13.683	0.485	13.752	3.776	11.226	1.554	17.456	3.010	12.603	0.552	9.907	3.286	7.335	0.717	13.765	0.391
MgO	15.837	0.528	15.746	0.348	14.662	3.172	17.059	1.304	11.198	1.408	17.382	0.560	17.391	1.888	18.828	0.688	15.234	0.266
CaO	6.268	0.428	6.484	0.736	7.360	1.081	6.904	0.780	8.071	1.137	6.347	0.414	7.327	0.862	7.573	1.002	6.958	0.423
Na_2O	0.043	0.037	0.057	0.040	0.065	0.060	0.045	0.046	0.097	0.069	0.077	0.041	0.072	0.064	0.075	0.081	0.068	0.024
Total	99.580	0.424	99.385	0.249	98.749	1.900	98.958	0.462	98.376	3.007	100.731	0.378	99.137	0.410	99.103	0.392	99.188	0.459
mineral formula calculation:																		
Si	2.998		3.000		3.000		3.000		3.000		2.973		3.000		3.000		2.982	
Al	0.002		0.000		0.000		0.000		0.000		0.027		0.000		0.000		0.018	
Z	**3.000**		**3.000**		**3.000**		**3.000**		**3.000**		**3.000**		**3.000**		**3.000**		**3.000**	
Si	0.000		0.004		0.045		0.016		0.075		0.000		0.000		0.012		0.000	
Al	1.866		1.891		1.854		1.876		1.818		1.850		1.923		1.938		1.881	
Fe^{3+}	0.078		0.051		0.000		0.046		0.000		0.115		0.040		0.025		0.063	
Ti	0.032		0.029		0.034		0.026		0.041		0.037		0.024		0.012		0.042	
Y	**1.976**		**1.971**		**1.888**		**1.948**		**1.860**		**2.002**		**1.987**		**1.975**		**1.986**	
Mg	1.729		1.720		1.620		1.853		1.267		1.859		1.876		2.008		1.671	
Fe^{2+}	0.797		0.788		0.852		0.638		1.108		0.641		0.559		0.414		0.784	
Ca	0.492		0.509		0.585		0.539		0.657		0.488		0.568		0.581		0.549	
X	**3.018**		**3.017**		**3.057**		**3.030**		**3.032**		**2.988**		**3.003**		**3.003**		**3.004**	
Total	**7.994**		**7.992**		**7.990**		**7.994**		**7.967**		**7.989**		**7.990**		**7.990**		**7.990**	
py	57.297		56.811		50.613		60.318		37.748		62.217		62.461		66.279		55.643	
alm	26.404		26.107		27.884		21.066		36.550		21.455		18.625		13.784		26.091	
andr	3.961		2.583		0.000		2.342		0.000		5.745		2.019		1.264		3.194	
grs	12.338		14.294		19.120		15.445		21.652		10.583		16.896		18.071		15.071	
ma	0.000		0.205		2.383		0.828		4.050		0.000		0.000		0.602		0.000	
Mg#	68.454		68.592		65.524		74.376		53.349		74.358		77.030		82.912		68.078	
x(g)	0.315		0.314		0.345		0.256		0.467		0.256		0.230		0.171		0.319	

Table 5.3.2 (continued): Garnet in MAOC 11 and 13 at 12.5, 15 and 20 kbar. Oxides are given in wt%, # is the number of the accordant analyses, sd is standard deviation. The formulae with ions on the basis of 12 O and the proportions of the end-members pyrope (py), almandine (alm), andradite (andr), grossular (gross) and majorite (ma), Mg# and the composition variable *x(g)* are calculated for the average values. Individual analyses are presented in Appendix B.

	MAOC 11 - garnet								**MAOC 13 - garnet**													
P	**20**								**12.5**				**15**									
T	**1050**						**1100**		**1050**		**1100**		**900**						**1050**		**1100**	
#/sd	11 tot	sd	8 dark	sd	3 light	sd	18	sd	8 dark	sd	9	sd	9 tot	sd	6 dark	sd	3 light	sd	13	sd	16	sd
SiO_2	41.013	0.909	41.245	0.916	40.393	0.635	41.317	0.219	41.350	0.239	40.952	0.651	41.196	0.888	41.515	0.945	40.557	0.081	41.717	0.384	41.985	0.560
TiO_2	0.599	0.383	0.580	0.415	0.649	0.356	0.721	0.203	0.413	0.126	0.441	0.136	0.479	0.123	0.490	0.120	0.457	0.153	0.590	0.078	0.442	0.196
Al_2O_3	22.140	0.523	22.094	0.599	22.263	0.281	22.217	0.471	22.349	0.442	22.347	0.427	21.893	0.874	22.065	1.009	21.550	0.498	22.485	0.436	22.983	0.645
FeO	11.517	2.793	10.213	1.951	14.997	0.850	12.777	0.561	11.703	0.283	11.599	0.393	11.952	2.776	10.235	1.292	15.387	0.340	10.112	0.569	9.364	1.162
MgO	16.325	2.859	17.629	2.011	12.847	1.328	15.846	0.522	17.489	0.280	17.333	0.375	16.922	1.941	18.168	0.658	14.430	0.089	19.605	0.555	18.839	1.035
CaO	7.264	1.032	6.806	0.738	8.483	0.590	7.520	0.436	6.054	0.413	6.001	0.282	6.372	0.392	6.230	0.385	6.657	0.248	5.710	0.358	6.269	0.529
Na_2O	0.052	0.022	0.047	0.020	0.064	0.028	0.068	0.025	0.066	0.029	0.100	0.058	0.068	0.058	0.080	0.067	0.045	0.033	0.092	0.086	0.066	0.045
Total	98.909	0.716	98.613	0.521	99.696	0.577	100.466	0.325	99.422	0.423	98.773	0.743	98.883	0.899	98.783	1.108	99.082	0.270	100.310	0.513	99.947	0.350
mineral formula calculation:																						
Si	2.999		3.000		2.991		2.990		2.994		2.984		3.000		3.000		3.000		2.963		2.995	
Al	0.001		0.000		0.009		0.010		0.006		0.016		0.000		0.000		0.000		0.037		0.005	
Z	**3.000**		**3.000**		**3.000**		**3.000**		**3.000**		**3.000**		**3.000**		**3.000**		**3.000**		**3.000**		**3.000**	
Si	0.000		0.002		0.000		0.000		0.000		0.000		0.009		0.009		0.007		0.000		0.000	
Al	1.907		1.895		1.935		1.885		1.902		1.903		1.884		1.885		1.883		1.845		1.927	
Fe^{3+}	0.036		0.045		0.011		0.056		0.068		0.078		0.055		0.054		0.058		0.142		0.041	
Ti	0.033		0.032		0.036		0.039		0.022		0.024		0.026		0.027		0.025		0.032		0.024	
Y	**1.976**		**1.972**		**1.982**		**1.980**		**1.992**		**2.006**		**1.966**		**1.975**		**1.974**		**2.018**		**1.991**	
Mg	1.779		1.913		1.418		1.710		1.888		1.883		1.842		1.963		1.595		2.076		2.003	
Fe^{2+}	0.669		0.577		0.918		0.717		0.641		0.629		0.675		0.566		0.896		0.459		0.518	
Ca	0.569		0.531		0.673		0.583		0.470		0.469		0.499		0.484		0.529		0.435		0.479	
X	**3.017**		**3.020**		**3.009**		**3.010**		**2.999**		**2.980**		**3.016**		3.014		3.020		**2.969**		**3.000**	
Total	**7.993**		**7.993**		**7.991**		**7.990**		**7.991**		**7.986**		**7.990**		**7.989**		**7.994**		**7.987**		**7.991**	
py	58.979		63.242		47.134		56.795		62.966		63.185		60.656		64.673		52.460		69.912		66.769	
alm	22.159		19.099		30.496		23.834		21.369		21.092		22.371		18.797		29.669		15.453		17.263	
andr	1.806		2.268		0.560		2.821		3.409		3.901		2.813		2.731		2.944		7.022		2.040	
grs	17.056		15.305		21.810		16.551		12.256		11.822		13.721		13.325		14.568		7.612		13.929	
ma	0.000		0.086		0.000		0.000		0.000		0.000		0.438		0.474		0.359		0.000		0.000	
Mg#	72.689		76.830		60.716		70.440		74.661		74.973		73.197		77.608		64.033		81.897		79.457	
x(g)	0.273		0.232		0.393		0.296		0.253		0.250		0.268		0.224		0.360		0.181		0.205	

Table 5.3.2 (continued): Garnet in MAOC 13 and 15 at 12.5, 15 and 20 kbar. Oxides are given in wt%, # is the number of the accordant analyses, sd is standard deviation. The formulae with ions on the basis of 12 O and the proportions of the end-members pyrope (py), almandine (alm), andradite (andr), grossular (gross) and majorite (ma), Mg# and the composition variable *x(g)* are calculated for the average values. Individual analyses are presented in Appendix B.

	MAOC 13 - garnet				**MAOC 15 - garnet**															
P	**20**				**12.5**				**15**										**20**	
T	**1050**		**1100**		**1050**		**1100**		**900**						**1050**		**1100**		**1050**		**1100**	
#/sd	10	sd	20	sd	5	sd	3 dark	sd	8 tot	sd	4 dark	sd	4 light	sd	6	sd	7	sd	11	sd	20	sd
SiO_2	41.500	0.699	41.874	0.439	42.098	0.361	42.122	1.240	40.911	1.161	41.243	1.034	40.580	1.335	41.968	0.593	42.173	0.647	42.437	0.375	42.279	0.561
TiO_2	0.411	0.123	0.626	0.207	0.266	0.092	0.435	0.132	0.359	0.079	0.355	0.092	0.364	0.079	0.501	0.138	0.330	0.177	0.446	0.182	0.423	0.146
Al_2O_3	22.714	1.035	22.277	0.372	21.680	0.762	20.973	2.179	22.558	1.601	22.963	1.414	22.153	1.882	22.488	0.600	23.653	0.535	22.267	0.577	22.816	0.494
FeO	10.820	1.182	11.641	1.015	10.692	0.288	9.903	0.749	10.876	2.770	8.558	1.570	13.195	1.047	9.573	0.498	7.589	1.088	9.007	1.133	10.192	1.410
MgO	17.583	0.999	17.874	1.170	18.098	0.757	18.173	0.634	17.854	2.152	19.598	1.498	16.110	0.673	20.052	0.493	20.294	1.002	19.472	1.011	19.421	0.909
CaO	6.303	0.611	6.190	0.597	6.492	1.132	6.945	1.758	6.139	0.500	6.113	0.259	6.165	0.718	5.508	0.468	5.900	0.575	5.990	0.630	5.436	0.851
Na_2O	0.081	0.038	0.069	0.020	0.146	0.103	0.282	0.214	0.155	0.174	0.134	0.150	0.176	0.217	0.078	0.041	0.056	0.024	0.095	0.061	0.097	0.092
Total	99.412	0.458	100.549	0.417	35.428	57.473	98.832	0.466	98.852	0.751	98.961	0.322	98.742	1.087	100.168	0.196	99.995	0.363	**99.714**	**0.449**	100.663	0.793
mineral formula calculation:																						
Si	2.998		2.998		3.000		3.000		2.966		2.952		2.979		2.976		2.977		3.000		2.994	
Al	0.002		0.002		0.000		0.000		0.034		0.048		0.021		0.024		0.023		0.000		0.006	
Z	**3.000**		**3.000**		**3.000**		**3.000**		**3.000**		**3.000**		**3.000**		**3.000**		**3.000**		**3.000**		**3.000**	
Si	0.000		0.000		0.034		0.049		0.000		0.000		0.000		0.000		0.000		0.026		0.000	
Al	1.931		1.877		1.841		1.789		1.893		1.890		1.896		1.856		1.945		1.872		1.898	
Fe^{3+}	0.037		0.067		0.082		0.106		0.124		0.138		0.109		0.125		0.051		0.041		0.076	
Ti	0.022		0.034		0.014		0.024		0.020		0.019		0.020		0.027		0.018		0.024		0.023	
Y	**1.991**		**1.978**		**1.938**		**1.918**		**2.036**		**2.047**		**2.025**		**2.008**		**2.013**		**1.963**		**1.997**	
Mg	1.893		1.908		1.944		1.961		1.929		2.091		1.763		2.120		2.136		2.070		2.050	
Fe^{2+}	0.616		0.630		0.562		0.494		0.536		0.374		0.701		0.443		0.397		0.496		0.527	
Ca	0.488		0.475		0.501		0.539		0.477		0.469		0.485		0.419		0.446		0.458		0.412	
X	**2.997**		**3.012**		**3.007**		**2.993**		**2.942**		**2.934**		**2.950**		**2.982**		**2.979**		**3.024**		**2.990**	
Total	**7.989**		**7.990**		**7.980**		**7.960**		**7.978**		**7.981**		**7.975**		**7.989**		**7.992**		**7.987**		**7.987**	
py	63.168		63.324		62.905		62.962		65.585		71.273		59.782		71.099		71.687		67.109		68.574	
alm	20.557		20.914		18.682		16.499		18.207		12.750		23.776		14.863		13.333		16.410		17.632	
andr	1.879		3.381		4.256		5.500		6.074		6.749		5.375		6.207		2.521		2.084		3.825	
grs	14.396		12.381		12.412		12.493		10.133		9.228		11.068		7.831		12.458		13.051		9.969	
ma	0.000		0.000		1.745		2.545		0.812		0.000		0.000		0.000		0.000		1.346		0.000	
Mg#	75.447		75.173		77.581		79.881		78.271		84.826		71.545		82.710		84.317		80.663		79.547	
x(g)	0.246		0.248		0.224		0.201		0.217		0.152		0.285		0.173		0.157		0.193		0.205	

The dominant end-member in garnet is pyrope with increasing values towards higher MgO in the bulk rock composition (Fig. 5.3.12). Mg# increases similarly from MAOC 11 to MAOC 15 and the average values vary in MAOC 11 between 65.5 (15 kbar/900 °C) and 77.0 (15 kbar/1100 °C), in MAOC 13 from 74.7 (12.5 kbar/ 1050 °C) and 81.9 (15 kbar/1050 °C) and in MAOC 15 between 77.6 (12.5 kbar/ 1050 °C) and 84.3 (15 kbar/1100 °C). No *P–T* dependent trend is apparent except of the fact that the highest Mg# and proportions of the pyrope component emerge at 15 kbar.

Al and Ti on the Y position and Fe^{2+} on the X position decrease from MAOC 11 to 15 and Ca on the X position decreases from MAOC 11 to 13 with scattering values in MAOC 15.

5.3.3.3 Amphibole

The proportion of amphibole increases from MAOC 11 to MAOC 15 beginning with an accessory amount in MAOC 11 (15 kbar/900 °C, 12.5 kbar/1050 °C) to a higher abundance of amphibole in MAOC 15 (in several assemblages from 10 to 15 kbar). Table 5.3.3 shows the average values of the microprobe analyses and the formula calculated according to Schumacher (1997, in: Leake *et al.*, 1997, their Appendix 2) given in terms of $AB_2C_5T_8O_{22}(OH)_2$, composed of one A site (A), two M4 sites (B), 2 M1, 2 M2 and 1 M3 sites (C), eight T sites (T) and OH (Leake *et al.*, 1997). The distribution of elements on sites as well as the formula calculation for the average values are presented in Tab. 5.3.3. The formulae given are the average from minimum and maximum calculations according to Schumacher (1997 in: Leake *et al.*, 1997, their Appendix 2) to allow a better estimation of the proportion of ferric iron according to several stoichiometric limits. The possible types of minimum and maximum calculations are *all* Fe^{2+}, *13eCNK* (13 cations excluding Ca, Na and K), *15eK* (15 cations excluding K), *15eNK* (15 cations excluding Na and K) and *all* Fe^{3+}. The resulting formulae correspond to different subdivisions of the calcic amphibole group (Leake *et al.,* 1997). Calcic amphiboles are defined by $(Ca + Na)_B \geq 1.00$ and $Na_B < 0.50$ (Leake *et al.*, 1997) and the composition varies within the calcic amphiboles with Mg#, the total number of Si in the formula and by (Na + K) on the A position (Fig. 5.3.13), whereas in this study no K was existent in the original oxide mixes (Tab. 5.2.3) The formula calculation of the averaged analyses in this study indicate that calcic amphiboles cover the compositional range of $Ca_2[Mg_4(Al,Fe^{3+})]Si_7AlO_{22}(OH)_2$ (magnesiohornblende),

$Ca_2(Mg_3AlFe^{3+})Si_6Al_2O_{22}(OH)_2$ (tschermakite) and $NaCa_2(Mg_4Al)Si_6Al_2O_{22}(OH)_2$ (pargasite).

Small amounts of magnesiohornblende (15 kbar/900 °C) and tschermakite (12.5 kbar/1050 °C) are developed in MAOC 11. Amphibole stability in MAOC 13 is limited to 10 kbar/1050 °C (pargasite and a small amount of tschermakite), 12.5 kbar/1050 °C (one magnesiohornblende) and 15 kbar/900 °C (mainly tschermakite and one magnesiohornblende). Amphibole is stable in five MAOC 15 assemblages, dominated by pargasite at 10 kbar/1050 °C, 12.5 kbar/1050 °C and 15 kbar/1100 °C as well as little tschermakite (10 kbar/1050 °C) and magnesiohornblende (12.5 kbar/ 1050 °C). Tschermakite also occurs at 15 kbar/900 °C together with a small amount of magnesiohornblende.

The most Si-rich amphiboles were generated under subsolidus conditions at 900 °C and the increasing MgO in the bulk compositions towards MAOC 15 is reflected in generally higher Mg on the C position, accompanied by an enrichment of Ti on the C position.

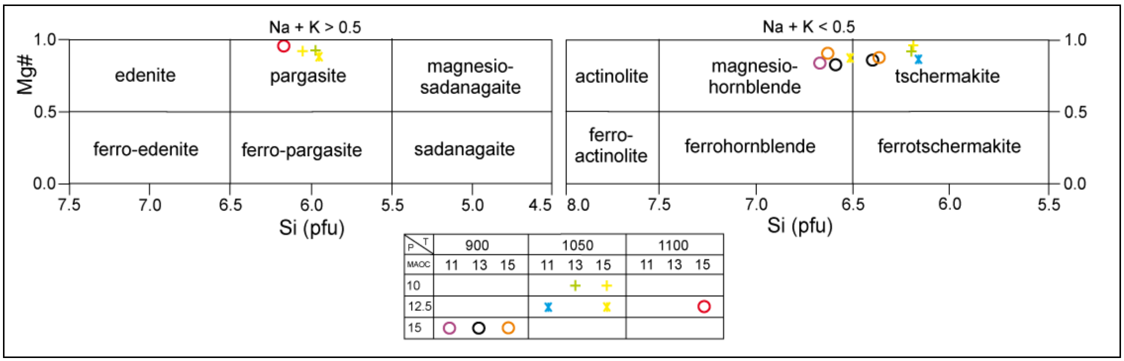

Figure 5.3.13: Classification of the calcic amphiboles in MAOC 11, 13 and 15 according to Leake *et al.* (1997), depending on Mg# and the total number of Si in the formula and separated by the amount of Na on the A position, since K is was not existent in the MAOC mixes. The amphiboles plot in the ranges of pargasite, magnesiohornblende and tschermakite. For some *P–T* conditions, two types of amphiboles were determined.

Table 5.3.3: Amphiboles in MAOC 11 and MAOC 13 at 10, 12.5 and 15 kbar. Oxides are given in wt%, # is the number of accordant analyses, sd is standard deviation. The formulae for the average values are calculated after Schumacher (1997, in: Leake *et al.*, 1997, their Appendix 2), with declaration of the form of minimum (min) and maximum (max) calculation as well as Mg#. Individual analyses are presented in Appendix B.

	MAOC 11 - amphibole				**MAOC 13 - amphibole**						
P	**12.5**		**15**		**10**			**12.5**	**15**		
T	**1050**		**900**		**1050**			**1050**	**900**		
#/sd	2	sd	2	sd	11	sd	1	1	8	sd	1
SiO_2	43.755	0.460	46.940	0.311	42.305	0.662	44.540	47.170	44.701	0.294	46.450
TiO_2	0.777	0.195	1.082	0.005	0.823	0.196	0.695	0.765	1.042	0.060	0.802
Al_2O_3	15.765	1.322	11.875	0.488	16.822	0.638	15.250	11.210	13.638	0.393	12.520
FeO	11.340	0.622	7.380	0.665	5.670	0.440	6.670	9.220	8.886	0.391	8.960
MgO	13.760	0.665	16.220	1.344	17.615	0.297	19.590	16.050	15.543	0.505	15.540
CaO	12.230	1.160	11.345	1.393	10.930	1.019	8.610	13.300	10.326	0.537	11.110
Na_2O	0.551	0.162	2.095	0.247	3.297	0.180	2.840	1.004	2.216	0.106	2.000
Total	98.178	0.630	96.937	0.290	97.462	0.510	98.195	98.719	96.352	0.530	97.382
name	tschermakite		mg-hbl.		parg.		tscherm.	mg-hbl.	tschermakite		mg-hbl.
min	*15 eNK*		*all Fe^{2+}*		*15 eNK*		*15 eNK*		*all Fe^{2+}*		*all Fe^{3+}*
max	*15 eK*		*13 eCNK*		*all Fe3^{+}*		*all Fe^{3+}*		*all Fe3^{+}*		*13 eCNK*
Si	6.160		6.665		5.978		6.195	formula	6.397		6.588
Al IV	1.840		1.335		2.022		1.805	calc.	1.603		1.412
<u>T</u>	**8.000**		**8.000**		**8.000**		**8.000**	failed	**8.000**		**8.000**
Al VI	0.776		0.652		0.779		0.694		0.697		0.681
Ti	0.082		0.115		0.087		0.073		0.112		0.086
Fe^{3+}	0.899		0.270		0.363		0.425		0.526		0.402
Mg	2.888		3.433		3.711		4.062		3.316		3.286
Fe^{2+}	0.355		0.529		0.060		0.000		0.350		0.545
<u>C</u>	**5.000**		**5.000**		**5.000**		**5.254**		**5.000**		**5.000**
Fe^{2+}	0.081		0.077		0.247		0.351		0.188		0.116
Ca	1.845		1.726		1.655		1.283		1.583		1.688
Na	0.075		0.197		0.099		0.367		0.229		0.196
<u>B</u>	**2.000**		**2.000**		**2.000**		**2.000**		**2.000**		**2.000**
Na	0.076		0.380		0.805		0.399		0.386		0.354
<u>A</u>	**0.076**		**0.380**		**0.805**		**0.399**		**0.386**		**0.354**
Total	**15.076**		**15.380**		**15.805**		**15.653**		**15.386**		**15.354**
Mg#	0.869		0.850		0.924		0.921		0.860		0.833

Table 5.3.3 (continued): Amphiboles in MAOC 15 at 10, 12.5, 15 and 20 kbar. Oxides are given in wt%, # is the number of accordant analyses, sd is standard deviation. The formulae for the average values are calculated after Schumacher (1997, in: Leake *et al.*, 1997, their Appendix 2), with declaration of the form of minimum (min) and maximum (max) calculation as well as Mg#. Individual analyses are presented in Appendix B.

	MAOC 15 - amphibole									
P	**10**			**12.5**			**15**			
T	**1050**			**1050**			**900**			**1100**
#/sd	7	sd	1	16	sd	1	3	sd	1	17	sd
SiO_2	42.669	0.350	44.950	41.658	0.507	47.410	44.583	0.530	47.620	44.084	0.781
TiO_2	1.091	0.360	1.186	1.611	0.147	0.602	0.924	0.153	0.534	1.044	0.151
Al_2O_3	16.326	0.995	14.820	16.826	0.490	14.690	14.413	0.578	11.310	15.741	0.893
FeO	5.089	0.630	5.530	7.381	0.171	8.500	7.483	0.719	8.710	2.861	0.365
MgO	17.804	0.724	21.330	16.035	0.278	15.970	15.970	0.385	20.610	19.661	0.429
CaO	10.556	0.335	8.310	9.380	0.232	11.480	10.310	0.137	7.010	10.001	0.623
Na_2O	3.156	0.183	2.360	3.830	0.118	0.893	2.460	0.105	1.660	3.748	0.135
Total	96.689	0.710	98.486	96.721	0.340	99.545	96.144	0.250	97.454	97.140	0.540
name	parg.		tscherm.	parg.		mg-hbl.	tschermakite		mg-hbl.	parg.	
min	*all Fe^{2+}*		*15 eNK*	*all Fe^{2+}*		*15 eNK*	*all Fe^{2+}*		*15 eNK*	*all Fe^{2+}*	
max	*all Fe^{3+}*		*all Fe^{3+}*	*all Fe^{3+}*		*15 eK*	*all Fe^{3+}*		*all Fe^{3+}*	*all Fe^{3+}*	
Si	6.056		6.184	5.957		6.509	6.366		6.625	6.175	
Al	1.944		1.816	2.043		1.491	1.634		1.375	1.825	
T	**8.000**		**8.000**	**8.000**		**8.000**	**8.000**		**8.000**	**8.000**	
Al	0.786		0.587	0.792		0.886	0.791		0.479	0.773	
Ti	0.116		0.123	0.173		0.062	0.099		0.056	0.110	
Fe^{3+}	0.300		0.465	0.437		0.478	0.442		0.601	0.167	
Mg	3.767		4.375	3.418		3.269	3.399		4.275	4.105	
Fe^{2+}	0.030		0.000	0.179		0.305	0.268		0.000	0.000	
C	**5.000**		**5.549**	**5.000**		**5.000**	**5.000**		**5.410**	**5.155**	
Fe^{2+}	0.274		0.171	0.266		0.193	0.183		0.413	0.168	
Ca	1.605		1.225	1.437		1.689	1.577		1.045	1.501	
Na	0.121		0.605	0.297		0.118	0.239		0.448	0.331	
B	**2.000**		**2.000**	**2.000**		**2.000**	**2.000**		**1.905**	**2.000**	
Na	0.747		0.025	0.765		0.120	0.442		0.000	0.687	
A	**0.747**		**0.025**	**0.765**		**0.120**	**0.442**		**0.000**	**0.687**	
Total	**15.747**		**15.574**	**15.765**		**15.120**	**15.442**		**15.316**	**15.842**	
Mg#	0.925		0.962	0.885		0.868	0.883		0.912	0.961	

5.3.3.4 Clinopyroxene

Clinopyroxene forms a major phase in all assemblages of this study and exhibits a wide range of chemical compositions. Pyroxenes have the general formula [(M2)(M1)$(Si,Al)_2O_6$] (Deer *et al.*, 1992), whereas clinopyroxene is a Ca-bearing monoclinic pyroxene and omphacite is an end-member of the calcium-sodium pyroxene subgroup (*Deer et al.*, 1992), which also needs to be considered in this study. The averaged microprobe analyses for clinopyroxenes in each experimental run with the appropriate formula, determined on the basis of six oxygen and elements distributed on X (M2 and M1) and Z ($(Si,Al)_2$) are presented in Tab. 5.3.4. The end-member proportions enstatite $Mg_2Si_2O_6$ (en), ferrosilite $Fe_2Si_2O_6$ (fs) and wollastonite $Ca_2Si_2O_6$ (wo) as well as Mg#, Q (Ca + Mg + Fe^{2+}) and J (2 Na) and the composition variable *j(di)* = xNaM2c + xNaM2n/2 as applied by THERMOCALC (Green *et al.*, 2007; subchapter 4.2.1) are also presented.

Morimoto *et al.* (1988) divided clinopyroxenes into the following four groups: Ca–Mg–Fe pyroxenes (Quad), Ca–Na pyroxenes (Ca–Na), Na pyroxenes (Na) and other pyroxenes (Others) of which Quad and Ca–Na pyroxenes are of interest in this study. Figures 5.3.14a-c present the classification of clinopyroxene in the Q–J diagram with Q = (Ca + Mg + Fe^{2+}) and J = 2 Na. Most of the average compositions of clinopyroxenes (Tab. 5.3.4) plot in the field for Quad, only those at 20 kbar/1100 °C (MAOC 13 and MAOC 15) plot at the border to Ca–Na pyroxenes, which implies the incorporation of a Na-component. The classification of the Na and Ca–Na pyroxenes is further presented in the Quad–Jd–Ae diagrams for the MAOC compositions (Fig. 5.3.15a) with Quad (Wo + En + Fs), Jd (jadeite $NaAlSi_2O_6$) and Ae (aegirine $NaFe^{3+}Si_2O_6$) components (Morimoto *et al,* 1988). The results from these diagrams match those of the Q–J diagrams (Fig. 5.3.14) where the compositions at 20 kbar/ 1100 °C (MAOC 13 and MAOC 15) are close to, but not really matching, the field of Ca–Na pyroxene (omphacite). The amount of Si increases with pressure whilst Al IV decreases. The remaining average compositions plot in the field for Quad and all clinopyroxenes (including the two Ca–Na pyroxenes at 20 kbar/1100 °C) are plotted in terms of Wo–En–Fs in the Ca–Mg–Fe pyroxene triangle diagram (Fig. 5.3.15b).

The clinopyroxene composition from MAOC 11 to 15 is sensitive to the bulk rock compositions and show accompanied increased proportions of the mean Mg on X and Mg#. The clinopyroxenes generally straddle the boundary of diopside and augite with no characteristic spreading within a bulk rock composition but with a trend to more augitic compositions towards higher MgO in the bulk rock composition (Fig 5.3.15b).

The compositions of clinopyroxenes in MAOC 11 straddle the boundary between augite and diopside, even in individual assemblages (Appendix B) and there is no obvious *P*–*T* trend (Fig. 5.3.15b). At 10 and 12.5 kbar/1100 °C and 15 kbar/900 °C the clinopyroxene plots in the augite field and at 15 and 20 kbar/1100 °C in the diopside field. To higher *P*, a trend of an increasing proportion of the omphacite end-member is apparent (Fig. 5.3.14), but no true omphacite is developed which is consistent with the thermodynamic calculations in subchapter 4.3.

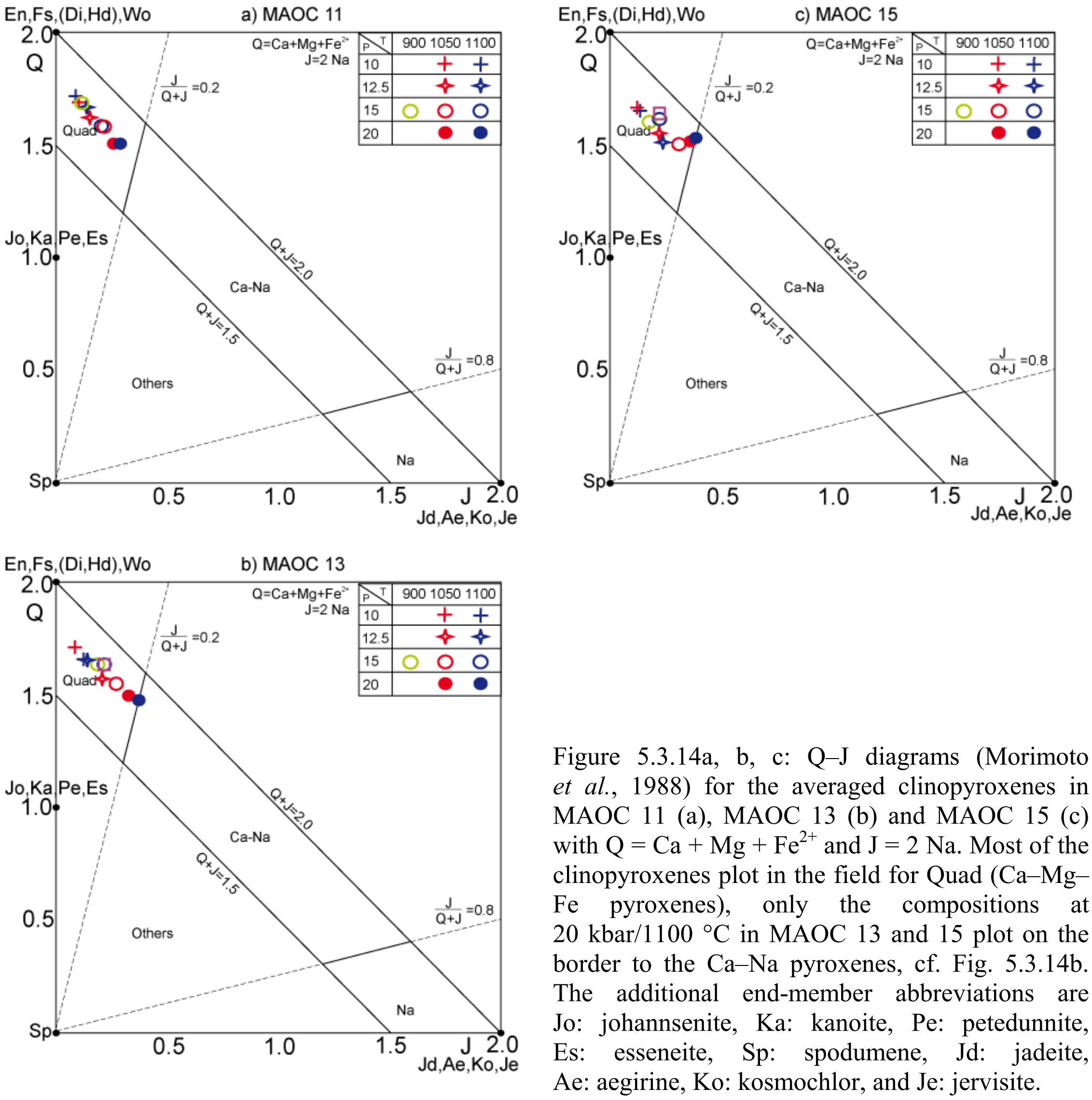

Figure 5.3.14a, b, c: Q–J diagrams (Morimoto *et al.*, 1988) for the averaged clinopyroxenes in MAOC 11 (a), MAOC 13 (b) and MAOC 15 (c) with Q = Ca + Mg + Fe^{2+} and J = 2 Na. Most of the clinopyroxenes plot in the field for Quad (Ca–Mg–Fe pyroxenes), only the compositions at 20 kbar/1100 °C in MAOC 13 and 15 plot on the border to the Ca–Na pyroxenes, cf. Fig. 5.3.14b. The additional end-member abbreviations are Jo: johannsenite, Ka: kanoite, Pe: petedunnite, Es: esseneite, Sp: spodumene, Jd: jadeite, Ae: aegirine, Ko: kosmochlor, and Je: jervisite.

Table 5.3.4: Clinopyroxenes in MAOC 11 at 10, 12.5, 15 and 20 kbar. Oxides are given in wt%, # is the number of accordant analyses, sd is standard deviation. The formulae with ions on the basis of 6 O and the proportions of the end-members enstatite (En), ferrosilite (Fs) and wollastonite (Wo), Mg#, Q (Ca + Mg + Fe^{2+}) and J (2 Na) are calculated for the average values. Individual analyses are presented in Appendix B.

	MAOC 11 - clinopyroxene																	
P	**10**				**12.5**				**15**						**20**			
T	**1050**		**1100**		**1050**		**1100**		**900**		**1050**		**1100**		**1050**		**1100**	
#/sd	11	sd	13	sd	10	sd	16	sd	10	sd	17	sd	12	sd	14	sd	20	sd
SiO_2	48.843	0.885	48.330	0.679	47.540	1.165	48.292	0.583	49.094	1.322	49.661	1.604	50.108	0.651	49.456	1.000	50.965	0.929
TiO_2	0.874	0.142	1.088	0.187	1.083	0.233	0.968	0.158	0.690	0.122	0.824	0.171	0.706	0.142	0.654	0.139	0.680	0.099
Al_2O_3	9.458	0.305	8.962	0.682	10.446	0.994	9.739	0.722	8.351	1.247	10.714	1.923	10.833	1.043	11.863	1.737	11.053	1.425
FeO	4.919	1.036	6.165	0.843	8.353	0.662	7.140	0.520	7.590	1.213	6.515	0.713	3.943	0.875	6.441	0.900	5.109	0.689
MgO	14.998	0.488	14.832	0.734	12.493	0.573	13.677	0.358	14.525	0.814	12.381	1.040	13.788	0.761	11.934	0.949	12.281	0.993
CaO	19.600	0.604	18.502	0.588	18.403	0.977	17.638	0.800	17.714	1.395	18.201	0.899	18.895	0.649	16.936	0.959	18.154	0.431
Na_2O	0.741	0.080	0.628	0.126	1.068	0.331	0.921	0.133	0.789	0.271	1.530	0.261	1.452	0.176	1.889	0.408	2.006	0.185
Total	99.433	0.916	98.507	0.236	99.386	0.842	98.374	0.539	98.753	0.690	99.826	0.635	99.725	0.318	99.173	0.315	100.246	0.533
mineral formula calculation:																		
Si	1.783		1.790		1.760		1.795		1.819		1.812		1.812		1.809		1.836	
Al IV	0.217		0.210		0.240		0.205		0.181		0.188		0.188		0.191		0.164	
Z	**2.000**		**2.000**		**2.000**		**2.000**		**2.000**		**2.000**		**2.000**		**2.000**		**2.000**	
Al VI	0.190		0.181		0.215		0.222		0.184		0.273		0.274		0.320		0.306	
Fe^{3+}	0.031		0.014		0.041		0.000		0.016		0.000		0.000		0.000		0.000	
Ti	0.024		0.030		0.030		0.027		0.019		0.023		0.019		0.018		0.018	
Mg	0.816		0.819		0.689		0.758		0.802		0.673		0.743		0.651		0.660	
Fe^{2+}	0.119		0.177		0.217		0.222		0.219		0.199		0.119		0.197		0.154	
Ca	0.767		0.734		0.730		0.703		0.703		0.712		0.732		0.664		0.701	
Na	0.052		0.045		0.077		0.066		0.057		0.108		0.102		0.134		0.140	
X	**2.000**		**2.000**		**2.000**		**1.998**		**2.000**		**1.988**		**1.989**		**1.983**		**1.979**	
Total	**4.000**		**4.000**		**4.000**		**3.998**		**4.000**		**3.988**		**3.989**		**3.983**		**3.979**	
En	47.955		47.335		42.123		45.050		46.511		42.521		46.612		43.052		43.557	
Fs	7.004		10.228		13.281		13.193		12.721		12.552		7.477		13.034		10.165	
Wo	45.042		42.437		44.597		41.757		40.768		44.927		45.912		43.913		46.278	
Mg#	87.256		82.231		76.029		77.349		78.523		77.208		86.177		76.760		81.079	
Q	1.702		1.730		1.637		1.682		1.725		1.584		1.594		1.511		1.515	
J	0.105		0.090		0.153		0.133		0.113		0.217		0.204		0.268		0.280	

Table 5.3.4 (continued): Clinopyroxenes in MAOC 13 at 10, 12.5, 15 and 20 kbar. Oxides are given in wt%, # is the number of accordant analyses, sd is standard deviation. The formulae with ions on the basis of 6 O and the proportions of the end-members enstatite (En), ferrosilite (Fs) and wollastonite (Wo), Mg#, Q (Ca + Mg + Fe^{2+}) and J (2 Na) are calculated for the average values. Individual analyses are presented in Appendix B.

	MAOC 13 - clinopyroxene																	
P	**10**				**12.5**				**15**						**20**			
T	**1050**		**1100**		**1050**		**1100**		**900**		**1050**		**1100**		**1050**		**1100**	
#/sd	20	sd	7	sd	19	sd	12	sd	7	sd	15	sd	9	sd	14	sd	17	sd
SiO_2	48.515	0.741	47.389	0.890	47.497	0.881	47.944	1.108	47.784	1.104	49.239	1.056	51.384	0.497	51.594	1.521	51.684	0.663
TiO_2	0.823	0.253	1.106	0.280	0.926	0.107	0.908	0.193	0.606	0.084	0.800	0.129	0.602	0.094	0.701	0.208	0.701	0.073
Al_2O_3	9.414	0.808	10.656	1.124	10.843	1.102	9.878	1.162	11.331	0.896	10.577	1.098	8.871	0.862	10.004	0.933	10.374	1.217
FeO	6.171	1.149	5.597	1.246	7.266	0.588	6.709	0.573	7.503	0.884	7.208	0.326	2.933	1.125	5.620	0.873	5.409	0.798
MgO	14.477	0.752	13.894	0.931	12.674	0.866	13.977	0.445	12.227	1.048	12.873	0.689	15.489	0.422	12.945	0.747	12.392	0.821
CaO	19.289	1.119	18.594	0.469	17.907	0.599	17.178	1.006	17.660	1.086	16.931	0.401	18.990	0.784	16.161	0.622	16.839	0.473
Na_2O	0.804	0.183	0.825	0.151	1.461	0.343	1.187	0.307	1.384	0.227	1.889	0.186	1.534	0.148	2.340	0.410	2.696	0.366
Total	99.455	0.570	98.060	0.360	98.575	0.381	97.780	0.983	98.496	0.284	99.517	0.405	99.803	0.790	99.365	0.700	100.094	0.333
mineral formula calculation:																		
Si	1.778		1.760		1.760		1.790		1.775		1.801		1.848		1.870		1.863	
Al IV	0.222		0.240		0.240		0.210		0.225		0.199		0.152		0.130		0.137	
Z	**2.000**		**2.000**		**2.000**		**2.000**		**2.000**		**2.000**		**2.000**		**2.000**		**2.000**	
Al VI	0.181		0.227		0.233		0.218		0.271		0.257		0.230		0.297		0.304	
Fe^{3+}	0.051		0.011		0.060		0.031		0.020		0.031		0.000		0.000		0.000	
Ti	0.023		0.031		0.026		0.025		0.017		0.022		0.016		0.019		0.019	
Mg	0.790		0.769		0.700		0.776		0.677		0.702		0.831		0.699		0.666	
Fe^{2+}	0.141		0.163		0.165		0.178		0.213		0.190		0.088		0.170		0.163	
Ca	0.760		0.740		0.711		0.685		0.703		0.664		0.732		0.628		0.651	
Na	0.058		0.059		0.105		0.086		0.100		0.134		0.107		0.164		0.188	
X	**1.999**		**2.000**		**2.000**		**1.999**		**2.000**		**1.999**		**1.998**		**1.978**		**1.991**	
Total	**3.999**		**4.000**		**4.000**		**3.999**		**4.000**		**3.999**		**3.998**		**3.978**		**3.991**	
En	47.165		46.006		44.428		47.328		42.516		45.138		50.317		46.711		45.014	
Fs	8.353		9.742		10.457		10.866		13.349		12.190		5.345		11.376		11.022	
Wo	44.482		44.251		45.115		41.806		44.135		42.671		44.339		41.913		43.965	
Mg#	84.955		82.525		80.947		81.328		76.105		78.736		90.398		80.416		80.331	
Q	1.691		1.672		1.576		1.639		1.592		1.555		1.651		1.497		1.480	
J	0.115		0.119		0.210		0.171		0.199		0.268		0.214		0.329		0.377	

Table 5.3.4 (continued): Clinopyroxenes in MAOC 15 at 10, 12.5, 15 and 20 kbar. Oxides are given in wt%, # is the number of accordant analyses, sd is standard deviation. The formulae with ions on the basis of 6 O and the proportions of the end-members enstatite (En), ferrosilite (Fs) and wollastonite (Wo), Mg#, Q (Ca + Mg + Fe^{2+}) and J (2 Na) are calculated for the average values. Individual analyses are presented in Appendix B.

	MAOC 15 - clinopyroxene																	
P	**10**				**12.5**				**15**						**20**			
T	**1050**		**1100**		**1050**		**1100**		**900**		**1050**		**1100**		**1050**		**1100**	
#/sd	16	sd	12	sd	20	sd	3	sd	9	sd	11	sd	12	sd	11	sd	16	sd
SiO_2	49.072	0.530	48.380	1.178	47.530	0.686	47.469	1.934	48.196	0.553	50.024	1.343	51.072	0.709	52.490	1.048	52.999	0.447
TiO_2	0.702	0.212	0.818	0.178	0.864	0.107	0.913	0.191	0.667	0.081	0.850	0.167	0.574	0.094	0.629	0.185	0.654	0.084
Al_2O_3	9.441	0.599	9.781	0.731	10.977	1.058	12.673	2.306	10.003	0.976	10.540	1.326	9.216	0.915	8.830	0.941	8.170	0.983
FeO	4.915	0.565	4.631	1.459	7.114	0.705	6.697	1.177	7.932	0.541	6.385	0.793	3.030	0.766	4.870	0.968	4.890	0.786
MgO	14.793	0.399	15.100	1.174	12.956	0.912	14.577	0.239	14.956	1.006	13.388	1.085	15.356	0.491	15.124	0.847	14.900	0.427
CaO	19.740	0.451	18.663	0.471	17.752	0.605	14.750	0.674	15.447	1.090	15.751	0.964	19.115	1.186	14.758	0.696	15.614	1.048
Na_2O	0.924	0.080	0.951	0.157	1.559	0.267	1.676	0.648	1.259	0.236	2.315	0.254	1.601	0.240	2.556	0.375	2.703	0.498
Total	99.586	0.254	98.325	0.531	98.751	0.418	98.755	0.377	98.459	0.379	99.252	0.284	99.964	0.193	99.258	0.500	99.931	0.479
mineral formula calculation:																		
Si	1.787		1.779		1.753		1.734		1.778		1.823		1.834		1.892		1.903	
Al IV	0.213		0.221		0.247		0.266		0.222		0.177		0.166		0.108		0.097	
Z	**2.000**		**2.000**		**2.000**		**2.000**		**2.000**		**2.000**		**2.000**		**2.000**		**2.000**	
Al VI	0.192		0.203		0.230		0.280		0.213		0.276		0.224		0.267		0.249	
Fe^{3+}	0.047		0.039		0.079		0.054		0.061		0.018		0.022		0.000		0.001	
Ti	0.019		0.023		0.024		0.025		0.019		0.023		0.016		0.017		0.018	
Mg	0.803		0.828		0.712		0.794		0.822		0.727		0.822		0.813		0.798	
Fe^{2+}	0.102		0.103		0.140		0.151		0.183		0.177		0.069		0.147		0.146	
Ca	0.770		0.735		0.702		0.577		0.610		0.615		0.736		0.570		0.601	
Na	0.065		0.068		0.111		0.119		0.090		0.164		0.112		0.179		0.188	
X	**1.999**		**1.999**		**1.999**		**2.000**		**1.999**		**2.000**		**2.000**		**1.993**		**2.000**	
Total	**3.999**		**3.999**		**3.999**		**4.000**		**3.999**		**4.000**		**4.000**		**3.993**		**4.000**	
En	47.923		49.685		45.838		52.167		50.882		47.877		50.541		53.135		51.642	
Fs	6.113		6.178		9.021		9.893		11.346		11.640		4.241		9.598		9.462	
Wo	45.964		44.137		45.141		37.940		37.772		40.483		45.218		37.267		38.896	
Mg#	88.687		88.940		83.556		84.059		81.767		80.442		92.258		84.700		84.516	
Q	1.675		1.666		1.554		1.522		1.616		1.519		1.627		1.530		1.545	
J	0.130		0.136		0.223		0.238		0.180		0.327		0.223		0.357		0.376	

The analyses of clinopyroxene in MAOC 13 predominantly plot in the field of augite and this type is developed exclusively at 12.5 kbar/1100 °C and 20 kbar/1050 °C. In addition, the composition also straddles the field of diopside, especially at 900 °C and 1050 °C at 10 and 12.5 kbar. At 12.5 kbar/1050 °C the analyses plot in the field of diopside. The proportion of the Ca–Na pyroxene component increases towards higher *P* to an omphacitic average composition at 20 kbar/1100 °C (Fig. 5.3.14).

Clinopyroxenes in MAOC 15 exhibit a decrease in their wollastonite end-member proportion giving way to more augitic compositions in MAOC 15 especially at higher *P*. The amount of diopside increases to lower *P* and it is the dominant clinopyroxene at 10 and 12.5 kbar/1050 °C. Omphacite has developed at 20 kbar/ 1100 °C (Fig. 5.3.14).

In summary, the composition of clinopyroxene changes with increasing MgO in the bulk rock composition from more diopsidic to augitic compositions and to higher pressures towards omphacite.

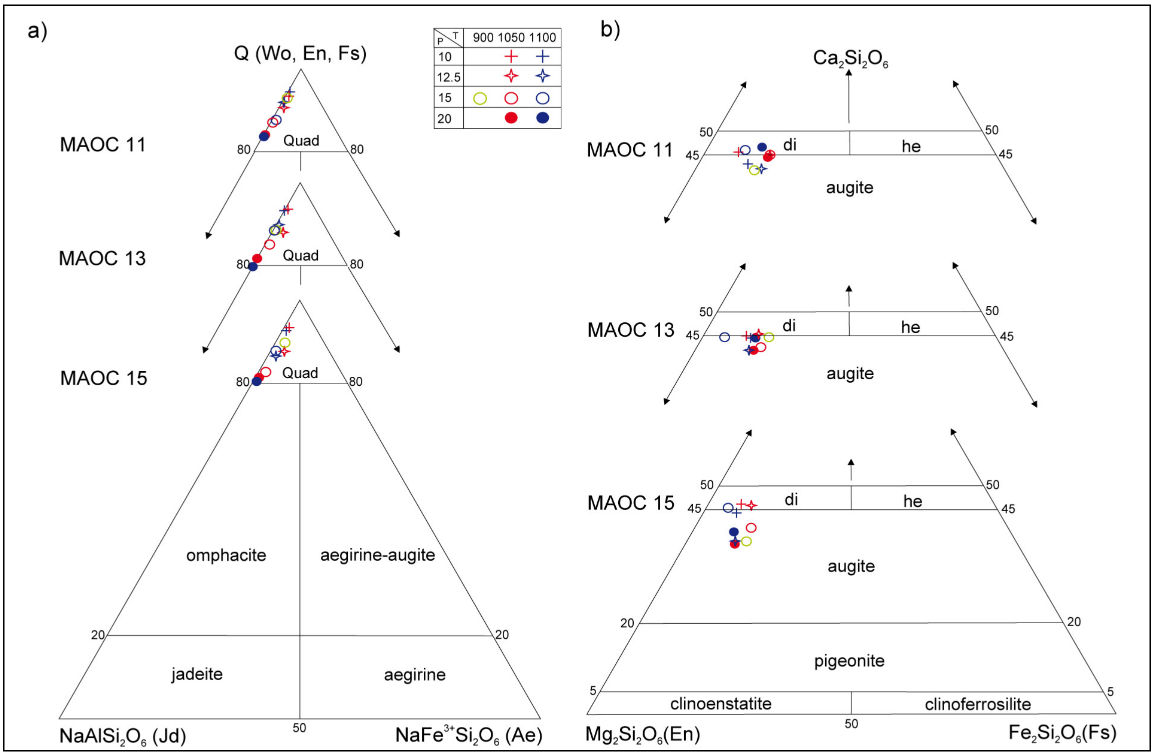

Figure 5.3.15 a, b: Plots for clinopyroxenes after Morimoto *et al.* (1988). Fig. 5.3.15a represents Ca–Mg–Fe and Na pyroxenes in the Q–jadeite–aegirine triangular with Q representing the Ca–Mg–Fe pyroxene area. The Ca–Mg–Fe pyroxenes are illustrated in Fig. 5.3.15b in the wollastonite–enstatite–ferrosilite triangular plot, being diopside and augite, whereas the augite end-member generally increases from MAOC 11 to 15. Note that for 20 kbar/1100 °C (MAOC 13 and 15) the compositions are outside the field for Quad, but regardless of this they are also plotted in Fig. 5.3.14b for comparison.

5.3.3.5 Orthopyroxene

The proportion of orthopyroxene in the assemblages increases from MAOC 11 to MAOC 15. Orthopyroxene is an orthorhombic, largely Ca-free pyroxene belonging to the magnesium-iron pyroxenes (Deer *et al.*, 1992) with the same general formula and mineral formula calculation as for clinopyroxene (subchapter 5.3.3.4). The distribution of Mg and Fe on M2 and M1 subdivides orthopyroxenes into enstatite (en; 50–100 en), and ferrosilite (fs; 0–50 en). The averaged oxides, the calculated mineral formulae, the end-members En, Fs and Wo, Mg# and the composition variable *x(opx)* (subchapter 3.1.2.2.5) for each assemblage are given in Tab. 5.3.5. Figure 5.3.16 illustrates the orthopyroxenes in the En–Fs–Wo triangle indicating that the composition is bronzite in most assemblages with a general increase in the proportion of enstatite related to the increase of MgO in the bulk rock composition.

Orthopyroxene is rare in MAOC 11, the phase occurs only at 10 kbar/1100 °C and in the 12.5 kbar assemblages, with the highest enstatite content reached at 10 kbar. The stability of orthopyroxene in MAOC 13 is enlarged to 10 kbar/1050 °C and 15 kbar/900 °C, whereas the highest proportion of the end-member enstatite is reached again at 10 kbar. Orthopyroxene in MAOC 15 is stable in most of the assemblages with the exception of 20 kbar/1100 °C. The proportion of the Mg end-member is higher than in MAOC 11 and 13 and at 10 kbar/1100 °C and 15 kbar/1100 °C the compositions of orthopyroxene in MAOC 15 have the highest enstatite content.

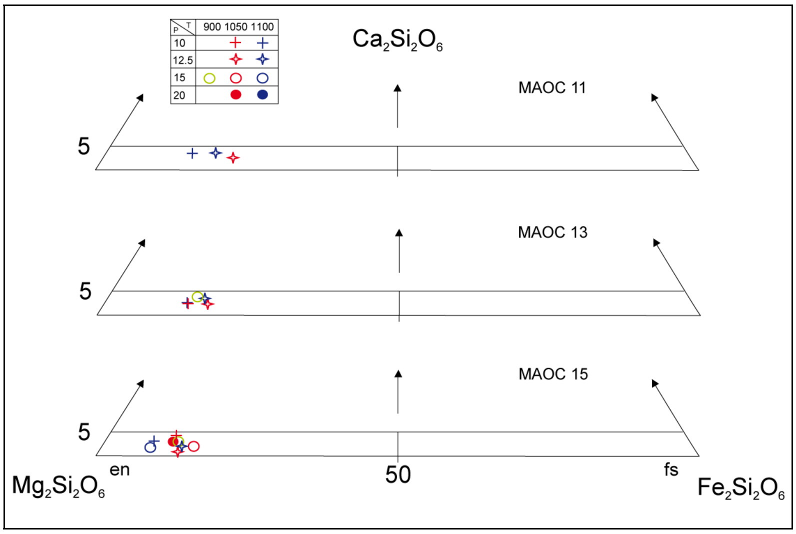

Figure 5.3.16: Classification of the orthopyroxenes in MAOC 11, 13 and 15. The stability of orthopyroxene increases in assemblages from MAOC 11 to MAOC 15 with an accompanying shift to Mg-richer compositions.

Table 5.3.5: Orthopyroxenes in MAOC 11 and MAOC 13 at 10, 12.5 and 15 kbar. Oxides are given in wt%, # is the accordant number of analyses, sd is standard deviation. The formula with ions on the basis of 6 O and the proportions of the end-members enstatite (En), ferrosilite (Fs) and wollastonite (Wo), Mg# and the composition variable *x(opx)* are calculated for the average values. Individual analyses are presented in Appendix B.

	MAOC 11 - orthopyroxene						**MAOC 13 - orthopyroxene**									
P	**10**		**12.5**				**10**				**12.5**				**15**	
T	**1100**		**1050**		**1100**		**1050**		**1100**		**1050**		**1100**		**900**	
#/sd	13	sd	11	sd	9	sd	4	sd	16	sd	9	sd	6	sd	2	sd
SiO_2	51.158	1.026	50.023	0.416	52.587	1.218	50.758	0.902	50.356	0.761	50.510	0.827	51.167	0.685	50.575	1.450
TiO_2	0.386	0.055	0.331	0.066	0.328	0.049	0.261	0.088	0.279	0.060	0.244	0.065	0.330	0.050	0.143	0.048
Al_2O_3	8.407	1.190	8.925	0.912	6.523	1.303	9.115	0.895	9.681	0.893	9.762	0.829	8.250	0.925	9.065	1.902
FeO	9.872	1.381	13.702	0.553	11.128	0.657	10.235	0.158	9.248	1.140	11.299	0.345	10.443	0.575	10.070	3.380
MgO	27.962	0.762	25.089	0.881	26.520	1.493	28.143	0.351	27.966	0.836	26.290	1.014	26.743	0.905	27.090	1.428
CaO	1.587	0.345	1.136	0.300	1.700	0.496	1.213	0.225	1.252	0.141	1.290	0.456	1.465	0.305	1.717	0.726
Na_2O	0.091	0.037	0.111	0.034	0.303	0.226	0.071	0.022	0.083	0.018	0.273	0.240	0.302	0.147	0.145	0.070
Total	99.463	0.350	99.317	0.640	99.089	0.272	99.794	0.437	98.866	0.316	99.668	0.718	98.700	0.471	98.804	1.560
mineral formula calculation:																
Si	1.808		1.801		1.876		1.786		1.784		1.790		1.829		1.802	
Al IV	0.192		0.199		0.124		0.214		0.216		0.210		0.171		0.198	
Z	**2.000**		**2.000**		**2.000**		**2.000**		**2.000**		**2.000**		**2.000**		**2.000**	
Al VI	0.158		0.179		0.150		0.164		0.188		0.200		0.176		0.182	
Fe^{3+}	0.019		0.008		0.000		0.040		0.019		0.100		0.000		0.019	
Ti	0.010		0.009		0.009		0.007		0.007		0.007		0.009		0.004	
Mg	1.473		1.346		1.410		1.476		1.477		1.390		1.425		1.439	
Fe^{2+}	0.273		0.404		0.332		0.261		0.255		0.320		0.312		0.281	
Ca	0.060		0.044		0.065		0.046		0.048		0.048		0.056		0.066	
Na	0.006		0.008		0.021		0.005		0.006		0.006		0.021		0.010	
X	**2.000**		**1.999**		**1.987**		**1.999**		**1.999**		**1.999**		**1.999**		**2.000**	
Total	**4.000**		**3.999**		**3.987**		**3.999**		**3.999**		**3.999**		**3.999**		**4.000**	
En	81.580		75.039		78.037		82.783		82.977		78.960		79.465		80.573	
Fs	15.092		22.519		18.368		14.654		14.352		18.260		17.407		15.758	
Wo	3.328		2.442		3.595		2.563		2.670		2.790		3.128		3.669	
Mg#	84.389		76.917		80.947		84.961		85.254		81.220		82.031		83.642	
x(opx)	0.156		0.231		0.191		0.150		0.147		0.187		0.180		0.164	

Table 5.3.5 (continued): Orthopyroxenes in MAOC 15 at 10, 12.5, 15 and 20 kbar. Oxides are given in wt%, # is the accordant number of analyses, sd is standard deviation. The formula with ions on the basis of 6 O and the proportions of the end-members enstatite(En), ferrosilite (Fs) and wollastonite (Wo), Mg# and the composition variable *x(opx)* are calculated for the average values. Individual analyses are presented in Appendix B.

	MAOC 15 - orthopyroxene															
P	**10**				**12.5**				**15**						**20**	
T	**1050**		**1100**		**1050**		**1100**		**900**		**1050**		**1100**		**1050**	
#/sd	5	sd	9	sd	7	sd	11	sd	2	sd	7	sd	6	sd	2	sd
SiO_2	52.708	0.660	52.143	0.988	50.679	0.794	50.817	0.480	52.380	0.339	52.654	1.104	53.531	0.533	55.020	0.481
TiO_2	0.188	0.098	0.226	0.057	0.203	0.036	0.309	0.078	0.160	0.019	0.285	0.053	0.230	0.058	0.263	0.054
Al_2O_3	9.198	0.916	7.840	1.781	9.353	0.990	9.165	0.795	8.520	0.820	6.999	1.628	6.662	0.524	5.360	0.552
FeO	7.612	0.540	6.273	0.708	10.090	0.263	9.125	0.860	8.275	0.007	9.541	0.803	6.022	0.312	6.950	0.311
MgO	27.940	1.936	30.740	0.944	28.570	0.536	28.333	0.534	29.085	1.478	27.881	1.295	31.828	0.370	29.940	0.877
CaO	2.253	0.846	1.626	0.767	0.902	0.199	1.034	0.100	1.460	0.170	1.065	0.098	1.069	0.065	1.630	0.042
Na_2O	0.285	0.200	0.135	0.070	0.138	0.029	0.304	0.140	0.203	0.185	0.416	0.125	0.156	0.023	0.391	0.146
Total	100.184	0.917	98.983	0.385	99.935	0.444	99.088	0.484	100.082	0.616	98.842	1.364	99.497	0.449	99.554	0.002
mineral formula calculation:																
Si	1.832		1.820		1.776		1.792		1.825		1.867		1.854		1.914	
Al IV	0.168		0.180		0.224		0.208		0.175		0.133		0.146		0.086	
Z	**2.000**		**2.000**		**2.000**		**2.000**		**2.000**		**2.000**		**2.000**		**2.000**	
Al VI	0.208		0.142		0.163		0.172		0.175		0.159		0.126		0.134	
Fe^{3+}	0.000		0.036		0.060		0.039		0.004		0.000		0.018		0.000	
Ti	0.005		0.006		0.005		0.008		0.004		0.008		0.006		0.007	
Mg	1.447		1.599		1.493		1.489		1.511		1.474		1.643		1.553	
Fe^{2+}	0.221		0.147		0.236		0.230		0.237		0.283		0.156		0.202	
Ca	0.084		0.061		0.034		0.039		0.054		0.040		0.040		0.061	
Na	0.019		0.009		0.009		0.021		0.014		0.029		0.010		0.026	
X	**1.985**		**2.000**		**2.000**		**1.999**		**2.000**		**1.992**		**2.000**		**1.982**	
Total	**3.985**		**4.000**		**4.000**		**3.999**		**4.000**		**3.992**		**4.000**		**3.982**	
En	82.591		88.483		84.683		84.697		83.842		82.006		89.359		85.518	
Fs	12.622		8.153		13.396		13.081		13.134		15.742		8.484		11.136	
Wo	4.787		3.364		1.921		2.223		3.024		2.251		2.157		3.346	
Mg#	86.743		91.563		86.341		86.622		86.457		83.895		91.329		88.479	
x(opx)	0.133		0.084		0.137		0.134		0.135		0.161		0.087		0.115	

5.3.3.6 Plagioclase

The proportion of plagioclase decreases with increasing MgO in the bulk rock composition and the phase does not occur at 15 and 20 kbar at 1100 °C. Plagioclase belongs to the feldspars with the formula XZ_4O_8 and is classified in the system Ab (albite $NaAlSi_3O_8$)–Or (orthoclase $KAlSi_3O_8$)–An (anorthite $CaAl_2Si_2O_8$). Compositions between Ab and Or are alkali feldspars, those between Ab and An are plagioclase feldspars, whereas only plagioclase feldspars are present in this study because the presence of alkali feldspars is excluded in the system NCFMASHTO. Plagioclase is subdivided according to the proportion of anorthite (0–10 albite, 10–30 oligoclase, 30–50 andesine, 50–70 labradorite, 70–90 bytownite and 90–100 anorthite). The results of the mineral formula calculation on the basis of 8 oxygen for the average composition in each assemblage and the corresponding contents of the end-members albite, orthoclase and anorthite are given in Tab. 5.3.6 and the composition variable *ca(pl)* = Ca/ Ca + Na (Holland & Powell, 2003) is given for comparison with the thermodynamic calculations (subchapter 6.2). The end-member data are additionally plotted in the ternary Ab–Or–An diagram (Fig. 5.3.17).

The amount of Ca on the X position increases with decreasing pressure coeval with increasing Al on the Z position (Tab. 5.3.6). The Ca end-member anorthite decreases in each bulk rock composition towards higher *P–T* conditions and there is a general trend towards a lower proportion of anorthite with increasing MgO in the bulk composition. The overall proportion of the Ca end-member (anorthite) varies between 29.7 at 15 kbar/1050 °C and 78.8 at 10 kbar/1050 °C, both achieved in MAOC 15, which therefore shows the broadest range of plagioclase compositions. However, it is a minor phase in MAOC 15 being not well developed in most cases, except for 15 kbar/1050 °C, where plagioclase fits the trend of the decreasing anorthite end-member. At 10 and 12.5 kbar/1050 °C the compositions are unusual due to their atypically high amounts of the anorthite component compared to the other analyses in this study and these analyses do not fit the overall trend of decreasing anorthite content from MAOC 11 to MAOC 15. Nevertheless, these plagioclase crystals are intergrown with pyroxenes within the assemblage and are not connected to unreacted material, which would have indicated a metastable phase.

Two types of plagioclase are developed in MAOC 11 at 10 kbar/1100 °C, the first occurring in the main assemblage and the second, lower anorthite plagioclase, appears enclosed in the melt.

Table 5.3.6: Plagioclase in MAOC 11 at 10, 12.5 and 15 kbar and MAOC 13 at 10 kbar. Oxides are given in wt%, # is the accordant number of analyses, sd is standard deviation. The formulae with ions on the basis of 8 O and the proportions of the end-members anorthite (An) and albite (Ab) as well as *ca(pl)* are calculated for the average values. Individual analyses are presented in Appendix B.

	MAOC 11 - plagioclase														**MAOC 13 - plagioclase**			
P	**10**						**12.5**				**15**				**10**			
T	**1050**		**1100**				**1050**		**1100**		**900**		**1050**		**1050**		**1100**	
#/sd	11	sd	6 (in)	sd	5 (rim)	sd	12	sd	14	sd	10	sd	11	sd	10	sd	1	
SiO$_2$	50.702	0.791	51.395	0.516	54.260	0.557	53.783	1.379	54.592	0.900	56.535	1.125	57.695	0.873	51.509	0.468	51.380	
TiO$_2$	0.041	0.030	0.056	0.049	0.237	0.133	0.070	0.044	0.069	0.078	0.062	0.034	0.040	0.038	0.034	0.041	0.011	
Al$_2$O$_3$	30.321	0.720	29.495	0.398	24.928	1.785	27.994	0.820	26.566	0.856	25.931	0.663	25.803	0.450	29.548	0.654	29.660	
FeO	0.267	0.128	0.411	0.127	1.090	0.619	0.649	0.204	0.450	0.167	0.497	0.149	0.388	0.143	0.491	0.247	0.240	
MgO	0.172	0.101	0.295	0.161	1.404	0.871	0.336	0.385	0.162	0.113	0.388	0.364	0.108	0.073	0.505	0.659	0.282	
CaO	13.784	0.654	13.138	0.264	10.450	0.944	11.003	0.697	10.314	0.658	9.678	0.570	8.710	0.569	12.874	0.336	13.150	
Na$_2$O	3.829	0.431	3.933	0.156	4.958	0.280	4.988	0.461	5.310	0.349	5.684	0.276	6.423	0.317	4.236	0.230	4.100	
Total	99.115	0.306	98.724	0.236	97.327	0.665	98.823	0.581	97.463	0.506	98.776	0.418	99.167	0.339	99.255	0.383	98.864	
mineral formula calculation:																		
Si	2.329		2.365		2.518		2.457		2.521		2.568		2.604		2.360		2.363	
Ti	0.001		0.002		0.008		0.002		0.002		0.002		0.001		0.001		0.000	
Al	1.642		1.600		1.363		1.507		1.446		1.388		1.372		1.596		1.607	
Fe^{3+}	0.010		0.016		0.042		0.025		0.017		0.019		0.015		0.019		0.009	
Mg	0.012		0.020		0.097		0.023		0.011		0.026		0.007		0.034		0.019	
Fe^{2+}	0.000		0.000		0.000		0.000		0.000		0.000		0.000		0.000		0.000	
Z	**3.994**		**4.002**		**4.029**		**4.015**		**3.997**		**4.004**		**3.999**		**4.011**		**3.998**	
Ca	0.678		0.648		0.520		0.539		0.510		0.471		0.421		0.632		0.648	
Na	0.341		0.351		0.446		0.442		0.475		0.501		0.562		0.376		0.366	
X	**1.020**		**0.999**		**0.966**		**0.981**		**0.986**		**0.972**		**0.983**		**1.008**		**1.013**	
Total	**5.014**		**5.001**		**4.994**		**4.995**		**4.983**		**4.976**		**4.982**		**5.019**		**5.012**	
An	66.547		64.862		53.805		54.934		51.771		48.478		42.838		62.680		63.931	
Ab	33.453		35.138		46.195		45.066		48.229		51.522		57.162		37.320		36.069	
Or	0.000		0.000		0.000		0.000		0.000		0.000		0.000		0.000		0.000	
ca(pl)	0.665		0.649		0.538		0.549		0.518		0.485		0.428		0.627		0.639	

Table 5.3.6 (continued): Plagioclase in MAOC 13 and MAOC 15 at 10, 12.5 and 15 kbar kbar. Oxides are given in wt%, # is the accordant number of analyses, sd is standard deviation. The formulae with ions on the basis of 8 O and the proportions of the end-members anorthite (An and albite (Ab) as well as *ca(pl)* are calculated for the average values. Individual analyses are presented in Appendix B.

	MAOC 13 - plagioclase								**MAOC 15 - plagioclase**									
P	**12.5**				**15**				**10**		**12.5**				**15**			
T	**1050**		**1100**		**900**		**1050**		**1050**		**1050**		**1100**		**900**		**1050**	
#/sd	8	sd	9	sd	6	sd	3	sd	8	sd	6	sd	3	sd	2	sd	13	sd
SiO_2	54.855	1.373	54.283	1.264	55.015	1.282	57.708	3.301	48.100	1.318	53.228	1.226	58.344	0.424	57.625	0.700	58.612	2.382
TiO_2	0.088	0.042	0.084	0.036	0.367	0.365	0.060	0.029	0.055	0.054	0.077	0.044	0.069	0.015	0.048	0.068	0.068	0.039
Al_2O_3	26.943	1.346	26.701	1.606	25.417	0.919	25.033	1.729	31.060	1.863	26.983	1.971	24.333	0.162	23.740	0.170	23.570	2.113
FeO	0.610	0.192	0.553	0.325	1.051	0.566	0.491	0.207	0.329	0.256	0.935	0.238	0.290	0.024	0.755	0.041	0.602	0.259
MgO	0.360	0.395	0.571	0.769	0.660	0.399	0.415	0.372	0.475	0.980	1.179	0.636	0.109	0.043	1.002	0.313	0.900	0.661
CaO	9.993	1.153	10.276	0.806	9.072	0.850	7.550	1.646	15.904	1.018	10.847	0.527	6.713	0.162	7.795	0.827	5.928	1.814
Na_2O	5.671	0.658	5.581	0.456	5.963	0.805	7.077	0.962	2.359	0.616	5.052	0.461	7.590	0.226	6.540	0.283	7.762	1.046
Total	98.569	0.642	98.098	0.306	97.592	0.427	98.360	0.768	98.336	1.172	98.390	0.478	97.542	0.396	97.582	0.005	97.513	0.768
mineral formula calculation:																		
Si	2.508		2.498		2.539		2.624		2.242		2.451		2.669		2.643		2.680	
Ti	0.003		0.003		0.013		0.002		0.002		0.003		0.002		0.002		0.002	
Al	1.452		1.448		1.383		1.341		1.706		1.464		1.312		1.283		1.270	
Fe^{3+}	0.023		0.021		0.041		0.019		0.013		0.036		0.011		0.029		0.023	
Mg	0.025		0.039		0.045		0.028		0.033		0.081		0.007		0.069		0.061	
Fe^{2+}	0.000		0.000		0.000		0.000		0.000		0.000		0.000		0.000		0.000	
Z	**4.011**		**4.009**		**4.021**		**4.014**		**3.996**		**4.035**		**4.002**		**4.025**		**4.037**	
Ca	0.489		0.507		0.449		0.368		0.794		0.535		0.329		0.383		0.290	
Na	0.503		0.498		0.534		0.624		0.213		0.451		0.673		0.582		0.688	
X	**0.992**		**1.005**		**0.982**		**0.992**		**1.007**		**0.986**		**1.002**		**0.965**		**0.978**	
Total	**5.003**		**5.014**		**5.003**		**5.006**		**5.003**		**5.021**		**5.004**		**4.990**		**5.015**	
An	49.334		50.432		45.672		37.090		78.840		54.266		32.831		39.711		29.679	
Ab	50.666		49.568		54.328		62.910		21.160		45.734		67.169		60.289		70.321	
Or	0.000		0.000		0.000		0.000		0.000		0.000		0.000		0.000		0.000	
ca(pl)	0.493		0.504		0.457		0.371		0.788		0.543		0.328		0.397		0.297	

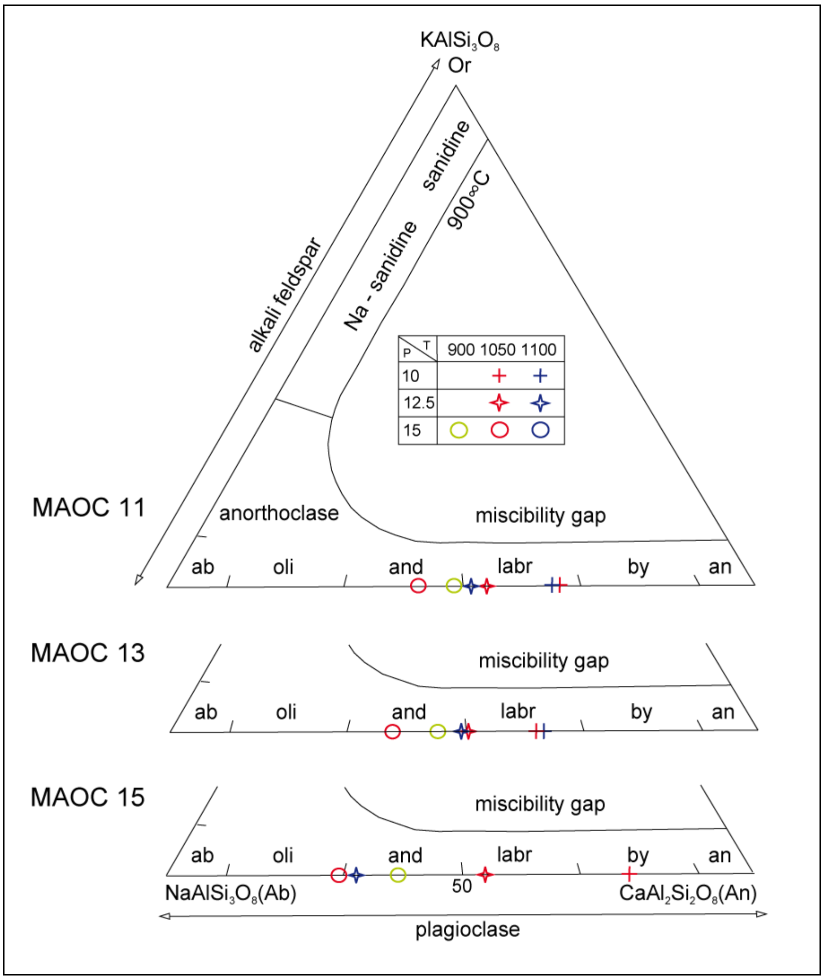

Figure 5.3.17: Classification of the plagioclase feldspars in the orthoclase (Or)–albite (Ab)–anorthite (An) ternary diagram. The Na end-member albite generally increases from MAOC 11 to 15 whereas the total amount of plagioclase decreases (cf. Tab. 5).

5.3.3.7 Melt

The proportion of melt decreases with increasing bulk rock MgO from the highest amount of melt in MAOC 11 to the lowest amount in MAOC 15. In MAOC 15 only small interstitial melt pools developed in the experimental runs that are typically too small to analyse. The degree of melting in each assemblage is given in Tab. 5.3.1 and a mass balance approach is given in subchapter 5.3.3.9 for most assemblages, depending on their inferred degree of equilibration. Table 5.3.7 presents the averaged values of the glass analyses representing the melt composition, the molecular Mg#, the alumina saturation index (A/CNK-ratio; molecular $Al_2O_3/(K_2O + Na_2O + CaO)$; in NCFMASHTO: A/CN-ratio) and the CIPW norm of the average values (Herrmann & Berry, 2002). The analyses of melt include a volatile proportion, expressed by the difference between 100 wt% and the total oxides. The composition of melt is predominantly distinguished by the SiO_2 content and it is either quartz-normative basaltic (50–55 wt% SiO_2), tonalitic (TTG-like) (> 60 wt% SiO_2) or intermediate between tonalitic and basaltic (Tab. 5.3.7, Figs 5.3.18–20). The CIPW normalised TTG-like and intermediate melt compositions generally have a tonalitic character in terms of quartz–alkali feldspar–plagioclase (Fig. 5.3.18; after Streckeisen, 1976) and albite–anorthite (Fig. 5.3.19, after Barker, 1979). The basaltic melt compositions are plotted in these diagrams for comparison and show a different composition towards diorite (gabbro). Based on the fact that K_2O is not incorporated in the oxide mixes (Tab. 5.2.3) all investigated melt compositions plot on the An–Ab arm of the An–Ab–Or triangle. The absence of K_2O excludes any granodioritic compositions for melt (Fig. 5.3.19) and trondhjemitic compositions are also not present. The three assemblages at 15 kbar/ 900 °C have equilibrated under subsolidus conditions and are not considered here.

In MAOC 11, melt is present in all experiments 1050 °C, whereas at 10 and 15 kbar generally more melt is developed than at 12.5 kbar (backbanded solidus, subchapter 5.3.4). The melt compositions in MAOC 11 are predominantly TTG-like (12.5 kbar/1100 °C, 15 kbar/1050 °C and 20 kbar), but also intermediate (15 kbar/ 1100 °C) and basaltic compositions (10 kbar/1100 °C, 12.5 kbar/1050 °C) are existent. At 12.5 kbar/1050 °C one of three analyses indicates a nepheline-normative basalt composition (Appendix B) causing the high standard deviations in Tab. 5.3.7. With the exception of 12.5 kbar/1050 °C, where no melt was identified, the melt-bearing assemblages in MAOC 13 are at the same *P–T* conditions than those in MAOC 11. Variation diagrams for the averaged melt compositions (Tab. 5.3.7) are presented in Fig. 5.3.20a-h and illustrate the variation in Mg#, MgO, MgO + FeO, FeO, Na_2O, Al_2O_3, CaO and TiO_2 with increasing SiO_2. The TTG-like melts have generally the lowest Mg#, MgO, MgO + FeO, Al_2O_3 and CaO, whereas FeO, $Na_2O + K_2O$ and TiO_2 do not show trends.

Most of the melt compositions in MAOC 13 are basaltic, plotting at the diorite (gabbro) field (Fig. 5.3.18). The tonalitic melts at 1050 °C (15 and 20 kbar) plot in the upper tonalite field (Fig. 5.3.18). Due to the minor amount of melt at 20 kbar/1100 °C only one analysis could be undertaken (Tab. 5.3.7). The melt in MAOC 15 is basaltic and its stability is restricted to 10 kbar/1100 °C and 15 kbar/1100 °C, where the highest degree of melting in MAOC 15 occurs. The analysis at 20 kbar/1050 °C presents the lowest amount of SiO_2 (42.1 wt %) of all melt compositions.

Table 5.3.7: Melt in MAOC 11 at 10, 12.5, 15 and 20 kbar. Oxides are given in wt%, # is the number of analyses, sd is standard deviation. The CIPW norm, Mg# and A/CNK (without K) are calculated for the average values. CIPW normative mineral abbreviations: Q (quartz), An (anorthite), Di (diopside), Hyp (hyperstene), Ab (albite), Ilm (ilmenite), C (corundum), Mag (magnetite). Individual analyses are presented in Appendix B.

	MAOC 11 - melt													
P	**10**		**12.5**				**15**				**20**			
T	**1100**		**1050**		**1100**		**1050**		**1100**		**1050**		**1100**	
#/sd	16	sd	3	sd	8	sd	12	sd	5	sd	9	sd	12	sd
SiO_2	52.414	0.483	52.777	7.600	61.719	0.986	64.886	1.404	57.956	0.274	65.453	0.710	62.382	0.867
TiO_2	0.721	0.041	0.828	0.397	1.136	0.102	0.769	0.075	0.883	0.089	0.912	0.051	1.094	0.056
Al_2O_3	19.643	0.541	14.420	7.290	14.871	0.607	16.244	0.714	19.896	0.357	15.032	0.196	17.096	0.227
FeO	3.854	0.320	4.667	2.757	3.386	0.127	2.593	0.307	1.974	0.146	1.833	0.162	2.572	0.265
MgO	4.230	1.333	5.030	5.470	2.441	0.123	1.378	0.284	2.812	0.570	0.865	0.173	1.475	0.584
CaO	8.755	0.539	9.663	7.005	5.096	0.140	4.675	0.413	6.602	0.371	3.743	0.396	5.589	0.641
Na_2O	1.372	0.586	2.163	1.780	3.285	0.157	2.366	0.797	3.094	0.193	1.924	0.248	1.872	0.173
Total	90.989	2.025	89.547	3.943	91.934	0.711	92.911	0.947	93.217	0.530	89.764	1.047	92.079	0.791
Mg#	0.662		0.658		0.562		0.487		0.717		0.457		0.506	
A/CNK	1.081		0.683		1.014		1.311		1.164		1.508		1.291	
CIPW norm of average values:														
Q	19.081		15.128		29.268		41.354		22.634		49.883		39.773	
An	47.725		33.085		27.484		24.954		35.124		20.687		30.113	
Di	0.000		16.437		0.000		0.000		0.000		0.000		0.000	
Hyp	16.302		11.949		9.291		5.128		8.668		2.771		5.603	
Ab	12.777		20.393		30.208		21.493		28.093		18.108		17.177	
Ilm	1.500		1.747		2.336		1.576		1.804		1.937		2.260	
C	1.595		0.000		0.214		4.146		2.996		5.628		4.184	
Mag	1.029		1.261		1.189		1.348		0.681		0.986		0.899	
Total	100.010		100.000		99.990		100.000		100.000		100.000		100.010	

Table 5.3.7 (continued): Melt in MAOC 13 and 15 at 10, 12.5, 15 and 20 kbar. Oxides are given in wt%, # is the number of analyses, sd is standard deviation. The CIPW norm, Mg# and A/CNK (without K) are calculated for the average values. CIPW normative mineral abbreviations: Q (quartz), An (anorthite), Di (diopside), Hyp (hyperstene), Ab (albite), Ilm (ilmenite), C (corundum), Mag (magnetite). Individual assemblages are presented in Appendix B.

	MAOC 13 - melt											**MAOC 15 - melt**					
P	**10**		**12.5**		**15**				**20**			**10**			**15**		**20**
T	**1100**		**1100**		**1050**		**1100**		**1050**		**1100**	**1050**	**1100**		**1100**		**1050**
#/sd	16	sd	5	sd	18	sd	14	sd	9	sd	1	1	7	sd	5	sd	1
SiO_2	51.387	0.428	53.895	0.669	61.726	2.386	52.115	2.590	64.914	1.407	53.360	50.200	50.901	0.463	49.600	0.381	42.080
TiO_2	0.707	0.076	1.420	0.111	0.936	0.059	0.974	0.196	0.935	0.064	1.236	0.490	0.761	0.074	0.959	0.031	0.913
Al_2O_3	21.960	0.792	18.578	0.816	16.274	0.687	20.405	0.909	14.103	0.613	17.610	20.450	21.616	0.438	20.190	0.247	18.710
FeO	3.474	0.201	3.992	0.332	3.205	0.509	2.159	0.628	2.118	0.281	3.900	3.600	2.310	0.179	2.054	0.401	8.460
MgO	3.111	0.880	2.890	1.312	2.142	1.267	3.518	2.020	1.513	0.643	3.320	5.520	4.389	0.737	1.011	0.488	15.390
CaO	8.283	0.630	5.668	0.910	4.252	1.463	7.834	1.777	3.452	0.976	4.680	8.180	7.917	0.208	8.812	0.213	5.090
Na_2O	2.356	0.573	3.996	0.355	2.322	0.913	2.835	0.246	1.835	0.267	1.610	2.590	2.102	1.379	2.304	0.075	0.431
Total	91.276	1.048	90.439	0.957	90.857	1.541	89.840	1.619	88.871	0.732	85.716	91.030	89.995	0.651	84.930	0.760	91.074
Mg#	0.615		0.563		0.544		0.744		0.560		0.603	0.732	0.772		0.467		0.764
A/CNK	1.160		1.101		1.409		1.079		1.517		1.578	1.069	1.211		1.019		1.878
CIPW norm of average values:																	
Q	14.621		13.994		38.211		14.410		49.850		31.936	7.919	15.635		17.760		0.462
An	44.996		31.056		23.217		43.260		19.249		27.087	44.550	43.607		51.445		27.682
Di	0.000		0.000		0.000		0.000		0.000		0.000	0.000	0.000		0.000		0.000
Hyp	13.155		11.628		8.711		11.371		4.914		13.722	20.376	14.754		4.878		54.875
Ab	21.831		37.401		21.577		26.654		17.431		15.908	24.031	19.800		22.931		3.977
Ilm	1.462		2.982		1.956		2.051		1.994		2.735	1.026	1.614		2.146		1.899
C	3.315		1.877		5.196		1.664		5.417		7.510	1.461	4.179		0.457		9.601
Mag	0.609		1.073		1.131		0.580		1.145		1.102	0.638	0.420		0.391		1.493
Total	99.990		100.010		100.000		99.990		100.000		100.000	100.000	100.010		100.010		99.990

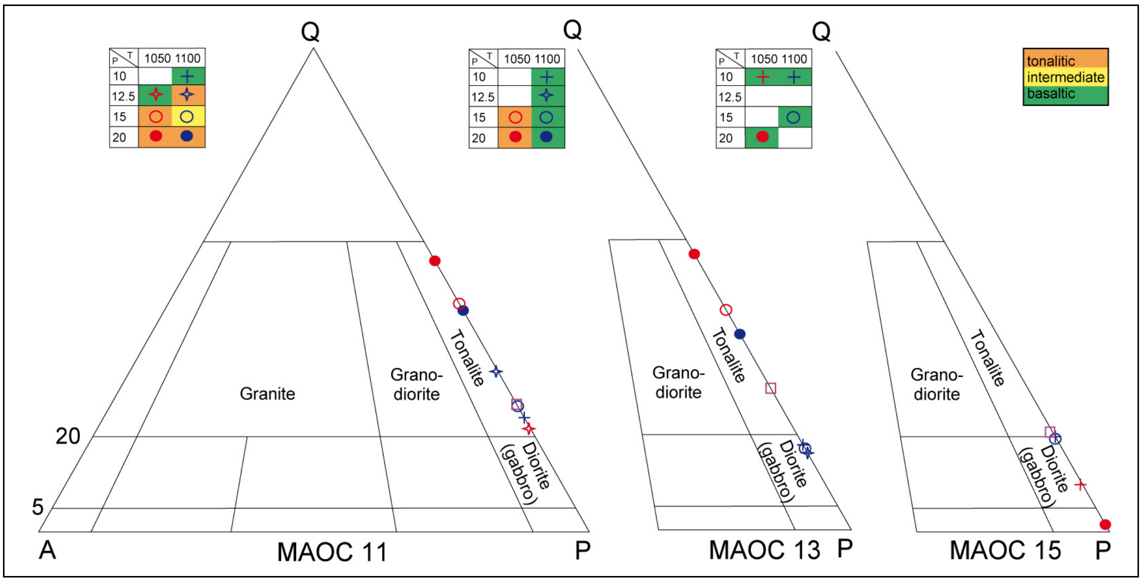

Figure 5.3.18: Triangular Q–A–P (quartz–alkali feldspar–plagioclase) plots of the averaged normative melt compositions for MAOC 11, 13 and 15 according to Streckeisen (1976). The compositions in MAOC 11 plot in the range of tonalite, the basaltic compositions near the diorite (gabbro) field. Most of the basaltic compositions in MAOC 13 plot in the diorite (gabbro) range and all MAOC 15 compositions plot in or near the field of gabbro. The legends for each composition present the type of melt.

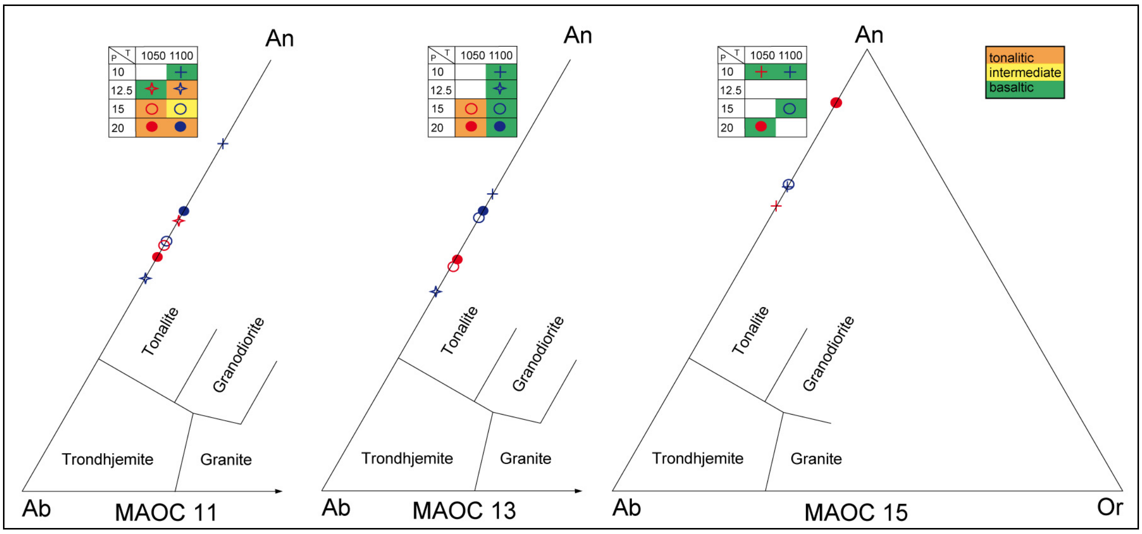

Figure 5.3.19: Triangular An–Ab–Or plots of the averaged normative melt compositions from MAOC 11, 13 and 15, redrawn from Barker (1979). The compositions plot on the Ab–An axis due to the absence of K_2O in the bulk rock composition. The compositions evolve from MAOC 11 to MAOC 15 towards the An end-member. The legends for each composition illustrate the type of melt.

Variation diagrams for the averaged melt compositions (Tab. 5.3.7) are presented in Fig. 5.3.20a-h and illustrate the variation in Mg#, MgO, MgO + FeO, FeO, Na_2O, Al_2O_3, CaO and TiO_2 with increasing SiO_2. The TTG-like melts have generally the lowest Mg#, MgO, MgO + FeO, Al_2O_3 and CaO, whereas FeO, $Na_2O + K_2O$ and TiO_2 do not show trends.

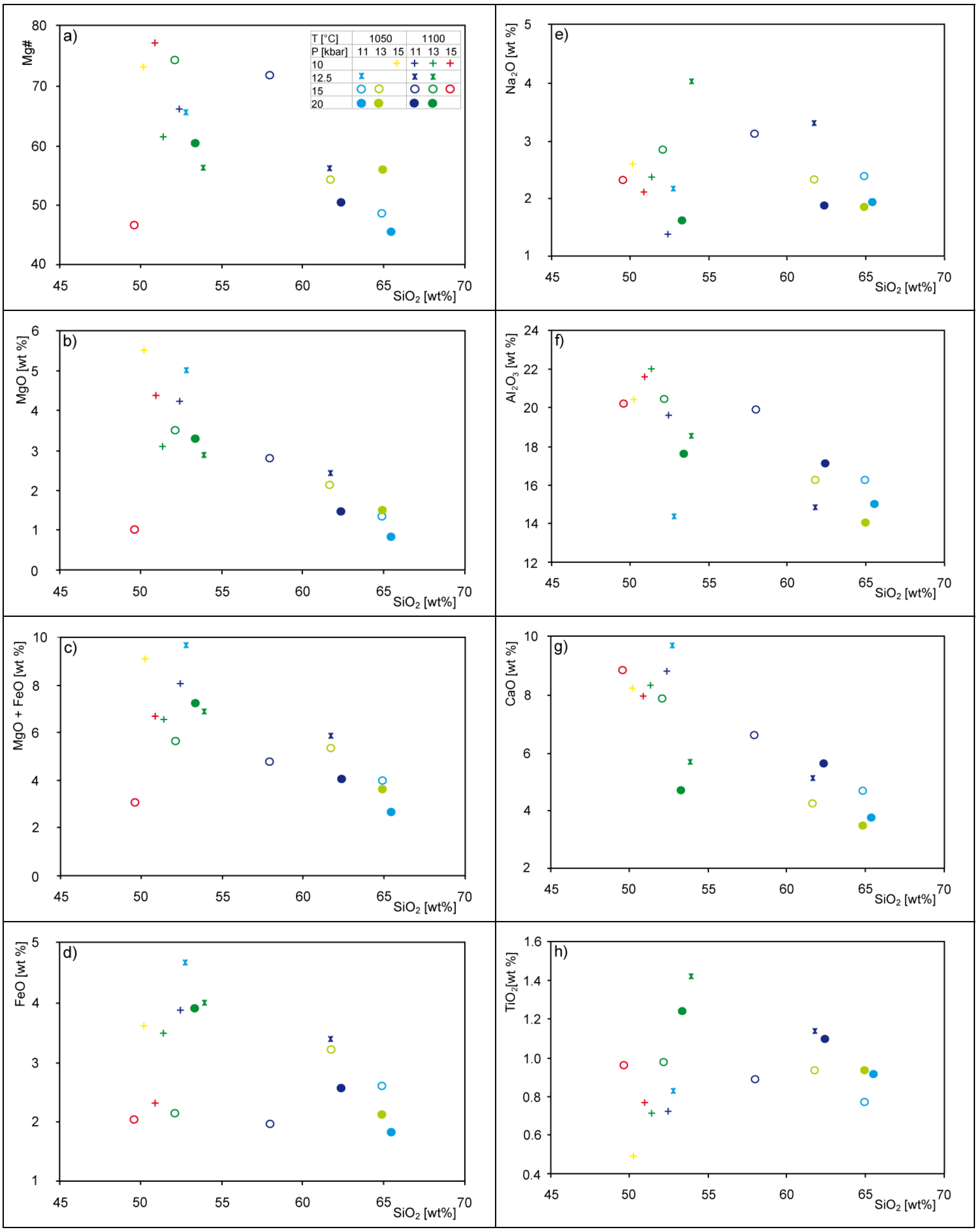

Figure 5.3.20a-h: Variation diagrams of Mg# (a), MgO (b), MgO + FeO (c), FeO (d) Na_2O (e), Al_2O_3 (f), CaO (g) and TiO_2 (h) against SiO_2 of the averaged melt compositions determined for MAOC 11–15, all oxides are given in wt %. Three groups of melt are shown: basaltic (< 55 wt % SiO_2), intermediate (55-60 wt % SiO_2) and TTG-like melt (> 60 wt % SiO_2). a) illustrates the fact that the groups of basaltic and intermediate melts generally have higher Mg# than the TTG-like ones. e) is a cutout of the total alkali-silica diagram (Le Bas *et al.*, 1986; LeMaitre, 1989). The variation of Na_2O is small and the important classification here is based on the silica content of a rock (ultrabasic < 45 > basic (basalt) < 52 > intermediate (basaltic andesite and andesite) < 63 > acid (dacite). b), f) and g) illustrate a decreasing trend of MgO, Al_2O_3 and CaO from the basaltic, low SiO_2-melts towards the TTG-like melts. FeO (d) and TiO_2 (h) do not show any trends and the values for the TTG-like melts plot in the same ranges like the other ones.

5.3.3.8 Trends and correlations of the melt and mineral compositions

The MAOC - oxide, *P* - oxide and *T* - oxide variation diagrams in Figs 5.3.21–5.3.27 represent the development of the amounts of the averaged values for the oxides SiO_2, Al_2O_3, TiO_2, MgO, FeO, CaO and Na_2O in each of the TTG-like, basaltic and intermediate melt compositions from MAOC 11 to MAOC 15 with varying pressure and temperature. The data points which represent identical *P–T* conditions from different MAOC compositions are connected with lines. The general trends of decreasing or increasing values with increasing pressure are interrupted for each oxide by positive or negative peaks at 12.5 kbar, which is probably caused firstly by the appearance of garnet or secondly due to the lower degrees of melt developed at 12.5 kbar (backbanded solidus, subchapter 5.4). The black rectangles indicate the initial amounts of the oxides in MAOC 11, 13 and 15.

The highest values of SiO_2 in melt (> 60 wt%) indicate the TTG-like melts (subchapter 3.3.3.7). The proportion of SiO_2 in melt is generally higher at higher pressures and the highest amounts of SiO_2 are present at 1050 °C at $P \geq 15$ kbar. SiO_2 is generally enriched in the melts compared to the bulk compositions but the SiO_2 content decreases in the melts from MAOC 11 to 15 (Fig. 5.3.21a-c).

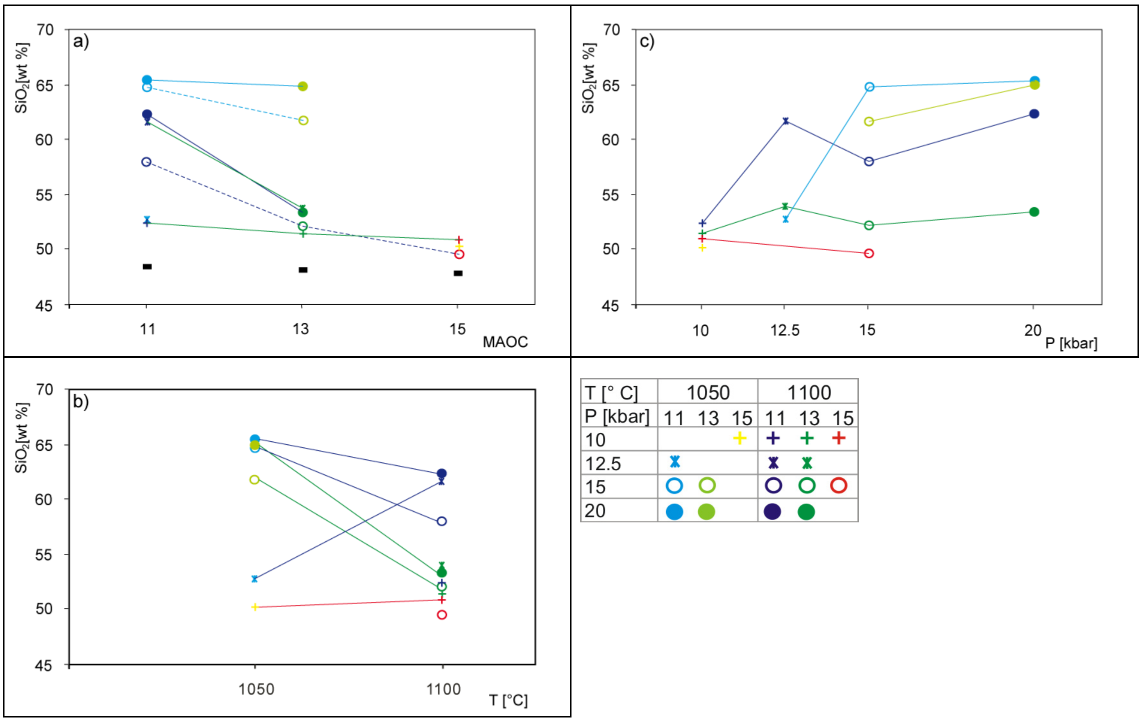

Figure 5.3.21a-c: MAOC - SiO_2 (a), *T* - SiO_2 (b) and *P* - SiO_2 (c) variation diagrams illustrate the evolution of SiO_2 in melts of similar *P–T* conditions in MAOC 11, 13 and 15. Similar conditions are interconnected. The black rectangles in the MAOC diagram indicate the bulk composition value.

The amount of SiO_2 in clinopyroxene (stable in each assemblage) and garnet (at $P \geq 12.5$ kbar) increases towards higher MAOC (Tabs 5.3.2, 5.3.4). SiO_2 in plagioclase increases with pressure in each MAOC composition and reaches highest values in MAOC 15 (Tab. 5.3.6).

The increase of Al_2O_3 in melt correlates with the decrease of SiO_2 (Fig. 5.3.20f) and the amount of Al_2O_3 in melt is less than that in the bulk rock at 12.5, 15 and 20 kbar/1050 °C, 12.5 kbar/1100 °C in MAOC 11 and 20/1050 °C in MAOC 13 (Fig. 5.3.22a). Troughs of Al_2O_3 content are obvious at 12.5 kbar (Fig. 5.3.22c), where an important change of the assemblages occurred in terms of the incoming of garnet. Al_2O_3 in melt compositions $\leq$ 15 kbar is higher if little or no plagioclase is stable in the appropriate assemblage and lower values are attained if more plagioclase is stabilised. At higher pressures, where garnet and clinopyroxene constitute the main assemblage, Al_2O_3 in melt is lower.

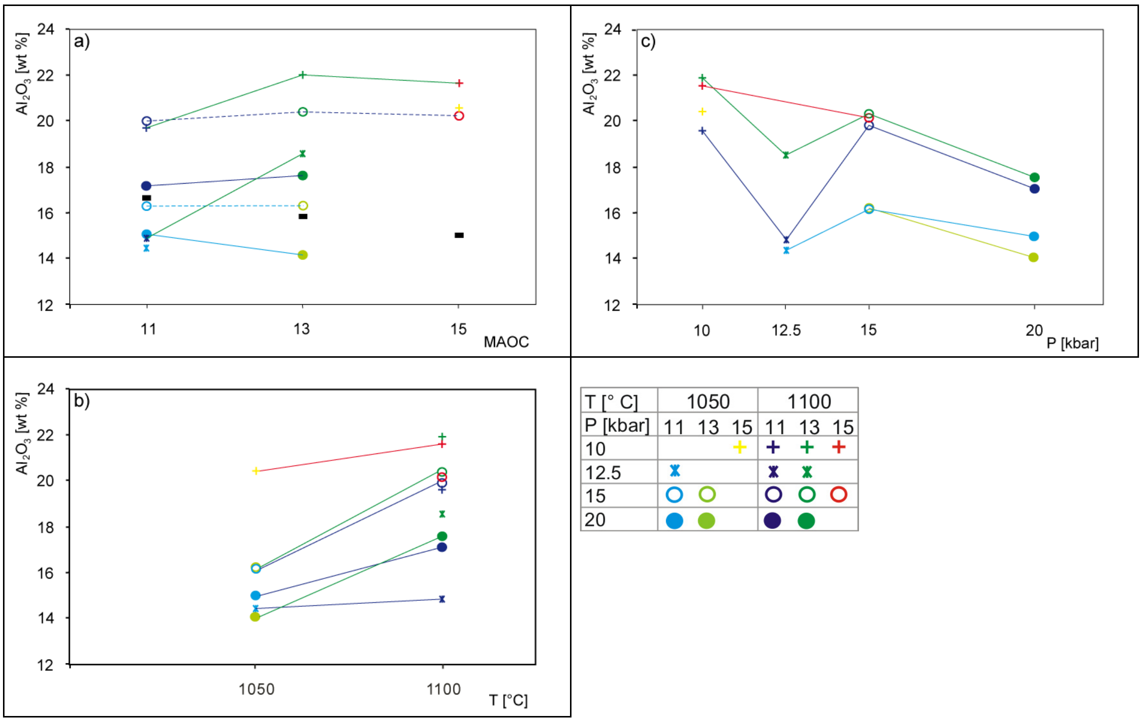

Figure 5.3.22a-c: MAOC - Al_2O_3 (a), T - Al_2O_3 (b) and P - Al_2O_3 (c) variation diagrams illustrate the evolution of Al_2O_3 in melts of similar P–T conditions in MAOC 11, 13 and 15. Similar conditions are interconnected. The black rectangles in the MAOC diagram indicate the bulk composition value.

TiO_2 is generally enriched in melts compared to the starting compositions except for 10 kbar/1050 °C in MAOC 15 (Fig. 5.3.23a). In the experimental runs of this study TiO_2 is not an indicator for TTG-like melts because the oxide plots in the middle ranges of values from the analysed melt pools (Fig. 5.3.20h). TiO_2 increases in the melt compositions towards 12.5 kbar and than decreases in the melts at 15 kbar terminating to an enrichment of TiO_2 in the melts at 20 kbar (Tab. 5.3.7) where rutile occurs at 1050 °C. The lowest values are present in MAOC 15 and TiO_2 in melt at 1100 °C has higher proportions than at lower temperatures.

TiO_2 is incorporated in garnet, amphibole, clinopyroxene and, to a smaller extent, in orthopyroxene. TiO_2 in plagioclase is very low (< 0.1 wt%) and shows no trends.

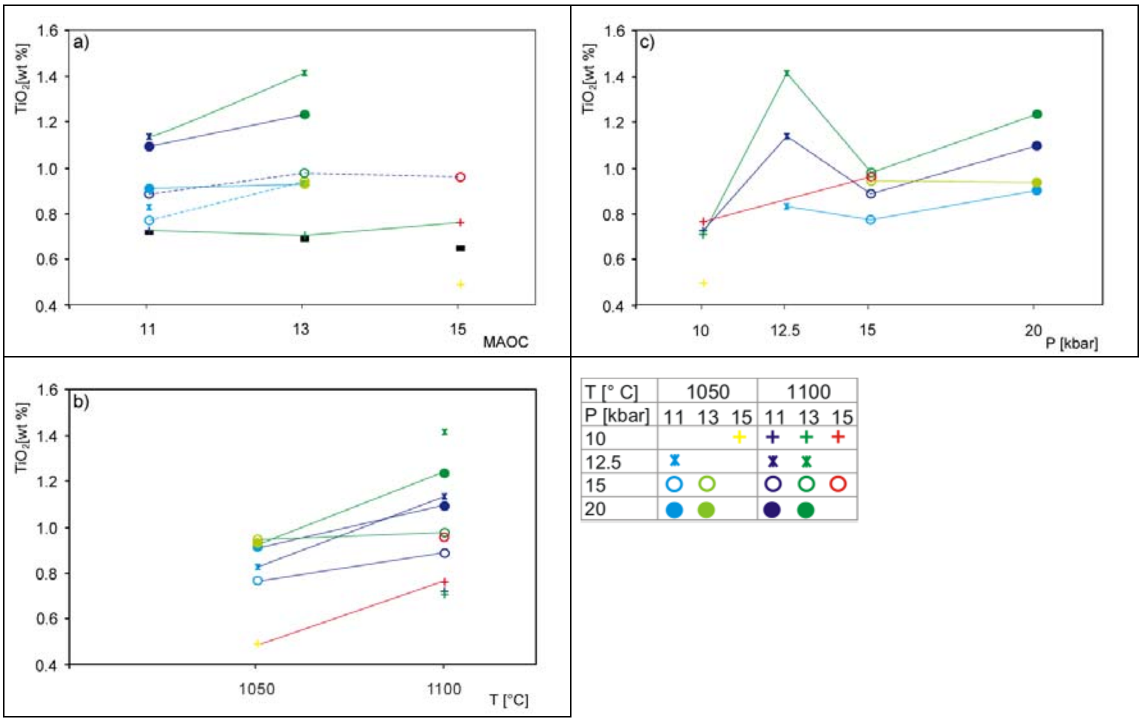

Figure 5.3.23a-c: MAOC - TiO_2 (a), *T* - TiO_2 (b) and *P* - TiO_2 (c) variation diagrams illustrate the evolution of TiO_2 in melts of similar *P–T* conditions in MAOC 11, 13 and 15. Similar conditions are interconnected. The black rectangles in the MAOC diagram indicate the bulk composition value.

MgO shows no obvious trends in the melt compositions between MAOC 11 and 15 or with temperature but the melt compositions at 10 and 12.5 kbar generally have higher MgO than at higher pressures (Fig. 5.3.24c). MgO is invariably depleted in the melt compositions in contrast to the bulk rock compositions, whereas the TTG-like melt compositions show the lowest amounts of MgO as well as low Mg# (Fig. 5.3.20a, b, Tab. 5.3.7). MgO is largely incorporated in the minerals garnet, amphibole, clinopyroxene and orthopyroxene. The mineral compositions reflect the bulk rock MgO from the initial MAOC compositions, which become more Mg-rich from MAOC 11 to MAOC 15 (Tabs 5.3.2–5.3.6). The higher amount of MgO in the bulk composition of MAOC 15 may account for the higher amount of amphiboles even on the high-*T* side of the solidus (Fig. 5.4.3f).

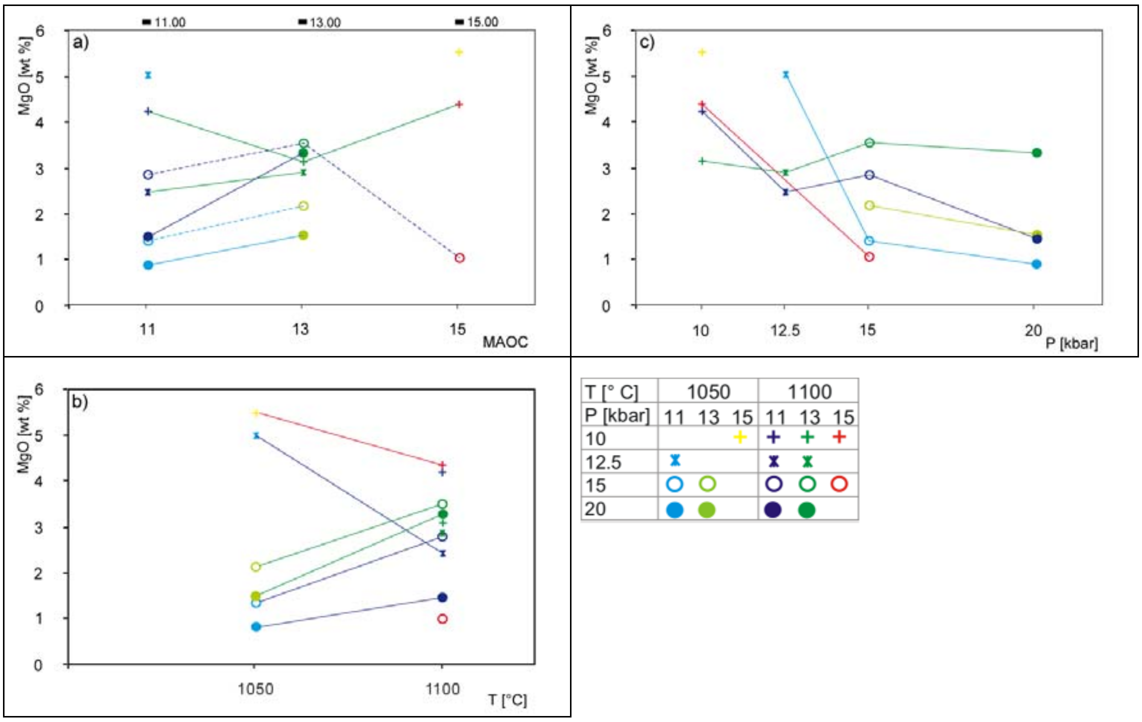

Figure 5.3.24: MAOC - MgO (a), *T* - MgO (b) and *P* - MgO (c) variation diagrams illustrate the evolution of MgO in melts of similar *P*–*T* conditions in MAOC 11, 13 and 15. Similar conditions are interconnected. The black rectangles in the MAOC diagram indicate the bulk composition value.

FeO is not a factor for the discrimination of TTG-like melts in this study because low values of FeO in the TTG-like melts also occur in the basaltic melts (Fig. 5.3.20d). FeO is depleted in the melt compositions in comparison with the initial proportions in MAOC 11–15. FeO in melt generally increases from MAOC 11 to 13 and then decreases towards MAOC 15 (Fig. 5.3.25a). The lowest values are present at 15 kbar and no overall *T*-dependent trend is obvious. To higher bulk MgO, Fe^{2+} decreases of the expense of Mg in garnet (Tab. 5.3.2), clinopyroxene (Tab. 5.3.4), orthopyroxene (Fig. 5.3.16, Tab. 5.3.5) and amphibole (Tab. 5.3.3).

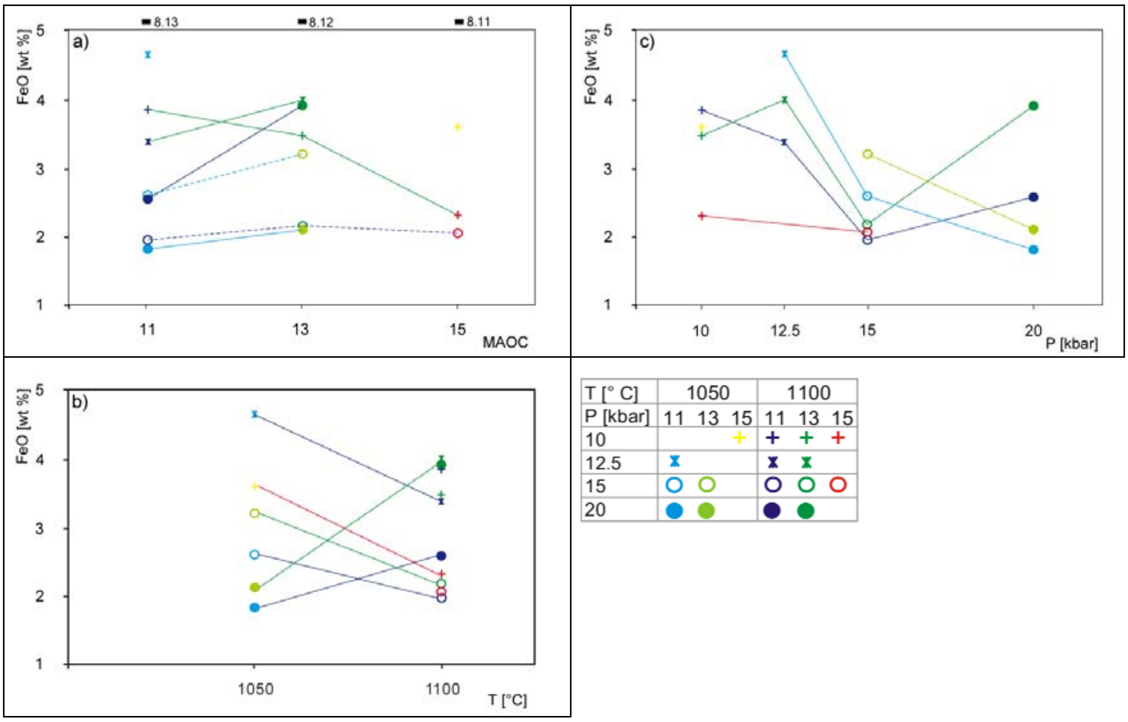

Figure 5.3.25a-c: MAOC - FeO (a), *T* - FeO (b) and *P* - FeO (c) variation diagrams illustrate the evolution of FeO in melts of similar *P*–*T* conditions in MAOC 11, 13 and 15. Similar conditions are interconnected. The black rectangles in the MAOC diagram indicate the bulk composition value. The exchange between MgO and FeO in amphiboles is illustrated in (d).

The melt compositions have lower CaO than the bulk rock MAOC compositions (Fig. 5.3.26a). CaO in melt compositions of MAOC 11 and 13 show no evident trends but it is obvious that CaO in the rare melt analyses of MAOC 15 always plot in the higher range. CaO contents in melt decrease with increasing pressure showing lower values at 12.5 kbar than at 15 kbar. With the exception of 12.5 kbar in MAOC 11 and 10 kbar in MAOC 15, CaO increases with increasing temperature. Figure 5.3.20g illustrates the decreasing CaO contents with increasing SiO_2 in direction to the TTG-like melt compositions. CaO is mainly present in clinopyroxene, plagioclase and garnet. In garnet, CaO broadly decreases from MAOC 11 to 13 towards a wider variety of values in MAOC 15. CaO in plagioclase (Fig. 5.3.17) also decreases with increasing pressure and with increasing bulk rock MgO.

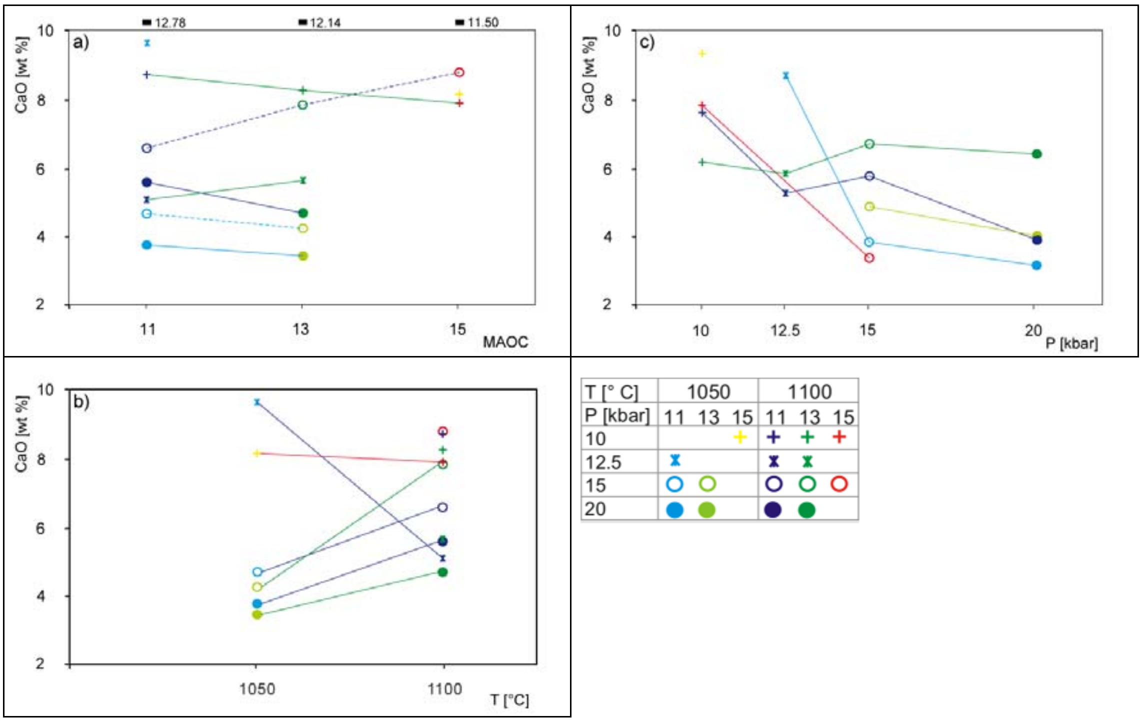

Figure 5.3.26a-c: MAOC - CaO (a), *T* - CaO (b) and *P* - CaO (c)variation diagrams illustrate the evolution of CaO in melts of similar *P*–*T* conditions in MAOC 11, 13 and 15. Similar conditions are interconnected. The black rectangles in the MAOC diagram indicate the bulk composition value.

Na_2O is generally enriched in the melt compositions of the experimental runs compared to the initial MAOC compositions except for 10kbar/1100 °C in MAOC 11 and 20 kbar/1100 °C in MAOC 13 (Fig. 5.3.27a). Changes in Na_2O content predominantly occur as a function of pressure, beginning with an increase from 10 to 12.5 kbar and followed by a decrease to 20 kbar. Towards higher pressures, Na_2O is incorporated to a greater extent into clinopyroxene, which evolves towards more omphacitic compositions at 20 kbar (Tab. 5.3.4 and Figs 5.3.14 and 5.3.15a).

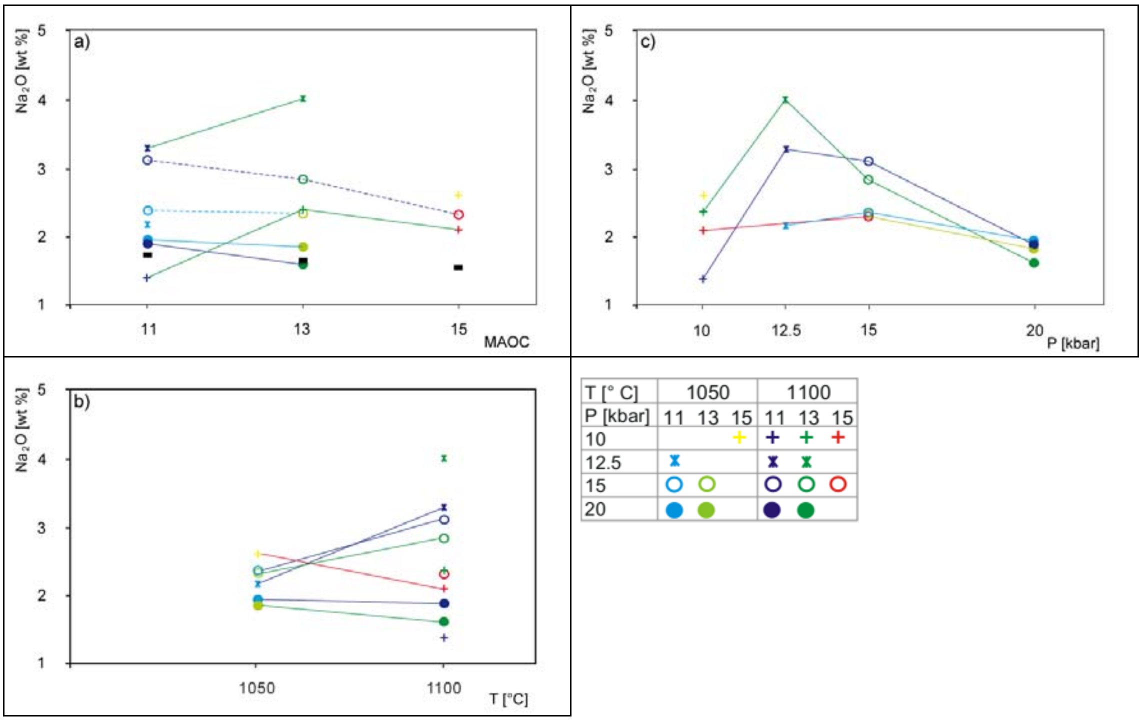

Figure 5.3.27a-c: MAOC - Na_2O (a), *T* - Na_2O (b) and *P* - Na_2O (c) variation diagrams illustrate the evolution of Na_2O in melts of similar *P*–*T* conditions in MAOC 11, 13 and 15. Similar conditions are interconnected. The black rectangles in the MAOC diagram indicate the bulk composition value.

5.3.3.9 Estimation of the phase abundances

The abundances of phases were estimated using pictures taken during the microprobe analysis in combination with a mass balance approach. The mass balance for the estimation of phase abundances was executed with the bulk rock compositions and the mineral compositions determined via microprobe analysis (subchapter 5.3.3.2–5.3.3.7) by using the “solver” function of Excel. The mass balance approach was used as a first estimate for the phase abundances. The results were enhanced with estimations of phase abundances from BSE pictures to eliminate errors originated during the mass balance calculations. Sources of error are that average values were considered for inhomogeneous phases, poor equilibration of some assemblages (especially in

MAOC 15) and/or the presence of undefined unreacted material. Taken together, this all would falsify or enable the mass balance approach calculations. Therefore, phase abundances given in brackets were estimated only by estimations on the basis of BSE images. This again is not exact in cases where the phases form a mush and are not completely distinguishable from each other by their colour and appearance in the images. If unreacted material was present, it was not considered and the phases were normalised to 100 %.

Table 5.3.8: Estimations of phase abundances for each assemblage combining a mass balance approach with phase abundance estimations on the basis of BSE images and estimations during microprobe analyses. The degree of melt correspond to Tab. 5.3.1. For assemblages with bracketed numbers no mass balance calculation was possible as unrected material was present or the assemblages were bad equilibrated. Mineral abbreviations are given in Tab. 3.3.1.

P [kbar]	T[°C]		g	amph	cpx	opx	pl	q	ru	m	degree of melt
10	1050	MAOC 11			x(60)		x(38)			x(2)	low
		MAOC 13		x(33)	x(45)	x(5)	x(15)			x(2)	low
		MAOC 15		x(12)	x(68)	x(6)	x(12)			x(2)	(low)
10	1100	MAOC 11			42	19	32			5	medium
		MAOC 13			x(75)	x(20)	x(1)			x(4)	medium
		MAOC 15			x(85)	x(12)				x(3)	low
12.5	1050	MAOC 11	20	1	43	9	24			2	low
		MAOC 13	25	1	50	7	17				
		MAOC 15	x(25)	x(15)	x(44)	x(15)	x(1)				
12.5	1100	MAOC 11	30		38	4	21	1		6	medium
		MAOC 13	30		42	6	15			7	medium
		MAOC 15	x(27)		x(50)	x(18)	x(5)				
15	900	MAOC 11	31	1	44		24				
		MAOC 13	25	8	48	3	16				
		MAOC 15	x(26)	x(10)	x(60)	x(2)	x(2)				
15	1050	MAOC 11	32		47		10			10	high
		MAOC 13	31		53		2	1		13	high
		MAOC 15	35		53	7	4			1	(low)
15	1100	MAOC 11	32		44					23	high
		MAOC 13	34		48					17	high
		MAOC 15	34	10	50	3				3	medium
20	1050	MAOC 11	32		51			1	1	15	high
		MAOC 13	34		54			1	1	10	medium
		MAOC 15	41		56	1			1	2	(low)
20	1100	MAOC 11	36		43					20	high
		MAOC 13	33		65					2	(low)
		MAOC 15	43		55						

5.4 Discussion of the high-pressure experiments

5.4.1 The location of the solidi and general changes in mineral assemblages

This subchapter presents the stability and modal proportions of phases in the investigated *P–T* area of different MAOC compositions. The investigated *P–T* conditions cover a range that transverses the solidus but these conditions are just points in a continuously evolving system. No data are available for the intervals between or beyond those points and additionally there is potential to miss accessory phases in the assemblages. The results of the high-pressure partial melting experiments in this study (subchapter 5.3.1–5.3.3) are summarised in Fig. 5.4.3, illustrating the stable mineral assemblages at the particular *P–T* conditions for MAOC 11, 13 and 15, the composition of melt as well as the estimated solidi and phase boundaries for garnet, amphibole, orthopyroxene and plagioclase. The results are further discussed considering the former experimental studies introduced in subchapter 2.3.4 and in the context of geodynamic settings.

Solidus

The positions of the solidi in MAOC 11, 13 and 15 are interpolated because the actual solidi at $P > 15$ kbar must occur at lower temperature than used in the experiments as all experiments at 20 kbar were melt bearing (Fig. 5.4.3). In MAOC 11, only one subsolidus assemblage occurs at 15 kbar/900 °C and therefore the only evidence for the location of the solidus is that it occurs between 900 °C and 1050 °C at 15 kbar. The existence of a low proportion of melt at 12.5 kbar/1050°C may suggest a backbending of the solidus to lower *T* at 12.5 kbar as apparent in MAOC 13 and 15. The shape of the interpolated solidus in MAOC 11 (Fig. 5.4.3a) is adjusted to the calculated solidus illustrated in the *P–T* pseudosections (Fig. 6.3.1) and also exhibits a backbend. The temperature condition of the solidus in MAOC 11 is estimated on the temperature difference between the calculated solidi in MAOC 11, 13 and 15 (Fig. 6.3.1) combined with the results of the experiments. The position of the solidi in MAOC 13 and 15 is further constrained by additional subsolidus assemblages at 12.5 kbar/1050 °C in MAOC 13, and at 12.5 kbar and 15 kbar/1050 °C in MAOC 15, in which also a minor amount of melt is identified at 10 kbar/1050 °C (Fig. 5.4.3b, c). It is possible that small proportions of initial melt were not detected, which would shift the solidi to slightly lower *T*. The backbend to higher *T* around 12.5 kbar is a characteristic feature of the solidi in MAOC 11, 13 and 15 is and these “S-“shaped, backbending solidi are decribed at higher pressure in the literature (e.g. Winther & Newton, 1991; Wyllie & Wolf, 1993; Vielzeuf & Schmidt, 2001) according to the breakdown of water-bearing phases and the induced melting owing to the accompanying water-release. Moyen & Stevens (2006) stated that a backbending solidus is typical for experimental investigations because the free water is not able to escape from the system as it is typical for natural rocks. This leads to increased melting at the conditions where H_2O-bearing minerals dehydrate and therefore lowering the melting point and may be also account for the backbends in the calculated solidi where H_2O remains in the system (Fig. 6.3.1).

Mineral phases

The phase-boundaries for garnet, amphibole, clinopyroxene, orthopyroxene and plagioclase are illustrated in Fig. 5.4.3d-f. The compositions of the phases garnet, amphibole, clinopyroxene and orthopyroxene are sensitive to the bulk rock MgO, showing increased Mg in their formula with increasing MgO in the bulk rock compositions from MAOC 11 to 15 (subchapter 5.3.3).

Garnet is stable in the assemblages of $P \geq 12.5$ kbar in MAOC 11, 13 and 15 and forms a major mineral phase in each of those assemblages. The increasing proportion of garnet towards higher pressures in all bulk compositions is accompanied by a limitation in the stability and/or the amount of the other phases at these conditions, whereas especially the proportions of amphibole and plagioclase which decrease. The proportion of the pyrope-component and Mg# are sensitive to the increasing MgO-content of the bulk rock composition from MAOC 11 towards MAOC 15 (Fig. 5.3.12). The zoning of garnets in some assemblages has little influence of the composition of melt as it predominantly occurs in the subsolidus assemblages at 900 °C (subchapter 5.3.3.2). The zoning also occurs in MAOC 11 at 15 kbar/1100 °C and 20 kbar/1050 °C, whereas both assemblages do not perfectly fit the TTG-like character because melt in the first one is of intermediate composition and melt in the second one is tonalitic but with rutile in the source (Tab. 5.3.1). The formula calculations on some of the averaged garnet compositions indicate a minor majorite component which is randomly distributed in MAOC 11, 13 and 15 (Tab. 5.3.2), predominantly in assemblages where zoned garnet crystals occur and/or in melt-free assemblages, both indicating experimental runs with imperfectly equilibrated phases. This may have allowed the incorporation of Si on the Y-position (Tab. 5.3.2) and the development of a majorite component, whereas majorite is usually common in the mantle transition zone (e.g. Ohtani *et al.*, 1991; Rollinson, 2007) and in meteorites (Smith & Mason, 1970).

The amount of *amphibole* in the assemblages of this study increases from MAOC 11 to MAOC 15 (Tab. 5.3.3). Since amphibole is involved in early partial melting reactions, the phase reacts out early or, in the case of the experiments in this study, was possibly not able to form at these high *P–T*. Therefore, amphibole is not implicitly apparent in the residue assemblages where the higher proportions of melt occur. The MAOC 11 assemblages host the smallest proportion of amphibole at 12.5 kbar/1050 °C and 15 kbar/900 °C (Tab. 5.3.8). Assemblages with a higher abundance of melt do not contain amphiboles as the H_2O in the system is primarily incorporated in melt after the breakdown of amphibole. The amphibole-out boundary is estimated to have a negative slope from slightly above 15 kbar/900 °C to around 12.5 kbar/1050 °C (minor proportion of amphibole) and bends back beneath by excluding the amphibole-free assemblage at 10 kbar/1050 °C. Although coexisting amphibole and melt in MAOC 11 is not well established at the experimental *P–T* conditions (only at 12.5 kbar/1050 °C), amphiboles and melt may occur together at conditions of $T < 1050$ °C where initial melting is induced by the breakdown of amphibole. The low–*T* conditions where amphibole and melt may occur together are not investigated in this study and the basaltic melt at 10 kbar/1100 °C and 12.5 kbar/ 1050 °C indicate that amphibole may be a contributor to these basaltic melts at 10 and 12.5 kbar, which are not present at 15 kbar. Amphibole is stable at 900 °C, thus indicating that amphibole is present at the solidus where tonalitic melts may have directly formed at 15 kbar. After the complete breakdown of amphibole, melt in the absence of amphibole and in the presence of plagioclase and quartz is tonalitic in MAOC 11. A limited coexistence of melt and amphibole is also developed for the MAOC 13 assemblages, where both phases only coexist at 10 kbar/1050 °C and amphibole forms a major phase together with two pyroxenes and plagioclase. The proportion of amphibole at 15 kbar/900 °C is higher than in the equivalent MAOC 11 assemblage, thus the amphibole-out boundary may proceed at higher *P–T* conditions and the amphibole-stability field is extended with the 10 kbar/1050 °C assemblage. The amphibole stability above 15 kbar/900 °C and below 1050 °C can not be determined due to the lack of data at these conditions yet it is likely that the curve becomes flatter towards lower temperature as it does in former experiments with basalts, but at different pressure (e.g. the subsolidus amphibole-out boundary at $P > 20$ kbar in Schmidt & Poli, 1998). The solidi and amphibole-out boundaries up to 15 kbar occur close to each other (Fig. 5.4.3d-f), suggesting that the breakdown of amphibole induces the generation of basaltic melts even in the presence of small proportions of plagioclase at 10 and 12.5 kbar and 1100 °C. The maximum proportion of amphibole was determined in MAOC 15, where the phase is absent only at 20 kbar and at 1100 °C (10 and 12.5 kbar). The highest proportions are achieved at 12.5 kbar/1050 °C and 15 kbar/1100 °C, where predominantely pargasite is developed. The curve is positively sloped at lower pressure and bends back between 15 and 20 kbar. Pargasitic amphiboles (Fig. 5.3.13, Tab. 5.3.3), coexistent with melt or in an assemblage close to the solidus, are coupled to melts of basaltic composition in MAOC 15 and at lowest pressure in MAOC 13. MAOC 15 is dominated by the pargasitic amphibole with minor proportions of magnesiohornblende and tschermakite, which are more frequently developed in MAOC 11 and 13 without showing a characteristic distribution.

Clinopyroxene is developed in all investigated assemblages as a dominat phase (Tab. 5.3.2). As described for garnet and amphibole, the clinopyroxene compositions from MAOC 11 to 15 are also sensitive to the bulk composition, they achieve increased proportions of the mean Mg on the X-Position as well as higher Mg# towards MAOC 15. The clinopyroxenes generally straddle the boundary of diopside and augite with a trend to more augitic compositions towards higher MgO in the bulk rock (Fig 5.3.15b). The clinopyroxenes at high pressures coexisting with garnet ± melt trend towards the Ca–Na pyroxene omphacite with an elevated jadeite component (Figs 5.3.14, 5.3.15a). It is noteworthy that the jadeite component in the clinopyroxenes in the eclogite facies realm is not high enough to be considered omphacite, thus leading to the term diopside-eclogite as introduced for the *P–T* pseudeusections (subchapter 4.2).

The stability field of *orthopyroxene* increases with higher bulk MgO from $P \leq 12.5$ kbar in MAOC 11 to a nearly overall presence of orthopyroxene in MAOC 15, except at 20 kbar/1100 °C. The orthopyroxene-bearing assemblages at $P \leq 12.5$ kbar in MAOC 11 and 13 are granulite facies assemblages, which occur in MAOC 15 also at 15 kbar. Orthopyroxene in MAOC 11 occurs in melt-bearing assemblages and in MAOC 13 and 15 it is also present under subsolidus conditions. Plagioclase-free pyroxenite as developed in experiments with the komatiite from Gorgona (Foley *et al*., 2003; subchapter 4.2.7) has developed in the experiments of this study in MAOC 15 at 10 kbar/1100 °C, whereas the proportion of plagioclase is also very low at 12.5 kbar (Tab. 5.3.8).

The stability of *plagioclase* in the experiments is restricted to pressures ≤ 15 kbar with the exception of 15 kbar/1100 °C. The composition generally evolves to Na-richer plagioclase (albite) with increasing *P–T* during progressive melting in MAOC 11 and 13 (Figs 5.3.17, 5.4.1a). Plagioclase in assemblages with TTG-like tonalitic melts exhibt the highest proportion of the albite component and therefore the lowest anorthite component (Fig. 5.4.1a). The albite component then increases from MAOC 11 to MAOC 13 but not strictly towards MAOC 15. Plagioclase in MAOC 15 coexists only in one assemblage (10 kbar/1050 °C) with melt of basaltic composition, where it exhibits the highest anorthite-component of all experiments (Tab. 5.3.6, Fig. 5.3.17). The coexistence of plagioclase and melt in the experimental runs decreases towards higher MgO in the bulk composition. The three tonalitic melts at pressures ≤ 15 kbar in MAOC 11 at 12.5 kbar/1100 °C (in the presence of quartz) and at 15 kbar/1050 °C in MAOC 11 and 13 have the lowest proportions of CaO in their compositions and coexist with plagioclase with the lowest anorthite component (Fig. 5.4.1a). This is shown vice versa for the plagioclase compositions in presence of Ca-richer basaltic melts. The proportion of melt in assemblages with coexisting plagioclase and tonaltic melt is higher (6–15 %) than that for basaltic melts (2–7 %) in the presence of plagioclase (Tab. 5.3.8), but the highest amounts of melt are developed in plagioclase-free assemblages. In contrast, the actual proportion of plagioclase in an assemblage is not responsible for the development of different melt compositions: basaltic melts have developed from rocks with 0–32 % plagioclase in the source, and tonalitic melts at pressures ≤ 15 kbar from assemblages with 2–21 % plagioclase (Fig. 5.4.1b). As introduced before, Na_2O in the melt shows no clear trend, even as a function of plagioclase stability and composition.

The breakdown of plagioclase allowed enhanced melting at 15 kbar/1100 °C, where the composition of melt evolves to an intermediate (MAOC 11) and a basaltic (MAOC 13) melt composition (Fig. 5.4.3a, b). The plagioclase-out boundaries in MAOC 13 and 15 are close to the solidus at the low and middle pressure range of the experimental conditions, indicating that the phase is involved in melting reactions over a narrow temperature range together with amphibole (Moyen & Stevens, 2006) and resulting in the peritectic phases garnet and clinopyroxene as well as in basaltic melt. The mode- and overall stability field of plagioclase in MAOC 11 and 13 is slightly greater than than those of amphibole, but this reverses over in MAOC 15 where amphibole is more abundant.

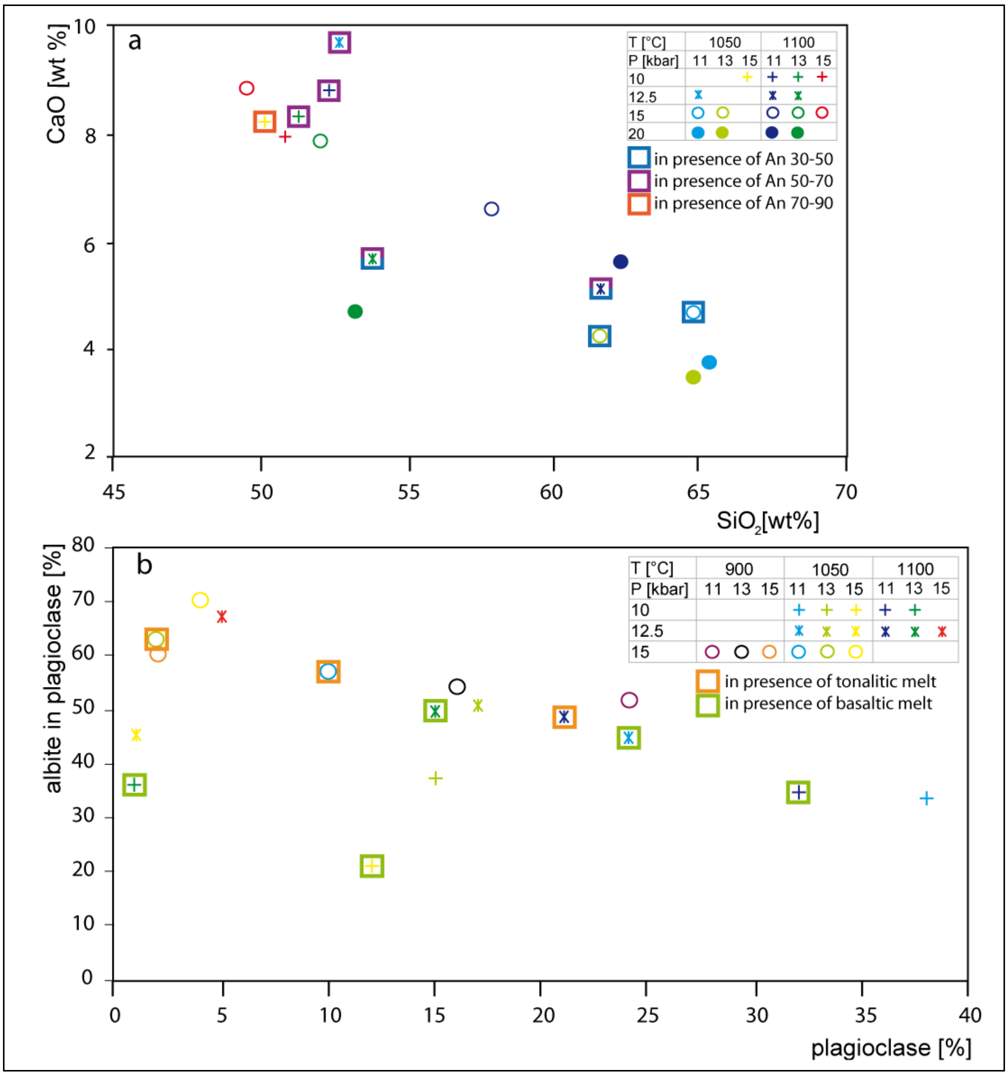

Fig. 5.4.1a, b: Variation diagram of SiO_2 against CaO (a) of the melt compositions (Tab. 5.3.7). The boxes indicate assemblages where melt coexists with plagioclase. The proportion of the anorthite component in plagioclase (Tab 5.3.7) is labelled with different colours and shows that the anorthite component decreases with icreasing pressure. The SiO_2 content in the melt divides the melt compositions into basaltic (< 55 wt% SiO_2), intermediate and tonalitic (> 60 wt% SiO_2). (b) illustrates proportion of the anorthite component in plagioclase with labelling of plagioclases coexisting with melt and the composition of melt.

Quartz is present in MAOC 11 at 12.5 kbar/1100 °C, in MAOC 13 at 15 kbar/1050 °C and in MAOC 11 and 13 at 20 kbar/1050 °C (Tab. 5.3.1). It is located at the upper margins of the capsules coexisting with tonalitic melt but tonalitic melt also occur swithout quartz at 15 kbar/1050 °C and 20 kbar/1100 °C in MAOC 11.

Rutile occurs in all MAOC compositions at 20 kbar/1050 °C, whereas in MAOC 15 basaltic melt is generated and the melt in MAOC 11 and 13 is of tonalitic composition. There is a debate whether the presence of rutile excludes these melts from belonging to the TTG-suite (subchapter 2.2.3 and 5.4.2)

Melt composition

The chemical classification of the averaged melt compositions in each assemblage is given in subchapter 5.3.3.7, whereas a general subdivision is made between tonalitic (TTG-like) melt (> 60 wt% SiO_2), transitional melt (55–60 wt% SiO_2) and basaltic melt (50–55 wt% SiO_2). TTG-like melts generated by partial melting high-pressure experiments of metamorphosed picrites (MAOC 11 and 13) are broadly tonalitic in terms of normative An–Ab–Or and Q–A–P (Figs 5.3.18, 5.3.19; Tab. 5.3.7) and they are developed in the following assemblages:

MAOC 11: 12.5 kbar/1100 °C, 15 kbar/1050°C, 20 kbar/1050 and 1100 °C
and to a smaller proportion in
MAOC 13: 15 kbar/1050 °C and 20 kbar/1050 °C

Tonalitic melts generally occur in assemblages such as garnet + clinopyroxene ± plagioclase ± quartz ± orthopyroxene, where orthopyroxene occurs as a minor phase at 12.5 kbar/1100 °C in MAOC 11. The presence of orthopyroxene does not preclude the generation of TTG-like tonalitic melts if plagioclase and quartz are present and orthopyroxene is not in contact with the melt as illustrated for the assemblage at 12.5 kbar/1100 °C in MAOC 11 (Fig. 5.4.2a). The tonalitic melts are located at the upper margin in the capsules, predominantly in contact with clinopyroxene, plagioclase and/or quartz (Figs 5.4.2a, 5.3.3) and in the inner part of the capsules interstitially between clinopyroxene and garnet (Figs 5.4.2b, 5.3.7a). Tonalitic melts in MAOC 11 and 13 at 20 kbar/1050 °C in the absence of plagioclase but in the presence of rutile may not belong to the TTG-like melts as introduced in subchapter 2.3.2 and further discussed in subchapter 5.4.2, but tonalitic melts at lower P in the presence of plagioclase do. Amphiboles do not occur in assemblages with tonalitic melt but in assemblages at lower T, even in MAOC 11 at 15 kbar/900 °C and 12.5 kbar/1050 °C. This indicates that amphibole-bearing assemblages (garnet-amphibolite) may have been present under subsolidus conditions, which produced basaltic melt as identified at 12.5 kbar/1050 °C. After the breakdown of amphibole tonalitic melts were produced at 1100 °C. Nevertheless, an amphibole-bearing assemblage at the solidus at 15 kbar in MAOC 11 and 13 may have produced initially tonalitic melt.

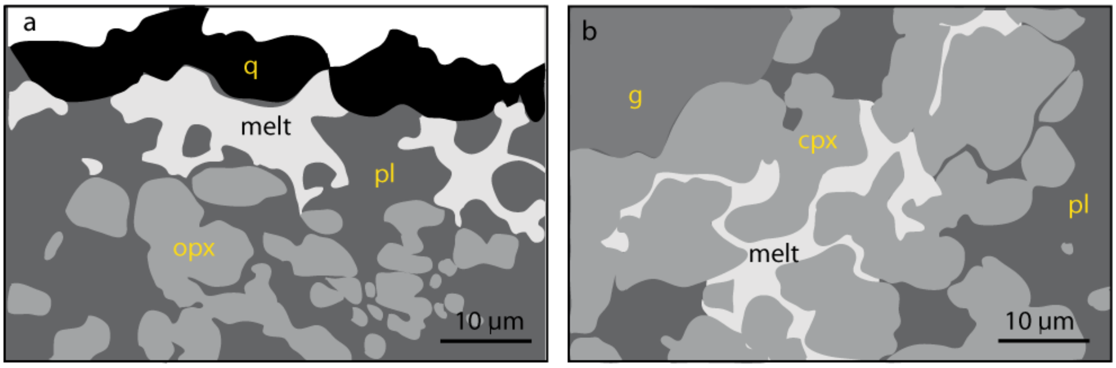

Figure 5.4.2a, b: Schematic scetches of the distrubition of tonalitic melt and the surrounding minerals in MAOC 11 at 12.5 kbar/1100 °C at the upper rim of the capsule (a) and half way down the capsule (b). Tonalitic melt is in contact with plagioclase and quartz at the margin whereas orthopyroxene is in contact with plagioclase (a). Tonalitic melt in (b) occurs interstitially between clinopyroxenes replacing plagioclase and melt usually is not in contact with garnet.

The *intermediate* melt composition in MAOC 11 at 15 kbar/1100 °C occurs in an assemblage with garnet and clinopyroxene. At 15 kbar/1050 °C and 12.5 kbar/ 1100 °C, where tonalitic melts occur, plagioclase was additionally stable. At slightly higher *P–T* conditions (15 kbar/1100 °C), the proportion of melt then is strongly increased (Tab. 5.3.8) and occupies the areas, which are filled with plagioclase in the plagioclase-bearing assemblages at lower *P–T* conditions. This indicates that progressive partial melting in the absence of plagioclase will result in melts which do not longer have TTG-like compositions at 15 kbar. In MAOC 13 at 15 kbar/1100 °C, basaltic melt developed in the presence of garnet and clinopyroxene. In contrast to MAOC 11, the tonalitic melt-bearing assemblage at 15 kbar/1050 °C comprises less plagioclase and quartz, and the assemblage at 12.5 kbar/1100 °C exhibit melt of basaltic composition.

Melt of *basaltic* composition generally occurs in assemblages with clinopyroxene ± garnet ± amphibole ± orthopyroxene ± plagioclase and is detected in MAOC 11 at 10 kbar/1100 °C with clinopyroxene + orthopyroxene + plagioclase and at 12.5 kbar/1050 °C with garnet + amphibole + clinopyroxene + orthopyroxene + plagioclase. Orthopyroxene crystals at 10 kbar occur in the melt area at the upper margin of the capsule (Fig. 5.3.5b) but it is not required for the generation of basaltic melts in assemblages that lack plagioclase and quartz, e.g. 15 kbar/1100 °C in MAOC 13 (Ta. 5.3.1). Basaltic melt in MAOC 13 is more abundant up to higher pressure (15 kbar) than in MAOC 11 and it is the dominant type of melt in MAOC 15. Amphibole, especially in MAOC 13, is not involved in the assemblages with basaltic melt at 1100 °C but it is supposed to be a contributor to these melts as it is stable in most of the melt-free assemblages at lower temperatures, which indicates that the amphibole breaks down between 1050 °C and 1100 °C induced the formation of basaltic melt. Amphibole in MAOC 15 occurs in 3 of 4 assemblages with basaltic melts and the plagioclase-out boundary is fairly close to the solidus which limits the coexistence of melt and plagioclase and the contribution of plagioclase to the melt, thus basaltic melt has developed (Fig. 5.4.3c).

In summary, the mineral compositions as well as the proportion of melt are not useful for a determination of the type of melt, they rather depend on the *P–T* conditions of the runs and the initial bulk rock composition. However, the assemblages coexisting with melts of tonalitic and basaltic composition differ in their composition. Tonalitic TTG-like melts always occur in the presence of garnet, clinopyroxene and, at $P \leq 15$ kbar, plagioclase as well as quartz in most assemblages that lack amphibole. Nevertheless, amphibole occurs at lower *P–T* and at 12.5 kbar in the presence of basaltic melt. The generation of tonalitic melt at $P \leq 15$ kbar is possible in a window of medium to high proportions of partial melting, which is best represented in MAOC 11 where (1) an increased degree of melting at 12.5 kbar changes the composition of the melt from basaltic to tonalitic over a *T*-interval of 50 °C and (2) by an increase in the proportion of melt at 15 kbar accompanied by the breakdown of plagioclase, which led to intermediate melt compositions over the same *T*-interval. Although the residue at 15 kbar/1050 °C contains no amphibole, it was present at 900 °C and may give rise to plagioclase-bearing garnet-amphibolite, which evolved with increasing *T* towards a diopside-eclogitic residue. Tonalitic melts generated at 20 kbar in the presence of rutile and a diopside-eclogitic residue are discussed in the next subchapter.

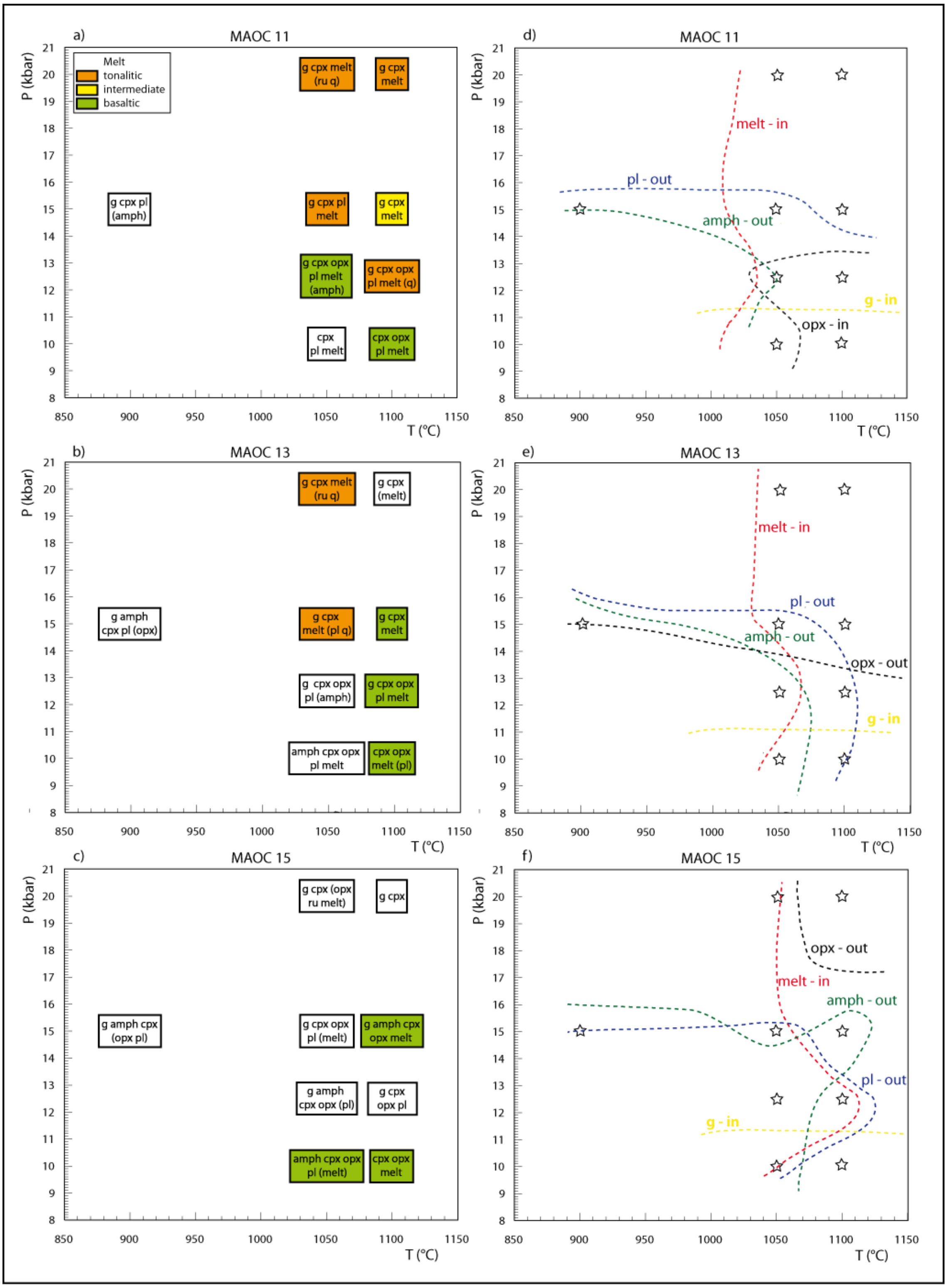

Figure 5.4.3a-f: Summary of the results from the high-pressure experiments deduced on MAOC 11, 13 and 15. a-c: The boxes include stable phases determined via microprobe analysis at given *P*–*T* conditions, phases in brackets are accessory. Different colours represent the types of melt (tonalitic, transitional or basaltic). Approximate phase-boundaries, resulting from the mineral assemlages are illustrated in d-f.

5.4.2 Comparison with previous studies

This subchapter relates the results from this study to those of earlier investigations and discusses similarities and differences between them.

It is inferred that melting in the *garnet* stability field is required for the generation of TTG-like melts (e.g. Drummond & Defant; 1990, Rapp *et al.*, 1991; Martin, 1999; Moyen & Stevens, 2006). The instability of garnet in the assemblages at 10 kbar (Tab. 5.3.1) as well as the melt compositions in this study (Tab. 5.3.7) excludes this *P*-condition as a possible source for the genesis of TTG-like melts from metamorphosed MgO-rich rocks, regardless of any potential geologic setting. Compared to earlier experiments with basaltic starting material (subchapter 2.3.4; summarised by Moyen & Stevens, 2006) the appearance of garnet here seems to be at slightly lower *P*, especially in the case of fluid-absent melting. This is in contrast to the appearance of garnet at higher *P–T* in komatiites (Foley *et al.*, 2003), whose MgO content is close to MAOC 15.

Several authors inferred that the generation of TTG-like melts requires *amphibole* in the source of melting (e.g. Martin, 1999; subchapter 2.3.2) but here amphibole does not occur in assemblages with tonalitic melts. As discussed above, the *P–T* conditions of the experiments containing tonalitic melt may be situated at too high temperatures where the instability of amphibole is achieved, but it may have been present at the solidus as indicated by the amphibole-bearing subsolidus assemblages at 15 kbar. This is consistent with the prediction of Moyen & Stevens (2006), who infers that melting of amphibolite quickly results in melts in equilibrium with amphibole-free eclogitic assemblages.

The observation that the stability of *orthopyroxene* increases with higher MgO in the bulk rock composition is consistent with the experiments for the komatiitic composition (Foley *et al.*, 2003), where the appearance of orthopyroxene gives rise to pyroxenite assemblages instead of garnet-amphibolite or eclogite assemblages in a MORB. However, the orthopyroxene-bearing assemblages in MAOC 11, 13 and 15 are rather granulitic than pyroxenitic assemblages. Orthopyroxene in MAOC 11 is a liquidus-phase, which is consistent with the experiments on basaltic starting material summarised by Moyen & Stevens (2006). In MAOC 13 and 15 the solidus appears at higher temperatures leading to an increasing stability of orthopyroxene also at subsolidus conditions. The assemblages in MAOC 15 trend towards plagioclase-free pyroxenites as reported from experiments with the Gorgona komatiite

(Foley *et al.*, 2003), but they do not perfectly fit as plagioclase is still present at least in MAOC 15 and these assemblages rather represent granulite facies assemblages.

As presented in subchapter 2.3.2, the presence of *plagioclase* in the source of melting is inferred to be required for the generation of early TTG-like melts from garnet-amphibolite at shallow depths (Martin & Moyen, 2002). The plagioclase-stability in the experiments is restricted to conditions ≤ 15 kbar with the exception of the plagioclase-free assemblage at 15 kbar/1100 °C in MAOC 11.

The presence of *rutile* in all three MAOC compositions at 20 kbar/1050 °C would permit high Nb/Ta ratios, which are supposed to develop in the melts in the presence of rutile and this would exclude these melts from beeing TTG-like according to Foley *et al.* (2002). This is debated by Rapp *et al.* (2003) who infers that TTGs have either variable or low Nb/Ta ratios and that TTGs could have formed also in equilibrium with eclogitic residues. Nevertheless, the tonalitic melt in MAOC 11 at 20 kbar/1100 °C occurs in a rutile-free diopside-eclogitic assemblage and can be regarded as TTG-like from both theories. The absence of plagioclase at 20 kbar has no influence as this pressure fits the model of Martin & Moyen (2002), who argued that plagioclase stability in the genesis of TTG-like melts will have decreased during melting in deepening subduction zones with time.

TTGs are *sodic granitoids* (Moyen & Stevens, 2006; subchapter 2.3.2), but the TTG-like melts generated during the high-pressure experiments in this study do not exhibit higher Na_2O-contents compared to the basaltic melts. Figure 5.3.20 e illustrates SiO_2 versus Na_2O and the TTG-like melts in this study plot rather in the lower ranges of Na_2O (Fig. 5.3.27). However, the amount of SiO_2 is used for the classification of TTG-like melts (subchapter 5.3.3.7). As shown simultaneously by thermodynamic modelling (Fig. 4.3.7a), the bulk MAOC compositions do not contain sufficient Na_2O to stabilise clinopyroxenes of omphacitic compositions and the analysed clinopyroxenes in the assemblages at 20 kbar do not exactly plot in the fields of the Ca–Na pyroxenes or omphacite (Figs 5.3.14 and 15a). This suggests that the bulk compositions for the models of Archean oceanic crust may contain too little Na_2O to stabilise omphacite in the eclogite facies realm and to reach the expected high values for TTG in the generated melts.

The fact that the TTG-like *melts* in this study are of broadly tonalitic composition (Tab. 5.3.7, Figs 5.3.18, 5.3.19) is consistent with the results of former melting experiments on alkali-basalts and tholeiites, leading to rather tonalitic than trondhjemitic liquids (e.g. Holloway & Burnham, 1972; Helz, 1976; Martin, 1999; subchapter 2.3.4). Moyen & Stevens (2006) proposed that TTGs are mostly metaluminous (molecular A/CNK < 1.1, with a small minority up to 1.2), a feature which can not be clearly confirmed by the experiments of this study, predominantly by the absence of K_2O in the system. The absence of K_2O in this study reduces the ratio to A/CN and the tonalitic melt here shows values of generally > 1 up to 1.5 (Tabs 5.3.7, 5.4.1). The high values of A/CN may be a consequence of the absent bulk K_2O which automatically shifts this ratio towards higher proportions. By adding a proportion of 1 respectively 2 wt% K_2O, which is valuable for Archean TTG, (Rollinson, 2007, tab. 4.2), the ratio of A/CNK decreases to lower values but these values are still slightly to high (Tab. 5.4.1). The high values may be additionally reinforced by the fact presented above that the bulk Na_2O in the MAOC compositions may also be too low and therefore the tonalitic melts also contain too little Na_2O.

Table 5.4.1: Molecular A/CNK ratios of tonalitic and intermediate* melt compositions with added 1 or 2 wt% K_2O are lower than the A/CN ratios from Tab. 5.3.7.

	MAOC 11				**MAOC 13**	
P	**12.5**	**15**	**15***	**20**	**12.5**	**15**
T	**1100**	**1050**	**1100**	**1050**	**1100**	**1050**
SiO_2	61.719	64.886	57.956	65.453	62.382	61.726
TiO_2	1.136	0.769	0.883	0.912	1.094	0.936
Al_2O_3	14.871	16.244	19.896	15.032	17.096	16.274
FeO	3.386	2.593	1.974	1.833	2.572	3.205
MgO	2.441	1.378	2.812	0.865	1.475	2.142
CaO	5.096	4.675	6.602	3.743	5.589	4.252
Na_2O	3.285	2.366	3.094	1.924	1.872	2.322
Total	91.934	92.911	93.217	89.764	92.079	90.857
Mg#	0.562	0.487	0.717	0.457	0.506	0.544
A/CN	**1.014**	**1.311**	**1.164**	**1.508**	**1.291**	**1.409**
A/CNK						
+ 1 wt% K_2O	0.944	1.206	1.095	1.360	1.194	1.288
+ 2 wt% K_2O	0.883	1.116	1.033	1.239	1.110	1.187

5.4.3 Genesis of TTG-like melts from MAOC 11, 13 and 15 related to geodynamic processes

The chemical classification of the averaged melt compositions in each assemblage is given in subchapter 5.3.3.7, whereas a general subdivision is made between tonalitic (> 60 wt% SiO_2), transitional (55–60 wt% SiO_2) and basaltic melt compositions (50–55 wt% SiO_2). Tonalitic melts are the important ones regarding the genesis of early TTG-like melts from metamorphosed picrites and these are present in the experimental runs of MAOC 11 at 12.5 kbar/1100 °C, 15 kbar/1050 °C, 20 kbar/1050 °C and 1100 °C and to a smaller degree of MAOC 13 at 15 kbar/1050 °C and 20 kbar/1050 °C.

As introduced in subchapter 2.3.3, early Archean TTG are comparable to modern high-silica-adakites (HSA) and have low Mg# and MgO due to the absent or limited interaction with overlying mantle material in low-angle dipping slabs or at the base of thick oceanic crust in a generally hotter environment. The hotter conditions on the early Earth may have caused a thicker oceanic crust with a higher proportion of MgO (Campbell & Jarvis, 1984; Foley *et al.*, 2003), and the melt compositions discussed here were generated by partial melting of such metamorphosed picrites with 11, 13 and 15 wt% MgO (Tab. 5.2.3). In MAOC 15 no TTG-like melts were generated in terms of SiO_2 (red symbols in Fig. 5.4.4a). The tonalitic melts at 20 kbar and at 15 kbar/1050 °C (MAOC 11) best fit the range for TTG > 3.5 Ga, but they do also fit into the fiels for the younger TTGs (Figs 5.4.4a, b). Furthermore, the tonalitic melts at 12.5 kbar/1100 °C in MAOC 11 and at 15 kbar/1050 °C in MAOC 13 plot in the field of TTG < 3.5 Ga. However, the averaged values for MAOC 13 show higher Mg# than those for MAOC 11 (Fig. 5.3.20a), which might be attributed to the bulk composition.

The interaction of partial melts with mantle material is not regarded and adjusted in the partial melting experiments of this study and the higher MgO and Mg# in MAOC 13 must have been generated by primary processes during the experiments according to the bulk composition. This indicates that formation of early TTGs with low MgO and Mg# is more likely to be generated by melting of oceanic crust with initial lower MgO and that the potential to lower Mg# rises with decreasing MgO in the bulk composition. Nevertheless, partial melts of MAOC 13 with SiO_2 > 60 wt% still plot within the fields of TTG > 3.5 Ga, which indicates that the formation of tonalitic melt is possible at some *P*–*T* (15 and 20 kbar/1050 °C) from MAOC 13 without consideration of possible further mantle interaction. Some degree of interaction between the initial TTG-like melts from metamorphosed MAOC 13 and the mantle would probably cause these melts to shift to rather adakitic compositions, but this is not considered in the experiments of this study.

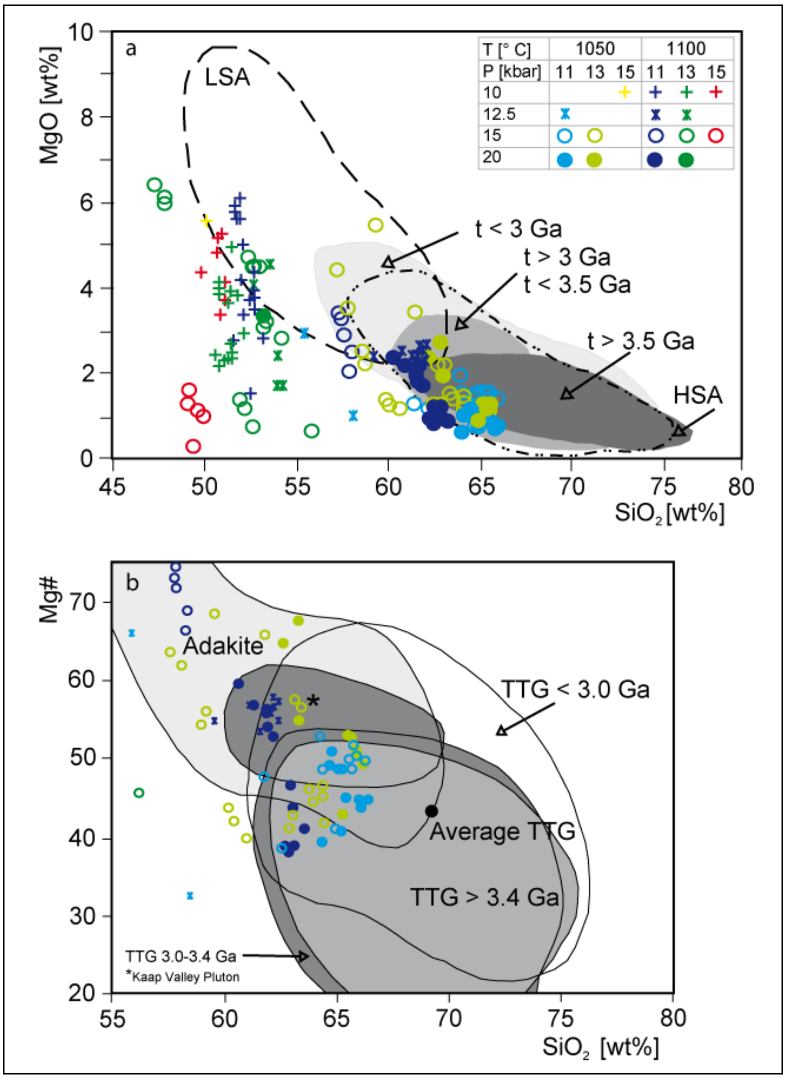

Figure 5.4.4a, b: Compositional ranges of SiO_2 vs. MgO (a, after Martin *et al.*, 2005, fig. 10) and Mg# (b, after Smithies 2000, fig. 4) for TTG of several ages and different types of adakite. The melt compositions of MAOC 11 (15 kbar/1050 °C and 20 kbar/1050 and 1100 °C) and MAOC 13 (15 and 20 kbar/1050 °C) best fit the ranges of TTGs > 3.5 (a) and 3.4 Ga (b).

Thermal gradients and geologic settings

Tonalitic melts were generated in the models of Archean oceanic crust with 11 and 13 wt% MgO at the *P*–*T* conditions described above. The results show a range of conditions for the generation of TTG-like melts in MAOC 11 from 12.5 to 20 kbar, representing thermal gradients of 15–25 °C/km or 525–880 °C/GPa (Fig. 5.4.4a, b) and in MAOC 13 from 15–20 kbar at 1050 °C (15–20 °C/km and 525–700 °C/GPa). The gradients at 15 and 20 kbar (< 750 °C/GPa) are similar to those of the medium-temperature eclogite–high-pressure granulite metamorphism (*E–HPG*) as known from Proterozoic and Phanerozoic rocks (Brown, 2006; subchapter 2.2.3) at depth of approximately 45–60 km. Related to the inferred scenarios for the formation of TTG-like melts through partial melting of metamorphosed oceanic crust in either shallowly subducted slabs, in delaminated material or at the base of thick oceanic crust (subchapter 2.3), 60 km seems to be too deep to represent a realistic scenario of the thickness of oceanic crust, even for a thicker Archean one. However, the formation of tonalitic melts is possible at 60 km depth (20 kbar) by slab melting in deeper subduction zones, but it is unlikely that these melts were extracted without any contamination with mantle material and accompanying modifications during their ascent. It is more likely that these melts would remain at mid-crustal levels. The absence of plagioclase in the diopside-eclogite assemblages at 20 kbar is consistent with the model of Martin & Moyen (2002), who stated that the plagioclase stability decreases with time during partial melting in deepening subduction zones induced by the progressive cooling of the Earth. The presence of rutile at 20 kbar may be a limiting factor for the formation of TTG-like melts as discussed in subchapter 5.4.2. However, rutile was not detected in the presence of tonalitic melt at 20 kbar/1100 °C in MAOC 11, hence the discussion is dispensable for the melt composition at this conditions. This tonalitic melt may be regarded as a TTG-like melt and would fit the scenario of slab melting in subduction zones. Most of the experiments were conducted at 1050 °C and higher in this study but slab melting in subduction zone settings is supposed to occur at lower temperatures from 700–900 °C and at 15–25 kbar or even deeper (10–30 °C/km) (Moyen & Stevens, 2006). However, the high proportion of melt at 20 kbar/1050 °C in MAOC 11 and 13 (ca. 15 % and 10 %; Tab. 5.3.8) indicates that the solidi are located at lower temperatures but that they are limited to be higher than the subsolidus assemblages at 900 °C at 15 kbar.

Another scenario for the genesis of TTG-like melts is partial melting at the base of thick oceanic plateaux at 700–1000 °C and 8–15 kbar (30–50 °C/km) (Moyen & Stevens, 2006), in a piece of delaminated lower crust or in subducted crust in depth around 45 km (15 kbar). The thickness of 45 km is more consistent with the inferred thicker Archean oceanic crust as modern oceanic plateaux reach depths of up to 35 km (subchapter 1.2, 2.2.2.1 and 2.3.3). The tonalitic melts at 12.5 kbar and especially at 15 kbar are equivalent to those settings and they show characteristics of TTG-like melts. These melts could have had more potential to migrate upwards without interacting with mantle material in a pile of thick crust or above delaminated parts/ shallow subduction zones where no asthenospheric mantle material exists above. The thermal gradients at 15 kbar (730 °C/GPa or 20 °C/km) still plot in the same range as for the *E–HPG* metamorphism (Fig. 5.4.5) but in direction to the ultrahigh-temperature granulite

(*G–UHT*) metamorphism. It is not excluded that garnet-amphibolite assemblages could occur at lower temperatures than 1050 °C as amphibole was detected at the subsolidus assemblages at 15 kbar/900 °C in MAOC 11 and 13 and is supported by the modelling.

The presence of plagioclase indicates that tonalitic melts generated at *P* ≤ 15 kbar may belong to early TTGs (Martin & Moyen, 2002), generated in either the base of thick oceanic crust or in shallow subduction zones. The generation of TTG-like melt at 12.5 kbar in the presence of a granulite facies assemblage rather correlates with melting at the base of a thick crust than in a subduction zone settings. The thermal gradient (880 °C/GPa and 525 °C/km) is comparable to that of *G–UHT* metamorphism and may be additionally associated with the unusually low pressure TTG genesis early in cratonic history described by De Wit & Hart (1993), introduced in subchapter 2.3.4.

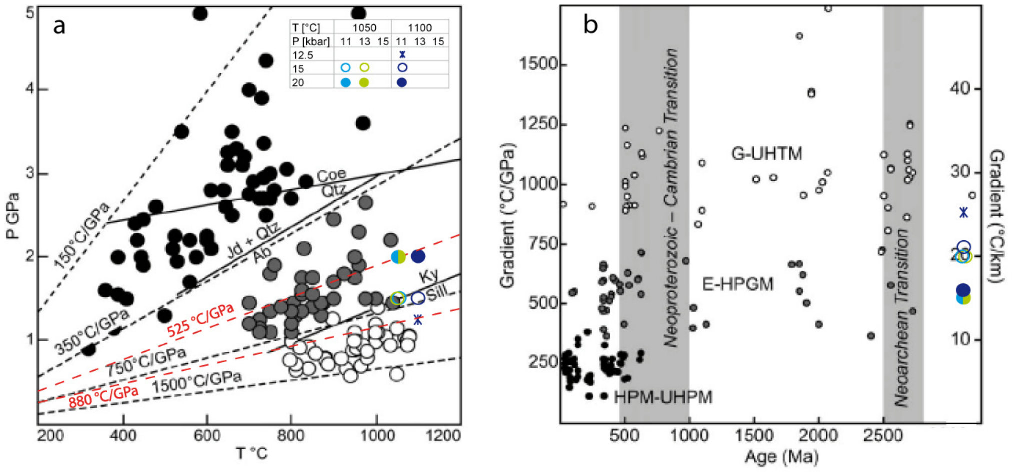

Figure 5.4.5: Metamorphic patterns based on representative *P–T* data by belt in apparent thermal gradients (a) and apparent thermal gradients versus age of peak *P–T* and for three main types of metamorphic belts (b) (Brown, 2006, figs 1, 2) including the thermal gradients for the tonalitic melt-bearing experiments in MAOC 11 and 13. Open circles: granulite and ultrahigh-temperature (*UHT*) granulite metamorphic belts, gray circles: medium-temperature eclogite-high-pressure granulite (*EHP–G*) metamorphic belts, and filled circles: high-pressure–ultrahigh-pressure (*HP–UHP*) metamorphic belts.

The fluid-absent conditions of the experiments precluded a higher proportion of hydrous phases even at 900 °C, but nevertheless, tonalitic melts were generated in the fluid-absent partial melting experiments despite the low H_2O contents of the initial bulk rock compositions. This is in conflict with the predications that TTG-like melts were generated by partial melting of a hydrous source (e.g Barker & Arth, 1976; Jahn *et al.*, 1981; Rapp *et al.*, 1991; Sen & Dunn, 1994; Rapp & Watson, 1995; Martin, 1999; Rapp *et al.*, 1999; Smithies, 2000; Martin & Moyen, 2002, Moyen & Stevens, 2006) and indicates on the one hand that TTG-like tonalitic melts may have been generated by melting of a largely anhydrous picritic source rock, as it is evident in MAOC 11 and 13 Nevertheless, the proportion of H_2O will affect the amount of TTG-like melts that can be produced. On the other hand, it is noteworthy that each experiment just displays a point in a continuously evolving system and it is likely that, even in natural systems, hydrous minerals are dehydrated at these *P–T* conditions and that garnet-amphibolite assemblages have transformed into granulite facies (lower *P*) or eclogite facies (higher *P*) residues (subchapter 2.3.2).

Melts at 10 kbar generated in the absence of garnet show basaltic features and thus exclude this pressure from the potential formation of TTG-like melts. This is consistent with the premise that garnet needs to be stable in the residue of melting (e.g. Drummond & Defant, 1990; Rapp *et al.*, 1991; Martin, 1999). TTG-like melts were not produced at all in the partial melting experiments with the MAOC 15 composition, which limits the proportion of MgO in the source rock from which TTG-like tonalitic melts are extractable by partial melting of metamorphosed picritic oceanic crust.

Chapter 6

Comparison of differences between thermodynamic equilibrium calculations and high-pressure partial melting experiments

6.1 Introduction

The results of the high-pressure partial melting experiments (Chapter 5) and the results of the thermodynamic modelling (Chapter 4) show similarities and differences that originate from several sources of uncertainties in both approaches, outlined in subchapter 6.1.4. In subchapter 6.1.2 each assemblage of the three MAOC compositions is discussed in the context of both approaches by comparing the *P–T* pseudosections for MAOC 11, 13 and 15 with the assemblages generated by the high-pressure partial melting experiments. The determination of the solidi is discussed in subchapter 6.1.3.

6.2 Comparison of the results from thermodynamic modelling and high-pressure experiments

The *P–T* pseudosections for the three models of metamorphosed Archean oceanic crust (subchapter 4.3) are attended to 1200 °C (Figs 6.2.1a, 6.2.2a, 6.2.3a) to cover the range of the investigated *P–T* conditions in the high-pressure partial melting experiments (Chapter 5). The composition variable isopleths for *x(g)*, *j(di)* and *ca(pl),* introduced in subchapter 5.3.3, are incorporated into these pseudosections and the variables *x(g)* and *ca(pl)* and *x(opx)* were predictable also from the microprobe analyses of garnet, plagioclase and orthopyroxene (Tab. 6.2.1). The composition variable *j(di)* describes the type of clinopyroxene. The calculated mineral modes for each experimental *P–T* condition are illustrated in pie charts and are compared to the assemblage determined by the experiments (Figs 6.2.1b, 6.2.2b, 6.2.3b, 5.4.3). Pseudosections with mineral mode isopleths for the main minerals are presented in Appendix A3.

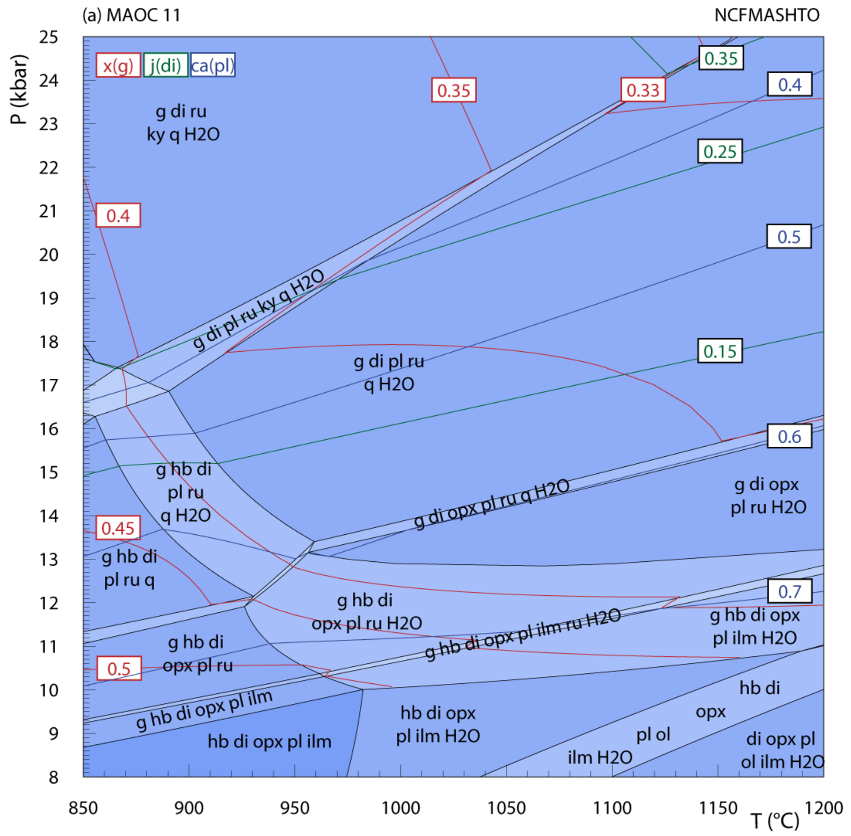

(b) modal proportions (NCFMASHTO) and experimental results

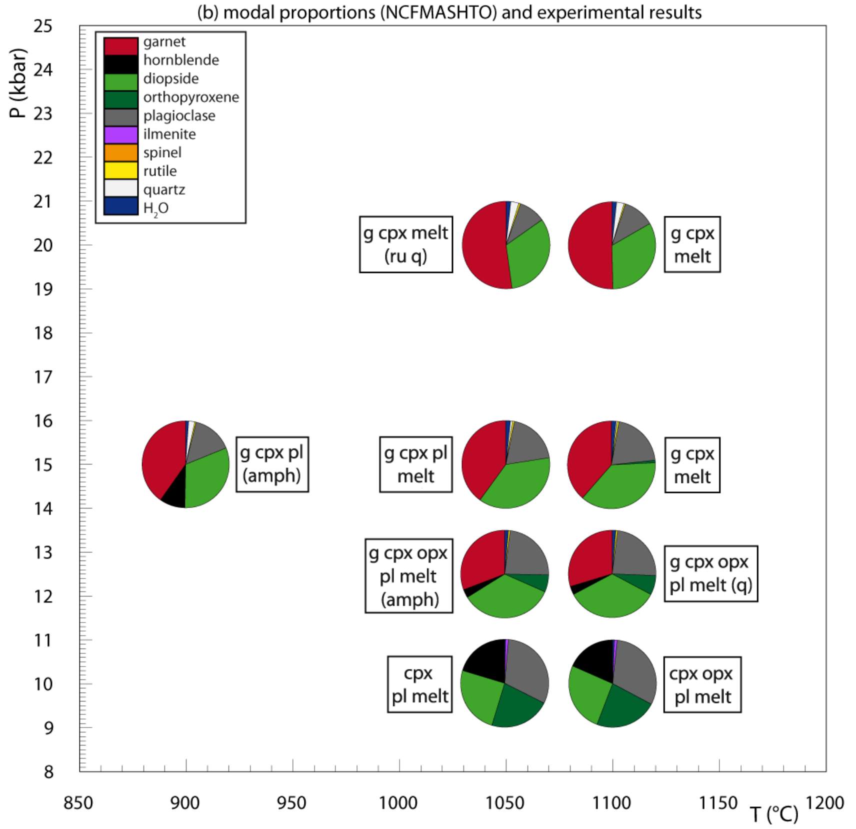

Figure 6.2.1a, b: (a) Extension of the *P–T* pseudosection for MAOC 11 (Fig. 4.3.2) covering the *P–T* range of the high-pressure experiments with composition variable isopleths for *x(g)*, *j(di)* and *ca(pl)*. (b) Comparison of the assemblages determined via microprobe analysis (boxes) with the modelled mineral abundances (pie charts with calculated abundances) at the experimental *P–T* conditions. The phases determined by the high-pressure experiments differ from the calculated results in some cases.

Garnet is a major mineral in the experimental assemblages ≥ 12.5 kbar and its appearance in the pseudosections lies slightly above 10 kbar at the experimental temperature conditions 1050 °C and 1100 °C. Towards higher pressures a rapid increase of the modal proportion of garnet occurs (Fig 6.2.2b), whereas the three models of MAOC have similar proportions of garnet at the equivalent *P–T* conditions. Microprobe analyses indicate an increasing proportion of the pyrope end-member with increasing MgO of the bulk rock composition as well as with increasing *P.* The composition variable *x(g)* = Fe/Fe+Mg in the calculations decreases vice versa to the increase of Mg# in the analyses garnets (Tab. 5.3.2, Figs 6.2.1a, 6.2.2a, 6.2.4a). *X(g)* is also calculated for the analysed garnets (Tab. 5.3.2) and shows lower values for *x(g)* than the calculated ones (Tab. 6.2.1).

In the thermodynamic calculations clinoamphiboles are divided into hornblende, glaucophane, actinolite and cummingtonite, depending on their composition variables (Appendix A1) and the location of solvi (e.g. Fig. 4.2.4). According to the high values of the compositional variables *a(hb)*, *y(hb)* and *c(hb)* the calculated amphiboles in the MAOC pseudosections are *hornblendes* (sensu lato). The classification into several types of calcic amphiboles according to Leake *et al.* (1997) subdivides the experimental amphiboles into pargasite, magnesiohornblende and tschermakite (Tab. 5.3.3 and Fig. 5.3.13). The high Mg# of those is equivalent to a low value of the composition variable *x(hb)* = Fe/Fe + Mg, whereas the remaining composition variables are not calculated for the experimental amphiboles because the required site distributions for this are not incorporated into the mineral formula calculation.

The stability of amphibole increases towards higher MgO in the bulk rock composition and in contrast to the calculated abundance of hornblende of ca. 20 % in MAOC 11 at 10 kbar, small amounts of amphibole were first detected at 12.5 kbar/ 1050 °C and 15 kbar/900 °C in the experimental assemblages (Fig. 6.2.1). Such difference might originate, if very small amounts of a phase were not detected or if a phase is overestimated in the calculations due to infelicities in the applied *a–x* models (subchapter 6.1.4). Representative amounts of amphibole in MAOC 13 are detected via microprobe at 10 kbar/1050 °C and 15 kbar/900 °C as well as an accessory amount at 12.5 kbar/1050 °C. The modelling predicted the stability of hornblende in those assemblages as well as for 10 and 12.5 kbar at 1100 °C. Hornblende in MAOC 15 was calculated up to 16 kbar and it was also developed in the experimental assemblages at these conditions except for 1100 °C and 15 kbar/1050 °C.

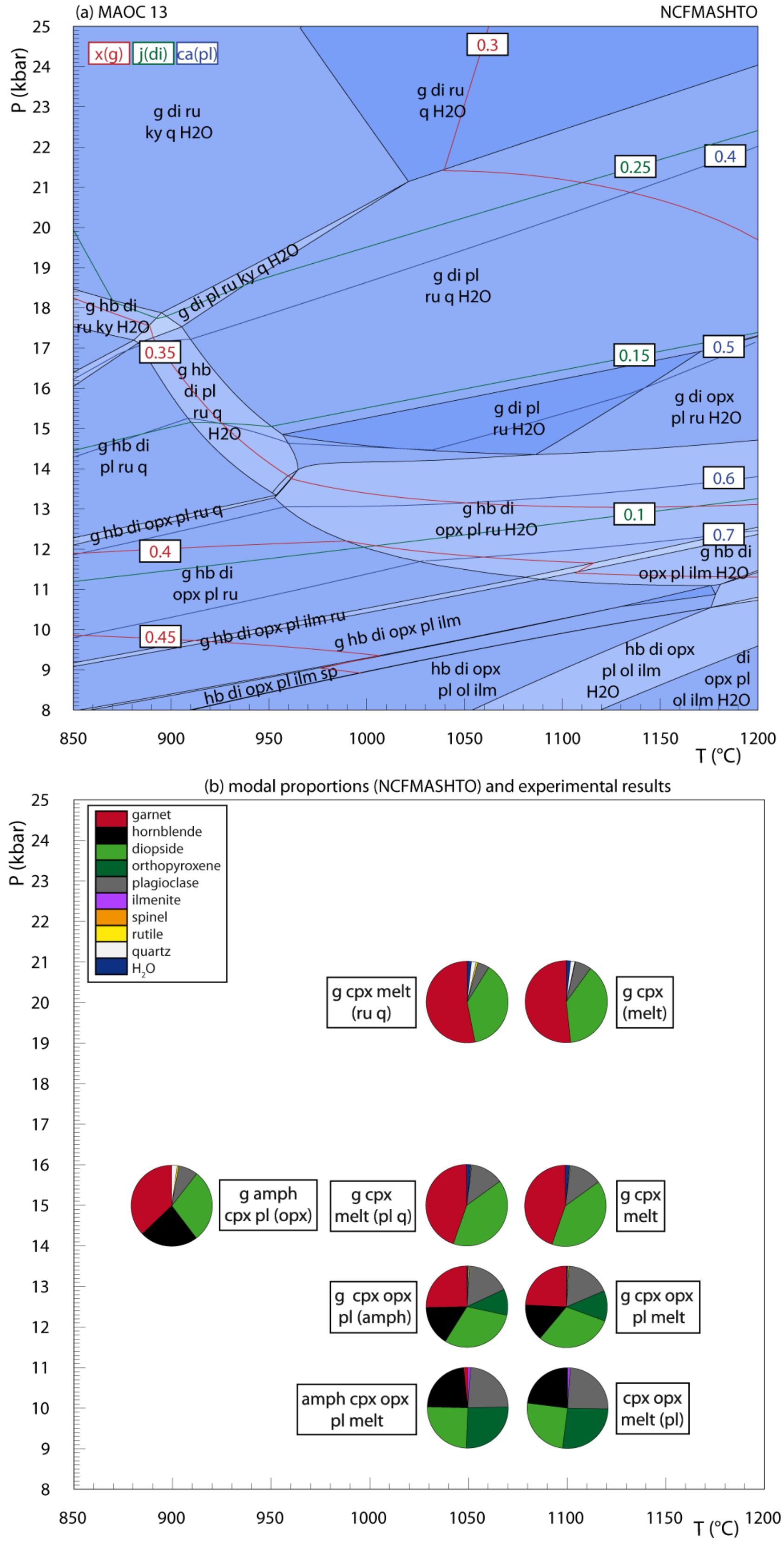

Figure 6.2.2a, b: (a) Extension of the *P–T* pseudosection for MAOC 13 (Fig. 4.3.3) covering the *P–T* range of the high-pressure experiments with composition variable isopleths for *x(g)*, *j(di)* and *ca(pl)*. (b) Comparison of the assemblages determined via microprobe analysis (boxes) with the modelled mineral abundances (pie charts with calculated abundances) at the experimental *P–T* conditions. The phases determined by the high-pressure experiments differ from the calculated results in some cases.

Clinopyroxene is the only phase that is stable in every experimental assemblage and its composition is best determined by summarising the results of both approaches. The calculation of clinopyroxenes with THERMOCALC allows a determination between diopside and omphacite, whereby the calculated clinopyroxenes are generally of diopsidic composition. This is underlined by the composition variable *j(di) = (xNaM2c + xNaM2n) / 2*, which is always < 0.25 at the equivalent experimental *P–T* conditions of the calculated pseudosections (subchapter 4.2.1). At 20 kbar *j(di)* trends towards omphacitic compositions, which is also confirmed by the analysed experimental clinopyroxenes developed at 20 kbar (Figs 5.3.14 and 5.3.15a). However, *j(di)* in the calculated MAOC compositions strongly depends on the amount of Na_2O as discussed in subchapter 4.3.6.2, but it is also *P*-sensitive in other compositions as shown in Fig. 4.2.2b. The mineral formula calculation of the analysed clinopyroxenes does not distinguish between M1 and M2 sites on the position X (Tab. 5.3.4) and the calculation of *j(di)* for the analysed clinopyroxenes is therefore not appropriate. The discrimination of diopside/augite from omphacite was executed by the the Q–J and Q–Jd–Ae diagrams (Figs 5.3.14 and 5.3.15a), where clinopyroxenes at 20 kbar plot on or near the border to the Na–Ca clinopyroxenes, confirming the results from the thermodynamic calculations The Ca–Mg–Fe clinopyroxenes at *P* < 20 kbar exhibit diopsidic or augitic compositions (Fig. 5.3.15).

The abundance of *orthopyroxene* in the experiments is well replicated by the calculations. The predicted stability in MAOC 11 and 13 is restricted to 10 and 12.5 kbar and orthopyroxene is developed in the appropriate experimental assemblages except at 10 kbar/1050 °C in MAOC 11, which is a larnite-contaminated assemblage (Fig. 5.3.5a). At 15 kbar/1100 °C (MAOC 11 and 15) the calculated results predict a small amount of orthopyroxene, which was either not detected by the analyses or actually no orthopyroxene occurs. In several assemblages of MAOC 15 (15 kbar/ 900 °C, 20 kbar/1050 °C) small amounts of orthopyroxene were detected although the phase was not calculated. The amount of the analysed Mg end-member (enstatite) increases with increasing MgO in the bulk rock composition, which is confirmed by the decreasing composition variable *x(opx)* = Fe/Fe+Mg towards higher MgO for both approaches but with varying values at some *P–T* conditions (Tabs 5.3.5, 6.2.1). No obvious trend is developed for the analysed orthopyroxenes in each MAOC and the calculated results indicate a decreasing *x(opx)* towards higher pressures indicating a decreasing amount of Fe^{2+} for the benefit of Mg.

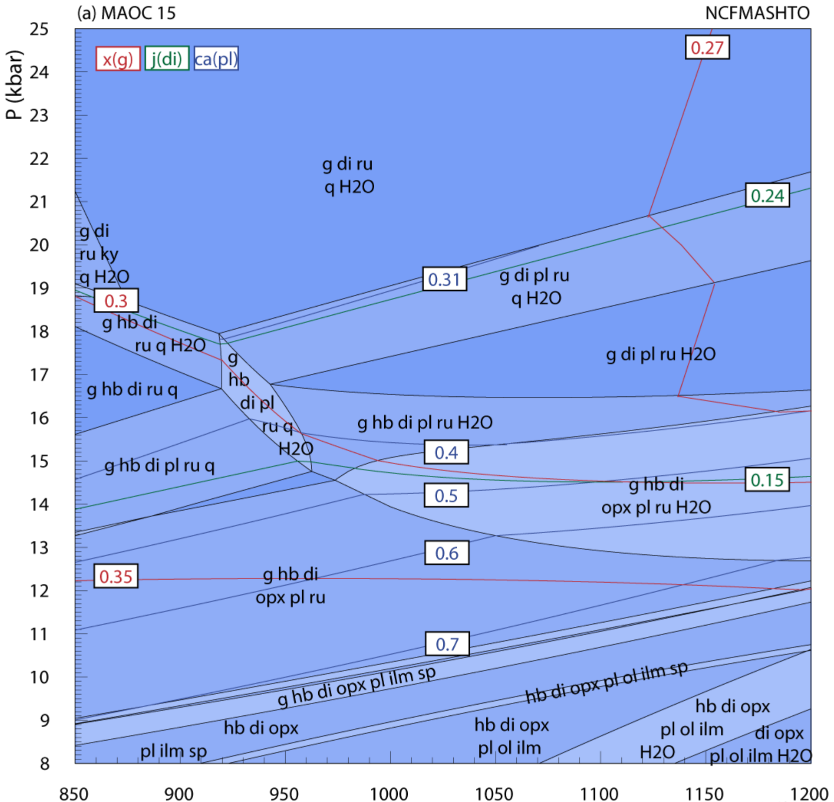

(b) modal proportions (NCFMASHTO) and experimental results

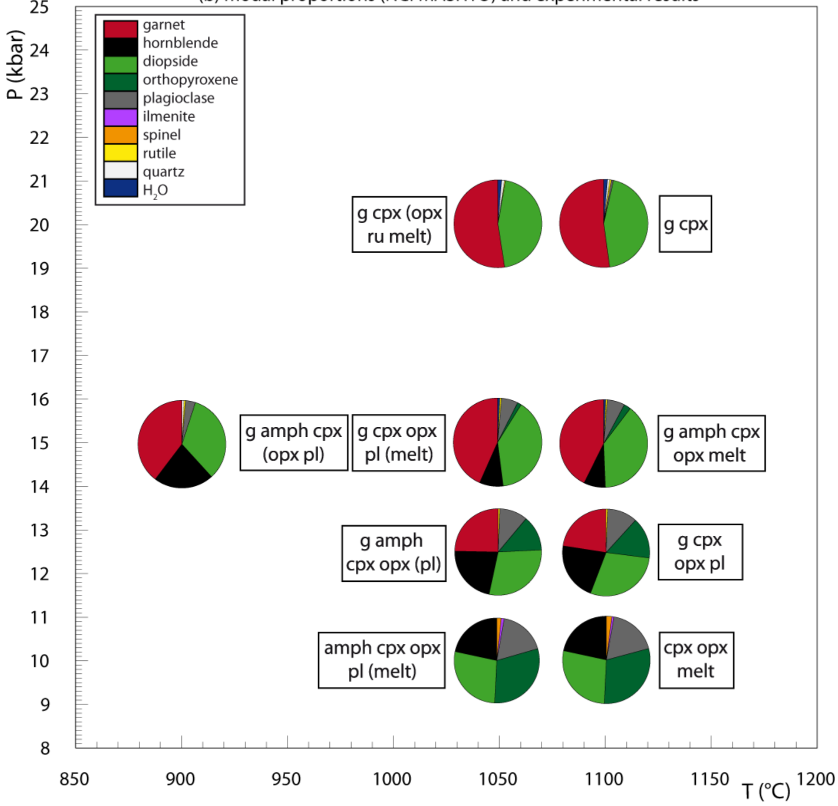

Figure 6.2.3a, b: (a) Extension of the *P–T* pseudosection for MAOC 15 (Fig. 4.3.4a) covering the *P–T* range of the high-pressure experiments with composition variable isopleths for *x(g)*, *j(di)* and *ca(pl)*. (b) Comparison of the assemblages determined via microprobe analysis (boxes) with the modelled mineral abundances (pie charts with calculated abundances) at the experimental *P–T* conditions. The phases determined by the high-pressure experiments differ from the calculated results in some cases.

Table 6.2.1: Composition variables *x(g), ca(pl)* and *x(opx)* for the analysed and calculated phases at the experimental *P–T* conditions. For each condition the composition variables of the analysed minerals are presented in the first line with the number of analyses #. The second line (*a–x*) presents the calculated composition variables.

		MAOC 11	MAOC 13	MAOC 15	MAOC 11	MAOC 13	MAOC 15	MAOC 11	MAOC 13	MAOC 15
P	T	x (g)	x (g)	x (g)	ca (pl)	ca (pl)	ca (pl)	x (opx)	x (opx)	x (opx)
10	1050				11 0.67	10 0.63	8 0.79		4 0.15	5 0.13
					a-x 0.77	a-x 0.78	a-x 0.77	a-x 0.30	a-x 0.26	a-x 0.23
	1100				6 (in) 0.65	1 0.64		13 0.16	16 0.15	9 0.08
					a-x 0.77	a-x 0.78		a-x 0.30	a-x 0.26	a-x 0.23
					5 (rim) 0.54					
					a-x 0.77					
12.5	1050	8 0.32	7 0.25	3 0.22	12 0.55	8 0.49	2 0.54	11 0.23	9 0.19	8 0.14
		a-x 0.39	a-x 0.37	a-x 0.35	a-x 0.63	a-x 0.50	a-x 0.64	a-x 0.22	a-x 0.21	a-x 0.19
	1100	9 0.31	9 0.25	4 0.20	14 0.52	9 0.50	3 0.33	9 0.19	6 0.18	11 0.13
		a-x 0.38	a-x 0.37	a-x 0.35	a-x 0.64	a-x 0.65	a-x 0.67	a-x 0.23	a-x 0.22	a-x 0.20
15	900	25 tot 0.35	9 0.27	8 0.22	10 0.49	6 0.46	2 0.40		2 0.16	2 0.14
		a-x 0.39	a-x 0.37	a-x 0.33	a-x 0.54	a-x 0.50	a-x 0.42			
		15 dark 0.26	6 0.22	4 0.15						
		a-x 0.39								
		10 light 0.47	3 0.36	4 0.28						
		a-x 0.39								
	1050	16 0.26	13 0.18	6 0.17	11 0.43	3 0.37	13 0.30			7 0.16
		a-x 0.36	a-x 0.31	a-x 0.29	a-x 0.57	a-x 0.50	a-x 0.44			a-x 0.15
	1100	10 0.32	16 0.20	7 0.16						6 0.09
		a-x 0.36	a-x 0.31	a-x 0.29	a-x 0.58	a-x 0.50	a-x 0.45	a-x 0.20		a-x 0.16
20	1050	11 tot 0.27	10 0.25	11 0.19						2 0.12
		a-x 0.34	a-x 0.30	a-x 0.27	a-x 0.44	a-x 0.38	a-x -			
		8 dark 0.23								
		a-x 0.34								
		3 light 0.39								
		a-x 0.34								
	1100	18 0.30	20 0.25	20 0.20						
		a-x 0.34	a-x 0.30	a-x 0.27	a-x 0.47	a-x 0.41	a-x 0.32			

The calculated stability of *plagioclase* is reduced to slightly lower pressures with increasing MgO in the bulk composition and the calculated proportions also decrease in each pseudosection with increasing pressure. The stability and the amount of plagioclase is highly overestimated in the thermodynamic models compared to the experimental assemblages (Figs 6.2.1–6.2.3) possibly reflecting limitations in the plagioclase thermodynamic model at high pressures (subchapter 6.1.4). The calculated plagioclase composition is defined amongst others by the compositional variable *ca(pl)* = Ca/Ca + Na. This variable decreases with increasing pressure from 10 to 20 kbar in the calculated plagioclase and indicates a higher amount of Na and a lower amount of Ca in the formule calculations (Tab. 5.3.6). This trend is confirmed by the microprobe analyses, which indicate a decrease of *ca(pl)* in the plagioclases from 10 to

15 kbar equivalent to the increasing Na-component (albite) towards higher pressures (Tab. 5.3.6, Fig. 5.3.17). With increasing MgO *ca(pl)* also decreases in both approaches at particular *P–T* conditions, especially from MAOC 11 to MAOC 13 (Tab. 5.3.6).

Within the series of the MAOC pseudosections H_2O appears at higher *P–T* conditions close to the hornblende-out boundary (subchapter 4.3). Free H_2O is not developed in the experiments since it is incorporated into the liquid phase, which can not be calculated for mafic rocks in NCFMASHTO. This aspect is treated in the next subchaper.

6.3 Determing the solidus

A marked difference between the thermodynamic calculations and the high-pressure partial melting experiments is the presence of a liquid phase (glass/melt) in the experiments. A liquid phase can not be calculated in the metabasic system NCFMASHTO and therefore the haplogranitic melt model in NCFMASH for metapelitic rocks from White *et al.* (2007) was adopted to model pseudosections for MAOC 11, 13 and 15 including the phase "liquid". While this melt model is not calibrated for metabasic rocks, it is used here in part to identify its shortcomings in these compositions. The calculated solidi (yellow in Fig. 6.2.4) and the liquid-bearing assemblages (purple in Fig. 6.2.4) illustrate an approximation of a potential shape of the solidi and shows the redistribution of the now liquid-bearing assemblages at the high-temperature side of the solidus. It is stated that the resulting backbending solidus displays artefacts of experimental investigations due to free water having no potential to escape the system (Moyen & Stevens, 2006, subchapter 5.4), which is comparable to thermodynamic calculations in a closed system. The estimated solidi determined by the results of the high-pressure experiments (Fig. 5.4.3) are integrated into these pseudosections. The estimated solidi in turn depend on the experimentally-determined mineral assemblages and additionally replicate the temperature differences of the calculated solidi at *P–T* conditions, where no experimental data are available. The bends in the solidi between 11 and 15 kbar are approximately reproduced, although at different *P–T*, by several melt-free experiments at 12.5 kbar in MAOC 13 and 15 as well as by an assemblage in MAOC 11 with just a small amount of melt. The temperature of melting generally increases towards higher MgO in both approaches and the solidi determined by the high-pressure experiments appears at lower temperatures than the calculated one, especially at higher pressures.

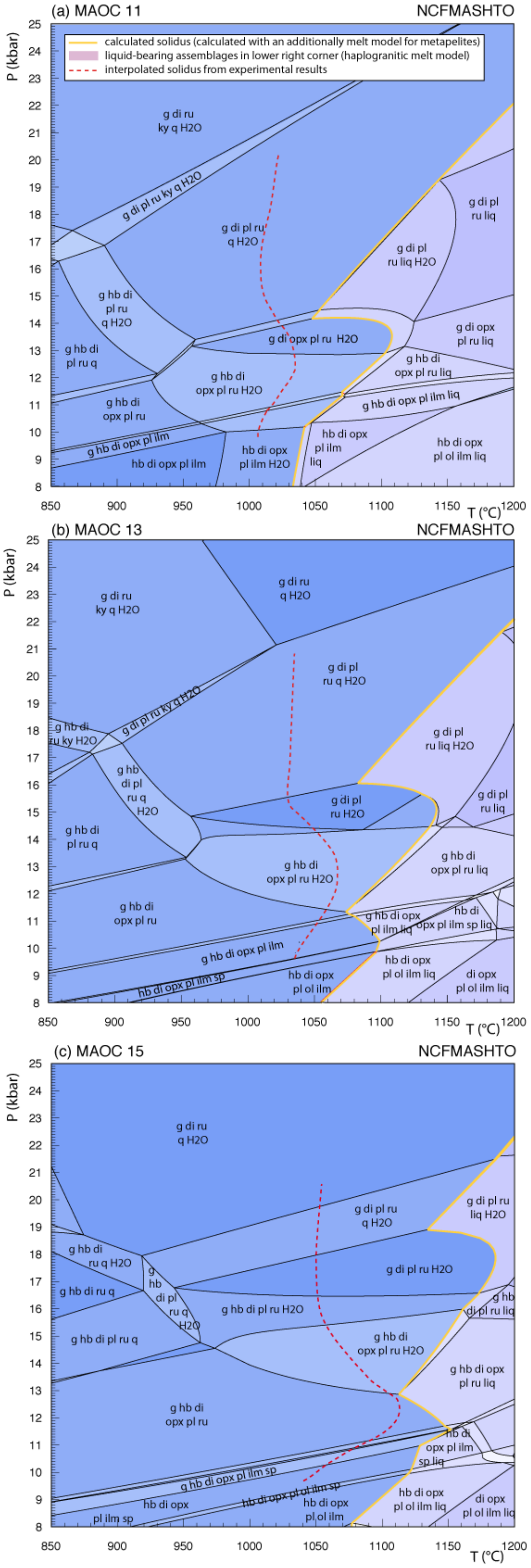

Figure 6.3.1 a-c: *P*–*T* pseudosections for MAOC 11 (a), 13 (b) and 15 (c) calculated with low H_2O. The solidi (yellow) are calculated with the melt model for metapelitic rocks (White *et al.*, 2007) and the accordant liquid-bearing assamblages are coloured in purple. The experimental determined solidi (red dotted lines) show the differences between the two approaches.

6.4 Sources of errors in the different methods

The similarities and discrepancies between the results of the thermodynamic calculations and high-pressure partial melting experiments are outlined above, whereas the origin of the differences is a consequence of uncertainties in both approaches. A direct comparison of both methods is problematic as they are based on different fundamentals but a careful combination of both approaches may serve as a good basis for an interpretation of the results. A fundamental difference is the absence of an appropriate melt model for the calculations in metabasic rocks, which indicates a higher reliability of the experimental results at supersolidus conditions. In contrast, the subsolidus assemblages of the experiments are not well equilibrated (subchapter 5.3.2), suggesting that here the calculations may be more reliable. Hornblende is absent towards high temperatures in the experiments despite its predicted abundance in the calculations for metabasic rocks in NCFMASHTO without the haplogranitic melt model. This might be caused by the breakdown of hornblende during melting in the experiments, which in turn cannot be calculated in the models. The fact that a liquid phase is not included in the calculations will also have influence on the assemblages and the composition of the phases therein. Some minerals, especially amphiboles, are additionally very complex and not all natural constitutions of the elements are considered in the *a*–*x* models, presenting a further source of errors. The calculated composition variables of amphibole allow to distinguish between hornblende, glaucophane, actinolite and cummingtonite (subchapter 4.2.1; Appendix A1), whereas the mineral formula calculation of the experimental amphiboles discriminates between several calcic amphiboles (pargasite, magnesiohornblende, tschermakite in this study, subchapter 5.3.3.3). The calculated mineral formulae also do not include the complete natural potential of site distributions and the microprobe analyses itself exhibit uncertainties (see below).

The overestimation of plagioclase in the thermodynamic calculations may originate from the plagioclase model, which is obviously not appropriate for the high *P*–*T* conditions required for the experimental conditions in this study. Additionally, the phase “liquid” which is not incorporated in the modelling is partially made up of the plagioclase components. The elements THERMOCALC uses to stabilise plagioclase are incorporated into the experimental melt compositions (Al, Na, Ca; Tab. 5.3.6) and would predominantly be incorporated in melt if a melt model would be included in the calculations. A similar effect may also have led to further accessory calculated phases, e.g. rutile, which is not detected in the experiments instead of 20 kbar/1050 °C. The present TiO_2 may be incorporated into the melt (up to 1 wt%; Tab. 5.3.7) or into other experimental phases, whose *a–x* models are written without Ti, e.g. amphibole (in NCFMASHO; Diener *et al.*, 2007), garnet (in CFMASO; White *et al.*, 2007) and clinopyroxene (in NCFF3MAS; Green *et al.*, 2007). Actually the amount of rutile in the calculations does not exceed 0.5 % and these minor amounts of rutile in the calculations may result from the non-consideration of Ti in the thermodynamic models of the other phases. Therefore, the presence of rutile in the *P–T* pseudosections possibly results from the necessity to distribute the Ti into phases whose *a–x* models can accomodate Ti such as rutile or ilmenite, which in turn were not detected in the experiments at $P < 20$ kbar. Nevertheless, there is also the potential to miss the detection of present accessory phases during the microprobe analyses although the experimental assemblages were studied in detail during the microprobe analyses.

As presented earlier, the amount of Fe^{3+} is controlled by the factor "O" in the thermodynamic calculations (Eq. 4.1.1). The estimation of the amount of Fe^{3+} from total FeO in the system is also an uncertainty, if no whole rock data are available for the amount of Fe^{3+}. Although Fe^{3+} was not added to the MAOC mixes, oxidation may have been taken place at some stage and the amount of Fe^{3+} from total FeO was set to approximately 10 % (O = 0.30) in the modelling of the MAOC compositions to allow the comparability with the *P–T* pseudosections for the bulk rock compositions in subchapter 4.2.

The influence of "O" is illustrated for three different values in MAOC 11, varying from "O" = 0.15 to 0.50, according to approximately 5 to 15% trivalent iron from total FeO (Fig. 6.4.1). The changes are insignificant in the scope of the comparison to experimental determined assemblages because the topology of the assemblage fields varies only slightly and the minerals made up the assemblages remain constant. The results from Fig. 6.4.1 exclude the amount of ferric iron as a huge source of uncertainties at those high *P–T* conditions. The effect of varying "O" is more important where Fe^{3+}-bearing phases like epidote become stable at lower *T* than used in the pseudosections for this study (Diener & Powell, 2010).

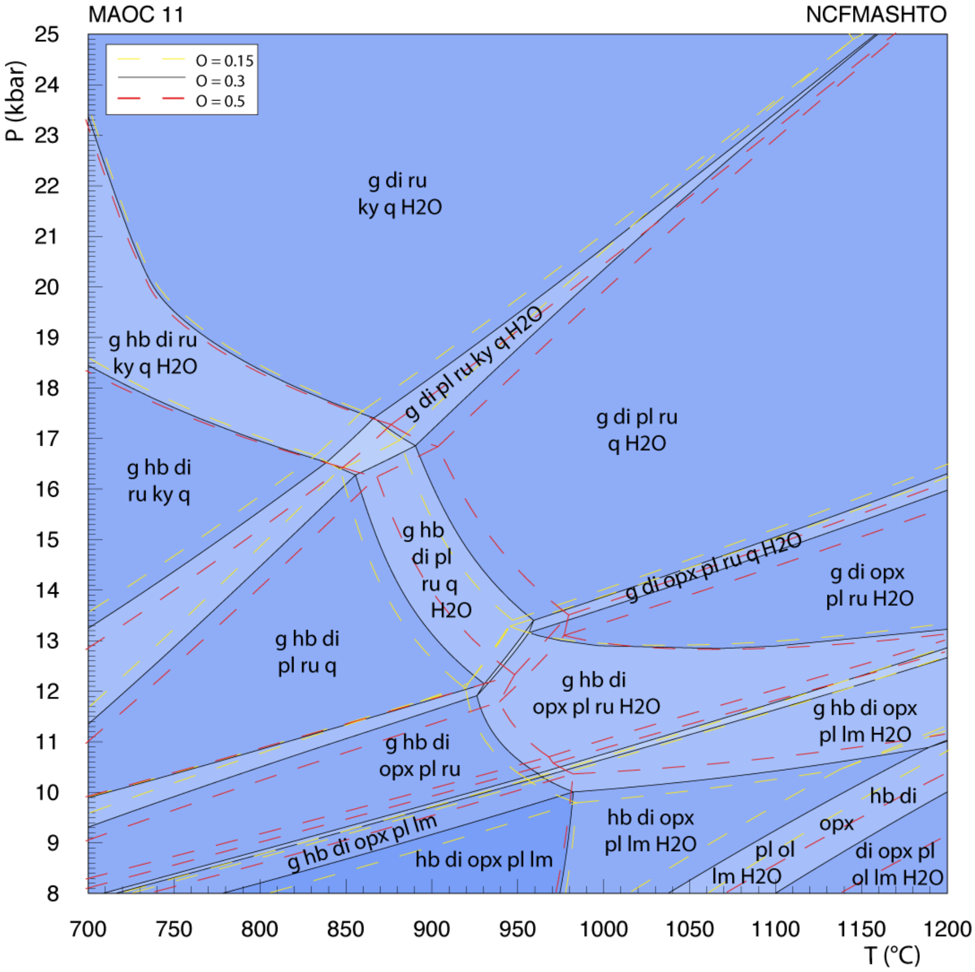

Figure 6.4.1: *P–T* pseudosection for MAOC 11 with different values for "O", indicating different amounts of ferric iron from the total FeO (5, 10 and 15 %). The small variations of the boundaries between the different Fe^{3+}-contents do not account for the differences between the calculated and the experimental results.

Uncertainties during the performance of the high-pressure partial melting experiments include variabilities in the *P–T* conditions (± 0.5 kbar, ± 1 °C) and a differing offset between the oven and the capsule. Furthermore, the amount of the MAOC mix used in a single experiment was very small and the mixes may have been inhomogeneous even though they were prepared conscientiously. The oxide mixes were stored in a heating furnace at 110 °C, but the amount of added H_2O may have changed during the period of conducting the high-pressure experiments, e.g. by the utilisation of the mixes or through leakages during the experiments itself. However, the *P–T* range in the pseudosections where the high-pressure experiments were conducted is not affected by modelling with varying H_2O-contents. This changes if the solidus, calculated with the haplogranitic melt model from White *et al.* (2007), is included in the pseudosection. Figure 6.4.2 illustrates examples for MORB and MAOC 11, both for calculations with H_2O in excess (as used for the natural bulk rock compositions in subchapter 4.2) and for low H_2O-contents (as used for MAOC bulk rock compositions in subchapter 4.3).

The *P–T* pseudosections with H_2O in excess are more complex at the low-*T* side than the low H_2O ones, but after the appearance of H_2O at high *T* (orange line in Fig. 6.4.2c and d) the pseudosections are identical up to the solidus (Fig. 6.4.2). The orange dotted lines in the H_2O-saturated pseudosections (Figs 6.4.2a, b) designate the appearance of H_2O in the pseudosections calculated for low H_2O and marks the beginning of identical fields up to the solidus.

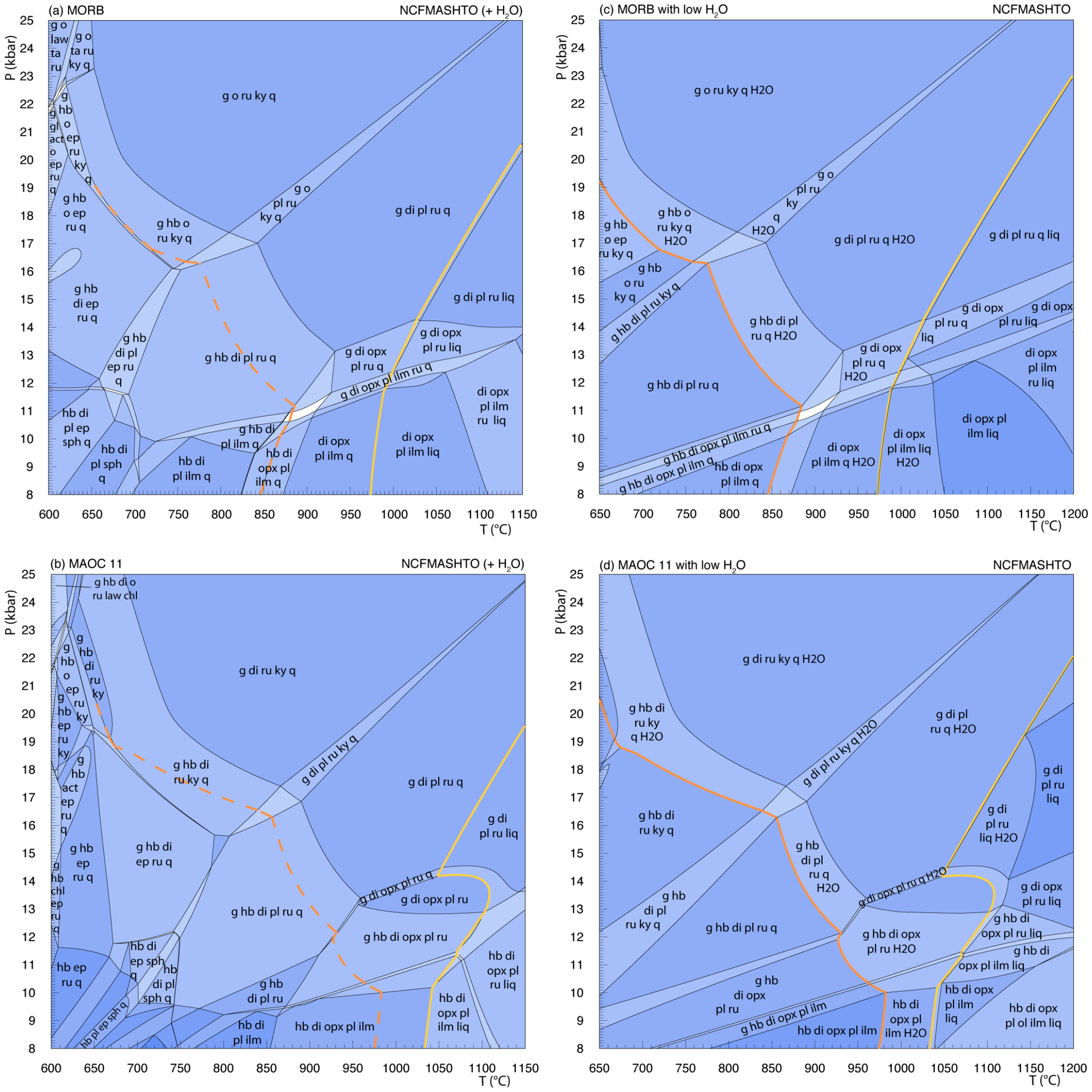

Figure 6.4.2a, b, c, d: Comparison of *P–T* pseudosections for MORB and MAOC 11, calculated with H_2O in excess (a, b) and with low H_2O (c, d), both with a solidus calculated with the melt model for metapelitic rocks. The boundary of the incoming of liquid (orange line in c and d) is assigned to (a) and (b) via the orange dotted line. H_2O-saturated assemblages are similar in the pseudosections with low and high H_2O up to the solidus. If H_2O is present, the position of the solidus is also equal but the pseudosections illustrate the difference in the liquid-bearing assemblages under different H_2O-conditions.

Pseudosections calculated without the haplogranitic melt model in the system NCFMASHTO would remain similar at high *T*, regardless of the amount of H_2O (not illustrated). The liquid-bearing assemblages for both H_2O-scenarios differ slightly from each other, predominantly by the higher stability of fluid in the calculations with H_2O in excess. The problems with the *a–x* models described above also occur in the modelling where the haplogranitic melt model is incorporated, especially the overestimation of plagioclase. This again indicates the higher reliability of the experimental results at supersolidus conditions.

The microprobe analyses also include sources of uncertainties. On the one hand, the analyses are affected by instabilities of the microprobe itself (e.g. beam current, standards) as well as by the surrounding conditions (e.g. air condition, weather) and on the other hand, the investigated section displays just a snapshot of the complete experiment, which allows the potential to miss accessory phases. Further uncertainties are based on the facts that the experimental assemblages host inhomogeneous phases and phases intergrown with each other, or that the initial mix was not completely equilibrated during the experimental runs. In these cases the assemblages contain unreacted material, which is not incorporated into the equilibrated volume. Additionally, the mineral formula calculations are based on simplified models and do not account for all possible distributions of elements on sites, but they allow an approximation to the chemistry of the phases observed in the experiments, even though the phases are commonly zoned or inhomogeneous (subchapter 5.3.2).

Chapter 7

Conclusions and future research

7.1 Conclusions

The main conclusion of the present study is that the formation of TTG-like tonalitic melts in terms of the main oxides is not limited to metamorphosed basalts and that the generation of those melts is also possible from model picritic Archean oceanic crust (MAOC) with higher MgO contents (MAOC 11 and 13) than that of mid-ocean ridge basalt.

The results of the high-pressure experiments in this study highlight a development with decreasing MgO contents from basaltic melts in MAOC 15 to predominantly tonalitic melts in MAOC 11 in the context of a continuously evolving early oceanic crust, emanating from komatiitic compositions in the Hadean towards lower MgO contents during the secular cooling of the Earth. The compositional threshold for the generation of TTG-like tonalitic melts occurs between 15 and 13 wt% MgO in the MAOC source rock compositions of this study; melting of more magnesian compositions will not produce tonalitic melts. The fact that the *P–T* conditions used for the experiments were consistent for MAOC 11, 13 and 15 gives rise to the conclusion that the *P–T* condition of an experiment alone does not account for the type of melt developed, with one exception: the melt compostions at 10 kbar in the absence of garnet are all basaltic. This is consistent with the inference that garnet needs to be present in the residuum during partial melting for the generation of TTGs (e.g. Drummond & Defant, 1990; Rapp *et al.*, 1991; Martin, 1999). The basaltic melts have generally formed in granulite facies assemblages (clinopyroxene ± garnet ± amphibole ± orthopyroxene ± plagioclase) at pressures ≤ 12.5 kbar in MAOC 11 und up to 15 kbar in MAOC 13 and 15.

A further conclusion is the assignment of assemblages with tonalitic melt to different geological settings for Archean continental crust formation, divided by their residual mineral assemblages that have developed on the different experimental *P–T* conditions. Tonalitic melts generated at 15 kbar and 1050 °C in MAOC 11 and 13 are related to early TTGs and to partial melting processes in either the base of a thick oceanic crust or in shallow subduction zones without further interaction with mantle material. The assemblages coexisting with tonalitic melts up to 15 kbar do not exactly confirm the theory that a potential source rock for the generation of TTG-like melts is garnet-amphibolite (e.g. Foley *et al.*, 2002, 2003; Schmidt *et al.*, 2004; Moyen & Stevens, 2006) because the tonalitic melts in this study were generated in assemblages like garnet + clinopyroxene ± plagioclase ± quartz in the lack of amphibole. A further conclusion of the experiments is that the solidi of the metamorphosed MAOC compositions occur at higher temperatures with increasing MgO. The solidi of MAOC 11 and 13 occur beyond the amphibole-bearing subsolidus assemblages at 900 °C and 15 kbar. The first tonalitic melt compostions then occur in the amphibole-free assemblages at 1050 °C, which permits the conclusions that (1) amphibole may have been present directly at the solidus and that garnet-amphibolitic assemblages were present at the onset of melting and/or that (2) the formation of tonalitic melts from metamorphosed picrites is also possible from amphibole-free rocks at higher temperatures and therefore from not primarily hydrated metamorphic rocks, comparable with conditions at the base of a thick crust. In contrast to amphibole, the presence of plagioclase is essential to the generation of tonalitic melts as the plagioclase-free assemblages at 15 kbar and 1100 °C produced intermediate (MAOC 11) or basaltic (MAOC 13) melt compositions. This is consistent with the prediction of Martin & Moyen (2002) that plagioclase is required for the genesis of early TTGs.

Tonalitic melts at 20 kbar were generated in eclogitic residues of MAOC 11 and 13 above the stability of plagioclase, these melts are related to younger TTGs and to processes in subduction zones that had deepened during the secular cooling of the Earth. The presence of rutile in most of these assemblages is a critical factor according to contradictory studies concerning an essential absence of rutile in the residuum (Foley *et al.*, 2002) or not (Rapp *et al.*, 2003). Apart from that, it is unlikely that melts generated at 20 kbar in deeper subduction zones could migrate upwards without interacting with overlying mantle material and consequently become richer in magnesium. However, the fact that tonalitic melts were generated at 20 kbar in this study is consistent with the declaration that TTG-like melts could have been generated by partial melting of eclogites (Rapp *et al.*, 2003).

The combination of mineral equilibria calculations with THERMOCALC and high-pressure partial melting experiments allows the investigation of a wider range of *P–T* conditions than by using only one of the approaches. The mineral equilibria modelling for metabasic rocks is limited by the absence of an adaptive metabasic melt model and appropriate mineral models for the high *P–T* conditions in the system NCFMASHTO, whereas the high-pressure partial melting experiments enable the determination of supersolidus assemblages as well as the composition of melt. In contrast, the experimental assemblages at subsolidus conditions are hindered by sluggish approach to equilibrium and these conditions are better investigated via mineral equilibria modelling. The comparison of both approaches in the realm of the experimental investigated *P–T* area (900–1100 °C and 10–20 kbar) indicates that the modelled and experimental determined stability, the proportion and the composition of the phases differ from each other. The differences originate from limitations in the applied *a–x* models, e.g. the Ti-bearing mineral rutile is present in the *P–T* pseudosections because the *a–x* models of effective Ti-bearing phases are written without Ti (e.g. amphibole). Another difference between the two approaches is the fact that the thermodynamic model for plagioclase overestimates the stability of plagioclase in the *P–T* pseudosections at conditions where the experimental assemblages are plagioclase-free.

A conclusion derived from both approaches used in this study is that the amount of Na_2O chosen in the MAOC compositions was too low. Omphacitic clinopyroxenes were not developed in the eclogite facies realm, neither the experimental nor the modelled clinopyroxenes exhibit compositions of omphacite and the tonalitic melt compositions should have higher Na_2O.

In summary, the calculation of pseudosections offered a definition of the initial MAOC compositions for the following more laborious high-pressure experiments in the scope of this study. Mineral equilibria modelling further provides valuable information in combination with the experimental results, e.g. for the influence of ferric iron (Fig. 6.1.5) and the evolution of the composition variable *j(di)* in clinopyroxenes by the help of *T–X* pseudosections (Figs 4.2.2b and 4.3.7). While there were differences in the location of the solidus between the modelling and the experiments, the topology of the solidus in both is similar, with both showing a distinct backbending. The temperature difference of the solidi in both approaches is broadly the same in MAOC 11, 13 and 15, which allows an estimation of the solidus temperature for modelled mafic compositions on which no experiments were conducted.

7.2 Suggestions for future research

This study provides a general overview of the contribution of source rocks richer in MgO than modern mid-ocean ridge basalts to the investigations on the formation of early Archean continental crust. Future reasearch is required to investigate aligned models of Archean oceanic crust with thermodynamic equilibria modelling under the considerations that (1) 15 wt% MgO in the source rock is identified to be already above the upper limit for the generation of TTG-like melts and that (2) the MAOC compositions in this study contain too little Na_2O. Further high-pressure experiments are required directly at or near the solidus to ascertain the mineral assemblages which are actually involved in the first melting reactions. The research needs to be expanded with trace-element investigations for Nb/Ta, Zr/Sm, Sr, Y and REE as these are important for an improved characterisation of the relevant melt compositions, e.g. for melts in eclogitic residues, whose affiliation to TTG-like melts in this study could not be satisfactorily determined. It could also be fruitful to relate the experimental results to selected TTGs whose genesis is well studied or to establish high-pressure partial melting experiments with samples of natural rocks, e.g. picrites from the base of oceanic plateaux - if available.

The improvement of existing thermodynamic models for phases, especially of plagioclase as well as the currently development of a melt model for metabasic rocks is important to model *P–T* and *T–X* pseudosections to ascertain approriate new models for Archean oceanic crust for further high-pressure experiments on the basis of the results of this study. The new datset from Holland & Powell (2011) already provides, amongst other things, an improvement of the models for many end-members, e.g. anorthite and albite. The new dataset may provide the foundation for further mineral equilibria calculations and a better understanding of the generation of early Archean continental crust from metamorphosed picritic rocks.

References

Abbott, D.H. & Hoffman, S.E. (1984): Archaean plate tectonics revisited. 1. Heat flow, spreading ridges, and the age of subducting oceanic lithosphere and their effects on the origin and evolution of continents. - *Tectonics* **3**, 429–448.

Abbott, D. & Mooney, W. (1995): The structural and geochemical evolution of the continental crust: Support for the oceanic plateau model of continental growth. - *Reviews of Geophys. Suppl., U.S. National Report to International Union of Geodesy and Geophysics 1991–1994*, 231–242.

Albarède, F. (1998): The growth of continental crust. - *Tectonophysics* **196**, 1–14

Allègre, C.J. & Rousseau, D. (1984): The growth of continents through geological time studied by Nd isotope analysis of shales. - *Earth and Planetary Science Letters* **67**, 19–34.

Atherton, M.P. & Petford, N. (1993): Generation of sodium-rich magmas from newly underplated basaltic crust. - *Nature* **362**, 144–146.

Arndt, N.T. (1983): Role of a thin, komatiite-rich oceanic crust in the Archean plate-tectonic process. - *Geology* **11**, 372–375.

Arndt, N. T., Ginibre, C., Chauvel, C., Albarède, F., Cheadle, M., Herzberg, C., Jenner, G. & Lahaye, Y. (1998): Were komatiites wet? - *Geology* **26**, 739–742.

Barker, F. & Arth, J.G. (1976): Generation of trondhjemitic-tonalitic liquids and Archean bimodal trondhjemite-basalt suites. - *Geology* **4**, 596–600.

Barker, F. ed. (1979): Trondhjemites, dacites and related rocks. - Developments in Petrology 6, *Elsevier, New York*. 676 pp.

Beard, J.S. & Lofgren, G.E. (1989): Effect of Water on the Composition of Partial Melts of Greenstone and Amphibolite. - *Science* **244**, 195–197

Beard, J.S. & Lofgren, G.E. (1991): Dehydration melting and Water-Saturated Melting of Basaltic and Andesitic Greenstones and Amphibolites at 1, 3 and 6.9 kbar. - *Journal of Petrology* **32**, 365–401.

Berman, R.G. (1988): Internally-consistent thermodynamic data for minerals in the system Na_2O–K_2O–CaO–MgO–FeO–Fe_2O_3–Al_2O_3–SiO_2–TiO_2–H_2O–CO_2. - *Journal of Petrology* **29**, 445–522.

Bickle, M.J. (1978): Heat loss from the earth: A constraint on Archean tectonics from the relation between geothermal gradients and the rate of plate production. - *Earth and Planetary Science Letters* **40**, 301–315.

Bickle, M.J., Nisbet, E.G. & Martin, A. (1994): Archean Greenstone Belts are not oceanic crust. - *The Journal of Geology* **102**, 121–138.

Bowring, S.A. & Williams, I.S. (1999): Priscoan (4.00–4.03 Ga) orthogneiss from northwestern Canada. - *Contributions To Mineralogy and Petrology* **134**, 3–16.

Brown, G.C. (1986): Processes and problems in the continental lithosphere: Geological history and physical implications. - In: *Snelling, N.J. ed., Geochronology and geological record: Geological Society, London, Memoirs* **10**, 326–446.

Brown, M. (2006): Duality of thermal regimes is the distinctive characteristic of plate tectonics since the Neoarchean. - *Geology* **34**, 961–964.

Brown, M. (2007): Metamorphic conditions in orogenic belts: A record of secular change. - *International Geology Review* **49**, 193–234.

Campbell, I.H. & Jarvis, G.T. (1984): Mantle Convection and early crustal evolution. - *Precambrian Research* **26**, 15–56.

Christensen, P.A., McSween, H. Y. Jr, Bandfield, J. L., Ruff, S. W., Rogers, A. D., Hamilton, V. E., Gorelick, N., Wyatt, M. B., Jakosky, B. M., Kieffer, H. H., Malin, M. C. & Moersch, J. E. (2005): Evidence for magmatic evolution and diversity on Mars from infrared observations. - *Nature* **436**, 504–509.

Clarke, G. L., Klepeis, K. A. & Daczko, N. R., (2000): Cretaceous high-*P* granulites at Milford Sound, New Zealand: their metamorphic history and emplacement in a convergent margin setting. - *Journal of Metamorphic Geology* **18**, 359–374.

Collerson, K.D. & Kamber, B.S. (1999): Evolution of the Continents and the Atmosphere inferred from Th-U-Nb Systematics of the Depleted Mantle. - *Science* **283**, 1519–1522.

Condie, K.C. (1981): Archean Greenstone Belts. - *Developments in Precambrian Geology. Elsevier Publishing Co., Amsterdam,* 434 pp.

Condie, K.C. (1997): *Plate Tectonics and Crustal Evolution. Fourth Edition.* - Butterworth-Heinemann, Oxford, UK, 282 pp.

Condie, K.C. (2000): Episodic continental growth models: afterthoughts and extensions. - *Tectonophysics* **322**, 153–162.

Connolly, J.A.D. (1990): Multivariable phase diagrams: An algorithm based on generalised thermodynamics. - *American Journal of Science* **290**, 666–718.

Coogan, L.A., Thompson, G., & MacLeod, C.J. (2002): A textural and geochemical investigation of high level gabbros from the Oman ophiolite: implications for the role of the axial magma chamber at fast-spreading ridges. - *Lithos* **63**, 67–82.

Dale, J., Powell, R., White, R.W., Elmer, F. L. & Holland, T.J.B. (2005): A thermodynamic model for Ca–Na clinoamphiboles in Na_2O–CaO–FeO–MgO–Al_2O3–SiO_2–H_2O–O for pertological calculations. - *Journal of metamorphic Geology* **23**, 771–791.

de Capitani, C. & Brown, T.H. (1987): The computation of chemical equilibrium in complex systems containing non-ideal solutions. - *Geochimica et Cosmochimica Acta* 51, 2639–2652.

Deer, W.A., Howie, R.A. & Zussmann, J. (1992): An Introduction to the Rock Forming Minerals. 2nd ed. - *Pearson Education Limited*, England, 696 pp.

Defant, M.J. & Drummond, M.S. (1990): Derivation of some modern arc magmas by melting of young subducted lithosphere. - *Nature* **347**, 662–665.

Demarest, H.H. & Haselton, H.T. Jr. (1981): Error analysis for bracketed phase equilibrium data. - *Geochimica et Cosmochimica Acta* **45**, 217–224.

De Wit, M.J. & Hart, R.A. (1993): Earth´s earliest continental lithosphere, hydrothermal flux and crustal recycling. - *Lithos* **30**, 309–335.

Diener, J.F.A., Powell, R., White, R.W. & Holland, T.J.B. (2007): A new thermodynamic model for clino-and orthoamphiboles in the system Na_2O–CaO–FeO–MgO–Al_2O_3–SiO_2–H_2O–O. - *Journal of metamorphic Geology* **25**, 631–656.

Diener (2009): *P–T* pseudosection tutorial for metabasic rocks. - http://www.metamorph.geo.uni-mainz.de/thermocalc/tutorials/index.html

Diener, J. F. A. and Powell, R. (2010): Influence of ferric iron on the stability of mineral assemblages. - *Journal of metamorphic Geology* **28**, 599-613.

Drummond, M.S. & Defant, M.J. (1990): A model for Trondhjemite-Tonalite-Dacite genesis and crustal growth via slab melting: Archean to modern comparisons. - *Journal of Geophysical Research* **95**, 21503–21521.

Elmer, F.L., White, R.W. & Powell, R., (2006): Devolatilisation of metabasic rocks during greenschist-amphibolite facies metamorphism. - *Journal of Metamorphic Geology* **24**, 497–513.

Escola, P. (1915): On the relation between chemical and mineralogical composition in the metamorphic rocks of the Orijävi region in south-western Finland. - *Bulletin de la Commission géologique de Finlande* **40**, 279 pp.

Escola, P. (1921): The mineral facies of rocks. - *Norsk Geologisk Tidsskrift* **6**, 143–194.

Falloon, T.J. & Green, D.H. (1988): Anhydrous Partial Melting of Peridotite from 8 to 35 kb and the Petrogenesis of MORB. - *Journal of Petrology*, *Special Lithosphere Issue*, 379–414.

Farnetari, C. G., Richards, M. A. & Ghiorso, M. S. (1996): Petrological models of magma evolution and deep crustal structure beneath hotspots and flood basalt provinces. - *Earth and Planetary Science Letters* **143**, 81–94.

Foley, S.F., Musselwhite, D.S. & van der Laan, S.R. (1999): Melt compositions from ultramafic vein assemblages in the lithospheric mantle: a comparison of cratonic and non-cratonic settings. - In: *Proceedings of Cape Town Kimberlite Conference, J.B.Dawson volume*, 238–246.

Foley, S.F., Tiepolo, M. & Vannucci, R. (2002): Growth of early continental crust controlled by melting of amphibolite in subduction zones. - *Nature* **417**, 837–840.

Foley, S.F., Buhre, S. & Jacob, D. E. (2003): Evolution of the Archean crust by delamination and shallow subduction. - *Nature* **421**, 249–252.

Forsyth, D. & Uyeda, S. (1975): On the Relative Importance of the Driving Forces of Plate Motion. - *Geophysical Journal of Royal Astronomical Society.* **43**, 163–200.

Fyfe, W-S. (1973): The granulite facies, partial melting and the Archean crust. - *Philosophical Transactions of the Royal Society London A.* **273**, 457–461.

Ghiorso, M.S. & Evans, B.W. (2002): Thermodynamics of the amphiboles; Ca–Mg–Fe^{2+} quadrilateral. - *American Mineralogist* **87**, 79–98.

Green, D.H. & Ringwood, A.E. (1967a): An experimental investigation of the gabbro to eclogite transformation and its petrological applications. - *Geochimica et Cosmochimica Acta* **31**, 767–833.

Green, D.H. & Ringwood, A.E. (1967b): The stability fields of aluminous pyroxene peridotite and their relevance in upper mantle structure. - *Earth and Planetary Science Letters* **3**, 151–160.

Green, D.H., Falloon T.J., Eggins, S.M. & Yaxley, G.M. (2001) : Primary magmas and mantle temperatures. - *European Journal of Mineralogy* **13**, 437–451.

Green, E., Holland, T. & Powell, R. (2007): An order-disorder model for omphacitic pyroxenes in the system jadeite-diopside-hedenbergite-acmite, with applications to eclogitic rocks. - *American Mineralogist* **92**, 1181–1189.

Gregoire, M., Mattielli, N., Nicollet, C., Cottin, J.Y., Leyrit, H., Weis, D., Shimizu, N. & Giret, A. (1994): Oceanic mafic granulite xenoliths from the Kerguelen archipelago. - *Nature* **367**, 360–363.

Guiraud, M., Powell, R. & Rebay, G. (2001): H_2O in metamorphism and uninspected behaviour in the preservation of metamorphic mineral assemblages. - *Journal of Metamorphic Geology* **19**, 445–454.

Halbach, H. & Chatterjee, N.D. (1982): The use of linear programming for determining consistent thermodynamic data for minerals. - In: *High Pressure Research in Geoscience* (ed. Schreyer, W., Schweizerbart´sche Verlagsbuchhandlung, Stuttgart.), 475–491.

Hargraves, R.B. (1986): Faster spreading or greater ridge length in the Archean? - *Geology* **14**, 750–752.

Hawkesworth, C.J. & Kemp, A.I.S. (2006): Evolution of the continental crust. - *Nature* **443**, 811–817.

Helgeson, H.C., Delany, J.M., Nesbitt, H.W. & Bird, D.K. (1978): Summary and critique of the thermodynamic properties of rock-forming minerals. - *American Journal of Science* **278A**, 229 pp.

Helz, R.T. (1976): Phase relations in basalts in their melting range at P(H2O) = 5 kb: II. Melt compositions. - *Journal of Petrology* **17**, 139–193.

Herrmann, W. & Berry, R.F. (2002): MINSQ – a least squares spreadsheet method for calculating mineral proportions from whole rock major element analyses. - *Geochemistry: Exploration, Environment, Analysis*, **2,** 361–368.

Holland, T.J.B. (1981): Thermodynamics of simple mineral systems. - In: *Thermodynamics of Minerals and Melts. (ed. Newton, R.C, Navrotsky, A. and Wood, B.J.J), Springer-Verlag, New York*, 19–34.

Holland, T.J.B. & Powell, R. (1985): An internally consistent dataset with uncertainties and correlations: 2. Data and results. - *Journal of Metamorphic Geology* **3**, 343–370.

Holland, T.J.B. (1990): Activities of components in omphacitic solid solutions. An application of Landau theory to mixtures. - *Contributions to Mineralogy and Petrology* **105**, 446–453.

Holland, T.J.B. & Powell, R. (1990): An enlarged and updated internally consistent dataset with uncertainties and correlations: the system K_2O–Na_2O–CaO–MgO–MnO–FeO–Fe_2O_3–Al_2O_3–TiO_2–SiO_2–C–H_2O. - *Journal of Metamorphic Geology* **8**, 89–124.

Holland, T.J.B. & Powell, R. (1996a): Thermodynamics of order-disorder in minerals: I. Symmetric formalism applied to minerals of fixed composition. - *American Mineralogist* **81**, 1413–1424.

Holland, T.J.B. & Powell, R. (1996b): Thermodynamics of order-disorder in minerals:II. Symmetric formalism applied to solid solutions. - *American Mineralogist* **81**, 1425–1437.

Holland, T.J.B., Baker, J.M. & Powell, R. (1998): Mixing properties and activity-composition relationships of chlorites in the system MgO–FeO–Al_2O_3–SiO_2–H_2O. - *European Journal of Mineralogy* **10**, 395–406.

Holland, T.J.B. & Powell, R. (1998): An internally consistent thermodynamic data set for phases of petrological interest. - *Journal of Metamorphic Geology* **16**, 309–343.

Holland, T.J.B. & Powell, R. (2003): Activity-composition relations for phases in petrological calculations: an asymmetric multicomponent formulation. - *Contributions to Mineralogy and Petrology* **145**, 492–501.

Holland, T.J.B. & Powell, R. (2006): Mineral activity-composition relations and petrological calculations involving cation equipartition in multisite minerals: a logical inconsistency. - *Journal of Metamorphic Geology* **24**, 851–861.

Holland, T.J.B. and Powell, R. (2011): An improved and extended internally consistent thermodynamic dataset for phases of petrological interest, involving new equation of state for solids. - *Journal of metamorphic Geology* **29**, 333-383.

Holland, T.J.B. (unpublished): *a-x* model for olivine.

Holloway, J.R. & Burnham, C.W. (1972): Melting relations of basalt with equilibrium water pressure less than total pressure. - *Journal of Petrology* **13**, 1–29.

Ishiwatari, A. (1985): Alpine ophiolites: product of low-degree mantle melting in a Mesozoic transcurrent rift zone. - *Earth and Planetary Science Letters* **76**, 93–108.

Jahn, B-M., Glikson, A.Y., Peucat, J.J. & Hickman, A.H. (1981): REE geochemistry and isotopic data of Archean silicic volcanics and granitoids from the Pilbara Block, Western Australia: implications for the early crustal evolution. - *Geochimica and Cosmochimica Acta* **45**, 1633–1652.

Jaques, A.L. & Green, D.H. (1980): Anhydrous melting of peridotite at 0-15Kb pressure and the genesis of tholeiitic basalts. - *Contributions to Mineralogy and Petrology* **73**, 287–310.

Johnson, K., Barnes, C.G. & Miller, C.A. (1997): Petrology, geochemistry, and genesis of high-Al tonalite and trondhjemites of the Cornucopia Stock, Blue Mountains, North-eastern Oregon. - *Journal of Petrology* **38**, 1585–1611.

Kay, R.W. (1978): Aleutian magnesian andesites: melts from subducted Pacific Ocean crust. - *Journal of Volcanology and Geotheral Research* **4**, 117–132.

Kay, R.W. & Mahlburg-Kay, I. (1991): Creation and destruction of lower continental crust. - *Geologische Rundschau* **80**, 259–278

Kerrick, D.M. & Jacobs, G.K (1981): A modified Redlich-Kwong equation for H_2O, CO_2 and H_2O–CO_2 mixtures at elevated pressures and temperatures. - *American Journal of Science* **281**, 735–767.

Kogiso, T., Hirschmann, M.M. & Pertermann, M. (2004): High-Pressure Partial Melting of Mafic Lithologies in the Mantle. - *Journal of Petrology* **45**, 2407–2422.

Krishnamurthy, P., Gopalan, K. & Macdougall, J.D. (2000): Olivine Compositions in Picrite Basalts and the Deccan Volcanic Cycle. - *Journal of Petrology* **41**, 1057–1069.

Kröner, A. (1985): Evolution of the Archean continental crust. - *Annual Reviews of Earth and Planetary Science* **13**, 49–74.

Kurepin, V.A. (1985): H_2O and CO_2 contents of cordierite as an indicator of thermodynamic conditions of formation. - *Geochemistry International* **22**, 148–156.

Laurie, A. & Stevens, G. (2010): Growth of early continental crust by water-present eclogite melting. - In: *Tyler, I.M. and Knox-Robinson, C.M. 2010, Fifth International Archean Symposium Abstracts: Geological Survey of Western Australia,* **Record 2010/18**, 410 pp.

Le Bas, M.J., Le Maitre, R.W., Streckeisen, A., Zanettin, B. (1986): A Chemical Classification of Volcanic Rocks Based on the Total Alkali-Silica Diagram. - *Journal of Petrology* **27**, 745–750.

Leake, B.E., Woolley, A.R., Arps, C.E.S., Birch, W.D., Gilbert, M.C., Grice, J.D., Hawthorne, F.C., Kato, A., Mandarino, J.A., Maresch, W.V., Nikel, E.H., Rock, N. M.S., Schumacher, J.C., Smith, D.C., Stephenson, N.C.N., Ungaretti, L.,Whittaker, E.J.W. & Youzhi, G. (1997): Nomenclature of amphiboles: Report of the Subcommittee on Amphiboles of the International Mineralogical Association, Commission on New Minerals and Mineral Names. - *American Mineralogist* **82**, 1019–1037.

LeMaitre, R.W. (2002): Igneous Rocks, A Classification and Glossary of Terms: Recommendations of the International Union of Geological Science Subcommission on the Sytematics of Igneous Rocks. - *Cambridge University Press*, pp 252.

Lucassen, F. & Franz, G. (1996): Magmatic arc metamorphism: Petrology and temperature history of metabasic rocks in the Coastal Cordillera of northern Chile. - *Journal of Metamorphic Geology* **14**, 249–265.

Macdonald, R., Hawkesworth, C.J. & Heath, E. (2000): The lesser Antilles volcanic chain: a study in arc magmatism. - *Earth-Science Reviews* **49**, 1–76.

Macpherson, C.G., Dreher, S.T. & Thierlwall, M.F. (2006): Adakites without slab melting: High pressure differentiation of island arc magma, Mindanao, the Philippines. - *Earth and Planetary Science Letters* **243**, 581–593.

Martin, E., Martin, H. & Sigmarsson, O. (2008): Could Iceland be a modern analogue for the Earth´s early continental crust? - *Terra Nova* **20**, 463–468.

Martin, E., Martin, H. & Sigmarsson, O. (2010): Comment on "Continental geochemical signatures in dacites from Iceland and implications for models of early Archaean crust formation" by Willbold, M., Hegner, E., Stracke, A. and Rocholl, A. - *Earth and Planetary Science Letters* **293**, 218–219.

Martin, H. (1986): Effect of steeper Archean geothermal gradient on geochemistry of subduction-zone magmas. - *Geology* **14**, 753–756.

Martin, H. (1994): The Archean grey gneisses and the genesis of the continental crust. - In: *K.C. Condie (ed.). Archean Crustal Evolution* Elsevier, Amsterdam, 205–259.

Martin, H. (1999): Adakitic magmas: modern analogues of Archean granitoids. - *Lithos* **46**, 411–429.

Martin, H. & Moyen, J.-F. (2002): Secular changes in tonalite-trondhjemite-granodiorite composition as markers of the progressive cooling of Earth. - *Geology* **30**, 319–322.

Martin, H., Smithies, R. H., Rapp, R., Moyen, J.-F. & Champion, D. (2005): An overview of adakite, tonalite-trondhjemite-granodiorite (TTG), and sanukitoid: relationships and some implications for crustal evolution. - *Lithos* **79**, 1–24.

Maruyama, S., Liou, J.G. & Terabayashi, M. (1996): Blueschists and eclogites of the world and their exhumation. - *International Geology Review* **38**, 490–596.

McKenzie, D. (1985): The extraction of magma from the crust and mantle. - *Earth and Planetary Science Letters* **74**, 81–91.

Morimoto, N., Fabries, J., Ferguson, A.K., Ginzburg, I.V., Ross, M., Seifert, F.A., Zussmann, J., Aolki, K., Gottardi, G. (1988): Nomenclature of pyroxenes. - *American Mineralogist* **73**,1123-1133.

Moyen, J.-F. & Stevens, G. (2004): Evolution of TTG geochemistry around the Barberton greenstone belt from 3.5 to 3.2 Ga: transition from shallow melting below under-plated crust to subduction-associated magmatism? - In: *Geocongress, Johannesbourg (South Africa).*

Moyen, J.-F. & Stevens, G. (2006): Experimental Constraints on TTG Petrogenesis: Implications for Archean Geodynamics. - In: *Archean Geodynamics and Environments. Editors: Benn, K., Mareschal, J.-C. and Condie, K.C.. Geophysical Monograph Series* **164**, 149–175.

Müller, R.D., Sdrolias, M., Gaina, C. & Roest, W.R. (2008): Age, spreading rates and spreading symmetry of the world's ocean crust - *Geochemistry, Geophysics Geosystems* 9, Q04006.

Muir, R.J., Weaver, S.D., Bradshaw, J.D., Eby, G.N. & Evans, J.A. (1995): The Cretaceous Separation Point batholith, New Zealand: granitoid magmas formed by melting of mafic lithosphere. - *Journal of the Geological Society Lond*on **152**, 689–701.

Mysen, B.O. & Kushiro, I. (1977): Compositional variation of coexisting phases with degrees of melting of peridotites in the upper mantle. - *American Mineralogist* **62**, 843–865.

Nagler, T.F. & Kramers, J.D. (1998): Nd isotopic evolution of the upper mantle during the Precambrian: models, data and the uncertainty of both. - *Precambrian Research* **91**, 233–252.

Newton, R.C. & Perkins, D. (1982): Thermodynamic calibration of geobarometers based on the assemblages garnet–plagioclase–orthopyroxene–clinopyroxene–quartz. - *American Mineralogist* **67**, 203–222.

Nicolas, A. (1989): Structures of ophiolites and dynamics of oceanic lithosphere. - *Petrology and Structural Geology* **4**. *Kluwer Academic Publishers Dordrecht/Boston/London*, 380 pp.

Nisbet, E.G. & Fowler, C.M.R (1983): Model for Archean Plate Tectonics. - *Geology* **11**, 376–379.

Nutman, A. P., McGregor, V. R., Friend, C. R. L., Bennett, V. C. & Kinney, P. D. (1996): The Itsaq Gneiss Complex of southern West Greenland; the world´s most extensive record of early crustal evolution (3900–3600 Ma). - *Precambrian Research* **78**, 1–39.

Ohtani, E., Kagawa, N. & Fujino, K (1991): Stability of majorite (Mg, Fe)SiO_3 at high pressures and 1800 °C. - *Earth and Planetary Science Letters* **102**, 158–166.

Okamoto, A. & Tourimi, M. (2004): Optimal mixing properties of calcic and subcalcic amphiboles: application of Gibbs´ method to the Sanbagawa shists, SW Japan. - *Contributions to Mineralogy and Petrology* **146**, 529–545.

Peacock, S.M., Rushmer, T. & Thompson, A.B. (1994): Partial melting of subducting oceanic crust. - *Earth and Planetary Science Letters* **121**, 227–244.

Pertermann, M. & Hirschmann, M.M. (2003): Anhydrous Partial Melting Experiments on MORB-like Eclogite: Phase Relations, Phase Compositions and Mineral-Melt Partitioning of Major Elements at 2–3 GPa. - *Journal of Petrology* **44**, 2173–2201.

Petford, N. & Atherton, M. (1996): Na-rich Partial Melts from Newly Underplated Basaltic Crust: the Cordillera Blanca Batholith, Peru. - *Journal of Petrology* **37**, 1491–1521.

Pichavant, M., Mysen, B.O. & Macdonald, R. (2002): Source and H_2O-content of high MgO-magmas in island arc settings: an experimental study of a primitive calc-alkaline basalt from St. Vincent, Lesser Antilles arc. - *Geochimica et Cosmochimica Acta* **66**, 2193–2209.

Powell, R. (1978*):* Equilibrium Thermodynamics in Petrology. - *Harper and Row, London*, 284 pp.

Powell, R. & Holland, T.J.B. (1985): An internally consistent dataset with uncertainties and correlations: 1. Methods and a worked example. - *Journal of Metamorphic Geology* **3**, 327–342.

Powell, R. (1987): Darken´s quadratic formalism and the thermodynamics of minerals. - *American Mineralogist* **72**, 1–11.

Powell, R. & Holland, T.J.B. (1988): An internally consistent dataset with uncertainties and correlations: 3. Applications to geobarometry, worked examples and a computer program. - *Journal of Metamorphic Geology* **6**, 173–204.

Powell, R. & Holland, T.J.B. (1993a): The applicability of least squares in the extraction of thermodynamic data from experimentally bracketed mineral equilibria. - *American Mineralogist* **78**, 107–112.

Powell, R. & Holland, T.J.B. (1993b): On the formulation of simple mixing models for complex phases. - *American Mineralogist* **78**, 1174–1180.

Powell, R., Holland, T.J.B. & Worley, B. (1998): Calculating phase diagrams involving solid solutions via non-linear equations, with examples using THERMOCALC. - *Journal of Metamorphic Geology* **16**, 577–588.

Powell, R. & Holland, T.J.B. (1999): Relating formulations of the thermodynamics of mineral solid solutions: Activity modelling of pyroxenes, amphiboles, and micas. - *American Mineralogist* **84**, 1–14.

Powell, R. & Holland, T.J.B. (2010): Using equilibrium thermodynamics to understand matamorphism and metamorphic rocks. - *Elements* **6**, 309–314.

Rapp, R.P., Watson, E.B. & Miller, C.F. (1991): Partial melting of amphibolite/eclogite and the origin of Archean trondhjemites and tonalites. - *Precambrian Research* **51**, 1–25.

Rapp, R.P. & Watson, B.E. (1995): Dehydration melting of metabasalt at 8-32 kbar: Implications for Continental Growth and crust-mantle recycling. - *Journal of Petrology* **36**, 891–931.

Rapp, R.P., Shimizu, N., Norman, M.D. & Applegate, G.S. (1999): Reaction between slab-derived melts and peridotite in the mantle wedge: experimental constraints at 3.8 GPa. - *Chemical Geology* **160**, 335-356.

Rapp, R.P., Shimizu, N. & Norman M.D. (2003): Growth of early continental crust by partial melting of eclogite. - *Nature* **425**, 605–609

Rollinson, H. (2007): Early Earth Systems. A Geochemical Approach. - *Blackwell Publishing, Oxford, Malden, Carlton*. viii + 285 pp.

Rudnick, R.L. (1995): Making continental crust. - *Nature* **378**, 571–578.

Rudnick, R.L. & Gao, S. (2003): Composition of the continental crust. - In: Holland, H.D. & Turekian, K.K. (eds). *Treatise on Geochemistry. Elsevier, Oxford*, **Vol. 3.01**, 1–63.

Rushmer, T. (1991): Partial melting of two amphibolites: contrasting experimental results under fluid-absent conditions. - *Contributions to Mineralogy and Petrology* **107**, 41–59.

Saunders, A.D., Tarney, J., Kerr, A.C. & Kent, R.W. (1996): The formation and fate of large oceanic igneous provinces. - *Lithos* **37**, 81–95.

Schilling, J.-G., Zajec, M., Evans, R., Johnston, T., White, W., Devine, J.D. & Kingsley, R. (1983): Petrologic and geochemical variations along the Mid-Atlantic Ridge from 29 °N to 73 °N. - *American Journal of Science* **283**, 510–586.

Schmidt, M. W. & Poli, S. (1998): Experimentally based water budgets for dehydrating slabs and consequences for arc magma generation. - *Earth and Planetary Science Letters* **163**, 361–379.

Schmidt, M.W., Dardon, A., Chazo, G. & Vannucci, R. (2004): The dependence of Nb and Ta rutile-melt partitioning on melt composition and Nb/Ta fractionation during subduction processes. - *Earth and Planetary Science Letters* **226**, 415–432.

Sen, C. & Dunn, T. (1994): Dehydration melting of a basaltic composition amphibolite at 1.5 and 2.0 GPa: implications for the origin of adakites. - *Contributions to Mineralogy and Petrology* **117**, 394–409.

Shafer, J.T., Neal, C.R. & Mahoney, J.J. (2005): Crustal xenoliths frtom Malaita, Solomon Islands: A window to the lower crust of the Ontong Java Plateau. - *Eos, Transactions of the American Geophysical Union* **86**, abstract T11C–0397.

Shirey, S.B. & Hanson, G.N. (1984): Mantle-derived Archaean monzodiorites and trachyandesites. - *Nature* **310**, 222–224.

Shirey, S. B., Klewin, K.W., Berg, J.H. & Carlson, R.W. (1994): Temporal changes in the sources of flood basalts: Isotopic and trace element evidence from the 1100 Ma old Keweenawan Mamainse Point Formation, Ontario, Canada. - *Geochimica et Cosmochimica Acta* **58**, 4475–4490.

Skjerle, K.P. & Patino Douce, A.E. (2002): The Fluid-absent Partial Melting of a Zoisite-bearing Quartz Eclogite from 1.0 to 3.2 GPa; Implications for Melting in Thickened Continental Crust and for Subduction-zone Processes. - *Journal of Petrology* **43**, 291–314.

Smith, J.V. & B. Mason (1970): Pyroxene-garnet transformation in Coorara meteorite. - *Science* **168**, 832–833.

Smithies, R.H. (2000): The Archean tonalite-trondhjemite-granodiorite (TTG) series is not an analogue of Cenozoic adakite. - *Earth and Planetary Science Letters* **182**, 115–125.

Springer, W. & Seck, H. (1997): Partial fusion of basic granulites at 5 to 15 kbar: implications for the origin of TTG magmas. - *Contributions to Mineralogy and Petrology* **127**, 30–45.

Stern, R.J. (2007): When and how did plate tectonics begin? Theoretical and empirical considerations. - *Chinese Science Bulletin* **52**, 578–591.

Streckeisen, A. (1976): To each plutonic rock its proper name. - *Earth Science Reviews. International Magazine for Geo-Scientists* **12**, 1–33.

Sun, S.S. & McDonough, W.F., (1989): Chemical and isotopic systematics of oceanic basalts: implications for mantle compositions and processes. - *In: Magmatism in the Ocean Basins, Special Publications (eds Saunders, A. & Norry, M.)* **42**, 313–345. Geological Society, London.

Taylor, S.R. & McLennan, S.M. (1981): The composition and evolution of the continental crust: rare earth elements evidence from sedimentary rocks. - *Philosophical Transactions of the Royal Society A.* **301**, 381–399.

Taylor, S.R. & McLennan, S.M. (1985): The Continental Crust: Its Composition and Evolution. - *Blackwell, Oxford*, 312 pp.

Taylor, S.R. (1989): Growth of planetary crusts. - *Tectonopysics* **161**, 147–156.

Taylor, S.R. & McLennan, S.M. (1995): The geochemical evolution of the continental crust. - *Reviews of Geophysics* **33**, 241–265.

Thorkelson, D.J. & Breitsprecher, K. (2005): Partial melting of slab window margins: genesis of adakitic and non-adakitic melts. - *Lithos* **79**, 25–41.

Turner, F.J. (1981): Metamorphic Petrology. Mineralogical and Field aspects. - Second edition. New York. McGraw-Hill, 403 pp.

Vernon, R.H. & Clarke, G.L. (2008): Principles of metamorphic petrology. - *Cambridge University Press, New York*, 460 pp.

Vielzeuf, D. & Schmidt, M.W. (2001): Melting relations in hydrous systems revisited: application to metapelites, metagreywackes and metabasalts. - *Contributions to Mineralogy and Petrology* **141**, 251–267.

Volodichev, O.I., Slabunov, A.I., Bibikova, E.V., Konilov, A.N. & Kuzenko, T.I., (2004) - Archean eclogites in the Belomorian Mobile Belt, Baltic Shield. - *Petrology* **12**, 540–560.

White, R.W., Powell, R. & Holland, T.J.B. (2001): Calculation of partial melting equilibria in the system $CaO–K_2O–FeO–MgO–Al_2O_3–SiO_2–H_2O$ (NCKFMASH). - *Journal of Metamorphic Geology* **19**, 139–153.

White, R.W., Powell, R., Holland, T.J.B. & Worley, B.A. (2000): The effect of TiO_2 and Fe_2O_3 on metapelitic assemblages at greenschist and amphibolite facies conditions: mineral equilibria calculations in the system $K_2O–FeO–MgO–Al_2O_3–SiO_2–H_2O–TiO_2–Fe_2O_33$. - *Journal of Metamorphic Geology* **18**, 497–511.

White, R.W., Powell, R. & Clarke, G.L. (2002): The interpretation of reaction textures in Fe-rich metapelitic granulites of the Musgrave Block, central Australia: constraints from mineral equilibria calculations in the system $K_2O–FeO–MgO–Al_2O_3–SiO_2–H_2O–TiO_2–Fe_2O_3$. - *Journal of Metamorphic Geology* **20**, 41–55.

White, R.W. & Powell, R. (2002): Melt loss and the preservation of granulite-facies mineral assemblages. - *Journal of Metamorphic Geology* **20**, 621–632.

White, R.W., Powell, R. & Holland, T.J.B. (2007): Progress relating to calculation of partial melting equilibria for metapelites. - *Journal of Metamorphic Geology* **25**, 511–527.

Wilde, S.A., Valley, J.W., Peck, W.H. & Graham, C.N. (2001): Evidence from detrical zircons for the existence of continental crust and oceans on the Earth 4.4 Gyr ago. - *Nature* **409**, 175–178.

Will, T.M., Powell, R. & Holland, T.J.B. (1990): A calculated petrogenetic grid for ultramafic rocks in the system CaO–FeO–MgO–Al_2O_3–SiO_2–CO_2–H_2O at low pressures. - *Contributions to Mineralogy and Petrology* **105**, 347–358.

Willbold, M., Hegner, E., Stracke, A. & Rocholl, A. (2009): Continental geochemical signatures in dacites from Iceland and implications for models of early Archaean crust formation. - *Earth and Planetary Science Letters* **279**, 44–52.

Willbold, M., Hegner, E., Stracke, A. & Rocholl, A. (2010): Reply to comment by E. Martin, M. Martin, and O. Sigmarssonon on "Continental geochemical signatures in dacites from Iceland and implications for models of early Archaean crust formation" by M. Willbold, E. Hegner, A. Stracke, and A. Rocholl. - *Earth and Planetary Science Letters* **293**, 220–222.

Winther, K.T. & Newton, R.C. (1991): Experimental melting of hydrous low-K tholeiite: evidence on the origin of Archean cratons. - *Bulletin of the Geological Society of Denmark* **39**, 213–228.

Winther, K.T. (1996): An experimentally based model for the origin of tonalitic and trondhjemitic melts. - *Chemical Geology* **127**, 43–59.

Wolf, M.B. & Wyllie, P.J. (1994): Dehydration-melting of amphibolite at 10 kbar: the effects of temperature and time. - *Contributions to Mineralogy and Petrology* **115**, 369–383.

Wood, B.J. & Holloway, J.R. (1984): A thermodynamic model for subsolidus equilibria in the system CaO–MgO–Al_2O_3–SiO_2. - *Geochimica et Cosmochimica Acta* **48**, 159–176.

Wyllie, P.J. & Wolf, M.B. (1993): Amphibolite dehydration-melting: sorting out the solidus. - *Geological Society, London, Special Publications* **76,** 405–416.

Zamora, D. (2000): Fusion de la croute océanique subductée: approche expérimentale et geochimique. - *Thèse d´université, Université Blaise-Pascal, Clermont-Ferrand.*

Zegers, T. E. & van Keken, P. E. (2001): Middle Archean continent formation by crustal delamination - *Geology*, 1083–1086.

Zen, E-an (1972): Gibbs free energy, enthalpy and entropy of ten rock-forming minerals. - *American Mineralogist* **57**, 524–553.

Internet:
Homepage THERMOCALC:
http://www.metamorph.geo.uni-mainz.de/thermocalc/documentation/index.html
http://www.metamorph.geo.uni-mainz.de/thermocalc/tutorials/index.html

Appendix A

THERMOCALC

Appendix A1:	Composition variables for amphibole
Appendix A2:	T–X_{MgO} pseudosections from MAOC 11–17 at different pressures
Appendix A3:	P–T pseudosections for MAOC 11, 13 and 15 with mineral mode isopleths of garnet, hornblende, diopside, orthopyroxene and plagioclase
Appendix A7:	Activity-composition models in the system NCFMASHTO (*a*–*x* file)

Appendix A1: Composition variables for amphibole

Composition variables of amphiboles (Diener *et al.*, 2007) :

variable		**glaucophane**	**hornblende**	**actinolite**	**cummingtonite**
x(hb)	Fe/Fe+Mg	0-1	0-1	0-1	0-1
y (hb)	octahedral Al	0.9-1	0.2-0.6	0-0.25	0-0.2
z (hb)	Na on the M4 site	0.8-1	0-0.6	0-0.25	0-0.05
a (hb)	A-site Na	0-0.2	0.2-0-6	0-0.25	0-0.05
c (hb)	Ca	0-0.2	0.6-0.9	0-7-1	0-0.05
f (hb)	Fe^{3+}	0-1	0-0.5	0-0.2	0-0.2

glaucophane: high z and y with low a and c
hornblende: high a,y and c
actinolite: high c with loq y and a
cummingtonite: low values for all

Composition variables of the calculated amphiboles in the *P–T* conditions for MAOC 11, 13 and 15 at the *P–T* conditions of the experiments (cf. subchapter 4.2.1 and 6.2)

		MAOC 11					
***P* [kbar]**	***T* [°C]**	**x(hb)**	**y (hb)**	**z (hb)**	**a (hb)**	**c (hb)**	**f (hb)**
10	**1050**						
12.5	**1050**	0.16	0.53	0.03	0.66	0.74	0.11
15	**900**	0.11	0.56	0.07	0.53	0.82	0.07
15	**1100**						

		MAOC 13					
***P* [kbar]**	***T* [°C]**	**x(hb)**	**y (hb)**	**z (hb)**	**a (hb)**	**c (hb)**	**f (hb)**
10	**1050**	0.19	0.61	0.02	0.80	0.78	0.10
12.5	**1050**	0.16	0.54	0.03	0.66	0.74	0.09
15	**900**	0.11	0.56	0.07	0.53	0.81	0.06
15	**1100**						

		MAOC 15					
***P* [kbar]**	***T* [°C]**	**x(hb)**	**y (hb)**	**z (hb)**	**a (hb)**	**c (hb)**	**f (hb)**
10	**1050**	0.17	0.62	0.02	0.83	0.79	0.10
12.5	**1050**	0.14	0.58	0.03	0.71	0.75	0.08
15	**900**	0.10	0.53	0.09	0.51	0.77	0.06
15	**1100**	0.12	0.57	0.06	0.72	0.69	0.07

Appendix A2: T–X_{MgO} pseudosections from MAOC 11–17 at 10, 12.5, 15, 17, 19 and 20 kbar

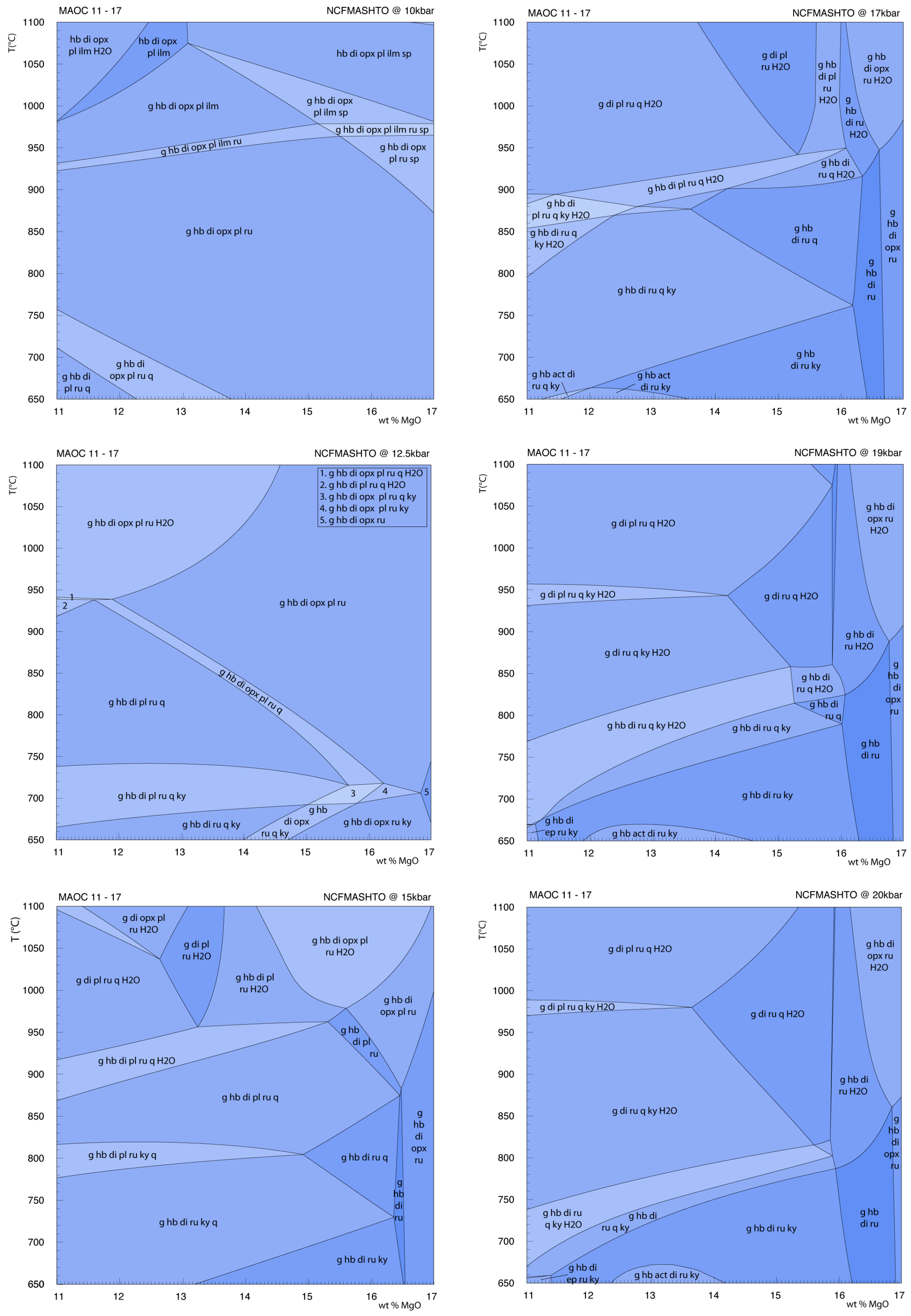

Figure A2: T–X_{MgO} pseudosections cover the range between MAOC 11 and 17 at 10, 12.5, 15, 17, 19 and 20 kbar. A further T–X pseudosection for 15 kbar is also illustrated in Fig. 4.3.1. Mineral abbreviations are given in Tab. 3.1.1.

Appendix A3: *P–T* pseudosections for MAOC 11, 13 and 15 with mineral mode isopleths of garnet, hornblende, diopside, orthopyroxene and plagioclase

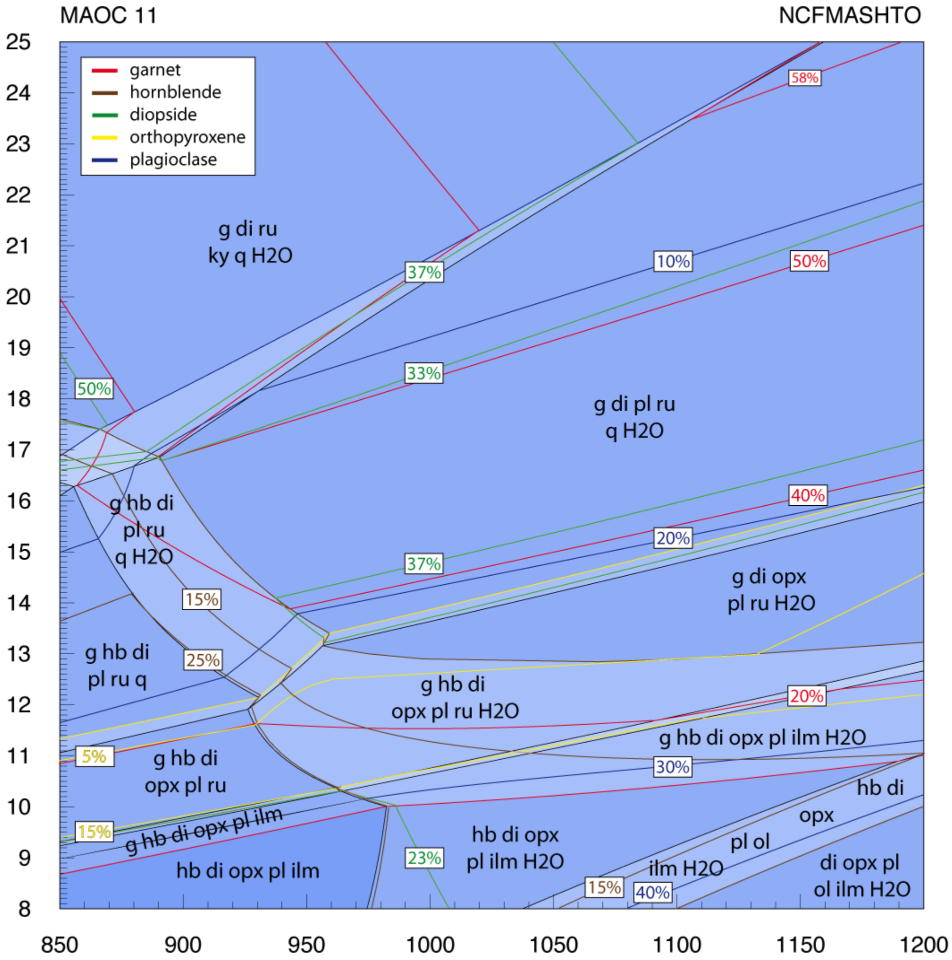

Figure A3.1: *P–T* pseudosection for MAOC 11 with mineral mode isopleths for garnet, hornblende, diopside, orthopyroxene and plagioclase complements the pie charts in Fig. 6.2.1.

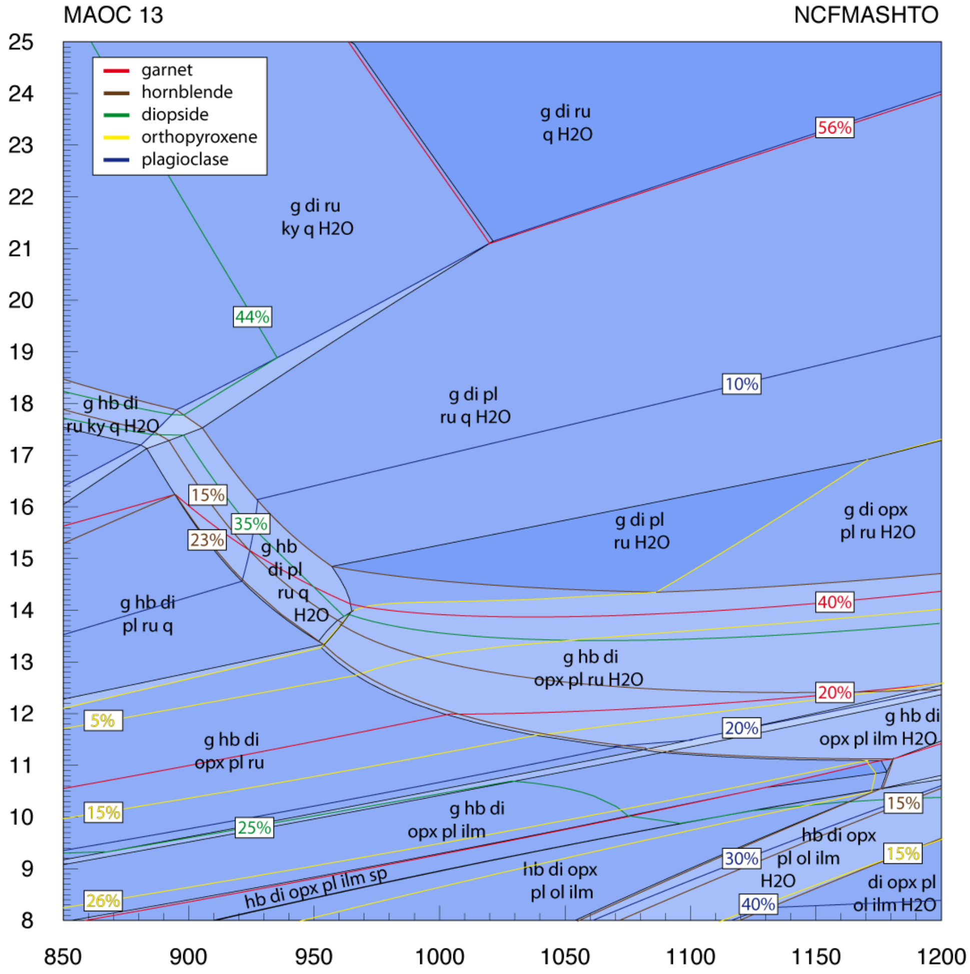

Figure A3.2: *P–T* pseudosection for MAOC 13 with mineral mode isopleths for garnet, hornblende, diopside, orthopyroxene and plagioclase complements the pie charts in Fig. 6.2.2.

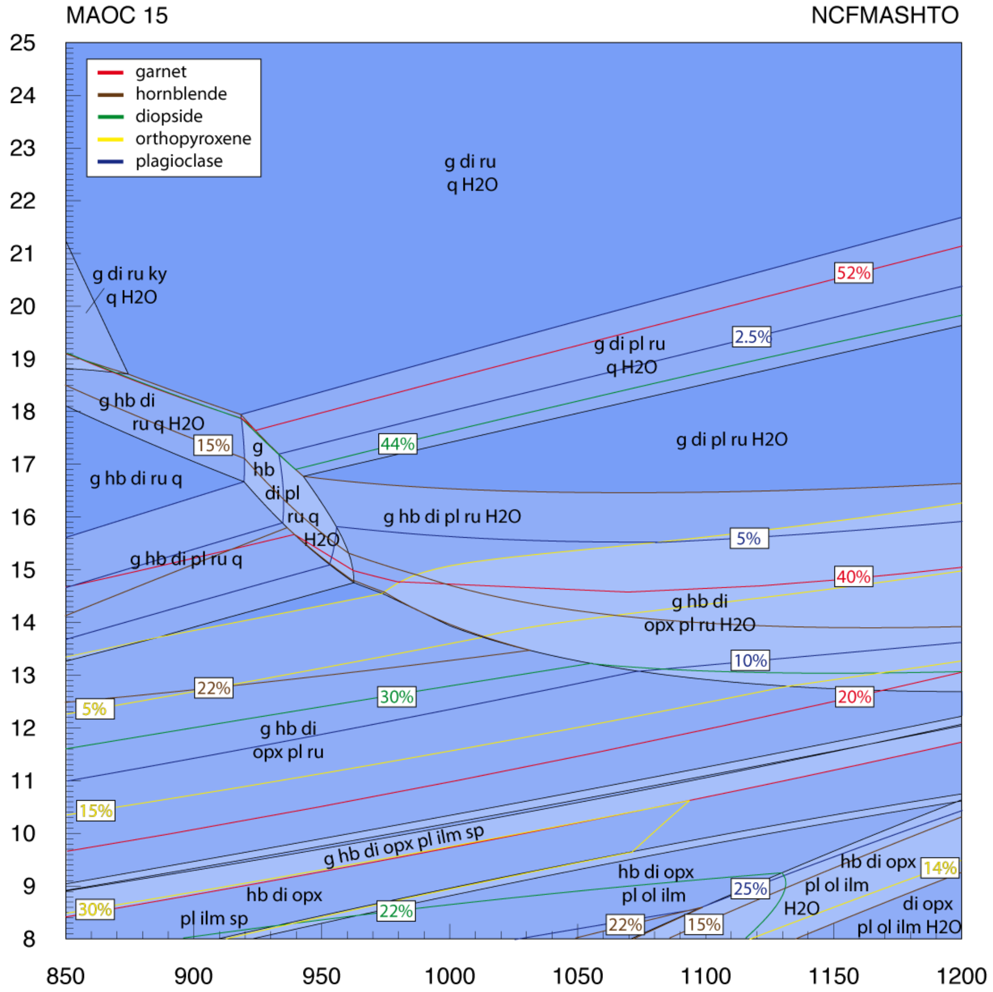

Figure A3.3: *P*–*T* pseudosection for MAOC 15 with mineral mode isopleths for garnet, hornblende, diopside, orthopyroxene and plagioclase complements the pie charts in Fig. 6.2.3.

Appendix A7: Activity-composition models in the system NCFMASHTO (*a–x* file “tc-NCFMASHTO”) and further applied *a–x* models

```
% ---------------------------------------------------------------------------------
%
% This is a NCFMASHTO datafile for metabasic rocks that contains coding for:
% gl, act, hb, cu, ged, anth, di, o, jd, chl, g, ep, pl, mt, ilm, hem.
%
% ---------------------------------------------------------------------------------
%
% When using this datafile, please cite the following references:
%
% Amphiboles:
% Diener, JFA, Powell, R, White, RW & Holland, TJB (2007) A new thermo-
% dynamic model for clino- and orthoamphiboles in Na2O-CaO-FeO-MgO-Al2O3-
% SiO2-H2O-O. Journal of Metamorphic Geology, 25, 631-656.
%
% Clinopyroxenes:
% Green, ECR, Holland, TJB & Powell, R (2007) An order-disorder model for
% omphacitic pyroxenes in the system jadeite-diopside-hedenbergite-acmite,
% with applications to eclogite rocks. American Mineralogist, 92, 1181-1189.
%
% Chlorite:
% Holland, TJB, Baker, JM & Powell, R (1998) Mixing properties and activity-
% composition relationships of chlorites in the system MgO-FeO-Al2O3-SiO2-H2O.
% European Journal of Mineralogy, 10, 395-406.
%
% Garnet:
% White, RW, Powell, R & Holland, TJB (2007) Progress relating to calculation
% of partial melting equilibria for metapelites. Journal of Metamorphic Geology,
% 25, 511-527.
%
% Epidote:
% Holland, TJB & Powell, R (1998) An internally consistent thermodynamic dataset
% for phases of petrological interest. Journal of Metamorphic Geology, 16, 309-343.
%
% Plagioclase:
% Holland, TJB & Powell, R (2003) Activity-composition relations for phases in
% petrological calculations: an asymmetric multicomponent formulation. Contributions
% to Mineralogy and Petrology, 145, 492-501.
%
% Magnetite:
% White, RW, Powell, R & Clarke, GL (2002) The interpretation of reaction textures
% in Fe-rich metapelitic granulites of the Musgrave Block, central Australia:
% constraints from mineral equilibria calculations in the system K2O-FeO-MgO-Al2O3-
% SiO2-H2O-TiO2-Fe2O3. Journal of Metamorphic Geology, 20, 41-55.
%
% Ilmenite and hematite:
% White, RW, Powell, R, Holland, TJB & Worley, BA (2000) The effect of TiO2 and
% Fe2O3 on metapelitic assemblages at greenschist and amphibolite facies conditions:
% mineral equilibria calculations in the system K2O-FeO-MgO-Al2O3-SiO2-H2O-TiO2-Fe2O3.
% Journal of Metamorphic Geology, 18, 497-511.
%
% ---------------------------------------------------------------------------------
%
% The coding for the 4 clinoamphiboles is identical - the different amphiboles are
% distinguished by different starting guesses. The same goes for the 2 ortho-
% amphiboles, the 3 clinopyroxenes and ilmenite and hematite.
%
% With all these minerals, watch that the calculated mineral composition hasn't
% "jumped" a solvus (ie check that the calculated mineral composition matches the
% mineral name)
%
% ---------------------------------------------------------------------------------
%
% WARNING: AMPHIBOLES ARE NOT GOOD FOR YOU.
% McDonald, J.C., Gibbs, G.W., Liddell, F.D.K and McDonald, A.D. (1978)
% Mortality after long exposure to cummingtonite-grunerite,
% American Review of Respiratory Disease, 118, 271-277.
%
% =================================================================================

% ---------------------------------------------
% clinoamphibole: NCFMASHO
%
% Diener, JFA, Powell, R, White, RW & Holland, TJB (2007) A new thermo-
% dynamic model for clino- and orthoamphiboles in Na2O-CaO-FeO-MgO-Al2O3-
% SiO2-H2O-O. Journal of Metamorphic Geology, 25, 631-656.
%
%       A         M13       M2                 M4                T1
%       v   Na    Mg  Fe    Mg  Fe  Al  Fe3    Ca  Mg  Fe  Na    Si  Al
% tr    1   0     3   0     2   0   0   0      2   0   0   0     4   0
% ts    1   0     3   0     0   0   2   0      2   0   0   0     2   2
% parg  0   1     3   0     1   0   1   0      2   0   0   0     2   2
% gl    1   0     3   0     0   0   2   0      0   0   0   2     4   0
% cumm  1   0     3   0     2   0   0   0      0   2   0   0     4   0
% grun  1   0     0   3     0   2   0   0      0   0   2   0     4   0
```

```
% a     1   0     3   0     0   2   0   0     0   0   2   0     4   0
% b     1   0     0   3     2   0   0   0     0   0   2   0     4   0
% mrb   1   0     3   0     0   0   0   2     0   0   0   2     4   0
%
%                     3 xFeM13 + 2 xFeM2 + 2 xFeM4
% x -> ------------------------------------------------------------
%      3 xFeM13 + 2 xFeM2 + 2 xFeM4 + 3 xMgM13 + 2 xMgM2 + 2 xMgM4
%
% y -> xAlM2
%
% z -> xNaM4
%
% a -> xNaA
%
% c -> xCaM4
%
% f -> xFe3M2
%
%               xFeM13
% Q1 -> x - ---------------
%           xFeM13 + xMgM13
%
%               xFeM2
% Q2 -> x - -------------
%           xFeM2 + xMgM2
% -------------------------------------------------

gl  9

  x(gl)         0.4263
  y(gl)         0.7618
  z(gl)         0.8817
  a(gl)         0.1185
  c(gl)         0.1161
  f(gl)        0.09158
  Q1(gl)      -0.01080 range -1 1
  Q2(gl)        0.1178 range -1 1

% -------------------------------------------------

p(tr)      1 1    0  5  -1/2  a   1  c  -1  f  -1  y   1  z

p(ts)      1 1    0  4  -1/2  a   1  f   1  y  -1  z

p(parg)    1 1    0  1  1  a

p(gl)      1 1    0  2  -1  f   1  z

p(cumm)    5 1    1  5  -1  c  -1  Q2  -1  x  -1  z  -3/2  Q1
            2    0  1  1  f    0  1  1  Q2
            2    0  1  1  c    0  1  1  x
            2    0  1  1  Q2    0  1  1  y
            2    0  1  1  x    0  1  1  z

p(grun)    7 1    0  3   1  x  -2  Q2  -5/2  Q1
            2    0  1  2  f    0  1  1  Q2
            2    0  1  1  c    0  1  1  x
            2    0  1  -1  f    0  1  1  x
            2    0  1  2  Q2    0  1  1  y
            2    0  1  -1  x    0  1  1  y
            2    0  1  1  x    0  1  1  z

p(a)       5 1    0  2   1  Q2  5/2  Q1
            2    0  1  -1  f    0  1  1  Q2
            2    0  1  -1  c    0  1  1  x
            2    0  1  -1  Q2    0  1  1  y
            2    0  1  -1  x    0  1  1  z

p(b)       7 1    0  2  2  Q2  3/2  Q1
            2    0  1  -2  f    0  1  1  Q2
            2    0  1  -1  c    0  1  1  x
            2    0  1  1  f    0  1  1  x
            2    0  1  -2  Q2    0  1  1  y
            2    0  1  1  x    0  1  1  y
            2    0  1  -1  x    0  1  1  z

p(mrb)     1 1    0  1  1  f

% -------------------------------------------------
asf
W(tr,ts)           20  0  0
W(tr,parg)         25  0  0
W(tr,gl)           65  0  0
W(tr,cumm)         45  0  0
W(tr,grun)         75  0  0
W(tr,a)            57  0  0
W(tr,b)            63  0  0
W(tr,mrb)          65  0  0 %
W(ts,parg)        -40  0  0
W(ts,gl)           25  0  0
```

```
W(ts,cumm)          70  0  0
W(ts,grun)          80  0  0
W(ts,a)             70  0  0
W(ts,b)           72.5  0  0
W(ts,mrb)           25  0  0 %
W(parg,gl)          50  0  0
W(parg,cumm)        90  0  0
W(parg,grun)     106.7  0  0
W(parg,a)         94.8  0  0
W(parg,b)         94.8  0  0
W(parg,mrb)         50  0  0 %
W(gl,cumm)         100  0  0
W(gl,grun)       113.5  0  0
W(gl,a)            100  0  0
W(gl,b)          111.2  0  0
W(gl,mrb)            0  0  0 %
W(cumm,grun)        33  0  0
W(cumm,a)           18  0  0
W(cumm,b)           23  0  0
W(cumm,mrb)        100  0  0 %
W(grun,a)           12  0  0
W(grun,b)            8  0  0
W(grun,mrb)      113.5  0  0 %
W(a,b)              20  0  0
W(a,mrb)           100  0  0
W(b,mrb)         111.2  0  0 %

tr             1  0  0
ts           1.5  0  0
parg         1.7  0  0
gl           0.8  0  0
cumm           1  0  0
grun           1  0  0
a              1  0  0
b              1  0  0
mrb          0.8  0  0

% ------------------------------------------------
14

xvA        1 1    1  1  -1  a

xNaA       1 1    0  1  1  a

xMgM13     1 1    1  2   1  Q1  -1  x

xFeM13     1 1    0  2  -1  Q1   1  x

xMgM2      5 1    1  4  -1  f   1  Q2  -1  x  -1  y
            2    0  1  -1  f    0  1  1  Q2
            2    0  1  1  f    0  1  1  x
            2    0  1  -1  Q2    0  1  1  y
            2    0  1  1  x    0  1  1  y

xFeM2      5 1    0  2  -1  Q2   1  x
            2    0  1  1  f    0  1  1  Q2
            2    0  1  -1  f    0  1  1  x
            2    0  1  1  Q2    0  1  1  y
            2    0  1  -1  x    0  1  1  y

xAlM2      1 1    0  1  1  y

xFe3M2     1 1    0  1  1  f

xCaM4      1 1    0  1  1  c

xMgM4      5 1    1  5  -1  c  -1  Q2  -1  x  -1  z  -3/2  Q1
            2    0  1  1  f    0  1  1  Q2
            2    0  1  1  c    0  1  1  x
            2    0  1  1  Q2    0  1  1  y
            2    0  1  1  x    0  1  1  z

xFeM4      5 1    0  3   1  Q2   1  x  3/2  Q1
            2    0  1  -1  f    0  1  1  Q2
            2    0  1  -1  c    0  1  1  x
            2    0  1  -1  Q2    0  1  1  y
            2    0  1  -1  x    0  1  1  z

xNaM4      1 1    0  1  1  z

xSiT1      1 1    1  4  -1/2  f  -1/2  y  1/2  z  -1/4  a

xAlT1      1 1    0  4  1/2  f  1/2  y  -1/2  z  1/4  a

% ------------------------------------------------

tr      1    5  xvA 1  xMgM13 3  xMgM2 2  xCaM4 2  xSiT1 1

ts      2    6  xvA 1  xMgM13 3  xAlM2 2  xCaM4 2  xSiT1 1/2  xAlT1 1/2
 DQF   10  0 0
```

```
parg    8    7  xNaA 1  xMgM13 3  xMgM2 1  xAlM2 1  xCaM4 2  xSiT1 1/2  xAlT1 1/2
 DQF   15  0 0

gl      1    5  xvA 1  xMgM13 3  xAlM2 2  xNaM4 2  xSiT1 1
 DQF   3  0 0

cumm    1    5  xvA 1  xMgM13 3  xMgM2 2  xMgM4 2  xSiT1 1
 DQF  -6.4 0 0

grun    1    5  xvA 1  xFeM13 3  xFeM2 2  xFeM4 2  xSiT1 1
 DQF  -5 0 0

a       1    5  xvA 1  xMgM13 3  xFeM2 2  xFeM4 2  xSiT1 1
 make   2  cumm 3/7  grun 4/7
 DQF    -15.1  0  0

b       1    5  xvA 1  xFeM13 3  xMgM2 2  xFeM4 2  xSiT1 1
 make   2  cumm 2/7  grun 5/7
 DQF    -17.1  0  0

mrb     1    5  xvA 1  xMgM13 3  xFe3M2 2  xNaM4 2  xSiT1 1
 make 3 gl 1 jd -2 acm 2
 DQF   8 0 0

% ======================================================================

% ------------------------------------------------
% clinoamphibole: NCFMASHO
%
% Diener, JFA, Powell, R, White, RW & Holland, TJB (2007) A new thermo-
% dynamic model for clino- and orthoamphiboles in Na2O-CaO-FeO-MgO-Al2O3-
% SiO2-H2O-O. Journal of Metamorphic Geology, 25, 631-656.
%
%       A         M13       M2                 M4                 T1
%       v   Na    Mg  Fe    Mg  Fe  Al  Fe3    Ca  Mg  Fe  Na     Si  Al
% tr    1   0     3   0     2   0   0   0      2   0   0   0      4   0
% ts    1   0     3   0     0   0   2   0      2   0   0   0      2   2
% parg  0   1     3   0     1   0   1   0      2   0   0   0      2   2
% gl    1   0     3   0     0   0   2   0      0   0   0   2      4   0
% cumm  1   0     3   0     2   0   0   0      0   2   0   0      4   0
% grun  1   0     0   3     0   2   0   0      0   0   2   0      4   0
% a     1   0     3   0     0   2   0   0      0   0   2   0      4   0
% b     1   0     0   3     2   0   0   0      0   0   2   0      4   0
% mrb   1   0     3   0     0   0   0   2      0   0   0   2      4   0
%
%                     3 xFeM13 + 2 xFeM2 + 2 xFeM4
% x -> ----------------------------------------------------------
%      3 xFeM13 + 2 xFeM2 + 2 xFeM4 + 3 xMgM13 + 2 xMgM2 + 2 xMgM4
%
% y -> xAlM2
%
% z -> xNaM4
%
% a -> xNaA
%
% c -> xCaM4
%
% f -> xFe3M2
%
%               xFeM13
% Q1 -> x - ---------------
%           xFeM13 + xMgM13
%
%               xFeM2
% Q2 -> x - -------------
%           xFeM2 + xMgM2
% ------------------------------------------------

act  9

  x(act)        0.3364
  y(act)        0.1934
  z(act)        0.2431
  a(act)        0.1133
  c(act)        0.7470
  f(act)       0.02325
  Q1(act)     -0.03874 range -1 1
  Q2(act)      0.08132 range -1 1
% ------------------------------------------------

p(tr)      1 1    0  5  -1/2  a   1  c  -1  f  -1  y   1  z

p(ts)      1 1    0  4  -1/2  a   1  f   1  y  -1  z

p(parg)    1 1    0  1  1  a

p(gl)      1 1    0  2  -1  f   1  z
```

```
p(cumm)     5 1    1  5  -1  c  -1  Q2  -1  x  -1  z  -3/2  Q1
             2    0  1  1  f    0  1  1  Q2
             2    0  1  1  c    0  1  1  x
             2    0  1  1  Q2    0  1  1  y
             2    0  1  1  x    0  1  1  z

p(grun)     7 1    0  3   1  x  -2  Q2  -5/2  Q1
             2    0  1  2  f    0  1  1  Q2
             2    0  1  1  c    0  1  1  x
             2    0  1  -1  f    0  1  1  x
             2    0  1  2  Q2    0  1  1  y
             2    0  1  -1  x    0  1  1  y
             2    0  1  1  x    0  1  1  z

p(a)        5 1    0  2   1  Q2  5/2  Q1
             2    0  1  -1  f    0  1  1  Q2
             2    0  1  -1  c    0  1  1  x
             2    0  1  -1  Q2    0  1  1  y
             2    0  1  -1  x    0  1  1  z

p(b)        7 1    0  2  2  Q2  3/2  Q1
             2    0  1  -2  f    0  1  1  Q2
             2    0  1  -1  c    0  1  1  x
             2    0  1  1  f    0  1  1  x
             2    0  1  -2  Q2    0  1  1  y
             2    0  1  1  x    0  1  1  y
             2    0  1  -1  x    0  1  1  z

p(mrb)      1 1    0  1  1  f
% ------------------------------------------------
asf
W(tr,ts)          20  0  0
W(tr,parg)        25  0  0
W(tr,gl)          65  0  0
W(tr,cumm)        45  0  0
W(tr,grun)        75  0  0
W(tr,a)           57  0  0
W(tr,b)           63  0  0
W(tr,mrb)         65  0  0 %
W(ts,parg)       -40  0  0
W(ts,gl)          25  0  0
W(ts,cumm)        70  0  0
W(ts,grun)        80  0  0
W(ts,a)           70  0  0
W(ts,b)         72.5  0  0
W(ts,mrb)         25  0  0 %
W(parg,gl)        50  0  0
W(parg,cumm)      90  0  0
W(parg,grun)   106.7  0  0
W(parg,a)       94.8  0  0
W(parg,b)       94.8  0  0
W(parg,mrb)       50  0  0 %
W(gl,cumm)       100  0  0
W(gl,grun)     113.5  0  0
W(gl,a)          100  0  0
W(gl,b)        111.2  0  0
W(gl,mrb)          0  0  0 %
W(cumm,grun)      33  0  0
W(cumm,a)         18  0  0
W(cumm,b)         23  0  0
W(cumm,mrb)      100  0  0 %
W(grun,a)         12  0  0
W(grun,b)          8  0  0
W(grun,mrb)    113.5  0  0 %
W(a,b)            20  0  0
W(a,mrb)         100  0  0
W(b,mrb)       111.2  0  0 %

tr             1  0  0
ts           1.5  0  0
parg         1.7  0  0
gl           0.8  0  0
cumm           1  0  0
grun           1  0  0
a              1  0  0
b              1  0  0
mrb          0.8  0  0

% ------------------------------------------------
14

xvA         1 1    1  1  -1  a

xNaA        1 1    0  1  1  a

xMgM13      1 1    1  2   1  Q1  -1  x

xFeM13      1 1    0  2  -1  Q1   1  x
```

```
xMgM2       5 1    1  4  -1  f   1  Q2  -1  x  -1  y
             2    0  1  -1  f    0  1  1  Q2
             2    0  1  1  f    0  1  1  x
             2    0  1  -1  Q2    0  1  1  y
             2    0  1  1  x    0  1  1  y

xFeM2       5 1    0  2  -1  Q2   1  x
             2    0  1  1  f    0  1  1  Q2
             2    0  1  -1  f    0  1  1  x
             2    0  1  1  Q2    0  1  1  y
             2    0  1  -1  x    0  1  1  y

xAlM2       1 1    0  1  1  y

xFe3M2      1 1    0  1  1  f

xCaM4       1 1    0  1  1  c

xMgM4       5 1    1  5  -1  c  -1  Q2  -1  x  -1  z  -3/2  Q1
             2    0  1  1  f    0  1  1  Q2
             2    0  1  1  c    0  1  1  x
             2    0  1  1  Q2    0  1  1  y
             2    0  1  1  x    0  1  1  z

xFeM4       5 1    0  3   1  Q2   1  x  3/2  Q1
             2    0  1  -1  f    0  1  1  Q2
             2    0  1  -1  c    0  1  1  x
             2    0  1  -1  Q2    0  1  1  y
             2    0  1  -1  x    0  1  1  z

xNaM4       1 1    0  1  1  z

xSiT1       1 1    1  4  -1/2  f  -1/2  y  1/2  z  -1/4  a

xAlT1       1 1    0  4  1/2  f  1/2  y  -1/2  z  1/4  a

% ------------------------------------------------

tr      1    5  xvA 1  xMgM13 3  xMgM2 2  xCaM4 2  xSiT1 1

ts      2    6  xvA 1  xMgM13 3  xAlM2 2  xCaM4 2  xSiT1 1/2  xAlT1 1/2
 DQF   10  0 0

parg    8    7  xNaA 1  xMgM13 3  xMgM2 1  xAlM2 1  xCaM4 2  xSiT1 1/2  xAlT1 1/2
 DQF   15  0 0

gl      1    5  xvA 1  xMgM13 3  xAlM2 2  xNaM4 2  xSiT1 1
 DQF   3  0 0

cumm    1    5  xvA 1  xMgM13 3  xMgM2 2  xMgM4 2  xSiT1 1
 DQF  -6.4 0 0

grun    1    5  xvA 1  xFeM13 3  xFeM2 2  xFeM4 2  xSiT1 1
 DQF  -5 0 0

a       1    5  xvA 1  xMgM13 3  xFeM2 2  xFeM4 2  xSiT1 1
 make   2  cumm 3/7  grun 4/7
 DQF    -15.1  0  0

b       1    5  xvA 1  xFeM13 3  xMgM2 2  xFeM4 2  xSiT1 1
 make   2  cumm 2/7  grun 5/7
 DQF    -17.1  0  0

mrb     1    5  xvA 1  xMgM13 3  xFe3M2 2  xNaM4 2  xSiT1 1
 make 3 gl 1 jd -2 acm 2
 DQF  8 0 0

% ===================================================================

% ------------------------------------------------
% clinoamphibole: NCFMASHO
%
% Diener, JFA, Powell, R, White, RW & Holland, TJB (2007) A new thermo-
% dynamic model for clino- and orthoamphiboles in Na2O-CaO-FeO-MgO-Al2O3-
% SiO2-H2O-O. Journal of Metamorphic Geology, 25, 631-656.
%
%       A         M13       M2                M4                T1
%       v   Na    Mg  Fe    Mg  Fe  Al  Fe3   Ca  Mg  Fe  Na    Si  Al
% tr    1   0     3   0     2   0   0   0     2   0   0   0     4   0
% ts    1   0     3   0     0   0   2   0     2   0   0   0     2   2
% parg  0   1     3   0     1   0   1   0     2   0   0   0     2   2
% gl    1   0     3   0     0   0   2   0     0   0   0   2     4   0
% cumm  1   0     3   0     2   0   0   0     0   2   0   0     4   0
% grun  1   0     0   3     0   2   0   0     0   0   2   0     4   0
% a     1   0     3   0     0   2   0   0     0   0   2   0     4   0
% b     1   0     0   3     2   0   0   0     0   0   2   0     4   0
% mrb   1   0     3   0     0   0   0   2     0   0   0   2     4   0
%
```

```
%                     3 xFeM13 + 2 xFeM2 + 2 xFeM4
% x -> -----------------------------------------------------------
%      3 xFeM13 + 2 xFeM2 + 2 xFeM4 + 3 xMgM13 + 2 xMgM2 + 2 xMgM4
%
% y -> xAlM2
%
% z -> xNaM4
%
% a -> xNaA
%
% c -> xCaM4
%
% f -> xFe3M2
%
%               xFeM13
% Q1 -> x - ---------------
%           xFeM13 + xMgM13
%
%               xFeM2
% Q2 -> x - -------------
%           xFeM2 + xMgM2
% -------------------------------------------------

hb  9

  x(hb)         0.4146
  y(hb)         0.6312
  z(hb)         0.4302
  a(hb)         0.4060
  c(hb)         0.5607
  f(hb)        0.07588
  Q1(hb)      -0.02510 range -1 1
  Q2(hb)        0.1443 range -1 1
% -------------------------------------------------

p(tr)      1 1    0  5  -1/2  a   1  c  -1  f  -1  y   1  z

p(ts)      1 1    0  4  -1/2  a   1  f   1  y  -1  z

p(parg)    1 1    0  1  1  a

p(gl)      1 1    0  2  -1  f   1  z

p(cumm)    5 1    1  5  -1  c  -1  Q2  -1  x  -1  z  -3/2  Q1
            2    0  1  1  f    0  1  1  Q2
            2    0  1  1  c    0  1  1  x
            2    0  1  1  Q2    0  1  1  y
            2    0  1  1  x    0  1  1  z

p(grun)    7 1    0  3   1  x  -2  Q2  -5/2  Q1
            2    0  1  2  f    0  1  1  Q2
            2    0  1  1  c    0  1  1  x
            2    0  1  -1  f    0  1  1  x
            2    0  1  2  Q2    0  1  1  y
            2    0  1  -1  x    0  1  1  y
            2    0  1  1  x    0  1  1  z

p(a)       5 1    0  2   1  Q2  5/2  Q1
            2    0  1  -1  f    0  1  1  Q2
            2    0  1  -1  c    0  1  1  x
            2    0  1  -1  Q2    0  1  1  y
            2    0  1  -1  x    0  1  1  z

p(b)       7 1    0  2  2  Q2  3/2  Q1
            2    0  1  -2  f    0  1  1  Q2
            2    0  1  -1  c    0  1  1  x
            2    0  1  1  f    0  1  1  x
            2    0  1  -2  Q2    0  1  1  y
            2    0  1  1  x    0  1  1  y
            2    0  1  -1  x    0  1  1  z

p(mrb)     1 1    0  1  1  f
% -------------------------------------------------
asf
W(tr,ts)           20  0  0
W(tr,parg)         25  0  0
W(tr,gl)           65  0  0
W(tr,cumm)         45  0  0
W(tr,grun)         75  0  0
W(tr,a)            57  0  0
W(tr,b)            63  0  0
W(tr,mrb)          65  0  0 %
W(ts,parg)        -40  0  0
W(ts,gl)           25  0  0
W(ts,cumm)         70  0  0
W(ts,grun)         80  0  0
W(ts,a)            70  0  0
W(ts,b)          72.5  0  0
W(ts,mrb)          25  0  0 %
W(parg,gl)         50  0  0
```

```
W(parg,cumm)       90  0  0
W(parg,grun)    106.7  0  0
W(parg,a)        94.8  0  0
W(parg,b)        94.8  0  0
W(parg,mrb)        50  0  0 %
W(gl,cumm)        100  0  0
W(gl,grun)      113.5  0  0
W(gl,a)           100  0  0
W(gl,b)         111.2  0  0
W(gl,mrb)           0  0  0 %
W(cumm,grun)       33  0  0
W(cumm,a)          18  0  0
W(cumm,b)          23  0  0
W(cumm,mrb)       100  0  0 %
W(grun,a)          12  0  0
W(grun,b)           8  0  0
W(grun,mrb)     113.5  0  0 %
W(a,b)             20  0  0
W(a,mrb)          100  0  0
W(b,mrb)        111.2  0  0 %

tr              1  0  0
ts            1.5  0  0
parg          1.7  0  0
gl            0.8  0  0
cumm            1  0  0
grun            1  0  0
a               1  0  0
b               1  0  0
mrb           0.8  0  0

% -------------------------------------------------
14

xvA        1 1    1  1  -1  a

xNaA       1 1    0  1  1  a

xMgM13     1 1    1  2   1  Q1  -1  x

xFeM13     1 1    0  2  -1  Q1   1  x

xMgM2      5 1    1  4  -1  f   1  Q2  -1  x  -1  y
            2    0  1  -1  f    0  1  1  Q2
            2    0  1  1  f    0  1  1  x
            2    0  1  -1  Q2    0  1  1  y
            2    0  1  1  x    0  1  1  y

xFeM2      5 1    0  2  -1  Q2   1  x
            2    0  1  1  f    0  1  1  Q2
            2    0  1  -1  f    0  1  1  x
            2    0  1  1  Q2    0  1  1  y
            2    0  1  -1  x    0  1  1  y

xAlM2      1 1    0  1  1  y

xFe3M2     1 1    0  1  1  f

xCaM4      1 1    0  1  1  c

xMgM4      5 1    1  5  -1  c  -1  Q2  -1  x  -1  z  -3/2  Q1
            2    0  1  1  f    0  1  1  Q2
            2    0  1  1  c    0  1  1  x
            2    0  1  1  Q2    0  1  1  y
            2    0  1  1  x    0  1  1  z

xFeM4      5 1    0  3   1  Q2   1  x  3/2  Q1
            2    0  1  -1  f    0  1  1  Q2
            2    0  1  -1  c    0  1  1  x
            2    0  1  -1  Q2    0  1  1  y
            2    0  1  -1  x    0  1  1  z

xNaM4      1 1    0  1  1  z

xSiT1      1 1    1  4  -1/2  f  -1/2  y  1/2  z  -1/4  a

xAlT1      1 1    0  4  1/2  f  1/2  y  -1/2  z  1/4  a

% -------------------------------------------------

tr      1    5  xvA 1  xMgM13 3  xMgM2 2  xCaM4 2  xSiT1 1

ts      2    6  xvA 1  xMgM13 3  xAlM2 2  xCaM4 2  xSiT1 1/2  xAlT1 1/2
 DQF   10  0 0

parg    8    7  xNaA 1  xMgM13 3  xMgM2 1  xAlM2 1  xCaM4 2  xSiT1 1/2  xAlT1 1/2
 DQF   15  0 0

gl      1    5  xvA 1  xMgM13 3  xAlM2 2  xNaM4 2  xSiT1 1
 DQF   3  0 0
```

```
cumm    1    5  xvA 1  xMgM13 3  xMgM2 2  xMgM4 2  xSiT1 1
 DQF  -6.4 0 0

grun    1    5  xvA 1  xFeM13 3  xFeM2 2  xFeM4 2  xSiT1 1
 DQF  -5 0 0

a       1    5  xvA 1  xMgM13 3  xFeM2 2  xFeM4 2  xSiT1 1
 make   2  cumm 3/7  grun 4/7
 DQF    -15.1  0  0

b       1    5  xvA 1  xFeM13 3  xMgM2 2  xFeM4 2  xSiT1 1
 make   2  cumm 2/7  grun 5/7
 DQF    -17.1  0  0

mrb     1    5  xvA 1  xMgM13 3  xFe3M2 2  xNaM4 2  xSiT1 1
 make 3 gl 1 jd -2 acm 2
 DQF  8 0 0

% ====================================================================
% ------------------------------------------------
% clinoamphibole: NCFMASHO
%
% Diener, JFA, Powell, R, White, RW & Holland, TJB (2007) A new thermo-
% dynamic model for clino- and orthoamphiboles in Na2O-CaO-FeO-MgO-Al2O3-
% SiO2-H2O-O. Journal of Metamorphic Geology, 25, 631-656.
%
%       A         M13       M2                M4                T1
%       v   Na    Mg  Fe    Mg  Fe  Al  Fe3   Ca  Mg  Fe  Na    Si  Al
% tr    1   0     3   0     2   0   0   0     2   0   0   0     4   0
% ts    1   0     3   0     0   0   2   0     2   0   0   0     2   2
% parg  0   1     3   0     1   0   1   0     2   0   0   0     2   2
% gl    1   0     3   0     0   0   2   0     0   0   0   2     4   0
% cumm  1   0     3   0     2   0   0   0     0   2   0   0     4   0
% grun  1   0     0   3     0   2   0   0     0   0   2   0     4   0
% a     1   0     3   0     0   2   0   0     0   0   2   0     4   0
% b     1   0     0   3     2   0   0   0     0   0   2   0     4   0
% mrb   1   0     3   0     0   0   0   2     0   0   0   2     4   0
%
%                     3 xFeM13 + 2 xFeM2 + 2 xFeM4
% x -> ----------------------------------------------------------
%      3 xFeM13 + 2 xFeM2 + 2 xFeM4 + 3 xMgM13 + 2 xMgM2 + 2 xMgM4
%
% y -> xAlM2
%
% z -> xNaM4
%
% a -> xNaA
%
% c -> xCaM4
%
% f -> xFe3M2
%
%              xFeM13
% Q1 -> x - ---------------
%          xFeM13 + xMgM13
%
%              xFeM2
% Q2 -> x - -------------
%          xFeM2 + xMgM2
% ------------------------------------------------

cu  9

 x(cu)         0.5837
  y(cu)        0.06607
  z(cu)        0.03172
  a(cu)        0.01462
  c(cu)        0.03891
  f(cu)        0.02175
  Q1(cu)       0.08125 range -1 1
  Q2(cu)        0.2080 range -1 1
% ------------------------------------------------

p(tr)      1 1    0  5  -1/2  a   1  c  -1  f  -1  y   1  z

p(ts)      1 1    0  4  -1/2  a   1  f   1  y  -1  z

p(parg)    1 1    0  1  1  a

p(gl)      1 1    0  2  -1  f   1  z

p(cumm)    5 1    1  5  -1  c  -1  Q2  -1  x  -1  z  -3/2  Q1
            2    0  1  1  f    0  1  1  Q2
            2    0  1  1  c    0  1  1  x
            2    0  1  1  Q2    0  1  1  y
            2    0  1  1  x    0  1  1  z
```

```
p(grun)     7 1    0  3   1  x  -2  Q2  -5/2  Q1
             2    0  1  2  f    0  1  1  Q2
             2    0  1  1  c    0  1  1  x
             2    0  1  -1  f    0  1  1  x
             2    0  1  2  Q2    0  1  1  y
             2    0  1  -1  x    0  1  1  y
             2    0  1  1  x    0  1  1  z

p(a)        5 1    0  2   1  Q2  5/2  Q1
             2    0  1  -1  f    0  1  1  Q2
             2    0  1  -1  c    0  1  1  x
             2    0  1  -1  Q2    0  1  1  y
             2    0  1  -1  x    0  1  1  z

p(b)        7 1    0  2  2  Q2  3/2  Q1
             2    0  1  -2  f    0  1  1  Q2
             2    0  1  -1  c    0  1  1  x
             2    0  1  1  f    0  1  1  x
             2    0  1  -2  Q2    0  1  1  y
             2    0  1  1  x    0  1  1  y
             2    0  1  -1  x    0  1  1  z

p(mrb)      1 1    0  1  1  f
% ---------------------------------------------------
asf
W(tr,ts)           20  0  0
W(tr,parg)         25  0  0
W(tr,gl)           65  0  0
W(tr,cumm)         45  0  0
W(tr,grun)         75  0  0
W(tr,a)            57  0  0
W(tr,b)            63  0  0
W(tr,mrb)          65  0  0 %
W(ts,parg)        -40  0  0
W(ts,gl)           25  0  0
W(ts,cumm)         70  0  0
W(ts,grun)         80  0  0
W(ts,a)            70  0  0
W(ts,b)          72.5  0  0
W(ts,mrb)          25  0  0 %
W(parg,gl)         50  0  0
W(parg,cumm)       90  0  0
W(parg,grun)    106.7  0  0
W(parg,a)        94.8  0  0
W(parg,b)        94.8  0  0
W(parg,mrb)        50  0  0 %
W(gl,cumm)        100  0  0
W(gl,grun)      113.5  0  0
W(gl,a)           100  0  0
W(gl,b)         111.2  0  0
W(gl,mrb)           0  0  0 %
W(cumm,grun)       33  0  0
W(cumm,a)          18  0  0
W(cumm,b)          23  0  0
W(cumm,mrb)       100  0  0 %
W(grun,a)          12  0  0
W(grun,b)           8  0  0
W(grun,mrb)     113.5  0  0 %
W(a,b)             20  0  0
W(a,mrb)          100  0  0
W(b,mrb)        111.2  0  0 %

tr             1  0  0
ts           1.5  0  0
parg         1.7  0  0
gl           0.8  0  0
cumm           1  0  0
grun           1  0  0
a              1  0  0
b              1  0  0
mrb          0.8  0  0

% ---------------------------------------------------
14

xvA         1 1    1  1  -1  a

xNaA        1 1    0  1  1  a

xMgM13      1 1    1  2   1  Q1  -1  x

xFeM13      1 1    0  2  -1  Q1   1  x

xMgM2       5 1    1  4  -1  f   1  Q2  -1  x  -1  y
             2    0  1  -1  f    0  1  1  Q2
             2    0  1  1  f    0  1  1  x
             2    0  1  -1  Q2    0  1  1  y
             2    0  1  1  x    0  1  1  y
```

```
xFeM2      5 1    0  2  -1  Q2   1  x
            2    0  1  1  f    0  1  1  Q2
            2    0  1  -1  f    0  1  1  x
            2    0  1  1  Q2    0  1  1  y
            2    0  1  -1  x    0  1  1  y

xAlM2      1 1    0  1  1  y

xFe3M2     1 1    0  1  1  f

xCaM4      1 1    0  1  1  c

xMgM4      5 1    1  5  -1  c  -1  Q2  -1  x  -1  z  -3/2  Q1
            2    0  1  1  f    0  1  1  Q2
            2    0  1  1  c    0  1  1  x
            2    0  1  1  Q2    0  1  1  y
            2    0  1  1  x    0  1  1  z

xFeM4      5 1    0  3   1  Q2   1  x  3/2  Q1
            2    0  1  -1  f    0  1  1  Q2
            2    0  1  -1  c    0  1  1  x
            2    0  1  -1  Q2    0  1  1  y
            2    0  1  -1  x    0  1  1  z

xNaM4      1 1    0  1  1  z

xSiT1      1 1    1  4  -1/2  f  -1/2  y  1/2  z  -1/4  a

xAlT1      1 1    0  4  1/2  f  1/2  y  -1/2  z  1/4  a

% -------------------------------------------------

tr      1    5  xvA 1  xMgM13 3  xMgM2 2  xCaM4 2  xSiT1 1

ts      2    6  xvA 1  xMgM13 3  xAlM2 2  xCaM4 2  xSiT1 1/2  xAlT1 1/2
 DQF   10  0 0

parg    8    7  xNaA 1  xMgM13 3  xMgM2 1  xAlM2 1  xCaM4 2  xSiT1 1/2  xAlT1 1/2
 DQF   15  0 0

gl      1    5  xvA 1  xMgM13 3  xAlM2 2  xNaM4 2  xSiT1 1
 DQF   3  0 0

cumm    1    5  xvA 1  xMgM13 3  xMgM2 2  xMgM4 2  xSiT1 1
 DQF  -6.4 0 0

grun    1    5  xvA 1  xFeM13 3  xFeM2 2  xFeM4 2  xSiT1 1
 DQF  -5 0 0

a       1    5  xvA 1  xMgM13 3  xFeM2 2  xFeM4 2  xSiT1 1
 make   2  cumm 3/7  grun 4/7
 DQF    -15.1  0  0

b       1    5  xvA 1  xFeM13 3  xMgM2 2  xFeM4 2  xSiT1 1
 make   2  cumm 2/7  grun 5/7
 DQF    -17.1  0  0

mrb     1    5  xvA 1  xMgM13 3  xFe3M2 2  xNaM4 2  xSiT1 1
 make 3 gl 1 jd -2 acm 2
 DQF 8 0 0

% =================================================

% -------------------------------------------------
% orthoamphibole: NCFMASHO
%
% Diener, JFA, Powell, R, White, RW & Holland, TJB (2007) A new thermo-
% dynamic model for clino- and orthoamphiboles in Na2O-CaO-FeO-MgO-Al2O3-
% SiO2-H2O-O. Journal of Metamorphic Geology, 25, 631-656.
%
%       A         M4                 M13       M2                 T1
%       v   Na    Ca  Na  Mg  Fe     Mg  Fe    Al  Fe3 Mg  Fe     Al  Si
% anth  1   0     0   0   2   0      3   0     0   0   2   0      0   4
% ged   1   0     0   0   2   0      3   0     2   0   0   0      2   2
% ompa  0   1     0   0   2   0      3   0     1   0   1   0      2   2
% omgl  1   0     0   2   0   0      3   0     2   0   0   0      0   4
% otr   1   0     2   0   0   0      3   0     0   0   2   0      0   4
% fanth 1   0     0   0   0   2      0   3     0   0   0   2      0   4
% omrb  1   0     0   2   0   0      3   0     0   2   0   0      0   4
% a     1   0     0   0   0   2      3   0     0   0   0   2      0   4
% b     1   0     0   0   0   2      0   3     0   0   2   0      0   4
%
%                     3 xFeM13 + 2 xFeM2 + 2 xFeM4
% x -> -----------------------------------------------------------
%      3 xFeM13 + 2 xFeM2 + 2 xFeM4 + 3 xMgM13 + 2 xMgM2 + 2 xMgM4
%
% y -> xAlM2
%
% z -> xNaM4
%
```

```
% a -> xNaA
%
% c -> xCaM4
%
% f -> xFe3M2
%
%              xFeM13
% Q1 -> x - ---------------
%          xFeM13 + xMgM13
%
%              xFeM2
% Q2 -> x - -------------
%          xFeM2 + xMgM2
% -------------------------------------------------

ged  9

 x(ged)   0.3
 y(ged)   0.5
 z(ged)   0.05
 a(ged)   0.4
 c(ged)   0.05
 f(ged)   0.05
 Q1(ged)  0 range -1 1
 Q2(ged)  0 range -1 1
% -------------------------------------------------

p(anth)     5 1    1  7  -1/2  a  -1  c  -1  f  -1  Q2  -1  x  -1  y  -3/2  Q1
             2    0  1  1  f    0  1  1  Q2
             2    0  1  1  c    0  1  1  x
             2    0  1  1  Q2    0  1  1  y
             2    0  1  1  x    0  1  1  z

p(ged)      1 1    0  4  -1/2  a   1  f   1  y  -1  z

p(ompa)     1 1    0  1  1  a

p(omgl)     1 1    0  2  -1  f   1  z

p(otr)      1 1    0  1  1  c

p(fanth)    7 1    0  3   1  x  -2  Q2  -5/2  Q1
             2    0  1  2  f    0  1  1  Q2
             2    0  1  1  c    0  1  1  x
             2    0  1  -1  f    0  1  1  x
             2    0  1  2  Q2    0  1  1  y
             2    0  1  -1  x    0  1  1  y
             2    0  1  1  x    0  1  1  z

p(omrb)     1 1    0  1  1  f

p(a)        5 1    0  2   1  Q2  5/2  Q1
             2    0  1  -1  f    0  1  1  Q2
             2    0  1  -1  c    0  1  1  x
             2    0  1  -1  Q2    0  1  1  y
             2    0  1  -1  x    0  1  1  z

p(b)        7 1    0  2  2  Q2  3/2  Q1
             2    0  1  -2  f    0  1  1  Q2
             2    0  1  -1  c    0  1  1  x
             2    0  1  1  f    0  1  1  x
             2    0  1  -2  Q2    0  1  1  y
             2    0  1  1  x    0  1  1  y
             2    0  1  -1  x    0  1  1  z
% -------------------------------------------------
asf
W(anth,ged)       25  0  0
W(anth,ompa)      25  0  0
W(anth,omgl)      65  0  0
W(anth,otr)       45  0  0
W(anth,fanth)     33  0  0
W(anth,omrb)      65  0  0 %
W(anth,a)         18  0  0
W(anth,b)         23  0  0
W(ged,ompa)      -40  0  0
W(ged,omgl)       25  0  0
W(ged,otr)        70  0  0
W(ged,fanth)    39.5  0  0
W(ged,omrb)       25  0  0 %
W(ged,a)          29  0  0
W(ged,b)        34.6  0  0
W(ompa,omgl)      50  0  0
W(ompa,otr)       90  0  0
W(ompa,fanth)     45  0  0
W(ompa,omrb)      50  0  0 %
W(ompa,a)       33.2  0  0
W(ompa,b)         36  0  0
W(omgl,otr)       65  0  0
W(omgl,fanth)   81.2  0  0
W(omgl,omrb)       0  0  0 %
```

```
W(omgl,a)       65.5  0  0
W(omgl,b)       78.4  0  0
W(otr,fanth)      75  0  0
W(otr,omrb)       65  0  0 %
W(otr,a)          57  0  0
W(otr,b)          63  0  0
W(fanth,omrb)   81.2  0  0 %
W(fanth,a)        12  0  0
W(fanth,b)         8  0  0
W(omrb,a)       65.5  0  0 %
W(omrb,b)       78.4  0  0 %
W(a,b)            20  0  0

anth    1  0  0
ged   1.5  0  0
ompa  1.7  0  0
omgl  0.8  0  0
otr     1  0  0
fanth   1  0  0
omrb  0.8  0  0
a       1  0  0
b       1  0  0

% ------------------------------------------------
14

xvA        1 1    1  1  -1  a

xNaA       1 1    0  1  1  a

xCaM4      1 1    0  1  1  c

xNaM4      1 1    0  1  1  z

xMgM4      5 1    1  5  -1  c  -1  Q2  -1  x  -1  z  -3/2  Q1
            2    0  1  1  f    0  1  1  Q2
            2    0  1  1  c    0  1  1  x
            2    0  1  1  Q2    0  1  1  y
            2    0  1  1  x    0  1  1  z

xFeM4      5 1    0  3   1  Q2   1  x  3/2  Q1
            2    0  1  -1  f    0  1  1  Q2
            2    0  1  -1  c    0  1  1  x
            2    0  1  -1  Q2    0  1  1  y
            2    0  1  -1  x    0  1  1  z

xMgM13     1 1    1  2   1  Q1  -1  x

xFeM13     1 1    0  2  -1  Q1   1  x

xAlM2      1 1    0  1  1  y

xFe3M2     1 1    0  1  1  f

xMgM2      5 1    1  4  -1  f   1  Q2  -1  x  -1  y
            2    0  1  -1  f    0  1  1  Q2
            2    0  1  1  f    0  1  1  x
            2    0  1  -1  Q2    0  1  1  y
            2    0  1  1  x    0  1  1  y

xFeM2      5 1    0  2  -1  Q2   1  x
            2    0  1  1  f    0  1  1  Q2
            2    0  1  -1  f    0  1  1  x
            2    0  1  1  Q2    0  1  1  y
            2    0  1  -1  x    0  1  1  y

xAlT1      1 1    0  4  1/2  f  1/2  y  -1/2  z  1/4  a

xSiT1      1 1    1  4  -1/2  f  -1/2  y  1/2  z  -1/4  a
% ------------------------------------------------

anth    1    5  xvA 1  xMgM4 2  xMgM13 3  xMgM2 2  xSiT1 1
 check 0  0  0  0  0  0  0  0

ged     2    6  xvA 1  xMgM4 2  xMgM13 3  xAlM2 2  xAlT1 1/2  xSiT1 1/2
 check 0  1  0  0  0  0  0  0
 DQF  22 0 0

ompa    8   7  xNaA 1  xMgM4 2  xMgM13 3  xAlM2 1  xMgM2 1  xAlT1 1/2 xSiT1 1/2
 check 0  1/2  0  1  0  0  0  0
 make  3 parg 1 tr -1 anth 1
 DQF  27 0 0

omgl    1    5  xvA 1  xNaM4 2  xMgM13 3  xAlM2 2  xSiT1 1
 check 0  1  1  0  0  0  0  0
 make  1 gl 1
 DQF 15 0 0
```

```
otr     1    5  xvA 1  xCaM4 2  xMgM13 3  xMgM2 2  xSiT1 1
 check 0  0  0  0  1  0  0  0
 make 1 tr 1
 DQF 0 0 0

fanth   1    5  xvA 1  xFeM4 2  xFeM13 3  xFeM2 2  xSiT1 1
 check 1  0  0  0  0  0  0  0
 DQF   7  0  0

omrb    1    5  xvA 1  xNaM4 2  xMgM13 3  xFe3M2 2  xSiT1 1
 check 0  0  1  0  0  1  0  0
 make 3 gl 1 jd -2 acm 2
 DQF   33 0 0

a       1    5  xvA 1  xFeM4 2  xMgM13 3  xFeM2 2  xSiT1 1
 check 4/7  0  0  0  0  0  4/7  -3/7
 make  2  anth 3/7 fanth 4/7
 DQF   -5.5  0  0

b       1    5  xvA 1  xFeM4 2  xFeM13 3  xMgM2 2  xSiT1 1
 check 5/7  0  0  0  0  0  -2/7  5/7
 make  2  anth 2/7 fanth 5/7
 DQF   -6.7  0  0

% ===============================================

% -----------------------------------------------
% orthoamphibole: NCFMASHO
%
% Diener, JFA, Powell, R, White, RW & Holland, TJB (2007) A new thermo-
% dynamic model for clino- and orthoamphiboles in Na2O-CaO-FeO-MgO-Al2O3-
% SiO2-H2O-O. Journal of Metamorphic Geology, 25, 631-656.
%
%       A         M4                 M13       M2                 T1
%       v   Na    Ca  Na  Mg  Fe    Mg  Fe    Al  Fe3 Mg  Fe    Al  Si
% anth  1   0     0   0   2   0     3   0     0   0   2   0     0   4
% ged   1   0     0   0   2   0     3   0     2   0   0   0     2   2
% ompa  0   1     0   0   2   0     3   0     1   0   1   0     2   2
% omgl  1   0     0   2   0   0     3   0     2   0   0   0     0   4
% otr   1   0     2   0   0   0     3   0     0   0   2   0     0   4
% fanth 1   0     0   0   0   2     0   3     0   0   0   2     0   4
% omrb  1   0     0   2   0   0     3   0     0   2   0   0     0   4
% a     1   0     0   0   0   2     3   0     0   0   0   2     0   4
% b     1   0     0   0   0   2     0   3     0   0   2   0     0   4
%
%                    3 xFeM13 + 2 xFeM2 + 2 xFeM4
% x -> ----------------------------------------------------------
%      3 xFeM13 + 2 xFeM2 + 2 xFeM4 + 3 xMgM13 + 2 xMgM2 + 2 xMgM4
%
% y -> xAlM2
%
% z -> xNaM4
%
% a -> xNaA
%
% c -> xCaM4
%
% f -> xFe3M2
%
%               xFeM13
% Q1 -> x - ---------------
%           xFeM13 + xMgM13
%
%               xFeM2
% Q2 -> x - -------------
%           xFeM2 + xMgM2
% -----------------------------------------------

anth  9

 x(anth)   0.28
 y(anth)   0.11
 z(anth)   0.05
 a(anth)   0.09
 c(anth)   0.05
 f(anth)   0.05
 Q1(anth)  0 range -1 1
 Q2(anth)  0 range -1 1
% -----------------------------------------------

p(anth)    5 1    1  7  -1/2  a  -1  c  -1  f  -1  Q2  -1  x  -1  y  -3/2  Q1
            2    0  1  1  f    0  1  1  Q2
            2    0  1  1  c    0  1  1  x
            2    0  1  1  Q2    0  1  1  y
            2    0  1  1  x    0  1  1  z

p(ged)     1 1    0  4  -1/2  a   1  f   1  y  -1  z

p(ompa)    1 1    0  1  1  a
```

```
p(omgl)    1 1    0  2  -1  f   1  z

p(otr)     1 1    0  1  1  c

p(fanth)   7 1    0  3   1  x  -2  Q2  -5/2  Q1
            2    0  1  2  f    0  1  1  Q2
            2    0  1  1  c    0  1  1  x
            2    0  1  -1  f    0  1  1  x
            2    0  1  2  Q2    0  1  1  y
            2    0  1  -1  x    0  1  1  y
            2    0  1  1  x    0  1  1  z

p(omrb)    1 1    0  1  1  f

p(a)       5 1    0  2   1  Q2  5/2  Q1
            2    0  1  -1  f    0  1  1  Q2
            2    0  1  -1  c    0  1  1  x
            2    0  1  -1  Q2    0  1  1  y
            2    0  1  -1  x    0  1  1  z

p(b)       7 1    0  2  2  Q2  3/2  Q1
            2    0  1  -2  f    0  1  1  Q2
            2    0  1  -1  c    0  1  1  x
            2    0  1  1  f    0  1  1  x
            2    0  1  -2  Q2    0  1  1  y
            2    0  1  1  x    0  1  1  y
            2    0  1  -1  x    0  1  1  z
% ------------------------------------------------
asf
W(anth,ged)        25  0  0
W(anth,ompa)       25  0  0
W(anth,omgl)       65  0  0
W(anth,otr)        45  0  0
W(anth,fanth)      33  0  0
W(anth,omrb)       65  0  0 %
W(anth,a)          18  0  0
W(anth,b)          23  0  0
W(ged,ompa)       -40  0  0
W(ged,omgl)        25  0  0
W(ged,otr)         70  0  0
W(ged,fanth)     39.5  0  0
W(ged,omrb)        25  0  0 %
W(ged,a)           29  0  0
W(ged,b)         34.6  0  0
W(ompa,omgl)       50  0  0
W(ompa,otr)        90  0  0
W(ompa,fanth)      45  0  0
W(ompa,omrb)       50  0  0 %
W(ompa,a)        33.2  0  0
W(ompa,b)          36  0  0
W(omgl,otr)        65  0  0
W(omgl,fanth)    81.2  0  0
W(omgl,omrb)        0  0  0 %
W(omgl,a)        65.5  0  0
W(omgl,b)        78.4  0  0
W(otr,fanth)       75  0  0
W(otr,omrb)        65  0  0 %
W(otr,a)           57  0  0
W(otr,b)           63  0  0
W(fanth,omrb)    81.2  0  0 %
W(fanth,a)         12  0  0
W(fanth,b)          8  0  0
W(omrb,a)        65.5  0  0 %
W(omrb,b)        78.4  0  0 %
W(a,b)             20  0  0

anth    1  0  0
ged   1.5  0  0
ompa  1.7  0  0
omgl  0.8  0  0
otr     1  0  0
fanth   1  0  0
omrb  0.8  0  0
a       1  0  0
b       1  0  0

% ------------------------------------------------
14

xvA        1 1    1  1  -1  a

xNaA       1 1    0  1  1  a

xCaM4      1 1    0  1  1  c

xNaM4      1 1    0  1  1  z
```

```
xMgM4      5 1    1  5  -1  c  -1  Q2  -1  x  -1  z  -3/2  Q1
            2    0  1  1  f    0  1  1  Q2
            2    0  1  1  c    0  1  1  x
            2    0  1  1  Q2    0  1  1  y
            2    0  1  1  x    0  1  1  z

xFeM4      5 1    0  3   1  Q2   1  x  3/2  Q1
            2    0  1  -1  f    0  1  1  Q2
            2    0  1  -1  c    0  1  1  x
            2    0  1  -1  Q2    0  1  1  y
            2    0  1  -1  x    0  1  1  z

xMgM13     1 1    1  2   1  Q1  -1  x

xFeM13     1 1    0  2  -1  Q1   1  x

xAlM2      1 1    0  1  1  y

xFe3M2     1 1    0  1  1  f

xMgM2      5 1    1  4  -1  f   1  Q2  -1  x  -1  y
            2    0  1  -1  f    0  1  1  Q2
            2    0  1  1  f    0  1  1  x
            2    0  1  -1  Q2    0  1  1  y
            2    0  1  1  x    0  1  1  y

xFeM2      5 1    0  2  -1  Q2   1  x
            2    0  1  1  f    0  1  1  Q2
            2    0  1  -1  f    0  1  1  x
            2    0  1  1  Q2    0  1  1  y
            2    0  1  -1  x    0  1  1  y

xAlT1      1 1    0  4  1/2  f  1/2  y  -1/2  z  1/4  a

xSiT1      1 1    1  4  -1/2  f  -1/2  y  1/2  z  -1/4  a
% -------------------------------------------------

anth    1    5  xvA 1  xMgM4 2  xMgM13 3  xMgM2 2  xSiT1 1
 check 0  0  0  0  0  0  0  0

ged     2    6  xvA 1  xMgM4 2  xMgM13 3  xAlM2 2  xAlT1 1/2  xSiT1 1/2
 check 0  1  0  0  0  0  0  0
 DQF  22 0 0

ompa    8   7  xNaA 1  xMgM4 2  xMgM13 3  xAlM2 1  xMgM2 1  xAlT1 1/2 xSiT1 1/2
 check 0  1/2  0  1  0  0  0  0
 make  3 parg 1 tr -1 anth 1
 DQF  27 0 0

omgl    1    5  xvA 1  xNaM4 2  xMgM13 3  xAlM2 2  xSiT1 1
 check 0  1  1  0  0  0  0  0
 make  1 gl 1
 DQF 15 0 0

otr     1    5  xvA 1  xCaM4 2  xMgM13 3  xMgM2 2  xSiT1 1
 check 0  0  0  0  1  0  0  0
 make 1 tr 1
 DQF 0 0 0

fanth   1    5  xvA 1  xFeM4 2  xFeM13 3  xFeM2 2  xSiT1 1
 check 1  0  0  0  0  0  0  0
 DQF   7  0  0

omrb    1    5  xvA 1  xNaM4 2  xMgM13 3  xFe3M2 2  xSiT1 1
 check 0  0  1  0  0  1  0  0
 make 3 gl 1 jd -2 acm 2
 DQF   33 0 0

a       1    5  xvA 1  xFeM4 2  xMgM13 3  xFeM2 2  xSiT1 1
 check 4/7  0  0  0  0  0  4/7  -3/7
 make  2  anth 3/7 fanth 4/7
 DQF   -5.5  0  0

b       1    5  xvA 1  xFeM4 2  xFeM13 3  xMgM2 2  xSiT1 1
 check 5/7  0  0  0  0  0  -2/7  5/7
 make  2  anth 2/7 fanth 5/7
 DQF   -6.7  0  0

% =====================================================================
% -------------------------------------------------
% cpx: NCFF3MAS
%
% Green, ECR, Holland, TJB & Powell, R (2007) An order-disorder model for
% omphacitic pyroxenes in the system jadeite-diopside-hedenbergite-acmite,
% with applications to eclogite rocks. American Mineralogist, 92, 1181-1189.
%
%       M1m               M1a               M2c       M2n
%       Mg  Fe  Fe3 Al    Mg  Fe  Fe3 Al    Na  Ca    Na  Ca
% jd    0   0   0   1/2   0   0   0   1/2   1/2 0     1/2 0
% di    1/2 0   0   0     1/2 0   0   0     0   1/2   0   1/2
```

```
% hed   0   1/2 0   0     0   1/2 0   0     0   1/2   0   1/2
% acm   0   0   1/2 0     0   0   1/2 0     1/2 0     1/2 0
% om    1/2 0   0   0     0   0   0   1/2   0   1/2   1/2 0
% cfm   0   1/2 0   0     1/2 0   0   0     0   1/2   0   1/2
% jac   0   0   0   1/2   0   0   1/2 0     1/2 0     1/2 0
%
%               xFe3M1a + xFe3M1m
% f -> -----------------------------------
%      xAlM1a + xAlM1m + xFe3M1a + xFe3M1m
%
%               xFeM1a + xFeM1m
% x -> ---------------------------------
%      xFeM1a + xFeM1m + xMgM1a + xMgM1m
%
%      xNaM2c + xNaM2n
% j -> ---------------
%             2
%
%      -xNaM2c + xNaM2n
% Q -> ----------------
%             2
%
%        xFe3M1a - xFe3M1m
% Qaf -> -----------------
%                2
%
%                 xFeM1a
% Qfm -> -x + ---------------
%             xFeM1a + xMgM1a
% -------------------------------------------------

di  7   % Qaf < f j

  x(di)         0.3481
  j(di)         0.1747
  f(di)         0.3345
  Q(di)        0.02126
  Qaf(di)     0.009286 range -0.5 0.5
  Qfm(di)      -0.1135  range -0.5 0.5
% -------------------------------------------------

p(jd)      2 1    0  3   1  j  -1  Q  -1  Qaf
            2    0  1  -1  f    0  1  1  j

p(di)      5 1    1  4  -1   j  -1  Q   1  Qfm  -1  x
            2    0  1  -1  j    0  1  1  Qfm
            2    0  1  -1  Q    0  1  1  Qfm
            2    0  1  1  j    0  1  1  x
            2    0  1  -1  Q    0  1  1  x

p(hed)     5 1    0  2   1  Qfm   1  x
            2    0  1  -1  j    0  1  1  Qfm
            2    0  1  -1  Q    0  1  1  Qfm
            2    0  1  -1  j    0  1  1  x
            2    0  1  -1  Q    0  1  1  x

p(acm)     2 1    0  1  -1  Qaf
            2    0  1  1  f    0  1  1  j

p(om)      1 1    0  1  2  Q

p(cfm)     4 1    0  1  -2  Qfm
            2    0  1  2  j    0  1  1  Qfm
            2    0  1  2  Q    0  1  1  Qfm
            2    0  1  2  Q    0  1  1  x

p(jac)     1 1    0  1  2  Qaf
% -------------------------------------------------
sf
W(jd,di)       26  0  0
W(jd,hed)      24  0  0
W(jd,acm)       5  0  0
W(jd,om)     15.5  0  0
W(jd,cfm)    25.2  0  0       % 14.8 + Wjdfom - y
W(jd,jac)       3  0  0
W(di,hed)       4  0  0
W(di,acm)      15  0  0
W(di,om)    15.75  0  0
W(di,cfm)       2  0  0
W(di,jac)   21.05  0  0
W(hed,acm)     14  0  0
W(hed,om)    17.2  0  0       % 6.3 + Whedfom - y
W(hed,cfm)      2  0  0
W(hed,jac)   20.1  0  0
W(acm,om)    12.8  0  0
W(acm,cfm)   15.5  0  0
W(acm,jac)      3  0  0
W(om,cfm)   18.45  0  0
W(om,jac)    19.3  0  0
W(cfm,jac)  21.05  0  0
```

```
% ------------------------------------------------
12

xMgM1m     5 1    1  4  -1  j   1  Q   1  Qfm  -1  x
            2    0  1  -1  j    0  1  1  Qfm
            2    0  1  -1  Q    0  1  1  Qfm
            2    0  1  1  j    0  1  1  x
            2    0  1  -1  Q    0  1  1  x

xFeM1m     5 1    0  2  -1  Qfm   1  x
            2    0  1  1  j    0  1  1  Qfm
            2    0  1  1  Q    0  1  1  Qfm
            2    0  1  -1  j    0  1  1  x
            2    0  1  1  Q    0  1  1  x

xFe3M1m    2 1    0  1  -1  Qaf
            2    0  1  1  f    0  1  1  j

xAlM1m     2 1    0  3   1  j  -1  Q   1  Qaf
            2    0  1  -1  f    0  1  1  j

xMgM1a     5 1    1  4  -1  j  -1  Q  -1  Qfm  -1  x
            2    0  1  1  j    0  1  1  Qfm
            2    0  1  1  Q    0  1  1  Qfm
            2    0  1  1  j    0  1  1  x
            2    0  1  1  Q    0  1  1  x

xFeM1a     5 1    0  2   1  Qfm   1  x
            2    0  1  -1  j    0  1  1  Qfm
            2    0  1  -1  Q    0  1  1  Qfm
            2    0  1  -1  j    0  1  1  x
            2    0  1  -1  Q    0  1  1  x

xFe3M1a    2 1    0  1   1  Qaf
            2    0  1  1  f    0  1  1  j

xAlM1a     2 1    0  3   1  j   1  Q  -1  Qaf
            2    0  1  -1  f    0  1  1  j

xNaM2c     1 1    0  2   1  j  -1  Q

xCaM2c     1 1    1  2  -1  j   1  Q

xNaM2n     1 1    0  2   1  j   1  Q

xCaM2n     1 1    1  2  -1  j  -1  Q
% ------------------------------------------------

jd      1    4  xAlM1m 1/2  xAlM1a 1/2  xNaM2c 1/2  xNaM2n 1/2

di      1    4  xMgM1m 1/2  xMgM1a 1/2  xCaM2c 1/2  xCaM2n 1/2

hed     1    4  xFeM1m 1/2  xFeM1a 1/2  xCaM2c 1/2  xCaM2n 1/2

acm     1    4  xFe3M1m 1/2  xFe3M1a 1/2  xNaM2c 1/2  xNaM2n 1/2

om      1    4  xMgM1m 1/2  xAlM1a 1/2  xCaM2c 1/2  xNaM2n 1/2
 make  2  jd 1/2  di 1/2
 DQF  -2.9  0  0

cfm     1    4  xFeM1m 1/2  xMgM1a 1/2  xCaM2c 1/2  xCaM2n 1/2
 make  2  di 1/2  hed 1/2
 DQF  -1.5  0  0

jac     1    4  xAlM1m 1/2  xFe3M1a 1/2  xNaM2c 1/2  xNaM2n 1/2
 make  2  jd 1/2  acm 1/2
 DQF  -1.0  0  0

% ================================================
% ------------------------------------------------
% cpx: NCFF3MAS
%
% Green, ECR, Holland, TJB & Powell, R (2007) An order-disorder model for
% omphacitic pyroxenes in the system jadeite-diopside-hedenbergite-acmite,
% with applications to eclogite rocks. American Mineralogist, 92, 1181-1189.
%
%       M1m                 M1a                 M2c       M2n
%       Mg  Fe  Fe3 Al      Mg  Fe  Fe3 Al      Na  Ca    Na  Ca
% jd    0   0   0   1/2     0   0   0   1/2     1/2 0     1/2 0
% di    1/2 0   0   0       1/2 0   0   0       0   1/2   0   1/2
% hed   0   1/2 0   0       0   1/2 0   0       0   1/2   0   1/2
% acm   0   0   1/2 0       0   0   1/2 0       1/2 0     1/2 0
% om    1/2 0   0   0       0   0   0   1/2     0   1/2   1/2 0
% cfm   0   1/2 0   0       1/2 0   0   0       0   1/2   0   1/2
% jac   0   0   0   1/2     0   0   1/2 0       1/2 0     1/2 0
%
%               xFe3M1a + xFe3M1m
% f -> ----------------------------------
%      xAlM1a + xAlM1m + xFe3M1a + xFe3M1m
%
```

```
%              xFeM1a + xFeM1m
% x -> --------------------------------
%      xFeM1a + xFeM1m + xMgM1a + xMgM1m
%
%      xNaM2c + xNaM2n
% j -> ---------------
%            2
%
%      -xNaM2c + xNaM2n
% Q -> ----------------
%            2
%
%        xFe3M1a - xFe3M1m
% Qaf -> -----------------
%               2
%
%                xFeM1a
% Qfm -> -x + ---------------
%             xFeM1a + xMgM1a
% ------------------------------------------------

o  7

  x(o)          0.43
  j(o)          0.45
  f(o)          0.12
  Q(o)          0.32
  Qaf(o)       0.020 range -0.5 0.5
  Qfm(o)      -0.079  range -0.5 0.5

% ------------------------------------------------

p(jd)      2 1    0  3   1  j  -1  Q  -1  Qaf
            2    0  1  -1  f    0  1  1  j

p(di)      5 1    1  4  -1  j  -1  Q   1  Qfm  -1  x
            2    0  1  -1  j    0  1  1  Qfm
            2    0  1  -1  Q    0  1  1  Qfm
            2    0  1  1  j    0  1  1  x
            2    0  1  -1  Q    0  1  1  x

p(hed)     5 1    0  2   1  Qfm   1  x
            2    0  1  -1  j    0  1  1  Qfm
            2    0  1  -1  Q    0  1  1  Qfm
            2    0  1  -1  j    0  1  1  x
            2    0  1  -1  Q    0  1  1  x

p(acm)     2 1    0  1  -1  Qaf
            2    0  1  1  f    0  1  1  j

p(om)      1 1    0  1  2  Q

p(cfm)     4 1    0  1  -2  Qfm
            2    0  1  2  j    0  1  1  Qfm
            2    0  1  2  Q    0  1  1  Qfm
            2    0  1  2  Q    0  1  1  x

p(jac)     1 1    0  1  2  Qaf
% ------------------------------------------------
sf
W(jd,di)       26  0  0
W(jd,hed)      24  0  0
W(jd,acm)       5  0  0
W(jd,om)     15.5  0  0
W(jd,cfm)    25.2  0  0       % 14.8 + Wjdfom - y
W(jd,jac)       3  0  0
W(di,hed)       4  0  0
W(di,acm)      15  0  0
W(di,om)    15.75  0  0
W(di,cfm)       2  0  0
W(di,jac)   21.05  0  0
W(hed,acm)     14  0  0
W(hed,om)    17.2  0  0       % 6.3 + Whedfom - y
W(hed,cfm)      2  0  0
W(hed,jac)   20.1  0  0
W(acm,om)    12.8  0  0
W(acm,cfm)   15.5  0  0
W(acm,jac)      3  0  0
W(om,cfm)   18.45  0  0
W(om,jac)    19.3  0  0
W(cfm,jac)  21.05  0  0
% ------------------------------------------------
12

xMgM1m     5 1    1  4  -1  j   1  Q   1  Qfm  -1  x
            2    0  1  -1  j    0  1  1  Qfm
            2    0  1  -1  Q    0  1  1  Qfm
            2    0  1  1  j    0  1  1  x
            2    0  1  -1  Q    0  1  1  x
```

```
xFeM1m     5 1    0  2  -1  Qfm   1  x
            2    0  1  1  j    0  1  1  Qfm
            2    0  1  1  Q    0  1  1  Qfm
            2    0  1  -1  j    0  1  1  x
            2    0  1  1  Q    0  1  1  x

xFe3M1m    2 1    0  1  -1  Qaf
            2    0  1  1  f    0  1  1  j

xAlM1m     2 1    0  3   1  j  -1  Q   1  Qaf
            2    0  1  -1  f    0  1  1  j

xMgM1a     5 1    1  4  -1  j  -1  Q  -1  Qfm  -1  x
            2    0  1  1  j    0  1  1  Qfm
            2    0  1  1  Q    0  1  1  Qfm
            2    0  1  1  j    0  1  1  x
            2    0  1  1  Q    0  1  1  x

xFeM1a     5 1    0  2   1  Qfm   1  x
            2    0  1  -1  j    0  1  1  Qfm
            2    0  1  -1  Q    0  1  1  Qfm
            2    0  1  -1  j    0  1  1  x
            2    0  1  -1  Q    0  1  1  x

xFe3M1a    2 1    0  1   1  Qaf
            2    0  1  1  f    0  1  1  j

xAlM1a     2 1    0  3   1  j   1  Q  -1  Qaf
            2    0  1  -1  f    0  1  1  j

xNaM2c     1 1    0  2   1  j  -1  Q

xCaM2c     1 1    1  2  -1  j   1  Q

xNaM2n     1 1    0  2   1  j   1  Q

xCaM2n     1 1    1  2  -1  j  -1  Q
% ---------------------------------------------------

jd      1    4  xAlM1m 1/2  xAlM1a 1/2  xNaM2c 1/2  xNaM2n 1/2

di      1    4  xMgM1m 1/2  xMgM1a 1/2  xCaM2c 1/2  xCaM2n 1/2

hed     1    4  xFeM1m 1/2  xFeM1a 1/2  xCaM2c 1/2  xCaM2n 1/2

acm     1    4  xFe3M1m 1/2  xFe3M1a 1/2  xNaM2c 1/2  xNaM2n 1/2

om      1    4  xMgM1m 1/2  xAlM1a 1/2  xCaM2c 1/2  xNaM2n 1/2
 make  2  jd 1/2  di 1/2
 DQF  -2.9  0  0

cfm     1    4  xFeM1m 1/2  xMgM1a 1/2  xCaM2c 1/2  xCaM2n 1/2
 make  2  di 1/2  hed 1/2
 DQF  -1.5  0  0

jac     1    4  xAlM1m 1/2  xFe3M1a 1/2  xNaM2c 1/2  xNaM2n 1/2
 make  2  jd 1/2  acm 1/2
 DQF  -1.0  0  0

% ===================================================
% ---------------------------------------------------
% cpx: NCFF3MAS
%
% Green, ECR, Holland, TJB & Powell, R (2007) An order-disorder model for
% omphacitic pyroxenes in the system jadeite-diopside-hedenbergite-acmite,
% with applications to eclogite rocks. American Mineralogist, 92, 1181-1189.
%
%       M1m                 M1a                 M2c       M2n
%       Mg  Fe  Fe3 Al      Mg  Fe  Fe3 Al      Na  Ca    Na  Ca
% jd    0   0   0   1/2     0   0   0   1/2     1/2 0     1/2 0
% di    1/2 0   0   0       1/2 0   0   0       0   1/2   0   1/2
% hed   0   1/2 0   0       0   1/2 0   0       0   1/2   0   1/2
% acm   0   0   1/2 0       0   0   1/2 0       1/2 0     1/2 0
% om    1/2 0   0   0       0   0   0   1/2     0   1/2   1/2 0
% cfm   0   1/2 0   0       1/2 0   0   0       0   1/2   0   1/2
% jac   0   0   0   1/2     0   0   1/2 0       1/2 0     1/2 0
%
%               xFe3M1a + xFe3M1m
% f -> -----------------------------------
%      xAlM1a + xAlM1m + xFe3M1a + xFe3M1m
%
%               xFeM1a + xFeM1m
% x -> ---------------------------------
%      xFeM1a + xFeM1m + xMgM1a + xMgM1m
%
%      xNaM2c + xNaM2n
% j -> ---------------
%             2
%
```

```
%      -xNaM2c + xNaM2n
% Q -> ----------------
%             2
%
%         xFe3M1a - xFe3M1m
% Qaf -> -----------------
%                2
%
%                 xFeM1a
% Qfm -> -x + ---------------
%             xFeM1a + xMgM1a
% -------------------------------------------------

jd  7

 x(jd)      0.45
 j(jd)      0.86
 f(jd)      0.01
 Q(jd)      0.04
 Qaf(jd)   0.001  range -0.5 0.5     % less than f j
 Qfm(jd)     0.1  range -0.5 0.5

% -------------------------------------------------

p(jd)      2 1    0  3   1  j  -1  Q  -1  Qaf
            2    0  1  -1  f    0  1  1  j

p(di)      5 1    1  4  -1  j  -1  Q   1  Qfm  -1  x
            2    0  1  -1  j    0  1  1  Qfm
            2    0  1  -1  Q    0  1  1  Qfm
            2    0  1  1  j    0  1  1  x
            2    0  1  -1  Q    0  1  1  x

p(hed)     5 1    0  2   1  Qfm   1  x
            2    0  1  -1  j    0  1  1  Qfm
            2    0  1  -1  Q    0  1  1  Qfm
            2    0  1  -1  j    0  1  1  x
            2    0  1  -1  Q    0  1  1  x

p(acm)     2 1    0  1  -1  Qaf
            2    0  1  1  f    0  1  1  j

p(om)      1 1    0  1  2  Q

p(cfm)     4 1    0  1  -2  Qfm
            2    0  1  2  j    0  1  1  Qfm
            2    0  1  2  Q    0  1  1  Qfm
            2    0  1  2  Q    0  1  1  x

p(jac)     1 1    0  1  2  Qaf
% -------------------------------------------------
sf
W(jd,di)       26  0  0
W(jd,hed)      24  0  0
W(jd,acm)       5  0  0
W(jd,om)     15.5  0  0
W(jd,cfm)    25.2  0  0       % 14.8 + Wjdfom - y
W(jd,jac)       3  0  0
W(di,hed)       4  0  0
W(di,acm)      15  0  0
W(di,om)    15.75  0  0
W(di,cfm)       2  0  0
W(di,jac)   21.05  0  0
W(hed,acm)     14  0  0
W(hed,om)    17.2  0  0       % 6.3 + Whedfom - y
W(hed,cfm)      2  0  0
W(hed,jac)   20.1  0  0
W(acm,om)    12.8  0  0
W(acm,cfm)   15.5  0  0
W(acm,jac)      3  0  0
W(om,cfm)   18.45  0  0
W(om,jac)    19.3  0  0
W(cfm,jac)  21.05  0  0
% -------------------------------------------------
12

xMgM1m     5 1    1  4  -1  j   1  Q   1  Qfm  -1  x
            2    0  1  -1  j    0  1  1  Qfm
            2    0  1  -1  Q    0  1  1  Qfm
            2    0  1  1  j    0  1  1  x
            2    0  1  -1  Q    0  1  1  x

xFeM1m     5 1    0  2  -1  Qfm   1  x
            2    0  1  1  j    0  1  1  Qfm
            2    0  1  1  Q    0  1  1  Qfm
            2    0  1  -1  j    0  1  1  x
            2    0  1  1  Q    0  1  1  x

xFe3M1m    2 1    0  1  -1  Qaf
            2    0  1  1  f    0  1  1  j
```

```
xAlM1m     2 1    0  3   1  j  -1  Q   1  Qaf
            2    0  1  -1  f    0  1  1  j

xMgM1a     5 1    1  4  -1  j  -1  Q  -1  Qfm  -1  x
            2    0  1  1  j    0  1  1  Qfm
            2    0  1  1  Q    0  1  1  Qfm
            2    0  1  1  j    0  1  1  x
            2    0  1  1  Q    0  1  1  x

xFeM1a     5 1    0  2   1  Qfm   1  x
            2    0  1  -1  j    0  1  1  Qfm
            2    0  1  -1  Q    0  1  1  Qfm
            2    0  1  -1  j    0  1  1  x
            2    0  1  -1  Q    0  1  1  x

xFe3M1a    2 1    0  1   1  Qaf
            2    0  1  1  f    0  1  1  j

xAlM1a     2 1    0  3   1  j   1  Q  -1  Qaf
            2    0  1  -1  f    0  1  1  j

xNaM2c     1 1    0  2   1  j  -1  Q

xCaM2c     1 1    1  2  -1  j   1  Q

xNaM2n     1 1    0  2   1  j   1  Q

xCaM2n     1 1    1  2  -1  j  -1  Q
% -------------------------------------------------

jd      1    4  xAlM1m 1/2  xAlM1a 1/2  xNaM2c 1/2  xNaM2n 1/2

di      1    4  xMgM1m 1/2  xMgM1a 1/2  xCaM2c 1/2  xCaM2n 1/2

hed     1    4  xFeM1m 1/2  xFeM1a 1/2  xCaM2c 1/2  xCaM2n 1/2

acm     1    4  xFe3M1m 1/2  xFe3M1a 1/2  xNaM2c 1/2  xNaM2n 1/2

om      1    4  xMgM1m 1/2  xAlM1a 1/2  xCaM2c 1/2  xNaM2n 1/2
 make  2  jd 1/2  di 1/2
 DQF  -2.9  0  0

cfm     1    4  xFeM1m 1/2  xMgM1a 1/2  xCaM2c 1/2  xCaM2n 1/2
 make  2  di 1/2  hed 1/2
 DQF  -1.5  0  0

jac     1    4  xAlM1m 1/2  xFe3M1a 1/2  xNaM2c 1/2  xNaM2n 1/2
 make  2  jd 1/2  acm 1/2
 DQF  -1.0  0  0

% =====================================================================
% Chlorite:
% Holland, TJB, Baker, JM & Powell, R (1998) Mixing properties and activity-
% composition relationships of chlorites in the system MgO-FeO-Al2O3-SiO2-H2O.
% European Journal of Mineralogy, 10, 395-406.

chl 4

  x(chl)        0.414
  y(chl)        0.508
  Q(chl)        0.4905

 % ---------------------------------------------------

 p(afchl) 1  1    1  2 -1  y -1  Q

 p(clin)  2  1    0  1  2  Q
             2    0  1 -2/5  x    3  1 -1  y

 p(daph)  1  2    0  1  2/5  x    3  1 -1  y

 p(ames)  1  1    0  2  1  y -1  Q

% ---------------------------------------------------
 sf

 W(afchl,clin)  18   0  0
 W(afchl,daph) 14.5 0  0
 W(afchl,ames) 20   0  0
 W(clin,daph)   2.5 0  0
 W(clin,ames)  18   0  0
 W(daph,ames)  13.5 0  0

 % ---------------------------------------------------
 10

 x(Fe,M23)  1  1    0  1  1  x
 x(Mg,M23)  1  1    1  1 -1  x
```

```
 x(Al,M1)   1  1    0  2  1  y -1  Q
 x(Fe,M1)   1  2    0  1  1  x     1  2 -1  y  1  Q
 x(Mg,M1)   1  2    1  1 -1  x     1  2 -1  y  1  Q

 x(Al,M4)   1  1    0  2  1  y  1  Q
 x(Fe,M4)   1  2    0  1  1  x     1  2 -1  y -1  Q
 x(Mg,M4)   1  2    1  1 -1  x     1  2 -1  y -1  Q

 x(Al,T2)   1  1    0  1  1  y
 x(Si,T2)   1  1    1  1 -1  y
 % ------------------------------------------------

 afchl  1  4    x(Mg,M23) 4   x(Mg,M1) 1   x(Mg,M4) 1   x(Si,T2) 2
  check 0 0 0

 clin   4  5    x(Mg,M23) 4   x(Mg,M1) 1   x(Al,M4) 1   x(Al,T2) 1  x(Si,T2) 1
  check 0 1/2 1/2

 daph   4  5    x(Fe,M23) 4   x(Fe,M1) 1   x(Al,M4) 1   x(Al,T2) 1  x(Si,T2) 1
  check 1 1/2 1/2

 ames   1  4    x(Mg,M23) 4   x(Al,M1) 1   x(Al,M4) 1   x(Al,T2) 2
  check 0 1 0

% ============================================================
% Garnet:
% White, RW, Powell, R & Holland, TJB (2007) Progress relating to calculation
% of partial melting equilibria for metapelites. Journal of Metamorphic Geology,
% 25, 511-527.
%
% this model is somewhat less asymmetric than used in the calculations
% of the above paper, but this is our currently preferred model
%
% x= Fe2/(Fe2 + Mg), z= Ca/(Fe2 + Mg + Ca), f = Fe3/2

g 4     % garnet with ferric (and van Laar)

  x(g)          0.87
  z(g)         0.235
  f(g)         0.046

% ------------------------------------------------

  p(alm)  1  2    1  1 -1  z    0  1  1  x

  p(py)   1  2    1  1 -1  z    1  1 -1  x

  p(gr)   1 1    0  2  1  z -1  f

  p(andr) 1 1    0  1  1  f


% ------------------------------------------------
 asf

 W(alm,py)      2.5  0  0
 W(alm,gr)       10  0  0
 W(alm,andr)     75  0  0

 W(py,gr)        45  0  0
 W(py,andr)      90  0  0

 W(gr,andr)       0  0  0

 alm      1 0 0
 py       1 0 0
 gr       3 0 0
 andr     3 0 0

% ------------------------------------------------
  5     % no of site fractions

  xFeX   1  2    1  1 -1  z    0  1  1  x

  xMgX   1  2    1  1 -1  z    1  1 -1  x

  xCaX   1  1    0  1  1  z

  xAlY   1 1     1  1 -1  f

  xFe3Y  1 1     0  1  1  f

% ------------------------------------------------
 alm     1  2      xFeX  3   xAlY 2

 py      1  2      xMgX  3   xAlY 2

 gr      1  2      xCaX  3   xAlY 2

 andr    1  2      xCaX  3   xFe3Y 2
```

```
% ==============================================================
% Epidote:
% Holland, TJB & Powell, R (1998) An internally consistent thermodynamic dataset
% for phases of petrological interest. Journal of Metamorphic Geology, 16, 309-343.
%
% Fe3+ - Al mixing on M1 & M3.  M2-all Al
%
%  f(ep) = Fe3+(m13)/(Fe3+(m13) + Al(m13))
%
%  Q(ep) = 1/2(Fe3+(m3) - Fe3+(m1))

ep 3

  f(ep)        0.25          % 0.117
  Q(ep)        0.24  range 0 0.5     %0.116

%--------------------------------------------------------------------


p(cz)    1  1    1  2 -1  f  -1  Q
p(ep)    1  1    0  1  2  Q
p(fep)   1  1    0  2  1  f  -1  Q

% --------------------------------------------------

sf
  W(cz,ep)         0  0  0
  W(cz,fep)     15.4  0  0
  W(ep,fep)        3  0  0

% --------------------------------------------------
  4   % 4 "site fractions"

  xFeM1   1  1    0  2  1  f  -1  Q

  xAlM1   1  1    1  2 -1  f   1  Q

  xFeM3   1  1    0  2  1  f   1  Q

  xAlM3   1  1    1  2 -1  f  -1  Q

% --------------------------------------------------
% ideal mixing activities

 cz      1  2      xAlM1  1  xAlM3   1

 ep      1  2      xAlM1  1  xFeM3   1

 fep     1  2      xFeM1  1  xFeM3   1



 %=================================================
opx 5   % no tet terms model

   x(opx)        0.5156
   y(opx)        0.1519
   N(opx)        0.3927
   f(opx)      0.006407

% --------------------------------------------------

p(en)   1  1  1  4 -1  x -1  y -1/2 N  -1  f

p(fs)   2  1  0  1       -1/2 N
        2  0  1  1  x    1  2 -1  y  -1  f

p(mgts) 1  1  0  1  1  y

p(fm)   2  1  0  1  1  N
        2  0  1  1  x     0  2  1  y 1  f

p(mots) 1  1  0  1  1  f

% --------------------------------------------------
 sf

  W(en,fs)     6.8  0  0
  W(en,mgts)     0  0  0
  W(en,fm)     4.5  0  0
  W(en,mots)   -14  0  0

  W(fs,mgts)    -1  0  0
  W(fs,fm)     4.5  0  0
  W(fs,mots)     6  0  0

  W(mgts,fm)   1.2  0  0
  W(mgts,mots)   0  0  0

  W(fm,mots)     6  0  0
```

```
 % --------------------------------------------------
6

 x(Al,M1)  1 1   0  1  1  y

 x(Fe3,M1) 1 1   0  1  1  f

 x(Mg,M1)  2 1   1  3 -1  y  -1  f  1/2 N
             2   0  1 -1  x    1  2 -1  y  -1  f

 x(Fe,M1)  2 1   0  1       -1/2 N
             2   0  1  1  x    1  2 -1  y -1  f

 x(Mg,M2)  1 1   1  2 -1  x -1/2 N

 x(Fe,M2)  1 1   0  2  1  x  1/2 N

% --------------------------------------------------

en      1  2      x(Mg,M1)  1   x(Mg,M2) 1
     check 0 0 0 0

fs      1  2      x(Fe,M1) 1   x(Fe,M2) 1
     check 1 0 0 0

mgts     1  2      x(Al,M1) 1   x(Mg,M2) 1
     check 0 1 0 0

fm      1  2      x(Mg,M1)  1   x(Fe,M2) 1
     check 1/2 0 1 0
     make       2       en 1/2    fs 1/2
     DQF    -6.95  0  0

mots    1  2      x(Fe3,M1)  1   x(Mg,M2) 1
     check 0 0 0 1
     make       3       mgts 1    cor -1/2   hem 1/2
     DQF    22  0  0


% ============================================================
% Plagioclase:
% Holland, TJB & Powell, R (2003) Activity-composition relations for phases in
% petrological calculations: an asymmetric multicomponent formulation. Contributions
% to Mineralogy and Petrology, 145, 492-501.
%
% from ternary plag mode for Cbar1 ASF

pl 2

   ca(pl) 0.3

% --------------------------------------------------

  p(ab)    1 1    1 1 -1 ca
  p(an)    1 1    0 1  1 ca

% --------------------------------------------------
  asf

    w(aban)   3.1   0     0

   ab   0.643  0  0
   an   1.0    0  0

% --------------------------------------------------
  2

  x(Na)    1 1    1 1 -1 ca
  x(Ca)    1 1    0 1  1 ca

% --------------------------------------------------

  abh      1 1     x(Na) 1
  an       1 1     x(Ca) 1
     DQF   7.03  -0.00466   0



% __________________________________________________________________

%==========================================================================
% Magnetite:
% White, RW, Powell, R & Clarke, GL (2002) The interpretation of reaction textures
% in Fe-rich metapelitic granulites of the Musgrave Block, central Australia:
% constraints from mineral equilibria calculations in the system K2O-FeO-MgO-Al2O3-
% SiO2-H2O-TiO2-Fe2O3. Journal of Metamorphic Geology, 20, 41-55.
%
% no Al, but proper od
```

```
mt 3

 x(mt) 0.9704   % prop "mt"
 Q(mt) 0.7472   % x(Fe3,tet)

% --------------------------------------------------
% psub = {pi -> 3Q - 2x, pd -> 3x - 3Q, pu -> 1 - x};

 p(i)  1 1    0  2 -2  x  3  Q

 p(d)  1 1    0  2  3  x -3  Q

 p(u)  1 1    1  1 -1  x

% --------------------------------------------------

sf

 W(i,d)    2.4  0  0
 W(i,u)      1  0  0
 W(d,u)     -5  0  0
% --------------------------------------------------
 5

% sfsub = {xFe3oct -> x - Q/2, xFe2oct -> 1/2 + Q/2 - x/2,   xTioct -> 1/2 - 1/2 x,
%          xFe3tet -> Q,       xFe2tet -> 1 - Q};

 x(Ti,oct)   1 1   1/2   1 -1/2  x
 x(Fe3,oct)  1 1    0    2   1   x -1/2 Q
 x(Fe2,oct)  1 1   1/2   2 -1/2  x  1/2 Q
 x(Fe3,tet)  1 1    0    1   1   Q
 x(Fe2,tet)  1 1    1    1  -1   Q
% --------------------------------------------------

% magnetic landau NOT included

imt      4  3    x(Fe3,oct)  1  x(Fe2,oct)  1  x(Fe3,tet)  1
    make  1  mt  1
    DQF      -1.8595  0.003166 0   % from dmt, - dHid - RT Log[16/27]
    check 1 1                      %      dHid = 3.19

dmt   27/4  4    x(Fe3,oct) 4/3 x(Fe2,oct) 2/3 x(Fe3,tet)  2/3 x(Fe2,tet) 1/3
    make  1  mt  1
    DQF   1.3305  -0.0011845  0    % taking off config dqf
    check 1 2/3

usp      4  3    x(Ti,oct)  1  x(Fe2,oct)  1  x(Fe2,tet)  1
    check 0 0

% =====================================================================
% Ilmenite - hematite:
% White, RW, Powell, R, Holland, TJB & Worley, BA (2000) The effect of TiO2 and
% Fe2O3 on metapelitic assemblages at greenschist and amphibolite facies conditions:
% mineral equilibria calculations in the system K2O-FeO-MgO-Al2O3-SiO2-H2O-TiO2-Fe2O3.
% Journal of Metamorphic Geology, 18, 497-511.

lm 3

 x(lm) 0.93                     % prop "ilm"
 Q(lm) 0.89   range -0.99 0.99  % x(Fe2,A) - x(Fe2,B)

% --------------------------------------------------

% psub = {ph -> 1 - x, po -> Q, pd -> x - Q};

 p(o)  1 1    0  1  1  Q

 p(d)  1 1    0  2  1  x -1  Q

 p(h)  1 1    1  1 -1  x

% --------------------------------------------------

sf

 W(o,d)   15.6  0  0
 W(o,h)   26.6  0  0
 W(d,h)     11  0  0
% --------------------------------------------------
 6

% sfsub = {xFe2A -> (x + Q)/2, xTiA -> (x - Q)/2, xFe3A -> 1 - x,
%          xFe2B -> (x - Q)/2, xTiB -> (x + Q)/2, xFe3B -> 1 - x};

 x(Fe2,A)  1 1    0  2  1/2  x  1/2  Q
 x(Ti,A)   1 1    0  2  1/2  x -1/2  Q
 x(Fe3,A)  1 1    1  1 -1  x
 x(Fe2,B)  1 1    0  2  1/2  x -1/2  Q
 x(Ti,B)   1 1    0  2  1/2  x  1/2  Q
 x(Fe3,B)  1 1    1  1 -1  x
```

```
% --------------------------------------------------

oilm      1  2    x(Fe2,A)  1  x(Ti,B)  1
   make  1  ilm  1
   DQF    -13.6075 0.009426 0  % DQF - dH + R Log[4]; dH = 15.6
   check 1 1

dilm      4  4    x(Fe2,A)  1/2   x(Ti,A)  1/2   x(Fe2,B)  1/2   x(Ti,B)  1/2
    make  1  ilm  1
    DQF     1.9928 -0.0021 0    % DQF = G(equil,Landau) - G(equil,SF)
    check 1 0

hem       1  2    x(Fe3,A)  1  x(Fe3,B)  1
    check 0 0
    make 1 hem 1

% ===================================================================
% Ilmenite - hematite:
% White, RW, Powell, R, Holland, TJB & Worley, BA (2000) The effect of TiO2 and
% Fe2O3 on metapelitic assemblages at greenschist and amphibolite facies conditions:
% mineral equilibria calculations in the system K2O-FeO-MgO-Al2O3-SiO2-H2O-TiO2-Fe2O3.
% Journal of Metamorphic Geology, 18, 497-511.

hem 3

  x(hem) 0.05                      % prop "ilm"
  Q(hem) 0.0002 range -0.05 0.05  % x(Fe2,A) - x(Fe2,B)

% --------------------------------------------------

% psub = {ph -> 1 - x, po -> Q, pd -> x - Q};

 p(o)  1 1    0  1  1  Q

 p(d)  1 1    0  2  1  x -1  Q

 p(h)  1 1    1  1 -1  x

% --------------------------------------------------

sf

 W(o,d)   15.6  0  0
 W(o,h)   26.6  0  0
 W(d,h)     11  0  0
% --------------------------------------------------
 6

% sfsub = {xFe2A -> (x + Q)/2, xTiA -> (x - Q)/2, xFe3A -> 1 - x,
%          xFe2B -> (x - Q)/2, xTiB -> (x + Q)/2, xFe3B -> 1 - x};

 x(Fe2,A)  1 1    0  2  1/2  x  1/2  Q
 x(Ti,A)   1 1    0  2  1/2  x -1/2  Q
 x(Fe3,A)  1 1    1  1 -1  x
 x(Fe2,B)  1 1    0  2  1/2  x -1/2  Q
 x(Ti,B)   1 1    0  2  1/2  x  1/2  Q
 x(Fe3,B)  1 1    1  1 -1  x

% --------------------------------------------------

oilm      1  2    x(Fe2,A)  1  x(Ti,B)  1
  make  1  ilm  1
  DQF    -13.6075 0.009426 0  % DQF - dH + R Log[4]; dH = 15.6
  check 1 1

dilm      4  4    x(Fe2,A)  1/2   x(Ti,A)  1/2   x(Fe2,B)  1/2   x(Ti,B)  1/2
  make  1  ilm  1
  DQF     1.9928 -0.0021 0    % DQF = G(equil,Landau) - G(equil,SF)
  check 1 0

hem       1  2    x(Fe3,A)  1  x(Fe3,B)  1
  check 0 0
  make 1 hem 1

% ==============================================================================
% ===================================================================
% Spinel: FMATO
% White, RW, Powell, R & Clarke, GL (2002) The interpretation of reaction textures
% in Fe-rich metapelitic granulites of the Musgrave Block, central Australia:
% constraints from mineral equilibria calculations in the system K2O-FeO-MgO-Al2O3-
% SiO2-H2O-TiO2-Fe2O3. Journal of Metamorphic Geology, 20, 41-55.
%
% x(he) = Fe2/(Mg + Fe2)
% y(he) = Al/(Al + Fe3 + 2Ti)
% z(he) = 2Ti/(Al + Fe3 + 2Ti)
```

```
sp 4

 x(he)    0.93    % Fe2/(Mg + Fe2)
 y(he)    0.80   % Al/(Al + Fe3 + 2Ti)
 z(he)    0.01   % 2Ti/(Al + Fe3 + 2Ti)

% -------------------------------------------------


  p(he)  2 1    0  1   1  y
           2   -1  1   1  x    1  1   1  z

  p(sp)  1 2    1  1  -1  x    1  1   1  z

  p(mt)  1 1    1  2  -1  y -1  z

  p(ulv) 1 1    0  1   1  z

% -------------------------------------------------

  sf

  W(he,sp)      0  0  0
  W(he,mt)    18.5 0  0
  W(he,ulv)   27  0  0
  W(sp,mt)    40  0  0
  W(sp,ulv)   30  0  0    % * free
  W(mt,ulv)    0  0  0

% -------------------------------------------------

  5     % site fractions

  x(Al)       1 1    0  1  1  y

  x(Fe3)      1 1    1  2 -1  y -1  z

  x(Ti)       1 1    0  1  1  z

  x(Mg)       1 1    1  1 -1  x

  x(Fe2)      1 1    0  1  1  x


% -------------------------------------------------

   herc    1  2    x(Al)  1    x(Fe2)  1

   sp      1  2    x(Al)  1    x(Mg)   1

   mt      1  2    x(Fe3) 1    x(Fe2)  1

   usp     1  2    x(Ti)  1    x(Fe2)  1

% ===================================================================

pa law ab ru sph ky q H2O
```

Further applied *a–x* models

Melt:

```
%===================================================================================
% Melt: FMASH
% White, RW, Powell, R & Holland, TJB (2007) Progress relating to calculation
% of partial melting equilibria for metapelites. Journal of Metamorphic Geology,
% 25, 511-527.

liq 5

      q(L)    0.06919
      ol(L)   0.02073
      x(L)    0.3945
      h2o(L)  0.8781

% --------------------------------------------------

   p(qL)    1 1      0  1  1  q

   p(silL)  1 1      1  3 -1 q -1  ol -1 h2o

   p(foL)   1 2      0  1  1  ol   1  1 -1  x

   p(faL)   1 2      0  1  1  ol   0  1  1  x
   p(h2oL)  1 1      0  1  1  h2o

% --------------------------------------------------
   sf

   W(qLsilL)       12  0     0
   W(qLfoL)        12  0  -0.4
   W(qLfaL)        14  0     0
   W(qLh2oL)       15  0     0

   W(silLfoL)      12  0     0
   W(silLfaL)      12  0     0
   W(silLh2oL)     16  0     0

   W(foLfaL)       18  0     0
   W(foLh2oL)      11  0  -0.5

   W(faLh2oL)      12  0     0

% --------------------------------------------------
   7

   fac   1 1      1  1 -1  h2o

   pq    1 1      0  1  1  q

   psil   1 1     1  3 -1 q -1 ol -1 h2o

   pol    1 1      0  1  1  ol

   xFe    1 1      0  1  1  x

   xMg    1 1      1  1 -1  x

   ph2o  1 1       0  1  1  h2o

% --------------------------------------------------
% ideal mixing activities

 qL     1  2      fac 1 pq 1
      make  1  qL 4

 silL   1  2      fac 1  psil 1
      make   1  silL  8/5
      DQF  -10 0 0

 foL    1  3      fac 1  pol 1  xMg  5
      make  1  foL 2
      DQF  -10 0 0

 faL    1  3      fac 1  pol 1  xFe  5
      make  1  faL 2
      DQF  -9 0 -1.3

 h2oL   1  1      ph2o 2


% ======================================================================
```

Talc:

```
% ==============================================================
% Talc: FMASH
% Holland, T.J.B., & Powell, R., 1998. An internally consistent thermodynamic dataset for
% phases of petrological interest. Journal of Metamorphic Geology, 16, 309-343.
%
% x(ta) = Fe/(Fe+Mg)
% y(ta) = x(Al,M3)

ta 3

   x(ta)  0.06
   y(ta)  0.04

% --------------------------------------------------
 p(ta)  2  1   1   1  -1  y
           2   0   1  -1  x    1  1  -1/3  y  % 1-y-x(1-1/3 y)
 p(fta) 1  2   0   1   1  x    1  1  -1/3  y  % x(1-1/3y)
 p(tats) 1  1  0   1   1  y

% --------------------------------------------------
 ideal

% --------------------------------------------------
 7
 x(Mg,M1)  1  1    1  1  -1  x
 x(Fe,M1)  1  1    0  1   1  x
 x(Mg,M3)  1  2    1  1  -1  x   1  1  -1  y
 x(Fe,M3)  1  2    0  1   1  x   1  1  -1  y
 x(Al,M3)  1  1    0  1   1  y
 x(Al,T1)  1  1    0  1  1/2 y
 x(Si,T1)  1  1    1  1 -1/2 y


% --------------------------------------------------
 ta  1  3   x(Mg,M1)  2   x(Mg,M3)  1   x(Si,T1)  2
 check  0  0
fta  1  3   x(Fe,M1)  2   x(Fe,M3)  1   x(Si,T1)  2
 check  1  0
tats 4  4   x(Mg,M1)  2   x(Al,M3)  1   x(Si,T1)  1   x(Al,T1)  1
 check  0  1
```

Olivine:

```
% ==============================================================
% olivine (Holland, T.J.B., unpublished)

ol 2
      x(ol) 0.1

  p(fo)   1 1      1  1 -1  x

  p(fa)   1 1      0  1  1  x

sf

  W(m,f) 8 0 0

2  x(Mg)   1 1      1  1 -1  x

   x(Fe)   1 1      0  1  1  x

      fo     1  1      x(Mg)  2

      fa     1  1      x(Fe)  2
```

Appendix B

Microprobe analyses

Microprobe analyses and formulae calculations for minerals in MAOC 11, 13 and 15. Oxides are given in wt%.

Appendix B1:	Garnet formulae with ions on the basis of 12 O, proportions of the end-members pyrope (py), almandine (alm), andradite (andr), grossular (gross) and majorite (ma), Mg# and the composition variable *x(g)*
Appendix B8:	Amphibole formulae calculated after Schumacher (1997), with declaration of the form of minimum (min) and maximum (max) calculation as well as Mg#
Appendix B10:	Clinopyroxene formulae with ions on the basis of 6 O, the proportions of the end-members enstatite (En), ferrosilite (Fs) and wollastonite (Wo), and Mg#, Q (Ca + Mg + Fe^{2+}) and J (2 Na)
Appendix B19:	Orthopyroxene formulae with ions on the basis of 6 O, the proportions of the end-members enstatite (En), ferrosilite (Fs) and wollastonite (Wo), Mg# and the composition variable *x(opx)*
Appendix B23:	Plagioclase formulae with ions on the basis of 8 O, proportions of the end-members anorthite (An) and albite (Ab) as well as *ca(pl)*
Appendix B27:	Melt Mg#, A/CNK (without K) and CIPW norm: Q (quartz), An (anorthite), Di (diopside), Hyp (hyperstene), Ab (albite), Ilm (ilmenite), C (corundum), Mag (magnetite), Neph (nepheline), Ol (olivine)

Garnet in MAOC 11

g	12.5 kbar/1050 °C												12.5 kbar/1100 °C			
MAOC 11											av	sd				
SiO_2	40.520	40.500	40.270	39.860	41.550	41.180	41.760	42.000	40.840	40.880	40.936	0.685	41.132	41.118	41.107	41.009
TiO_2	0.559	0.558	0.862	0.803	0.775	0.425	0.455	0.461	0.678	0.226	0.580	0.199	0.497	0.600	0.707	0.431
Al_2O_3	21.890	22.010	21.420	21.540	19.990	22.390	21.620	20.820	21.930	22.670	21.628	0.772	22.390	21.620	20.820	22.400
FeO	14.300	14.470	15.020	15.080	14.760	14.160	13.370	14.170	13.710	13.840	14.288	0.560	13.430	13.340	13.060	13.020
MgO	15.350	15.760	15.240	15.060	16.090	16.470	15.670	16.700	16.000	16.030	15.837	0.528	16.300	15.830	15.320	16.270
CaO	6.630	6.370	6.390	6.530	5.930	5.370	6.900	6.050	6.420	6.090	6.268	0.428	5.990	6.980	8.030	6.130
Na_2O	0.000	0.010	0.034	0.045	0.070	0.000	0.115	0.063	0.071	0.024	0.043	0.037	0.007	0.117	0.097	0.056
Total	**99.249**	**99.678**	**99.236**	**98.918**	**99.165**	**99.995**	**99.890**	**100.264**	**99.649**	**99.760**	**99.580**	**0.424**	**99.746**	**99.605**	**99.141**	**99.316**
formula																
Si	2.983	2.964	2.973	2.953	3.000	2.994	3.000	3.000	2.983	2.978	2.998		2.995	3.000	3.000	2.995
Al	0.017	0.036	0.027	0.047	0.000	0.006	0.000	0.000	0.017	0.022	0.002		0.005	0.000	0.000	0.005
Z	**3.000**	**3.000**	**3.000**	**3.000**	**3.000**	**3.000**	**3.000**	**3.000**	**3.000**	**3.000**	**3.000**		**3.000**	**3.000**	**3.000**	**3.000**
Si	0.000	0.000	0.000	0.000	0.063	0.000	0.044	0.048	0.000	0.000	0.000		0.000	0.004	0.025	0.000
Al	1.882	1.863	1.837	1.833	1.737	1.912	1.858	1.781	1.871	1.925	1.866		1.917	1.861	1.805	1.923
Fe^{3+}	0.074	0.113	0.099	0.131	0.061	0.047	0.020	0.082	0.082	0.076	0.078		0.034	0.082	0.081	0.043
Ti	0.031	0.031	0.048	0.045	0.043	0.023	0.025	0.025	0.037	0.012	0.032		0.027	0.033	0.039	0.024
Y	**1.986**	0.031	**1.984**	**2.009**	**1.904**	**1.983**	**1.947**	**1.936**	**1.990**	**2.013**	**1.976**		**1.978**	**1.976**	**1.926**	**1.990**
Mg	1.684	1.720	1.677	1.663	1.768	1.785	1.703	1.807	1.742	1.741	1.729		1.770	1.724	1.680	1.771
Fe^{2+}	0.806	0.773	0.828	0.803	0.849	0.814	0.795	0.778	0.756	0.767	0.797		0.784	0.733	0.723	0.752
Ca	0.523	0.500	0.505	0.518	0.468	0.418	0.539	0.470	0.502	0.475	0.492		0.467	0.546	0.633	0.480
X	**3.014**	**2.992**	**3.011**	**2.985**	**3.086**	**3.017**	**3.037**	**3.055**	**3.000**	**2.984**	**3.018**		**3.021**	**3.004**	**3.036**	**3.002**
Total	**8.000**	**7.999**	**7.995**	**7.994**	**7.990**	**8.000**	**7.984**	**7.991**	**7.990**	**7.997**	**7.994**		**7.999**	**7.983**	**7.986**	**7.992**
py			55.703	55.724	53.976	59.164	53.804	56.649	58.070	58.346	57.297		58.582	57.204	54.075	58.990
alm	26.755	25.834	27.511	26.910	27.523	26.972	26.174	25.472	25.183	25.722	26.404		25.945	24.415	23.799	25.035
andr	3.723	366.697	4.986	6.521	3.182	2.376	1.039	4.219	4.115	3.760	3.961		1.726	4.131	4.209	2.181
gross	13.628	11.080	11.801	10.845	11.996	11.488	16.708	11.178	12.631	12.172	12.338		13.746	14.059	16.643	13.793
ma	0.000	0.000	0.000	0.000	3.324	0.000	2.275	2.482	0.000	0.000	0.000		0.000	0.192	1.275	0.000
Mg#	67.628	68.988	66.939	67.434	67.552	68.687	68.179	69.892	69.752	69.404	68.454		69.306	70.157	69.931	70.205
x(g)	0.324	0.310	0.331	0.326	0.324	0.313	0.318	0.301	0.302	0.306	0.315		0.307	0.298	0.301	0.298

g	12.5 kbar/1100 °C							15 kbar/900 °C dark								
MAOC 11						av	sd									
SiO_2	41.214	40.692	40.945	40.688	41.031	40.993	0.189	42.370	42.840	41.800	41.820	41.130	40.940	41.770	41.640	41.480
TiO_2	0.611	0.532	0.566	0.439	0.382	0.529	0.103	1.196	0.604	0.539	0.487	0.380	0.498	0.370	0.253	0.262
Al_2O_3	20.800	22.270	22.160	22.400	22.170	21.892	0.659	21.500	19.940	21.900	21.880	22.050	22.330	22.540	22.350	22.570
FeO	13.810	14.040	14.110	14.360	13.980	13.683	0.485	12.090	11.730	10.690	10.700	9.260	12.600	10.210	9.560	9.380
MgO	15.540	15.480	15.700	15.460	15.810	15.746	0.348	15.740	15.160	17.450	17.160	18.800	16.180	17.680	18.270	19.180
CaO	7.120	6.000	6.020	5.840	6.250	6.484	0.736	6.630	9.240	7.310	7.050	6.460	6.620	6.680	6.320	5.880
Na_2O	0.093	0.075	0.035	0.011	0.025	0.057	0.040	0.038	0.185	0.056	0.076	0.014	0.027	0.000	0.031	0.020
Total	**99.188**	**99.089**	**99.536**	**99.198**	**99.648**	**99.385**	**0.274**	**99.564**	**99.699**	**99.745**	**99.173**	**98.094**	**99.195**	**99.250**	**98.424**	**98.772**
formula																
Si	3.000	2.994	2.999	2.993	2.999	3.000		3.000	3.000	3.000	3.000	2.988	2.993	3.000	3.000	2.988
Al	0.000	0.006	0.001	0.007	0.001	0.000		0.000	0.000	0.000	0.000	0.012	0.007	0.000	0.000	0.012
Z	**3.000**	**3.000**	**3.000**	**3.000**	**3.000**	**3.000**		**3.000**	**3.000**	**3.000**	**3.000**	**3.000**	**3.000**	**3.000**	**3.000**	**3.000**
Si	0.033	0.000	0.000	0.000	0.000	0.004		0.077	0.128	0.015	0.036	0.000	0.000	0.020	0.022	0.000
Al	1.804	1.925	1.913	1.935	1.909	1.891		1.840	1.716	1.862	1.872	1.876	1.917	1.920	1.912	1.904
Fe^{3+}	0.076	0.033	0.031	0.025	0.054	0.051		0.000	0.000	0.058	0.014	0.097	0.040	0.000	0.021	0.082
Ti	0.034	0.029	0.031	0.024	0.021	0.029		0.065	0.033	0.029	0.027	0.021	0.027	0.020	0.014	0.014
Y	**1.914**	**1.987**	**1.974**	**1.984**	**1.984**	**1.971**		**1.905**	**1.749**	**1.948**	**1.912**	**1.993**	**1.984**	**1.941**	**1.947**	**2.000**
Mg	1.705	1.698	1.714	1.695	1.723	1.720		1.704	1.650	1.876	1.857	2.036	1.763	1.905	1.977	2.060
Fe^{2+}	0.774	0.831	0.834	0.859	0.801	0.788		0.734	0.716	0.587	0.636	0.466	0.731	0.617	0.559	0.483
Ca	0.561	0.473	0.472	0.460	0.489	0.509		0.516	0.723	0.565	0.548	0.503	0.519	0.517	0.491	0.454
X	**3.040**	**3.002**	**3.021**	**3.014**	**3.013**	**3.017**		**2.954**	**3.090**	**3.029**	**3.041**	**3.005**	**3.013**	**3.040**	**3.027**	**2.997**
Total	**7.987**	**7.989**	**7.995**	**7.998**	**7.996**	**7.992**		**7.936**	**7.967**	**7.992**	**7.989**	**7.998**	**7.996**	**8.000**	**7.996**	**7.997**
py	54.358	56.559	56.760	56.247	57.177	56.811		53.666	46.078	61.183	59.192	67.759	58.531	61.674	64.172	68.734
alm	25.458	27.685	27.597	28.483	26.577	26.107		24.854	23.184	19.391	20.902	15.506	24.257	20.296	18.466	16.122
andr	3.965	1.648	1.557	1.252	2.710	2.583		0.000	0.000	2.952	0.727	4.847	1.991	0.014	1.089	4.096
gross	14.501	14.108	14.086	14.019	13.536	14.294		17.463	23.400	15.702	17.305	11.887	15.220	17.008	15.145	11.049
ma	1.718	0.000	0.000	0.000	0.000	0.205		4.017	7.338	0.772	1.873	0.000	0.000	1.008	1.127	0.000
Mg#	68.776	67.138	67.285	66.384	68.268	68.592		69.888	69.733	76.162	74.499	81.377	70.700	75.540	77.955	81.001
x(g)	0.312	0.329	0.327	0.336	0.317	0.314		0.301	0.303	0.238	0.255	0.186	0.293	0.245	0.220	0.190

g	15 kbar/900 °C dark								15 kbar/900 °C light							
MAOC 11							av dark	sd dark								
SiO_2	41.500	40.760	40.930	41.500	40.740	40.740	41.399	0.583	41.490	41.180	41.230	42.630	42.310	37.060	39.980	39.590
TiO_2	0.275	0.706	0.577	0.457	0.760	0.579	0.482	0.160	0.826	0.546	0.649	0.517	0.837	0.258	0.810	1.166
Al_2O_3	22.160	21.770	21.810	21.840	21.090	21.580	21.844	0.675	20.550	21.290	21.080	18.750	17.410	20.470	21.410	20.340
FeO	9.670	12.450	12.280	11.190	13.460	13.980	11.226	1.554	17.500	18.470	18.620	14.370	16.170	11.250	18.200	20.880
MgO	18.500	16.620	16.450	16.420	15.710	15.240	17.059	1.304	11.320	10.530	10.790	12.870	11.270	13.570	11.270	9.490
CaO	6.460	6.670	6.680	7.390	7.010	6.890	6.904	0.780	7.950	7.720	7.550	9.600	10.610	7.190	7.730	7.840
Na_2O	0.026	0.023	0.023	0.014	0.072	0.056	0.045	0.046	0.067	0.067	0.076	0.194	0.245	0.107	0.027	0.076
Total	**98.591**	**98.999**	**98.750**	**98.811**	**98.842**	**99.065**	**98.958**	**0.570**	**99.703**	**99.803**	**99.995**	**98.931**	**98.852**	**89.905**	**99.427**	**99.382**
formula																
Si	3.000	2.983	3.000	3.000	3.000	3.000	3.000		3.000	3.000	3.000	3.000	3.000	2.997	3.000	3.000
Al	0.000	0.017	0.000	0.000	0.000	0.000	0.000		0.000	0.000	0.000	0.000	0.000	0.003	0.000	0.000
Z	**3.000**	**3.000**	**3.000**	**3.000**	**3.000**	**3.000**	**3.000**		**3.000**	**3.000**	**3.000**	**3.000**	**3.000**	**3.000**	**3.000**	**3.000**
Si	0.006	0.000	0.002	0.035	0.004	0.004	0.016		0.099	0.083	0.082	0.180	0.202	0.000	0.011	0.026
Al	1.891	1.860	1.885	1.883	1.833	1.875	1.876		1.809	1.878	1.857	1.648	1.553	1.948	1.900	1.833
Fe^{3+}	0.071	0.083	0.049	0.000	0.085	0.061	0.046		0.000	0.000	0.000	0.000	0.000	0.041	0.000	0.000
Ti	0.015	0.039	0.032	0.025	0.042	0.032	0.026		0.046	0.031	0.036	0.029	0.048	0.016	0.046	0.067
Y	**1.978**	**1.982**	**1.967**	**1.908**	**1.960**	**1.969**	**1.948**		**1.856**	**1.909**	**1.894**	**1.677**	**1.600**	**2.004**	**1.946**	**1.900**
Mg	1.997	1.813	1.799	1.790	1.727	1.675	1.853		1.261	1.175	1.202	1.431	1.271	1.636	1.265	1.082
Fe^{2+}	0.515	0.679	0.704	0.684	0.745	0.800	0.638		1.093	1.156	1.164	0.896	1.023	0.720	1.146	1.335
Ca	0.501	0.523	0.525	0.579	0.554	0.544	0.539		0.636	0.619	0.605	0.767	0.860	0.623	0.624	0.642
X	**3.013**	**3.015**	**3.028**	**3.054**	**3.026**	**3.020**	**3.030**		**2.990**	**2.951**	**2.971**	**3.095**	**3.155**	**2.979**	**3.035**	**3.058**
Total	**7.996**	**7.997**	**7.997**	**7.997**	**7.990**	**7.992**	**7.994**		**7.945**	**7.942**	**7.947**	**7.953**	**7.957**	**7.983**	**7.991**	**7.985**
py	66.005	60.134	59.297	56.771	56.870	55.286	60.318		36.810	35.493	36.130	35.507	27.704	54.913	41.142	33.967
alm	17.078	22.520	23.245	22.411	24.619	26.507	21.066		36.560	39.187	39.176	28.964	32.434	24.175	37.763	43.643
andr	3.593	4.181	2.516	0.000	4.342	3.123	2.342		0.000	0.000	0.000	0.000	0.000	2.026	0.000	0.000
gross	13.043	13.164	14.825	18.964	13.963	14.901	15.445		21.280	20.986	20.353	24.792	27.267	18.886	20.550	20.996
ma	0.282	0.000	0.117	1.855	0.206	0.183	0.828		5.349	4.334	4.340	10.737	12.594	0.000	0.544	1.394
Mg#	79.514	72.754	71.878	72.344	69.865	67.665	74.376		53.556	50.405	50.813	61.488	55.406	69.433	52.469	44.758
x(g)	0.205	0.272	0.281	0.277	0.301	0.323	0.256		0.464	0.496	0.492	0.385	0.446	0.306	0.475	0.552

g	**15 kbar/900 °C light**				**15 kbar/900 °C**		**15 kbar/1050 °C**									
MAOC 11			**av light**	**sd light**	**av all**	**sd all**										
SiO_2	39.140	40.470	40.508	1.652	41.082	1.214	40.800	41.180	41.180	41.680	41.230	41.140	41.490	41.520	41.220	42.320
TiO_2	0.985	0.669	0.726	0.257	0.608	0.261	0.617	0.638	0.665	0.810	0.769	0.755	0.772	0.659	0.720	0.698
Al_2O_3	20.510	21.390	20.320	1.287	21.220	1.198	22.130	22.310	22.410	21.930	22.140	22.310	22.230	22.010	22.230	21.330
FeO	21.600	17.500	17.456	3.010	13.752	3.776	13.550	13.220	13.190	12.440	12.760	12.960	13.130	12.640	12.420	12.610
MgO	8.900	11.970	11.198	1.408	14.662	3.172	16.690	16.620	16.820	18.270	17.700	17.470	17.780	17.580	17.770	17.210
CaO	7.560	6.960	8.071	1.137	7.360	1.081	6.010	6.640	6.340	5.700	5.740	5.970	5.900	6.160	6.300	6.920
Na_2O	0.060	0.047	0.097	0.069	0.065	0.060	0.075	0.041	0.078	0.112	0.076	0.068	0.060	0.062	0.064	0.171
Total	**98.755**	**99.006**	**98.376**	**3.395**	**98.749**	**2.323**	**99.872**	**100.649**	**100.683**	**100.942**	**100.415**	**100.673**	**101.362**	**100.631**	**100.724**	**101.259**
formula																
Si	3.000	3.000	3.000		3.000		2.963	2.968	2.964	2.975	2.965	2.954	2.958	2.980	2.952	3.000
Al	0.000	0.000	0.000		0.000		0.037	0.032	0.036	0.025	0.035	0.046	0.042	0.020	0.048	0.000
Z	**3.000**	**3.000**	**3.000**		**3.000**		**3.000**	**3.000**	**3.000**	**3.000**	**3.000**	**3.000**	**3.000**	**3.000**	**3.000**	**3.000**
Si	0.020	0.040	0.075		0.045		0.000	0.000	0.000	0.000	0.000	0.000	0.000	0.000	0.000	0.025
Al	1.865	1.894	1.818		1.854		1.858	1.864	1.865	1.819	1.841	1.842	1.827	1.842	1.828	1.797
Fe^{3+}	0.000	0.000	0.000		0.000		0.122	0.104	0.109	0.135	0.122	0.132	0.140	0.115	0.151	0.102
Ti	0.057	0.038	0.041		0.034		0.034	0.035	0.036	0.043	0.042	0.041	0.041	0.036	0.039	0.038
Y	**1.922**	**1.932**	**1.860**		**1.888**		**2.013**	**2.003**	**2.011**	**1.997**	**2.004**	**2.015**	**2.008**	**1.993**	**2.018**	**1.937**
Mg	1.024	1.340	1.267		1.620		1.807	1.786	1.805	1.944	1.897	1.870	1.890	1.881	1.897	1.834
Fe^{2+}	1.394	1.099	1.108		0.852		0.701	0.693	0.685	0.607	0.646	0.647	0.643	0.644	0.592	0.651
Ca	0.625	0.560	0.657		0.585		0.468	0.513	0.489	0.436	0.442	0.459	0.451	0.474	0.483	0.530
X	**3.043**	**3.000**	**3.032**		**3.057**		**2.976**	**2.992**	**2.978**	**2.987**	**2.985**	**2.976**	**2.983**	**2.999**	**2.973**	**3.015**
Total	**7.985**	**7.972**	**7.967**		**7.990**		**7.989**	**7.994**	**7.989**	**7.985**	**7.989**	**7.991**	**7.992**	**7.991**	**7.991**	**7.976**
py	32.594	42.604	37.748		50.613		60.725	59.701	60.599	65.073	63.561	62.840	63.353	62.735	63.813	59.546
alm	45.809	36.644	36.550		27.884		23.559	23.156	22.984	20.336	21.624	21.726	21.537	21.466	19.927	21.600
andr	0.000	0.000	0.000		0.000		6.054	5.202	5.441	6.758	6.075	6.536	6.991	5.772	7.500	5.291
gross	20.543	18.673	21.652		19.120		9.662	11.941	10.976	7.834	8.740	8.898	8.118	10.027	8.760	12.287
ma	1.054	2.078	4.050		2.383		0.000	0.000	0.000	0.000	0.000	0.000	0.000	0.000	0.000	1.276
Mg#	42.348	54.942	53.349		65.524		72.048	72.053	72.502	76.190	74.615	74.309	74.630	74.506	76.204	73.793
x(g)	0.577	0.451	0.467		0.345		0.280	0.279	0.275	0.238	0.254	0.257	0.254	0.255	0.238	0.262

g	**15 kbar/1050 °C**								**15 kbar/1100 °C dark**							
MAOC 11							**av**	**sd**								
SiO_2	42.080	41.360	41.510	41.050	41.650	41.600	41.438	0.384	44.122	41.665	42.009	41.722	42.330	42.286	42.114	41.694
TiO_2	0.534	0.839	0.494	0.565	0.588	0.716	0.677	0.100	0.318	0.343	0.243	0.090	0.130	0.234	0.238	0.182
Al_2O_3	22.740	21.870	22.500	22.620	22.450	22.100	22.207	0.335	19.530	23.440	23.490	23.600	23.320	22.900	22.790	23.330
FeO	12.540	11.840	11.630	12.810	11.820	12.080	12.603	0.552	6.310	7.860	7.890	7.470	6.520	6.370	7.330	7.140
MgO	16.400	18.190	17.700	16.920	17.280	17.710	17.382	0.560	17.930	18.160	18.850	18.810	19.870	19.790	18.580	19.120
CaO	6.790	6.210	6.510	6.860	6.900	6.600	6.347	0.414	10.560	7.270	7.100	7.300	7.240	7.730	7.850	6.960
Na_2O	0.171	0.050	0.046	0.037	0.058	0.066	0.077	0.041	0.308	0.113	0.027	0.052	0.045	0.097	0.090	0.025
Total	**101.255**	**100.359**	**100.390**	**100.862**	**100.746**	**100.872**	**100.731**	**0.419**	**99.078**	**98.851**	**99.609**	**99.044**	**99.455**	**99.407**	**98.992**	**98.451**
formula																
Si	3.000	2.967	2.976	2.945	2.983	2.974	2.973		3.000	2.997	2.994	2.985	3.000	3.000	3.000	2.997
Al	0.000	0.033	0.024	0.055	0.017	0.026	0.027		0.000	0.003	0.006	0.015	0.000	0.000	0.000	0.003
Z	**3.000**	**3.000**	**3.000**	**3.000**	**3.000**	**3.000**	**3.000**		**3.000**	**3.000**	**3.000**	**3.000**	**3.000**	**3.000**	**3.000**	**3.000**
Si	0.010	0.000	0.000	0.000	0.000	0.000	0.000		0.171	0.000	0.000	0.000	0.001	0.000	0.020	0.000
Al	1.917	1.815	1.878	1.858	1.878	1.837	1.850		1.654	1.984	1.968	1.975	1.949	1.915	1.926	1.973
Fe^{3+}	0.028	0.134	0.099	0.140	0.084	0.121	0.115		0.011	0.000	0.016	0.037	0.041	0.073	0.021	0.014
Ti	0.029	0.045	0.027	0.030	0.032	0.039	0.037		0.017	0.019	0.013	0.005	0.007	0.012	0.013	0.010
Y	**1.974**	**1.995**	**2.003**	**2.029**	**1.993**	**1.996**	**2.002**		**1.683**	**2.003**	**1.996**	**2.017**	**1.997**	**2.000**	**1.960**	**1.997**
Mg	1.749	1.945	1.892	1.810	1.845	1.888	1.859		1.921	1.947	2.003	2.006	2.100	2.093	1.986	2.049
Fe^{2+}	0.722	0.576	0.598	0.628	0.624	0.601	0.641		0.368	0.473	0.455	0.410	0.346	0.305	0.418	0.415
Ca	0.520	0.477	0.500	0.527	0.529	0.506	0.488		0.813	0.560	0.542	0.560	0.550	0.588	0.603	0.536
X	**2.992**	**2.998**	**2.990**	**2.966**	**2.999**	**2.995**	**2.988**		**3.103**	**2.980**	**3.000**	**2.975**	**2.996**	**2.986**	**3.008**	**3.000**
Total	**7.976**	**7.993**	**7.994**	**7.995**	**7.992**	**7.991**	**7.989**		**7.957**	**7.983**	**7.996**	**7.993**	**7.994**	**7.987**	**7.987**	**7.997**
py	57.934	64.877	63.272	61.028	61.529	63.037	62.217		51.729	65.337	66.768	67.426	70.037	70.085	65.023	68.298
alm	24.140	19.203	20.002	21.189	20.813	20.079	21.455		11.868	15.863	15.156	13.766	11.537	10.220	13.911	13.833
andr	1.419	6.740	4.953	6.912	4.205	6.061	5.745		0.656	0.000	0.782	1.850	2.051	3.638	1.078	0.712
gross	15.978	9.179	11.773	10.871	13.453	10.823	10.583		25.555	18.799	17.293	16.957	16.308	16.041	18.975	17.157
ma	0.529	0.000	0.000	0.000	0.000	0.000	0.000		10.192	0.000	0.000	0.000	0.067	0.016	1.013	0.000
Mg#	70.776	77.161	75.980	74.228	74.723	75.842	74.358		83.916	80.464	81.500	83.045	85.869	87.276	82.599	83.158
x(g)	0.292	0.228	0.240	0.258	0.253	0.242	0.256		0.161	0.195	0.185	0.170	0.141	0.127	0.174	0.168

g	**15 kbar/1100 °C dark**						**15 kbar/1100 °C light**									
MAOC 11					**av dark**	**sd dark**									**av light**	**sd light**
SiO_2	41.696	40.965	41.888	42.611	42.092	0.765	39.897	39.979	40.191	40.323	40.685	41.117	40.839	41.042	40.509	0.476
TiO_2	0.232	0.193	0.180	0.262	0.220	0.072	0.753	0.760	0.721	0.913	0.883	0.621	0.631	0.754	0.755	0.104
Al_2O_3	23.740	23.470	23.690	22.450	22.979	1.154	21.720	21.960	21.790	21.810	21.740	22.450	22.190	21.540	21.900	0.292
FeO	7.240	7.550	7.490	8.850	7.335	0.717	13.940	14.170	13.530	14.240	14.120	13.430	13.320	13.370	13.765	0.391
MgO	19.210	18.920	19.120	17.580	18.828	0.688	14.740	15.340	15.420	15.540	15.200	15.170	15.460	15.000	15.234	0.266
CaO	6.970	7.320	6.760	7.820	7.573	1.002	7.410	6.710	7.070	6.280	6.480	7.150	7.140	7.420	6.958	0.423
Na_2O	0.018	0.043	0.000	0.078	0.075	0.081	0.044	0.055	0.089	0.087	0.079	0.038	0.050	0.101	0.068	0.024
Total	**99.106**	**98.461**	**99.128**	**99.651**	**99.103**	**0.374**	**98.504**	**98.974**	**98.811**	**99.193**	**99.187**	**99.976**	**99.630**	**99.227**	**99.188**	**0.459**
formula																
Si	2.977	2.947	2.993	3.000	3.000		2.963	2.949	2.964	2.968	2.999	3.000	2.986	3.000	2.982	
Al	0.023	0.053	0.007	0.000	0.000		0.037	0.051	0.036	0.032	0.001	0.000	0.014	0.000	0.018	
Z	**3.000**	**3.000**	**3.000**	**3.000**	**3.000**		**3.000**	**3.000**	**3.000**	**3.000**	**3.000**	**3.000**	**3.000**	**3.000**	**3.000**	
Si	0.000	0.000	0.000	0.055	0.012		0.000	0.000	0.000	0.000	0.000	0.001	0.000	0.021	0.000	
Al	1.975	1.936	1.988	1.897	1.938		1.864	1.858	1.859	1.860	1.887	1.931	1.899	1.869	1.881	
Fe^{3+}	0.026	0.102	0.000	0.000	0.025		0.095	0.116	0.110	0.083	0.027	0.005	0.052	0.020	0.063	
Ti	0.012	0.010	0.010	0.014	0.012		0.042	0.042	0.040	0.051	0.049	0.034	0.035	0.042	0.042	
Y	**2.013**	**2.049**	**1.998**	**1.911**	**1.975**		**2.001**	**2.016**	**2.008**	**1.994**	**1.963**	**1.970**	**1.986**	**1.931**	**1.986**	
Mg	2.045	2.029	2.037	1.879	2.008		1.632	1.687	1.696	1.705	1.670	1.650	1.685	1.646	1.671	
Fe^{2+}	0.407	0.352	0.448	0.531	0.414		0.771	0.758	0.725	0.793	0.843	0.815	0.762	0.803	0.784	
Ca	0.533	0.564	0.518	0.601	0.581		0.590	0.530	0.559	0.495	0.512	0.559	0.559	0.585	0.549	
X	**2.985**	**2.945**	**3.002**	**3.010**	**3.003**		**2.992**	**2.976**	**2.979**	**2.994**	**3.025**	**3.024**	**3.007**	**3.034**	**3.004**	
Total	**7.998**	**7.994**	**8.000**	**7.977**	**7.990**		**7.994**	**7.992**	**7.987**	**7.988**	**7.989**	**7.995**	**7.993**	**7.986**	**7.990**	
py	68.509	68.888	67.849	59.533	66.279		54.536	56.692	56.917	56.958	55.210	54.545	56.049	53.165	55.643	
alm	13.625	11.956	14.910	17.626	13.784		25.759	25.485	24.327	26.498	27.873	26.936	25.346	26.458	26.091	
andr	1.273	4.980	0.000	0.000	1.264		4.744	5.742	5.470	4.174	1.381	0.257	2.639	1.049	3.194	
gross	16.593	14.175	17.241	19.956	18.071		14.961	12.081	13.286	12.370	15.535	18.231	15.966	18.239	15.071	
ma	0.000	0.000	0.000	2.885	0.602		0.000	0.000	0.000	0.000	0.000	0.032	0.000	1.088	0.000	
Mg#	83.411	85.211	81.984	77.979	82.912		67.919	68.988	70.057	68.249	66.451	66.955	68.861	67.218	68.078	
x(g)	0.166	0.148	0.180	0.220	0.171		0.321	0.310	0.299	0.318	0.335	0.330	0.311	0.328	0.319	

g	15 kbar/1100 °C		20 kbar/1050 °C dark									
MAOC 11	av all	sd all									av dark	sd dark
SiO_2	41.459	1.027	42.450	42.140	41.780	40.370	40.700	39.790	41.120	41.610	41.245	0.916
TiO_2	0.434	0.281	0.229	0.298	0.356	0.449	0.616	1.533	0.691	0.468	0.580	0.415
Al_2O_3	22.548	1.047	22.400	22.340	22.420	23.120	21.360	21.540	21.500	22.070	22.094	0.599
FeO	9.907	3.286	7.250	8.250	8.740	11.650	12.160	12.600	10.740	10.310	10.213	1.951
MgO	17.391	1.888	20.470	19.790	19.350	15.690	15.790	15.550	16.580	17.810	17.629	2.011
CaO	7.327	0.862	6.150	6.080	5.930	7.370	7.330	6.610	8.000	6.980	6.806	0.738
Na_2O	0.072	0.064	0.052	0.021	0.055	0.037	0.072	0.072	0.021	0.047	0.047	0.020
Total	**99.137**	**0.406**	**99.001**	**98.919**	**98.631**	**98.686**	**98.028**	**97.695**	**98.652**	**99.295**	**98.613**	**0.521**
formula												
Si	3.000		3.000	3.000	3.000	2.961	3.000	2.967	3.000	3.000	3.000	
Al	0.000		0.000	0.000	0.000	0.039	0.000	0.033	0.000	0.000	0.000	
Z	**3.000**		**3.000**	**3.000**	**3.000**	**3.000**	**3.000**	**3.000**	**3.000**	**3.000**	**3.000**	
Si	0.000		0.024	0.019	0.009	0.000	0.014	0.000	0.010	0.007	0.002	
Al	1.923		1.881	1.887	1.903	1.960	1.864	1.861	1.855	1.879	1.895	
Fe^{3+}	0.040		0.053	0.045	0.049	0.034	0.050	0.010	0.052	0.063	0.045	
Ti	0.024		0.012	0.016	0.019	0.025	0.034	0.086	0.038	0.025	0.032	
Y	**1.987**		**1.946**	**1.948**	**1.971**	**2.019**	**1.949**	**1.957**	**1.945**	**1.968**	**1.972**	
Mg	1.876		2.174	2.114	2.077	1.716	1.743	1.729	1.809	1.918	1.913	
Fe^{2+}	0.559		0.379	0.449	0.478	0.681	0.703	0.776	0.605	0.560	0.577	
Ca	0.568		0.469	0.467	0.458	0.579	0.582	0.528	0.627	0.540	0.531	
X	**3.003**		**3.022**	**3.030**	**3.013**	**2.976**	**3.027**	**3.033**	**3.042**	**3.019**	**3.020**	
Total	**7.990**		**7.993**	**7.997**	**7.992**	**7.995**	**7.990**	**7.990**	**7.997**	**7.993**	**7.993**	
py	62.461		70.689	68.776	68.506	57.662	56.871	57.007	58.962	63.212	63.242	
alm	18.625		12.530	14.820	15.859	22.871	23.215	25.576	19.899	18.551	19.099	
andr	2.019		2.736	2.328	2.464	1.688	2.575	0.520	2.677	3.199	2.268	
gross	16.896		12.797	13.079	12.724	17.779	16.635	16.897	17.948	14.702	15.305	
ma	0.000		1.247	0.998	0.448	0.000	0.705	0.000	0.513	0.337	0.086	
Mg#	77.030		85.166	82.481	81.301	71.600	71.265	69.030	74.930	77.404	76.830	
x(g)	0.230		0.148	0.175	0.187	0.284	0.287	0.310	0.251	0.226	0.232	

g	20 kbar/1050 °C light					20 kbar/1050 °C		20 kbar/1100 °C								
MAOC 11				av light	sd light	av all	sd all									
SiO_2	40.740	39.660	40.780	40.393	0.635	41.013	0.909	41.300	41.280	41.450	41.700	41.470	40.950	41.150	40.970	41.290
TiO_2	0.435	1.060	0.451	0.649	0.356	0.599	0.383	0.570	0.705	0.665	0.694	0.868	0.981	0.954	0.547	1.088
Al_2O_3	22.230	22.000	22.560	22.263	0.281	22.140	0.523	22.360	23.080	22.020	22.080	21.950	21.590	21.500	22.280	21.670
FeO	14.020	15.570	15.400	14.997	0.850	11.517	2.793	13.140	12.380	12.290	12.490	12.150	13.060	13.900	13.530	13.300
MgO	14.220	11.570	12.750	12.847	1.328	16.325	2.859	15.260	15.750	16.400	16.960	16.940	15.840	15.810	15.100	15.880
CaO	8.030	9.150	8.270	8.483	0.590	7.264	1.032	7.830	7.400	7.100	6.760	6.690	7.300	6.900	7.580	7.470
Na_2O	0.077	0.084	0.032	0.064	0.028	0.052	0.022	0.066	0.079	0.048	0.081	0.094	0.081	0.076	0.037	0.056
Total	**99.752**	**99.094**	**100.243**	**99.696**	**0.577**	**98.909**	**0.716**	**100.526**	**100.674**	**99.973**	**100.765**	**100.162**	**99.802**	**100.290**	**100.044**	**100.754**
formula																
Si	2.992	2.975	3.000	2.991		2.999		2.994	2.977	3.000	2.995	2.995	2.988	2.994	2.989	2.988
Al	0.008	0.025	0.000	0.009		0.001		0.006	0.023	0.000	0.005	0.005	0.012	0.006	0.011	0.012
Z	**3.000**	**3.000**	**3.000**	**3.000**		**3.000**		**3.000**	**3.000**	**3.000**	**3.000**	**3.000**	**3.000**	**3.000**	**3.000**	**3.000**
Si	0.000	0.000	0.004	0.000		0.000		0.000	0.000	0.006	0.000	0.000	0.000	0.000	0.000	0.000
Al	1.916	1.920	1.959	1.935		1.907		1.905	1.939	1.882	1.865	1.864	1.844	1.838	1.905	1.836
Fe^{3+}	0.056	0.000	0.000	0.011		0.036		0.047	0.019	0.041	0.076	0.059	0.072	0.074	0.052	0.066
Ti	0.024	0.060	0.025	0.036		0.033		0.031	0.038	0.036	0.037	0.047	0.054	0.052	0.030	0.059
Y	**1.995**	**1.980**	**1.984**	**1.982**		**1.976**		**1.984**	**1.996**	**1.959**	**1.978**	**1.971**	**1.970**	**1.964**	**1.986**	**1.961**
Mg	1.557	1.294	1.400	1.418		1.779		1.649	1.693	1.773	1.816	1.824	1.723	1.715	1.642	1.713
Fe^{2+}	0.805	0.977	0.949	0.918		0.669		0.749	0.728	0.704	0.674	0.674	0.725	0.772	0.774	0.739
Ca	0.632	0.735	0.653	0.673		0.569		0.608	0.572	0.552	0.520	0.518	0.571	0.538	0.593	0.579
X	**2.994**	**3.006**	**3.002**	**3.009**		**3.017**		**3.007**	**2.993**	**3.028**	**3.010**	**3.016**	**3.019**	**3.025**	**3.008**	**3.031**
Total	**7.989**	**7.986**	**7.989**	**7.991**		**7.993**		**7.991**	**7.989**	**7.993**	**7.989**	**7.987**	**7.989**	**7.989**	**7.995**	**7.992**
py	51.997	43.043	46.442	47.134		58.979		54.853	56.572	58.256	60.331	60.475	57.074	56.693	54.587	56.511
alm	26.899	32.492	31.606	30.496		22.159		24.918	24.325	23.245	22.386	22.359	24.021	25.524	25.719	24.383
andr	2.790	0.000	0.000	0.560		1.806		2.390	0.929	2.107	3.860	3.019	3.640	3.753	2.602	3.351
gross	18.314	24.465	21.747	21.810		17.056		17.839	18.175	16.108	13.423	14.147	15.264	14.031	17.092	15.756
ma	0.000	0.000	0.205	0.000		0.000		0.000	0.000	0.284	0.000	0.000	0.000	0.000	0.000	0.000
Mg#	65.906	56.984	59.611	60.716		72.689		68.763	69.931	71.577	72.936	73.007	70.379	68.956	67.974	69.859
x(g)	0.341	0.430	0.404	0.393		0.273		0.312	0.301	0.284	0.271	0.270	0.296	0.310	0.320	0.301

g	20 kbar/1100 °C										
MAOC 11										av	sd
SiO_2	41.190	41.670	41.080	41.380	41.110	41.320	41.370	41.610	41.410	41.317	0.219
TiO_2	0.975	0.662	0.913	0.643	0.361	0.384	0.672	0.639	0.649	0.721	0.203
Al_2O_3	21.860	22.490	22.100	22.400	22.930	23.150	22.290	22.050	22.110	22.217	0.471
FeO	13.480	12.050	13.250	12.800	12.840	12.040	12.500	12.460	12.330	12.777	0.561
MgO	15.700	15.890	15.220	15.570	15.650	15.320	15.700	16.080	16.160	15.846	0.522
CaO	7.760	7.830	7.610	7.620	7.790	8.310	8.090	7.600	7.720	7.520	0.436
Na_2O	0.127	0.072	0.102	0.027	0.035	0.050	0.063	0.060	0.078	0.068	0.025
Total	**101.092**	**100.664**	**100.275**	**100.440**	**100.716**	**100.574**	**100.685**	**100.499**	**100.457**	**100.466**	**0.361**
formula											
Si	2.971	3.000	2.989	2.999	2.966	2.983	2.987	3.000	2.990	2.990	
Al	0.029	0.000	0.011	0.001	0.034	0.017	0.013	0.000	0.010	0.010	
Z	**3.000**	**3.000**	**3.000**	**3.000**	**3.000**	**3.000**	**3.000**	**3.000**	**3.000**	**3.000**	
Si	0.000	0.004	0.000	0.000	0.000	0.000	0.000	0.006	0.000	0.000	
Al	1.829	1.911	1.885	1.912	1.916	1.953	1.884	1.878	1.872	1.885	
Fe^{3+}	0.113	0.019	0.040	0.023	0.084	0.029	0.065	0.049	0.078	0.056	
Ti	0.053	0.036	0.050	0.035	0.020	0.021	0.036	0.035	0.035	0.039	
Y	**1.994**	**1.966**	**1.975**	**1.970**	**2.019**	**2.003**	**1.985**	**1.961**	**1.985**	**1.980**	
Mg	1.688	1.708	1.651	1.682	1.683	1.649	1.690	1.732	1.740	1.710	
Fe^{2+}	0.700	0.707	0.766	0.752	0.690	0.698	0.690	0.704	0.667	0.717	
Ca	0.600	0.605	0.593	0.592	0.602	0.643	0.626	0.588	0.597	0.583	
X	**2.988**	**3.020**	**3.011**	**3.026**	**2.976**	**2.990**	**3.006**	**3.024**	**3.004**	**3.010**	
Total	**7.982**	**7.990**	**7.986**	**7.996**	**7.995**	**7.993**	**7.991**	**7.992**	**7.989**	**7.990**	
py	56.492	56.341	54.843	55.584	56.564	55.146	56.220	56.949	57.916	56.795	
alm	23.440	23.422	25.448	24.865	23.199	23.356	22.959	23.277	22.198	23.834	
andr	5.646	0.974	2.035	1.179	4.175	1.427	3.255	2.491	3.920	2.821	
gross	14.422	19.054	17.674	18.372	16.061	20.072	17.566	16.963	15.966	16.551	
ma	0.000	0.209	0.000	0.000	0.000	0.000	0.000	0.320	0.000	0.000	
Mg#	70.675	70.713	68.306	69.092	70.915	70.248	71.004	71.100	72.292	70.440	
x(g)	0.293	0.293	0.317	0.309	0.291	0.298	0.290	0.289	0.277	0.296	

Garnet in MAOC 13

g	12.5 kbar/1050 °C											12.5 kbar/1100 °C				
MAOC 13	light	dark								av	sd					
SiO_2	43.710	41.370	41.640	40.930	41.560	41.510	41.420	41.260	41.110	41.350	0.239	41.140	41.146	41.419	41.261	42.014
TiO_2	0.695	0.592	0.235	0.560	0.403	0.342	0.503	0.337	0.331	0.413	0.126	0.509	0.475	0.242	0.406	0.386
Al_2O_3	16.900	21.670	22.720	21.860	22.350	22.880	22.080	22.480	22.750	22.349	0.442	22.330	22.490	22.580	22.940	21.940
FeO	9.840	11.670	12.060	12.140	11.330	11.790	11.430	11.600	11.600	11.703	0.283	11.270	11.510	12.060	11.820	11.080
MgO	14.870	17.030	17.270	17.370	17.800	17.640	17.320	17.750	17.730	17.489	0.280	17.930	17.770	17.260	17.460	17.300
CaO	12.320	6.840	6.100	6.240	6.100	5.700	6.160	5.460	5.830	6.054	0.413	5.780	6.090	5.640	5.620	6.200
Na_2O	0.702	0.086	0.099	0.060	0.041	0.038	0.109	0.038	0.054	0.066	0.029	0.075	0.020	0.117	0.156	0.204
Total	**99.037**	**99.258**	**100.124**	**99.160**	**99.584**	**99.900**	**99.022**	**98.925**	**99.405**	**99.422**	**0.423**	**99.034**	**99.501**	**99.318**	**99.663**	**99.124**
formula																
Si	3.000	3.000	3.000	2.978	3.000	2.990	3.000	2.998	2.972	2.994		2.983	2.974	3.000	2.978	3.000
Al	0.000	0.000	0.000	0.022	0.000	0.010	0.000	0.002	0.028	0.006		0.017	0.026	0.000	0.022	0.000
Z	**3.000**	**3.000**	**3.000**	**3.000**	**3.000**	**3.000**	**3.000**	**3.000**	**3.000**	**3.000**		**3.000**	**3.000**	**3.000**	**3.000**	**3.000**
Si	0.053	0.007	0.052	0.000	0.000	0.000	0.012	0.000	0.000	0.000		0.000	0.000	0.004	0.000	0.048
Al	1.760	1.911	1.847	1.852	1.901	1.932	1.892	1.923	1.911	1.902		1.891	1.890	1.930	1.929	1.876
Fe^{3+}	0.131	0.062	0.049	0.117	0.061	0.046	0.044	0.047	0.089	0.068		0.081	0.088	0.052	0.070	0.013
Ti	0.020	0.008	0.011	0.031	0.022	0.019	0.028	0.018	0.018	0.022		0.028	0.026	0.013	0.022	0.021
Y	**1.911**	**1.981**	**1.907**	**2.000**	**1.984**	**1.997**	**1.964**	**1.989**	**2.017**	**1.992**		**2.000**	**2.003**	**1.995**	**2.022**	**1.911**
Mg	1.864	1.998	1.919	1.884	1.915	1.894	1.878	1.923	1.911	1.888		1.938	1.915	1.866	1.879	1.871
Fe^{2+}	0.499	0.592	0.577	0.621	0.623	0.664	0.651	0.658	0.612	0.641		0.603	0.608	0.680	0.643	0.659
Ca	0.635	0.417	0.525	0.486	0.472	0.440	0.480	0.425	0.452	0.470		0.449	0.472	0.438	0.435	0.482
X	**2.998**	**3.008**	**3.021**	**2.991**	**3.010**	**2.998**	**3.009**	**3.006**	**2.975**	**2.999**		**2.990**	**2.994**	**2.984**	**2.956**	**3.012**
Total	**7.962**	**7.996**	**7.979**	**7.992**	**7.994**	**7.995**	**7.985**	**7.995**	**7.992**	**7.991**		**7.989**	**7.997**	**7.984**	**7.978**	**7.971**
py	59.377	66.066	60.812	62.975	63.628	63.184	61.790	63.968	64.232	62.966		64.826	63.948	62.327	63.544	59.588
alm	16.643	19.679	19.093	20.765	20.700	22.142	21.644	21.890	20.588	21.369		20.154	20.300	22.780	21.756	21.873
andr	6.847	3.110	2.557	5.870	3.063	2.322	2.232	2.359	4.403	3.409		4.041	4.386	2.588	3.473	0.704
gross	14.348	10.771	14.834	10.390	12.609	12.352	13.720	11.784	10.777	12.256		10.978	11.365	12.099	11.227	15.298
ma	2.786	0.375	2.703	0.000	0.000	0.000	0.614	0.000	0.000	0.000		0.000	0.000	0.206	0.000	2.537
Mg#	78.881	77.149	76.887	75.203	75.453	74.050	74.248	74.505	75.728	74.661		76.284	75.904	73.298	74.495	73.960
x(g)	0.211	0.229	0.231	0.248	0.245	0.260	0.258	0.255	0.243	0.253		0.237	0.241	0.267	0.255	0.260

g	12.5 kbar/1100 °C						15 kbar/900 °C dark								15 kbar/900 °C light	
MAOC 13					av	sd							av dark	sd dark		
SiO_2	40.637	40.927	40.070	39.953	40.952	0.651	41.640	41.200	40.700	42.070	40.460	43.020	41.515	0.945	40.500	40.650
TiO_2	0.301	0.451	0.720	0.482	0.441	0.136	0.361	0.493	0.367	0.459	0.626	0.634	0.490	0.120	0.328	0.417
Al_2O_3	22.960	21.890	21.860	22.130	22.347	0.427	21.800	22.010	22.090	20.890	21.670	23.930	22.065	1.009	21.970	21.680
FeO	11.130	11.630	11.690	12.200	11.599	0.393	9.230	9.780	10.370	12.300	11.000	8.730	10.235	1.292	15.040	15.720
MgO	17.330	17.160	17.160	16.630	17.333	0.375	19.170	18.470	18.270	18.200	17.340	17.560	18.168	0.658	14.500	14.460
CaO	5.900	6.420	6.090	6.270	6.001	0.282	6.380	6.310	6.000	5.570	6.610	6.510	6.230	0.385	6.730	6.380
Na_2O	0.097	0.130	0.052	0.050	0.100	0.058	0.070	0.030	0.039	0.088	0.041	0.210	0.080	0.067	0.012	0.045
Total	**98.355**	**98.608**	**97.642**	**97.715**	**98.773**	**0.260**	**98.651**	**98.293**	**97.836**	**99.577**	**97.747**	**100.594**	**98.783**	**1.108**	**99.080**	**99.352**
formula																
Si	2.967	2.990	2.958	2.954	2.984		3.000	2.995	2.976	3.000	2.978	3.000	3.000		2.998	3.000
Al	0.033	0.010	0.042	0.046	0.016		0.000	0.005	0.024	0.000	0.022	0.000	0.000		0.002	0.000
Z	**3.000**	**3.000**	**3.000**	**3.000**	**3.000**		**3.000**	**3.000**	**3.000**	**3.000**	**3.000**	**3.000**	**3.000**		**3.000**	**3.000**
Si	0.000	0.000	0.000	0.000	0.000		0.005	0.000	0.000	0.043	0.000	0.038	0.009		0.000	0.007
Al	1.942	1.875	1.860	1.882	1.903		1.854	1.881	1.879	1.781	1.858	1.991	1.885		1.915	1.890
Fe^{3+}	0.071	0.104	0.109	0.118	0.078		0.108	0.074	0.111	0.095	0.100	0.000	0.054		0.052	0.055
Ti	0.017	0.025	0.040	0.027	0.024		0.020	0.027	0.020	0.025	0.035	0.034	0.027		0.018	0.023
Y	**2.030**	**2.004**	**2.009**	**2.027**	**2.006**		**1.981**	**1.982**	**2.010**	**1.901**	**1.993**	**2.025**	**1.975**		**1.985**	**1.969**
Mg	1.886	1.869	1.889	1.833	1.883		2.062	2.002	1.991	1.963	1.903	1.848	1.963		1.600	1.595
Fe^{2+}	0.608	0.607	0.613	0.637	0.629		0.449	0.520	0.523	0.649	0.577	0.515	0.566		0.879	0.917
Ca	0.462	0.503	0.482	0.497	0.469		0.493	0.492	0.470	0.432	0.521	0.492	0.484		0.534	0.506
X	**2.956**	**2.978**	**2.983**	**2.966**	**2.980**		**3.005**	**3.014**	**2.985**	**3.044**	**3.001**	**2.856**	3.014		**3.013**	**3.017**
Total	**7.986**	**7.982**	**7.993**	**7.993**	**7.986**		**7.990**	**7.996**	**7.994**	**7.988**	**7.994**	**7.919**	**7.989**		**7.998**	**7.994**
py	63.810	62.758	63.305	61.791	63.185		68.402	66.421	66.715	62.210	63.401	62.859	64.673		53.110	52.483
alm	20.576	20.367	20.547	21.465	21.092		14.953	17.270	17.538	21.329	19.228	18.047	18.797		29.172	30.393
andr	3.512	5.191	5.411	5.802	3.901		5.435	3.738	5.500	4.992	5.019	0.000	2.731		2.625	2.814
gross	12.102	11.684	10.736	10.942	11.822		10.982	12.571	10.247	9.193	12.351	17.242	13.325		15.092	13.945
ma	0.000	0.000	0.000	0.000	0.000		0.229	0.000	0.000	2.276	0.000	1.852	0.474		0.000	0.366
Mg#	**75.616**	**75.499**	**75.496**	**74.218**	**74.973**		**82.110**	**79.364**	**79.184**	**75.145**	**76.729**	**78.193**	**77.608**		**64.546**	**63.488**
x(g)	0.244	0.245	0.245	0.258	0.250		0.179	0.206	0.208	0.249	0.233	0.218	0.224		0.355	0.365

g	15 kbar/900 °C light			15 kbar/900 °C		15 kbar/1050 °C										
MAOC 13		av light	sd light	av all	sd all											
SiO_2	40.520	40.557	0.081	41.196	0.888	41.970	41.760	42.020	41.650	41.500	42.570	41.900	41.780	41.660	41.390	40.910
TiO_2	0.626	0.457	0.153	0.479	0.123	0.515	0.579	0.570	0.585	0.585	0.396	0.586	0.695	0.650	0.633	0.700
Al_2O_3	21.000	21.550	0.498	21.893	0.874	22.830	22.340	22.440	22.570	23.090	21.270	22.700	22.530	22.370	22.770	22.160
FeO	15.400	15.387	0.340	11.952	2.776	9.670	9.240	10.680	10.860	11.100	10.360	9.720	9.920	10.020	9.450	10.600
MgO	14.330	14.430	0.089	16.922	1.941	20.250	20.110	19.310	19.410	19.300	18.280	20.450	19.830	19.730	19.770	19.220
CaO	6.860	6.657	0.248	6.372	0.392	5.420	5.490	5.630	5.460	5.450	6.670	5.300	5.730	5.760	5.780	5.600
Na_2O	0.077	0.045	0.033	0.068	0.058	0.066	0.109	0.125	0.023	0.045	0.360	0.058	0.053	0.113	0.075	0.083
Total	**98.813**	99.082	0.270	**98.883**	**1.108**	**100.721**	**99.628**	**100.775**	**100.558**	**101.070**	**99.906**	**100.714**	**100.538**	**100.303**	**99.868**	**99.273**
formula																
Si	3.000	3.000		3.000		2.959	2.974	2.978	2.959	2.935	3.000	2.953	2.959	2.957	2.946	2.942
Al	0.000	0.000		0.000		0.041	0.026	0.022	0.041	0.065	0.000	0.047	0.041	0.043	0.054	0.058
Z	**3.000**	**3.000**		**3.000**		**3.000**	**3.000**	**3.000**	**3.000**	**3.000**	**3.000**	**3.000**	**3.000**	**3.000**	**3.000**	**3.000**
Si	0.016	0.007		0.009		0.000	0.000	0.000	0.000	0.000	0.049	0.000	0.000	0.000	0.000	0.000
Al	1.842	1.883		1.884		1.856	1.849	1.852	1.849	1.859	1.795	1.839	1.840	1.829	1.855	1.821
Fe^{3+}	0.067	0.058		0.055		0.140	0.129	0.127	0.133	0.150	0.114	0.153	0.135	0.160	0.142	0.173
Ti	0.035	0.025		0.026		0.027	0.031	0.030	0.031	0.031	0.021	0.031	0.037	0.035	0.034	0.038
Y	**1.944**	**1.974**		**1.966**		**2.023**	**2.010**	**2.009**	**2.013**	**2.040**	**1.931**	**2.024**	**2.011**	**2.024**	**2.031**	**2.031**
Mg	1.590	1.595		1.842		2.128	2.135	2.040	2.056	2.035	1.952	2.149	2.094	2.088	2.097	2.061
Fe^{2+}	0.892	0.896		0.675		0.430	0.421	0.506	0.513	0.506	0.507	0.419	0.453	0.435	0.421	0.465
Ca	0.547	0.529		0.499		0.409	0.419	0.427	0.416	0.413	0.512	0.400	0.435	0.438	0.441	0.432
X	**3.029**	3.020		**3.016**		**2.968**	**2.975**	**2.974**	**2.984**	**2.953**	**2.970**	**2.969**	**2.982**	**2.961**	**2.959**	**2.957**
Total	**7.989**	**7.994**		**7.990**		**7.991**	**7.985**	**7.983**	**7.997**	**7.994**	**7.950**	**7.992**	**7.993**	**7.984**	**7.990**	**7.988**
py	51.676	52.460		60.656		71.703	71.767	68.598	68.893	68.889	63.171	72.386	70.223	70.516	70.889	69.689
alm	29.439	29.669		22.371		14.504	14.151	17.027	17.178	17.130	17.058	14.130	15.193	14.688	14.215	15.717
andr	3.441	2.944		2.813		6.902	6.434	6.300	6.589	7.374	5.896	7.584	6.689	7.903	6.982	8.505
gross	14.622	14.568		13.721		6.892	7.648	8.075	7.340	6.607	11.336	5.900	7.895	6.893	7.914	6.089
ma	0.821	0.359		0.438		0.000	0.000	0.000	0.000	0.000	2.538	0.000	0.000	0.000	0.000	0.000
Mg#	64.071	64.033		73.197		83.176	83.530	80.115	80.042	80.086	79.391	83.668	82.212	82.761	83.297	81.597
x(g)	0.359	0.360		0.268		0.168	0.165	0.199	0.200	0.199	0.206	0.163	0.178	0.172	0.167	0.184

g	15 kbar/1050 °C				15 kbar/1100 °C											
MAOC 13			av	sd												
SiO_2	41.680	41.530	41.717	0.384	42.310	41.930	41.260	41.910	42.120	41.700	42.180	41.430	41.980	42.210	41.770	42.420
TiO_2	0.584	0.594	0.590	0.078	0.655	0.377	0.671	0.219	0.427	0.607	0.225	0.217	0.651	0.690	0.679	0.211
Al_2O_3	22.680	22.550	22.485	0.436	22.150	23.120	22.960	24.030	23.760	22.640	23.750	23.220	22.470	21.720	22.450	23.880
FeO	9.750	10.080	10.112	0.569	10.170	9.590	10.250	8.780	8.360	9.990	8.730	11.300	9.840	9.680	9.650	7.370
MgO	19.830	19.380	19.605	0.555	17.080	18.810	17.530	19.330	19.260	18.800	19.830	17.890	19.040	18.650	18.530	20.840
CaO	5.870	6.070	5.710	0.358	6.870	6.140	7.190	5.640	6.000	5.980	5.800	5.570	5.770	7.020	6.770	5.790
Na_2O	0.045	0.037	0.092	0.086	0.196	0.039	0.091	0.038	0.099	0.075	0.034	0.014	0.070	0.090	0.062	0.052
Total	**100.439**	**100.241**	**100.310**	**0.560**	**99.431**	**100.006**	**99.952**	**99.947**	**100.026**	**99.792**	**100.549**	**99.641**	**99.821**	**100.060**	**99.911**	**100.563**
formula																
Si	2.952	2.955	2.963		3.000	2.990	2.963	2.976	2.988	2.985	2.973	2.984	3.000	3.000	2.989	2.970
Al	0.048	0.045	0.037		0.000	0.010	0.037	0.024	0.012	0.015	0.027	0.016	0.000	0.000	0.011	0.030
Z	**3.000**	**3.000**	**3.000**		**3.000**	**3.000**	**3.000**	**3.000**	**3.000**	**3.000**	**3.000**	**3.000**	**3.000**	**3.000**	**3.000**	**3.000**
Si	0.000	0.000	0.000		0.053	0.000	0.000	0.000	0.000	0.000	0.000	0.000	0.002	0.017	0.000	0.000
Al	1.846	1.845	1.845		1.884	1.934	1.906	1.987	1.975	1.894	1.947	1.955	1.894	1.830	1.882	1.941
Fe^{3+}	0.146	0.142	0.142		0.000	0.041	0.072	0.019	0.005	0.066	0.061	0.039	0.043	0.074	0.065	0.074
Ti	0.031	0.032	0.032		0.036	0.020	0.036	0.012	0.023	0.033	0.012	0.012	0.035	0.037	0.037	0.011
Y	**2.023**	**2.019**	**2.018**		**1.919**	**1.995**	**2.014**	**2.018**	**2.003**	**1.993**	**2.019**	**2.006**	**1.971**	**1.941**	**1.983**	**2.026**
Mg	2.094	2.055	2.076		1.838	2.000	1.877	2.046	2.037	2.006	2.084	1.921	2.030	1.987	1.977	2.175
Fe^{2+}	0.432	0.458	0.459		0.614	0.531	0.544	0.502	0.491	0.532	0.454	0.641	0.546	0.504	0.513	0.357
Ca	0.446	0.463	0.435		0.531	0.469	0.553	0.429	0.456	0.459	0.438	0.430	0.442	0.538	0.519	0.434
X	**2.971**	**2.976**	**2.969**		**2.982**	**3.000**	**2.974**	**2.977**	**2.984**	**2.996**	**2.976**	**2.992**	**3.017**	**3.029**	**3.008**	**2.967**
Total	**7.994**	**7.995**	**7.987**		**7.955**	**7.995**	**7.987**	**7.995**	**7.986**	**7.990**	**7.995**	**7.998**	**7.990**	**7.988**	**7.991**	**7.993**
py	70.478	69.062	69.912		58.829	66.666	63.105	68.729	68.269	66.943	70.023	64.204	67.177	64.721	65.708	73.312
alm	14.527	15.391	15.453		20.578	17.694	18.292	16.858	16.445	17.752	15.257	21.429	18.086	16.649	17.038	12.049
andr	7.213	7.016	7.022		0.000	2.064	3.553	0.965	0.264	3.311	3.000	1.969	2.165	3.827	3.272	3.654
gross	7.781	8.531	7.612		17.811	13.577	15.049	13.448	15.022	11.993	11.720	12.399	12.486	13.921	13.982	10.985
ma	0.000	0.000	0.000		2.781	0.000	0.000	0.000	0.000	0.000	0.000	0.000	0.087	0.882	0.000	0.000
Mg#	82.910	81.776	81.897		74.962	79.026	77.528	80.304	80.587	79.040	82.109	74.976	78.810	79.759	79.409	85.885
x(g)	0.171	0.182	0.181		0.250	0.210	0.225	0.197	0.194	0.210	0.179	0.250	0.212	0.202	0.206	0.141

g	15 kbar/1100 °C						20 kbar/1050 °C									
MAOC 13					av	sd										
SiO_2	43.690	41.540	41.730	41.580	41.985	0.560	39.650	41.850	42.040	41.560	41.710	41.820	42.040	41.540	41.610	41.180
TiO_2	0.185	0.503	0.319	0.428	0.442	0.196	0.434	0.557	0.398	0.217	0.429	0.308	0.374	0.422	0.650	0.323
Al_2O_3	23.010	22.670	23.040	22.860	22.983	0.645	25.500	22.170	22.290	22.870	22.710	22.730	22.470	22.590	21.940	21.870
FeO	6.600	9.730	10.170	9.610	9.364	1.162	10.020	10.270	8.880	9.860	10.800	10.860	10.920	11.910	11.590	13.090
MgO	20.820	18.580	18.110	18.320	18.839	1.035	18.390	16.860	19.750	18.200	16.880	17.360	17.710	17.440	17.010	16.230
CaO	6.140	6.700	6.200	6.720	6.269	0.529	5.750	7.460	5.490	5.770	6.730	6.210	6.000	6.120	6.920	6.580
Na_2O	0.101	0.034	0.021	0.037	0.066	0.045	0.062	0.169	0.062	0.047	0.082	0.111	0.059	0.080	0.099	0.038
Total	**100.546**	**99.757**	**99.590**	**99.555**	**99.947**	**0.324**	**99.806**	**99.336**	**98.910**	**98.524**	**99.341**	**99.399**	**99.573**	**100.102**	**99.819**	**99.311**
formula																
Si	3.000	2.975	2.999	2.984	2.995		2.829	3.000	3.000	3.000	3.000	3.000	3.000	2.990	3.000	3.000
Al	0.000	0.025	0.001	0.016	0.005		0.171	0.000	0.000	0.000	0.000	0.000	0.000	0.010	0.000	0.000
Z	**3.000**	**3.000**	**3.000**	**3.000**	**3.000**		**3.000**	**3.000**	**3.000**	**3.000**	**3.000**	**3.000**	**3.000**	**3.000**	**3.000**	**3.000**
Si	0.056	0.000	0.000	0.000	0.000		0.000	0.031	0.017	0.014	0.021	0.023	0.032	0.000	0.009	0.010
Al	1.897	1.888	1.951	1.918	1.927		1.974	1.893	1.885	1.954	1.938	1.936	1.910	1.906	1.870	1.884
Fe^{3+}	0.000	0.088	0.018	0.057	0.041		0.158	0.007	0.047	0.001	0.000	0.000	0.000	0.070	0.054	0.067
Ti	0.010	0.027	0.017	0.023	0.024		0.023	0.030	0.021	0.012	0.023	0.017	0.020	0.023	0.035	0.018
Y	**1.906**	**2.003**	**1.986**	**1.998**	**1.991**		**2.156**	**1.930**	**1.953**	**1.968**	**1.962**	**1.953**	**1.930**	**1.999**	**1.960**	**1.968**
Mg	2.171	1.983	1.940	1.960	2.003		1.956	1.821	2.113	1.967	1.822	1.871	1.904	1.871	1.834	1.768
Fe^{2+}	0.386	0.495	0.593	0.520	0.518		0.440	0.615	0.486	0.597	0.654	0.656	0.659	0.647	0.647	0.733
Ca	0.460	0.514	0.477	0.517	0.479		0.440	0.579	0.422	0.448	0.522	0.481	0.464	0.472	0.536	0.515
X	**3.017**	**2.992**	**3.011**	**2.997**	**3.000**		**2.836**	**3.014**	**3.021**	**3.012**	**2.999**	**3.008**	**3.026**	**2.990**	**3.017**	**3.017**
Total	**7.979**	**7.995**	**7.997**	**7.995**	**7.991**		**7.991**	**7.976**	**7.991**	**7.993**	**7.981**	**7.984**	**7.989**	**7.989**	**7.986**	**7.995**
py	69.028	66.285	64.451	65.402	66.769		68.993	58.768	69.074	64.624	59.721	61.013	61.260	62.577	60.308	58.132
alm	12.795	16.535	19.690	17.356	17.263		15.502	20.393	16.091	19.804	21.812	21.823	21.762	21.640	21.438	24.301
andr	0.000	4.388	0.929	2.834	2.040		7.346	0.382	2.394	0.068	0.000	0.000	0.000	3.488	2.766	3.401
gross	15.251	12.792	14.930	14.408	13.929		8.159	18.825	11.578	14.814	17.415	15.989	15.320	12.294	15.008	13.679
ma	2.926	0.000	0.000	0.000	0.000		0.000	1.631	0.862	0.689	1.053	1.176	1.658	0.000	0.480	0.487
Mg#	84.902	80.035	76.599	79.028	79.457		81.653	74.759	81.296	76.733	73.589	74.024	74.301	74.304	73.928	70.693
x(g)	0.151	0.200	0.234	0.210	0.205		0.183	0.252	0.187	0.233	0.264	0.260	0.257	0.257	0.261	0.293

g	20 kbar/1050 °C		20 kbar/1100 °C													
MAOC 13	av	sd														
SiO_2	41.500	0.699	42.120	41.970	42.490	42.600	42.050	42.530	41.170	41.550	41.140	41.900	41.600	41.320	41.280	42.070
TiO_2	0.411	0.123	0.366	0.402	0.674	0.717	0.441	0.458	0.714	0.879	0.322	0.362	0.894	0.892	0.871	0.448
Al_2O_3	22.714	1.035	22.740	22.320	22.270	21.940	22.340	22.290	22.260	22.000	22.940	22.930	21.730	22.530	21.780	22.640
FeO	10.820	1.182	11.590	13.120	9.960	9.870	12.490	9.610	12.720	12.050	13.200	12.290	12.530	12.030	11.870	11.320
MgO	17.583	0.999	18.550	17.270	20.170	20.250	17.210	19.580	16.220	17.120	16.930	16.840	16.850	16.950	16.940	18.210
CaO	6.303	0.611	5.730	5.930	5.410	5.450	5.950	6.120	6.700	6.700	5.680	6.560	6.900	6.100	7.350	5.720
Na_2O	0.081	0.038	0.067	0.097	0.068	0.066	0.092	0.079	0.109	0.038	0.056	0.074	0.044	0.049	0.060	0.052
Total	**99.412**	**0.458**	**101.163**	**101.109**	**101.042**	**100.893**	**100.573**	**100.667**	**99.893**	**100.337**	**100.268**	**100.956**	**100.548**	**99.871**	**100.151**	**100.460**
formula																
Si	2.998		2.987	3.000	2.993	3.000	3.000	3.000	2.990	2.995	2.968	3.000	2.999	2.991	2.981	3.000
Al	0.002		0.013	0.000	0.007	0.000	0.000	0.000	0.010	0.005	0.032	0.000	0.001	0.009	0.019	0.000
Z	**3.000**		**3.000**	**3.000**	**3.000**	**3.000**	**3.000**	**3.000**	**3.000**	**3.000**	**3.000**	**3.000**	**3.000**	**3.000**	**3.000**	**3.000**
Si	0.000		0.000	0.002	0.000	0.005	0.021	0.009	0.000	0.000	0.000	0.000	0.000	0.000	0.000	0.007
Al	1.931		1.888	1.882	1.842	1.824	1.891	1.859	1.896	1.864	1.918	1.934	1.846	1.914	1.835	1.907
Fe^{3+}	0.037		0.096	0.084	0.103	0.099	0.032	0.086	0.052	0.051	0.086	0.038	0.064	0.005	0.098	0.038
Ti	0.022		0.020	0.022	0.036	0.038	0.024	0.024	0.039	0.048	0.017	0.019	0.048	0.049	0.047	0.024
Y	**1.991**		**2.003**	**1.987**	**1.981**	**1.961**	**1.948**	**1.969**	**1.986**	**1.963**	**2.022**	**1.991**	**1.958**	**1.967**	**1.980**	**1.969**
Mg	1.893		1.961	1.842	2.118	2.130	1.843	2.065	1.756	1.840	1.821	1.797	1.811	1.829	1.824	1.940
Fe^{2+}	0.616		0.592	0.701	0.484	0.484	0.718	0.483	0.721	0.675	0.710	0.698	0.691	0.724	0.619	0.638
Ca	0.488		0.435	0.454	0.408	0.412	0.458	0.464	0.521	0.517	0.439	0.503	0.533	0.473	0.569	0.438
X	**2.997**		**2.988**	**2.997**	**3.010**	**3.025**	**3.019**	**3.012**	**2.998**	**3.032**	**2.970**	**2.998**	**3.035**	**3.026**	**3.012**	**3.016**
Total	**7.989**		**7.991**	**7.987**	**7.991**	**7.991**	**7.987**	**7.989**	**7.985**	**7.995**	**7.992**	**7.990**	**7.994**	**7.993**	**7.992**	**7.993**
py	63.168		65.630	61.338	70.364	70.134	59.987	68.122	58.570	60.674	61.311	59.936	59.663	60.449	60.556	63.975
alm	20.557		19.799	23.384	16.072	15.988	23.781	16.025	24.042	22.260	23.905	23.283	22.777	23.915	20.559	21.158
andr	1.879		4.779	4.227	5.196	5.029	1.663	4.364	2.602	2.620	4.273	1.889	3.272	0.233	4.933	1.947
gross	14.396		9.792	10.938	8.368	8.588	13.507	11.040	14.787	14.446	10.511	14.892	14.288	15.402	13.951	12.574
ma	0.000		0.000	0.112	0.000	0.261	1.062	0.448	0.000	0.000	0.000	0.000	0.000	0.000	0.000	0.346
Mg#	75.447		76.824	72.436	81.406	81.492	71.967	81.056	70.898	73.160	71.948	72.022	72.372	71.653	74.654	75.248
x(g)	0.246		0.232	0.276	0.186	0.185	0.280	0.189	0.291	0.268	0.281	0.280	0.276	0.283	0.253	0.248

g	20 kbar/1100 °C							
MAOC 13							**av**	**sd**
SiO_2	42.250	41.600	41.960	41.760	42.060	42.060	41.874	0.439
TiO_2	0.643	0.755	0.484	0.663	0.562	0.964	0.626	0.207
Al_2O_3	21.960	22.270	22.670	22.030	22.130	21.760	22.277	0.372
FeO	11.740	11.600	10.810	11.630	10.870	11.510	11.641	1.015
MgO	17.650	17.210	19.000	17.490	18.630	18.410	17.874	1.170
CaO	6.540	6.740	4.970	6.790	6.160	6.300	6.190	0.597
Na_2O	0.101	0.052	0.061	0.064	0.056	0.087	0.069	0.020
Total	**100.884**	**100.227**	**99.955**	**100.427**	**100.468**	**101.091**	**100.549**	**0.430**
formula								
Si	3.000	2.996	3.000	2.998	3.000	2.993	2.998	
Al	0.000	0.004	0.000	0.002	0.000	0.007	0.002	
Z	**3.000**	**3.000**	**3.000**	**3.000**	**3.000**	**3.000**	**3.000**	
Si	0.019	0.000	0.001	0.000	0.001	0.000	0.000	
Al	1.850	1.886	1.911	1.863	1.861	1.818	1.877	
Fe^{3+}	0.057	0.044	0.043	0.076	0.085	0.098	0.067	
Ti	0.035	0.041	0.026	0.036	0.030	0.052	0.034	
Y	**1.941**	**1.971**	**1.980**	**1.975**	**1.976**	**1.967**	**1.978**	
Mg	1.880	1.848	2.026	1.872	1.981	1.953	1.908	
Fe^{2+}	0.645	0.654	0.604	0.622	0.563	0.587	0.630	
Ca	0.501	0.520	0.381	0.522	0.471	0.480	0.475	
X	**3.026**	**3.022**	**3.010**	**3.016**	**3.015**	**3.021**	**3.012**	
Total	**7.986**	**7.993**	**7.992**	**7.991**	**7.992**	**7.988**	**7.990**	
py	61.149	61.135	67.240	62.064	65.678	64.656	63.324	
alm	21.309	21.657	20.048	20.618	18.674	19.442	20.914	
andr	2.926	2.236	2.174	3.867	4.323	4.965	3.381	
gross	13.623	14.972	10.478	13.450	11.293	10.938	12.381	
ma	0.993	0.000	0.059	0.000	0.032	0.000	0.000	
Mg#	74.465	73.842	77.047	75.063	77.871	76.882	75.173	
x(g)	0.255	0.262	0.230	0.249	0.221	0.231	0.248	

Garnet in MAOC 15

g	12.5 kbar/1050 °C							12.5 kbar/1100 °C						15 kbar/900 °C dark		
MAOC 15						**av**	**sd**	**light**	**dark**			**av dark**	**sd dark**			
SiO_2	42.280	41.710	41.960	41.910	42.630	42.098	0.361	41.395	43.968	41.401	41.726	42.122	1.240	42.100	41.510	41.620
TiO_2	0.261	0.341	0.372	0.149	0.208	0.266	0.092	0.314	0.501	0.337	0.589	0.435	0.132	0.285	0.461	0.272
Al_2O_3	21.490	21.900	20.520	22.600	21.890	21.680	0.762	22.580	17.980	22.600	20.730	20.973	2.179	22.460	22.430	21.910
FeO	11.030	10.740	10.350	10.890	10.450	10.692	0.288	10.540	8.940	10.450	9.680	9.903	0.749	7.070	7.440	10.380
MgO	19.030	17.620	17.180	18.680	17.980	18.098	0.757	18.550	17.630	18.870	17.640	18.173	0.634	21.080	20.680	18.120
CaO	5.440	6.590	8.150	5.430	6.850	6.492	1.132	5.520	9.180	5.560	7.520	6.945	1.758	5.900	6.450	6.180
Na_2O	0.060	0.223	0.268	0.028	0.151	0.146	0.103	0.141	0.562	0.091	0.335	0.282	0.214	0.021	0.096	0.064
Total	**99.591**	**99.124**	**98.800**	**99.687**	**100.159**	**99.472**	**0.526**	**99.040**	**98.761**	**99.309**	**98.220**	**98.832**	**0.466**	**98.916**	**99.067**	**98.546**
formula																
Si	3.000	3.000	3.000	3.000	3.000	3.000		2.986	3.000	2.976	3.000	3.000		2.994	2.953	3.000
Al	0.000	0.000	0.000	0.000	0.000	0.000		0.014	0.000	0.024	0.000	0.000		0.006	0.047	0.000
Z	**3.000**	**3.000**	**3.000**	**3.000**	**3.000**	**3.000**		**3.000**	**3.000**	**3.000**	**3.000**	**3.000**		**3.000**	**3.000**	**3.000**
Si	0.053	0.007	0.052	0.007	0.052	0.034		0.000	0.191	0.000	0.043	0.049		0.000	0.000	0.025
Al	1.760	1.911	1.847	1.911	1.847	1.841		1.906	1.538	1.891	1.782	1.789		1.877	1.834	1.877
Fe^{3+}	0.131	0.062	0.049	0.062	0.049	0.082		0.094	0.104	0.110	0.115	0.106		0.101	0.176	0.054
Ti	0.020	0.008	0.011	0.008	0.011	0.014		0.017	0.027	0.018	0.032	0.024		0.015	0.025	0.015
Y	**1.911**	**1.981**	**1.907**	**1.981**	**1.907**	**1.938**		**2.017**	**1.669**	**2.018**	**1.929**	**1.918**		**1.993**	**2.035**	**1.945**
Mg	1.864	1.998	1.919	1.998	1.919	1.944		1.995	1.908	2.022	1.918	1.961		2.235	2.193	1.963
Fe^{2+}	0.499	0.592	0.577	0.592	0.577	0.562		0.542	0.439	0.519	0.475	0.494		0.319	0.266	0.577
Ca	0.635	0.417	0.525	0.417	0.525	0.501		0.427	0.714	0.428	0.588	0.539		0.450	0.492	0.481
X	**2.998**	**3.008**	**3.021**	**3.008**	**3.021**	**3.007**		**2.964**	**3.060**	**2.969**	**2.981**	**2.993**		**3.004**	**2.952**	**3.021**
Total	**7.962**	**7.996**	**7.979**	**7.996**	**7.979**	**7.980**		**7.980**	**7.921**	**7.987**	**7.953**	**7.960**		**7.997**	**7.987**	**7.991**
py	59.377	66.066	60.812	66.066	60.812	62.905		67.309	50.870	68.111	62.118	62.962		74.409	74.314	63.709
alm	16.643	19.679	19.093	19.679	19.093	18.682		18.295	14.342	17.465	15.942	16.499		10.622	9.027	19.103
andr	6.847	3.110	2.557	3.110	2.557	4.256		4.642	6.213	5.432	5.970	5.500		5.088	8.660	2.757
gross	14.348	10.771	14.834	10.771	14.834	12.412		9.754	17.114	8.992	13.745	12.493		9.880	7.999	13.169
ma	2.786	0.375	2.703	0.375	2.703	1.745		0.000	11.461	0.000	2.225	2.545		0.000	0.000	1.262
Mg#	78.881	77.149	76.887	77.149	76.887	77.581		78.628	81.295	79.591	80.143	79.881		87.508	89.169	77.279
x(g)	0.211	0.229	0.231	0.229	0.231	0.224		0.214	0.187	0.204	0.199	0.201		0.125	0.108	0.227

g	15 kbar/900 °C dark			15 kbar/900 °C light						15 kbar/900 °C		15 kbar/1050 °C				
MAOC 15		**av dark**	**sd dark**					**av light**	**sd light**	**av**	**sd**					
SiO_2	39.740	41.243	1.034	41.410	40.900	41.400	38.610	40.580	1.335	40.911	1.161	42.200	42.260	42.150	42.480	40.820
TiO_2	0.401	0.355	0.092	0.298	0.437	0.427	0.294	0.364	0.079	0.359	0.079	0.518	0.733	0.530	0.337	0.387
Al_2O_3	25.050	22.963	1.414	22.290	21.030	20.540	24.750	22.153	1.882	22.558	1.601	22.400	22.060	22.410	22.070	23.670
FeO	9.340	8.558	1.570	13.700	13.400	11.670	14.010	13.195	1.047	10.876	2.770	9.870	9.150	8.920	9.460	10.280
MgO	18.510	19.598	1.498	16.400	15.220	16.800	16.020	16.110	0.673	17.854	2.152	19.300	20.350	20.130	20.680	20.180
CaO	5.920	6.113	0.259	5.760	7.010	6.480	5.410	6.165	0.718	6.139	0.500	5.920	5.750	5.660	5.050	4.800
Na_2O	0.354	0.134	0.150	0.096	0.499	0.062	0.045	0.176	0.217	0.155	0.174	0.151	0.054	0.037	0.059	0.094
Total	**99.315**	**98.961**	**0.322**	**99.954**	**98.496**	**97.379**	**99.139**	**98.742**	**1.087**	**98.852**	**0.268**	**100.359**	**100.357**	**99.837**	**100.136**	**100.231**
formula																
Si	2.839	2.952		3.000	3.000	3.000	2.821	2.979		2.966		2.997	2.990	2.996	3.000	2.890
Al	0.161	0.048		0.000	0.000	0.000	0.179	0.021		0.034		0.003	0.010	0.004	0.000	0.110
Z	**3.000**	3.000		**3.000**	**3.000**	**3.000**	**3.000**	3.000		**3.000**		**3.000**	**3.000**	**3.000**	**3.000**	**3.000**
Si	0.000	0.000		0.007	0.019	0.072	0.000	0.000		0.000		0.000	0.000	0.000	0.007	0.000
Al	1.947	1.890		1.908	1.829	1.797	1.953	1.896		1.893		1.872	1.830	1.873	1.841	1.864
Fe^{3+}	0.220	0.138		0.059	0.156	0.020	0.200	0.109		0.124		0.097	0.109	0.080	0.117	0.218
Ti	0.022	0.019		0.016	0.024	0.024	0.016	0.020		0.020		0.028	0.039	0.028	0.018	0.021
Y	**2.189**	2.047		**1.983**	**2.010**	**1.840**	**2.169**	2.025		**2.036**		**1.996**	**1.978**	**1.981**	**1.976**	**2.103**
Mg	1.971	2.091		1.775	1.675	1.859	1.745	1.763		1.929		2.043	2.147	2.133	2.182	2.130
Fe^{2+}	0.338	0.374		0.773	0.671	0.705	0.656	0.701		0.536		0.489	0.432	0.450	0.443	0.391
Ca	0.453	0.469		0.448	0.554	0.515	0.424	0.485		0.477		0.450	0.436	0.431	0.383	0.364
X	**2.762**	2.934		**2.996**	**2.900**	**3.078**	**2.825**	2.950		**2.942**		**2.983**	**3.014**	**3.014**	**3.009**	**2.884**
Total	**7.951**	**7.981**		**7.986**	**7.929**	**7.991**	**7.994**	**7.975**		**7.978**		**7.979**	**7.993**	**7.995**	**7.992**	**7.987**
py	71.360	71.273		58.896	56.808	56.439	61.780	59.782		65.585		68.497	71.210	70.767	72.167	73.831
alm	12.237	12.750		25.791	23.142	22.885	23.225	23.776		18.207		16.402	14.328	14.931	14.739	13.547
andr	10.047	6.749		2.983	7.758	1.073	9.223	5.375		6.074		4.854	5.535	4.045	5.897	10.357
gross	6.357	9.228		11.974	11.357	15.665	5.772	11.068		10.133		10.247	8.926	10.256	6.833	2.265
ma	0.000	0.000		0.356	0.935	3.938	0.000	0.000		0.812		0.000	0.000	0.000	0.363	0.000
Mg#	85.362	84.826		69.673	71.389	72.514	72.678	71.545		78.271		80.681	83.249	82.577	83.111	84.496
x(g)	0.146	0.152		0.303	0.286	0.275	0.273	0.285		0.217		0.193	0.168	0.174	0.169	0.155

g	15 kbar/1050 °C			15 kbar/1100 °C									20 kbar/1050 °C			
MAOC 15		av	sd								av	sd				
SiO_2	41.900	41.968	0.593	41.770	41.200	42.810	42.520	43.010	42.150	41.750	42.173	0.647	42.620	42.780	41.530	42.480
TiO_2	0.498	0.501	0.138	0.542	0.585	0.122	0.198	0.237	0.250	0.374	0.330	0.177	0.653	0.292	0.448	0.848
Al_2O_3	22.320	22.488	0.600	22.770	24.010	24.030	23.970	23.210	24.200	23.380	23.653	0.535	21.450	22.520	22.100	21.470
FeO	9.760	9.573	0.498	9.250	8.760	6.770	7.400	6.270	6.890	7.780	7.589	1.088	8.050	8.310	11.920	7.960
MgO	19.670	20.052	0.493	19.040	18.780	21.190	21.020	21.080	20.750	20.200	20.294	1.002	20.250	20.610	17.160	20.550
CaO	5.870	5.508	0.468	6.470	6.530	5.240	5.340	6.410	5.400	5.910	5.900	0.575	6.740	5.290	5.230	6.660
Na_2O	0.072	0.078	0.041	0.057	0.101	0.029	0.050	0.071	0.034	0.052	0.056	0.024	0.094	0.049	0.209	0.049
Total	**100.090**	**100.168**	**0.215**	**99.899**	**99.966**	**100.191**	**100.498**	**100.288**	**99.674**	**99.446**	**99.995**	**0.363**	**99.857**	**99.851**	**98.597**	**100.017**
formula																
Si	2.980	2.976		2.979	2.931	3.000	2.977	3.000	2.973	2.965	2.977		3.000	3.000	3.000	3.000
Al	0.020	0.024		0.021	0.069	0.000	0.023	0.000	0.027	0.035	0.023		0.000	0.000	0.000	0.000
Z	**3.000**	**3.000**		**3.000**	**3.000**	**3.000**	**3.000**	**3.000**	**3.000**	**3.000**	**3.000**		**3.000**	**3.000**	**3.000**	**3.000**
Si	0.000	0.000		0.000	0.000	0.000	0.000	0.013	0.000	0.000	0.000		0.025	0.029	0.035	0.009
Al	1.850	1.856		1.893	1.944	1.985	1.955	1.916	1.985	1.922	1.945		1.794	1.879	1.903	1.792
Fe^{3+}	0.127	0.125		0.078	0.076	0.005	0.054	0.044	0.019	0.080	0.051		0.099	0.038	0.007	0.106
Ti	0.027	0.027		0.029	0.031	0.006	0.010	0.012	0.013	0.020	0.018		0.035	0.016	0.025	0.045
Y	**2.004**	**2.008**		**2.000**	**2.052**	**1.997**	**2.019**	**1.972**	**2.018**	**2.022**	**2.013**		**1.928**	**1.933**	**1.935**	**1.944**
Mg	2.085	2.120		2.024	1.992	2.214	2.194	2.201	2.182	2.139	2.136		2.143	2.176	1.869	2.170
Fe^{2+}	0.454	0.443		0.474	0.445	0.391	0.379	0.324	0.387	0.382	0.397		0.379	0.454	0.721	0.365
Ca	0.447	0.419		0.494	0.498	0.393	0.401	0.481	0.408	0.450	0.446		0.513	0.401	0.410	0.505
X	**2.986**	**2.982**		**2.992**	**2.934**	**2.999**	**2.974**	**3.006**	**2.977**	**2.971**	**2.979**		**3.034**	**3.031**	**3.000**	**3.041**
Total	**7.990**	**7.989**		**7.992**	**7.986**	**7.996**	**7.993**	**7.990**	**7.995**	**7.993**	**7.992**		**7.987**	**7.993**	**7.970**	**7.993**
py	69.825	71.099		67.651	67.873	73.804	73.775	72.596	73.291	71.991	71.687		69.325	70.256	60.503	70.906
alm	15.198	14.863		15.826	15.165	13.054	12.755	10.765	13.001	12.871	13.333		12.485	14.990	24.043	12.013
andr	6.315	6.207		3.905	3.711	0.266	2.672	2.215	0.960	3.941	2.521		5.134	1.950	0.365	5.465
gross	8.662	7.831		12.618	13.251	12.855	10.799	13.790	12.748	11.197	12.458		11.760	11.290	13.284	11.158
ma	0.000	0.000		0.000	0.000	0.021	0.000	0.634	0.000	0.000	0.000		1.295	1.514	1.805	0.459
Mg#	82.124	82.710		81.041	81.737	84.975	85.259	87.184	84.934	84.833	84.317		84.976	82.723	72.156	85.592
x(g)	0.179	0.173		0.190	0.183	0.150	0.147	0.128	0.151	0.152	0.157		0.150	0.173	0.278	0.144

g	20 kbar/1050 °C									20 kbar/1100 °C						
MAOC 15								av	sd							
SiO_2	42.210	42.610	42.230	42.320	42.890	42.410	42.730	42.437	0.375	41.730	41.990	41.420	41.980	41.550	42.370	42.480
TiO_2	0.304	0.306	0.316	0.324	0.604	0.357	0.452	0.446	0.182	0.425	0.561	0.686	0.331	0.483	0.329	0.426
Al_2O_3	22.660	22.750	22.790	22.470	21.450	23.020	22.260	22.267	0.577	22.860	22.460	22.700	23.120	22.760	22.780	22.470
FeO	9.300	9.240	9.590	8.980	9.300	8.080	8.350	9.007	1.133	10.570	10.750	10.980	10.760	10.620	10.650	10.740
MgO	19.390	19.720	18.940	19.130	18.630	20.270	19.540	19.472	1.011	18.470	18.820	18.070	19.400	18.640	19.170	19.010
CaO	5.800	4.970	5.810	6.100	6.510	6.090	6.690	5.990	0.630	6.220	5.600	5.960	4.100	5.230	5.640	5.640
Na_2O	0.036	0.083	0.073	0.063	0.206	0.056	0.126	0.095	0.061	0.043	0.085	0.076	0.082	0.086	0.072	0.124
Total	**99.700**	**99.679**	**99.749**	**99.387**	**99.590**	**100.283**	**100.148**	**99.714**	**0.449**	**100.318**	**100.266**	**99.892**	**99.773**	**99.369**	**101.011**	**100.890**
formula																
Si	3.000	3.000	3.000	3.000	3.000	2.991	3.000	3.000		2.978	2.997	2.976	3.000	2.990	2.996	3.000
Al	0.000	0.000	0.000	0.000	0.000	0.009	0.000	0.000		0.022	0.003	0.024	0.000	0.010	0.004	0.000
Z	**3.000**	**3.000**	**3.000**	**3.000**	**3.000**	**3.000**	**3.000**	**3.000**		**3.000**	**3.000**	**3.000**	**3.000**	**3.000**	**3.000**	**3.000**
Si	0.012	0.036	0.018	0.030	0.076	0.000	0.030	0.026		0.000	0.000	0.000	0.000	0.000	0.000	0.010
Al	1.906	1.910	1.919	1.896	1.813	1.905	1.860	1.872		1.900	1.886	1.898	1.947	1.920	1.895	1.877
Fe^{3+}	0.043	0.000	0.021	0.017	0.000	0.073	0.050	0.041		0.082	0.069	0.062	0.029	0.050	0.084	0.074
Ti	0.016	0.016	0.017	0.017	0.033	0.019	0.024	0.024		0.023	0.030	0.037	0.018	0.026	0.017	0.023
Y	**1.965**	**1.927**	**1.958**	**1.931**	**1.846**	**1.997**	**1.934**	**1.963**		**2.005**	**1.985**	**1.997**	**1.994**	**1.996**	**1.996**	**1.973**
Mg	2.063	2.094	2.018	2.042	1.992	2.131	2.065	2.070		1.965	2.002	1.936	2.067	2.000	2.021	2.008
Fe^{2+}	0.512	0.551	0.552	0.520	0.558	0.403	0.446	0.496		0.548	0.573	0.598	0.614	0.589	0.546	0.562
Ca	0.443	0.379	0.445	0.468	0.500	0.460	0.508	0.458		0.476	0.428	0.459	0.314	0.403	0.427	0.428
X	**3.018**	**3.024**	**3.015**	**3.030**	**3.050**	**2.995**	**3.019**	**3.024**		**2.989**	**3.003**	**2.992**	**2.995**	**2.992**	**2.994**	**2.999**
Total	**7.995**	**7.987**	**7.990**	**7.991**	**7.971**	**7.992**	**7.983**	**7.987**		**7.994**	**7.988**	**7.989**	**7.989**	**7.988**	**7.990**	**7.983**
py	67.727	67.394	66.022	65.829	61.204	71.165	66.873	67.109		65.741	66.670	64.691	69.005	66.830	67.499	66.436
alm	16.971	18.202	18.311	17.168	18.288	13.467	14.757	16.410		18.347	19.072	19.974	20.513	19.693	18.228	18.755
andr	2.173	0.000	1.078	0.906	0.000	3.667	2.562	2.084		4.110	3.465	3.110	1.437	2.497	4.211	3.749
gross	12.518	12.544	13.679	14.539	16.402	11.700	14.272	13.051		11.802	10.793	12.225	9.045	10.980	10.062	10.530
ma	0.610	1.859	0.910	1.559	4.105	0.000	1.536	1.346		0.000	0.000	0.000	0.000	0.000	0.000	0.529
Mg#	80.106	79.187	78.519	79.697	78.124	84.087	82.256	80.663		78.182	77.756	76.408	77.085	77.240	78.737	78.120
x(g)	0.199	0.208	0.215	0.203	0.219	0.159	0.177	0.193		0.218	0.222	0.236	0.229	0.228	0.213	0.219

g	20 kbar/1100 °C														
MAOC 15														av	sd
SiO_2	42.360	41.910	42.350	43.270	42.020	42.940	41.920	42.260	43.110	42.300	42.300	43.510	41.810	42.279	0.561
TiO_2	0.308	0.453	0.423	0.178	0.312	0.571	0.322	0.329	0.585	0.268	0.288	0.736	0.438	0.423	0.146
Al_2O_3	22.870	23.170	22.610	22.900	23.290	22.350	22.830	23.250	22.480	23.140	23.510	21.290	23.480	22.816	0.494
FeO	10.310	9.190	10.380	7.410	11.740	8.540	11.440	11.430	6.630	11.630	11.590	8.980	9.490	10.192	1.410
MgO	20.280	19.870	18.760	21.570	19.250	19.540	19.030	19.630	21.710	19.250	19.270	18.990	19.680	19.421	0.909
CaO	4.740	5.350	4.530	4.930	4.890	6.950	4.810	5.100	6.460	4.830	4.780	7.540	5.410	5.436	0.851
Na_2O	0.037	0.073	0.210	0.042	0.083	0.154	0.036	0.037	0.073	0.067	0.071	0.443	0.054	0.097	0.092
Total	**100.905**	**100.016**	**99.263**	**100.300**	**101.585**	**101.045**	**100.388**	**102.036**	**101.048**	**101.485**	**101.809**	**101.489**	**100.362**	**100.663**	**0.594**
formula															
Si	2.984	2.974	3.000	3.000	2.959	3.000	2.988	2.959	2.999	2.981	2.971	3.000	2.960	2.994	
Al	0.016	0.026	0.000	0.000	0.041	0.000	0.012	0.041	0.001	0.019	0.029	0.000	0.040	0.006	
Z	**3.000**	**3.000**	**3.000**	**3.000**	**3.000**	**3.000**	**3.000**	**3.000**	**3.000**	**3.000**	**3.000**	**3.000**	**3.000**	**3.000**	
Si	0.000	0.000	0.043	0.034	0.000	0.021	0.000	0.000	0.000	0.000	0.000	0.056	0.000	0.000	
Al	1.883	1.912	1.915	1.892	1.891	1.853	1.906	1.877	1.841	1.904	1.917	1.762	1.920	1.898	
Fe^{3+}	0.105	0.076	0.000	0.028	0.128	0.066	0.076	0.135	0.109	0.096	0.091	0.109	0.081	0.076	
Ti	0.016	0.024	0.023	0.009	0.017	0.030	0.017	0.017	0.031	0.014	0.015	0.039	0.023	0.023	
Y	**2.004**	**2.012**	**1.938**	**1.929**	**2.036**	**1.950**	**2.000**	**2.029**	**1.981**	**2.013**	**2.024**	**1.910**	**2.024**	**1.997**	
Mg	2.130	2.102	2.009	2.254	2.021	2.049	2.022	2.049	2.251	2.023	2.018	1.988	2.077	2.050	
Fe^{2+}	0.503	0.469	0.624	0.407	0.563	0.436	0.606	0.535	0.277	0.590	0.589	0.418	0.481	0.527	
Ca	0.358	0.407	0.349	0.370	0.369	0.524	0.367	0.383	0.481	0.365	0.360	0.567	0.410	0.412	
X	**2.991**	**2.978**	**2.982**	**3.032**	**2.953**	**3.009**	**2.996**	**2.966**	**3.009**	**2.977**	**2.967**	**2.974**	**2.969**	**2.990**	
Total	**7.995**	**7.990**	**7.962**	**7.994**	**7.989**	**7.979**	**7.995**	**7.995**	**7.990**	**7.991**	**7.990**	**7.940**	**7.993**	**7.987**	
py	71.223	70.582	65.175	72.623	68.436	67.048	67.509	69.077	74.802	67.936	68.007	63.938	69.969	68.574	
alm	16.813	15.760	20.916	13.420	19.069	14.487	20.227	18.025	9.201	19.813	19.869	14.069	16.206	17.632	
andr	5.219	3.778	0.000	1.430	6.298	3.411	3.804	6.633	5.490	4.747	4.510	5.707	3.991	3.825	
gross	6.745	9.881	11.695	10.786	6.197	13.999	8.460	6.266	10.507	7.504	7.615	13.371	9.834	9.969	
ma	0.000	0.000	2.214	1.741	0.000	1.055	0.000	0.000	0.000	0.000	0.000	2.916	0.000	0.000	
Mg#	80.902	81.747	76.314	84.712	78.208	82.460	76.946	79.306	89.047	77.420	77.390	82.615	81.194	79.547	
x(g)	0.191	0.183	0.237	0.153	0.218	0.175	0.231	0.207	0.110	0.226	0.226	0.174	0.188	0.205	

Amphibole in MAOC 11

amph	12.5 kbar/1050 °C (tschermakite)				15 kbar/900 °C (magnesiohornblende)			
MAOC 11			av	sd			av	sd
SiO_2	44.080	43.430	43.755	0.460	46.720	47.160	46.940	0.311
TiO_2	0.915	0.639	0.777	0.195	1.078	1.085	1.082	0.005
Al_2O_3	14.830	16.700	15.765	1.322	12.220	11.530	11.875	0.488
FeO	10.900	11.780	11.340	0.622	6.910	7.850	7.380	0.665
MgO	13.290	14.230	13.760	0.665	17.170	15.270	16.220	1.344
CaO	13.050	11.410	12.230	1.160	10.360	12.330	11.345	1.393
Na_2O	0.665	0.436	0.551	0.162	2.270	1.920	2.095	0.247
Total	**97.730**	**98.625**	**98.178**	**0.633**	**96.728**	**97.145**	**96.937**	**0.295**
min	15 eNK	15 eNK	15 eNK		all Fe2+	all Fe2+	all Fe2+	
max	13 eCNK	10SFe3+	15 eK		all Fe3+	13 eCNK	13 eCNK	
Si	6.287	6.072	6.160		6.602	6.747	6.665	
Al IV	1.713	1.928	1.840		1.398	1.253	1.335	
T	**8.000**	**8.000**	**8.000**		**8.000**	**8.000**	**8.000**	
Al VI	0.779	0.823	0.776		0.637	0.691	0.652	
Ti	0.098	0.067	0.082		0.115	0.117	0.115	
Fe^{3+}	0.561	0.969	0.899		0.405	0.011	0.270	
Mg	2.826	2.966	2.888		3.617	3.257	3.433	
Fe^{2+}	0.736	0.175	0.355		0.227	0.925	0.529	
C	**5.000**	**5.000**	**5.000**		**5.000**	**5.000**	**5.000**	
Fe^{2+}	0.003	0.233	0.081		0.185	0.003	0.077	
Ca	1.994	1.709	1.845		1.568	1.890	1.726	
Na	**0.003**	**0.058**	**0.075**		**0.247**	**0.107**	**0.197**	
B	**2.000**	**2.000**	**2.000**		**2.000**	**2.000**	**2.000**	
Na	0.181	0.060	0.076		0.375	0.425	0.380	
A	**0.181**	**0.060**	**0.076**		**0.375**	**0.425**	**0.380**	
Total	**15.181**	**15.060**	**15.076**		**15.375**	**15.425**	**15.380**	
Mg#	0.793	0.879	0.869		0.898	0.778	0.850	

Amphibole in MAOC 13

amph	10 kbar/1050 °C (pargasite, 1 tschermakite)													
MAOC 13												av	sd	tscherm.
SiO_2	42.130	42.390	42.200	42.000	42.770	43.440	42.430	41.500	42.250	41.120	43.120	42.305	0.662	44.540
TiO_2	0.768	0.781	0.834	0.832	0.710	0.732	1.203	0.514	1.084	0.640	0.953	0.823	0.196	0.695
Al_2O_3	16.430	16.780	16.910	17.040	17.220	16.330	16.790	17.580	16.760	17.780	15.420	16.822	0.638	15.250
FeO	5.870	6.140	6.110	5.830	5.810	5.600	5.950	4.740	5.690	4.970	5.660	5.670	0.440	6.670
MgO	17.720	17.770	17.770	17.420	17.620	17.900	17.770	17.190	17.550	17.040	18.020	17.615	0.297	19.590
CaO	10.120	10.180	10.470	10.170	10.380	10.670	10.350	12.740	10.970	13.010	11.170	10.930	1.019	8.610
Na_2O	3.230	3.290	3.310	3.550	3.390	3.210	3.440	3.080	3.500	2.940	3.330	3.297	0.180	2.840
Total	**96.268**	**97.331**	**97.604**	**96.842**	**97.900**	**97.882**	**97.933**	**97.344**	**97.804**	**97.500**	**97.673**	**97.462**	**0.511**	**98.195**
min	15 eNK	15 eNK	15 eNK	all Fe2+	all Fe2+	all Fe2+	all Fe2+	15 eNK	all Fe2+	15 eNK	15 eNK	15 eNK		15 eNK
max	all Fe3+	all Fe3+	all Fe3+	all Fe3+	all Fe3+	all Fe3+	all Fe3+	all Fe3+	all Fe3+	13 eCNK	all Fe3+	all Fe3+		all Fe3+
Si	6.018	5.994	5.955	5.972	6.006	6.095	5.970	5.868	5.961	5.810	6.085	5.978		6.195
Al IV	1.982	2.006	2.045	2.028	1.994	1.905	2.030	2.132	2.039	2.190	1.915	2.022		1.805
T	**8.000**	**8.000**	**8.000**	**8.000**	**8.000**	**8.000**	**8.000**	**8.000**	**8.000**	**8.000**	**8.000**	**8.000**		**8.000**
Al VI	0.784	0.790	0.767	0.827	0.856	0.795	0.754	0.797	0.748	0.770	0.650	0.779		0.694
Ti	0.083	0.083	0.089	0.089	0.075	0.077	0.127	0.055	0.115	0.068	0.101	0.087		0.073
Fe^{3+}	0.359	0.374	0.401	0.344	0.339	0.326	0.347	0.452	0.333	0.512	0.354	0.363		0.425
Mg	3.774	3.746	3.738	3.692	3.689	3.744	3.727	3.623	3.692	3.589	3.791	3.711		4.062
Fe^{2+}	0.001	0.007	0.005	0.048	0.042	0.057	0.044	0.073	0.112	0.061	0.104	0.060		0.000
C	**5.000**	**5.000**	**5.000**	**5.000**	**5.000**	**5.000**	**5.000**	**5.000**	**5.000**	**5.000**	**5.000**	**5.000**		**5.254**
Fe^{2+}	0.341	0.345	0.314	0.301	0.302	0.274	0.308	0.035	0.226	0.014	0.210	0.247		0.351
Ca	1.549	1.542	1.583	1.549	1.562	1.604	1.560	1.930	1.658	1.969	1.689	1.655		1.283
Na	**0.110**	**0.113**	**0.103**	**0.149**	**0.137**	**0.122**	**0.132**	**0.035**	**0.115**	**0.016**	**0.101**	**0.099**		**0.367**
B	**2.000**	**2.000**	**2.000**	**2.000**	**2.000**	**2.000**	**2.000**	**2.000**	**2.000**	**2.000**	**2.000**	**2.000**		**2.000**
Na	0.784	0.789	0.803	0.829	0.786	0.751	0.807	0.809	0.842	0.789	0.810	0.805		0.399
A	**0.784**	**0.789**	**0.803**	**0.829**	**0.786**	**0.751**	**0.807**	**0.809**	**0.842**	**0.789**	**0.810**	**0.805**		**0.399**
Total	**15.784**	**15.789**	**15.803**	**15.829**	**15.786**	**15.751**	**15.807**	**15.809**	**15.842**	**15.789**	**15.810**	**15.805**		**15.653**
Mg#	0.917	0.914	0.921	0.914	0.915	0.919	0.914	0.971	0.916	0.979	0.923	0.924		0.921

amph	12.5 kbar/	15 kbar/900 °C (tschermakite, 1 magnesiohornblende)										
MAOC 13	1050°C									av	sd	mg-hbl.
SiO_2	47.17	44.590	44.950	44.540	44.300	44.590	45.270	44.620	44.750	44.701	0.294	46.450
TiO_2	0.77	0.949	0.988	1.087	1.033	1.020	1.031	1.131	1.098	1.042	0.060	0.802
Al_2O_3	11.21	13.770	13.570	14.370	13.530	13.220	13.360	13.280	14.000	13.638	0.393	12.520
FeO	9.22	9.350	9.070	9.110	9.130	9.060	8.460	8.710	8.200	8.886	0.391	8.960
MgO	16.05	16.680	14.940	15.680	15.450	15.290	15.460	15.440	15.400	15.543	0.505	15.540
CaO	13.30	9.790	10.870	9.700	10.200	11.310	10.410	10.160	10.170	10.326	0.537	11.110
Na_2O	1.00	2.050	2.140	2.300	2.400	2.160	2.210	2.210	2.260	2.216	0.106	2.000
Total	**98.72**	**97.179**	**96.528**	**96.787**	**96.043**	**96.650**	**96.201**	**95.551**	**95.878**	**96.352**	**0.532**	**97.382**
min		15 eNK	all Fe2+	all Fe2+	all Fe2+	all Fe2+	all Fe2+	all Fe2+	all Fe2+	all Fe2+		all Fe2+
max		all Fe3+	13 eCNK	all Fe3+	all Fe3+	13 eCNK	13 eCNK	all Fe3+	all Fe3+	all Fe3+		13 eCNK
Si	formula	6.320	6.444	6.339	6.373	6.406	6.473	6.432	6.413	6.397		6.588
Al IV	calc.	1.680	1.556	1.661	1.627	1.594	1.527	1.568	1.587	1.603		1.412
T	failed	**8.000**	**8.000**	**8.000**	**8.000**	**8.000**	**8.000**	**8.000**	**8.000**	**8.000**		**8.000**
Al VI		0.621	0.736	0.749	0.667	0.644	0.724	0.689	0.777	0.697		0.681
Ti		0.101	0.107	0.116	0.112	0.110	0.111	0.123	0.118	0.112		0.086
Fe^{3+}		0.611	0.427	0.536	0.543	0.410	0.494	0.519	0.486	0.526		0.402
Mg		3.525	3.193	3.327	3.314	3.275	3.296	3.318	3.290	3.316		3.286
Fe^{2+}		0.143	0.537	0.273	0.365	0.561	0.375	0.352	0.328	0.350		0.545
C		**5.000**	**5.000**	**5.000**	**5.000**	**5.000**	**5.000**	**5.000**	**5.000**	**5.000**		**5.000**
Fe^{2+}		0.355	0.123	0.276	0.190	0.118	0.143	0.179	0.168	0.188		0.116
Ca		1.487	1.669	1.479	1.572	1.741	1.595	1.569	1.561	1.583		1.688
Na		**0.159**	**0.208**	**0.245**	**0.238**	0.141	0.263	0.251	0.270	0.229		0.196
B		**2.000**	**2.000**	**2.000**	**2.000**	**2.000**	**2.000**	**2.000**	**2.000**	**2.000**		**2.000**
Na		0.405	0.387	0.389	0.432	0.460	0.350	0.366	0.358	0.386		0.354
A		**0.405**	**0.387**	**0.389**	**0.432**	**0.460**	**0.350**	**0.366**	**0.358**	**0.386**		**0.354**
Total		**15.405**	**15.387**	**15.389**	**15.432**	**15.460**	**15.350**	**15.366**	**15.358**	**15.386**		**15.354**
Mg#		0.876	0.829	0.858	0.856	0.828	0.864	0.862	0.869	0.860		0.833

Amphibole in MAOC 15

amph	**10 kbar/1050 °C (pargasite, 1 tschermakite)**										**12.5 kbar/1050 °C (pargasite, 1 magnesiohornblende)**					
MAOC 15								**av**	**sd**	**tscherm.**						
SiO_2	42.130	42.410	42.760	42.960	43.040	42.420	42.960	42.669	0.350	44.950	41.810	42.290	41.590	41.800	41.950	41.420
TiO_2	1.082	1.304	0.818	1.720	0.637	1.197	0.878	1.091	0.360	1.186	1.388	1.457	1.830	1.483	1.476	1.790
Al_2O_3	16.780	16.920	17.490	17.130	14.960	15.770	15.230	16.326	0.995	14.820	16.860	16.500	16.780	16.480	16.500	16.360
FeO	6.010	4.310	5.600	4.340	5.370	4.950	5.040	5.089	0.630	5.530	7.290	7.250	7.470	7.370	7.770	7.590
MgO	17.400	18.100	16.490	17.590	18.370	18.000	18.680	17.804	0.724	21.330	16.170	16.350	16.000	15.660	16.810	15.980
CaO	10.870	10.640	10.150	10.510	11.090	10.340	10.290	10.556	0.335	8.310	9.520	9.180	9.590	9.440	8.750	9.390
Na_2O	3.280	3.330	2.820	3.330	3.080	3.080	3.170	3.156	0.183	2.360	3.810	3.800	4.090	3.980	3.520	3.800
Total	**97.552**	**97.014**	**96.128**	**97.580**	**96.547**	**95.757**	**96.248**	**96.689**	**0.712**	**98.486**	**96.848**	**96.827**	**97.350**	**96.213**	**96.776**	**96.330**
min	15 eNK	all Fe2+	all Fe2+	all Fe2+	15 eNK	all Fe2+	15 eNK	all Fe2+		15 eNK	all Fe2+	all Fe2+	all Fe2+	all Fe2+	all Fe2+	all Fe2+
max	all Fe3+	all Fe3+	all Fe3+	all Fe3+	all Fe3+	all Fe3+	all Fe3+	all Fe3+		all Fe3+	all Fe3+	all Fe3+	all Fe3+	all Fe3+	all Fe3+	all Fe3+
Si	5.957	5.991	6.082	6.024	6.123	6.076	6.120	6.056		6.184	5.969	6.027	5.924	6.010	5.984	5.956
Al IV	2.043	2.009	1.918	1.976	1.877	1.924	1.880	1.944		1.816	2.031	1.973	2.076	1.990	2.016	2.044
T	**8.000**	**8.000**	**8.000**	**8.000**	**8.000**	**8.000**	**8.000**	**8.000**		**8.000**	**8.000**	**8.000**	**8.000**	**8.000**	**8.000**	**8.000**
Al VI	0.753	0.809	1.014	0.854	0.632	0.738	0.677	0.786		0.587	0.805	0.798	0.740	0.802	0.758	0.729
Ti	0.115	0.139	0.088	0.181	0.068	0.129	0.094	0.116		0.123	0.149	0.156	0.196	0.160	0.158	0.194
Fe^{3+}	0.376	0.253	0.331	0.253	0.408	0.295	0.320	0.300		0.465	0.431	0.428	0.441	0.439	0.459	0.452
Mg	3.668	3.812	3.497	3.677	3.896	3.843	3.967	3.767		4.375	3.441	3.474	3.397	3.357	3.575	3.426
Fe^{2+}	0.088	0.000	0.072	0.034	0.000	0.000	0.000	0.030		0.000	0.174	0.145	0.226	0.242	0.050	0.200
C	**5.000**	**5.012**	**5.000**	**5.000**	**5.004**	**5.005**	**5.058**	**5.000**		**5.549**	**5.000**	**5.000**	**5.000**	**5.000**	**5.000**	**5.000**
Fe^{2+}	0.246	0.256	0.264	0.222	0.231	0.298	0.281	0.274		0.171	0.266	0.291	0.224	0.205	0.418	0.261
Ca	1.647	1.610	1.547	1.579	1.690	1.587	1.571	1.605		1.225	1.456	1.402	1.463	1.454	1.337	1.447
Na	0.107	0.134	0.189	0.200	0.079	0.115	0.149	0.121		0.605	0.279	0.307	0.313	0.341	0.245	0.292
B	**2.000**	**2.000**	**2.000**	**2.000**	**2.000**	**2.000**	**2.000**	**2.000**		**2.000**	**2.000**	**2.000**	**2.000**	**2.000**	**2.000**	**2.000**
Na	0.792	0.778	0.588	0.706	0.771	0.740	0.727	0.747		0.025	0.776	0.743	0.816	0.769	0.728	0.767
A	**0.792**	**0.778**	**0.588**	**0.706**	**0.771**	**0.740**	**0.727**	**0.747**		**0.025**	**0.776**	**0.743**	**0.816**	**0.769**	**0.728**	**0.767**
Total	**15.792**	**15.791**	**15.588**	**15.706**	**15.775**	**15.745**	**15.785**	**15.747**		**15.574**	**15.776**	**15.743**	**15.816**	**15.769**	**15.728**	**15.767**
Mg#	0.916	0.937	0.912	0.935	0.944	0.928	0.934	0.925		0.962	0.887	0.888	0.883	0.882	0.884	0.881

amph	**12.5 kbar/1050 °C (pargasite, 1 magnesiohornblende)**													**15 kbar/900 °C**		
MAOC 15											**av**	**sd**	**mg-hbl.**	**(tschermakite, 1 mg-hbl.)**		
SiO_2	40.440	40.980	41.700	41.860	41.480	41.290	41.700	42.010	42.650	41.560	41.658	0.507	47.41	44.100	45.150	44.500
TiO_2	1.810	1.557	1.619	1.680	1.527	1.690	1.740	1.622	1.392	1.710	1.611	0.147	0.60	1.077	0.925	0.771
Al_2O_3	17.500	18.270	17.060	16.750	16.980	16.900	16.710	16.750	16.250	16.570	16.826	0.490	14.69	14.060	14.100	15.080
FeO	7.620	7.440	7.490	7.240	7.290	7.330	7.210	7.250	7.140	7.350	7.381	0.171	8.50	8.310	7.140	7.000
MgO	15.680	16.090	16.080	16.150	15.850	16.120	15.950	15.790	16.050	15.830	16.035	0.278	15.97	15.590	16.360	15.960
CaO	9.460	9.040	9.270	9.590	9.620	9.380	9.410	9.330	9.600	9.510	9.380	0.232	11.48	10.190	10.280	10.460
Na_2O	3.870	3.880	3.840	3.720	3.870	3.840	3.800	3.800	3.860	3.800	3.830	0.118	0.89	2.570	2.450	2.360
Total	**96.380**	**97.257**	**97.059**	**96.990**	**96.617**	**96.550**	**96.520**	**96.552**	**96.942**	**96.330**	**96.721**	**0.340**	**99.55**	**95.897**	**96.405**	**96.131**
min	all Fe2+	all Fe2+	all Fe2+	all Fe2+	all Fe2+	all Fe2+	all Fe2+	all Fe2+	all Fe2+	all Fe2+	all Fe2+		15 eNK	all Fe2+	all Fe2+	all Fe2+
max	all Fe3+	all Fe3+	all Fe3+	all Fe3+	all Fe3+	all Fe3+	all Fe3+	all Fe3+	all Fe3+	all Fe3+	all Fe3+		15 eK	all Fe3+	all Fe3+	all Fe3+
Si	5.822	5.826	5.941	5.966	5.942	5.919	5.971	6.007	6.073	5.970	5.957		6.51	6.340	6.416	6.341
Al IV	2.178	2.174	2.059	2.034	2.058	2.081	2.029	1.993	1.927	2.030	2.043		1.49	1.660	1.584	1.659
T	**8.000**	**8.000**	**8.000**	**8.000**	**8.000**	**8.000**	**8.000**	**8.000**	**8.000**	**8.000**	**8.000**		**8.00**	**8.000**	**8.000**	**8.000**
Al VI	0.792	0.886	0.806	0.780	0.808	0.774	0.791	0.830	0.800	0.775	0.792		0.89	0.722	0.778	0.873
Ti	0.196	0.166	0.173	0.180	0.165	0.182	0.187	0.174	0.149	0.185	0.173		0.06	0.116	0.099	0.083
Fe^{3+}	0.454	0.438	0.442	0.427	0.432	0.435	0.428	0.429	0.421	0.437	0.437		0.48	0.494	0.420	0.413
Mg	3.366	3.410	3.415	3.432	3.385	3.445	3.405	3.366	3.407	3.390	3.418		3.27	3.341	3.466	3.390
Fe^{2+}	0.193	0.099	0.164	0.181	0.210	0.164	0.189	0.201	0.223	0.214	0.179		0.30	0.327	0.237	0.240
C	**5.000**	**5.000**	**5.000**	**5.000**	**5.000**	**5.000**	**5.000**	**5.000**	**5.000**	**5.000**	**5.000**		**5.00**	**5.000**	**5.000**	**5.000**
Fe^{2+}	0.271	0.347	0.287	0.255	0.231	0.280	0.247	0.237	0.206	0.232	0.266		0.19	0.178	0.191	0.181
Ca	1.459	1.377	1.415	1.464	1.476	1.441	1.444	1.429	1.464	1.463	1.437		1.69	1.569	1.565	1.597
Na	0.270	0.276	0.298	0.281	0.293	0.280	0.310	0.334	0.329	0.305	0.297		0.12	0.252	0.244	0.223
B	**2.000**	**2.000**	**2.000**	**2.000**	**2.000**	**2.000**	**2.000**	**2.000**	**2.000**	**2.000**	**2.000**		**2.00**	**2.000**	**2.000**	**2.000**
Na	0.810	0.793	0.763	0.747	0.782	0.787	0.745	0.719	0.737	0.754	0.765		0.12	0.464	0.431	0.429
A	**0.810**	**0.793**	**0.763**	**0.747**	**0.782**	**0.787**	**0.745**	**0.719**	**0.737**	**0.754**	**0.765**		**0.12**	**0.464**	**0.431**	**0.429**
Total	**15.810**	**15.793**	**15.763**	**15.747**	**15.782**	**15.787**	**15.745**	**15.719**	**15.737**	**15.754**	**15.765**		**15.12**	**15.464**	**15.431**	**15.429**
Mg#	0.879	0.884	0.883	0.887	0.885	0.886	0.887	0.885	0.888	0.884	0.885		0.87	0.869	0.890	0.890

amph	**15 kbar/900 °C**			**15 kbar/1100 °C (pargasite)**												
MAOC 15	**av**	**sd**	**mg-hbl.**													
SiO_2	44.583	0.530	47.62	44.500	44.230	44.100	43.810	43.250	43.910	43.640	44.500	44.980	45.930	44.950	43.520	44.170
TiO_2	0.924	0.153	0.53	1.069	1.095	1.044	0.911	0.936	0.732	0.980	1.186	0.971	1.039	1.125	1.241	1.082
Al_2O_3	14.413	0.578	11.31	15.450	16.010	15.300	16.060	17.420	16.090	16.100	15.510	15.130	13.740	15.450	15.970	15.500
FeO	7.483	0.719	8.71	2.460	2.570	3.380	2.860	2.470	2.910	2.710	2.670	2.940	3.730	3.080	2.920	2.750
MgO	15.970	0.385	20.61	20.190	19.810	19.420	19.650	19.050	19.340	18.820	20.070	19.900	20.270	20.340	19.620	19.380
CaO	10.310	0.137	7.01	9.990	10.320	9.830	10.040	10.540	10.670	10.720	10.080	9.580	8.430	9.360	9.710	10.120
Na_2O	2.460	0.105	1.66	3.820	3.850	3.800	3.880	3.520	3.750	3.620	3.760	3.610	4.060	3.920	3.680	3.620
Total	**96.144**	**0.254**	**97.45**	**97.479**	**97.885**	**96.874**	**97.211**	**97.186**	**97.402**	**96.590**	**97.776**	**97.111**	**97.199**	**98.225**	**96.661**	**96.622**
min	all Fe2+		15 eNK	all Fe2+	all Fe2+	all Fe2+	all Fe2+	all Fe2+	all Fe2+	all Fe2+	all Fe2+	all Fe2+	all Fe2+	all Fe2+	all Fe2+	all Fe2+
max	all Fe3+		all Fe3+	all Fe3+	all Fe3+	all Fe3+	all Fe3+	all Fe3+	all Fe3+	all Fe3+	all Fe3+	all Fe3+	all Fe3+	all Fe3+	all Fe3+	all Fe3+
Si	6.366		6.62	6.203	6.150	6.203	6.137	6.051	6.147	6.154	6.190	6.283	6.410	6.218	6.126	6.214
Al IV	1.634		1.38	1.797	1.850	1.797	1.863	1.949	1.853	1.846	1.810	1.717	1.590	1.782	1.874	1.786
T	**8.000**		**8.00**	**8.000**	**8.000**	**8.000**	**8.000**	**8.000**	**8.000**	**8.000**	**8.000**	**8.000**	**8.000**	**8.000**	**8.000**	**8.000**
Al VI	0.791		0.48	0.741	0.773	0.739	0.789	0.924	0.801	0.830	0.732	0.773	0.670	0.736	0.775	0.784
Ti	0.099		0.06	0.112	0.115	0.110	0.096	0.098	0.077	0.104	0.124	0.102	0.109	0.117	0.131	0.114
Fe^{3+}	0.442		0.60	0.143	0.149	0.198	0.167	0.144	0.170	0.159	0.155	0.171	0.217	0.177	0.171	0.161
Mg	3.399		4.27	4.196	4.106	4.072	4.104	3.974	4.036	3.957	4.162	4.144	4.218	4.195	4.117	4.065
Fe^{2+}	0.268		0.00	0.000	0.000	0.000	0.000	0.000	0.000	0.000	0.000	0.000	0.000	0.000	0.000	0.000
C	**5.000**		**5.41**	**5.192**	**5.143**	**5.120**	**5.156**	**5.140**	**5.084**	**5.050**	**5.173**	**5.190**	**5.214**	**5.226**	**5.194**	**5.124**
Fe^{2+}	0.183		0.41	0.144	0.150	0.200	0.168	0.145	0.171	0.160	0.156	0.172	0.219	0.179	0.172	0.162
Ca	1.577		1.04	1.492	1.537	1.481	1.507	1.580	1.600	1.620	1.502	1.434	1.260	1.387	1.464	1.525
Na	0.239		0.45	0.364	0.313	0.319	0.325	0.275	0.229	0.220	0.342	0.394	0.521	0.434	0.363	0.312
B	**2.000**		**1.91**	**2.000**	**2.000**	**2.000**	**2.000**	**2.000**	**2.000**	**2.000**	**2.000**	**2.000**	**2.000**	**2.000**	**2.000**	**2.000**
Na	0.442		0.00	0.668	0.725	0.717	0.729	0.680	0.789	0.770	0.672	0.583	0.578	0.617	0.641	0.675
A	**0.442**		**0.00**	**0.668**	**0.725**	**0.717**	**0.729**	**0.680**	**0.789**	**0.770**	**0.672**	**0.583**	**0.578**	**0.617**	**0.641**	**0.675**
Total	**15.442**		**15.32**	**15.860**	**15.868**	**15.837**	**15.884**	**15.819**	**15.873**	**15.819**	**15.845**	**15.773**	**15.791**	**15.843**	**15.835**	**15.799**
Mg#	0.883		0.91	0.967	0.965	0.953	0.961	0.965	0.959	0.961	0.964	0.960	0.951	0.959	0.960	0.962

amph	15 kbar/1100 °C (pargasite)					
MAOC 15					av	sd
SiO_2	43.790	44.280	42.530	43.330	44.084	0.781
TiO_2	1.325	1.003	0.807	1.199	1.044	0.151
Al_2O_3	15.500	14.860	17.680	15.820	15.741	0.893
FeO	2.670	3.420	2.420	2.680	2.861	0.365
MgO	19.970	19.610	19.270	19.530	19.661	0.429
CaO	9.760	9.780	11.240	9.850	10.001	0.623
Na_2O	3.780	3.690	3.620	3.740	3.748	0.135
Total	**96.795**	**96.643**	**97.567**	**96.149**	**97.140**	**0.544**
min	all Fe2+	all Fe2+	all Fe2+	all Fe2+	all Fe2+	
max	all Fe3+	all Fe3+	all Fe3+	all Fe3+	all Fe3+	
Si	6.154	6.240	5.952	6.132	6.175	
Al IV	1.846	1.760	2.048	1.868	1.825	
T	**8.000**	**8.000**	**8.000**	**8.000**	**8.000**	
Al VI	0.721	0.709	0.869	0.770	0.773	
Ti	0.140	0.106	0.085	0.128	0.110	
Fe^{3+}	0.156	0.201	0.141	0.158	0.167	
Mg	4.184	4.120	4.021	4.120	4.105	
Fe^{2+}	0.000	0.000	0.000	0.000	0.000	
C	**5.202**	**5.136**	**5.115**	**5.177**	**5.155**	
Fe^{2+}	0.157	0.202	0.142	0.159	0.168	
Ca	1.470	1.477	1.685	1.493	1.501	
Na	0.373	0.321	0.173	0.347	0.331	
B	**2.000**	**2.000**	**2.000**	**2.000**	**2.000**	
Na	0.657	0.687	0.810	0.679	0.687	
A	**0.657**	**0.687**	**0.810**	**0.679**	**0.687**	
Total	**15.859**	**15.823**	**15.925**	**15.855**	**15.842**	
Mg#	0.964	0.953	0.966	0.963	0.961	

Clinopyroxene in MAOC 11

cpx	10 kbar/1050 °C												10 kbar/1100 °C		
MAOC 11											av	sd			
SiO_2	48.450	49.670	49.210	48.400	48.010	46.740	49.710	49.140	49.190	49.260	49.490	48.843	0.885	48.670	49.600	47.390
TiO_2	0.886	0.790	0.940	0.757	0.863	1.266	0.808	0.875	0.862	0.781	0.781	0.874	0.142	1.227	1.089	1.262
Al_2O_3	9.090	9.520	9.890	9.240	9.360	9.280	9.390	9.550	10.080	9.520	9.120	9.458	0.305	8.160	8.580	9.800
FeO	6.850	4.770	5.070	6.110	5.100	6.050	3.580	4.320	4.130	4.030	4.100	4.919	1.036	6.050	5.420	7.000
MgO	14.550	14.970	14.890	14.430	15.640	14.350	15.230	15.770	14.670	14.980	15.500	14.998	0.488	15.410	16.230	13.770
CaO	19.190	20.400	19.470	19.590	18.370	19.930	20.250	19.550	19.770	18.930	20.150	19.600	0.604	18.330	17.170	18.260
Na_2O	0.707	0.752	0.841	0.747	0.686	0.549	0.717	0.739	0.815	0.802	0.801	0.741	0.080	0.771	0.695	0.710
Total	**99.723**	**100.872**	**100.311**	**99.274**	**98.029**	**98.165**	**99.685**	**99.944**	**99.517**	**98.303**	**99.942**	**99.433**	**0.916**	**98.618**	**98.784**	**98.192**
formula															
Si	1.775	1.787	1.781	1.777	1.772	1.739	1.804	1.777	1.791	1.810	1.791	1.783		1.796	1.816	1.767
Al IV	0.225	0.213	0.219	0.223	0.228	0.261	0.196	0.223	0.209	0.190	0.209	0.217		0.204	0.184	0.233
Z	**2.000**	**2.000**	**2.000**	**2.000**	**2.000**	**2.000**	**2.000**	**2.000**	**2.000**	**2.000**	**2.000**	**2.000**		**2.000**	**2.000**	**2.000**
Al VI	0.168	0.190	0.203	0.177	0.179	0.146	0.206	0.185	0.224	0.222	0.179	0.190		0.151	0.187	0.198
Fe^{3+}	0.059	0.031	0.023	0.056	0.048	0.085	0.000	0.042	0.000	0.000	0.043	0.031		0.039	0.000	0.013
Ti	0.024	0.021	0.026	0.021	0.024	0.035	0.022	0.024	0.024	0.022	0.021	0.024		0.034	0.030	0.035
Mg	0.795	0.803	0.804	0.790	0.860	0.796	0.824	0.850	0.796	0.821	0.836	0.816		0.848	0.886	0.766
Fe^{2+}	0.151	0.112	0.130	0.131	0.109	0.104	0.109	0.089	0.126	0.124	0.081	0.119		0.147	0.166	0.205
Ca	0.753	0.786	0.755	0.771	0.726	0.794	0.787	0.758	0.771	0.745	0.781	0.767		0.725	0.674	0.730
Na	0.050	0.052	0.059	0.053	0.049	0.040	0.050	0.052	0.058	0.057	0.056	0.052		0.055	0.049	0.051
X	**2.000**	**1.997**	**2.000**	**2.000**	**1.996**	**1.999**	**1.998**	**1.999**	**1.998**	**1.991**	**1.998**	**2.000**		**2.000**	**1.992**	**1.999**
Total	**4.000**	**3.997**	**4.000**	**4.000**	**3.996**	**3.999**	**3.998**	**3.999**	**3.998**	**3.991**	**3.998**	**4.000**		**4.000**	**3.992**	**3.999**
En	46.772	47.182	47.577	46.691	50.729	46.982	47.904	50.123	47.025	48.564	49.225	47.955		49.294	51.343	45.031
Fs	8.891	6.606	7.710	7.751	6.446	6.121	6.317	5.218	7.426	7.329	4.781	7.004		8.563	9.618	12.051
Wo	44.337	46.212	44.713	45.558	42.825	46.897	45.779	44.659	45.548	44.108	45.994	45.042		42.142	39.039	42.918
Mg#	84.027	87.718	86.054	85.762	88.725	88.473	88.350	90.571	86.362	86.888	91.147	87.256		85.199	84.223	78.888
Q	1.699	1.702	1.689	1.692	1.696	1.694	1.720	1.697	1.693	1.690	1.698	1.702		1.720	1.726	1.700
J	0.100	0.105	0.118	0.106	0.098	0.079	0.101	0.104	0.115	0.114	0.112	0.105		0.110	0.099	0.103

cpx	10 kbar/1100°C												12.5 kbar/1050°C			
MAOC 11											av	sd				
SiO_2	48.120	48.310	47.850	47.500	48.960	48.280	48.710	47.580	49.220	48.100	48.330	0.679	46.760	47.530	47.520	46.490
TiO_2	1.135	1.109	1.371	1.013	0.787	0.879	0.924	1.125	0.870	1.352	1.088	0.187	1.420	0.861	1.003	0.994
Al_2O_3	9.190	8.690	10.630	8.120	8.750	9.270	9.010	8.500	8.670	9.130	8.962	0.682	10.750	11.410	10.800	11.140
FeO	6.510	6.300	4.810	6.920	5.260	6.530	6.550	7.810	5.400	5.590	6.165	0.843	8.500	8.590	8.320	9.210
MgO	14.740	15.080	13.980	15.020	15.550	14.970	14.310	13.780	15.350	14.630	14.832	0.734	12.180	12.130	12.100	12.240
CaO	18.350	18.380	19.210	19.070	18.710	17.930	18.390	19.430	18.380	18.910	18.502	0.588	18.420	17.250	18.410	18.120
Na_2O	0.676	0.691	0.587	0.333	0.645	0.785	0.634	0.457	0.650	0.531	0.628	0.126	1.145	1.325	1.140	0.976
Total	**98.721**	**98.560**	**98.438**	**97.976**	**98.662**	**98.644**	**98.528**	**98.682**	**98.540**	**98.243**	**98.507**	**0.236**	**99.175**	**99.096**	**99.293**	**99.170**
formula																
Si	1.779	1.785	1.766	1.774	1.800	1.781	1.805	1.775	1.813	1.786	1.790		1.736	1.761	1.761	1.728
Al IV	0.221	0.215	0.234	0.226	0.200	0.219	0.195	0.225	0.187	0.214	0.210		0.264	0.239	0.239	0.272
Z	**2.000**	**2.000**	**2.000**	**2.000**	**2.000**	**2.000**	**2.000**	**2.000**	**2.000**	**2.000**	**2.000**		**2.000**	**2.000**	**2.000**	**2.000**
Al VI	0.179	0.164	0.228	0.131	0.179	0.184	0.199	0.149	0.190	0.185	0.181		0.206	0.260	0.232	0.216
Fe^{3+}	0.027	0.038	0.000	0.062	0.021	0.042	0.000	0.046	0.000	0.000	0.014		0.061	0.026	0.032	0.071
Ti	0.032	0.031	0.038	0.028	0.022	0.024	0.026	0.032	0.024	0.038	0.030		0.040	0.024	0.028	0.028
Mg	0.812	0.831	0.769	0.836	0.852	0.823	0.791	0.766	0.843	0.810	0.819		0.674	0.670	0.668	0.678
Fe^{2+}	0.174	0.157	0.148	0.154	0.141	0.160	0.203	0.197	0.166	0.174	0.177		0.203	0.240	0.226	0.215
Ca	0.727	0.728	0.760	0.763	0.737	0.709	0.730	0.777	0.725	0.752	0.734		0.733	0.685	0.731	0.722
Na	0.048	0.050	0.042	0.024	0.046	0.056	0.046	0.033	0.046	0.038	0.045		0.082	0.095	0.082	0.070
X	**2.000**	**1.997**	**1.986**	**1.999**	**1.998**	**1.998**	**1.994**	**2.000**	**1.995**	**1.996**	**2.000**		**1.999**	**2.000**	**1.999**	**2.000**
Total	**4.000**	**3.997**	**3.986**	**3.999**	**3.998**	**3.998**	**3.994**	**4.000**	**3.995**	**3.996**	**4.000**		**3.999**	**4.000**	**3.999**	**4.000**
En	47.406	48.429	45.859	47.703	49.269	48.668	45.863	44.032	48.592	46.656	47.335		41.887	42.015	41.133	41.992
Fs	10.177	9.146	8.851	8.766	8.124	9.436	11.776	11.345	9.589	10.000	10.228		12.585	15.042	13.887	13.328
Wo	42.417	42.424	45.290	43.531	42.607	41.896	42.361	44.623	41.819	43.343	42.437		45.528	42.943	44.980	44.680
Mg#	82.326	84.114	83.822	84.477	85.844	83.760	79.570	79.513	83.519	82.350	82.231		76.896	73.636	74.759	75.908
Q	1.714	1.715	1.677	1.753	1.730	1.692	1.724	1.740	1.735	1.735	1.730		1.609	1.595	1.625	1.615
J	0.097	0.099	0.084	0.048	0.092	0.112	0.091	0.066	0.093	0.076	0.090		0.165	0.190	0.164	0.141

cpx	12.5 kbar/1050 °C								12.5 kbar/1100 °C							
MAOC 11							av	sd								
SiO_2	47.360	46.820	49.180	50.000	47.260	46.480	47.540	1.165	48.785	48.911	48.074	47.682	49.535	48.138	48.021	48.063
TiO_2	1.210	1.465	1.017	0.942	0.741	1.176	1.083	0.233	0.933	0.776	1.213	0.930	0.730	0.872	0.949	0.652
Al_2O_3	9.820	9.570	11.810	11.020	9.330	8.810	10.446	0.994	9.450	8.880	9.130	11.140	9.160	10.190	10.050	9.870
FeO	8.290	8.360	7.650	7.550	7.550	9.510	8.353	0.662	6.750	6.830	7.780	6.420	6.580	6.810	7.970	7.270
MgO	12.750	12.780	11.550	12.500	13.340	13.360	12.493	0.573	14.220	13.730	13.200	13.080	13.660	13.450	14.460	13.530
CaO	18.000	19.380	17.890	17.510	20.640	18.410	18.403	0.977	17.360	18.480	18.390	18.520	18.040	18.260	16.740	17.990
Na_2O	0.999	0.873	1.590	1.440	0.590	0.600	1.068	0.331	0.990	0.969	0.706	1.016	1.170	0.914	0.770	0.964
Total	**98.429**	**99.248**	**100.687**	**100.962**	**99.451**	**98.346**	**99.386**	**0.842**	**98.488**	**98.576**	**98.493**	**98.788**	**98.875**	**98.634**	**98.960**	**98.339**
formula																
Si	1.769	1.739	1.787	1.807	1.746	1.745	1.760		1.806	1.814	1.795	1.762	1.827	1.785	1.774	1.787
Al IV	0.231	0.261	0.213	0.193	0.254	0.255	0.240		0.194	0.186	0.205	0.238	0.173	0.215	0.226	0.213
Z	**2.000**	**2.000**	**2.000**	**2.000**	**2.000**	**2.000**	**2.000**		**2.000**	**2.000**	**2.000**	**2.000**	**2.000**	**2.000**	**2.000**	**2.000**
Al VI	0.202	0.158	0.292	0.277	0.152	0.134	0.215		0.218	0.202	0.196	0.247	0.225	0.230	0.212	0.220
Fe^{3+}	0.031	0.084	0.000	0.000	0.103	0.096	0.041		0.000	0.009	0.000	0.010	0.000	0.002	0.017	0.026
Ti	0.034	0.041	0.028	0.026	0.021	0.033	0.030		0.026	0.022	0.034	0.026	0.020	0.024	0.026	0.018
Mg	0.710	0.708	0.626	0.674	0.735	0.748	0.689		0.785	0.759	0.735	0.721	0.751	0.743	0.796	0.750
Fe^{2+}	0.228	0.175	0.232	0.228	0.130	0.203	0.217		0.209	0.203	0.243	0.188	0.203	0.209	0.229	0.200
Ca	0.720	0.771	0.696	0.678	0.817	0.740	0.730		0.689	0.734	0.736	0.733	0.713	0.725	0.663	0.717
Na	0.072	0.063	0.112	0.101	0.042	0.044	0.077		0.071	0.070	0.051	0.073	0.084	0.066	0.055	0.069
X	**1.998**	**2.000**	**1.987**	**1.983**	**2.000**	**1.998**	**2.000**		**1.997**	**1.999**	**1.994**	**1.998**	**1.996**	**2.000**	**1.998**	**2.000**
Total	**3.998**	**4.000**	**3.987**	**3.983**	**4.000**	**3.998**	**4.000**		**3.997**	**3.999**	**3.994**	**3.998**	**3.996**	**4.000**	**3.998**	**4.000**
En	42.813	42.778	40.245	42.633	43.679	44.222	42.123		46.648	44.752	42.883	43.876	45.057	44.312	47.171	45.007
Fs	13.746	10.598	14.953	14.445	7.749	11.981	13.281		12.421	11.956	14.178	11.474	12.175	12.451	13.580	11.983
Wo	43.441	46.624	44.803	42.923	48.572	43.797	44.597		40.931	43.292	42.939	44.650	42.768	43.238	39.249	43.010
Mg#	75.695	80.145	72.911	74.693	84.933	78.683	76.029		78.972	78.916	75.153	79.269	78.727	78.065	77.646	78.973
Q	1.659	1.654	1.554	1.580	1.682	1.691	1.637		1.682	1.696	1.713	1.642	1.667	1.678	1.688	1.666
J	0.145	0.126	0.224	0.202	0.085	0.087	0.153		0.142	0.139	0.102	0.146	0.167	0.131	0.110	0.139

cpx	12.5 kbar/1100 °C										15 kbar/900 °C					
MAOC 11									av	sd						
SiO_2	47.786	47.346	48.699	47.843	48.066	48.969	47.982	48.775	48.292	0.583	47.950	49.490	47.100	49.130	48.900	50.550
TiO_2	1.221	1.015	1.028	1.145	0.986	1.045	0.995	0.990	0.968	0.158	0.831	0.662	0.649	0.793	0.939	0.640
Al_2O_3	8.830	10.640	11.010	9.570	8.940	9.480	9.830	9.650	9.739	0.722	8.120	11.060	7.410	9.540	9.180	7.750
FeO	8.160	6.680	6.860	7.110	7.540	6.920	7.580	6.980	7.140	0.520	8.770	7.510	8.730	7.520	8.860	6.630
MgO	13.700	13.590	13.760	13.560	13.970	13.940	13.260	13.720	13.677	0.358	16.160	14.750	14.910	13.920	14.270	13.260
CaO	17.830	16.410	15.610	17.650	18.210	17.570	17.620	17.530	17.638	0.800	16.980	15.570	19.430	15.930	16.420	18.390
Na_2O	0.715	1.064	0.912	0.955	0.772	0.846	0.899	1.069	0.921	0.133	0.495	0.975	0.329	1.118	0.803	0.895
Total	**98.242**	**96.745**	**97.879**	**97.833**	**98.484**	**98.770**	**98.166**	**98.714**	**98.374**	**0.539**	**99.306**	**100.017**	**98.558**	**97.951**	**99.372**	**98.115**
formula																
Si	1.789	1.781	1.800	1.790	1.788	1.807	1.792	1.804	1.795		1.764	1.795	1.756	1.824	1.805	1.876
Al IV	0.211	0.219	0.200	0.210	0.212	0.193	0.208	0.196	0.205		0.236	0.205	0.244	0.176	0.195	0.124
Z	**2.000**	**2.000**	**2.000**	**2.000**	**2.000**	**2.000**	**2.000**	**2.000**	**2.000**		**2.000**	**2.000**	**2.000**	**2.000**	**2.000**	**2.000**
Al VI	0.179	0.252	0.280	0.212	0.180	0.219	0.224	0.225	0.222		0.116	0.268	0.081	0.242	0.205	0.215
Fe^{3+}	0.016	0.000	0.000	0.003	0.032	0.000	0.000	0.000	0.000		0.109	0.000	0.150	0.000	0.000	0.000
Ti	0.034	0.029	0.029	0.032	0.028	0.029	0.028	0.028	0.027		0.023	0.018	0.018	0.022	0.026	0.018
Mg	0.765	0.762	0.758	0.756	0.775	0.767	0.738	0.757	0.758		0.886	0.798	0.829	0.771	0.785	0.734
Fe^{2+}	0.240	0.210	0.212	0.220	0.203	0.214	0.237	0.216	0.222		0.161	0.228	0.122	0.234	0.274	0.206
Ca	0.715	0.661	0.618	0.707	0.726	0.695	0.705	0.695	0.703		0.669	0.605	0.776	0.634	0.649	0.731
Na	0.052	0.078	0.065	0.069	0.056	0.061	0.065	0.077	0.066		0.035	0.069	0.024	0.080	0.057	0.064
X	**2.000**	**1.992**	**1.963**	**1.999**	**1.999**	**1.984**	**1.997**	**1.996**	**1.998**		**1.999**	**1.985**	**2.000**	**1.982**	**1.997**	**1.969**
Total	**4.000**	**3.992**	**3.963**	**3.999**	**3.999**	**3.984**	**3.997**	**3.996**	**3.998**		**3.999**	**3.985**	**4.000**	**3.982**	**3.997**	**3.969**
En	44.464	46.651	47.732	44.920	45.490	45.780	43.942	45.378	45.050		51.635	48.917	47.994	47.047	45.971	43.912
Fs	13.944	12.863	13.349	13.056	11.891	12.748	14.091	12.950	13.193		9.370	13.971	7.054	14.257	16.011	12.316
Wo	41.592	40.487	38.919	42.023	42.618	41.472	41.967	41.672	41.757		38.995	37.112	44.952	38.696	38.018	43.771
Mg#	76.127	78.387	78.146	77.480	79.277	78.219	75.719	77.798	77.349		84.641	77.784	87.186	76.743	74.168	78.096
Q	1.720	1.633	1.589	1.683	1.703	1.675	1.680	1.667	1.682		1.716	1.630	1.726	1.638	1.708	1.671
J	0.104	0.155	0.131	0.139	0.111	0.121	0.130	0.153	0.133		0.071	0.137	0.048	0.161	0.115	0.129

cpx	15 kbar/900 °C						15 kbar/1050 °C									
MAOC 11					av	sd										
SiO_2	50.440	50.640	47.170	49.570	49.094	1.322	49.920	49.470	49.880	49.090	47.920	47.260	49.430	49.480	48.650	50.460
TiO_2	0.561	0.603	0.598	0.625	0.690	0.122	0.708	0.849	0.692	0.887	0.825	0.804	1.089	0.858	0.807	0.804
Al_2O_3	7.590	6.780	8.140	7.940	8.351	1.247	10.450	10.950	9.780	10.630	12.890	13.490	9.700	11.380	11.650	10.470
FeO	6.190	5.940	9.130	6.620	7.590	1.213	6.090	6.150	6.340	7.530	7.090	7.890	7.000	6.790	6.550	5.200
MgO	13.840	14.170	15.130	14.840	14.525	0.814	11.940	11.440	12.460	12.360	11.230	12.610	13.060	11.760	11.720	12.940
CaO	18.910	19.090	18.600	17.820	17.714	1.395	19.020	18.500	19.120	17.830	17.380	15.910	18.320	18.070	18.530	19.170
Na_2O	1.067	0.962	0.473	0.768	0.789	0.271	1.730	1.770	1.540	1.480	1.740	1.242	1.281	1.820	1.550	1.560
Total	**98.598**	**98.185**	**99.241**	**98.183**	**98.753**	**0.690**	**99.858**	**99.129**	**99.812**	**99.807**	**99.075**	**99.206**	**99.880**	**100.158**	**99.457**	**100.604**
formula																
Si	1.865	1.880	1.742	1.840	1.819		1.823	1.818	1.825	1.801	1.765	1.737	1.810	1.802	1.785	1.820
Al IV	0.135	0.120	0.258	0.160	0.181		0.177	0.182	0.175	0.199	0.235	0.263	0.190	0.198	0.215	0.180
Z	**2.000**	**2.000**	**2.000**	**2.000**	**2.000**		**2.000**	**2.000**	**2.000**	**2.000**	**2.000**	**2.000**	**2.000**	**2.000**	**2.000**	**2.000**
Al VI	0.196	0.176	0.097	0.188	0.184		0.272	0.292	0.247	0.260	0.325	0.321	0.229	0.290	0.289	0.265
Fe^{3+}	0.000	0.000	0.161	0.000	0.016		0.000	0.000	0.000	0.000	0.000	0.000	0.000	0.000	0.000	0.000
Ti	0.016	0.017	0.017	0.017	0.019		0.019	0.023	0.019	0.024	0.023	0.022	0.030	0.024	0.022	0.022
Mg	0.763	0.784	0.833	0.821	0.802		0.650	0.627	0.680	0.676	0.617	0.691	0.713	0.638	0.641	0.696
Fe^{2+}	0.191	0.184	0.121	0.206	0.219		0.186	0.189	0.194	0.231	0.218	0.242	0.214	0.207	0.201	0.157
Ca	0.749	0.759	0.736	0.709	0.703		0.744	0.728	0.750	0.701	0.686	0.626	0.719	0.705	0.729	0.741
Na	0.076	0.069	0.034	0.055	0.057		0.122	0.126	0.109	0.105	0.124	0.088	0.091	0.129	0.110	0.109
X	**1.991**	**1.990**	**1.999**	**1.996**	**2.000**		**1.994**	**1.985**	**1.999**	**1.998**	**1.993**	**1.991**	**1.996**	**1.993**	**1.993**	**1.989**
Total	**3.991**	**3.990**	**3.999**	**3.996**	**4.000**		**3.994**	**3.985**	**3.999**	**3.998**	**3.993**	**3.991**	**3.996**	**3.993**	**3.993**	**3.989**
En	44.785	45.384	49.302	47.320	46.511		41.135	40.587	41.870	42.042	40.544	44.291	43.311	41.182	40.819	43.665
Fs	11.236	10.672	7.137	11.841	12.721		11.769	12.239	11.951	14.368	14.359	15.545	13.022	13.338	12.797	9.843
Wo	43.979	43.944	43.561	40.839	40.768		47.096	47.173	46.179	43.590	45.098	40.164	43.667	45.480	46.384	46.492
Mg#	79.943	80.962	87.355	79.985	78.523		77.754	76.831	77.795	74.530	73.847	74.020	76.884	75.535	76.132	81.605
Q	1.703	1.728	1.690	1.736	1.725		1.580	1.544	1.624	1.608	1.521	1.560	1.646	1.550	1.571	1.593
J	0.153	0.138	0.068	0.111	0.113		0.245	0.252	0.219	0.211	0.249	0.177	0.182	0.257	0.221	0.218

cpx	15 kbar/1050 °C									15 kbar/1100 °C						
MAOC 11								av	sd							
SiO_2	48.780	47.040	51.520	52.010	51.690	48.990	52.650	49.661	1.604	50.430	51.430	49.560	50.710	50.420	49.370	50.030
TiO_2	1.237	0.907	0.832	0.663	0.448	0.875	0.721	0.824	0.171	0.954	0.592	0.819	0.696	0.855	0.589	0.675
Al_2O_3	10.200	13.840	9.340	8.700	5.640	11.910	11.120	10.714	1.923	9.240	9.030	10.260	10.220	11.020	12.250	11.270
FeO	6.340	7.310	5.710	5.460	6.570	6.240	6.500	6.515	0.713	5.060	4.320	5.450	2.970	3.670	3.130	3.660
MgO	12.730	11.050	13.320	13.020	15.410	11.730	11.690	12.381	1.040	15.290	14.510	14.250	14.240	14.020	13.430	13.090
CaO	19.360	17.600	17.450	18.220	19.100	18.600	17.230	18.201	0.899	18.070	18.370	18.000	19.300	18.310	19.220	19.830
Na_2O	0.969	1.540	1.660	1.690	1.039	1.530	1.870	1.530	0.261	1.140	1.560	1.249	1.450	1.400	1.390	1.680
Total	**99.616**	**99.287**	**99.832**	**99.763**	**99.897**	**99.875**	**101.781**	**99.826**	**0.635**	**100.184**	**99.812**	**99.588**	**99.586**	**99.695**	**99.379**	**100.235**
formula																
Si	1.791	1.733	1.864	1.885	1.885	1.787	1.867	1.812		1.821	1.857	1.804	1.829	1.816	1.785	1.803
Al IV	0.209	0.267	0.136	0.115	0.115	0.213	0.133	0.188		0.179	0.143	0.196	0.171	0.184	0.215	0.197
Z	**2.000**	**2.000**	**2.000**	**2.000**	**2.000**	**2.000**	**2.000**	**2.000**		**2.000**	**2.000**	**2.000**	**2.000**	**2.000**	**2.000**	**2.000**
Al VI	0.232	0.334	0.262	0.257	0.128	0.298	0.331	0.273		0.214	0.241	0.245	0.264	0.284	0.307	0.282
Fe^{3+}	0.000	0.000	0.000	0.000	0.034	0.000	0.000	0.000		0.000	0.000	0.000	0.000	0.000	0.000	0.000
Ti	0.034	0.025	0.023	0.018	0.012	0.024	0.019	0.023		0.026	0.016	0.022	0.019	0.023	0.016	0.018
Mg	0.697	0.607	0.718	0.704	0.838	0.638	0.618	0.673		0.823	0.781	0.773	0.766	0.753	0.724	0.703
Fe^{2+}	0.195	0.225	0.173	0.165	0.166	0.190	0.193	0.199		0.153	0.130	0.166	0.090	0.111	0.095	0.110
Ca	0.762	0.695	0.676	0.708	0.746	0.727	0.654	0.712		0.699	0.711	0.702	0.746	0.707	0.745	0.766
Na	0.069	0.110	0.116	0.119	0.073	0.108	0.129	0.108		0.080	0.109	0.088	0.101	0.098	0.097	0.117
X	**1.989**	**1.996**	**1.969**	**1.970**	**1.998**	**1.985**	**1.944**	**1.988**		**1.995**	**1.988**	**1.998**	**1.985**	**1.975**	**1.983**	**1.997**
Total	**3.989**	**3.996**	**3.969**	**3.970**	**3.998**	**3.985**	**3.944**	**3.988**		**3.995**	**3.988**	**3.998**	**3.985**	**3.975**	**3.983**	**3.997**
En	42.151	39.748	45.829	44.623	47.862	41.016	42.172	42.521		49.139	48.148	47.116	47.821	47.950	46.311	44.531
Fs	11.776	14.750	11.020	10.497	9.502	12.240	13.154	12.552		9.122	8.041	10.108	5.595	7.041	6.054	6.984
Wo	46.073	45.502	43.151	44.880	42.637	46.745	44.674	44.927		41.739	43.811	42.775	46.584	45.009	47.635	48.485
Mg#	78.163	72.935	80.615	80.956	83.436	77.017	76.225	77.208		84.343	85.689	82.336	89.526	87.196	88.438	86.442
Q	1.653	1.527	1.568	1.577	1.751	1.555	1.465	1.584		1.675	1.622	1.641	1.601	1.570	1.563	1.579
J	0.138	0.220	0.233	0.238	0.147	0.216	0.257	0.217		0.160	0.218	0.176	0.203	0.196	0.195	0.235

cpx	15 kbar/1100 °C							20 kbar/1050 °C								
MAOC 11						av	sd									
SiO_2	49.720	50.300	48.970	50.230	50.130	50.108	0.651	49.680	51.670	49.980	49.560	48.980	48.630	49.980	49.420	49.020
TiO_2	0.913	0.545	0.634	0.577	0.620	0.706	0.142	0.811	0.711	0.764	0.586	0.738	0.610	0.900	0.690	0.586
Al_2O_3	12.130	11.080	12.040	10.850	10.610	10.833	1.043	12.150	9.240	11.990	13.080	9.470	12.750	11.030	12.220	12.860
FeO	2.530	4.200	4.730	3.420	4.170	3.943	0.875	5.710	5.950	5.700	5.960	7.690	6.860	5.920	6.090	6.210
MgO	13.150	14.000	12.400	13.590	13.480	13.788	0.761	10.970	12.590	11.450	11.430	13.790	11.840	12.540	11.240	11.320
CaO	19.860	18.420	18.890	19.300	19.170	18.895	0.649	17.420	17.520	17.490	16.390	17.410	16.040	17.140	17.440	16.440
Na_2O	1.680	1.410	1.540	1.650	1.279	1.452	0.176	2.310	2.150	1.970	2.160	0.994	1.890	1.830	2.130	2.170
Total	**99.983**	**99.955**	**99.204**	**99.617**	**99.459**	**99.725**	**0.318**	**99.051**	**99.831**	**99.344**	**99.166**	**99.072**	**98.620**	**99.340**	**99.230**	**98.606**
formula																
Si	1.788	1.812	1.788	1.816	1.819	1.812		1.817	1.874	1.819	1.803	1.808	1.789	1.821	1.807	1.800
Al IV	0.212	0.188	0.212	0.184	0.181	0.188		0.183	0.126	0.181	0.197	0.192	0.211	0.179	0.193	0.200
Z	**2.000**	**2.000**	**2.000**	**2.000**	**2.000**	**2.000**		**2.000**	**2.000**	**2.000**	**2.000**	**2.000**	**2.000**	**2.000**	**2.000**	**2.000**
Al VI	0.302	0.282	0.306	0.278	0.272	0.274		0.340	0.269	0.334	0.364	0.220	0.341	0.294	0.334	0.356
Fe^{3+}	0.000	0.000	0.000	0.000	0.000	0.000		0.000	0.000	0.000	0.000	0.000	0.000	0.000	0.000	0.000
Ti	0.025	0.015	0.017	0.016	0.017	0.019		0.022	0.019	0.021	0.016	0.020	0.017	0.025	0.019	0.016
Mg	0.705	0.752	0.675	0.732	0.729	0.743		0.598	0.681	0.621	0.620	0.759	0.649	0.681	0.613	0.619
Fe^{2+}	0.076	0.127	0.144	0.103	0.127	0.119		0.175	0.180	0.174	0.181	0.237	0.211	0.180	0.186	0.191
Ca	0.765	0.711	0.739	0.748	0.745	0.732		0.682	0.681	0.682	0.639	0.688	0.632	0.669	0.683	0.647
Na	0.117	0.098	0.109	0.116	0.090	0.102		0.164	0.151	0.139	0.152	0.071	0.135	0.129	0.151	0.154
X	**1.989**	**1.985**	**1.990**	**1.993**	**1.980**	**1.989**		**1.981**	**1.982**	**1.971**	**1.973**	**1.996**	**1.985**	**1.978**	**1.986**	**1.983**
Total	**3.989**	**3.985**	**3.990**	**3.993**	**3.980**	**3.989**		**3.981**	**3.982**	**3.971**	**3.973**	**3.996**	**3.985**	**3.978**	**3.986**	**3.983**
En	45.591	47.305	43.311	46.256	45.545	46.612		41.096	44.145	42.068	43.046	45.041	43.503	44.500	41.337	42.525
Fs	4.920	7.961	9.268	6.530	7.903	7.477		11.999	11.703	11.747	12.591	14.089	14.139	11.784	12.564	13.086
Wo	49.488	44.734	47.421	47.214	46.552	45.912		46.904	44.152	46.185	44.364	40.870	42.358	43.716	46.099	44.388
Mg#	90.259	85.596	82.374	87.630	85.213	86.177		77.400	79.045	78.171	77.369	76.172	75.471	79.063	76.691	76.468
Q	1.546	1.589	1.558	1.583	1.601	1.594		1.455	1.542	1.477	1.440	1.684	1.492	1.530	1.482	1.457
J	0.234	0.197	0.218	0.231	0.180	0.204		0.328	0.302	0.278	0.305	0.142	0.270	0.259	0.302	0.309

cpx	20 kbar/1050 °C							20 kbar/1100 °C								
MAOC 11						av	sd									
SiO_2	48.410	50.960	47.770	49.280	49.050	49.456	1.000	49.920	51.420	51.050	50.050	49.900	48.990	51.760	51.300	50.020
TiO_2	0.431	0.795	0.473	0.537	0.528	0.654	0.139	0.659	0.625	0.667	0.719	0.659	0.745	0.651	0.592	0.717
Al_2O_3	13.090	11.830	15.550	11.660	9.160	11.863	1.737	12.840	10.860	11.260	11.710	13.100	13.510	10.820	11.480	12.670
FeO	7.810	4.680	7.230	7.410	6.950	6.441	0.900	5.790	5.130	5.050	5.530	5.730	6.700	4.330	4.460	4.980
MgO	12.030	10.830	10.860	12.840	13.340	11.934	0.949	10.820	11.830	11.760	11.640	10.890	10.840	12.510	12.240	11.340
CaO	15.820	17.860	15.510	15.760	18.860	16.936	0.959	18.060	18.120	18.120	17.820	18.370	17.380	18.430	17.460	17.910
Na_2O	1.850	2.360	1.920	1.580	1.132	1.889	0.408	2.160	2.140	2.150	1.860	2.190	2.120	2.090	2.050	2.000
Total	**99.441**	**99.315**	**99.313**	**99.067**	**99.020**	**99.173**	**0.315**	**100.249**	**100.125**	**100.057**	**99.329**	**100.839**	**100.285**	**100.591**	**99.582**	**99.637**
formula																
Si	1.773	1.846	1.743	1.805	1.809	1.809		1.805	1.854	1.842	1.822	1.795	1.777	1.852	1.847	1.811
Al IV	0.227	0.154	0.257	0.195	0.191	0.191		0.195	0.146	0.158	0.178	0.205	0.223	0.148	0.153	0.189
Z	**2.000**	**2.000**	**2.000**	**2.000**	**2.000**	**2.000**		**2.000**	**2.000**	**2.000**	**2.000**	**2.000**	**2.000**	**2.000**	**2.000**	**2.000**
Al VI	0.338	0.352	0.411	0.309	0.208	0.320		0.352	0.315	0.321	0.325	0.351	0.354	0.309	0.335	0.351
Fe^{3+}	0.000	0.000	0.000	0.000	0.032	0.000		0.000	0.000	0.000	0.000	0.000	0.000	0.000	0.000	0.000
Ti	0.012	0.022	0.013	0.015	0.015	0.018		0.018	0.017	0.018	0.020	0.018	0.020	0.018	0.016	0.020
Mg	0.657	0.585	0.591	0.701	0.734	0.651		0.583	0.636	0.633	0.632	0.584	0.586	0.667	0.657	0.612
Fe^{2+}	0.239	0.142	0.221	0.227	0.182	0.197		0.175	0.155	0.152	0.168	0.172	0.203	0.130	0.134	0.151
Ca	0.621	0.693	0.606	0.619	0.745	0.664		0.700	0.700	0.701	0.695	0.708	0.675	0.707	0.674	0.695
Na	0.131	0.166	0.136	0.112	0.081	0.134		0.151	0.150	0.150	0.131	0.153	0.149	0.145	0.143	0.140
X	**1.998**	**1.959**	**1.978**	**1.982**	**1.997**	**1.983**		**1.979**	**1.972**	**1.975**	**1.971**	**1.986**	**1.989**	**1.975**	**1.959**	**1.968**
Total	**3.998**	**3.959**	**3.978**	**3.982**	**3.997**	**3.983**		**3.979**	**3.972**	**3.975**	**3.971**	**3.986**	**3.989**	**3.975**	**3.959**	**3.968**
En	43.302	41.192	41.668	45.333	44.166	43.052		40.003	42.660	42.584	42.251	39.879	40.015	44.385	44.850	41.991
Fs	15.770	9.985	15.561	14.675	10.955	13.034		12.008	10.377	10.258	11.260	11.771	13.874	8.618	9.167	10.344
Wo	40.928	48.823	42.771	39.992	44.879	43.913		47.989	46.963	47.158	46.489	48.350	46.111	46.997	45.982	47.665
Mg#	73.304	80.489	72.809	75.544	80.126	76.760		76.913	80.434	80.588	78.958	77.211	74.255	83.741	83.029	80.235
Q	1.517	1.420	1.418	1.547	1.661	1.511		1.458	1.490	1.486	1.495	1.464	1.465	1.504	1.465	1.457
J	0.263	0.332	0.272	0.224	0.162	0.268		0.303	0.299	0.301	0.263	0.306	0.298	0.290	0.286	0.281

cpx	20 kbar/1100 °C												
MAOC 11												**av**	**sd**
SiO_2	51.930	51.030	50.910	50.690	50.410	52.670	52.530	51.290	50.450	51.520	51.450	50.965	0.929
TiO_2	0.648	0.639	0.659	0.785	0.739	0.570	0.475	0.652	0.961	0.644	0.799	0.680	0.099
Al_2O_3	9.820	9.130	9.720	12.360	12.430	9.740	8.450	10.660	9.880	10.450	10.160	11.053	1.425
FeO	4.470	5.320	5.860	4.400	4.830	4.150	4.330	5.190	6.190	4.810	4.930	5.109	0.689
MgO	12.890	13.790	13.130	11.860	11.780	13.160	14.530	12.140	12.780	12.490	13.190	12.281	0.993
CaO	18.420	17.290	18.350	18.180	18.280	18.350	17.850	18.530	18.810	18.780	18.570	18.154	0.431
Na_2O	2.050	1.730	1.770	2.070	2.050	2.090	1.940	2.140	1.470	2.180	1.860	2.006	0.185
Total	**100.228**	**98.929**	**100.399**	**100.345**	**100.519**	**100.730**	**100.105**	**100.602**	**100.541**	**100.874**	**100.959**	**100.246**	**0.533**
formula													
Si	1.866	1.862	1.841	1.818	1.810	1.878	1.886	1.844	1.827	1.846	1.842	1.836	
Al IV	0.134	0.138	0.159	0.182	0.190	0.122	0.114	0.156	0.173	0.154	0.158	0.164	
Z	**2.000**	**2.000**	**2.000**	**2.000**	**2.000**	**2.000**	**2.000**	**2.000**	**2.000**	**2.000**	**2.000**	**2.000**	
Al VI	0.282	0.255	0.255	0.341	0.336	0.288	0.243	0.296	0.249	0.288	0.271	0.306	
Fe^{3+}	0.000	0.000	0.000	0.000	0.000	0.000	0.000	0.000	0.000	0.000	0.000	0.000	
Ti	0.018	0.018	0.018	0.021	0.020	0.015	0.013	0.018	0.026	0.017	0.022	0.018	
Mg	0.690	0.750	0.708	0.634	0.631	0.700	0.778	0.651	0.690	0.667	0.704	0.660	
Fe^{2+}	0.134	0.162	0.177	0.132	0.145	0.124	0.130	0.156	0.187	0.144	0.148	0.154	
Ca	0.709	0.676	0.711	0.699	0.703	0.701	0.687	0.714	0.730	0.721	0.712	0.701	
Na	0.143	0.122	0.124	0.144	0.143	0.145	0.135	0.149	0.103	0.151	0.129	0.140	
X	**1.976**	**1.984**	**1.993**	**1.971**	**1.978**	**1.972**	**1.986**	**1.983**	**1.985**	**1.991**	**1.986**	**1.979**	
Total	**3.976**	**3.984**	**3.993**	**3.971**	**3.978**	**3.972**	**3.986**	**3.983**	**3.985**	**3.991**	**3.986**	**3.979**	
En	45.013	47.224	44.349	43.293	42.638	45.891	48.778	42.793	42.927	43.541	45.014	43.557	
Fs	8.756	10.220	11.103	9.010	9.807	8.118	8.154	10.262	11.663	9.406	9.438	10.165	
Wo	46.231	42.556	44.547	47.697	47.555	45.991	43.068	46.945	45.410	47.053	45.549	46.278	
Mg#	83.715	82.209	79.977	82.774	81.301	84.969	85.678	80.657	78.635	82.235	82.667	81.079	
Q	1.534	1.589	1.596	1.465	1.479	1.525	1.594	1.521	1.607	1.533	1.564	1.515	
J	0.286	0.245	0.248	0.288	0.285	0.289	0.270	0.298	0.206	0.303	0.258	0.280	

Clinopyroxene in MAOC 13

cpx	10 kbar/1050 °C															
MAOC 13																
SiO_2	47.020	48.140	49.180	47.820	47.250	48.720	47.600	48.170	48.640	50.100	48.990	49.120	48.820	48.550	47.900	48.950
TiO_2	1.598	0.731	0.825	0.908	0.906	0.835	0.844	1.164	1.070	0.411	0.681	0.573	0.784	1.029	0.817	0.836
Al_2O_3	9.300	9.800	9.530	9.250	10.010	8.280	9.730	9.240	8.330	8.480	9.610	10.560	7.580	9.470	10.110	8.980
FeO	7.000	6.130	6.240	7.610	7.970	7.500	7.370	7.260	6.800	5.620	4.190	4.450	6.540	6.520	6.420	6.480
MgO	13.630	13.870	14.150	14.060	13.320	15.840	14.260	14.210	14.270	15.030	15.000	14.070	15.290	14.510	15.740	14.610
CaO	19.350	19.780	20.090	18.860	18.540	17.820	18.410	19.300	18.820	19.340	19.540	19.760	20.480	19.100	16.990	19.190
Na_2O	0.720	0.928	0.937	0.678	0.984	0.532	0.797	0.782	0.531	0.740	0.940	1.059	0.403	0.740	1.073	0.671
Total	**98.618**	**99.379**	**100.952**	**99.186**	**98.980**	**99.527**	**99.011**	**100.126**	**98.461**	**99.721**	**98.951**	**99.592**	**99.897**	**99.919**	**99.050**	**99.717**
formula																
Si	1.750	1.765	1.776	1.767	1.749	1.785	1.756	1.760	1.809	1.827	1.790	1.787	1.785	1.773	1.748	1.793
Al IV	0.250	0.235	0.224	0.233	0.251	0.215	0.244	0.240	0.191	0.173	0.210	0.213	0.215	0.227	0.252	0.207
Z	**2.000**	**2.000**	**2.000**	**2.000**	**2.000**	**2.000**	**2.000**	**2.000**	**2.000**	**2.000**	**2.000**	**2.000**	**2.000**	**2.000**	**2.000**	**2.000**
Al VI	0.158	0.189	0.182	0.170	0.186	0.143	0.179	0.158	0.174	0.191	0.204	0.240	0.112	0.181	0.183	0.180
Fe^{3+}	0.055	0.070	0.060	0.061	0.084	0.064	0.074	0.074	0.000	0.011	0.035	0.015	0.086	0.040	0.098	0.029
Ti	0.045	0.020	0.022	0.025	0.025	0.023	0.023	0.032	0.030	0.011	0.019	0.016	0.022	0.028	0.022	0.023
Mg	0.756	0.758	0.762	0.775	0.735	0.865	0.784	0.774	0.791	0.817	0.817	0.763	0.833	0.790	0.856	0.798
Fe^{2+}	0.163	0.118	0.128	0.174	0.163	0.166	0.153	0.148	0.212	0.161	0.094	0.120	0.114	0.159	0.098	0.170
Ca	0.772	0.777	0.778	0.747	0.735	0.700	0.728	0.755	0.750	0.756	0.765	0.770	0.802	0.747	0.664	0.753
Na	0.052	0.066	0.066	0.049	0.071	0.038	0.057	0.055	0.038	0.052	0.067	0.075	0.029	0.052	0.076	0.048
X	**2.000**	**1.999**	**1.998**	**2.000**	**1.999**	**1.998**	**1.999**	**1.998**	**1.996**	**1.999**	**2.000**	**1.999**	**1.997**	**1.998**	**1.998**	**2.000**
Total	**4.000**	**3.999**	**3.998**	**4.000**	**3.999**	**3.998**	**3.999**	**3.998**	**3.996**	**3.999**	**4.000**	**3.999**	**3.997**	**3.998**	**3.998**	**4.000**
En	44.726	45.856	45.691	45.691	45.011	49.992	47.090	46.151	45.143	47.132	48.763	46.155	47.639	46.564	52.903	46.363
Fs	9.638	7.144	7.684	10.259	9.960	9.586	9.216	8.798	12.067	9.280	5.582	7.256	6.500	9.383	6.054	9.868
Wo	45.636	47.001	46.625	44.050	45.029	40.422	43.694	45.051	42.790	43.589	45.655	46.589	45.862	44.053	41.043	43.769
Mg#	82.272	86.521	85.604	81.664	81.881	83.909	83.632	83.989	78.907	83.550	89.729	86.414	87.994	83.229	89.732	82.451
Q	1.691	1.654	1.668	1.695	1.633	1.731	1.665	1.677	1.753	1.733	1.676	1.653	1.749	1.697	1.619	1.720
J	0.104	0.132	0.131	0.097	0.141	0.076	0.114	0.111	0.077	0.105	0.133	0.149	0.057	0.105	0.152	0.095

cpx	10 kbar/1050 °C						10 kbar/1100 °C								
MAOC 13					**av**	**sd**								**av**	**sd**
SiO_2	49.030	48.600	49.230	49.000	48.542	0.750	47.220	48.410	45.680	46.990	47.660	47.730	48.030	47.389	0.890
TiO_2	0.733	0.594	0.771	0.645	0.838	0.250	1.191	1.531	1.274	1.241	0.771	0.797	0.934	1.106	0.280
Al_2O_3	9.840	9.760	9.770	8.930	9.328	0.723	11.160	8.670	11.490	10.760	9.680	11.950	10.880	10.656	1.124
FeO	4.720	4.940	5.310	6.270	6.267	1.090	6.080	5.680	7.020	5.690	6.480	5.080	3.150	5.597	1.246
MgO	14.690	15.200	14.760	14.720	14.562	0.661	13.030	14.570	12.680	13.430	14.210	13.960	15.380	13.894	0.931
CaO	19.230	19.370	19.170	19.010	19.108	0.770	18.190	18.910	18.850	18.510	18.600	17.850	19.250	18.594	0.469
Na_2O	0.916	0.940	0.884	0.975	0.812	0.184	0.981	0.645	1.004	0.749	0.817	0.930	0.647	0.825	0.151
Total	**99.159**	**99.404**	**99.895**	**99.550**	**99.455**	**0.570**	**97.852**	**98.416**	**97.998**	**97.370**	**98.218**	**98.297**	**98.271**	**98.060**	**0.360**
formula															
Si	1.792	1.769	1.789	1.791	1.778		1.760	1.795	1.706	1.759	1.769	1.758	1.762	1.760	
Al IV	0.208	0.231	0.211	0.209	0.222		0.240	0.205	0.294	0.241	0.231	0.242	0.238	0.240	
Z	**2.000**	**2.000**	**2.000**	**2.000**	**2.000**		**2.000**	**2.000**	**2.000**	**2.000**	**2.000**	**2.000**	**2.000**	**2.000**	
Al VI	0.216	0.187	0.208	0.175	0.181		0.251	0.174	0.212	0.234	0.193	0.277	0.232	0.227	
Fe^{3+}	0.018	0.078	0.022	0.068	0.051		0.000	0.000	0.083	0.000	0.054	0.000	0.000	0.011	
Ti	0.020	0.016	0.021	0.018	0.023		0.033	0.043	0.036	0.035	0.022	0.022	0.026	0.031	
Mg	0.800	0.825	0.800	0.802	0.790		0.724	0.805	0.706	0.750	0.786	0.767	0.841	0.769	
Fe^{2+}	0.126	0.072	0.140	0.124	0.141		0.190	0.176	0.136	0.178	0.147	0.156	0.097	0.163	
Ca	0.753	0.755	0.746	0.744	0.760		0.727	0.751	0.754	0.743	0.740	0.705	0.757	0.740	
Na	0.065	0.066	0.062	0.069	0.058		0.071	0.046	0.073	0.054	0.059	0.066	0.046	0.059	
X	**2.000**	**2.000**	**1.998**	**2.000**	**1.999**		**1.995**	**1.996**	**2.000**	**1.994**	**2.000**	**1.993**	**1.998**	**2.000**	
Total	**4.000**	**4.000**	**3.998**	**4.000**	**3.999**		**3.995**	**3.996**	**4.000**	**3.994**	**4.000**	**3.993**	**3.998**	**4.000**	
En	47.659	49.909	47.440	48.013	47.165		44.148	46.479	44.222	44.878	47.000	47.100	49.641	46.006	
Fs	7.501	4.379	8.276	7.422	8.353		11.556	10.164	8.528	10.666	8.784	9.615	5.703	9.742	
Wo	44.840	45.712	44.284	44.565	44.482		44.296	43.357	47.250	44.456	44.216	43.285	44.656	44.251	
Mg#	86.401	91.934	85.146	86.612	84.955		79.255	82.056	83.833	80.797	84.254	83.048	89.695	82.525	
Q	1.679	1.652	1.686	1.670	1.691		1.640	1.733	1.597	1.670	1.673	1.628	1.694	1.672	
J	0.130	0.133	0.125	0.138	0.115		0.142	0.093	0.145	0.109	0.118	0.133	0.092	0.119	

cpx	**12.5 kbar/1050 °C**															
MAOC 13																
SiO_2	46.720	46.420	47.140	46.460	47.770	47.900	47.470	47.470	47.800	48.860	47.550	46.590	49.280	46.500	49.110	47.780
TiO_2	0.840	1.025	1.004	0.883	0.796	0.801	0.977	1.091	1.028	0.672	1.006	0.965	0.799	0.924	0.860	1.005
Al_2O_3	11.450	10.780	11.280	11.300	9.960	10.200	9.670	10.770	9.830	9.370	11.940	11.350	13.880	11.840	9.790	10.200
FeO	7.120	7.960	6.850	8.000	6.930	7.240	7.970	7.300	7.860	7.010	7.180	8.080	5.760	7.540	6.360	7.500
MgO	12.340	12.480	12.480	12.120	13.070	13.170	13.380	12.390	14.020	13.440	11.780	12.400	10.210	12.120	13.340	13.720
CaO	18.530	18.550	18.230	17.940	18.360	17.510	18.430	18.090	17.010	18.010	17.710	17.930	16.840	18.380	18.090	16.410
Na_2O	1.560	1.203	1.430	1.460	1.420	1.460	1.142	1.350	1.136	1.231	1.520	1.450	2.750	1.460	1.660	1.305
Total	**98.560**	**98.418**	**98.414**	**98.163**	**98.306**	**98.281**	**99.039**	**98.461**	**98.684**	**98.593**	**98.686**	**98.765**	**99.519**	**98.764**	**99.210**	**97.920**
formula																
Si	1.728	1.729	1.749	1.733	1.772	1.777	1.755	1.765	1.768	1.809	1.763	1.725	1.791	1.721	1.800	1.780
Al IV	0.272	0.271	0.251	0.267	0.228	0.223	0.245	0.235	0.232	0.191	0.237	0.275	0.209	0.279	0.200	0.220
Z	**2.000**	**2.000**	**2.000**	**2.000**	**2.000**	**2.000**	**2.000**	**2.000**	**2.000**	**2.000**	**2.000**	**2.000**	**2.000**	**2.000**	**2.000**	**2.000**
Al VI	0.227	0.202	0.242	0.229	0.208	0.223	0.176	0.237	0.197	0.218	0.285	0.220	0.386	0.238	0.222	0.227
Fe^{3+}	0.109	0.099	0.056	0.094	0.078	0.060	0.095	0.034	0.057	0.024	0.005	0.104	0.000	0.094	0.047	0.031
Ti	0.023	0.029	0.028	0.025	0.022	0.022	0.027	0.031	0.029	0.019	0.028	0.027	0.022	0.026	0.024	0.028
Mg	0.680	0.693	0.690	0.674	0.723	0.728	0.737	0.687	0.773	0.742	0.651	0.684	0.553	0.669	0.729	0.762
Fe^{2+}	0.111	0.149	0.156	0.156	0.138	0.165	0.151	0.193	0.187	0.193	0.218	0.146	0.175	0.140	0.147	0.203
Ca	0.734	0.740	0.725	0.717	0.730	0.696	0.730	0.721	0.674	0.715	0.704	0.711	0.656	0.729	0.710	0.655
Na	0.112	0.087	0.103	0.106	0.102	0.105	0.082	0.097	0.081	0.088	0.109	0.104	0.194	0.105	0.118	0.094
X	**1.997**	**1.999**	**2.000**	**2.000**	**2.000**	**2.000**	**1.999**	**2.000**	**1.998**	**1.999**	**2.000**	**1.997**	**1.985**	**2.000**	**1.998**	**2.000**
Total	**3.997**	**3.999**	**4.000**	**4.000**	**4.000**	**4.000**	**3.999**	**4.000**	**3.998**	**3.999**	**4.000**	**3.997**	**3.985**	**4.000**	**3.998**	**4.000**
En	44.595	43.789	43.931	43.577	45.458	45.828	45.564	42.899	47.320	44.966	41.406	44.382	39.970	43.502	45.936	47.045
Fs	7.275	9.431	9.947	10.064	8.647	10.379	9.327	12.083	11.416	11.727	13.854	9.494	12.649	9.082	9.293	12.512
Wo	48.130	46.780	46.122	46.359	45.895	43.792	45.108	45.017	41.264	43.307	44.740	46.124	47.382	47.415	44.771	40.442
Mg#	85.975	82.279	81.537	81.238	84.018	81.534	83.007	78.023	80.564	79.315	74.929	82.379	75.961	82.728	83.173	78.992
Q	1.526	1.582	1.571	1.546	1.590	1.590	1.618	1.601	1.634	1.650	1.573	1.542	1.384	1.538	1.586	1.619
J	0.224	0.174	0.206	0.211	0.204	0.210	0.164	0.195	0.163	0.177	0.219	0.208	0.388	0.210	0.236	0.188

cpx	**12.5 kbar/1050 °C**					**12.5 kbar/1100 °C**										
MAOC 13				**av**	**sd**											
SiO_2	47.780	47.370	46.480	47.497	0.881	48.253	48.741	48.134	47.656	48.699	49.852	47.635	47.260	48.953	47.446	47.229
TiO_2	1.009	0.967	0.946	0.926	0.107	0.858	0.977	0.635	0.789	0.850	0.569	0.946	1.107	1.057	1.214	1.084
Al_2O_3	9.750	10.860	11.800	10.843	1.102	8.910	10.040	9.420	10.100	10.540	8.890	11.080	10.720	8.250	8.100	10.720
FeO	7.150	6.990	7.260	7.266	0.588	7.230	5.830	6.680	7.300	5.680	6.260	6.800	6.620	6.470	7.500	7.040
MgO	13.370	12.860	12.120	12.674	0.866	14.210	14.100	14.050	14.010	14.020	14.200	13.210	13.390	14.750	14.460	13.450
CaO	18.030	17.700	18.480	17.907	0.599	18.950	16.910	18.070	17.110	16.870	17.420	16.500	17.730	16.330	18.250	16.870
Na_2O	1.266	1.450	1.510	1.461	0.343	0.716	1.360	1.198	1.175	1.540	1.520	1.450	1.261	1.300	0.521	1.158
Total	**98.355**	**98.197**	**98.596**	**98.575**	**0.381**	**99.127**	**97.958**	**98.187**	**98.140**	**98.199**	**98.711**	**97.621**	**98.088**	**97.110**	**97.491**	**97.551**
formula																
Si	1.774	1.760	1.721	1.760		1.782	1.804	1.783	1.768	1.794	1.832	1.776	1.755	1.831	1.785	1.767
Al IV	0.226	0.240	0.279	0.240		0.218	0.196	0.217	0.232	0.206	0.168	0.224	0.245	0.169	0.215	0.233
Z	**2.000**	**2.000**	**2.000**	**2.000**		**2.000**	**2.000**	**2.000**	**2.000**	**2.000**	**2.000**	**2.000**	**2.000**	**2.000**	**2.000**	**2.000**
Al VI	0.201	0.235	0.236	0.233		0.170	0.242	0.195	0.209	0.251	0.217	0.263	0.224	0.195	0.144	0.239
Fe^{3+}	0.059	0.056	0.096	0.060		0.052	0.000	0.073	0.061	0.015	0.025	0.012	0.048	0.007	0.039	0.017
Ti	0.028	0.027	0.026	0.026		0.024	0.027	0.018	0.022	0.024	0.016	0.027	0.031	0.030	0.034	0.030
Mg	0.740	0.712	0.669	0.700		0.782	0.778	0.776	0.775	0.770	0.778	0.734	0.741	0.822	0.811	0.750
Fe^{2+}	0.163	0.161	0.128	0.165		0.171	0.180	0.134	0.165	0.160	0.167	0.200	0.158	0.195	0.197	0.203
Ca	0.717	0.704	0.733	0.711		0.750	0.671	0.717	0.680	0.666	0.686	0.659	0.705	0.654	0.736	0.676
Na	0.091	0.104	0.108	0.105		0.051	0.098	0.086	0.085	0.110	0.108	0.105	0.091	0.094	0.038	0.084
X	**2.000**	**2.000**	**1.998**	**2.000**		**2.000**	**1.996**	**1.999**	**1.997**	**1.996**	**1.998**	**1.999**	**1.997**	**1.998**	**1.999**	**2.000**
Total	**4.000**	**4.000**	**3.998**	**4.000**		**4.000**	**3.996**	**3.999**	**3.997**	**3.996**	**3.998**	**3.999**	**3.997**	**3.998**	**3.999**	**4.000**
En	45.683	45.136	43.710	44.428		45.930	47.758	47.678	47.829	48.237	47.693	46.094	46.203	49.184	46.519	46.037
Fs	10.039	10.215	8.389	10.457		10.048	11.077	8.249	10.189	10.046	10.256	12.526	9.826	11.680	11.283	12.462
Wo	44.278	44.649	47.901	45.115		44.023	41.165	44.073	41.982	41.717	42.051	41.380	43.971	39.136	42.198	41.501
Mg#	81.984	81.545	83.898	80.947		82.051	81.173	85.251	82.439	82.763	82.301	78.631	82.463	80.810	80.480	78.697
Q	1.620	1.578	1.531	1.576		1.703	1.629	1.628	1.620	1.596	1.631	1.593	1.604	1.672	1.743	1.629
J	0.182	0.209	0.217	0.210		0.103	0.195	0.172	0.169	0.220	0.217	0.210	0.182	0.189	0.076	0.168

cpx	**12.5 kbar/1100 °C**			**15 kbar/900 °C**									**15 kbar/1050 °C**			
MAOC 13		**av**	**sd**								**av**	**sd**				
SiO_2	45.475	47.944	1.108	47.500	47.440	47.280	46.520	47.490	48.250	50.010	47.784	1.104	48.760	47.860	48.880	49.100
TiO_2	0.811	0.908	0.193	0.586	0.696	0.516	0.547	0.704	0.674	0.517	0.606	0.084	0.806	0.721	0.958	0.807
Al_2O_3	11.760	9.878	1.162	11.370	10.820	11.700	12.390	12.180	9.740	11.120	11.331	0.896	11.280	11.990	11.180	10.510
FeO	7.100	6.709	0.573	7.860	7.630	8.260	8.510	7.310	7.110	5.840	7.503	0.884	7.310	7.950	7.030	7.300
MgO	13.870	13.977	0.445	13.050	11.750	12.850	13.060	10.660	13.140	11.080	12.227	1.048	12.340	11.970	12.580	12.750
CaO	15.120	17.178	1.006	16.250	18.810	17.110	16.320	18.340	18.140	18.650	17.660	1.086	17.430	16.960	17.270	17.120
Na_2O	1.046	1.187	0.307	1.500	1.290	1.203	1.215	1.770	1.161	1.550	1.384	0.227	1.890	2.050	1.780	1.820
Total	**95.182**	**97.780**	**0.983**	**98.116**	**98.436**	**98.919**	**98.562**	**98.454**	**98.215**	**98.767**	**98.496**	**0.284**	**99.816**	**99.501**	**99.678**	**99.407**
formula																
Si	1.736	1.790		1.763	1.769	1.748	1.723	1.767	1.796	1.837	1.775		1.781	1.753	1.787	1.799
Al IV	0.264	0.210		0.237	0.231	0.252	0.277	0.233	0.204	0.163	0.225		0.219	0.247	0.213	0.201
Z	**2.000**	**2.000**		**2.000**	**2.000**	**2.000**	**2.000**	**2.000**	**2.000**	**2.000**	**2.000**		**2.000**	**2.000**	**2.000**	**2.000**
Al VI	0.265	0.218		0.261	0.245	0.258	0.264	0.301	0.223	0.318	0.271		0.266	0.271	0.269	0.253
Fe^{3+}	0.030	0.031		0.049	0.041	0.052	0.069	0.019	0.027	0.000	0.020		0.042	0.082	0.016	0.031
Ti	0.023	0.025		0.016	0.020	0.014	0.015	0.020	0.019	0.014	0.017		0.022	0.020	0.026	0.022
Mg	0.789	0.776		0.722	0.653	0.708	0.721	0.591	0.729	0.607	0.677		0.672	0.654	0.686	0.697
Fe^{2+}	0.197	0.178		0.195	0.197	0.204	0.195	0.209	0.195	0.179	0.213		0.181	0.161	0.199	0.193
Ca	0.618	0.685		0.646	0.752	0.678	0.648	0.731	0.723	0.734	0.703		0.682	0.666	0.676	0.672
Na	0.077	0.086		0.108	0.093	0.086	0.087	0.128	0.084	0.110	0.100		0.134	0.146	0.126	0.129
X	**2.000**	**1.999**		**1.998**	**2.000**	**2.000**	**1.999**	**1.999**	**2.000**	**1.963**	**2.000**		**1.999**	**1.999**	**1.998**	**1.997**
Total	**4.000**	**3.999**		**3.998**	**4.000**	**4.000**	**3.999**	**3.999**	**4.000**	**3.963**	**4.000**		**3.999**	**3.999**	**3.998**	**3.997**
En	49.196	47.328		46.184	40.773	44.546	46.114	38.613	44.263	39.913	42.516		43.761	44.146	43.922	44.596
Fs	12.258	10.866		12.484	12.315	12.823	12.469	13.641	11.818	11.801	13.349		11.813	10.899	12.742	12.365
Wo	38.545	41.806		41.333	46.912	42.631	41.417	47.746	43.919	48.286	44.135		44.426	44.956	43.337	43.038
Mg#	80.053	81.328		78.721	76.802	77.648	78.715	73.895	78.927	77.180	76.105		78.744	80.200	77.513	78.292
Q	1.604	1.639		1.564	1.602	1.590	1.564	1.531	1.647	1.520	1.592		1.535	1.481	1.561	1.562
J	0.155	0.171		0.216	0.187	0.172	0.175	0.255	0.168	0.221	0.199		0.268	0.291	0.252	0.259

cpx	15 kbar/1050 °C													15 kbar/1100 °C		
MAOC 13												av	sd			
SiO_2	47.700	47.810	50.600	49.420	51.420	49.300	49.960	49.190	48.670	50.400	49.510	49.239	1.056	51.620	51.790	50.720
TiO_2	0.792	1.038	0.722	0.974	0.629	0.642	0.719	0.769	0.808	0.653	0.956	0.800	0.129	0.638	0.546	0.630
Al_2O_3	11.720	12.530	9.600	9.980	8.740	10.340	9.940	10.150	11.510	8.970	10.220	10.577	1.098	8.230	8.870	9.100
FeO	7.280	7.020	7.030	7.540	6.570	7.050	7.140	7.130	7.580	6.870	7.320	7.208	0.326	3.480	3.610	2.240
MgO	12.090	11.940	14.040	13.840	13.580	12.670	13.190	12.970	12.260	13.420	13.450	12.873	0.689	15.510	15.130	15.020
CaO	17.390	17.210	15.830	16.950	17.180	16.860	16.780	16.740	16.840	16.940	16.470	16.931	0.401	18.150	19.110	19.010
Na_2O	1.770	1.950	1.930	1.530	2.050	2.090	1.750	2.080	1.910	2.160	1.580	1.889	0.186	1.560	1.550	1.600
Total	**98.742**	**99.498**	**99.752**	**100.234**	**100.169**	**98.952**	**99.479**	**99.029**	**99.578**	**99.413**	**99.506**	**99.517**	**0.405**	**99.188**	**100.606**	**98.320**
formula																
Si	1.761	1.750	1.841	1.797	1.863	1.811	1.829	1.804	1.782	1.840	1.813	1.801		1.867	1.853	1.847
Al IV	0.239	0.250	0.159	0.203	0.137	0.189	0.171	0.196	0.218	0.160	0.187	0.199		0.133	0.147	0.153
Z	**2.000**	**2.000**	**2.000**	**2.000**	**2.000**	**2.000**	**2.000**	**2.000**	**2.000**	**2.000**	**2.000**	**2.000**		**2.000**	**2.000**	**2.000**
Al VI	0.271	0.290	0.252	0.224	0.237	0.258	0.257	0.243	0.279	0.226	0.254	0.257		0.218	0.227	0.237
Fe^{3+}	0.048	0.040	0.004	0.032	0.007	0.047	0.000	0.056	0.032	0.052	0.000	0.031		0.000	0.000	0.000
Ti	0.022	0.029	0.020	0.027	0.017	0.018	0.020	0.021	0.022	0.018	0.026	0.022		0.017	0.015	0.017
Mg	0.666	0.651	0.761	0.750	0.734	0.694	0.720	0.709	0.669	0.730	0.734	0.702		0.836	0.807	0.815
Fe^{2+}	0.176	0.175	0.210	0.197	0.192	0.170	0.219	0.163	0.200	0.158	0.224	0.190		0.105	0.108	0.068
Ca	0.688	0.675	0.617	0.660	0.667	0.663	0.658	0.658	0.661	0.663	0.646	0.664		0.703	0.733	0.742
Na	0.127	0.138	0.136	0.108	0.144	0.149	0.124	0.148	0.136	0.153	0.112	0.134		0.109	0.108	0.113
X	**1.998**	**1.998**	**2.000**	**1.998**	**1.998**	**2.000**	**1.998**	**1.998**	**2.000**	**1.999**	**1.997**	**1.999**		**1.990**	**1.996**	**1.992**
Total	**3.998**	**3.998**	**4.000**	**3.998**	**3.998**	**4.000**	**3.998**	**3.998**	**4.000**	**3.999**	**3.997**	**3.999**		**3.990**	**3.996**	**3.992**
En	43.501	43.383	47.940	46.658	46.069	45.424	45.086	46.364	43.746	47.095	45.758	45.138		50.841	48.980	50.168
Fs	11.528	11.674	13.211	12.272	12.042	11.132	13.690	10.626	13.067	10.179	13.970	12.190		6.399	6.556	4.197
Wo	44.971	44.943	38.849	41.070	41.889	43.444	41.224	43.009	43.187	42.726	40.272	42.671		42.760	44.464	45.635
Mg#	79.051	78.796	78.397	79.176	79.278	80.317	76.707	81.354	76.999	82.227	76.611	78.736		88.821	88.196	92.280
Q	1.530	1.502	1.588	1.608	1.592	1.527	1.596	1.530	1.530	1.551	1.604	1.555		1.645	1.647	1.625
J	0.253	0.277	0.272	0.216	0.288	0.298	0.248	0.296	0.271	0.306	0.224	0.268		0.219	0.215	0.226

cpx	15 kbar/1100 °C								20 kbar/1050 °C							
MAOC 13							av	sd								
SiO_2	51.710	51.960	50.480	51.570	51.390	51.220	51.384	0.497	49.930	49.090	51.500	51.300	49.890	52.190	52.550	51.690
TiO_2	0.585	0.645	0.739	0.430	0.688	0.516	0.602	0.094	0.808	0.407	0.652	0.534	1.111	0.762	0.959	0.794
Al_2O_3	7.660	9.570	10.210	9.730	8.540	7.930	8.871	0.862	9.370	12.110	10.280	9.880	11.490	8.710	9.870	10.360
FeO	2.340	1.096	2.530	3.220	2.740	5.140	2.933	1.125	6.640	7.290	5.820	6.340	5.940	5.400	4.500	4.470
MgO	16.040	15.960	15.410	15.190	16.040	15.100	15.489	0.422	13.560	13.180	12.840	12.930	12.220	12.740	12.280	11.820
CaO	20.070	19.790	18.900	18.630	19.620	17.630	18.990	0.784	17.440	14.860	16.420	15.910	16.220	16.720	16.310	16.270
Na_2O	1.500	1.730	1.510	1.560	1.182	1.610	1.534	0.148	1.480	1.980	2.400	2.530	2.100	2.430	2.890	2.720
Total	**99.905**	**100.751**	**99.779**	**100.330**	**100.200**	**99.146**	**99.803**	**0.790**	**99.228**	**98.917**	**99.912**	**99.424**	**98.971**	**98.952**	**99.359**	**98.124**
formula																
Si	1.856	1.837	1.813	1.844	1.843	1.866	1.848		1.832	1.798	1.860	1.866	1.820	1.900	1.896	1.887
Al IV	0.144	0.163	0.187	0.156	0.157	0.134	0.152		0.168	0.202	0.140	0.134	0.180	0.100	0.104	0.113
Z	**2.000**	**2.000**	**2.000**	**2.000**	**2.000**	**2.000**	**2.000**		**2.000**	**2.000**	**2.000**	**2.000**	**2.000**	**2.000**	**2.000**	**2.000**
Al VI	0.180	0.236	0.245	0.254	0.203	0.207	0.230		0.237	0.320	0.297	0.289	0.314	0.274	0.315	0.332
Fe^{3+}	0.037	0.006	0.009	0.000	0.000	0.012	0.000		0.000	0.000	0.000	0.000	0.000	0.000	0.000	0.000
Ti	0.016	0.017	0.020	0.012	0.019	0.014	0.016		0.022	0.011	0.018	0.015	0.030	0.021	0.026	0.022
Mg	0.858	0.841	0.825	0.810	0.857	0.820	0.831		0.742	0.720	0.691	0.701	0.664	0.692	0.660	0.643
Fe^{2+}	0.033	0.026	0.067	0.096	0.082	0.144	0.088		0.204	0.223	0.176	0.193	0.181	0.164	0.136	0.136
Ca	0.772	0.750	0.727	0.714	0.754	0.688	0.732		0.686	0.583	0.635	0.620	0.634	0.652	0.630	0.636
Na	0.104	0.119	0.105	0.108	0.082	0.114	0.107		0.105	0.141	0.168	0.178	0.149	0.172	0.202	0.192
X	**2.000**	**1.995**	**2.000**	**1.993**	**1.997**	**2.000**	**1.998**		**1.996**	**1.998**	**1.986**	**1.996**	**1.972**	**1.975**	**1.970**	**1.962**
Total	**4.000**	**3.995**	**4.000**	**3.993**	**3.997**	**4.000**	**3.998**		**3.996**	**3.998**	**3.986**	**3.996**	**3.972**	**3.975**	**3.970**	**3.962**
En	51.608	52.021	50.956	49.990	50.634	49.621	50.317		45.474	47.156	46.011	46.309	44.910	45.850	46.293	45.425
Fs	1.980	1.618	4.127	5.944	4.852	8.740	5.345		12.491	14.631	11.699	12.737	12.246	10.902	9.516	9.636
Wo	46.412	46.361	44.918	44.066	44.514	41.639	44.339		42.035	38.213	42.290	40.954	42.844	43.248	44.191	44.939
Mg#	96.305	96.983	92.508	89.373	91.256	85.025	90.398		78.451	76.320	79.728	78.428	78.575	80.791	82.949	82.499
Q	1.663	1.617	1.619	1.620	1.693	1.653	1.651		1.631	1.526	1.502	1.514	1.479	1.508	1.426	1.416
J	0.209	0.237	0.210	0.216	0.164	0.227	0.214		0.211	0.281	0.336	0.357	0.297	0.343	0.404	0.385

cpx	20 kbar/1050 °C								20 kbar/1100 °C							
MAOC 13							av	sd								
SiO_2	52.480	51.170	51.710	50.640	52.980	55.190	51.594	1.521	51.750	52.280	50.320	51.150	51.160	52.370	52.540	52.480
TiO_2	0.790	0.491	0.693	0.344	0.697	0.777	0.701	0.208	0.853	0.768	0.701	0.622	0.679	0.697	0.635	0.673
Al_2O_3	8.940	9.960	9.930	10.400	9.010	9.750	10.004	0.933	10.410	9.220	10.430	9.340	10.190	9.130	9.250	10.440
FeO	4.700	5.570	5.280	6.660	4.870	5.200	5.620	0.873	5.790	5.610	7.220	6.520	6.350	5.510	5.620	4.950
MgO	13.140	14.220	13.250	14.300	12.760	11.990	12.945	0.747	12.610	12.980	11.870	12.790	12.450	13.010	12.990	12.500
CaO	16.090	16.010	16.450	15.250	16.520	15.780	16.161	0.622	16.060	17.080	16.810	17.330	16.970	17.210	17.110	16.300
Na_2O	2.740	1.910	2.460	1.860	2.700	2.560	2.340	0.410	2.510	2.640	2.440	2.220	2.450	2.550	2.540	3.130
Total	**98.880**	**99.331**	**99.773**	**99.454**	**99.537**	**101.247**	**99.365**	**0.700**	**99.983**	**100.578**	**99.791**	**99.972**	**100.249**	**100.477**	**100.685**	**100.473**
formula																
Si	1.904	1.853	1.867	1.839	1.911	1.943	1.870		1.865	1.879	1.836	1.859	1.851	1.883	1.884	1.877
Al IV	0.096	0.147	0.133	0.161	0.089	0.057	0.130		0.135	0.121	0.164	0.141	0.149	0.117	0.116	0.123
Z	**2.000**	**2.000**	**2.000**	**2.000**	**2.000**	**2.000**	**2.000**		**2.000**	**2.000**	**2.000**	**2.000**	**2.000**	**2.000**	**2.000**	**2.000**
Al VI	0.286	0.279	0.289	0.284	0.294	0.347	0.297		0.307	0.269	0.285	0.259	0.286	0.270	0.275	0.317
Fe^{3+}	0.000	0.000	0.000	0.000	0.000	0.000	0.000		0.000	0.000	0.013	0.003	0.000	0.000	0.000	0.000
Ti	0.022	0.013	0.019	0.009	0.019	0.021	0.019		0.023	0.021	0.019	0.017	0.018	0.019	0.017	0.018
Mg	0.711	0.768	0.713	0.774	0.686	0.629	0.699		0.678	0.695	0.646	0.693	0.672	0.697	0.694	0.667
Fe^{2+}	0.143	0.169	0.159	0.202	0.147	0.153	0.170		0.175	0.169	0.207	0.195	0.192	0.166	0.169	0.148
Ca	0.626	0.621	0.636	0.593	0.638	0.595	0.628		0.620	0.658	0.657	0.675	0.658	0.663	0.657	0.625
Na	0.193	0.134	0.172	0.131	0.189	0.175	0.164		0.175	0.184	0.173	0.156	0.172	0.178	0.177	0.217
X	**1.980**	**1.984**	**1.989**	**1.994**	**1.973**	**1.920**	**1.978**		**1.978**	**1.996**	**2.000**	**1.998**	**1.997**	**1.993**	**1.989**	**1.992**
Total	**3.980**	**3.984**	**3.989**	**3.994**	**3.973**	**3.920**	**3.978**		**3.978**	**3.996**	**4.000**	**3.998**	**3.997**	**3.993**	**3.989**	**3.992**
En	48.060	49.287	47.263	49.316	46.629	45.679	46.711		46.021	45.700	42.757	44.332	44.135	45.697	45.675	46.310
Fs	9.643	10.830	10.565	12.884	9.983	11.113	11.376		11.853	11.080	13.723	12.495	12.627	10.856	11.085	10.287
Wo	42.297	39.883	42.173	37.800	43.389	43.208	41.913		42.126	43.221	43.520	43.173	43.238	43.447	43.240	43.403
Mg#	83.289	81.986	81.730	79.286	82.366	80.432	80.416		79.519	80.486	75.704	78.012	77.754	80.803	80.471	81.824
Q	1.479	1.558	1.509	1.570	1.471	1.378	1.497		1.472	1.522	1.510	1.563	1.522	1.526	1.520	1.439
J	0.386	0.268	0.344	0.262	0.378	0.349	0.329		0.351	0.368	0.345	0.313	0.344	0.356	0.353	0.434

cpx	20 kbar/1100 °C										
MAOC 13										av	sd
SiO_2	51.230	51.620	51.190	50.780	51.790	51.290	52.010	52.420	52.250	51.684	0.663
TiO_2	0.687	0.690	0.622	0.873	0.695	0.691	0.709	0.710	0.604	0.701	0.073
Al_2O_3	13.430	11.700	11.610	10.260	10.980	10.650	10.820	10.390	8.100	10.374	1.217
FeO	4.550	4.780	5.610	5.670	4.880	5.320	4.180	4.320	5.070	5.409	0.798
MgO	9.850	11.430	12.180	12.770	12.050	12.540	12.610	12.440	13.590	12.392	0.821
CaO	17.340	16.540	16.330	16.770	16.470	17.110	16.490	16.470	17.880	16.839	0.473
Na_2O	3.280	3.170	2.550	2.280	3.040	2.410	3.150	3.150	2.320	2.696	0.366
Total	**100.367**	**99.930**	**100.092**	**99.403**	**99.905**	**100.011**	**99.969**	**99.900**	**99.814**	**100.094**	**0.333**
formula											
Si	1.835	1.856	1.843	1.847	1.864	1.851	1.865	1.882	1.893	1.863	
Al IV	0.165	0.144	0.157	0.153	0.136	0.149	0.135	0.118	0.107	0.137	
Z	**2.000**	**2.000**	**2.000**	**2.000**	**2.000**	**2.000**	**2.000**	**2.000**	**2.000**	**2.000**	
Al VI	0.402	0.352	0.336	0.287	0.329	0.304	0.323	0.321	0.239	0.304	
Fe^{3+}	0.000	0.000	0.000	0.000	0.000	0.000	0.000	0.000	0.000	0.000	
Ti	0.019	0.019	0.017	0.024	0.019	0.019	0.019	0.019	0.016	0.019	
Mg	0.526	0.613	0.654	0.692	0.646	0.675	0.674	0.666	0.734	0.666	
Fe^{2+}	0.136	0.144	0.169	0.172	0.147	0.161	0.125	0.130	0.154	0.163	
Ca	0.666	0.637	0.630	0.654	0.635	0.662	0.634	0.634	0.694	0.651	
Na	0.228	0.221	0.178	0.161	0.212	0.169	0.219	0.219	0.163	0.188	
X	**1.977**	**1.986**	**1.983**	**1.990**	**1.988**	**1.988**	**1.994**	**1.989**	**1.999**	**1.991**	
Total	**3.977**	**3.986**	**3.983**	**3.990**	**3.988**	**3.988**	**3.994**	**3.989**	**3.999**	**3.991**	
En	39.614	43.963	45.005	45.601	45.258	45.073	47.041	46.590	46.406	45.014	
Fs	10.265	10.313	11.628	11.358	10.282	10.726	8.747	9.076	9.712	11.022	
Wo	50.121	45.724	43.367	43.041	44.460	44.201	44.212	44.334	43.882	43.965	
Mg#	79.421	80.999	79.468	80.060	81.488	80.777	84.321	83.696	82.694	80.331	
Q	1.328	1.394	1.453	1.518	1.428	1.497	1.433	1.429	1.581	1.480	
J	0.456	0.442	0.356	0.322	0.424	0.337	0.438	0.439	0.326	0.377	

Clinopyroxene in MAOC 15

cpx	10 kbar/1050 °C															
MAOC 15																
SiO_2	49.290	49.470	48.500	49.770	49.790	49.240	48.380	49.070	49.310	49.660	49.620	48.900	48.230	48.930	48.650	48.340
TiO_2	0.648	0.493	0.710	0.556	0.515	0.740	0.706	0.649	0.674	0.641	0.538	0.838	1.040	0.504	0.667	1.306
Al_2O_3	9.060	9.290	10.210	8.130	8.600	10.290	9.590	9.390	9.670	9.020	9.200	9.580	9.780	9.050	10.040	10.160
FeO	5.840	5.050	5.420	5.070	5.080	5.080	5.670	4.200	4.870	4.030	4.680	3.830	4.810	5.370	5.170	4.470
MgO	14.620	14.330	14.040	14.960	15.290	14.770	14.400	15.310	14.780	15.230	14.790	15.300	14.490	14.980	14.320	15.070
CaO	19.050	20.050	19.800	20.710	19.070	19.200	19.620	19.710	19.330	19.970	19.710	20.030	20.410	19.750	19.810	19.620
Na_2O	1.077	0.896	0.950	0.771	0.880	0.880	0.947	0.929	0.984	0.853	0.967	0.919	0.865	1.041	0.999	0.830
Total	**99.585**	**99.579**	**99.630**	**99.967**	**99.225**	**100.200**	**99.313**	**99.258**	**99.618**	**99.404**	**99.505**	**99.397**	**99.625**	**99.625**	**99.656**	**99.796**
formula																
Si	1.798	1.805	1.770	1.809	1.819	1.783	1.771	1.785	1.794	1.806	1.807	1.776	1.757	1.779	1.771	1.755
Al IV	0.202	0.195	0.230	0.191	0.181	0.217	0.229	0.215	0.206	0.194	0.193	0.224	0.243	0.221	0.229	0.245
Z	**2.000**	**2.000**	**2.000**	**2.000**	**2.000**	**2.000**	**2.000**	**2.000**	**2.000**	**2.000**	**2.000**	**2.000**	**2.000**	**2.000**	**2.000**	**2.000**
Al VI	0.188	0.204	0.210	0.158	0.189	0.222	0.185	0.188	0.209	0.193	0.201	0.186	0.177	0.167	0.202	0.189
Fe^{3+}	0.054	0.026	0.048	0.056	0.026	0.016	0.073	0.055	0.030	0.023	0.031	0.056	0.069	0.100	0.059	0.042
Ti	0.018	0.014	0.019	0.015	0.014	0.020	0.019	0.018	0.018	0.018	0.015	0.023	0.028	0.014	0.018	0.036
Mg	0.795	0.779	0.764	0.811	0.833	0.797	0.786	0.830	0.802	0.826	0.803	0.828	0.787	0.812	0.777	0.815
Fe^{2+}	0.124	0.128	0.117	0.098	0.129	0.137	0.101	0.073	0.118	0.099	0.112	0.060	0.078	0.063	0.098	0.094
Ca	0.745	0.784	0.774	0.807	0.746	0.745	0.769	0.768	0.754	0.778	0.769	0.779	0.797	0.769	0.773	0.763
Na	0.076	0.063	0.067	0.054	0.062	0.062	0.067	0.066	0.069	0.060	0.068	0.065	0.061	0.073	0.071	0.058
X	**2.000**	**1.999**	**2.000**	**1.999**	**2.000**	**2.000**	**2.000**	**1.997**	**2.000**	**1.998**	**1.999**	**1.997**	**1.996**	**1.999**	**1.998**	**1.998**
Total	**4.000**	**3.999**	**4.000**	**3.999**	**4.000**	**4.000**	**4.000**	**3.997**	**4.000**	**3.998**	**3.999**	**3.997**	**3.996**	**3.999**	**3.998**	**3.998**
En	47.795	46.074	46.153	47.251	48.741	47.470	47.453	49.664	47.898	48.478	47.683	49.661	47.367	49.367	47.148	48.762
Fs	7.445	7.594	7.068	5.735	7.567	8.179	6.079	4.382	7.079	5.836	6.645	3.612	4.680	3.853	5.973	5.610
Wo	44.760	46.332	46.780	47.014	43.692	44.351	46.469	45.954	45.023	45.686	45.672	46.727	47.953	46.780	46.878	45.628
Mg#	86.522	85.850	86.720	89.176	86.562	85.303	88.645	91.892	87.123	89.255	87.769	93.221	91.008	92.759	88.755	89.682
Q	1.664	1.692	1.655	1.716	1.708	1.680	1.656	1.672	1.674	1.704	1.684	1.668	1.661	1.645	1.648	1.672
J	0.152	0.127	0.134	0.109	0.125	0.124	0.134	0.131	0.139	0.120	0.137	0.129	0.122	0.147	0.141	0.117

cpx	10 kbar/1050 °C		10kbar/1100 °C													
MAOC 15	av	sd													av	sd
SiO_2	49.072	0.530	47.903	49.048	47.591	48.380	47.440	48.050	47.850	47.450	48.820	50.400	50.710	46.920	48.380	1.178
TiO_2	0.702	0.212	0.878	0.641	0.791	0.664	1.020	0.885	0.621	0.750	0.866	0.808	0.662	1.233	0.818	0.178
Al_2O_3	9.441	0.599	10.430	9.780	10.360	9.800	9.780	10.680	10.180	10.100	9.210	8.390	8.500	10.160	9.781	0.731
FeO	4.915	0.565	5.770	4.620	5.950	4.860	5.460	3.900	5.630	6.210	4.440	1.480	2.280	4.970	4.631	1.459
MgO	14.793	0.399	14.090	15.480	13.980	14.440	14.490	15.460	14.230	14.340	15.790	16.710	17.740	14.450	15.100	1.174
CaO	19.740	0.451	18.520	18.520	18.640	19.140	18.980	17.780	18.930	17.900	18.650	19.440	18.610	18.850	18.663	0.471
Na_2O	0.924	0.080	0.997	1.058	1.123	1.080	0.743	0.865	1.006	1.133	0.665	1.008	0.754	0.984	0.951	0.157
Total	**99.586**	**0.254**	**98.588**	**99.147**	**98.435**	**98.364**	**97.913**	**97.620**	**98.447**	**97.883**	**98.441**	**98.236**	**99.256**	**97.567**	**98.325**	**0.531**
formula																
Si	1.787		1.765	1.785	1.756	1.781	1.760	1.773	1.763	1.759	1.793	1.835	1.827	1.744	1.779	
Al IV	0.213		0.235	0.215	0.244	0.219	0.240	0.227	0.237	0.241	0.207	0.165	0.173	0.256	0.221	
Z	**2.000**		**2.000**	**2.000**	**2.000**	**2.000**	**2.000**	**2.000**	**2.000**	**2.000**	**2.000**	**2.000**	**2.000**	**2.000**	**2.000**	
Al VI	0.192		0.218	0.204	0.206	0.206	0.188	0.238	0.206	0.200	0.192	0.194	0.188	0.189	0.203	
Fe^{3+}	0.047		0.036	0.049	0.072	0.054	0.045	0.002	0.066	0.080	0.014	0.000	0.000	0.069	0.039	
Ti	0.019		0.024	0.018	0.022	0.018	0.028	0.025	0.017	0.021	0.024	0.022	0.018	0.034	0.023	
Mg	0.803		0.774	0.840	0.769	0.792	0.802	0.851	0.782	0.792	0.865	0.907	0.953	0.801	0.828	
Fe^{2+}	0.102		0.142	0.091	0.111	0.095	0.125	0.119	0.108	0.112	0.122	0.045	0.068	0.085	0.103	
Ca	0.770		0.731	0.722	0.737	0.755	0.755	0.703	0.747	0.711	0.734	0.758	0.718	0.751	0.735	
Na	0.065		0.071	0.075	0.080	0.077	0.053	0.062	0.072	0.081	0.047	0.071	0.053	0.071	0.068	
X	**1.999**		**1.997**	**1.998**	**1.998**	**1.998**	**1.995**	**1.998**	**1.998**	**1.998**	**1.998**	**1.998**	**1.999**	**2.000**	**1.999**	
Total	**3.999**		**3.997**	**3.998**	**3.998**	**3.998**	**3.995**	**3.998**	**3.998**	**3.998**	**3.998**	**3.998**	**3.999**	**4.000**	**3.999**	
En	47.923		46.994	50.799	47.548	48.235	47.688	50.859	47.761	49.048	50.246	53.027	54.772	48.923	49.685	
Fs	6.113		8.611	5.519	6.887	5.814	7.416	7.101	6.574	6.949	7.100	2.635	3.931	5.208	6.178	
Wo	45.964		44.395	43.681	45.565	45.951	44.896	42.039	45.665	44.004	42.654	44.338	41.297	45.869	44.137	
Mg#	88.687		84.514	90.200	87.349	89.243	86.542	87.748	87.901	87.591	87.619	95.267	93.303	90.378	88.940	
Q	1.675		1.647	1.653	1.617	1.643	1.681	1.672	1.637	1.615	1.721	1.710	1.740	1.637	1.666	
J	0.130		0.142	0.149	0.161	0.154	0.107	0.124	0.144	0.163	0.095	0.142	0.105	0.142	0.136	

cpx	**12.5 kbar/1050 °C**															
MAOC 15																
SiO_2	49.280	47.050	47.290	47.390	47.630	47.880	47.440	46.790	48.650	47.100	47.160	47.510	48.080	47.180	47.520	46.740
TiO_2	0.907	0.893	1.015	0.891	0.822	0.830	0.997	0.844	0.617	0.943	0.943	0.736	0.728	0.819	0.688	0.910
Al_2O_3	8.900	11.520	10.890	8.710	12.060	11.440	10.960	11.990	10.480	10.100	11.920	11.740	10.970	11.600	11.550	11.870
FeO	6.830	7.040	7.500	9.290	6.830	6.500	7.560	6.840	6.190	7.920	6.360	6.610	6.780	6.350	6.890	7.100
MgO	14.860	12.180	12.650	14.360	12.330	12.610	12.830	12.330	12.950	13.000	12.080	12.480	12.570	12.520	12.900	12.570
CaO	16.850	17.940	18.060	17.820	17.900	17.670	17.740	18.430	17.860	19.090	18.110	17.970	17.800	18.120	17.820	17.690
Na_2O	1.520	1.680	1.660	0.804	1.820	1.610	1.590	1.760	1.830	1.169	1.670	1.690	1.690	1.680	1.680	1.630
Total	**99.147**	**98.303**	**99.065**	**99.265**	**99.392**	**98.540**	**99.117**	**98.984**	**98.577**	**99.322**	**98.243**	**98.736**	**98.618**	**98.269**	**99.048**	**98.510**
formula																
Si	1.803	1.745	1.742	1.752	1.744	1.769	1.746	1.720	1.791	1.737	1.749	1.749	1.774	1.746	1.744	1.726
Al IV	0.197	0.255	0.258	0.248	0.256	0.231	0.254	0.280	0.209	0.263	0.251	0.251	0.226	0.254	0.256	0.274
Z	**2.000**	**2.000**	**2.000**	**2.000**	**2.000**	**2.000**	**2.000**	**2.000**	**2.000**	**2.000**	**2.000**	**2.000**	**2.000**	**2.000**	**2.000**	**2.000**
Al VI	0.186	0.249	0.215	0.132	0.264	0.267	0.221	0.239	0.245	0.177	0.269	0.259	0.251	0.251	0.244	0.243
Fe^{3+}	0.069	0.076	0.106	0.123	0.076	0.033	0.089	0.119	0.060	0.117	0.050	0.069	0.052	0.078	0.094	0.096
Ti	0.025	0.025	0.028	0.025	0.023	0.023	0.028	0.023	0.017	0.026	0.026	0.020	0.020	0.023	0.019	0.025
Mg	0.810	0.673	0.695	0.791	0.673	0.694	0.704	0.676	0.711	0.715	0.668	0.685	0.691	0.691	0.706	0.692
Fe^{2+}	0.140	0.142	0.126	0.164	0.133	0.167	0.143	0.091	0.130	0.127	0.148	0.134	0.157	0.118	0.117	0.124
Ca	0.660	0.713	0.713	0.706	0.702	0.699	0.699	0.726	0.704	0.755	0.719	0.709	0.704	0.718	0.701	0.700
Na	0.108	0.121	0.119	0.058	0.129	0.115	0.113	0.125	0.131	0.084	0.120	0.121	0.121	0.121	0.120	0.117
X	**1.999**	**1.999**	**2.000**	**1.999**	**2.000**	**2.000**	**1.998**	**2.000**	**1.998**	**2.000**	**2.000**	**1.998**	**1.996**	**2.000**	**2.000**	**1.996**
Total	**3.999**	**3.999**	**4.000**	**3.999**	**4.000**	**4.000**	**3.998**	**4.000**	**3.998**	**4.000**	**4.000**	**3.998**	**3.996**	**4.000**	**4.000**	**3.996**
En	50.310	44.064	45.314	47.633	44.624	44.482	45.513	45.274	45.992	44.782	43.505	44.820	44.538	45.212	46.314	45.656
Fs	8.689	9.289	8.189	9.883	8.814	10.719	9.257	6.089	8.419	7.954	9.618	8.797	10.133	7.757	7.704	8.164
Wo	41.001	46.647	46.497	42.484	46.561	44.799	45.230	48.638	45.589	47.264	46.877	46.384	45.329	47.030	45.983	46.180
Mg#	85.273	82.589	84.695	82.816	83.506	80.581	83.098	88.145	84.527	84.917	81.895	83.593	81.465	85.355	85.739	84.831
Q	1.611	1.528	1.533	1.662	1.508	1.561	1.546	1.492	1.545	1.596	1.535	1.529	1.552	1.527	1.524	1.516
J	0.216	0.242	0.237	0.115	0.258	0.231	0.227	0.251	0.261	0.167	0.240	0.241	0.242	0.241	0.239	0.233

cpx	**12.5 kbar/1050 °C**						**12.5 kbar/1100 °C**					**15 kbar/900 °C**				
MAOC 15					**av**	**sd**				**av**	**sd**					
SiO_2	48.420	46.980	46.540	47.970	47.530	0.686	46.912	45.874	49.620	47.469	1.934	47.630	48.690	48.340	47.880	45.870
TiO_2	0.833	0.999	0.954	0.902	0.864	0.107	1.010	0.693	1.036	0.913	0.191	0.515	0.909	0.537	0.652	1.032
Al_2O_3	9.350	11.670	11.900	9.920	10.977	1.058	12.930	14.840	10.250	12.673	2.306	10.640	9.770	9.600	10.710	10.130
FeO	7.880	7.300	7.250	7.260	7.114	0.705	6.780	7.830	5.480	6.697	1.177	7.790	8.180	7.930	7.920	9.990
MgO	15.420	12.700	12.200	13.580	12.956	0.912	14.650	14.770	14.310	14.577	0.239	14.510	13.860	14.970	14.060	13.550
CaO	16.250	17.070	17.900	16.950	17.752	0.605	14.880	14.020	15.350	14.750	0.674	16.030	15.130	15.580	15.260	16.370
Na_2O	0.988	1.650	1.540	1.510	1.559	0.267	1.480	1.149	2.400	1.676	0.648	1.071	1.960	1.180	1.680	1.510
Total	**99.141**	**98.369**	**98.284**	**98.092**	**98.751**	**0.418**	**98.642**	**99.176**	**98.446**	**98.755**	**0.377**	**98.186**	**98.499**	**98.137**	**98.162**	**98.452**
formula																
Si	1.777	1.740	1.729	1.780	1.753		1.717	1.673	1.812	1.734		1.764	1.796	1.789	1.770	1.704
Al IV	0.223	0.260	0.271	0.220	0.247		0.283	0.327	0.188	0.266		0.236	0.204	0.211	0.230	0.296
Z	**2.000**	**2.000**	**2.000**	**2.000**	**2.000**		**2.000**	**2.000**	**2.000**	**2.000**		**2.000**	**2.000**	**2.000**	**2.000**	**2.000**
Al VI	0.181	0.249	0.249	0.214	0.230		0.275	0.310	0.253	0.280		0.229	0.221	0.208	0.237	0.148
Fe^{3+}	0.067	0.074	0.080	0.062	0.079		0.057	0.060	0.047	0.054		0.054	0.072	0.055	0.077	0.197
Ti	0.023	0.028	0.027	0.025	0.024		0.028	0.019	0.028	0.025		0.014	0.025	0.015	0.018	0.029
Mg	0.843	0.701	0.675	0.751	0.712		0.799	0.803	0.779	0.794		0.801	0.762	0.826	0.775	0.750
Fe^{2+}	0.175	0.152	0.146	0.163	0.140		0.150	0.179	0.120	0.151		0.187	0.181	0.191	0.168	0.113
Ca	0.639	0.677	0.712	0.674	0.702		0.584	0.548	0.601	0.577		0.636	0.598	0.618	0.605	0.652
Na	0.070	0.118	0.111	0.109	0.111		0.105	0.081	0.170	0.119		0.077	0.140	0.085	0.120	0.109
X	**1.998**	**2.000**	**2.000**	**1.998**	**1.999**		**1.999**	**2.000**	**1.999**	**2.000**		**1.999**	**1.999**	**1.997**	**2.000**	**1.998**
Total	**3.998**	**4.000**	**4.000**	**3.998**	**3.999**		**3.999**	**4.000**	**3.999**	**4.000**		**3.999**	**3.999**	**3.997**	**4.000**	**3.998**
En	50.887	45.805	44.052	47.308	45.838		52.131	52.501	51.952	52.167		49.313	49.462	50.527	50.077	49.520
Fs	10.571	9.946	9.494	10.253	9.021		9.813	11.681	7.995	9.893		11.531	11.731	11.679	10.860	7.481
Wo	38.542	44.249	46.454	42.439	45.141		38.056	35.818	40.053	37.940		39.156	38.807	37.795	39.064	42.999
Mg#	82.800	82.161	82.270	82.188	83.556		84.158	81.800	86.663	84.059		81.048	80.830	81.226	82.179	86.876
Q	1.658	1.531	1.533	1.588	1.554		1.534	1.529	1.500	1.522		1.625	1.541	1.635	1.548	1.515
J	0.141	0.237	0.222	0.217	0.223		0.210	0.162	0.340	0.238		0.154	0.280	0.169	0.241	0.218

cpx	**15 kbar/900 °C**						**15 kbar/1050 °C**									
MAOC 15					**av**	**sd**										
SiO_2	48.670	48.760	48.500	49.420	48.196	0.553	50.720	48.830	51.870	49.000	49.990	51.550	50.110	48.910	49.220	51.960
TiO_2	0.629	0.698	0.543	0.489	0.667	0.081	1.043	1.158	0.849	0.588	0.728	0.725	0.924	0.702	0.792	0.862
Al_2O_3	11.560	10.610	8.830	8.180	10.003	0.976	9.640	12.610	9.900	12.220	10.470	8.670	11.010	10.770	9.930	8.770
FeO	6.940	6.610	8.390	7.640	7.932	0.541	5.950	6.710	5.260	6.520	6.260	5.880	5.960	7.320	7.400	5.410
MgO	15.300	15.060	16.610	16.680	14.956	1.006	15.900	12.390	13.670	13.210	13.470	13.940	13.250	12.630	12.530	14.280
CaO	14.640	15.090	15.260	15.660	15.447	1.090	13.990	14.890	14.960	15.800	16.340	16.420	15.730	16.380	17.070	14.870
Na_2O	1.092	1.142	0.696	0.996	1.259	0.236	1.980	2.380	2.780	2.070	2.020	2.300	2.200	2.260	2.340	2.670
Total	**98.831**	**97.970**	**98.829**	**99.065**	**98.459**	**0.379**	**99.223**	**98.968**	**99.289**	**99.408**	**99.278**	**99.485**	**99.184**	**98.972**	**99.282**	**98.822**
formula																
Si	1.779	1.799	1.782	1.806	1.778		1.837	1.786	1.874	1.783	1.823	1.873	1.824	1.795	1.803	1.888
Al IV	0.221	0.201	0.218	0.194	0.222		0.163	0.214	0.126	0.217	0.177	0.127	0.176	0.205	0.197	0.112
Z	**2.000**	**2.000**	**2.000**	**2.000**	**2.000**		**2.000**	**2.000**	**2.000**	**2.000**	**2.000**	**2.000**	**2.000**	**2.000**	**2.000**	**2.000**
Al VI	0.277	0.260	0.164	0.159	0.213		0.248	0.330	0.296	0.307	0.273	0.245	0.297	0.260	0.231	0.264
Fe^{3+}	0.000	0.000	0.075	0.077	0.061		0.000	0.000	0.000	0.024	0.004	0.004	0.000	0.067	0.088	0.000
Ti	0.017	0.019	0.015	0.013	0.019		0.028	0.032	0.023	0.016	0.020	0.020	0.025	0.019	0.022	0.024
Mg	0.834	0.828	0.910	0.909	0.822		0.858	0.676	0.736	0.717	0.732	0.755	0.719	0.691	0.684	0.774
Fe^{2+}	0.212	0.204	0.183	0.156	0.183		0.180	0.205	0.159	0.174	0.187	0.175	0.181	0.158	0.138	0.164
Ca	0.573	0.597	0.601	0.613	0.610		0.543	0.584	0.579	0.616	0.639	0.639	0.614	0.644	0.670	0.579
Na	0.077	0.082	0.050	0.071	0.090		0.139	0.169	0.195	0.146	0.143	0.162	0.155	0.161	0.166	0.188
X	**1.991**	**1.990**	**1.998**	**1.998**	**1.999**		**1.997**	**1.995**	**1.988**	**2.000**	**1.998**	**2.000**	**1.992**	**2.000**	**2.000**	**1.992**
Total	**3.991**	**3.990**	**3.998**	**3.998**	**3.999**		**3.997**	**3.995**	**3.988**	**4.000**	**3.998**	**4.000**	**3.992**	**4.000**	**4.000**	**3.992**
En	51.489	50.855	53.736	54.144	50.882		54.280	46.135	49.940	47.550	47.022	48.131	47.493	46.290	45.848	50.996
Fs	13.101	12.521	10.782	9.321	11.346		11.394	14.016	10.779	11.574	11.981	11.122	11.984	10.561	9.261	10.838
Wo	35.410	36.624	35.482	36.535	37.772		34.326	39.849	39.281	40.876	40.997	40.747	40.523	43.149	44.892	38.167
Mg#	79.717	80.243	83.288	85.313	81.767		82.650	76.699	82.247	80.424	79.694	81.230	79.852	81.423	83.196	82.473
Q	1.619	1.629	1.693	1.679	1.616		1.582	1.464	1.474	1.507	1.557	1.569	1.514	1.492	1.492	1.517
J	0.155	0.163	0.099	0.141	0.180		0.278	0.338	0.389	0.292	0.286	0.324	0.311	0.322	0.332	0.376

cpx	15 kbar/1050 °C			15 kbar/1100 °C											
MAOC 15		av	sd												
SiO_2	48.100	50.024	1.343	50.700	51.530	50.380	51.810	51.860	51.860	51.400	50.730	51.700	50.030	50.870	49.990
TiO_2	0.974	0.850	0.167	0.554	0.439	0.475	0.514	0.584	0.516	0.623	0.644	0.610	0.522	0.611	0.794
Al_2O_3	11.950	10.540	1.326	9.960	8.080	9.910	8.430	8.400	8.210	8.470	9.940	8.770	10.810	9.620	9.990
FeO	7.570	6.385	0.793	2.900	2.490	2.500	3.580	4.270	3.640	4.260	3.200	2.520	2.040	2.120	2.840
MgO	12.000	13.388	1.085	14.460	15.420	14.980	16.210	15.390	15.670	15.720	15.530	15.830	14.720	15.090	15.250
CaO	16.810	15.751	0.964	19.490	20.390	20.340	18.220	17.290	18.330	17.730	18.070	19.110	20.810	20.360	19.240
Na_2O	2.460	2.315	0.254	1.880	1.470	1.450	1.570	2.130	1.790	1.670	1.670	1.370	1.326	1.360	1.530
Total	**99.864**	**99.252**	**0.284**	**99.944**	**99.819**	**100.035**	**100.334**	**99.924**	**100.016**	**99.873**	**99.784**	**99.910**	**100.258**	**100.031**	**99.634**
formula															
Si	1.750	1.823		1.821	1.854	1.808	1.852	1.863	1.861	1.850	1.822	1.853	1.792	1.827	1.801
Al IV	0.250	0.177		0.179	0.146	0.192	0.148	0.137	0.139	0.150	0.178	0.147	0.208	0.173	0.199
Z	**2.000**	**2.000**		**2.000**	**2.000**	**2.000**	**2.000**	**2.000**	**2.000**	**2.000**	**2.000**	**2.000**	**2.000**	**2.000**	**2.000**
Al VI	0.262	0.276		0.243	0.197	0.227	0.207	0.218	0.209	0.210	0.243	0.224	0.248	0.234	0.225
Fe^{3+}	0.107	0.018		0.037	0.027	0.041	0.021	0.036	0.026	0.022	0.016	0.000	0.024	0.001	0.039
Ti	0.027	0.023		0.015	0.012	0.013	0.014	0.016	0.014	0.017	0.017	0.016	0.014	0.017	0.022
Mg	0.651	0.727		0.774	0.827	0.801	0.864	0.824	0.838	0.844	0.832	0.846	0.786	0.808	0.819
Fe^{2+}	0.123	0.177		0.050	0.048	0.035	0.086	0.092	0.083	0.107	0.080	0.076	0.037	0.063	0.047
Ca	0.655	0.615		0.750	0.786	0.782	0.698	0.665	0.705	0.684	0.695	0.734	0.799	0.783	0.743
Na	0.174	0.164		0.131	0.103	0.101	0.109	0.148	0.125	0.117	0.116	0.095	0.092	0.095	0.107
X	**1.999**	**2.000**		**2.000**	**2.000**	**1.999**	**1.998**	**2.000**	**2.000**	**1.999**	**2.000**	**1.991**	**2.000**	**2.000**	**2.000**
Total	**3.999**	**4.000**		**4.000**	**4.000**	**3.999**	**3.998**	**4.000**	**4.000**	**3.999**	**4.000**	**3.991**	**4.000**	**4.000**	**4.000**
En	45.527	47.877		49.186	49.800	49.530	52.438	52.096	51.560	51.627	51.748	51.100	48.462	48.844	50.911
Fs	8.635	11.640		3.166	2.871	2.133	5.199	5.839	5.092	6.523	4.975	4.563	2.296	3.790	2.923
Wo	45.837	40.483		47.648	47.329	48.337	42.362	42.065	43.348	41.850	43.276	44.337	49.242	47.366	46.165
Mg#	84.056	80.442		93.952	94.548	95.872	90.979	89.921	91.012	88.782	91.229	91.802	95.476	92.799	94.570
Q	1.429	1.519		1.574	1.661	1.618	1.647	1.582	1.626	1.634	1.607	1.655	1.622	1.654	1.608
J	0.347	0.327		0.262	0.205	0.202	0.218	0.297	0.249	0.233	0.233	0.190	0.184	0.189	0.214

cpx	15 kbar/1100 °C		20 kbar/1050 °C												
MAOC 15	av	sd												av	sd
SiO_2	51.072	0.709	52.530	52.710	51.280	52.950	53.570	53.450	52.730	52.360	52.040	53.640	50.130	52.490	1.048
TiO_2	0.574	0.094	0.525	1.071	0.421	0.520	0.663	0.525	0.541	0.492	0.675	0.660	0.831	0.629	0.185
Al_2O_3	9.216	0.915	7.750	7.740	8.950	8.900	8.810	8.030	8.440	8.750	9.990	8.860	10.910	8.830	0.941
FeO	3.030	0.766	5.200	5.280	6.400	4.460	3.490	4.290	4.950	5.640	5.360	3.080	5.420	4.870	0.968
MgO	15.356	0.491	15.550	14.110	15.920	15.150	14.490	16.630	15.520	15.320	15.270	14.810	13.590	15.124	0.847
CaO	19.115	1.186	15.430	15.850	14.700	14.530	14.490	13.610	15.060	14.680	13.710	15.510	14.770	14.758	0.696
Na_2O	1.601	0.240	2.230	3.030	2.030	2.580	3.090	2.520	2.220	2.370	2.380	3.130	2.540	2.556	0.375
Total	**99.964**	**0.193**	**99.215**	**99.791**	**99.701**	**99.090**	**98.603**	**99.055**	**99.461**	**99.612**	**99.425**	**99.690**	**98.191**	**99.258**	**0.500**
formula															
Si	1.834		1.901	1.900	1.849	1.905	1.926	1.917	1.897	1.886	1.869	1.913	1.834	1.892	
Al IV	0.166		0.099	0.100	0.151	0.095	0.074	0.083	0.103	0.114	0.131	0.087	0.166	0.108	
Z	**2.000**		**2.000**	**2.000**	**2.000**	**2.000**	**2.000**	**2.000**	**2.000**	**2.000**	**2.000**	**2.000**	**2.000**	**2.000**	
Al VI	0.224		0.232	0.229	0.230	0.282	0.300	0.256	0.255	0.258	0.292	0.285	0.305	0.267	
Fe^{3+}	0.022		0.000	0.024	0.040	0.000	0.000	0.000	0.000	0.000	0.000	0.000	0.000	0.000	
Ti	0.016		0.014	0.029	0.011	0.014	0.018	0.014	0.015	0.013	0.018	0.018	0.023	0.017	
Mg	0.822		0.839	0.758	0.856	0.812	0.777	0.889	0.832	0.823	0.818	0.787	0.741	0.813	
Fe^{2+}	0.069		0.157	0.135	0.153	0.134	0.105	0.129	0.149	0.170	0.161	0.092	0.166	0.147	
Ca	0.736		0.598	0.612	0.568	0.560	0.558	0.523	0.580	0.567	0.528	0.593	0.579	0.570	
Na	0.112		0.156	0.212	0.142	0.180	0.215	0.175	0.155	0.166	0.166	0.216	0.180	0.179	
X	**2.000**		**1.997**	**2.000**	**2.000**	**1.983**	**1.973**	**1.987**	**1.986**	**1.996**	**1.983**	**1.991**	**1.995**	**1.993**	
Total	**4.000**		**3.997**	**4.000**	**4.000**	**3.983**	**3.973**	**3.987**	**3.986**	**3.996**	**3.983**	**3.991**	**3.995**	**3.993**	
En	50.541		52.610	50.363	54.278	53.924	53.942	57.706	53.295	52.764	54.283	53.494	49.879	53.135	
Fs	4.241		9.869	8.976	9.701	8.905	7.288	8.351	9.535	10.897	10.688	6.241	11.159	9.598	
Wo	45.218		37.521	40.661	36.021	37.171	38.770	33.943	37.170	36.339	35.029	40.265	38.962	37.267	
Mg#	92.258		84.204	84.873	84.838	85.827	88.097	87.359	84.824	82.884	83.549	89.553	81.718	84.700	
Q	1.627		1.595	1.506	1.577	1.507	1.440	1.541	1.562	1.559	1.506	1.472	1.486	1.530	
J	0.223		0.313	0.424	0.284	0.360	0.431	0.350	0.310	0.331	0.332	0.433	0.360	0.357	

cpx	20 kbar/1100 °C														
MAOC 15															
SiO_2	52.730	53.160	53.330	52.750	53.660	52.890	53.990	52.530	52.910	52.170	53.160	52.460	52.870	53.120	53.150
TiO_2	0.693	0.684	0.680	0.652	0.644	0.536	0.616	0.528	0.663	0.684	0.577	0.525	0.739	0.839	0.696
Al_2O_3	9.230	9.110	9.120	9.210	8.340	8.580	9.060	6.370	6.850	9.170	6.630	7.800	8.350	7.940	7.490
FeO	4.430	4.410	4.830	4.460	4.490	4.530	4.650	6.060	6.010	5.370	6.030	6.180	3.790	3.860	4.580
MgO	14.200	14.380	14.370	14.540	14.590	14.960	14.780	15.180	15.360	15.580	15.560	14.630	14.870	15.000	15.200
CaO	14.560	14.420	14.150	14.400	14.830	15.280	14.130	16.350	16.330	15.580	16.480	16.560	16.520	16.740	16.640
Na_2O	3.380	3.260	3.340	3.250	3.100	2.950	3.240	2.290	2.270	1.940	2.180	2.300	2.650	2.420	2.300
Total	**99.223**	**99.424**	**99.820**	**99.262**	**99.654**	**99.726**	**100.466**	**99.308**	**100.393**	**100.494**	**100.617**	**100.455**	**99.789**	**99.919**	**100.056**
formula															
Si	1.897	1.907	1.908	1.897	1.922	1.896	1.915	1.909	1.900	1.865	1.907	1.886	1.896	1.904	1.908
Al IV	0.103	0.093	0.092	0.103	0.078	0.104	0.085	0.091	0.100	0.135	0.093	0.114	0.104	0.096	0.092
Z	**2.000**	**2.000**	**2.000**	**2.000**	**2.000**	**2.000**	**2.000**	**2.000**	**2.000**	**2.000**	**2.000**	**2.000**	**2.000**	**2.000**	**2.000**
Al VI	0.288	0.292	0.293	0.287	0.274	0.258	0.294	0.181	0.190	0.251	0.187	0.216	0.249	0.239	0.225
Fe^{3+}	0.012	0.000	0.000	0.007	0.000	0.022	0.000	0.042	0.030	0.000	0.027	0.029	0.000	0.000	0.000
Ti	0.019	0.018	0.018	0.018	0.017	0.014	0.016	0.014	0.018	0.018	0.016	0.014	0.020	0.023	0.019
Mg	0.761	0.769	0.767	0.779	0.779	0.799	0.781	0.822	0.822	0.830	0.832	0.784	0.795	0.801	0.813
Fe^{2+}	0.121	0.132	0.145	0.127	0.134	0.114	0.138	0.142	0.150	0.161	0.154	0.156	0.114	0.116	0.137
Ca	0.561	0.554	0.543	0.555	0.569	0.587	0.537	0.637	0.628	0.597	0.633	0.638	0.635	0.643	0.640
Na	0.236	0.227	0.232	0.227	0.215	0.205	0.223	0.161	0.158	0.134	0.152	0.160	0.184	0.168	0.160
X	**1.998**	**1.993**	**1.997**	**2.000**	**1.989**	**2.000**	**1.989**	**2.000**	**1.997**	**1.991**	**2.000**	**1.999**	**1.998**	**1.990**	**1.995**
Total	**3.998**	**3.993**	**3.997**	**4.000**	**3.989**	**4.000**	**3.989**	**4.000**	**3.997**	**3.991**	**4.000**	**3.999**	**3.998**	**3.990**	**3.995**
En	52.732	52.833	52.735	53.339	52.544	53.285	53.659	51.376	51.374	52.299	51.387	49.679	51.508	51.376	51.129
Fs	8.408	9.089	9.943	8.694	9.071	7.599	9.470	8.852	9.371	10.112	9.496	9.905	7.364	7.416	8.642
Wo	38.860	38.078	37.322	37.967	38.386	39.117	36.870	39.772	39.256	37.589	39.117	40.416	41.128	41.208	40.229
Mg#	86.248	85.322	84.136	85.984	85.278	87.520	84.999	85.302	84.574	83.798	84.402	83.377	87.491	87.386	85.541
Q	1.444	1.456	1.454	1.461	1.483	1.500	1.456	1.600	1.601	1.587	1.619	1.578	1.544	1.560	1.591
J	0.471	0.454	0.463	0.453	0.431	0.410	0.446	0.323	0.316	0.269	0.303	0.321	0.369	0.336	0.320

cpx	**20 kbar/1100 °C**		
MAOC 15		**av**	**sd**
SiO_2	53.110	52.999	0.447
TiO_2	0.714	0.654	0.084
Al_2O_3	7.470	8.170	0.983
FeO	4.560	4.890	0.786
MgO	15.200	14.900	0.427
CaO	16.860	15.614	1.048
Na_2O	2.370	2.703	0.498
Total	**100.284**	**99.931**	**0.479**
formula			
Si	1.904	1.903	
Al IV	0.096	0.097	
Z	**2.000**	**2.000**	
Al VI	0.219	0.249	
Fe^{3+}	0.003	0.001	
Ti	0.019	0.018	
Mg	0.812	0.798	
Fe^{2+}	0.134	0.146	
Ca	0.648	0.601	
Na	0.165	0.188	
X	**2.000**	**2.000**	
Total	**4.000**	**4.000**	
En	50.970	51.642	
Fs	8.396	9.462	
Wo	40.634	38.896	
Mg#	85.857	84.516	
Q	1.594	1.545	
J	0.329	0.376	

Orthopyroxene in MAOC 11

opx	**10 kbar/1100 °C**														
MAOC 11														**av**	**sd**
SiO_2	52.530	51.680	50.830	51.000	51.750	51.820	50.710	50.890	49.800	49.300	51.790	52.780	50.180	51.158	1.026
TiO_2	0.424	0.479	0.398	0.382	0.324	0.261	0.375	0.409	0.373	0.419	0.386	0.345	0.438	0.386	0.055
Al_2O_3	6.730	7.150	8.170	8.180	7.140	8.230	8.920	7.980	9.840	10.810	8.360	7.860	9.920	8.407	1.190
FeO	8.570	10.770	9.780	11.550	10.630	8.570	9.400	12.220	11.210	9.710	8.720	7.340	9.870	9.872	1.381
MgO	29.490	27.240	28.470	27.550	28.120	28.840	28.170	26.820	26.970	27.330	28.260	28.220	28.030	27.962	0.762
CaO	1.680	2.000	1.500	1.480	1.373	1.480	1.342	1.322	1.386	1.350	1.870	2.490	1.360	1.587	0.345
Na_2O	0.114	0.162	0.092	0.117	0.089	0.114	0.086	0.082	0.026	0.073	0.099	0.100	0.024	0.091	0.037
Total	**99.538**	**99.481**	**99.240**	**100.259**	**99.426**	**99.315**	**99.003**	**99.723**	**99.605**	**98.992**	**99.485**	**99.135**	**99.822**	**99.463**	**0.350**
formula															
Si	1.843	1.837	1.797	1.798	1.834	1.823	1.795	1.811	1.766	1.748	1.823	1.853	1.765	1.808	
Al IV	0.157	0.163	0.203	0.202	0.166	0.177	0.205	0.189	0.234	0.252	0.177	0.147	0.235	0.192	
Z	**2.000**	**2.000**	**2.000**	**2.000**	**2.000**	**2.000**	**2.000**	**2.000**	**2.000**	**2.000**	**2.000**	**2.000**	**2.000**	**2.000**	
Al VI	0.121	0.136	0.137	0.138	0.132	0.164	0.167	0.146	0.178	0.200	0.170	0.178	0.176	0.158	
Fe^{3+}	0.020	0.012	0.051	0.052	0.022	0.006	0.024	0.026	0.036	0.035	0.000	0.000	0.035	0.019	
Ti	0.011	0.013	0.011	0.010	0.009	0.007	0.010	0.011	0.010	0.011	0.010	0.009	0.012	0.010	
Mg	1.542	1.443	1.500	1.448	1.485	1.512	1.486	1.423	1.426	1.445	1.483	1.477	1.470	1.473	
Fe^{2+}	0.231	0.308	0.238	0.288	0.293	0.246	0.254	0.337	0.297	0.253	0.257	0.215	0.256	0.273	
Ca	0.063	0.076	0.057	0.056	0.052	0.056	0.051	0.050	0.053	0.051	0.071	0.094	0.051	0.060	
Na	0.008	0.011	0.006	0.008	0.006	0.008	0.006	0.006	0.000	0.005	0.007	0.007	0.000	0.006	
X	**1.997**	**2.000**	**2.000**	**2.000**	**1.999**	**1.999**	**1.999**	**1.999**	**1.999**	**2.000**	**1.997**	**1.979**	**1.999**	**2.000**	
Total	**3.997**	**4.000**	**4.000**	**4.000**	**3.999**	**3.999**	**3.999**	**3.999**	**3.999**	**4.000**	**3.997**	**3.979**	**3.999**	**4.000**	
En	83.969	78.986	83.592	80.794	81.164	83.363	82.960	78.582	80.327	82.588	81.924	82.691	82.729	81.580	
Fs	12.593	16.846	13.242	16.087	15.987	13.563	14.199	18.634	16.706	14.480	14.180	12.065	14.386	15.092	
Wo	3.438	4.168	3.165	3.119	2.848	3.075	2.841	2.784	2.967	2.932	3.896	5.244	2.885	3.328	
Mg#	86.958	82.421	86.325	83.395	83.544	86.007	85.385	80.832	82.783	85.083	85.245	87.267	85.187	84.389	
x (opx)	0.130	0.176	0.137	0.166	0.165	0.140	0.146	0.192	0.172	0.149	0.148	0.127	0.148	0.156	

opx	**12.5 kbar/1050 °C**												
MAOC 11												**av**	**sd**
SiO_2	49.210	50.370	49.470	50.460	50.120	49.750	50.510	49.860	50.060	50.340	50.100	50.023	0.416
TiO_2	0.321	0.444	0.252	0.260	0.332	0.358	0.413	0.352	0.261	0.386	0.266	0.331	0.066
Al_2O_3	9.880	8.240	9.040	8.190	9.440	8.060	7.420	8.700	9.400	10.580	9.230	8.925	0.912
FeO	14.060	14.210	13.430	14.030	13.340	14.380	13.940	14.290	13.220	12.860	12.960	13.702	0.553
MgO	24.860	25.210	24.850	25.320	23.130	26.120	25.950	25.380	25.960	24.040	25.160	25.089	0.881
CaO	1.530	1.108	1.750	1.017	1.248	0.648	0.837	1.060	1.065	1.158	1.074	1.136	0.300
Na_2O	0.112	0.089	0.116	0.125	0.152	0.071	0.073	0.076	0.094	0.175	0.133	0.111	0.034
Total	**99.973**	**99.671**	**98.908**	**99.402**	**97.762**	**99.387**	**99.143**	**99.718**	**100.060**	**99.539**	**98.923**	**99.317**	**0.640**
formula													
Si	1.760	1.810	1.786	1.816	1.827	1.786	1.821	1.790	1.780	1.798	1.804	1.801	
Al IV	0.240	0.190	0.214	0.184	0.173	0.214	0.179	0.210	0.220	0.202	0.196	0.199	
Z	**2.000**	**2.000**	**2.000**	**2.000**	**2.000**	**2.000**	**2.000**	**2.000**	**2.000**	**2.000**	**2.000**	**2.000**	
Al VI	0.177	0.159	0.171	0.164	0.232	0.127	0.136	0.158	0.174	0.244	0.196	0.179	
Fe^{3+}	0.052	0.011	0.036	0.014	0.000	0.070	0.025	0.039	0.037	0.000	0.000	0.008	
Ti	0.009	0.012	0.007	0.007	0.009	0.010	0.011	0.010	0.007	0.010	0.007	0.009	
Mg	1.326	1.351	1.338	1.359	1.257	1.398	1.395	1.358	1.376	1.280	1.351	1.346	
Fe^{2+}	0.369	0.417	0.370	0.408	0.407	0.362	0.395	0.390	0.356	0.384	0.390	0.404	
Ca	0.059	0.043	0.068	0.039	0.049	0.025	0.032	0.041	0.041	0.044	0.041	0.044	
Na	0.008	0.006	0.008	0.009	0.011	0.005	0.005	0.005	0.006	0.012	0.009	0.008	
X	**1.998**	**1.998**	**1.997**	**2.000**	**1.964**	**1.997**	**2.000**	**2.000**	**1.998**	**1.975**	**1.995**	**1.999**	
Total	**3.998**	**3.998**	**3.997**	**4.000**	**3.964**	**3.997**	**4.000**	**4.000**	**3.998**	**3.975**	**3.995**	**3.999**	
En	75.607	74.629	75.356	75.235	73.405	78.329	76.548	75.929	77.612	74.923	75.779	75.039	
Fs	21.049	23.014	20.830	22.593	23.748	20.274	21.678	21.792	20.100	22.483	21.896	22.519	
Wo	3.344	2.357	3.814	2.172	2.847	1.397	1.775	2.279	2.288	2.594	2.325	2.442	
Mg#	78.223	76.430	78.344	76.905	75.556	79.438	77.930	77.700	79.429	76.919	77.583	76.917	
x (opx)	0.218	0.236	0.217	0.231	0.244	0.206	0.221	0.223	0.206	0.231	0.224	0.231	

opx	**12.5/1100 °C**										
MAOC 11										**av**	**sd**
SiO_2	53.749	51.152	53.235	51.317	53.120	51.313	53.376	54.339	51.682	52.587	1.218
TiO_2	0.299	0.330	0.365	0.330	0.327	0.373	0.213	0.357	0.355	0.328	0.049
Al_2O_3	3.850	7.160	5.720	7.320	7.120	8.040	5.480	7.530	6.490	6.523	1.303
FeO	11.260	11.630	10.830	11.850	10.810	11.480	10.890	9.720	11.680	11.128	0.657
MgO	28.440	27.130	27.410	26.500	25.740	26.470	26.920	23.060	27.010	26.520	1.493
CaO	1.550	1.308	1.470	1.360	1.890	1.342	1.830	2.900	1.650	1.700	0.496
Na_2O	0.142	0.144	0.181	0.190	0.570	0.208	0.373	0.771	0.147	0.303	0.226
Total	**99.290**	**98.854**	**99.211**	**98.867**	**99.577**	**99.226**	**99.082**	**98.677**	**99.014**	**99.089**	**0.272**
formula											
Si	1.914	1.832	1.891	1.842	1.881	1.832	1.902	1.929	1.851	1.876	
Al IV	0.086	0.168	0.109	0.158	0.119	0.168	0.098	0.071	0.149	0.124	
Z	**2.000**	**2.000**	**2.000**	**2.000**	**2.000**	**2.000**	**2.000**	**2.000**	**2.000**	**2.000**	
Al VI	0.075	0.134	0.131	0.151	0.178	0.170	0.132	0.244	0.125	0.150	
Fe^{3+}	0.002	0.026	0.000	0.002	0.000	0.000	0.000	0.000	0.015	0.000	
Ti	0.008	0.009	0.010	0.009	0.009	0.010	0.006	0.010	0.010	0.009	
Mg	1.510	1.448	1.452	1.418	1.359	1.408	1.430	1.220	1.442	1.410	
Fe^{2+}	0.333	0.322	0.322	0.354	0.320	0.343	0.325	0.289	0.335	0.332	
Ca	0.059	0.050	0.056	0.052	0.072	0.051	0.070	0.110	0.063	0.065	
Na	0.010	0.010	0.012	0.013	0.039	0.014	0.026	0.053	0.010	0.021	
X	**1.997**	**2.000**	**1.983**	**1.999**	**1.977**	**1.997**	**1.988**	**1.926**	**2.000**	**1.987**	
Total	**3.997**	**4.000**	**3.983**	**3.999**	**3.977**	**3.997**	**3.988**	**3.926**	**4.000**	**3.987**	
En	79.361	79.550	79.353	77.722	77.618	78.142	78.383	75.367	78.370	78.037	
Fs	17.530	17.694	17.588	19.411	18.286	19.011	17.787	17.820	18.189	18.368	
Wo	3.109	2.757	3.059	2.867	4.096	2.847	3.830	6.812	3.441	3.595	
Mg#	81.907	81.805	81.857	80.016	80.933	80.432	81.505	80.877	81.163	80.947	
x (opx)	0.181	0.182	0.181	0.200	0.191	0.196	0.185	0.191	0.188	0.191	

Orthopyroxene in MAOC 13

opx	**10 kbar/1050 °C**						**10 kbar/1100 °C**									
MAOC 13					**av**	**sd**										
SiO_2	49.980	50.500	50.490	52.060	50.758	0.902	51.130	51.480	50.430	51.090	51.030	49.340	50.510	49.270	49.120	50.410
TiO_2	0.392	0.203	0.235	0.214	0.261	0.088	0.322	0.279	0.341	0.265	0.344	0.351	0.273	0.330	0.242	0.265
Al_2O_3	10.000	9.340	9.250	7.870	9.115	0.895	9.230	8.330	9.360	8.120	8.660	10.230	9.730	10.790	11.140	9.300
FeO	10.130	10.120	10.460	10.230	10.235	0.158	8.110	8.730	9.550	10.150	9.750	11.510	8.030	10.370	10.270	9.610
MgO	27.790	28.510	27.900	28.370	28.143	0.351	28.940	28.640	27.580	27.680	27.740	26.550	28.760	26.970	26.930	27.440
CaO	1.098	1.104	1.098	1.550	1.213	0.225	1.440	1.382	1.271	1.336	1.324	0.975	1.336	1.059	1.017	1.365
Na_2O	0.041	0.076	0.071	0.095	0.071	0.022	0.079	0.115	0.078	0.105	0.087	0.054	0.086	0.080	0.051	0.102
Total	**99.431**	**99.853**	**99.504**	**100.389**	**99.794**	**0.437**	**99.251**	**98.956**	**98.610**	**98.746**	**98.935**	**99.010**	**98.725**	**98.869**	**98.770**	**98.492**
formula																
Si	1.766	1.772	1.783	1.823	1.786		1.795	1.819	1.795	1.820	1.812	1.762	1.782	1.753	1.748	1.797
Al IV	0.234	0.228	0.217	0.177	0.214		0.205	0.181	0.205	0.180	0.188	0.238	0.218	0.247	0.252	0.203
Z	**2.000**	**2.000**	**2.000**	**2.000**	**2.000**		**2.000**	**2.000**	**2.000**	**2.000**	**2.000**	**2.000**	**2.000**	**2.000**	**2.000**	**2.000**
Al VI	0.182	0.158	0.168	0.148	0.164		0.177	0.166	0.187	0.161	0.174	0.192	0.186	0.206	0.215	0.188
Fe^{3+}	0.034	0.063	0.040	0.023	0.040		0.014	0.008	0.004	0.011	0.000	0.031	0.023	0.029	0.026	0.007
Ti	0.010	0.005	0.006	0.006	0.007		0.009	0.007	0.009	0.007	0.009	0.009	0.007	0.009	0.006	0.007
Mg	1.464	1.491	1.469	1.481	1.476		1.515	1.509	1.463	1.470	1.468	1.413	1.512	1.431	1.429	1.458
Fe^{2+}	0.265	0.234	0.269	0.277	0.261		0.224	0.250	0.280	0.292	0.289	0.313	0.214	0.280	0.280	0.280
Ca	0.042	0.041	0.042	0.058	0.046		0.054	0.052	0.048	0.051	0.050	0.037	0.050	0.040	0.039	0.052
Na	0.003	0.005	0.005	0.006	0.005		0.005	0.008	0.005	0.007	0.006	0.004	0.006	0.006	0.004	0.007
X	**2.000**	**1.998**	**1.999**	**1.999**	**1.999**		**1.999**	**2.000**	**1.997**	**1.999**	**1.998**	**2.000**	**1.999**	**2.000**	**1.998**	**1.998**
Total	**4.000**	**3.998**	**3.999**	**3.999**	**3.999**		**3.999**	**4.000**	**3.997**	**3.999**	**3.998**	**4.000**	**3.999**	**4.000**	**3.998**	**3.998**
En	82.665	84.399	82.538	81.564	82.783		84.484	83.318	81.650	81.098	81.204	80.130	85.099	81.706	81.757	81.465
Fs	14.988	13.252	15.127	15.233	14.654		12.494	13.792	15.645	16.089	16.010	17.755	12.060	15.988	16.024	15.623
Wo	2.347	2.349	2.335	3.203	2.563		3.021	2.890	2.704	2.813	2.786	2.115	2.841	2.306	2.219	2.913
Mg#	84.652	86.429	84.511	84.263	84.961		87.116	85.797	83.920	83.445	83.531	81.861	87.587	83.634	83.613	83.909
x (opx)	0.153	0.136	0.155	0.157	0.150		0.129	0.142	0.161	0.166	0.165	0.181	0.124	0.164	0.164	0.161

opx	**10 kbar/1100 °C**								**12.5 kbar/1050 °C**						
MAOC 13							**av**	**sd**							
SiO_2	49.080	50.530	50.360	50.730	50.870	50.310	50.356	0.761	49.890	49.870	51.220	50.180	51.000	49.760	50.050
TiO_2	0.348	0.246	0.187	0.215	0.155	0.307	0.279	0.060	0.265	0.164	0.249	0.231	0.380	0.234	0.283
Al_2O_3	10.730	9.480	10.510	9.650	9.240	10.400	9.681	0.893	10.350	10.000	8.000	9.930	9.430	9.790	10.440
FeO	9.470	9.920	7.140	7.790	9.140	8.430	9.248	1.140	11.550	11.770	11.570	11.390	11.040	11.180	11.170
MgO	27.350	27.780	29.530	28.660	28.390	28.510	27.966	0.836	26.440	26.400	27.700	26.310	25.940	25.940	25.280
CaO	1.156	1.370	1.194	1.377	1.228	1.205	1.252	0.141	1.029	0.924	0.877	0.956	0.999	2.170	1.620
Na_2O	0.072	0.075	0.083	0.098	0.067	0.101	0.083	0.018	0.204	0.227	0.107	0.173	0.220	0.253	0.271
Total	**98.206**	**99.401**	**99.004**	**98.520**	**99.090**	**99.263**	**98.866**	**0.316**	**99.728**	**99.355**	**99.723**	**99.170**	**99.009**	**99.327**	**99.114**
formula															
Si	1.752	1.785	1.762	1.793	1.796	1.767	1.784		1.768	1.773	1.814	1.790	1.816	1.772	1.787
Al IV	0.248	0.215	0.238	0.207	0.204	0.233	0.216		0.232	0.227	0.186	0.210	0.184	0.228	0.213
Z	**2.000**	**2.000**	**2.000**	**2.000**	**2.000**	**2.000**	**2.000**		**2.000**	**2.000**	**2.000**	**2.000**	**2.000**	**2.000**	**2.000**
Al VI	0.203	0.179	0.195	0.195	0.181	0.198	0.188		0.201	0.193	0.148	0.207	0.212	0.183	0.226
Fe^{3+}	0.031	0.027	0.038	0.007	0.020	0.024	0.019		0.031	0.039	0.032	0.003	0.000	0.049	0.000
Ti	0.009	0.007	0.005	0.006	0.004	0.008	0.007		0.007	0.004	0.007	0.006	0.010	0.006	0.008
Mg	1.455	1.463	1.540	1.510	1.494	1.493	1.477		1.397	1.400	1.462	1.399	1.377	1.377	1.345
Fe^{2+}	0.252	0.266	0.171	0.223	0.250	0.223	0.255		0.311	0.311	0.310	0.337	0.329	0.283	0.333
Ca	0.044	0.052	0.045	0.052	0.046	0.045	0.048		0.039	0.035	0.033	0.037	0.038	0.083	0.062
Na	0.005	0.005	0.006	0.007	0.005	0.007	0.006		0.014	0.016	0.007	0.012	0.015	0.017	0.019
X	**2.000**	**1.999**	**2.000**	**2.000**	**2.000**	**1.999**	**1.999**		**2.000**	**1.997**	**2.000**	**2.000**	**1.982**	**2.000**	**1.993**
Total	**4.000**	**3.999**	**4.000**	**4.000**	**4.000**	**3.999**	**3.999**		**4.000**	**3.997**	**4.000**	**4.000**	**3.982**	**4.000**	**3.993**
En	83.103	82.130	87.731	84.585	83.433	84.750	82.977		79.954	80.182	80.981	78.945	78.963	78.992	77.285
Fs	14.373	14.959	9.720	12.494	13.973	12.675	14.352		17.810	17.801	17.176	18.994	18.852	16.259	19.156
Wo	2.525	2.911	2.550	2.921	2.594	2.575	2.670		2.236	2.017	1.843	2.062	2.186	4.749	3.560
Mg#	85.255	84.593	90.026	87.130	85.654	86.990	85.254		81.783	81.833	82.501	80.606	80.727	82.930	80.137
x (opx)	0.147	0.154	0.100	0.129	0.143	0.130	0.147		0.182	0.182	0.175	0.194	0.193	0.171	0.199

opx	**12.5 kbar/1050 °C**				**12.5/1100 °C**								**15 kbar/900 °C**			
MAOC 13			**av**	**sd**							**av**	**sd**			**av**	**sd**
SiO_2	50.370	52.250	50.510	0.827	51.837	52.038	51.375	50.757	50.380	50.613	51.167	0.685	49.550	51.600	50.575	1.450
TiO_2	0.165	0.226	0.244	0.065	0.300	0.290	0.336	0.337	0.422	0.295	0.330	0.050	0.109	0.177	0.143	0.048
Al_2O_3	9.150	10.770	9.762	0.829	7.850	8.070	6.970	8.290	9.790	8.530	8.250	0.925	10.410	7.720	9.065	1.902
FeO	11.410	10.610	11.299	0.345	10.540	9.930	11.510	10.150	10.050	10.480	10.443	0.575	12.460	7.680	10.070	3.380
MgO	27.870	24.730	26.290	1.014	26.840	27.220	27.300	26.790	24.960	27.350	26.743	0.905	26.080	28.100	27.090	1.428
CaO	1.287	1.750	1.290	0.456	1.323	1.384	1.309	1.520	2.050	1.201	1.465	0.305	1.203	2.230	1.717	0.726
Na_2O	0.107	0.893	0.273	0.240	0.238	0.391	0.185	0.274	0.554	0.169	0.302	0.147	0.095	0.194	0.145	0.070
Total	**100.359**	**101.229**	**99.668**	**0.718**	**98.928**	**99.323**	**98.985**	**98.118**	**98.206**	**98.638**	**98.700**	**0.471**	**99.907**	**97.701**	**98.804**	**1.560**
formula																
Si	1.768	1.818	1.790		1.846	1.841	1.836	1.823	1.809	1.805	1.829		1.759	1.843	1.802	
Al IV	0.232	0.182	0.210		0.154	0.159	0.164	0.177	0.191	0.195	0.171		0.241	0.157	0.198	
Z	**2.000**	**2.000**	**2.000**		**2.000**	**2.000**	**2.000**	**2.000**	**2.000**	**2.000**	**2.000**		**2.000**	**2.000**	**2.000**	
Al VI	0.147	0.260	0.200		0.175	0.178	0.130	0.174	0.223	0.164	0.176		0.194	0.168	0.182	
Fe^{3+}	0.084	0.000	0.100		0.000	0.000	0.029	0.004	0.000	0.024	0.000		0.047	0.000	0.019	
Ti	0.004	0.006	0.007		0.008	0.008	0.009	0.009	0.011	0.008	0.009		0.003	0.005	0.004	
Mg	1.458	1.283	1.390		1.425	1.436	1.454	1.434	1.336	1.454	1.425		1.380	1.496	1.439	
Fe^{2+}	0.251	0.309	0.320		0.314	0.294	0.315	0.301	0.302	0.288	0.312		0.323	0.229	0.281	
Ca	0.048	0.065	0.048		0.050	0.052	0.050	0.058	0.079	0.046	0.056		0.046	0.085	0.066	
Na	0.007	0.060	0.006		0.016	0.027	0.013	0.019	0.039	0.012	0.021		0.007	0.013	0.010	
X	**2.000**	**1.983**	**1.999**		**1.988**	**1.994**	**2.000**	**2.000**	**1.990**	**1.996**	**1.999**		**1.999**	**1.997**	**2.000**	
Total	**4.000**	**3.983**	**3.999**		**3.988**	**3.994**	**4.000**	**4.000**	**3.990**	**3.996**	**3.999**		**3.999**	**3.997**	**4.000**	
En	82.964	77.428	78.960		79.636	80.568	79.941	79.958	77.827	81.316	79.465		78.921	82.621	80.573	
Fs	14.283	18.634	18,26		17.543	16.487	17.304	16.782	17.578	16.117	17.407		18.463	12.667	15.758	
Wo	2.754	3.938	2.790		2.821	2.944	2.755	3.261	4.594	2.566	3.128		2.616	4.713	3.669	
Mg#	85.313	80.602	81.220		81.948	83.012	82.206	82.653	81.575	83.458	82.031		81.041	86.707	83.642	
x (opx)	0.147	0.194	0.187		0.181	0.170	0.178	0.173	0.184	0.165	0.180		0.190	0.133	0.164	

Orthopyroxene in MAOC 15

opx	**10 kbar/1050 °C**							**10 kbar/1100 °C**								
MAOC 15						**av**	**sd**									
SiO_2	51.730	52.340	53.300	53.170	53.000	52.708	0.660	52.341	52.524	54.157	51.830	52.485	50.409	52.080	51.780	51.680
TiO_2	0.210	0.339	0.085	0.184	0.120	0.188	0.098	0.166	0.260	0.292	0.319	0.231	0.242	0.181	0.160	0.185
Al_2O_3	9.880	10.230	9.120	8.870	7.890	9.198	0.916	7.470	7.130	3.740	9.000	8.750	10.140	8.150	7.740	8.440
FeO	8.080	7.050	7.340	7.300	8.290	7.612	0.540	6.270	6.580	6.730	5.600	5.240	6.580	7.600	6.150	5.710
MgO	29.780	26.500	26.610	26.490	30.320	27.940	1.936	30.830	31.440	31.740	28.860	31.150	30.440	29.660	31.500	31.040
CaO	1.315	2.880	2.920	2.810	1.341	2.253	0.846	1.385	1.330	1.810	3.620	1.334	1.239	1.290	1.321	1.304
Na_2O	0.174	0.464	0.534	0.167	0.087	0.285	0.200	0.146	0.074	0.141	0.308	0.139	0.105	0.082	0.115	0.103
Total	**101.169**	**99.803**	**99.909**	**98.991**	**101.048**	**100.184**	**0.917**	**98.608**	**99.338**	**98.610**	**99.537**	**99.329**	**99.155**	**99.043**	**98.766**	**98.462**
formula																
Si	1.776	1.823	1.856	1.864	1.826	1.832		1.832	1.826	1.901	1.804	1.817	1.754	1.828	1.804	1.807
Al IV	0.224	0.177	0.144	0.136	0.174	0.168		0.168	0.174	0.099	0.196	0.183	0.246	0.172	0.196	0.193
Z	**2.000**	**2.000**	**2.000**	**2.000**	**2.000**	**2.000**		**2.000**	**2.000**	**2.000**	**2.000**	**2.000**	**2.000**	**2.000**	**2.000**	**2.000**
Al VI	0.176	0.242	0.230	0.231	0.146	0.208		0.140	0.118	0.056	0.173	0.174	0.169	0.165	0.122	0.155
Fe^{3+}	0.046	0.000	0.000	0.000	0.028	0.000		0.028	0.047	0.037	0.025	0.007	0.070	0.002	0.073	0.036
Ti	0.005	0.009	0.002	0.005	0.003	0.005		0.004	0.007	0.008	0.008	0.006	0.006	0.005	0.004	0.005
Mg	1.525	1.376	1.381	1.385	1.557	1.447		1.609	1.629	1.661	1.498	1.607	1.579	1.552	1.636	1.618
Fe^{2+}	0.186	0.205	0.214	0.214	0.211	0.221		0.156	0.144	0.161	0.138	0.145	0.121	0.221	0.106	0.131
Ca	0.048	0.107	0.109	0.106	0.049	0.084		0.052	0.050	0.068	0.135	0.049	0.046	0.049	0.049	0.049
Na	0.012	0.031	0.036	0.011	0.006	0.019		0.010	0.005	0.010	0.021	0.009	0.007	0.006	0.008	0.007
X	**1.998**	**1.971**	**1.973**	**1.951**	**2.000**	**1.985**		**1.999**	**2.000**	**2.000**	**1.998**	**1.998**	**1.999**	**1.999**	**1.999**	**2.000**
Total	**3.998**	**3.971**	**3.973**	**3.951**	**4.000**	**3.985**		**3.999**	**4.000**	**4.000**	**3.998**	**3.998**	**3.999**	**3.999**	**3.999**	**4.000**
En	86.686	81.477	81.064	81.246	85.682	82.591		88.555	89.390	87.901	84.566	89.210	90.424	85.198	91.319	89.991
Fs	10.562	12.159	12.543	12.559	11.594	12.622		8.585	7.892	8.497	7.810	8.044	6.930	12.139	5.929	7.292
Wo	2.751	6.364	6.393	6.194	2.724	4.787		2.859	2.718	3.603	7.624	2.746	2.645	2.663	2.752	2.717
Mg#	89.139	87.014	86.600	86.611	88.081	86.743		91.162	91.887	91.186	91.546	91.728	92.881	87.529	93.904	92.505
x (opx)	0.109	0.130	0.134	0.134	0.119	0.133		0.088	0.081	0.088	0.085	0.083	0.071	0.125	0.061	0.075

opx	**10 kbar/1100 °C**		**12.5 kbar/1050 °C**									**12.5/1100 °C**				
MAOC 15	**av**	**sd**								**av**	**sd**					
SiO_2	52.143	0.988	51.690	50.210	51.140	50.440	49.720	49.960	51.590	50.679	0.794	51.338	50.861	51.344	50.727	51.119
TiO_2	0.226	0.057	0.234	0.197	0.190	0.268	0.194	0.163	0.177	0.203	0.036	0.279	0.249	0.187	0.337	0.235
Al_2O_3	7.840	1.781	8.260	10.620	8.950	9.210	10.220	10.110	8.100	9.353	0.990	8.340	9.110	8.440	10.580	9.770
FeO	6.273	0.708	10.390	9.880	10.200	10.440	9.790	9.850	10.080	10.090	0.263	9.180	8.850	8.440	6.830	9.350
MgO	30.740	0.944	29.150	28.280	28.210	28.410	29.200	27.790	28.950	28.570	0.536	29.060	27.780	29.330	27.960	28.150
CaO	1.626	0.767	0.718	1.069	0.781	0.850	0.822	1.277	0.794	0.902	0.199	1.002	1.000	1.029	1.255	1.083
Na_2O	0.135	0.070	0.116	0.147	0.169	0.183	0.104	0.117	0.133	0.138	0.029	0.214	0.465	0.271	0.649	0.308
Total	**98.983**	**0.385**	**100.558**	**100.403**	**99.640**	**99.801**	**100.050**	**99.267**	**99.824**	**99.935**	**0.444**	**99.413**	**98.315**	**99.041**	**98.338**	**100.015**
formula																
Si	1.820		1.801	1.751	1.801	1.772	1.733	1.764	1.810	1.776		1.803	1.807	1.804	1.788	1.788
Al IV	0.180		0.199	0.249	0.199	0.228	0.267	0.236	0.190	0.224		0.197	0.193	0.196	0.212	0.212
Z	**2.000**		**2.000**	**2.000**	**2.000**	**2.000**	**2.000**	**2.000**	**2.000**	**2.000**		**2.000**	**2.000**	**2.000**	**2.000**	**2.000**
Al VI	0.142		0.141	0.187	0.172	0.153	0.153	0.185	0.145	0.163		0.148	0.188	0.153	0.228	0.191
Fe^{3+}	0.036		0.052	0.062	0.029	0.072	0.110	0.050	0.043	0.060		0.048	0.023	0.051	0.010	0.029
Ti	0.006		0.006	0.005	0.005	0.007	0.005	0.004	0.005	0.005		0.007	0.007	0.005	0.009	0.006
Mg	1.599		1.515	1.470	1.481	1.488	1.518	1.463	1.514	1.493		1.521	1.471	1.536	1.469	1.468
Fe^{2+}	0.147		0.251	0.226	0.271	0.234	0.175	0.241	0.253	0.236		0.222	0.240	0.197	0.192	0.244
Ca	0.061		0.027	0.040	0.029	0.032	0.031	0.048	0.030	0.034		0.038	0.038	0.039	0.047	0.041
Na	0.009		0.008	0.010	0.012	0.012	0.007	0.008	0.009	0.009		0.015	0.032	0.018	0.044	0.021
X	**2.000**		**1.999**	**2.000**	**1.999**	**1.999**	**1.999**	**2.000**	**1.999**	**2.000**		**1.998**	**1.999**	**1.999**	**1.999**	**2.000**
Total	**4.000**		**3.999**	**4.000**	**3.999**	**3.999**	**3.999**	**4.000**	**3.999**	**4.000**		**3.998**	**3.999**	**3.999**	**3.999**	**4.000**
En	88.483		84.518	84.676	83.109	84.821	88.059	83.476	84.280	84.683		85.416	84.096	86.696	86.006	83.759
Fs	8.153		13.986	13.023	15.237	13.355	10.159	13.767	14.059	13.396		12.467	13.728	11.118	11.219	13.925
Wo	3.364		1.496	2.301	1.654	1.824	1.782	2.757	1.661	1.921		2.117	2.176	2.186	2.775	2.316
Mg#	91.563		85.801	86.670	84.507	86.396	89.657	85.843	85.704	86.341		87.263	85.967	88.634	88.461	85.745
x (opx)	0.084		0.142	0.133	0.155	0.136	0.103	0.142	0.143	0.137		0.127	0.140	0.114	0.115	0.143

opx	**12.5/1100 °C**								**15 kbar/900 °C**				**15 kbar/1050 °C**			
MAOC 15							**av**	**sd**			**av**	**sd**				
SiO_2	49.716	50.393	51.289	50.814	50.767	50.620	50.817	0.480	52.620	52.140	52.380	0.339	51.734	52.957	51.950	53.232
TiO_2	0.218	0.355	0.344	0.397	0.394	0.401	0.309	0.078	0.146	0.173	0.160	0.019	0.306	0.228	0.371	0.255
Al_2O_3	10.220	9.600	8.100	8.920	8.690	9.050	9.165	0.795	7.940	9.100	8.520	0.820	8.170	6.350	8.690	5.470
FeO	9.640	9.780	9.620	9.690	9.500	9.490	9.125	0.860	8.270	8.280	8.275	0.007	9.200	8.820	9.170	9.430
MgO	27.970	28.180	28.610	27.590	28.540	28.490	28.333	0.534	30.130	28.040	29.085	1.478	26.560	27.700	26.500	28.140
CaO	1.023	0.973	0.974	1.173	0.918	0.949	1.034	0.100	1.339	1.580	1.460	0.170	1.174	0.903	1.196	1.051
Na_2O	0.239	0.218	0.222	0.358	0.207	0.198	0.304	0.140	0.072	0.333	0.203	0.185	0.579	0.443	0.555	0.438
Total	**99.026**	**99.499**	**99.159**	**98.942**	**99.016**	**99.198**	**99.088**	**0.484**	**100.517**	**99.646**	**100.082**	**0.616**	**97.723**	**97.401**	**98.432**	**98.016**
formula																
Si	1.755	1.773	1.811	1.801	1.794	1.785	1.792		1.822	1.826	1.825		1.853	1.896	1.846	1.902
Al IV	0.245	0.227	0.189	0.199	0.206	0.215	0.208		0.178	0.174	0.175		0.147	0.104	0.154	0.098
Z	**2.000**	**2.000**	**2.000**	**2.000**	**2.000**	**2.000**	**2.000**		**2.000**	**2.000**	**2.000**		**2.000**	**2.000**	**2.000**	**2.000**
Al VI	0.180	0.171	0.148	0.174	0.156	0.161	0.172		0.146	0.201	0.175		0.198	0.164	0.210	0.132
Fe^{3+}	0.067	0.051	0.037	0.027	0.043	0.045	0.039		0.029	0.000	0.004		0.000	0.000	0.000	0.000
Ti	0.006	0.009	0.009	0.011	0.010	0.011	0.008		0.004	0.005	0.004		0.008	0.006	0.010	0.007
Mg	1.472	1.478	1.506	1.458	1.504	1.497	1.489		1.555	1.464	1.511		1.418	1.478	1.404	1.499
Fe^{2+}	0.217	0.237	0.247	0.260	0.238	0.235	0.230		0.210	0.242	0.237		0.276	0.264	0.273	0.282
Ca	0.039	0.037	0.037	0.045	0.035	0.036	0.039		0.050	0.059	0.054		0.045	0.035	0.046	0.040
Na	0.016	0.015	0.015	0.025	0.014	0.014	0.021		0.005	0.023	0.014		0.040	0.031	0.038	0.030
X	**1.998**	**1.997**	**1.999**	**1.998**	**2.000**	**1.998**	**1.999**		**1.999**	**1.993**	**2.000**		**1.985**	**1.980**	**1.981**	**1.990**
Total	**3.998**	**3.997**	**3.999**	**3.998**	**4.000**	**3.998**	**3.999**		**3.999**	**3.993**	**4.000**		**3.985**	**3.980**	**3.981**	**3.990**
En	85.176	84.393	84.146	82.715	84.651	84.683	84.697		85.691	82.909	83.842		81.561	83.192	81.530	82.316
Fs	12.585	13.512	13.795	14.757	13.392	13.290	13.081		11.571	13.733	13.134		15.848	14.859	15.826	15.474
Wo	2.239	2.094	2.059	2.528	1.957	2.027	2.223		2.737	3.358	3.024		2.591	1.949	2.645	2.210
Mg#	87.127	86.199	85.915	84.860	86.341	86.435	86.622		88.103	85.789	86.457		83.731	84.845	83.744	84.176
x (opx)	0.129	0.138	0.141	0.151	0.137	0.136	0.134		0.119	0.142	0.135		0.163	0.152	0.163	0.158

opx	**15 kbar/1050 °C**					**15 kbar/1100 °C**							
MAOC 15				**av**	**sd**							**av**	**sd**
SiO_2	51.885	52.030	54.790	52.654	1.104	54.145	52.668	53.951	53.364	53.747	53.310	53.531	0.533
TiO_2	0.278	0.327	0.232	0.285	0.053	0.235	0.298	0.154	0.196	0.198	0.297	0.230	0.058
Al_2O_3	7.840	8.110	4.360	6.999	1.628	6.140	7.450	6.020	6.710	6.750	6.900	6.662	0.524
FeO	9.650	11.270	9.250	9.541	0.803	6.230	5.960	5.690	6.410	6.200	5.640	6.022	0.312
MgO	27.890	27.990	30.390	27.881	1.295	31.930	31.210	32.310	31.980	31.890	31.650	31.828	0.370
CaO	1.059	1.028	1.044	1.065	0.098	1.037	1.110	1.166	1.000	1.008	1.093	1.069	0.065
Na_2O	0.368	0.264	0.268	0.416	0.125	0.158	0.151	0.157	0.139	0.132	0.199	0.156	0.023
Total	**98.970**	**101.019**	**100.334**	**98.842**	**1.364**	**99.875**	**98.847**	**99.448**	**99.799**	**99.925**	**99.089**	**99.497**	**0.449**
formula													
Si	1.839	1.815	1.908	1.867		1.871	1.836	1.866	1.843	1.855	1.852	1.854	
Al IV	0.161	0.185	0.092	0.133		0.129	0.164	0.134	0.157	0.145	0.148	0.146	
Z	**2.000**	**2.000**	**2.000**	**2.000**		**2.000**	**2.000**	**2.000**	**2.000**	**2.000**	**2.000**	**2.000**	
Al VI	0.167	0.149	0.087	0.159		0.121	0.142	0.111	0.117	0.129	0.135	0.126	
Fe^{3+}	0.004	0.035	0.008	0.000		0.007	0.015	0.025	0.039	0.015	0.011	0.018	
Ti	0.007	0.009	0.006	0.008		0.006	0.008	0.004	0.005	0.005	0.008	0.006	
Mg	1.474	1.456	1.578	1.474		1.644	1.622	1.665	1.647	1.641	1.639	1.643	
Fe^{2+}	0.282	0.294	0.261	0.283		0.173	0.159	0.140	0.146	0.164	0.153	0.156	
Ca	0.040	0.038	0.039	0.040		0.038	0.041	0.043	0.037	0.037	0.041	0.040	
Na	0.025	0.018	0.018	0.029		0.011	0.010	0.011	0.009	0.009	0.013	0.010	
X	**2.000**	**1.998**	**1.997**	**1.992**		**2.000**	**1.997**	**1.999**	**2.000**	**2.000**	**2.000**	**2.000**	
Total	**4.000**	**3.998**	**3.997**	**3.992**		**4.000**	**3.997**	**3.999**	**4.000**	**4.000**	**4.000**	**4.000**	
En	82.059	81.414	84.013	82.006		88.625	88.993	90.101	89.999	89.054	89.427	89.359	
Fs	15.701	16.437	13.913	15.742		9.306	8.733	7.562	7.978	8.923	8.354	8.484	
Wo	2.239	2.149	2.074	2.251		2.069	2.275	2.337	2.023	2.023	2.220	2.157	
Mg#	83.939	83.202	85.793	83.895		90.497	91.064	92.257	91.857	90.893	91.457	91.329	
x (opx)	0.161	0.168	0.142	0.161		0.095	0.089	0.077	0.081	0.091	0.085	0.087	

opx	**20 kbar/1050 °C**			
MAOC 15			**av**	**sd**
SiO_2	54.680	55.360	55.020	0.481
TiO_2	0.224	0.301	0.263	0.054
Al_2O_3	4.970	5.750	5.360	0.552
FeO	7.170	6.730	6.950	0.311
MgO	30.560	29.320	29.940	0.877
CaO	1.660	1.600	1.630	0.042
Na_2O	0.288	0.494	0.391	0.146
Total	**99.552**	**99.555**	**99.554**	**0.002**
formula				
Si	1.906	1.920	1.914	
Al IV	0.094	0.080	0.086	
Z	**2.000**	**2.000**	**2.000**	
Al VI	0.111	0.155	0.134	
Fe^{3+}	0.000	0.000	0.000	
Ti	0.006	0.008	0.007	
Mg	1.588	1.516	1.553	
Fe^{2+}	0.209	0.195	0.202	
Ca	0.062	0.059	0.061	
Na	0.019	0.033	0.026	
X	**1.995**	**1.969**	**1.982**	
Total	**3.995**	**3.969**	**3.982**	
En	85.423	85.618	85.518	
Fs	11.243	11.024	11.136	
Wo	3.335	3.358	3.346	
Mg#	88.370	88.593	88.479	
x (opx)	0.116	0.114	0.115	

Plagioclase in MAOC 11

pl	**10 kbar/1050 °C**													**10 kbar/1100 °C (rim)**	
MAOC 11												**av**	**sd**			
SiO_2	51.880	49.800	50.430	51.270	49.990	52.220	50.730	50.370	50.070	50.130	50.830	50.702	0.791	55.040	53.790	53.730
TiO_2	0.053	0.083	0.018	0.035	0.053	0.000	0.086	0.020	0.065	0.000	0.034	0.041	0.030	0.333	0.322	0.075
Al_2O_3	28.940	30.860	30.580	30.110	31.040	28.980	30.360	30.840	30.500	30.770	30.550	30.321	0.720	24.160	23.690	27.370
FeO	0.574	0.196	0.271	0.365	0.203	0.215	0.192	0.199	0.382	0.218	0.119	0.267	0.128	1.224	1.550	0.332
MgO	0.420	0.106	0.222	0.222	0.088	0.176	0.087	0.083	0.226	0.176	0.091	0.172	0.101	1.465	1.990	0.392
CaO	12.860	14.630	14.280	13.860	14.320	12.640	13.010	13.800	14.130	14.090	14.000	13.784	0.654	9.960	10.820	11.620
Na_2O	4.390	3.240	3.630	3.870	3.530	4.550	4.380	3.760	3.560	3.420	3.790	3.829	0.431	5.390	4.690	4.730
Total	**99.117**	**98.915**	**99.431**	**99.732**	**99.224**	**98.781**	**98.845**	**99.072**	**98.933**	**98.804**	**99.414**	**99.115**	**0.306**	**97.572**	**96.852**	**98.249**
formula																
Si	2.380	2.296	2.313	2.341	2.297	2.399	2.335	2.315	2.308	2.310	2.328	2.329		2.547	2.517	2.470
Ti	0.002	0.003	0.000	0.001	0.002	0.000	0.003	0.000	0.002	0.000	0.001	0.001		0.012	0.011	0.003
Al	1.565	1.677	1.653	1.620	1.681	1.569	1.647	1.671	1.657	1.671	1.649	1.642		1.317	1.306	1.483
Fe^{3+}	0.022	0.008	0.010	0.014	0.008	0.008	0.007	0.008	0.015	0.008	0.005	0.010		0.047	0.061	0.013
Mg	0.029	0.007	0.015	0.015	0.006	0.012	0.006	0.006	0.016	0.012	0.006	0.012		0.101	0.139	0.027
Fe^{2+}	0.000	0.000	0.000	0.000	0.000	0.000	0.000	0.000	0.000	0.000	0.000	0.000		0.000	0.000	0.000
Z	**3.997**	**3.991**	**3.992**	**3.991**	**3.994**	**3.988**	**3.998**	**3.999**	**3.997**	**4.002**	**3.989**	**3.994**		**4.024**	**4.034**	**3.996**
Ca	0.632	0.723	0.702	0.678	0.705	0.622	0.642	0.680	0.698	0.696	0.687	0.678		0.494	0.542	0.572
Na	0.390	0.290	0.323	0.343	0.315	0.405	0.391	0.335	0.318	0.306	0.337	0.341		0.484	0.425	0.422
X	**1.023**	**1.012**	**1.025**	**1.021**	**1.020**	**1.027**	**1.032**	**1.015**	**1.016**	**1.001**	**1.024**	**1.020**		**0.977**	**0.968**	**0.994**
Total	**5.020**	**5.003**	**5.016**	**5.012**	**5.014**	**5.015**	**5.030**	**5.013**	**5.013**	**5.003**	**5.012**	**5.014**		**5.001**	**5.001**	**4.990**
An	61.815	71.390	68.493	66.433	69.153	60.555	62.142	66.977	68.685	69.482	67.120	66.547		50.524	56.042	57.584
Ab	38.185	28.610	31.507	33.567	30.847	39.445	37.858	33.023	31.315	30.518	32.880	33.453		49.476	43.958	42.416
Or	0.000	0.000	0.000	0.000	0.000	0.000	0.000	0.000	0.000	0.000	0.000	0.000		0.000	0.000	0.000
ca(pl)	0.618	0.714	0.685	0.664	0.692	0.606	0.621	0.670	0.687	0.695	0.671	0.665		0.505	0.560	0.576

pl	**10 kbar/1100 °C (rim)**				**10 kbar/1100 °C (in)**								**12.5 kbar/1050 °C**			
MAOC 11			**av rim**	**sd rim**							**av in**	**sd in**				
SiO_2	54.140	54.600	54.260	0.557	51.260	52.060	51.370	51.290	51.820	50.570	51.395	0.516	53.610	53.190	53.690	53.790
TiO_2	0.109	0.346	0.237	0.133	0.031	0.147	0.068	0.051	0.009	0.032	0.056	0.049	0.033	0.028	0.086	0.131
Al_2O_3	26.220	23.200	24.928	1.785	29.440	28.810	29.550	29.540	29.580	30.050	29.495	0.398	28.020	29.200	28.500	26.600
FeO	0.573	1.770	1.090	0.619	0.508	0.610	0.297	0.418	0.327	0.305	0.411	0.127	0.548	0.476	0.819	0.951
MgO	0.694	2.480	1.404	0.871	0.391	0.576	0.177	0.259	0.209	0.159	0.295	0.161	0.233	0.162	0.648	0.814
CaO	10.720	9.130	10.450	0.944	13.120	12.810	13.310	13.100	12.940	13.550	13.138	0.264	11.690	12.010	10.190	11.540
Na_2O	4.970	5.010	4.958	0.280	3.780	3.940	3.830	4.050	4.180	3.820	3.933	0.156	4.860	4.360	5.380	4.520
Total	**97.426**	**96.536**	**97.327**	**0.665**	**98.530**	**98.953**	**98.602**	**98.708**	**99.065**	**98.486**	**98.724**	**0.236**	**98.994**	**99.426**	**99.313**	**98.346**
formula																
Si	2.506	2.550	2.518		2.363	2.388	2.366	2.362	2.375	2.336	2.365		2.450	2.419	2.440	2.474
Ti	0.004	0.012	0.008		0.001	0.005	0.002	0.002	0.000	0.001	0.002		0.001	0.000	0.003	0.005
Al	1.430	1.277	1.363		1.599	1.557	1.604	1.603	1.598	1.636	1.600		1.509	1.565	1.527	1.442
Fe^{3+}	0.022	0.069	0.042		0.020	0.023	0.011	0.016	0.013	0.012	0.016		0.021	0.018	0.031	0.037
Mg	0.048	0.173	0.097		0.027	0.039	0.012	0.018	0.014	0.011	0.020		0.016	0.011	0.044	0.056
Fe^{2+}	0.000	0.000	0.000		0.000	0.000	0.000	0.000	0.000	0.000	0.000		0.000	0.000	0.000	0.000
Z	**4.010**	**4.081**	**4.029**		**4.010**	**4.013**	**3.996**	**4.000**	**3.999**	**3.997**	**4.002**		**3.997**	**4.013**	**4.045**	**4.012**
Ca	0.532	0.457	0.520		0.648	0.629	0.657	0.646	0.635	0.671	0.648		0.572	0.585	0.496	0.569
Na	0.446	0.454	0.446		0.338	0.350	0.342	0.362	0.371	0.342	0.351		0.431	0.384	0.474	0.403
X	**0.978**	**0.911**	**0.966**		**0.986**	**0.980**	**0.999**	**1.008**	**1.007**	**1.013**	**0.999**		**1.003**	**0.970**	**0.970**	**0.972**
Total	**4.987**	**4.992**	**4.994**		**4.996**	**4.992**	**4.995**	**5.008**	**5.006**	**5.010**	**5.001**		**5.000**	**4.982**	**5.015**	**4.984**
An	54.379	50.176	53.805		65.731	64.244	65.759	64.125	63.110	66.219	64.862		57.068	60.353	51.141	58.522
Ab	45.621	49.824	46.195		34.269	35.756	34.241	35.875	36.890	33.781	35.138		42.932	39.647	48.859	41.478
Or	0.000	0.000	0.000		0.000	0.000	0.000	0.000	0.000	0.000	0.000		0.000	0.000	0.000	0.000
ca(pl)	0.544	0.502	0.538		0.657	0.642	0.658	0.641	0.631	0.662	0.649		0.571	0.604	0.511	0.585

pl	**12.5 kbar/1050 °C**										**12.5 kbar/1100 °C**					
MAOC 11									**av**	**sd**						
SiO_2	54.100	54.900	55.090	55.140	52.270	54.870	50.350	54.390	53.783	1.379	52.953	54.346	55.518	55.421	55.214	55.327
TiO_2	0.145	0.029	0.027	0.090	0.085	0.010	0.105	0.075	0.070	0.044	0.095	0.010	0.010	0.043	0.130	0.043
Al_2O_3	27.640	27.560	27.690	27.590	28.470	27.450	29.580	27.630	27.994	0.820	28.540	26.530	25.890	26.200	25.740	26.020
FeO	0.695	0.444	0.587	0.534	0.558	0.544	1.097	0.529	0.649	0.204	0.469	0.440	0.376	0.364	0.581	0.434
MgO	0.131	0.091	0.199	0.191	0.096	0.089	1.304	0.074	0.336	0.385	0.126	0.119	0.231	0.096	0.166	0.229
CaO	10.800	10.560	10.380	10.300	12.270	10.730	10.710	10.860	11.003	0.697	11.830	10.720	10.050	9.990	10.000	9.990
Na_2O	4.630	5.580	5.510	5.470	4.480	5.250	4.570	5.250	4.988	0.461	4.540	5.170	5.610	5.490	5.240	5.550
Total	**98.141**	**99.164**	**99.483**	**99.315**	**98.229**	**98.943**	**97.716**	**98.808**	**98.823**	**0.581**	**98.553**	**97.335**	**97.685**	**97.604**	**97.071**	**97.593**
formula																
Si	2.482	2.496	2.495	2.499	2.412	2.499	2.337	2.483	2.457		2.430	2.516	2.555	2.550	2.555	2.548
Ti	0.005	0.000	0.000	0.003	0.003	0.000	0.004	0.003	0.002		0.003	0.000	0.000	0.001	0.005	0.001
Al	1.494	1.477	1.478	1.474	1.549	1.473	1.618	1.487	1.507		1.543	1.447	1.404	1.421	1.404	1.412
Fe^{3+}	0.027	0.017	0.022	0.020	0.022	0.021	0.043	0.020	0.025		0.018	0.017	0.014	0.014	0.022	0.017
Mg	0.009	0.006	0.013	0.013	0.007	0.006	0.090	0.005	0.023		0.009	0.008	0.016	0.007	0.011	0.016
Fe^{2+}	0.000	0.000	0.000	0.000	0.000	0.000	0.000	0.000	0.000		0.000	0.000	0.000	0.000	0.000	0.000
Z	**4.016**	**3.996**	**4.009**	**4.010**	**3.992**	**3.999**	**4.091**	**3.997**	**4.015**		**4.003**	**3.988**	**3.990**	**3.993**	**3.997**	**3.995**
Ca	0.531	0.514	0.504	0.500	0.607	0.524	0.533	0.531	0.539		0.582	0.532	0.496	0.493	0.496	0.493
Na	0.412	0.492	0.484	0.481	0.401	0.464	0.411	0.465	0.442		0.404	0.464	0.501	0.490	0.470	0.496
X	**0.943**	**1.006**	**0.988**	**0.981**	**1.008**	**0.987**	**0.944**	**0.996**	**0.981**		**0.985**	**0.996**	**0.996**	**0.982**	**0.966**	**0.989**
Total	**4.959**	**5.003**	**4.997**	**4.991**	**5.000**	**4.986**	**5.035**	**4.993**	**4.995**		**4.988**	**4.984**	**4.986**	**4.976**	**4.963**	**4.983**
An	56.314	51.120	51.006	50.994	60.215	53.039	56.429	53.339	54.934		59.016	53.399	49.748	50.139	51.329	49.868
Ab	43.686	48.880	48.994	49.006	39.785	46.961	43.571	46.661	45.066		40.984	46.601	50.252	49.861	48.671	50.132
Or	0.000	0.000	0.000	0.000	0.000	0.000	0.000	0.000	0.000		0.000	0.000	0.000	0.000	0.000	0.000
ca(pl)	0.563	0.511	0.510	0.510	0.602	0.530	0.564	0.533	0.549		0.590	0.534	0.497	0.501	0.513	0.499

pl	12.5 kbar/1100 °C										15 kbar/ 900 °C					
MAOC 11									av	sd						
SiO_2	54.110	55.987	55.110	54.123	54.116	54.922	53.235	53.908	54.592	0.900	58.580	56.250	58.280	56.830	56.790	55.280
TiO_2	0.313	0.017	0.074	0.041	0.027	0.036	0.061	0.068	0.069	0.078	0.057	0.111	0.021	0.020	0.074	0.093
Al_2O_3	25.710	25.510	26.350	27.150	26.930	26.400	27.530	27.420	26.566	0.856	25.390	25.250	25.440	26.700	25.150	25.870
FeO	0.965	0.467	0.309	0.390	0.458	0.278	0.342	0.429	0.450	0.167	0.340	0.516	0.307	0.435	0.618	0.815
MgO	0.502	0.091	0.097	0.080	0.107	0.072	0.120	0.227	0.162	0.113	0.119	0.767	0.079	0.139	0.484	1.095
CaO	10.060	9.070	9.760	10.680	10.560	10.020	10.980	10.690	10.314	0.658	8.540	10.140	8.850	9.680	9.540	10.010
Na_2O	4.750	5.810	5.660	5.330	5.220	5.540	5.120	5.310	5.310	0.349	6.290	5.400	5.890	5.770	5.720	5.450
Total	**96.410**	**96.952**	**97.360**	**97.794**	**97.418**	**97.268**	**97.388**	**98.052**	**97.463**	**0.506**	**99.316**	**98.434**	**98.867**	**99.574**	**98.376**	**98.613**
formula																
Si	2.524	2.587	2.543	2.495	2.503	2.538	2.468	2.480	2.521		2.633	2.569	2.631	2.560	2.590	2.526
Ti	0.011	0.000	0.003	0.001	0.000	0.001	0.002	0.002	0.002		0.002	0.004	0.000	0.000	0.003	0.003
Al	1.414	1.389	1.433	1.475	1.468	1.438	1.504	1.487	1.446		1.345	1.359	1.353	1.418	1.352	1.393
Fe^{3+}	0.038	0.018	0.012	0.015	0.018	0.011	0.013	0.017	0.017		0.013	0.020	0.012	0.016	0.024	0.031
Mg	0.035	0.006	0.007	0.005	0.007	0.005	0.008	0.016	0.011		0.008	0.052	0.005	0.009	0.033	0.075
Fe^{2+}	0.000	0.000	0.000	0.000	0.000	0.000	0.000	0.000	0.000		0.000	0.000	0.000	0.000	0.000	0.000
Z	**4.021**	**4.000**	**3.997**	**3.992**	**3.996**	**3.992**	**3.996**	**4.002**	**3.997**		**4.001**	**4.003**	**4.001**	**4.004**	**4.001**	**4.028**
Ca	0.503	0.449	0.482	0.528	0.523	0.496	0.545	0.527	0.510		0.411	0.496	0.428	0.467	0.466	0.490
Na	0.430	0.520	0.506	0.476	0.468	0.496	0.460	0.474	0.475		0.548	0.478	0.515	0.504	0.506	0.483
X	**0.932**	**0.969**	**0.989**	**1.004**	**0.992**	**0.992**	**1.006**	**1.001**	**0.986**		**0.959**	**0.974**	**0.944**	**0.971**	**0.972**	**0.973**
Total	**4.954**	**4.970**	**4.986**	**4.996**	**4.988**	**4.985**	**5.001**	**5.002**	**4.983**		**4.960**	**4.977**	**4.945**	**4.975**	**4.973**	**5.000**
An	53.925	46.314	48.795	52.546	52.784	49.988	54.236	52.663	51.771		42.867	50.925	45.365	48.109	47.962	50.372
Ab	46.075	53.686	51.205	47.454	47.216	50.012	45.764	47.337	48.229		57.133	49.075	54.635	51.891	52.038	49.628
Or	0.000	0.000	0.000	0.000	0.000	0.000	0.000	0.000	0.000		0.000	0.000	0.000	0.000	0.000	0.000
ca(pl)	0.539	0.463	0.488	0.525	0.528	0.500	0.542	0.527	0.518		0.429	0.509	0.454	0.481	0.480	0.504

pl	15 kbar/ 900 °C						15 kbar/1050 °C							
MAOC 11					av	sd								
SiO_2	55.390	56.210	56.030	55.710	56.535	1.125	56.640	56.520	57.460	58.110	57.090	58.010	57.910	58.660
TiO_2	0.054	0.109	0.031	0.050	0.062	0.034	0.000	0.054	0.044	0.030	0.107	0.032	0.000	0.000
Al_2O_3	26.850	26.400	25.580	26.680	25.931	0.663	26.430	26.480	25.280	25.820	25.720	25.670	25.860	25.470
FeO	0.517	0.484	0.380	0.562	0.497	0.149	0.387	0.397	0.334	0.384	0.761	0.380	0.286	0.255
MgO	0.130	0.234	0.750	0.085	0.388	0.364	0.061	0.065	0.285	0.055	0.150	0.150	0.060	0.046
CaO	10.130	9.870	10.270	9.750	9.678	0.570	9.440	9.370	8.780	8.660	8.800	8.380	8.720	8.090
Na_2O	5.420	5.780	5.460	5.660	5.684	0.276	6.010	6.210	6.490	6.610	6.000	6.590	6.600	6.770
Total	**98.491**	**99.087**	**98.501**	**98.497**	**98.776**	**0.418**	**98.968**	**99.096**	**98.673**	**99.669**	**98.628**	**99.212**	**99.436**	**99.291**
formula														
Si	2.528	2.549	2.558	2.541	2.568		2.567	2.561	2.609	2.609	2.592	2.614	2.607	2.637
Ti	0.002	0.004	0.001	0.002	0.002		0.000	0.002	0.002	0.001	0.004	0.001	0.000	0.000
Al	1.444	1.411	1.376	1.434	1.388		1.412	1.414	1.353	1.366	1.376	1.363	1.372	1.349
Fe^{3+}	0.020	0.018	0.015	0.021	0.019		0.015	0.015	0.013	0.014	0.029	0.014	0.011	0.010
Mg	0.009	0.016	0.051	0.006	0.026		0.004	0.004	0.019	0.004	0.010	0.010	0.004	0.003
Fe^{2+}	0.000	0.000	0.000	0.000	0.000		0.000	0.000	0.000	0.000	0.000	0.000	0.000	0.000
Z	**4.003**	**3.998**	**4.001**	**4.003**	**4.004**		**3.997**	**3.996**	**3.995**	**3.995**	**4.010**	**4.003**	**3.993**	**3.999**
Ca	0.495	0.480	0.502	0.476	0.471		0.458	0.455	0.427	0.417	0.428	0.405	0.421	0.390
Na	0.480	0.508	0.483	0.500	0.501		0.528	0.545	0.571	0.575	0.528	0.576	0.576	0.590
X	**0.975**	**0.988**	**0.986**	**0.977**	**0.972**		**0.986**	**1.000**	**0.998**	**0.992**	**0.956**	**0.980**	**0.997**	**0.980**
Total	**4.978**	**4.986**	**4.987**	**4.980**	**4.976**		**4.984**	**4.996**	**4.993**	**4.987**	**4.966**	**4.984**	**4.990**	**4.979**
An	50.808	48.551	50.967	48.769	48.478		46.467	45.469	42.779	41.996	44.767	41.271	42.201	39.772
Ab	49.192	51.449	49.033	51.231	51.522		53.533	54.531	57.221	58.004	55.233	58.729	57.799	60.228
Or	0.000	0.000	0.000	0.000	0.000		0.000	0.000	0.000	0.000	0.000	0.000	0.000	0.000
ca(pl)	0.508	0.486	0.510	0.488	0.485		0.465	0.455	0.428	0.420	0.448	0.413	0.422	0.398

pl	15 kbar/1050 °C				
MAOC 11				av	sd
SiO_2	58.910	58.660	56.670	57.695	0.873
TiO_2	0.022	0.048	0.105	0.040	0.038
Al_2O_3	25.090	25.710	26.300	25.803	0.450
FeO	0.268	0.313	0.504	0.388	0.143
MgO	0.106	0.052	0.162	0.108	0.073
CaO	7.920	8.080	9.570	8.710	0.569
Na_2O	6.680	6.740	5.950	6.423	0.317
Total	**98.996**	**99.603**	**99.261**	**99.167**	**0.339**
formula					
Si	2.653	2.629	2.563	2.604	
Ti	0.000	0.002	0.004	0.001	
Al	1.332	1.358	1.402	1.372	
Fe^{3+}	0.010	0.012	0.019	0.015	
Mg	0.007	0.003	0.011	0.007	
Fe^{2+}	0.000	0.000	0.000	0.000	
Z	**4.002**	**4.004**	**3.998**	**3.999**	
Ca	0.382	0.388	0.464	0.421	
Na	0.583	0.586	0.522	0.562	
X	**0.965**	**0.974**	**0.985**	**0.983**	
Total	**4.968**	**4.977**	**4.984**	**4.982**	
An	39.584	39.849	47.057	42.838	
Ab	60.416	60.151	52.943	57.162	
Or	0.000	0.000	0.000	0.000	
ca(pl)	0.396	0.398	0.471	0.428	

Plagioclase in MAOC 13

pl	10 kbar/1050 °C												10 kbar	12.5 kbar/1050 °C		
MAOC 13											av	sd	1100 °C			
SiO_2	51.960	51.830	50.860	51.650	50.760	52.270	51.590	51.540	51.360	51.270	51.509	0.468	51.380	55.270	55.050	53.600
TiO_2	0.000	0.000	0.094	0.010	0.104	0.018	0.053	0.000	0.000	0.061	0.034	0.041	0.011	0.118	0.000	0.101
Al_2O_3	29.880	29.900	29.410	29.940	28.330	28.950	29.580	30.250	30.360	28.880	29.548	0.654	29.660	24.900	26.850	27.710
FeO	0.384	0.339	0.440	0.382	1.087	0.580	0.629	0.371	0.171	0.525	0.491	0.247	0.240	0.953	0.508	0.778
MgO	0.076	0.107	0.510	0.103	2.200	0.398	0.489	0.110	0.101	0.953	0.505	0.659	0.282	1.238	0.192	0.324
CaO	13.160	12.500	13.120	13.140	12.460	12.310	12.800	13.070	12.960	13.220	12.874	0.336	13.150	9.800	9.560	10.930
Na_2O	4.460	4.600	4.020	4.290	3.810	4.400	4.170	4.070	4.260	4.280	4.236	0.230	4.100	5.920	5.900	5.000
Total	**99.921**	**99.311**	**98.597**	**99.592**	**98.791**	**98.988**	**99.331**	**99.429**	**99.314**	**99.277**	**99.255**	**0.383**	**98.864**	**98.217**	**98.074**	**98.464**
formula																
Si	2.365	2.370	2.350	2.360	2.341	2.396	2.361	2.354	2.351	2.356	2.360		2.363	2.541	2.524	2.459
Ti	0.000	0.000	0.003	0.000	0.004	0.000	0.002	0.000	0.000	0.002	0.001		0.000	0.004	0.000	0.003
Al	1.603	1.611	1.602	1.612	1.540	1.564	1.595	1.629	1.638	1.564	1.596		1.607	1.349	1.451	1.498
Fe^{3+}	0.015	0.013	0.017	0.015	0.042	0.022	0.024	0.014	0.007	0.020	0.019		0.009	0.037	0.019	0.030
Mg	0.005	0.007	0.035	0.007	0.151	0.027	0.033	0.007	0.007	0.065	0.034		0.019	0.085	0.013	0.022
Fe^{2+}	0.000	0.000	0.000	0.000	0.000	0.000	0.000	0.000	0.000	0.000	0.000		0.000	0.000	0.000	0.000
Z	**3.988**	**4.002**	**4.007**	**3.994**	**4.078**	**4.010**	**4.015**	**4.004**	**4.002**	**4.008**	**4.011**		**3.998**	**4.016**	**4.008**	**4.013**
Ca	0.642	0.612	0.650	0.643	0.616	0.605	0.628	0.640	0.636	0.651	0.632		0.648	0.483	0.470	0.537
Na	0.394	0.408	0.360	0.380	0.341	0.391	0.370	0.360	0.378	0.381	0.376		0.366	0.528	0.525	0.445
X	**1.035**	**1.020**	**1.010**	**1.023**	**0.956**	**0.996**	**0.998**	**1.000**	**1.014**	**1.032**	**1.008**		**1.013**	**1.010**	**0.994**	**0.982**
Total	**5.023**	**5.022**	**5.017**	**5.017**	**5.035**	**5.006**	**5.013**	**5.005**	**5.016**	**5.040**	**5.019**		**5.012**	**5.026**	**5.003**	**4.995**
An	61.986	60.027	64.331	62.862	64.378	60.724	62.912	63.959	62.703	63.058	62.680		63.931	47.775	47.242	54.711
Ab	38.014	39.973	35.669	37.138	35.622	39.276	37.088	36.041	37.297	36.942	37.320		36.069	52.225	52.758	45.289
Or	0.000	0.000	0.000	0.000	0.000	0.000	0.000	0.000	0.000	0.000	0.000		0.000	0.000	0.000	0.000
ca(pl)	0.620	0.600	0.643	0.629	0.644	0.607	0.629	0.640	0.627	0.631	0.627		0.639	0.478	0.472	0.547

pl	12.5 kbar/1050 °C							12.5 kbar/1100 °C								
MAOC 13						av	sd									
SiO_2	55.410	57.240	53.470	55.640	53.160	54.855	1.373	54.255	53.484	56.387	55.850	54.862	52.986	54.479	53.631	52.614
TiO_2	0.143	0.074	0.097	0.098	0.074	0.088	0.042	0.137	0.114	0.019	0.086	0.086	0.101	0.080	0.039	0.096
Al_2O_3	26.960	26.200	28.750	25.660	28.510	26.943	1.346	23.790	27.980	25.200	25.160	26.990	28.250	27.080	27.580	28.280
FeO	0.647	0.433	0.594	0.620	0.349	0.610	0.192	1.400	0.475	0.501	0.535	0.426	0.524	0.350	0.415	0.349
MgO	0.191	0.112	0.132	0.618	0.072	0.360	0.395	2.530	0.196	0.600	0.768	0.316	0.367	0.136	0.134	0.092
CaO	9.170	8.790	11.500	8.720	11.470	9.993	1.153	11.120	11.020	8.900	9.590	9.950	10.180	9.770	10.640	11.310
Na_2O	6.020	6.530	4.910	6.250	4.840	5.671	0.658	5.340	5.150	6.370	5.990	5.740	5.320	5.960	5.370	4.990
Total	**98.602**	**99.396**	**99.586**	**97.685**	**98.531**	**98.569**	**0.642**	**98.583**	**98.450**	**97.996**	**98.039**	**98.420**	**97.803**	**97.907**	**97.938**	**97.749**
formula																
Si	2.526	2.582	2.431	2.560	2.439	2.508		2.503	2.455	2.584	2.565	2.511	2.445	2.507	2.474	2.434
Ti	0.005	0.003	0.003	0.003	0.003	0.003		0.005	0.004	0.000	0.003	0.003	0.004	0.003	0.001	0.003
Al	1.449	1.393	1.541	1.391	1.542	1.452		1.294	1.514	1.361	1.362	1.456	1.537	1.469	1.500	1.542
Fe^{3+}	0.025	0.016	0.023	0.024	0.013	0.023		0.054	0.018	0.019	0.021	0.016	0.020	0.013	0.016	0.014
Mg	0.013	0.008	0.009	0.042	0.005	0.025		0.174	0.013	0.041	0.053	0.022	0.025	0.009	0.009	0.006
Fe^{2+}	0.000	0.000	0.000	0.000	0.000	0.000		0.000	0.000	0.000	0.000	0.000	0.000	0.000	0.000	0.000
Z	**4.018**	**4.001**	**4.007**	**4.021**	**4.002**	**4.011**		**4.030**	**4.004**	**4.006**	**4.003**	**4.008**	**4.031**	**4.001**	**4.000**	**4.000**
Ca	0.448	0.425	0.560	0.430	0.564	0.489		0.550	0.542	0.437	0.472	0.488	0.503	0.482	0.526	0.561
Na	0.532	0.571	0.433	0.557	0.431	0.503		0.478	0.458	0.566	0.533	0.509	0.476	0.532	0.480	0.448
X	**0.980**	**0.996**	**0.993**	**0.987**	**0.994**	**0.992**		**1.027**	**1.000**	**1.003**	**1.005**	**0.997**	**0.979**	**1.014**	**1.006**	**1.008**
Total	**4.998**	**4.997**	**5.000**	**5.008**	**4.996**	**5.003**		**5.057**	**5.004**	**5.009**	**5.008**	**5.005**	**5.011**	**5.015**	**5.007**	**5.008**
An	45.705	42.657	56.414	43.535	56.703	49.334		53.505	54.181	43.570	46.942	48.926	51.396	47.531	52.266	55.605
Ab	54.295	57.343	43.586	56.465	43.297	50.666		46.495	45.819	56.430	53.058	51.074	48.604	52.469	47.734	44.395
Or	0.000	0.000	0.000	0.000	0.000	0.000		0.000	0.000	0.000	0.000	0.000	0.000	0.000	0.000	0.000
ca(pl)	0.457	0.427	0.564	0.435	0.567	0.493		0.535	0.542	0.436	0.469	0.489	0.514	0.475	0.523	0.556

pl	12.5 kbar/1100 °C		15 kbar/900 °C								15 kbar/1050 °C				
MAOC 13	av	sd							av	sd				av	sd
SiO_2	54.283	1.264	55.510	56.110	54.310	53.100	54.510	56.550	55.015	1.282	56.296	55.349	61.480	57.708	3.301
TiO_2	0.084	0.036	0.519	0.113	1.040	0.279	0.095	0.154	0.367	0.365	0.059	0.089	0.032	0.060	0.029
Al_2O_3	26.701	1.606	25.320	23.870	25.460	26.720	25.370	25.760	25.417	0.919	26.650	25.240	23.210	25.033	1.729
FeO	0.553	0.325	0.823	1.224	2.130	0.669	0.787	0.675	1.051	0.566	0.508	0.688	0.276	0.491	0.207
MgO	0.571	0.769	0.523	1.158	0.475	0.666	1.058	0.081	0.660	0.399	0.248	0.841	0.156	0.415	0.372
CaO	10.276	0.806	9.540	9.210	8.470	8.480	10.480	8.250	9.072	0.850	7.600	9.170	5.880	7.550	1.646
Na_2O	5.581	0.456	5.540	5.460	6.140	7.200	4.970	6.470	5.963	0.805	6.700	6.360	8.170	7.077	0.962
Total	**98.098**	**0.306**	**97.867**	**97.198**	**98.082**	**97.158**	**97.270**	**97.975**	**97.592**	**0.427**	**98.112**	**97.746**	**99.221**	**98.360**	**0.768**
formula															
Si	2.498		2.553	2.595	2.503	2.473	2.526	2.586	2.539		2.567	2.551	2.750	2.624	
Ti	0.003		0.018	0.004	0.036	0.010	0.003	0.005	0.013		0.002	0.003	0.001	0.002	
Al	1.448		1.372	1.301	1.383	1.467	1.386	1.388	1.383		1.432	1.371	1.224	1.341	
Fe^{3+}	0.021		0.032	0.047	0.082	0.026	0.031	0.026	0.041		0.019	0.027	0.010	0.019	
Mg	0.039		0.036	0.080	0.033	0.046	0.073	0.006	0.045		0.017	0.058	0.010	0.028	
Fe^{2+}	0.000		0.000	0.000	0.000	0.000	0.000	0.000	0.000		0.000	0.000	0.000	0.000	
Z	**4.009**		**4.010**	**4.026**	**4.036**	**4.022**	**4.019**	**4.011**	**4.021**		**4.038**	**4.010**	**3.996**	**4.014**	
Ca	0.507		0.470	0.456	0.418	0.423	0.520	0.404	0.449		0.371	0.453	0.282	0.368	
Na	0.498		0.494	0.490	0.549	0.650	0.447	0.574	0.534		0.592	0.568	0.709	0.624	
X	**1.005**		**0.964**	**0.946**	**0.967**	**1.073**	**0.967**	**0.978**	**0.982**		**0.964**	**1.021**	**0.990**	**0.992**	
Total	**5.014**		**4.974**	**4.972**	**5.003**	**5.096**	**4.986**	**4.989**	**5.003**		**5.001**	**5.031**	**4.986**	**5.006**	
An	50.432		48.761	48.245	43.257	39.426	53.817	41.337	45.672		38.532	44.345	28.455	37.090	
Ab	49.568		51.239	51.755	56.743	60.574	46.183	58.663	54.328		61.468	55.655	71.545	62.910	
Or	0.000		0.000	0.000	0.000	0.000	0.000	0.000	0.000		0.000	0.000	0.000	0.000	
ca(pl)	0.504		0.488	0.482	0.433	0.394	0.538	0.413	0.457		0.385	0.443	0.285	0.371	

Plagioclase in MAOC 15

pl	10 kbar/1050 °C										12.5 kbar/1050 °C				
MAOC 15									av	sd					
SiO_2	49.260	49.320	47.580	47.500	49.300	49.120	46.650	46.070	48.100	1.318	53.430	53.840	54.220	53.930	53.090
TiO_2	0.000	0.102	0.061	0.047	0.142	0.091	0.000	0.000	0.055	0.054	0.106	0.000	0.127	0.060	0.080
Al_2O_3	31.590	31.520	32.720	31.640	27.190	30.640	30.010	33.170	31.060	1.863	26.430	27.710	24.660	25.550	27.240
FeO	0.162	0.182	0.203	0.286	0.946	0.350	0.264	0.241	0.329	0.256	0.945	0.511	1.149	1.138	0.845
MgO	0.121	0.075	0.071	0.347	2.890	0.101	0.100	0.094	0.475	0.980	1.105	0.254	1.940	1.483	1.640
CaO	15.120	15.030	16.560	15.900	15.440	14.660	17.250	17.270	15.904	1.018	11.250	10.480	10.890	10.430	10.360
Na_2O	3.050	3.150	2.090	2.270	2.390	2.800	1.540	1.580	2.359	0.616	5.080	5.480	5.630	5.000	4.730
Total	**99.398**	**99.380**	**99.334**	**98.100**	**98.349**	**97.818**	**95.872**	**98.438**	**98.336**	**1.172**	**98.414**	**98.368**	**98.698**	**97.704**	**98.075**
formula															
Si	2.266	2.267	2.197	2.221	2.303	2.291	2.237	2.152	2.242		2.463	2.472	2.497	2.497	2.446
Ti	0.000	0.004	0.002	0.002	0.005	0.003	0.000	0.000	0.002		0.004	0.000	0.004	0.002	0.003
Al	1.713	1.708	1.781	1.743	1.497	1.684	1.696	1.826	1.706		1.436	1.500	1.339	1.394	1.479
Fe^{3+}	0.006	0.007	0.008	0.011	0.037	0.014	0.011	0.009	0.013		0.036	0.020	0.044	0.044	0.033
Mg	0.008	0.005	0.005	0.024	0.201	0.007	0.007	0.007	0.033		0.076	0.017	0.133	0.102	0.113
Fe^{2+}	0.000	0.000	0.000	0.000	0.000	0.000	0.000	0.000	0.000		0.000	0.000	0.000	0.000	0.000
Z	**3.993**	**3.991**	**3.993**	**4.001**	**4.044**	**3.998**	**3.951**	**3.994**	**3.996**		**4.015**	**4.009**	**4.018**	**4.040**	**4.073**
Ca	0.745	0.740	0.819	0.796	0.773	0.732	0.886	0.864	0.794		0.556	0.516	0.537	0.517	0.511
Na	0.272	0.281	0.187	0.206	0.216	0.253	0.143	0.143	0.213		0.454	0.488	0.503	0.449	0.423
X	**1.017**	**1.021**	**1.007**	**1.002**	**0.989**	**0.986**	**1.030**	**1.007**	**1.007**		**1.010**	**1.003**	**1.040**	**0.966**	**0.934**
Total	**5.011**	**5.012**	**5.000**	**5.003**	**5.033**	**4.984**	**4.981**	**5.002**	**5.003**		**5.024**	**5.012**	**5.058**	**5.006**	**5.007**
An	73.259	72.503	81.408	79.469	78.118	74.315	86.092	85.796	78.840		55.032	51.382	51.666	53.548	54.759
Ab	26.741	27.497	18.592	20.531	21.882	25.685	13.908	14.204	21.160		44.968	48.618	48.334	46.452	45.241
Or	0.000	0.000	0.000	0.000	0.000	0.000	0.000	0.000	0.000		0.000	0.000	0.000	0.000	0.000
ca(pl)	0.733	0.725	0.814	0.795	0.781	0.743	0.861	0.858	0.788		0.550	0.514	0.517	0.535	0.548

pl	12.5 kbar/1050 °C			12.5 kbbar/1100 °C					15 kbar/900 °C			
MAOC 15		av	sd				av	sd			av	sd
SiO_2	50.860	53.228	1.226	58.329	58.775	57.928	58.344	0.424	58.120	57.130	57.625	0.700
TiO_2	0.086	0.077	0.044	0.054	0.071	0.083	0.069	0.015	0.096	0.000	0.048	0.068
Al_2O_3	30.310	26.983	1.971	24.230	24.250	24.520	24.333	0.162	23.860	23.620	23.740	0.170
FeO	1.020	0.935	0.238	0.268	0.316	0.285	0.290	0.024	0.726	0.784	0.755	0.041
MgO	0.651	1.179	0.636	0.137	0.060	0.131	0.109	0.043	0.781	1.223	1.002	0.313
CaO	11.670	10.847	0.527	6.900	6.620	6.620	6.713	0.162	7.210	8.380	7.795	0.827
Na_2O	4.390	5.052	0.461	7.350	7.800	7.620	7.590	0.226	6.740	6.340	6.540	0.283
Total	**99.080**	**98.390**	**0.478**	**97.349**	**97.997**	**97.280**	**97.542**	**0.396**	**97.585**	**97.578**	**97.582**	**0.005**
formula												
Si	2.332	2.451		2.672	2.677	2.658	2.669		2.658	2.627	2.643	
Ti	0.003	0.003		0.002	0.002	0.003	0.002		0.003	0.000	0.002	
Al	1.638	1.464		1.308	1.302	1.326	1.312		1.286	1.280	1.283	
Fe^{3+}	0.039	0.036		0.010	0.012	0.011	0.011		0.028	0.030	0.029	
Mg	0.045	0.081		0.009	0.004	0.009	0.007		0.053	0.084	0.069	
Fe^{2+}	0.000	0.000		0.000	0.000	0.000	0.000		0.000	0.000	0.000	
Z	**4.057**	**4.035**		**4.002**	**3.997**	**4.007**	**4.002**		**4.029**	**4.022**	**4.025**	
Ca	0.573	0.535		0.339	0.323	0.325	0.329		0.353	0.413	0.383	
Na	0.390	0.451		0.653	0.689	0.678	0.673		0.598	0.565	0.582	
X	**0.964**	**0.986**		**0.992**	**1.012**	**1.003**	**1.002**		**0.951**	**0.978**	**0.965**	
Total	**5.021**	**5.021**		**4.993**	**5.008**	**5.010**	**5.004**		**4.980**	**5.000**	**4.990**	
An	59.498	54.266		34.158	31.927	32.437	32.831		37.153	42.211	39.711	
Ab	40.502	45.734		65.842	68.073	67.563	67.169		62.847	57.789	60.289	
Or	0.000	0.000		0.000	0.000	0.000	0.000		0.000	0.000	0.000	
ca(pl)	0.595	0.543		0.342	0.319	0.324	0.328		0.372	0.422	0.397	

pl	15 kbar/1050 °C														
MAOC 15														av	sd
SiO_2	55.272	58.014	52.957	60.770	60.303	60.956	57.908	59.761	60.368	60.291	56.880	59.450	59.020	58.612	2.382
TiO_2	0.085	0.014	0.086	0.079	0.049	0.049	0.163	0.082	0.113	0.049	0.035	0.045	0.036	0.068	0.039
Al_2O_3	25.400	24.660	27.320	20.940	20.910	22.110	22.320	22.900	21.830	21.910	26.260	24.660	25.190	23.570	2.113
FeO	0.954	0.416	0.650	0.916	0.921	0.377	0.867	0.391	0.812	0.532	0.263	0.360	0.367	0.602	0.259
MgO	1.288	0.419	0.887	2.000	1.860	0.322	1.627	0.189	1.333	0.913	0.094	0.395	0.376	0.900	0.661
CaO	7.500	6.690	9.320	3.960	4.130	4.110	6.740	5.080	4.030	3.990	8.050	6.690	6.770	5.928	1.814
Na_2O	6.690	7.380	5.840	8.550	8.360	9.040	7.540	8.610	8.680	9.110	6.490	7.470	7.140	7.762	1.046
Total	**97.279**	**97.730**	**97.096**	**97.315**	**96.611**	**97.027**	**97.214**	**97.052**	**97.277**	**96.887**	**98.127**	**99.120**	**98.929**	**97.513**	**0.768**
formula															
Si	2.553	2.651	2.461	2.773	2.771	2.783	2.669	2.737	2.756	2.764	2.591	2.672	2.655	2.680	
Ti	0.003	0.000	0.003	0.003	0.002	0.002	0.006	0.003	0.004	0.002	0.001	0.002	0.001	0.002	
Al	1.383	1.328	1.497	1.126	1.132	1.190	1.212	1.236	1.175	1.184	1.410	1.306	1.336	1.270	
Fe^{3+}	0.037	0.016	0.025	0.035	0.035	0.014	0.033	0.015	0.031	0.020	0.010	0.014	0.014	0.023	
Mg	0.089	0.029	0.061	0.136	0.127	0.022	0.112	0.013	0.091	0.062	0.006	0.026	0.025	0.061	
Fe^{2+}	0.000	0.000	0.000	0.000	0.000	0.000	0.000	0.000	0.000	0.000	0.000	0.000	0.000	0.000	
Z	**4.064**	**4.023**	**4.048**	**4.072**	**4.068**	**4.011**	**4.032**	**4.003**	**4.056**	**4.032**	**4.018**	**4.019**	**4.031**	**4.037**	
Ca	0.371	0.328	0.464	0.194	0.203	0.201	0.333	0.249	0.197	0.196	0.393	0.322	0.326	0.290	
Na	0.599	0.654	0.526	0.756	0.745	0.800	0.674	0.764	0.768	0.810	0.573	0.651	0.623	0.688	
X	**0.970**	**0.981**	**0.990**	**0.950**	**0.948**	**1.001**	**1.007**	**1.014**	**0.965**	**1.006**	**0.966**	**0.973**	**0.949**	**0.978**	
Total	**5.034**	**5.004**	**5.038**	**5.022**	**5.016**	**5.013**	**5.039**	**5.017**	**5.022**	**5.037**	**4.984**	**4.992**	**4.980**	**5.015**	
An	38.254	33.376	46.863	20.379	21.446	20.080	33.065	24.588	20.418	19.487	40.669	33.107	34.382	29.679	
Ab	61.746	66.624	53.137	79.621	78.554	79.920	66.935	75.412	79.582	80.513	59.331	66.893	65.618	70.321	
Or	0.000	0.000	0.000	0.000	0.000	0.000	0.000	0.000	0.000	0.000	0.000	0.000	0.000	0.000	
ca(pl)	0.383	0.334	0.469	0.204	0.214	0.201	0.331	0.246	0.204	0.195	0.407	0.331	0.344	0.297	

Melt in MAOC 11

melt	10kbar/1100 °C															
MAOC 11																
SiO_2	52.660	51.870	51.890	52.330	51.780	53.430	52.650	52.700	52.900	52.330	52.890	52.100	52.070	51.860	52.240	52.930
TiO_2	0.723	0.736	0.758	0.691	0.678	0.665	0.689	0.719	0.673	0.722	0.714	0.781	0.745	0.732	0.814	0.692
Al_2O_3	20.460	19.160	18.920	19.700	19.490	20.230	20.360	19.890	20.270	19.090	20.000	18.970	19.100	19.040	19.700	19.910
FeO	3.890	4.210	4.040	3.540	3.350	3.640	3.060	3.990	3.760	4.210	3.810	4.130	4.060	4.070	3.930	3.970
MgO	3.690	5.760	5.620	3.350	2.740	2.790	1.505	3.950	3.460	5.010	3.740	5.600	6.050	5.930	4.160	4.320
CaO	8.010	9.410	9.040	7.980	8.500	7.690	8.190	8.930	8.720	9.110	8.990	9.330	9.280	8.970	9.300	8.630
Na_2O	2.620	1.910	1.480	0.571	0.500	0.787	0.463	1.490	1.075	1.280	1.460	1.810	1.930	1.610	1.590	1.380
Total	92.053	93.056	91.748	88.162	87.038	89.232	86.917	91.669	90.858	91.752	91.604	92.721	93.235	92.212	91.734	91.832
Mg#	0.628	0.709	0.713	0.628	0.593	0.577	0.467	0.638	0.621	0.680	0.636	0.707	0.727	0.722	0.654	0.660
A/CNK	1.084	0.946	1.003	1.275	1.197	1.324	1.301	1.064	1.150	1.023	1.067	0.951	0.953	1.004	1.009	1.109
Q																
An																
Di																
Hyp																
Ab																
Ilm																
C																
Mag																
Total																

melt	10kbar/1100 °C		12.5kbar/1050 °C					12.5kbar/1100 °C							
MAOC 11	av	sd				av	sd								
SiO_2	52.414	0.483	44.140	55.750	58.440	52.777	7.600	62.258	62.471	62.064	62.227	62.440	61.598	61.141	59.551
TiO_2	0.721	0.041	0.951	0.384	1.149	0.828	0.397	1.135	1.078	1.124	1.161	1.233	1.278	1.138	0.938
Al_2O_3	19.643	0.541	6.330	20.480	16.450	14.420	7.290	14.860	14.950	15.070	14.860	14.220	13.990	15.000	16.020
FeO	3.854	0.320	7.800	2.610	3.590	4.667	2.757	3.400	3.270	3.280	3.280	3.460	3.640	3.320	3.440
MgO	4.230	1.333	11.250	2.870	0.970	5.030	5.470	2.500	2.250	2.370	2.540	2.640	2.390	2.480	2.360
CaO	8.755	0.539	17.490	7.520	3.980	9.663	7.005	4.880	5.120	5.040	5.200	5.070	4.980	5.340	5.140
Na_2O	1.372	0.586	0.858	4.190	1.440	2.163	1.780	3.130	3.470	3.250	3.230	3.340	3.050	3.510	3.300
Total	90.989	2.025	88.819	93.804	86.019	89.547	3.943	92.163	92.609	92.198	92.498	92.403	90.926	91.929	90.749
Mg#	0.662		0.720	0.662	0.325	0.658		0.658	0.551	0.563	0.580	0.576	0.539	0.571	0.550
A/CNK	1.081		0.191	0.996	1.713	0.683		1.060	0.996	1.039	1.006	0.967	0.994	0.969	1.084
	CIPW		CIPW	CIPW	CIPW	CIPW									
Q/ Neph*	19.081		1.32*	10.290	44.902	15.128									
An	47.725		15.073	39.518	22.920	33.085									
Di	0.000		66.106	0.177	0.000	16.437									
Hyp/ Ol*	16.302		7.58*	10.829	6.524	11.949									
Ab	12.777		5.779	37.739	14.131	20.393									
Ilm	1.500		2.032	0.760	2.545	1.747									
C	1.595		0.000	0.000	7.963	0.000									
Mag	1.029		2.117	0.667	1.015	1.261									
Total	100.010		100.000	99.980	100.000	100.000									

melt	12.5kbar/1100 °C		15kbar/1050 °C													
MAOC 11	av	sd													av	sd
SiO_2	61.719	0.986	61.790	62.580	66.410	65.860	65.330	65.320	65.970	65.100	64.440	65.650	65.810	64.370	64.886	1.404
TiO_2	1.136	0.102	0.759	0.964	0.674	0.763	0.760	0.755	0.731	0.665	0.782	0.776	0.816	0.787	0.769	0.075
Al_2O_3	14.871	0.607	17.460	16.540	15.870	15.880	15.880	16.020	15.920	17.840	15.490	15.910	15.750	16.370	16.244	0.714
FeO	3.386	0.127	2.410	2.980	2.430	2.410	2.770	2.600	2.650	1.850	2.790	2.640	2.580	3.000	2.593	0.307
MgO	2.441	0.123	1.242	1.055	1.369	1.470	1.488	1.401	1.517	0.725	1.499	1.487	1.384	1.900	1.378	0.284
CaO	5.096	0.140	5.890	4.570	4.350	4.690	4.630	4.550	4.710	4.720	4.690	4.550	4.560	4.190	4.675	0.413
Na_2O	3.285	0.157	4.130	2.370	2.000	2.230	2.020	2.090	1.910	3.940	2.070	1.960	1.940	1.730	2.366	0.797
Total	91.934	0.711	93.681	91.059	93.103	93.303	92.878	92.736	93.408	94.840	91.761	92.973	92.840	92.347	92.911	0.947
Mg#	0.562		0.479	0.387	0.501	0.521	0.489	0.490	0.505	0.411	0.489	0.501	0.489	0.530	0.487	
A/CNK	1.014		0.998	1.355	1.417	1.302	1.353	1.368	1.360	1.184	1.298	1.384	1.372	1.564	1.311	
	CIPW														CIPW	
Q	29.268														41.354	
An	27.484														24.954	
Di	0.000														0.000	
Hyp	9.291														5.128	
Ab	30.208														21.493	
Ilm	2.336														1.576	
C	0.214														4.146	
Mag	1.189														1.348	
Total	99.990														100.000	

melt	15kbar/1100 °C							20kbar/1050 °C								
MAOC 11						av	sd									
SiO_2	58.310	57.740	57.720	58.190	57.820	57.956	0.274	66.230	66.520	65.540	66.130	65.210	65.320	64.470	64.780	64.880
TiO_2	0.783	0.931	0.810	0.892	1.000	0.883	0.089	0.927	0.882	0.924	0.928	1.007	0.831	0.897	0.865	0.945
Al_2O_3	19.970	19.750	19.430	20.410	19.920	19.896	0.357	15.110	15.210	15.180	15.050	15.280	14.790	14.680	15.000	14.990
FeO	1.980	1.960	2.190	1.780	1.960	1.974	0.146	1.770	1.500	1.990	1.990	1.970	1.830	1.700	1.930	1.820
MgO	2.510	3.290	3.390	2.010	2.860	2.812	0.570	0.775	0.685	0.916	0.913	1.054	0.708	0.621	1.053	1.064
CaO	6.560	6.680	7.100	6.060	6.610	6.602	0.371	3.210	3.240	3.920	3.960	4.000	3.490	3.460	4.180	4.230
Na_2O	3.390	3.160	3.020	3.020	2.880	3.094	0.193	1.480	1.710	1.990	2.070	2.060	1.850	1.740	2.200	2.220
Total	93.503	93.511	93.660	92.362	93.050	93.217	0.530	89.502	89.747	90.460	91.041	90.581	88.819	87.568	90.008	90.149
Mg#	0.693	0.750	0.734	0.668	0.722	0.717		0.438	0.449	0.451	0.450	0.488	0.408	0.394	0.493	0.510
A/CNK	1.141	1.139	1.087	1.277	1.189	1.164		1.827	1.748	1.460	1.419	1.433	1.575	1.604	1.337	1.322
						CIPW										
Q						22.634										
An						35.124										
Di						0.000										
Hyp						8.668										
Ab						28.093										
Ilm						1.804										
C						2.996										
Mag						0.681										
Total						100.000										

melt	**20kbar/1050 °C**		**20kbar/1100 °C**													
MAOC 11	**av**	**sd**													**av**	**sd**
SiO_2	65.453	0.710	63.160	63.620	62.230	61.330	61.930	61.950	61.900	60.660	63.200	62.900	62.720	62.980	62.382	0.867
TiO_2	0.912	0.051	1.091	0.993	1.105	1.130	1.197	1.132	1.168	1.075	1.063	1.060	1.067	1.044	1.094	0.056
Al_2O_3	15.032	0.196	16.930	17.230	16.830	16.910	16.900	16.950	17.200	16.810	17.290	17.440	17.320	17.340	17.096	0.227
FeO	1.833	0.162	2.770	2.150	2.640	2.850	2.970	2.790	2.480	2.770	2.340	2.210	2.470	2.420	2.572	0.265
MgO	0.865	0.173	1.217	0.845	1.670	2.130	2.180	1.860	1.770	2.340	0.834	0.764	0.883	1.204	1.475	0.584
CaO	3.743	0.396	5.220	4.810	5.880	6.370	6.310	6.080	5.920	6.410	4.720	4.910	5.060	5.380	5.589	0.641
Na_2O	1.924	0.248	1.850	1.670	1.940	1.980	2.110	2.020	2.030	2.060	1.670	1.750	1.620	1.760	1.872	0.173
Total	**89.764**	**1.047**	**92.238**	**91.318**	**92.295**	**92.700**	**93.597**	**92.782**	**92.468**	**92.125**	**91.117**	**91.034**	**91.140**	**92.128**	**92.079**	**0.791**
Mg#	0.457		0.439	0.412	0.530	0.571	0.567	0.543	0.560	0.601	0.389	0.381	0.389	0.470	0.506	
A/CNK	1.508		1.351	1.499	1.212	1.140	1.131	1.179	1.220	1.117	1.526	1.477	1.460	1.368	1.291	
	CIPW														**CIPW**	
Q	49.883														39.773	
An	20.687														30.113	
Di	0.000														0.000	
Hyp	2.771														5.603	
Ab	18.108														17.177	
Ilm	1.937														2.260	
C	5.628														4.184	
Mag	0.986														0.899	
Total	**100.000**														**100.010**	

Melt in MAOC 13

melt	**10kbar/1100 °C**															
MAOC 13																
SiO_2	52.330	51.960	51.450	51.640	51.320	50.920	50.890	50.930	51.590	51.220	51.570	51.300	51.630	51.670	51.000	50.770
TiO_2	0.567	0.768	0.599	0.823	0.656	0.773	0.753	0.716	0.703	0.750	0.708	0.715	0.621	0.627	0.706	0.823
Al_2O_3	21.770	20.840	22.670	20.830	21.400	21.290	21.510	21.200	21.070	22.720	22.540	23.090	22.800	22.340	22.770	22.520
FeO	3.400	3.700	3.410	3.720	3.480	3.520	3.490	3.700	3.600	3.530	3.140	3.610	3.370	2.990	3.320	3.600
MgO	2.890	3.790	2.300	4.920	3.630	3.900	3.820	4.130	3.870	2.180	2.700	2.280	2.480	2.330	2.160	2.390
CaO	8.370	8.550	8.140	9.000	8.960	9.050	8.910	9.170	8.650	7.820	7.260	7.380	7.760	7.960	7.740	7.800
Na_2O	1.188	1.343	1.161	2.670	2.740	2.860	2.730	2.610	2.450	2.550	2.640	2.600	2.690	2.330	2.650	2.480
Total	**90.515**	**90.951**	**89.730**	**93.603**	**92.186**	**92.313**	**92.103**	**92.456**	**91.933**	**90.770**	**90.558**	**90.975**	**91.351**	**90.247**	**90.346**	**90.383**
Mg#	0.602	0.646	0.546	0.702	0.650	0.664	0.661	0.666	0.657	0.524	0.605	0.530	0.567	0.581	0.537	0.542
A/CNK	1.268	1.174	1.357	1.004	1.029	1.006	1.040	1.011	1.066	1.234	1.285	1.305	1.230	1.220	1.235	1.233
Q																
An																
Di																
Hyp																
Ab																
Ilm																
C																
Mag																
Total																

melt	**10kbar/1100 °C**		**12.5kbar/1100 °C**							**15kbar/1050 °C**						
MAOC 13	**av**	**sd**						**av**	**sd**							
SiO_2	51.387	0.428	54.240	54.023	54.581	53.825	52.808	53.895	0.669	62.940	63.480	61.890	63.840	63.240	64.550	59.570
TiO_2	0.707	0.076	1.588	1.373	1.356	1.471	1.310	1.420	0.111	0.854	0.907	0.867	0.985	0.925	0.991	0.943
Al_2O_3	21.960	0.792	18.750	19.540	19.080	17.520	18.000	18.578	0.816	16.820	16.290	15.090	16.210	15.820	16.540	14.580
FeO	3.474	0.201	4.280	3.650	3.740	4.400	3.890	3.992	0.332	3.150	2.900	3.070	3.100	2.760	2.860	4.390
MgO	3.111	0.880	2.390	1.740	1.750	4.530	4.040	2.890	1.312	1.230	2.150	3.370	1.501	2.120	1.153	5.500
CaO	8.283	0.630	5.320	4.830	4.940	6.370	6.880	5.668	0.910	3.490	3.180	6.090	3.630	4.820	3.370	8.680
Na_2O	2.356	0.573	4.190	4.490	3.970	3.690	3.640	3.996	0.355	2.250	1.820	1.900	2.260	1.930	2.050	2.020
Total	**91.276**	**1.048**	**90.758**	**89.646**	**89.417**	**91.806**	**90.568**	**90.439**	**0.957**	**90.734**	**90.727**	**92.277**	**91.526**	**91.615**	**91.514**	**95.683**
Mg#	0.615		0.499	0.459	0.455	0.647	0.649	0.563		0.410	0.569	0.662	0.463	0.578	0.418	0.691
A/CNK	1.160		1.132	1.209	1.230	0.993	0.973	1.101		1.674	1.856	1.063	1.571	1.325	1.741	0.763
	CIPW							**CIPW**								
Q	14.621							13.994								
An	44.996							31.056								
Di	0.000							0.000								
Hyp	13.155							11.628								
Ab	21.831							37.401								
Ilm	1.462							2.982								
C	3.315							1.877								
Mag	0.609							1.073								
Total	**99.990**							**100.010**								

melt	**15kbar/1050 °C**													**15kbar/1100 °C**		
MAOC 13												**av**	**sd**			
SiO_2	64.510	64.040	63.160	64.510	58.063	57.536	60.209	60.432	61.015	59.160	58.923	62.787	1.637	53.230	53.600	53.360
TiO_2	0.911	0.969	1.031	1.050	0.896	0.896	0.929	1.013	0.932	0.875	0.873	0.925	0.053	1.230	1.109	1.042
Al_2O_3	16.130	16.700	16.770	16.460	15.210	16.960	16.990	16.710	16.760	16.220	16.670	15.907	0.807	19.890	20.720	20.780
FeO	2.870	3.050	3.040	2.790	3.770	4.400	2.970	2.850	2.980	3.060	3.680	3.176	0.554	2.320	2.100	2.040
MgO	1.411	1.374	1.276	1.301	3.490	4.390	1.301	1.171	1.110	2.220	2.480	2.432	1.550	4.440	3.130	3.040
CaO	3.480	3.550	3.460	3.240	6.540	4.020	3.490	3.460	3.410	4.650	3.980	4.751	2.019	7.040	6.470	6.410
Na_2O	1.390	0.699	0.519	2.200	3.100	2.790	3.620	3.410	3.460	2.920	3.460	2.033	0.170	2.900	2.940	2.930
Total	**90.702**	**90.382**	**89.256**	**91.551**	**91.069**	**90.992**	**89.509**	**89.046**	**89.667**	**89.105**	**90.066**	**90.857**	**1.541**	**91.050**	**90.069**	**89.602**
Mg#	0.467	0.445	0.428	0.454	0.623	0.640	0.439	0.423	0.399	0.564	0.546	0.544		0.773	0.727	0.727
A/CNK	1.873	2.196	2.347	1.731	0.895	1.425	1.381	1.404	1.409	1.223	1.289	1.409		1.132	1.248	1.261
												CIPW				
Q												38.211				
An												23.217				
Di												0.000				
Hyp												8.711				
Ab												21.577				
Ilm												1.956				
C												5.196				
Mag												1.131				
Total												**100.000**				

melt	15kbar/1100 °C												
MAOC 13												av	sd
SiO_2	54.480	47.900	47.880	47.330	52.490	52.800	52.050	53.140	52.610	52.650	56.090	53.397	0.188
TiO_2	1.054	0.854	0.899	0.984	0.835	0.533	0.861	1.231	1.104	1.143	0.756	1.127	0.095
Al_2O_3	20.700	20.160	20.180	20.340	21.190	21.900	21.500	19.000	19.220	18.960	21.130	20.463	0.497
FeO	2.080	2.780	2.760	2.850	1.161	1.048	1.910	2.570	2.750	2.610	1.243	2.153	0.147
MgO	2.820	6.020	6.070	6.380	1.151	0.691	1.285	4.490	4.690	4.460	0.590	3.537	0.784
CaO	6.500	10.800	10.800	10.700	8.820	7.630	7.060	7.340	7.420	7.460	5.230	6.640	0.348
Na_2O	3.080	2.850	3.080	2.940	2.240	2.510	2.490	2.950	2.840	2.930	3.010	2.923	0.021
Total	**90.714**	**91.364**	**91.669**	**91.524**	**87.887**	**87.112**	**87.156**	**90.721**	**90.634**	**90.213**	**88.049**	**89.840**	**1.619**
Mg#	0.707	0.794	0.797	0.800	0.639	0.540	0.545	0.757	0.753	0.753	0.458	0.744	
A/CNK	1.226	0.829	0.817	0.837	1.075	1.217	1.270	1.044	1.058	1.031	1.461	1.079	
												CIPW	
Q												14.410	
An												43.260	
Di												0.000	
Hyp												11.371	
Ab												26.654	
Ilm												2.051	
C												1.664	
Mag												0.580	
Total												**99.990**	

melt	20kbar/1050 °C											20 kbar
MAOC 13										av	sd	1100°C
SiO_2	62.620	63.300	65.960	66.240	65.820	65.580	66.020	65.340	63.350	64.914	1.407	53.360
TiO_2	1.004	0.934	0.870	0.833	0.947	0.877	0.938	1.003	1.008	0.935	0.064	1.236
Al_2O_3	13.130	13.150	14.220	14.210	14.100	14.260	14.270	14.550	15.040	14.103	0.613	17.610
FeO	2.210	2.270	2.030	1.950	2.040	2.010	1.860	1.910	2.780	2.118	0.281	3.900
MgO	2.310	2.700	1.207	1.065	1.278	1.273	1.068	0.805	1.910	1.513	0.643	3.320
CaO	4.700	5.550	3.040	2.890	3.100	3.090	2.950	2.820	2.930	3.452	0.976	4.680
Na_2O	1.276	1.890	1.910	1.850	1.840	1.890	2.280	1.940	1.640	1.835	0.267	1.610
Total	**87.250**	**89.794**	**89.237**	**89.038**	**89.125**	**88.980**	**89.386**	**88.368**	**88.658**	**88.871**	**0.732**	**85.716**
Mg#	0.651	0.680	0.515	0.493	0.528	0.530	0.506	0.429	0.551	0.560		0.603
A/CNK	1.234	0.996	1.640	1.713	1.628	1.634	1.566	1.749	1.874	1.517		1.578
										CIPW		CIPW
Q										49.850		31.936
An										19.249		27.087
Di										0.000		0.000
Hyp										4.914		13.722
Ab										17.431		15.908
Ilm										1.994		2.735
C										5.417		7.510
Mag										1.145		1.102
Total										**100.000**		**100.000**

Melt in MAOC 15

melt	10 kbar	10kbar/1100 °C								
MAOC 15	1050°C								av	sd
SiO_2	50.200	50.860	51.130	50.850	51.260	51.243	51.046	49.918	50.901	0.463
TiO_2	0.490	0.822	0.872	0.743	0.800	0.714	0.714	0.660	0.761	0.074
Al_2O_3	20.450	21.320	21.390	21.050	21.660	21.720	22.430	21.740	21.616	0.438
FeO	3.600	2.380	2.400	2.530	2.440	2.110	2.040	2.270	2.310	0.179
MgO	5.520	4.840	5.240	5.200	4.080	3.670	3.360	4.330	4.389	0.737
CaO	8.180	8.010	7.900	8.010	8.190	7.780	7.540	7.990	7.917	0.208
Na_2O	2.590	1.119	0.649	1.135	1.133	3.660	3.680	3.340	2.102	1.379
Total	**91.030**	**89.351**	**89.581**	**89.518**	**89.563**	**90.897**	**90.810**	**90.248**	**89.995**	**0.651**
Mg#	0.732	0.784	0.796	0.786	0.749	0.756	0.746	0.773	0.772	
A/CNK	1.069	1.300	1.386	1.281	1.293	1.077	1.135	1.086	1.211	
	CIPW								CIPW	
Q	7.919								15.635	
An	44.550								43.607	
Di	0.000								0.000	
Hyp	20.376								14.754	
Ab	24.031								19.800	
Ilm	1.026								1.614	
C	1.461								4.179	
Mag	0.638								0.420	
Total	**100.000**								**100.010**	

melt	15kbar/1100 °C							20 kbar
MAOC 15						av	sd	1050 °C
SiO_2	49.570	50.200	49.680	49.240	49.310	49.600	0.381	42.080
TiO_2	0.965	0.922	0.949	0.951	1.006	0.959	0.031	0.913
Al_2O_3	19.960	20.270	20.370	20.450	19.900	20.190	0.247	18.710
FeO	1.390	1.980	2.210	2.310	2.380	2.054	0.401	8.460
MgO	0.255	0.889	1.096	1.261	1.556	1.011	0.488	15.390
CaO	9.150	8.570	8.830	8.790	8.720	8.812	0.213	5.090
Na_2O	2.300	2.320	2.340	2.180	2.380	2.304	0.075	0.431
Total	**83.590**	**85.151**	**85.475**	**85.182**	**85.252**	**84.930**	**0.760**	**91.074**
Mg#	0.246	0.445	0.469	0.493	0.538	0.467		0.764
A/CNK	0.978	1.045	1.023	1.045	1.007	1.019		1.878
						CIPW		CIPW
Q						17.760		0.462
An						51.445		27.682
Di						0.000		0.000
Hyp						4.878		54.875
Ab						22.931		3.977
Ilm						2.146		1.899
C						0.457		9.601
Mag						0.391		1.493
Total						**100.010**		**99.990**